

THE UNIVERSITY OF HULL

**Towards the synthesis of Multifunctional Constructs:  
Coupling PET and PDT for the Targeted Diagnosis  
and Therapy of CXCR4 Expressing Tumours**

being a Thesis submitted for the Degree of  
Doctor of Philosophy in the University of Hull

by

Rachel Smith, MChem (Hons)

December 2012

## Abstract

To establish accurate and early stage tumour diagnosis, quantitative molecular imaging modalities such as positron emission tomography (PET) are being employed. Molecular probes containing a positron emitting isotope (e.g.  $^{18}\text{F}$ ,  $^{64}\text{Cu}$ ) are designed to target biomarkers or metabolic processes within the tumour. A therapeutic molecule could then be conjugated to this diagnostic probe to create a multifunctional construct (MFC). MFCs are a new concept in drug design offering the potential for both diagnosis and therapy. This work exploits the chelating properties of saturated tetraazamacrocycles known herein as macrocycles as well as their known affinity for the chemokine receptor CXCR4, a cell surface receptor involved in embryonic development and cell migration known to be overexpressed in at least twenty three different tumour types, along with the photodynamic activity of porphyrin molecules to create novel MFCs with diagnostic and therapeutic properties.

A series of configurationally restricted copper(II), zinc(II) and nickel(II) mono-ring macrocycles bearing a methylamine pendant arm are presented. Monomacrocycles possess the potential for improved pharmacological properties. Biological studies assessing the affinity and potency of these macrocycles as CXCR4 antagonists demonstrated that zinc(II) monomacrocycles were the most potent in their class. A side bridged (SB) zinc(II) monocyclen compound;  $[\text{Zn}\mathbf{9}]^{2+}$  synthesised in 64% yield, demonstrated the highest affinity for CXCR4 in its class showing a 2.5-fold higher affinity in comparison to the clinically licensed antagonist AMD3100 ( $\text{IC}_{50} = 12 \text{ nM}$  vs.  $31 \text{ nM}$ ).

In response to the high affinity observed for a *meta*-substituted biscyclen ligand ( $\text{L}^{48}$ ) a novel cross bridged (CB) *meta*-substituted biscyclen compound bearing a methylamine pendant arm **20** was synthesised along with its copper(II), nickel(II) and zinc(II) complexes in 77%, 88% and 90% yields, respectively. These metal complexes displayed high affinity for CXCR4 when competed with a CXCR4 specific antibody (% inhibition >85%) and required sub-micromolar concentrations to reduce the 'normal' signalling of CXCR4 by 50%.  $[\text{Cu}_2\mathbf{20}]^{4+}$  has the potential to be a

targeted PET probe through the use of  $^{64}\text{Cu}$  and so a detailed biological evaluation into its binding mode was undertaken. These assays concluded that  $[\text{Cu}_2\mathbf{20}]^{4+}$  exerts its antagonistic effect by locking the receptor on the surface of the cell, stopping the internalisation and recycling processes, which would result in formation of a new receptor. An analogous *meta*-substituted biscyclam ligand (**28**) and its copper(II), zinc(II) and nickel(II) complexes were synthesised in 74%, 58% and 46% yields, respectively. These metal complexes also demonstrated high affinity for CXCR4 ( $\text{IC}_{50} < 0.1 \mu\text{M}$ ). In fact  $[\text{Cu}_2\mathbf{28}]^{4+}$  showed unexpectedly high affinity for CXCR4 demonstrating almost a 3-fold higher affinity than AMD3100 ( $\text{IC}_{50} = 11\text{nM}$  vs. 31 nM), the potential of  $[\text{Cu}_2\mathbf{28}]^{4+}$  as a targeted PET probe should also be considered.

Various organic spacer arms were attached to bismacrocycle **20**, to produce a CXCR4 targeting probe with a functional arm for further conjugation which would also act to prevent steric hindrance. An acidic terminating chain was successfully attached to bismacrocycle **20** in quantitative yield, via ring-opening of diglycolic anhydride as well as an amine terminating variant (93% yield). A biotin tag was also attached to bismacrocycle **20** and its copper(II) complex was successfully isolated in a 94% yield. Addition of a spacer arm was found to have no significantly detrimental effect on binding affinity to CXCR4.

A series of known water and organic soluble metalloporphyrins were synthesised. Subsequent conjugation to macrocyclic compounds proved challenging but analytical data for the conjugation of bismacrocycle **20** and metalloporphyrin  $[\text{Zn}\mathbf{59}]$  indicated a successful reaction had occurred. This reaction represents important steps towards the synthesis of MFCs with diagnostic and therapeutic properties.

## **Risk Assessment**

All experiments were carried out in accordance with the University of Hull's Health and Safety guidelines. A full COSHH and risk assessment was carried out for each new experiment, signed by the undertaking student, supervisor (Dr S. J. Archibald) and the departmental safety officer (Dr T. McCreedy) before any practical work started. The COSHH forms carry the reference numbers RSSJA01-RSSJA54.

## Acknowledgements

Firstly, I would like to thank my supervisors Dr S. J. Archibald and Dr R. W. Boyle. Steve as my principal supervisor I would like to thank you for all the knowledge you have imparted to me and opportunities you have given me. Ross I would like to thank you for all the ideas and support you have given me. I would also like to acknowledge Dr Francesca Giuntini at this point for her help and involvement with my project.

I would like to take this opportunity to thank all the technical staff for their help throughout my PhD. Especially Carol Kennedy for performing all my CHN analysis and for being a continual source of help. I would also like to thank the EPSRC National Mass Spectrometry Service Centre, Dr Kevin Welham (Hull) and Karl Heaton (York) for performing mass spectrometry analysis on my behalf as well as Prof. Erik De Clercq's group for performing the calcium(II) signalling studies and Prof. Tony Ng's group for performing the internalisation, phosphorylation and degradation assays.

I would like to acknowledge all my friends and family for their support and encouragement throughout my PhD. In particular, my wonderful boyfriend Marc, you have had to endure all the up and downs of my PhD. You have been there through the hard times and the good and so my achievements are your achievements. You have been my constant source of support and I am forever thankful. To my parents I would like to thank you for always believing in me, always supporting me and always encouraging me to aim high, this ones for you. I wouldn't be the person I am today without you and I am blessed to have parents like you. Fran, Louis and Kati – my three muskateers what would I have done without you guys, your madness has kept me sane! You have been my support network and I thank you all for the time you have put into helping me both chemically and emotionally.

## Abbreviations

$\lambda_{\max}$	Maximum Wavelength
ACCP	Activatable Cell Penetrating Peptide
Ac <sub>2</sub> O	Acetic Anhydride
AcOH	Acetic Acid
AIBN	Azobisisobutyronitrile
Asp	Aspartate
ATCC	American Type Culture Collection
$\beta^-$	Electron (beta minus)
$\beta^+$	Positron (beta plus)
BCA	Bicinchoninic Acid
BFC	Bifunctional Chelator
Boc	<i>tert</i> -Butyloxycarbonyl
BOP	(Benzotriazol-1-yloxy)tris(dimethylamino)phosphonium hexafluorophosphate
br	Broad
BSA	Bovine Serum Albumin
CB	Cross Bridge
CC <sub>50</sub>	The cytotoxic concentration required to reduce a population by 50%
CCD	Charge Coupled Device
CEA	Carcinoembryonic Antigen
CHN	Carbon, Hydrogen, Nitrogen analysis
CHX	Cycloheximide
COSHH	Control of Sustances Hazardous to Health
CPP	Cell Penetrating Peptide
CT	Computed Tomography
Cy 5	Cyanine 5
Cy 5.5	Cyanine 5.5
$\delta$	Chemical Shift
d	Doublet
DABCO	1,4-Diaza[2.2.2]bicyclooctane
DCC	Dicyclohexylcarbodiimide
DCM	Dichloromethane
DCU	Dicyclohexylurea
DIC	Diisopropylcarbodiimide
DIPEA	Diisopropylethylamine
DIU	Diisopropylurea
DMAP	4-Dimethylaminopyridine
DMF	<i>N,N'</i> -Dimethylformamide
DMSO	Dimethylsulfoxide
DNA	Deoxyribose Nucleic Acid
DO2A	4,10-bis(Carboxymethyl)-1,4,7,10-tetraazabicyclo[5.5.2]tetradecane
DOTA	1,4,7,10-Tetraazacyclododecane-1,4,7,10-tetraacetic Acid
DTPA	Diethylenetriamine Pentaacetic Acid
DTT	Dithiothreitol

$\epsilon$	Molar Absorptivity
EC <sub>50</sub>	Effective concentration required to reduce an effect by 50%
ECL 1, 2 or 3	Extra Cellular Loop 1, 2 or 3
ECL	Enhanced Luminol-based Chemiluminescent
EcoRI	<i>Escherichia coli</i> RY13 first identified
EDC	1-Ethyl-3-(3-dimethylaminopropyl) Carbodiimide
EDTA	Ethylene Diamine Tetra-acetic Acid
EEA1	Early Endosome Antigen 1
EGFP	Enhanced Green Fluorescent Protein
ERK1/2	Extracellular Regulated Kinase 1/2
ESI	Electrospray Ionisation
FACS	Fluorescence Activated Cell Sorting
FBS	Foetal Bovine Serum
FDG	2-Deoxy-2-fluoro-D-glucose
FITC	Fluorescein Isothiocyanate
FLIPR	Fluorometric Imaging Plate Reader
Fmoc	Fluorenylmethyloxycarbonyl Chloride
GAPDH	Glyceraldehydephosphate Dehydrogenase
GFP	Green Fluorescent Protein
Glu	Glutamate
GPCR	G-Protein Coupled Receptor
HBTU	<i>O</i> -Benzotriazole- <i>N,N,N',N'</i> -tetramethyl-uronium-hexafluoro phosphate
HEPES	4-(2-Hydroxyethyl)-1-piperazineethanesulfonic acid
HindIII	Haemophilus Influenza III
HIV	Human Immunodeficiency Virus
HOBt	<i>N</i> -Hydroxybenzotriazole
HRMS	High Resolution Mass Spectrometry
HPLC	High Pressure Liquid Chromatography
HRP	Horseradish peroxidase
Hsp27	Heat Shock Protein 27
HTLV-1	Human T-lymphotropic Virus 1
IC <sub>50</sub>	Concentration required to inhibit binding by 50%
IVM	Intravital Microscopy
J	Coupling Constant
kDa	Kilodaltons
keV	Kiloelectronvolts
m	Multiplet
mAb	Monoclonal Antibody
MACE	Mono Aspartyl Chlorin e <sub>6</sub>
MeCN	Acetonitrile
MEM	Minimum Essential Medium
MeOH	Methanol
MFC	Multifunctional Construct
M	Molar
mCi	Millicurie

MHz	Megahertz
mm	Millimetres
$\mu$ M	Micromolar
$\mu$ mol	Micromolar
MRI	Magnetic Resonance Imaging
MRL	Medical Research Laboratory
MS	Mass Spectrometry
MT-4	Meta Trader 4
NBS	<i>N</i> -Bromosuccinimide
NCS	Isothiocyanate
NIR	Near Infra-Red
NHS	<i>N</i> -Hydroxysuccinimide
nm	Nanometres
nM	Nanomolar
NMR	Nuclear Magnetic Resonance
OI	Optical Imaging
p38MAPK	p38 Mitogen Activated Protein Kinase
PAA	Plains All America
PBMC	Peripheral Blood Mononuclear Cell
PBS	Phosphate Buffer Solution
PDT	Photodynamic Therapy
PEG	Polyethyleneglycol
PET	Positron Emission Tomography
PFA	Paraformaldehyde
ppm	Parts Per Million
PS	Photosensitiser
PVDT	Poly(vinylidiaminotriazine)
pVSV-G	Vesicular Stomatitis Virus-Glycoprotein
PyBOP	(Benzotriazol-1-yloxy)tripyrrolidino phosphonium hexafluorophosphate
q	Quartet
QD	Quantum Dots
quin	Qunitet
RDG	Arginine-Glycine-Aspartate
R <sub>f</sub>	Retention factor
RPMI	Roswell Park Memorial Institute
RT	Room Temperature
s	Singlet
SB	Side Bridge
SDS-PAGE	Sodium Dodecyl Sulfate Polyacrylamide Gel Electrophoresis
SEM	Standard Error of the Mean
SI	Selectivity Index
SIV	Simian Immunodeficiency Virus
SOD	Superoxide Dismutase
SPECT	Single Photon Emission Computed Tomography
t	Triplet

TBS-T	Tris Buffered Saline-Tween
TBTU	<i>O</i> -(Benzotriazol-1-yl)- <i>N,N,N',N'</i> -tetramethyluronium tetrafluoroborate
TCP	1,1'-Thiocarbonyldi-2(1H)-pyridone
TE2A	4,11-bis(Carboxymethyl)-1,4,8,11-tetraazabicyclo[6.6.2]hexadecane
TETA	1,4,8,11-Tetraazacyclotetradecane-1,4,8,11-tetraacetic Acid
TFA	Trifluoroacetic Acid
THF	Tetrahydrofuran
TLC	Thin Layer Chromatography
TM	Transmembrane
TMS	Tetramethylsilane
TPP	Tetraphenyl Porphyrin
TPP-NO <sub>2</sub>	Nitro-tetraphenyl Porphyrin
TPP-NH <sub>2</sub>	Amino-tetraphenyl Porphyrin
TPP-NCS	Isothiocyano-tetraphenyl Porphyrin
UK	United Kingdom
US	Ultrasound
USA	United States of America
UV	Ultra-Violet
UV-vis	Ultra-Violet-visible
VWR	Van Waters and Rodgers
W	Watts

## List of Figures

- Figure 1.** A) White light image of mouse xenograft after tumour exposure. B) Fluorescence image of GFP-labelled tumour cells. C) Fluorescence image 6 hours after administration of the ACCP probe. D) Overlay of images B and C to show co-localisation. Following tumour excision, E) White light image showing apparent complete excision of the tumour mass. F) Fluorescence imaging with GFP also appears to show complete excision. Imaging with the ACCP probe shows a residual fluorescent signal (see \*) in the pectoralis muscle (G and H). Upon excision, K and L show this mass is fluorescent indicating that it is tumour tissue. (Reproduced from Proc. Nat. Acad. Sci.)<sup>4</sup>
- Figure 2.** Summary of the potential uses and advantages of MFCs.
- Figure 3.** A comparison of PET, CT, US (Ultrasound), MRI and SPECT. The box for each imaging modality spans the resolution over which the modality is best suited on the y-axis and demonstrates the maximum depth of penetration it can achieve on the x-axis. The colour of the box is related to its sensitivity (see key). The number of pluses indicates how quantitative the imaging modality is, with [+] being the least and [+++] being the most. (Adapted from Curr. Top. Med. Chem.)<sup>19</sup>
- Figure 4.** Examples of molecular specific contrast agents. Small molecules, peptides and antibodies need to be labelled with a fluorescent moiety for OI. (Nanoparticles include quantum dots (QD)). (Reproduced from J. Mater. Sci: Mater. Med.)<sup>26</sup>
- Figure 5.** Imaging of different sized QD targeting cancer cells in a mouse model. (Reproduced from Methods Mol. Biol.)<sup>29</sup>
- Figure 6.** Helical wheel (A) and serpentine diagram (B) of the CXCR4 receptor. (Reproduced from J. Biol. Chem.)<sup>36</sup>

- Figure 7.** Structure of the small molecule antagonist IT1t.
- Figure 8.** (Left) Overall fold of the CXCR4-IT1t complex. The receptor is coloured blue. The *N*-terminus, ECL1, ECL2 and ECL3 are coloured brown, blue, green and red, respectively. IT1t is shown as a stick representation in magenta with the disulfide bonds in yellow. Conserved water molecules are shown in red. (Right) CXCR4 ligand-binding cavity for IT1t (magenta) the residues of the receptor involved in ligand interactions are shown in green. Nitrogen atoms are blue, oxygen atoms are red and sulfur atoms are yellow. (Reproduced from Science.)<sup>31</sup>
- Figure 9.** Chemokines and chemokine receptor families. (Reproduced from Trends in Mol. Med.)<sup>41</sup>
- Figure 10.** CXCL12 expression in normal human organs. Values are expressed as femtograms of target gene in 100 ng of total cDNA. (Adapted from Nature.)<sup>43</sup>
- Figure 11.** Structure of the tetraazamacrocycles; cyclam (left) and cyclen (right).
- Figure 12.** Molecular structure of AMD3100.
- Figure 13.** Curtis' macrocycle; 5,7,7,12,14,14-hexamethyl-1,4,8,11-tetraazacyclo tetradecane.
- Figure 14.** Molecular structure of AMD3465.
- Figure 15.** Molecular model of the main ligand binding pocket of the CXCR4 receptor with AMD3100 docked into favourable interactions with Asp171 and Asp262. (Reproduced from J. Biol. Chem.)<sup>36</sup>
- Figure 16.** Representations of the six configurational arrangements cyclam derived structures containing metal ions can adopt. (Adapted from Chem. Soc. Rev.)<sup>62</sup>

- Figure 17.** With the addition of an ethylene bridge between adjacent nitrogens a *trans-II* configuration is adopted (when mono-alkylated). With the addition of an ethylene bridge between opposite nitrogens a *cis-V* configuration is adopted. (Reproduced from *Curr. Med. Chem.*)<sup>32</sup>
- Figure 18.** Molecular structures of biscyclams.
- Figure 19.** Photosensitiser initiated cell death. Adapted from *Metal based drugs*)<sup>73</sup>
- Figure 20.** Structure of the porphine macrocycle.
- Figure 21.** Relationship between the absorption profile of a porphyrin and the amount of transmitted light. The transmittance of light increases towards the red end of the spectrum. (Adapted from *Chem. Soc. Rev.*)<sup>75</sup>
- Figure 22.** A bar chart showing the relationship between wavelength and tissue penetration.
- Figure 23.** Clinically licensed porphyrins; photofrin (left) and temoporfin (right).
- Figure 24.** A porphyrin-peptide conjugate shown to selectively accumulate in prostate tumours.<sup>71</sup>
- Figure 25.** Thyroid imaging in a mouse model using PET. Accumulation of radioactivity can also be seen in the liver and bladder due to metabolism and excretion. Colour scale represents the amount of radioactivity accumulated; black = minimum, white = maximum. Image obtained from Prof. P. Blower, Kings College, London. `
- Figure 26.** Schematic of imaging with a PET scanner. (Reproduced from *Acc. Chem. Res.*)<sup>9</sup>
- Figure 27.** The process of PET radiotracer production. From top left: a commercially available biomedical cyclotron; an automated

radiolabelling system controlled from outside the hot cell; analysis and quality-control laboratory; a PET scanner (Siemens); and a processed PET image (bottom left). The whole process typically takes a few hours. (Reproduced from Angew. Chem. Int. Ed.)<sup>93</sup>

- Figure 28.** Structure of <sup>18</sup>F-fluorodeoxyglucose (<sup>18</sup>F-FDG).
- Figure 29.** <sup>18</sup>F-FDG PET image of a patient with non-Hodgkins lymphoma before and after chemotherapy. Scan A shows disease sites in the left neck, mediastinum, lungs and lymph nodes in the upper abdomen. Scan B shows complete resolution of the disease after chemotherapy. (Reproduced from Cancer Metast. Rev.)<sup>25</sup>
- Figure 30.** Examples of a) a sarcophagine, b) a bis-thiosemicarbazone and c) a diphosphine ligand.
- Figure 31.** Structures of macrocyclic <sup>64</sup>Cu chelators.
- Figure 32.** Whole body images of <sup>64</sup>Cu-AMD3100 (left), 50 mg/kg of AMD3100 blocking dose followed by <sup>64</sup>Cu-AMD3100 (middle), and [<sup>64</sup>Cu]CuCl<sub>2</sub> alone (right). All images were scaled to the same maximum threshold value. L = Liver, K= Kidney, B = Bladder. (Reproduced from Cancer Res.)<sup>111</sup>
- Figure 33.** Schematic representing the key components of a proposed MFC with diagnostic and therapeutic properties.
- Figure 34.** Structures of C-functionalised aminomethyl bearing monomacrocycles L<sup>1</sup>-L<sup>4</sup> as reported by Parker and co-workers.<sup>114</sup>
- Figure 35.** C-functionalised ligands L<sup>5</sup>-L<sup>7</sup> as outlined by Archibald and co-workers and the structures of TETA and CB-TE2A.<sup>115, 116</sup>
- Figure 36.** Structures of dioxocyclam ligands; L<sup>8</sup>-L<sup>11</sup>.<sup>62</sup>

- Figure 37.** Structures of aminomethyl C-functionalised macrocycles; L<sup>12</sup> and L<sup>13</sup> as outlined by Rousselin *et al.*<sup>120</sup>
- Figure 38.** Structure of a SB macrocycle published by Wainwright (L<sup>14</sup>).<sup>122</sup>
- Figure 39.** SB monocyclam ligands bearing functional pendant arms; L<sup>15</sup>, L<sup>16</sup>, HSBTE1A, L<sup>17</sup> and HSBTE1A1P.<sup>53, 123</sup>
- Figure 40.** Structures of rigidified macrocycles published by Weisman (L<sup>18</sup>) and Bencini (L<sup>19</sup>).<sup>66, 124</sup>
- Figure 41.** Structures of CB monomacrocycles bearing functional pendant arms; CB-DO2A and L<sup>20</sup>-L<sup>25</sup>, synthesised by Weisman, Wong and co-workers.<sup>128, 129</sup>
- Figure 42.** Molecular structure of bridged cyclam showing a *cis* configuration (left). Ball and stick representation, indicating the presence of two *exo* and two *endo* lone pairs (right). Grey = carbon atoms, blue = nitrogen atoms. Note hydrogen atoms have been omitted for clarity.
- Figure 43.** Representative structures of copper(II), zinc(II) and nickel(II) complexes of monomacrocyclic ligands **8**, **9**, **14** and **15**. Note in some cases anions and/or solvent molecules may coordinate to the metal centre.
- Figure 44.** *ortho*-, *meta*- and *para*-substituted 12-14-membered azamacrocycles; L<sup>26</sup>-L<sup>31</sup> as outlined by De Clercq and co-workers.<sup>141</sup>
- Figure 45.** Structures of configurationally restricted biscyclams L<sup>32</sup> and L<sup>33</sup>.<sup>58, 63</sup>
- Figure 46.** Structures of linear biscyclams; L<sup>34</sup> and L<sup>35</sup> as outlined by Lindoy and co-workers.<sup>143</sup>
- Figure 47.** Structures of a family of configurationally restricted biscyclens; L<sup>36</sup>-L<sup>39</sup>, linked by a *para*- or *meta*-substituted xylyl bridge synthesised by Bernier *et al.*<sup>144</sup>

- Figure 48.** Structure of *meta*- and *para*-substituted biscyclen ligands; L<sup>40</sup> and L<sup>41</sup> bearing protecting groups outlined by Costa *et al.*<sup>145</sup>
- Figure 49.** Structures of the *ortho*- and pyridyl substituted biscyclen ligands; L<sup>42</sup> and L<sup>43</sup> outlined by Develay *et al.*<sup>148</sup>
- Figure 50.** Structures of *meta*- and *para*-substituted bismacrocycles L<sup>44</sup>-L<sup>47</sup>.<sup>149</sup>
- Figure 51.** Structure of a high affinity CXCR4 antagonist L<sup>48</sup>.
- Figure 52.** Representative structures of metal complexes of bismacrocycles **19** and **20**. Note in some cases anions and/or solvent molecules may coordinate to the metal centres.
- Figure 53.** A bis[Zn(cyclen)]<sup>4+</sup> compound synthesised by Oltmanns *et al.*<sup>157</sup>
- Figure 54.** Representative structures of copper(II), zinc(II) and nickel(II) complexes of the CB biscyclam ligand **28**. Note in some cases anions and/or solvent molecules may coordinate to the metal centres.
- Figure 55.** General scheme outlining the formation of an amide bond using an activated acid species. (Adapted from Tetrahedron.)<sup>159</sup>
- Figure 56.** Utilising the NHS ester functionality to conjugate a targeted antagonistic peptide to a DTPA chelate bearing a fluorescent dye. (Reproduced from Bioconj. Chem.)<sup>160</sup>
- Figure 57.** Structure of the fragment observed in the MS analysis in an attempt to isolate acid chloride **29**.
- Figure 58.** Components to produce a targeted multimodal *in vitro* evaluation probe. Note in the case of the copper(II) complex some anions and/or solvent molecules may be bound to the metal centres.
- Figure 59.** Structures of successfully isolated bismacrocycles bearing spacer arms.

- Figure 60.** HIV cell entry: A) interaction of gp120 with CD4, B) interaction of gp120 with CXCR4 or CCR5, C) conformational change in gp41 followed by fusion. (Reproduced from *Curr. Med. Chem.*)<sup>32</sup>
- Figure 61.** Ball and stick representation of the interactions of [Zn<sub>2</sub>AMD3100]<sup>4+</sup> with Asp262, Asp171 and Glu288 of CXCR4. (Reproduced from *J. Am. Chem. Soc.*)<sup>113</sup>
- Figure 62.** *ortho*-, *meta*- and *para*-substituted 12-14-membered azamacrocycles; L<sup>26</sup>-L<sup>31</sup> as outlined by De Clercq and co-workers.<sup>141</sup>
- Figure 63.** Key nitrogen atoms required for potency are highlighted in the structure of AMD3100 along with the structures of AMD3465, L<sup>49</sup> and L<sup>50, 198</sup>.
- Figure 64.** Structures of configurationally restricted bicyclams L<sup>32</sup> and L<sup>33, 58, 63</sup>.
- Figure 65.** Structures of the *meta*-substituted bismacrocycles L<sup>48</sup> and L<sup>51</sup>.
- Figure 66.** Structure of unsymmetrical bismacrocycles L<sup>46</sup> and L<sup>47, 149</sup>.
- Figure 67.** Downstream pathways caused by the stimulation of CXCR4 by its sole natural ligand CXCL12/SDF1 $\alpha$ .<sup>200</sup>
- Figure 68.** A representation of the crystal structure of CXCR4 showing the distance between Asp262 and Asp171 (the residues key for binding to AMD3100) *ca.* 16 Å. (Pymol using pdb data file).
- Figure 69.** A homology model of the crystal structure of CXCR4 outlining the distance between the two metal centres in AMD3100 *ca.* 12 Å. (pymol using the pdb data file).
- Figure 70.** Microscope images showing the co-localisation of CXCR4 and EEA-1 in the presence of CXCL12 and how this co-localisation is affected upon addition of increasing concentrations of [Cu<sub>2</sub>20]<sup>4+</sup>.

- Figure 71.** Microscope images showing how the co-localisation of CXCR4 and EEA-1 with CXCL12 stimulation is affected in the presence of AMD3100.
- Figure 72.** A bar chart comparing the effectiveness of antagonists  $[\text{Cu}_2\mathbf{20}]^{4+}$  and AMD3100 to interfere with an internalisation process with increasing concentration.
- Figure 73.** A bar chart depicting the levels of phosphorylation enzymes present upon addition of increasing concentrations of  $[\text{Cu}_2\mathbf{20}]^{4+}$ . Note 1 AU on the y-axis is the normal activation level.
- Figure 74.** Western blot assay depicting the level of degradation observed with and without the presence of CXCL12 with increasing concentration of the antagonist  $[\text{Cu}_2\mathbf{20}]^{4+}$ .
- Figure 75.** A bar chart showing the decrease in degradation observed with increasing concentrations of antagonist  $[\text{Cu}_2\mathbf{20}]^{4+}$ .
- Figure 76.** Strategies to form either thiourea or amide bonds between porphyrins and targeted biomolecules. (Adapted from Photochem. Photobiol. Sci.)<sup>76</sup>
- Figure 77.** Conjugation of an RDG peptide to a carboxy functionalised porphyrin to give  $\text{L}^{52}$  outlined by Boisbrun *et al.*<sup>204</sup>
- Figure 78.** A bis-carboxy functionalised porphyrin conjugated to two cyclic peptides ( $\text{L}^{53}$ ) outlined by Starkey *et al.*<sup>205</sup>
- Figure 79.** Conversion of  $\text{L}^{54}$  two different amine-reactive groups; carboxy ( $\text{L}^{55}$ ) and isothiocyanate ( $\text{L}^{56}$ ) outlined by Sibrian-Vasquez *et al.*<sup>209</sup>
- Figure 80.** The six possible porphyrin products from [3 + 1] condensation reactions.

**Figure 81.** The nitration products ( $L^{59}$ - $L^{62}$ ) observed from nitration of metalloporphyrins  $L^{57}$  and  $L^{58}$  using various nitrating agents outlined by Wickramasinghe *et al.*<sup>222</sup>

**Figure 82.** Addition of specific equivalents of  $[\text{NO}_2]\text{BF}_4$  to TPP allows the clean isolation of mono-, bis- and tris-nitration products. Reproduced from Arkivoc.)<sup>233</sup>

**Figure 83.** Structures of the 'building blocks' synthesised to make novel MFCs.

## List of Schemes

- Scheme 1.** The synthetic pathway to produce cyclam (**1**).
- Scheme 2.** Synthetic route to obtain bridged cyclam (**2**) and bridged cyclen (**3**).
- Scheme 3.** Synthetic route to produce a range of structurally related CB and SB cyclam and cyclen compounds.
- Scheme 4.** Synthetic route to obtain a novel amine terminating CB biscyclen compound; **20**.
- Scheme 5.** A possible route to obtain 3,5-di(bromomethyl)benzotrile.
- Scheme 6.** Bromination of 3,5-dimethylbenzotrile using NBS and a radical initiator.
- Scheme 7.** The bromination products of the synthesis of 3,5-di(bromomethyl) benzotrile (**16**) using NBS and AIBN as the initiator. Products include the desired 3,5-di(bromomethyl)benzotrile (**16**) and two further brominated products **B** and **C**.
- Scheme 8.** Synthetic route to **24**; a *meta*-substituted biscyclen ligand and its metal complexes  $[\text{Zn}_2\mathbf{24}]^{4+}$  and  $[\text{Cu}_2\mathbf{24}]^{4+}$ . Note in the case of metal complexes anions and/or solvent molecules may coordinate to the metal centres.
- Scheme 9.** Synthetic route to obtain a CB biscyclam compound, isolated as a hydrochloride salt (**28**).
- Scheme 10.** Synthetic route to append an *in situ* generated acid chloride; **29** to bismacrocycle **20** to produce bismacrocycle **31**.
- Scheme 11.** Ring-opening of diglycolic anhydride to produce an acid terminating monomacrocycle **33**.
- Scheme 12.** Ring-opening of diglycolic anhydride and subsequent copper(II) complexation of macrocycle **34**. Note in the case of the metal

complex anions and/or solvent molecules may coordinate to the metal centres.

- Scheme 13.** Attempted reactions to activate bismacrocycle **34** by means of an NHS ester.
- Scheme 14.** Proposed synthetic route to attach phenylethylamine to bismacrocycle **34** using various coupling reagents.
- Scheme 15.** Synthetic scheme to attach a *p*-nitrophenol activated vinylpyridine linker (**D**) to a C-functionalised macrocycle and subsequent conjugation to a mAb as outlined by Parker and co-workers.<sup>114</sup>
- Scheme 16.** Activation of bismacrocycle **34** with *p*-nitrophenol to give an activated ester **38**.
- Scheme 17.** Formation of 4-nitrophenyl 6-((*tert*-butoxycarbonyl)amino) hexanoate (**39**).
- Scheme 18.** Synthetic route to obtain an amine terminating monomacrocycle (**41**) utilising *p*-nitrophenol chemistry.
- Scheme 19.** Synthetic route to obtain an amine terminating bismacrocycle (**31**) utilising *p*-nitrophenol chemistry.
- Scheme 20.** Formation of an activated ester analogue of biotin (**43**) following conditions outlined by Bodanszky *et al.*<sup>177</sup>
- Scheme 21.** Conjugation of biotin-*p*-nitrophenyl ester **43** to bismacrocycle **20** and subsequent complexation of copper(II) acetate to form  $[\text{Cu}_2\mathbf{44}]^{4+}$ . Note in the case of  $[\text{Cu}_2\mathbf{44}]^{4+}$ , anions and/or solvent molecules may coordinate to the metal centres.
- Scheme 22.** Mechanism for the formation of tetraphenyl porphyrin using Adler-Longo conditions.<sup>216</sup>

- Scheme 23.** Synthetic route to produce zinc-5-[4-(succinimide-*N*-oxycarbonyl)phenyl]-10,15,20-tris-(4-*N*-methylpyridinium)porphyrin trichloride [Zn**48**].
- Scheme 24.** Synthetic route to produce zinc-5-(4-isothiocyanatophenyl)-10,15,20-tris(4-*N*-methylpyridiniumyl) porphyrin trichloride [Zn**53**].
- Scheme 25.** Attempted conjugation reactions between porphyrins **48** and **53** and monomacrocycle **15** to produce conjugated products; **54** and **55**.
- Scheme 26.** Synthetic route to synthesise organic soluble porphyrins and their zinc complexes. Conditions: i) propionic acid, 1 hour reflux, ii) [NO<sub>2</sub>][BF<sub>4</sub>], DCM, RT, iii) HCl and SnCl<sub>2</sub>·2H<sub>2</sub>O at 60°C for 1 hour, iv) TCP in DCM for 6 hours at RT, v) zinc(II) acetate in MeOH, 15 min at RT, vi) ethylenediamine for 18 hours at RT.
- Scheme 27.** Addition of acyl halides to Zn-TPP-NH<sub>2</sub> to produce [Zn**61**] and [Zn**62**].
- Scheme 28.** An example of copper(II) insertion into saturated azamacrocyclic cavities producing a novel MFC. Note anions and/or solvent molecules may coordinate to the copper(II) centres.

## List of Tables

- Table 1.** Frequently used radionuclides, their production method, positron energy and type of radiolabelling chemistry. (Adapted from Methods)<sup>20</sup>
- Table 2.** Anti-HIV activity of bismacrocycles with varying ring size. (Adapted from J. Med. Chem.)<sup>141</sup>
- Table 3.** Anti-HIV activity, cytotoxicity (CC<sub>50</sub>) and selectivity index (SI) for L<sup>32</sup>, L<sup>33</sup> and their metal complexes.
- Table 4.** Calcium signalling and anti-HIV data for metal containing *meta*-substituted bismacrocycles using AMD3100 as a control.
- Table 5.** The IC<sub>50</sub> (calcium signalling), CC<sub>50</sub> and SI of a series of novel metal containing monomacrocycles in the cell line U87.CD4.CXCR4 are presented along with their % of inhibition of anti-CXCR4 mAb binding in Jurkat cells.
- Table 6.** The IC<sub>50</sub> (calcium signalling), CC<sub>50</sub> and SI of a series of novel bismacrocycles and their metal complexes in the cell line U87.CD4.CXCR4 are presented along with their % of inhibition of anti-CXCR4 mAb binding in Jurkat cells.
- Table 7.** Anti-HIV data; IC<sub>50</sub>, CC<sub>50</sub> and SI of a series of bismacrocycles tested in MT-4 cells.
- Table 8.** The IC<sub>50</sub> (calcium signalling), CC<sub>50</sub> and SI of a series of novel metal containing bismacrocycles bearing spacer arms in the cell line U87.CD4.CXCR4 are presented along with their % of inhibition of anti-CXCR4 mAb binding in Jurkat cells.
- Table 9.** Structures of the expected conjugation products obtained from reacting amine terminating bismacrocyclic species with metalloporphyrins.

**Table 10.** Structures of the expected conjugation products obtained from reacting an acid or an activated ester terminating bismacrocylic species with metalloporphyrins.

## Table of Contents

1. Introduction .....	1
1.1. Designing clinical drugs.....	2
1.1.1. Multifunctional constructs.....	2
1.1.2. Cancer .....	4
1.1.3. Molecular imaging .....	5
1.1.4. Targeted therapy .....	7
1.1.4.1. <i>Quantum dots as molecular specific contrast agents.</i> .....	9
1.2. Chemokines and chemokine receptors .....	10
1.2.1. The chemokine receptor CXCR4 .....	10
1.3. Saturated tetraazamacrocycles as small molecule receptor antagonists .....	15
1.3.1. The chelate effect .....	16
1.3.2. Monomacrocycles.....	16
1.3.3. Metal complexes of monomacrocycles .....	18
1.3.4. Configurationally restricted macrocycles .....	19
1.4. Targeted MFCs using porphyrin bioconjugates .....	21
1.4.1. Photodynamic therapy .....	22
1.4.2. Porphyrins as photosensitisers.....	23
1.4.3. Development of porphyrin photosensitisers.....	25
1.4.4. Third generation porphyrins – improved PDT agents .....	26
1.5. Imaging cancers using the nuclear imaging modality PET.....	28
1.5.1. Current radiopharmaceuticals.....	31
1.5.1.2. <i><sup>18</sup>F-Fluorodeoxyglucose</i> .....	32
1.6. The advantages of <sup>64</sup> Cu as a radiopharmaceutical .....	34
1.6.1. Chelators based on cyclam and cyclen backbones.....	36

1.7. Research aims .....	39
1.8. Summary .....	40
2. Synthesis of novel saturated tetraazamacrocycles and their metal complexes.....	41
2.1. Synthetic strategy .....	42
2.2. Past strategies.....	42
2.2.1. C-functionalised monomacrocycles.....	43
2.2.2. N-functionalised monomacrocycles .....	45
2.2.2.1. <i>SB monomacrocycles bearing functional pendant arms</i> .....	45
2.2.2.2. <i>CB monomacrocycles bearing functional pendant arms</i> .....	47
2.3. Synthesis of monomacrocyclic ligands .....	48
2.3.1. Configurationally restricted monomacrocycles.....	50
2.3.2. Reduction methods.....	52
2.3.3. Novel metal-containing monomacrocycles .....	53
2.4. Design and synthesis of novel high affinity bismacrocycles and their metal complexes. ....	56
2.4.1. Past strategies – bismacrocycles .....	56
2.4.2. Synthesis of a novel CB biscyclen ligand; 1,1'-[3,5-dimethylaminobenzyl]-7,7'-[methyl]-bis(1,4,7,10-tetraazabicyclo[5.5.2]dodecane ( <b>20</b> )).....	60
2.4.2.1. <i>Synthesis of 3,5-di(bromomethyl)benzotrile</i> .....	61
<b>2.4.2.1.1. Using benzoyl peroxide as the initiator</b> .....	62
<b>2.4.2.1.2. Using AIBN as the initiator</b> .....	64
2.4.2.2. <i>Configurational restriction</i> .....	65
2.4.2.3. <i>Metal complexes of CB biscyclen ligand 20</i> .....	66
2.5. Bismacrocycles as CXCR4 antagonists?.....	67
2.6. Synthesis of a novel CB biscyclam ligand; 1,1'-[3,5-dimethylamino benzyl]-8, 8'-[methyl]-bis-1,4,8,11-tetraazabicyclo [10.2.2]hexadecane octahydrochloride ( <b>28</b> ).....	69
2.6.1. Metal complexes of CB biscyclam ligand <b>28</b> .....	70
3. Development of a spacer arm.....	72

3.1. Introduction .....	73
3.1.1. Synthetic strategy .....	73
3.2. The formation of amide bonds .....	73
3.2.1. <i>N</i> -hydroxysuccinimide ester functionalities .....	74
3.3. Formation of an acid chloride.....	75
3.4. Ring-opening of diglycolic anhydride.....	77
3.4.1. Activation of bismacrocycle <b>34</b> .....	79
3.4.2. Activation using <i>p</i> -nitrophenol .....	83
3.4.2.1. Previous strategy .....	83
3.4.2.2. <i>Activation of bismacrocycle 33 with p-nitrophenol</i> .....	84
3.4.2.3. <i>Synthesis to attach amine terminating spacer arms to macrocycles utilising p-nitrophenol chemistry</i> .....	85
3.4.3. A biotin activated ester; towards the synthesis of an <i>in vitro</i> evaluation probe. ....	88
3.5. Conclusions .....	90
4. Biological evaluation of mono and bismacrocycles as CXCR4 antagonists.....	92
4.1. Introduction .....	93
4.1.1. CXCR4 – role in cancer and HIV .....	93
4.1.2. CXCR4 antagonists .....	95
4.1.2.1. <i>AMD3100</i> .....	95
4.2. Previous studies .....	96
4.2.1. Strategy.....	102
4.3. Biological assays.....	102
4.3.1. Antibody competition binding assay .....	102
4.3.2. Calcium(II) flux studies.....	103
4.4. Monomacrocycles as CXCR4 antagonists .....	104
4.5. Bismacrocycles as CXCR4 antagonists .....	107

4.5.1. Evaluation of binding affinity.....	107
4.5.2. Antibody competition and signal blocking assays .....	109
4.5.2.1. <i>Anti-HIV activity</i> .....	113
4.5.3. Detailed biological evaluation of [Cu <sub>2</sub> 20] <sup>4+</sup> .....	114
4.5.3.1. <i>Downstream signalling: Does an antagonist inhibit the co-localisation of CXCR4 with early endosome antigen 1 (EEA1) upon CXCL12 stimulation?</i> .....	115
4.5.3.2. <i>CXCR4 phosphorylation and downstream signalling events</i> .....	118
4.5.3.3. <i>Reduced CXCR4 receptor degradation in the presence of [Cu<sub>2</sub>20]<sup>4+</sup></i> .....	120
4.6. Addition of spacer arms – acidic and a biotin tag.....	121
4.7. Conclusions .....	123
5. Synthesis of porphyrin compounds; towards the formation of novel MFCs.....	125
5.1. Introduction .....	126
5.2. Synthetic strategy .....	126
5.2.1. Previous strategies.....	126
5.3. Synthesis of water soluble porphyrins.....	130
5.3.1. Characterisation of porphyrin products. ....	135
5.3.1.1. <i>UV-vis analysis</i> .....	136
5.4. Towards the synthesis of water soluble MFCs .....	137
5.5. Organic soluble porphyrins; useful models .....	139
5.5.1. Tetraphenylporphyrin and its derivatives .....	139
5.5.1.1. <i>Mono-nitration of TPP</i> .....	140
5.5.1.2. <i>Formation of acyl halide derivatives</i> .....	143
5.6. Towards the synthesis of organic soluble MFCs .....	144
5.7. Conclusions .....	150
6. Conclusions and future work .....	151
6.1. Conclusions .....	152
6.1.1. Overview .....	152

6.1.2. Main achievements.....	152
6.1.3. Overall achievements in relation to the field .....	155
6.2. Future work.....	156
6.2.1. Short-term goals .....	156
6.2.2. Long-term goals .....	157
7. Experimental .....	159
7.1. General methods .....	160
7.1.1. Materials .....	160
7.2. Synthetic procedures .....	161
7.2.1. Synthesis of 1,4,8,11-tetraazacyclotetradecane ( <b>1</b> ) .....	161
7.2.2. Synthesis of <i>cis</i> -3a,5a,8a,10a-tetraazaperhydropyrene ( <b>2</b> ) and <i>cis</i> -13-1,4,7,10-tetraazatetracyclo[5.5.1.0 <sup>4,14</sup> .0 <sup>10,13</sup> ]tetradecane ( <b>3</b> ) .....	162
7.2.3. Synthesis of 3a-[4-cyanobenzyl]-decahydro-3a,5a,8a,10a-tetraaza-pyrenium bromide ( <b>4</b> ) and 2a-[4-cyanobenzyl]-decahydro-2a,4a,6a,8a-tetraaza-pyrenium bromide ( <b>5</b> ) .....	164
7.2.4. Synthesis of 1-[4-cyanobenzyl]-1,4,8,11-tetraazabicyclo[10.2.2]hexadecane ( <b>6</b> ) and 1-[4-cyanobenzyl]-1,4,7,10-tetraazabicyclo[8.2.2]dodecane ( <b>7</b> ) .....	166
7.2.5. Synthesis of 1-[4-aminomethylbenzyl]-1,4,8,11-tetraazabicyclo[10.2.2]hexadecane ( <b>8</b> ) .....	168
7.2.6. Synthesis of 1-[4-aminomethylbenzyl]-1,4,7,10-tetraazabicyclo[8.2.2]dodecane ( <b>9</b> ) .....	171
7.2.7. Synthesis of 3a-[4-cyanobenzyl]-8a-[methyl]-decahydro-3a,5a,8a,10a-tetraaza-pyrenium diiodide ( <b>10</b> ) and 2a-[4-cyanobenzyl]-6a-[methyl]-decahydro-2a,4a,6a,8a-tetraaza-pyrenium diiodide ( <b>11</b> ) .....	173
7.2.8. Synthesis of 1-[4-cyanobenzyl]-8-[methyl]-1,4,8,11-tetraazabicyclo[6.6.2]hexadecane ( <b>12</b> ) and 1-[4-cyanobenzyl]-7-[methyl]-1,4,7,10-tetraazabicyclo[5.5.2]dodecane ( <b>13</b> ) .....	175

7.2.9. Synthesis of 1-[4-aminomethylbenzyl]-8-[methyl]-1,4,8,11-tetraazabicyclo[6.6.2]hexadecane ( <b>14</b> ) and 1-[4-aminomethylbenzyl]-7-[methyl]-1,4,7,10-tetraazabicyclo[5.5.2]dodecane ( <b>15</b> ) .....	177
7.2.10. Synthesis of metal complexes of ligands 1-[4-aminomethylbenzyl]-1,4,8,11-tetraazabicyclo[10.2.2]hexadecane ( <b>8</b> ) and 1-[4-aminomethylbenzyl]-1,4,7,10-tetraazabicyclo[8.2.2]dodecane ( <b>9</b> ) .....	179
7.2.11. Synthesis of metal complexes of ligands 1-[4-aminomethylbenzyl]-8-[methyl]-1,4,8,11-tetraazabicyclo[6.6.2]hexadecane ( <b>14</b> ) and 1-[4-aminomethyl benzyl]-7-[methyl]-1,4,7,10-tetraazabicyclo[5.5.2]dodecane ( <b>15</b> ) .....	182
7.2.12. Synthesis of 3,5-bis(bromomethyl) benzonitrile ( <b>16</b> ) .....	185
7.2.13. Synthesis of 2a,2a'-[3,5-dimethylbenzonitrile]-bis(decahydro-2a,4a,6a,8a-tetraaza pyrenium) dibromide ( <b>17</b> ) .....	187
7.2.14. Synthesis of 2a,2a'-[3,5-dimethylbenzonitrile]-6a,6a'-[methyl]-bis (decahydro-2a,4a,6a,8a-tetraazapyrenium) tetraiodide ( <b>18</b> ) .....	188
7.2.15. Synthesis of 1,1'-[3,5-dimethylbenzonitrile]-7,7'-[methyl]-bis(1,4,7,10-tetraaza bicyclo[5.5.2]dodecane) ( <b>19</b> ) .....	189
7.2.16. Synthesis of 1,1'-[3,5-dimethylbenzonitrile]-7,7'-[methyl]-bis(1,4,7,10-tetraaza bicyclo[5.5.2]dodecane) copper acetate [Cu <sub>2</sub> <b>19</b> ] <sup>4+</sup> .....	190
7.2.17. Synthesis of 1,1'-[3,5-dimethylaminobenzyl]-7,7'-[methyl]-bis(1,4,7,10-tetraaza bicyclo[5.5.2]dodecane) ( <b>20</b> ) .....	191
7.2.18. Synthesis of metal complexes of 1,1'-[3,5-dimethylaminobenzyl]-7,7'-[methyl]-bis(1,4,7,10-tetraazabicyclo[5.5.2]dodecane) ( <b>20</b> ) .....	192
7.2.19. Synthesis of 1,1'-[3,5-dimethylaminobenzyl]-7,7'-[methyl]-bis(1,4,7,10-tetraaza bicyclo[5.5.2]dodecane) octahydrochloride ( <b>21</b> ) .....	194
7.2.20. Synthesis of 1,4,7-tri- <i>tert</i> -butylcarbonate-1,4,7,10-tetraazacyclododecane ( <b>22</b> ) .....	195
7.2.21. Synthesis of 10,10'-(3,5-dimethylbenzonitrile)-bis-(1,4,7,10-tetraazacyclo dodecane)-1,4,7-hexa- <i>tert</i> -butylcarbonate ( <b>23</b> ) .....	196

7.2.22. Synthesis of 10,10'-(3,5-dimethylbenzotrile)-bis(1,4,7,10-tetraazacyclo dodecane) octahydrochloride ( <b>24</b> ) .....	197
7.2.23. Synthesis of metal complexes of 10,10'-(3,5-dimethylbenzotrile)-bis(1,4,7,10- tetraazacyclododecane) ( <b>24</b> ) .....	198
7.2.24. Synthesis of 3a,3a'-[3,5-dimethylbenzotrile]-bis(decahydro-3a,5a,8a,10a, tetraaza-pyrenium) dibromide ( <b>25</b> ) .....	200
7.2.25. Synthesis of 3a,3a'-[3,5-dimethylbenzotrile]-8a,8a'-[methyl]-bis (decahydro- 3a,5a,8a,10a-tetraaza-pyrenium) tetraiodide ( <b>26</b> ).....	201
7.2.26. Synthesis of 1,1'-[3,5-dimethylbenzotrile]-8,8'-[methyl]-bis(1,4,8,11-tetraaza bicyclo[10.2.2]hexadecane) ( <b>27</b> ).....	202
7.2.27. Synthesis of 1,1'-[3,5-dimethylbenzotrile]-8,8'-[methyl]-bis(1,4,8,11- tetraazabicyclo[10.2.2]hexadecane) copper(II) acetate [Cu <sub>2</sub> <b>27</b> ] <sup>4+</sup> .....	203
7.2.28. Synthesis of 1,1'-[3,5-dimethylaminobenzyl]-8,8'-[methyl]-bis(1,4,8,11-tetraaza bicyclo[10.2.2]hexadecane) octahydrochloride ( <b>28</b> ) .....	204
7.2.29. Synthesis of metal complexes of 1,1'-[3,5-dimethylaminobenzyl]-8,8'-[methyl]- bis(1,4,8,11-tetraazabicyclo[10.2.2]hexadecane) octahydrochloride ( <b>28</b> ) .....	206
7.2.30. Synthesis of 6-(( <i>tert</i> -butoxycarbonyl)amino)hexanoic acid ( <b>29</b> ) .....	208
7.2.31. Attempted synthesis of <i>tert</i> -butyl(6-chloro-6-oxohexyl)carbamate ( <b>30</b> ).....	209
7.2.32. Synthesis of <i>tert</i> -butyl(6-((3,5-bis((7,7'-[methyl]-1,4,7,10-tetraazabicyclo [5.5.2]tetradecan-4-yl)methyl)benzyl)amino)-6-oxohexyl) carbamate ( <b>31</b> ) .....	210
7.2.33. Synthesis of 6-amino- <i>N</i> -(3,5-bis((7,7'-[methyl]-1,4,7,10-tetraazabicyclo[5.5.2] tetradecan-4-yl)methyl)benzyl)hexanamide ( <b>32</b> ).....	212
7.2.34. Synthesis of 2-(2-((4-((7-[methyl]-1,4,7,10-tetraazabicyclo[5.5.2] tetradecan-4- yl)methyl)benzyl)amino)-2-oxoethoxy)acetic acid ( <b>33</b> ).....	214
7.2.35. Synthesis of 2-(2-((3,5-bis((7,7'-[methyl]-1,4,7,10-tetraazabicyclo[5.5.2] tetradecan-4-yl)methyl)benzyl)amino)-2-oxoethoxy)acetic acid ( <b>34</b> ).....	215

7.2.36. Synthesis of 2-(2-((3,5-bis((7,7'-[methyl]-1,4,7,10-tetraazabicyclo[5.5.2]tetradecan-4-yl)methyl)benzyl)amino)-2-oxoethoxy)acetic acid copper(II) acetate [Cu <sub>2</sub> <b>34</b> ] <sup>4+</sup> .....	216
7.2.37. Attempted synthesis of <i>N</i> -(2-aminoethyl)-2-(2-((3,5-bis((7,7'-[methyl]-1,4,7,10-tetraazabicyclo[5.5.2]tetradecan-4-yl)methyl)benzyl)amino)-2-oxoethoxy)acetamide ( <b>35</b> ).....	217
7.2.38. Attempted synthesis of 2,5-dioxocyclopentyl-2-(2-((3,5-bis((7,7'-[methyl]-1,4,7,10-tetraazabicyclo[5.5.2]tetradecan-4-yl)methyl)benzyl)amino)-2-oxoethoxy)ester ( <b>36</b> ) .....	218
7.2.39. Synthesis of <i>N</i> -(3,5-bis((7,7'-[methyl]-1,4,7,10-tetraazabicyclo[5.5.2]tetradecan-4-yl)methyl)benzyl)-2-(2-oxo-2-(phenethylamino)ethoxy)acetamide ( <b>37</b> ) .....	219
7.2.40. Synthesis of 2-(2-((3,5-bis((7,7'-[methyl]-1,4,7,10-tetraazabicyclo[5.5.2]tetradecan-4-yl)methyl)benzyl)amino)-2-oxoethoxy)nitrophenyl ester ( <b>38</b> ).....	222
7.2.41. Synthesis of 4-nitrophenyl-6-(( <i>tert</i> -butoxycarbonyl)amino)hexanoate ( <b>39</b> ).....	223
7.2.42. Synthesis of <i>tert</i> -butyl-(6-((1,4-((7-[methyl]-1,4,7,10-tetraazabicyclo[5.5.2]tetradecan-4-yl)methyl)benzyl)amino)-6-oxohexyl)carbamate ( <b>40</b> ).....	224
7.2.43. Synthesis of 6-amino- <i>N</i> -(6-((1,4-((7-[methyl]-1,4,7,10-tetraazabicyclo[5.5.2]tetradecan-4-yl)methyl)benzyl))hexanamide ( <b>41</b> ).....	225
7.2.44. Synthesis of <i>N</i> -trifluoroacetyl-biotin- <i>p</i> -nitrophenyl ester ( <b>42</b> ).....	226
7.2.45. Synthesis of biotin- <i>p</i> -nitrophenyl ester ( <b>43</b> ).....	227
7.2.46. Synthesis of 1,1'-[3,5-dimethylamino-(biotin- <i>p</i> -nitrophenyl ester)benzyl]-7,7'-[methyl]-bis(1,4,7,10-tetraazabicyclo[5.5.2]dodecane) ( <b>44</b> ).....	228
7.2.47. Synthesis of 1,1'-[3,5-dimethylamino-(biotin- <i>p</i> -nitrophenyl ester)benzyl]-7,7'-[methyl]-bis(1,4,7,10-tetraazabicyclo[5.5.2]dodecane) copper(II) acetate [Cu <sub>2</sub> <b>44</b> ] <sup>4+</sup> .....	229
7.2.48. Synthesis of 5-(4-carboxyphenyl)-10,15,20-tris-(4-pyridyl) porphyrin ( <b>45</b> ).....	230
7.2.49. Synthesis of 5-[4-(succinimide- <i>N</i> -oxycarbonyl)phenyl]-10,15,20-tris-(4-pyridyl) porphyrin ( <b>46</b> ) .....	231

7.2.50. Synthesis of 5-[4-(succinimide- <i>N</i> -oxycarbonyl)phenyl]-10,15,20-tris-(4- <i>N</i> -methyl pyridinium)porphyrin triiodide ( <b>47</b> ).....	232
7.2.51. Synthesis of 5-[4-(succinimide- <i>N</i> -oxycarbonyl)phenyl]-10,15,20-tris-(4- <i>N</i> -methyl pyridinium)porphyrin trichloride ( <b>48</b> ) .....	233
7.2.52. Synthesis of zinc-5-[4-(succinimide- <i>N</i> -oxycarbonyl)phenyl]-10,15,20-tris-(4- <i>N</i> -methylpyridinium)porphyrin trichloride [Zn <b>48</b> ] .....	234
7.2.53. Synthesis of 5-(4-acetamidophenyl)-10,15,20-tris-(4-pyridyl)porphyrin ( <b>49</b> ) .....	235
7.2.54. Synthesis of 5-(4-aminophenyl)-10,15,20-tris-(4-pyridyl)porphyrin ( <b>50</b> ).....	236
7.2.55. Synthesis of 5-(4-isothiocyanatophenyl)-10,15,20-tris-(4-pyridyl)porphyrin ( <b>51</b> ) .....	237
7.2.56. Synthesis of 5-(4-isothiocyanatophenyl)-10,15,20-tris-(4- <i>N</i> -methyl pyridiniumyl) porphyrin triiodide ( <b>52</b> ) .....	238
7.2.57. Synthesis of 5-(4-isothiocyanatophenyl)-10,15,20-tris-(4- <i>N</i> -methyl pyridiniumyl) porphyrin trichloride ( <b>53</b> ) .....	239
7.2.58. Synthesis of zinc-5-(4-isothiocyanatophenyl)-10,15,20-tris-(4- <i>N</i> -methyl pyridiniumyl) porphyrin trichloride [Zn <b>53</b> ] .....	240
7.2.59. Attempted conjugation of 1-[4-aminomethylbenzyl]-7-[methyl]-1,4,7,10-tetraaza bicyclo[5.5.2]dodecane ( <b>15</b> ) with 5-[4-(succinimide- <i>N</i> -oxycarbonyl)phenyl]-10,15,20-tris-(4- <i>N</i> -methylpyridinium)porphyrin trichloride ( <b>48</b> ) .....	241
7.2.60. Attempted conjugation of 1-[4-aminomethylbenzyl]-7-[methyl]-1,4,7,10-tetraaza bicyclo[5.5.2]dodecane ( <b>15</b> ) with 5-(4-isothiocyanatophenyl)-10,15,20-tris-(4- <i>N</i> -methyl pyridiniumyl) porphyrin trichloride ( <b>53</b> ) .....	242
7.2.61. Synthesis of tetraphenyl porphyrin (TPP) ( <b>56</b> ) .....	243
7.2.62. Synthesis of nitro-tetraphenyl porphyrin (TPP-NO <sub>2</sub> ) ( <b>57</b> ) .....	244
7.2.63. Synthesis of amino-tetraphenyl porphyrin (TPP-NH <sub>2</sub> ) ( <b>58</b> ) .....	245
7.2.64. Synthesis of isothiocyano-tetraphenyl porphyrin (TPP-NCS) ( <b>59</b> ).....	246

7.2.65. Synthesis of zinc-amino-tetraphenyl porphyrin [Zn58] and zinc-isothiocyano-tetraphenyl porphyrin [Zn59] .....	247
7.2.66. Synthesis of zinc-(aminoethyl)thiourea-tetraphenyl porphyrin [Zn60] .....	249
7.2.67. Synthesis of zinc-chloroacetamido-tetraphenyl porphyrin [Zn61] and zinc-2-bromo acetamido-tetraphenyl porphyrin [Zn62] .....	250
7.2.68. Attempted conjugation of 1,1'-[3,5-dimethylaminobenzyl]-7,7'-[methyl]-bis (1,4,7,10-tetraazabicyclo [5.5.2]dodecane ( <b>20</b> ) with zinc-chloroacetamido-tetraphenyl porphyrin [Zn61] or zinc-bromoacetamido-tetraphenyl porphyrin [Zn62].....	252
7.2.69. Conjugation of 1,1'-[3,5-dimethylaminobenzyl]-7,7'-[methyl]-bis (1,4,7,10-tetraazabicyclo [5.5.2]dodecane ( <b>20</b> ) and Zn-TPP-NCS [Zn59].....	253
7.2.70. Attempted conjugation of 6-amino- <i>N</i> -(3,5-bis((10-methyl-1,4,7,10-tetraazabicyclo [5.5.2] tetradecan-4-yl)methyl)benzyl)hexanamide ( <b>32</b> ) and zinc-chloroacetamido-tetraphenyl porphyrin [Zn61] .....	254
7.2.71. Attempted conjugation of 6-amino- <i>N</i> -(3,5-bis((10-methyl-1,4,7,10-tetraazabicyclo [5.5.2]tetradecan-4-yl)methyl)benzyl)hexanamide ( <b>32</b> ) and Zn-TPP-NCS [Zn59].....	255
7.2.72. Attempted conjugation of 2-(2-((3,5-bis((10-methyl-1,4,7,10-tetraaza bicyclo[5.5.2]tetradecan-4-yl)methyl)benzyl)amino)-2-oxoethoxy) nitrophenyl ester ( <b>38</b> ) and zinc-(aminoethyl)thiourea-tetraphenyl porphyrin [Zn60] .....	256
7.2.73. Attempted conjugation of 2-(2-((3,5-bis((10-methyl-1,4,7,10-tetraaza bicyclo[5.5.2]tetradecan-4-yl)methyl)benzyl)amino)-2-oxoethoxy) nitrophenyl ester ( <b>38</b> ) or 2-(2-((3,5-bis((10-methyl-1,4,7,10-tetraazabicyclo[5.5.2]tetradecan-4-yl)methyl)benzyl)amino)-2-oxoethoxy)acetic acid ( <b>34</b> ) with Zn-TPP-NH <sub>2</sub> [Zn58].....	257
7.3. Biological experimental .....	259
7.3.1. Experimental for competition binding assays .....	259
7.3.1.1. <i>General methods and preparation of cell cultures</i> .....	259
7.3.1.2. <i>Antibodies and fluorescent dyes</i> .....	259
7.3.1.3. <i>Cell counting</i> .....	259
7.3.1.4. <i>Antibody binding and subsequent fluorescent tagging for flow cytometry</i> 260	

7.4. Experimental for calcium signaling assays.....	260
7.4.1. Cell cultures .....	260
7.4.2. Loading of the cells with the Ca <sup>2+</sup> indicator Fluo-3.....	261
7.4.3. Measurement of intracellular Ca <sup>2+</sup> mobilization and evaluation of receptor antagonists by the Fluorometric Imaging Plate Reader (FLIPR) .....	261
7.5. Experimental for anti-HIV assays.....	262
7.6. Experimental for internalisation, phosphorylation and degradation assays.....	263
7.6.1. Antibodies and reagents.....	263
7.6.2. Plasmids, cell lines, and cell culture conditions.....	263
7.6.3. Receptor degradation assay .....	264
7.6.4. Immunoblot analysis.....	264
7.6.5. Confocal microscopy.....	265
7.6.6. Statistical methods .....	265
References .....	266
Appendix .....	277
A. Dot plot – gridded area was used for histogram plots B - E.....	277
B. Histogram plot for the copper(II), zinc(II) and nickel(II) complexes for ligand <b>8</b> .....	277
C. Histogram plot for the copper(II), zinc(II) and nickel(II) complexes for ligand <b>9</b> .....	278
D. Histogram plot for the copper(II), zinc(II) and nickel(II) complexes for ligand <b>14</b> .....	278
E. Histogram plot for the copper(II), zinc(II) and nickel(II) complexes for ligand <b>15</b> .....	279
F. Dot plot – gridded area was used for histogram plots G, H and M - Q.....	279
G. Histogram plot for ligand <b>20</b> and its copper(II), zinc(II) and nickel(II) complexes.....	280
H. Histogram plot comparing the copper(II) complexes of ligand <b>19</b> and <b>20</b> .....	280
I. Dot plot – gridded area was used for histogram J.....	281
J. Histogram plot for ligand <b>28</b> and its copper(II) complex.....	281

K. Dot plot – gridded area was used for histogram L. ....	282
L. Histogram plot for the zinc(II) and nickel(II) complexes of ligand <b>28</b> . ....	282
M. Histogram plot comparing the copper(II) complexes of ligand <b>27</b> and <b>28</b> . ....	283
N. Histogram plot for ligand <b>24</b> and its zinc(II) complex. ....	283
O. Histogram plot for $[\text{Cu}_2\mathbf{24}]^{4+}$ ....	284
P. Histogram plot comparing the methylamine terminating ligand <b>20</b> with the acid terminating ligand <b>34</b> along with their respective copper(II) complexes. ....	284
Q. Histogram plot comparing the methylamine terminating ligand $[\text{Cu}_2\mathbf{20}]^{4+}$ with the biotin tagged ligand $[\text{Cu}_2\mathbf{44}]^{4+}$ ....	285

# **Chapter 1**

## **Introduction**

## **1.1. Designing clinical drugs**

Designing diagnostic and therapeutic drugs is of paramount importance in order to prevent and/or treat many of the diseases prevalent in our society. Diagnostic drugs are aimed at distinguishing diseased from healthy tissue, this can be achieved via detection of specific antigens, cell surface receptors, proteins or imbalances in normal tissues. Therapeutic drugs influence the system under study either by blocking the life cycle of the disease i.e. for viral and bacterial infections, or by causing cell death and preventing the spread of the disease i.e. cancers.

### **1.1.1. Multifunctional constructs**

Multifunctional constructs (MFCs) are a relatively new idea, bringing into focus the need for a multidisciplinary approach to the control and management of diseases. MFCs encapsulate the idea of dual modality, combinations of various components offer multifunctional platforms which can allow for complementary imaging techniques or imaging and therapy. Such constructs combine several areas of science including biochemistry, chemistry, physics and medicine.

Multimodal imaging probes make it possible to combine the advantages of different imaging techniques to enhance the quality and validity of images obtained. For an imaging agent to be detectable using different imaging modalities it must contain more than one diagnostic label.

A popular choice for clinical imaging is to couple magnetic resonance imaging (MRI) and optical imaging (OI), due to the potential to obtain anatomical as well as physiological information from MRI in combination with the rapid screening capability of OI, with nanoparticles proving to be a useful platform to build such probes.<sup>1-3</sup> Nguyen *et al.* however, took a different approach and were able to develop an activatable cell penetrating peptide (ACCP) dually labelled with a fluorescent dye (Cy 5) and a gadolinium chelate.<sup>4</sup> This probe could provide an objective way to assess tumour margins as well as surgical efficiency. Initial tests in mice demonstrated that pre-operative MRI imaging was accessible due to the gadolinium chelate, this provided information on the exact location and size of the

tumour. The fluorescent dye then allowed for intra-operative real time fluorescence imaging giving a means to assess whether the entire tumour mass had been excised. A residual fluorescent signal was observed under the pectoralis muscle in the mouse after excision of the main tumour mass and a small piece of residual tumour was then removed, see Figure 1. This example demonstrates the clinical relevance of such a multimodal probe and also how they can directly influence the completeness of tumour excision. Kim *et al.* have published a thorough review of multimodal imaging probes.<sup>5</sup>

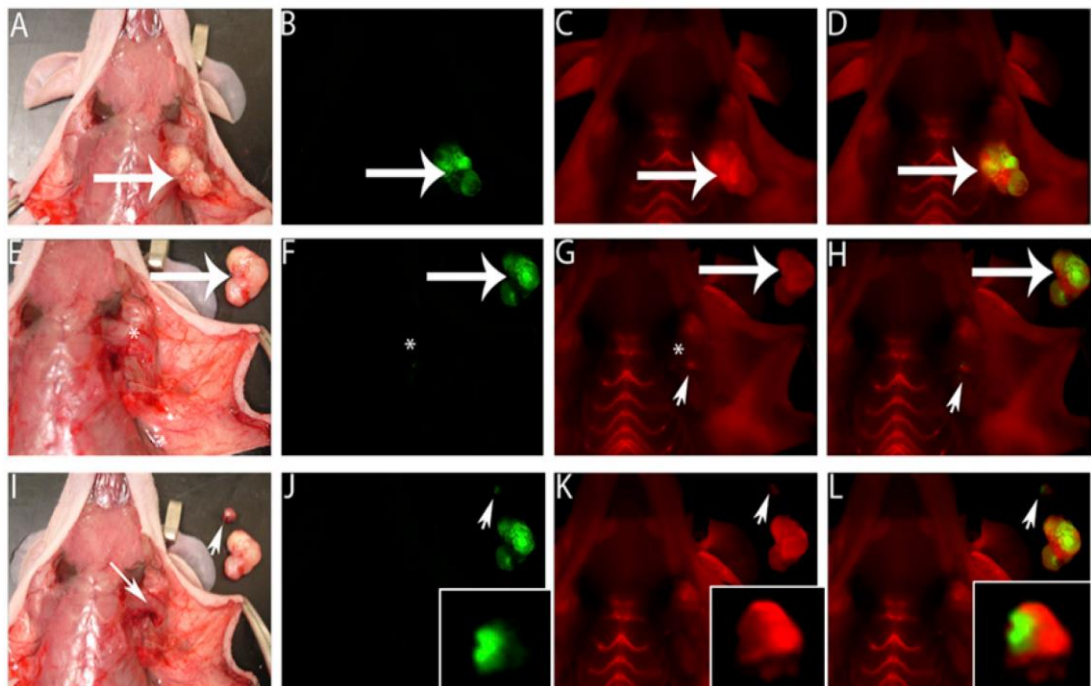


*Figure 1: A) White light image of mouse xenograft after tumour exposure. B) Fluorescence image of GFP-labelled tumour cells. C) Fluorescence image 6 hours after administration of the ACCP probe. D) Overlay of images B and C to show co-localisation. Following tumour excision, E) White light image showing apparent complete excision of the tumour mass. F) Fluorescence imaging with GFP also appears to show complete excision. Imaging with the ACCP probe shows a residual fluorescent signal (see \*) in the pectoralis muscle (G and H). Upon excision, K and L show this mass is fluorescent indicating that it is tumour tissue.*

*(Reproduced from Proc. Nat. Acad. Sci.)<sup>4</sup>*

Multifunctional probes for synergistic imaging and therapy are also receiving a lot of attention.<sup>6, 7</sup> Current therapeutic modalities include photosensitisers (PS) and anti-

cancer drugs; their limitation is that they possess no targeting properties and can cause systemic side effects. Coupling a therapeutic molecule to a targeting vehicle could offer many advantages in these areas. Hsiue and co-workers designed polymer micelles filled with the anti-cancer drug doxorubicin functionalised with an organic dye (FITC) via PEG linking chains.<sup>8</sup> This probe could not only be used for OI but also displayed cytotoxicity towards the targeted cancer cell line.

MFCs are a new addition to the array of drugs for diagnosis and therapy but offer many distinct advantages. Some of their potential uses and advantages are summarised, see Figure 2.

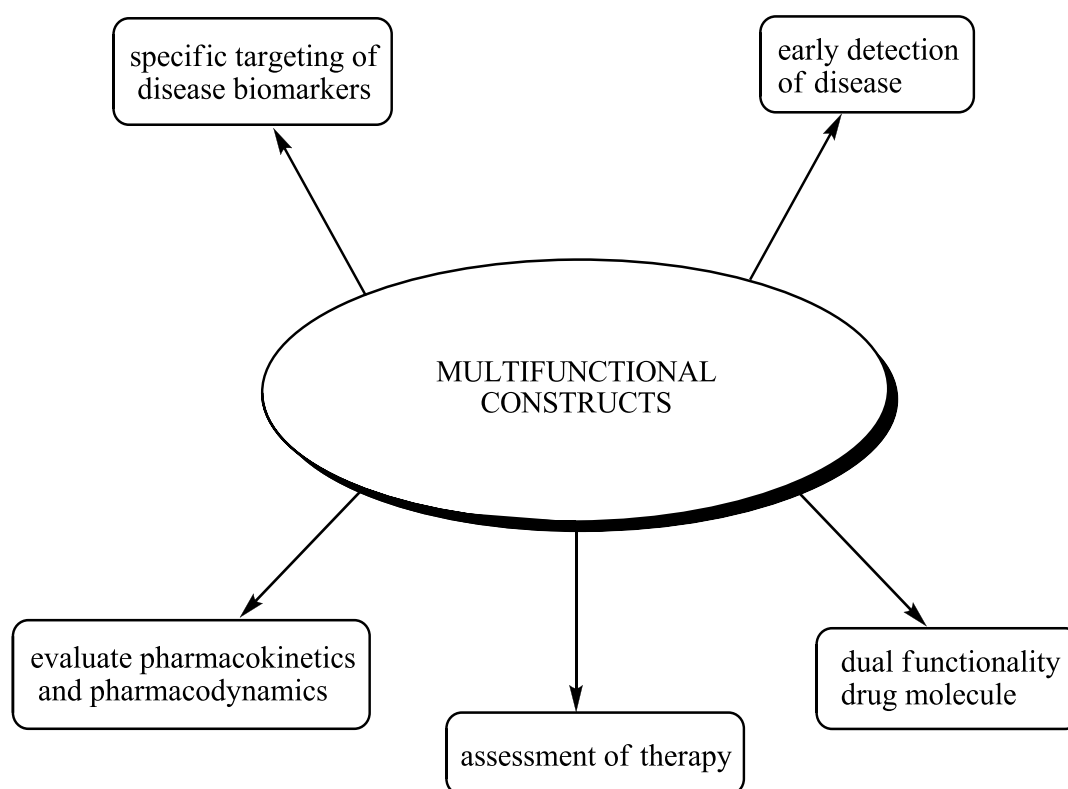


*Figure 2: Summary of the potential uses and advantages of MFCs.*

### **1.1.2. Cancer**

Cancer is a challenging disease, characterised by heterogeneity, uncontrolled cell division, and the ability of cancer cells to invade other tissues.<sup>9</sup> Cancer can affect any region in the body including all organs, soft tissue, bones and the lymphatic

system. Several factors cause the transformation of a healthy cell into a tumour cell including carcinogens, radiation, infectious agents and genetic abnormalities, which can either be hereditary or occur during DNA replication.<sup>10</sup> The body is unable to rid itself of these 'abnormal' cells because they become resistant to apoptosis; programmed cell death, which is an essential component of normal cell growth. This resistance is caused by mutations in the suppressor gene p53<sup>11</sup> which can lead to the survival and growth of cancer cells, indeed the spread of cancer is as much a failure of apoptosis as it is a result of unchecked proliferation.<sup>12</sup> Tumours gain as many nutrients from their surrounding environment as possible to facilitate proliferated growth. This results in increased levels of certain cell surface receptors in comparison to healthy tissue. To sustain proliferation, tumours require a network of blood vessels. The physiological process of growing a new network of blood vessels from pre-existing vessels is called angiogenesis. In tumour cells, angiogenesis is enabled providing the tumour with a blood supply and a network of blood vessels. Tumour cells can then access the blood stream and lymphatic system. Metastasis which is the ability of cancer to spread to a secondary location requires angiogenesis and occurs in some cancers but not all. The cancer cells access the blood stream or lymphatic system where they circulate then invade and localise in previously healthy tissue forming secondary cancers known as metastases. Metastasis is the final step in cancer progression and is the primary cause of death from solid tumours.<sup>13</sup>

The effects of cancer are widespread, in the UK in 2004, over a quarter of a million people were diagnosed with cancer.<sup>14</sup> This alarming fact has led to much attention from the medical world with a huge emphasis on detection, diagnosis and therapy. Early detection of cancer is paramount to allow intervention at a stage that can influence overall survival.

### **1.1.3. Molecular imaging**

There are several imaging modalities which are capable of imaging the structure and function of tumours including; CT (Computed Tomography), MRI, PET and

SPECT (Single Photon Emission Computed Tomography). Current clinical imaging techniques are focused mainly on structural imaging (CT, MRI) and whilst these techniques are useful and provide high resolution anatomical images with detailed structural information<sup>15</sup> they do not provide all the information necessary to fully characterise or monitor those with or at risk of cancer,<sup>16</sup> often being limited by the depth to which they can image. The chemical changes which occur in a tumour often precede structural changes; opening up the field of medical imaging toward the use of molecular imaging.<sup>12, 17, 18</sup>

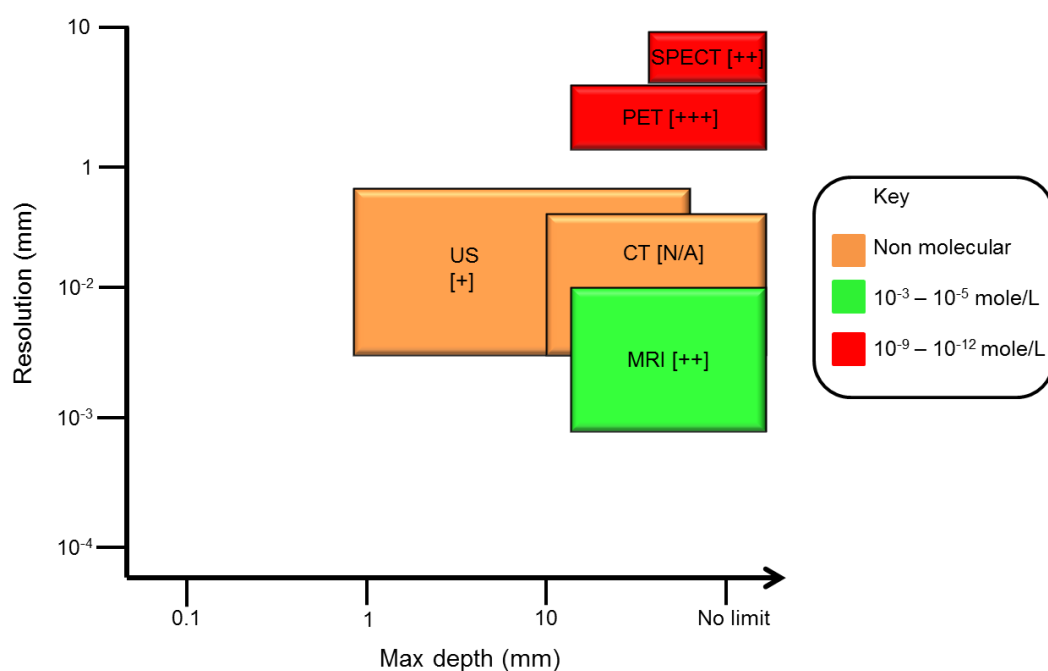


Figure 3: A comparison of PET, CT, US (Ultrasound), MRI and SPECT. The box for each imaging modality spans the resolution over which the modality is best suited on the y-axis and demonstrates the maximum depth of penetration it can achieve on the x-axis. The colour of the box is related to its sensitivity (see key). The number of pluses indicates how quantitative the imaging modality is, with [+] being the least and [+++] being the most.

(Adapted from *Curr. Top. Med. Chem.*)<sup>19</sup>

Molecular imaging is a rapidly expanding area<sup>20</sup> and has had a major impact in the fields of drug discovery and clinical oncology. Molecular imaging allows visualisation of molecular processes in a non-invasive manner and is used to study the physiology of tumours as well as the molecular processes, which occur during tumour growth.

The nuclear imaging modality PET is emerging as a particularly useful diagnostic tool for molecular imaging providing the most quantitative data of all the clinical imaging techniques available, see Figure 3.<sup>19</sup> PET can also penetrate deep within tissue making it an ideal technique for imaging tumours (which are often located deep within the body). PET agents can also be administered at concentrations low enough ( $10^{-9}$  –  $10^{-12}$  M) so as not to elicit a physiological response.<sup>17</sup>

Molecular imaging using PET makes it possible to observe specific biochemical events such as cell trafficking, gene expression and receptor binding<sup>19</sup> using carefully designed molecular probes. Much attention has centred on evidence that tumours overexpress receptors on the surface of cells.<sup>21, 22</sup> The identification of a unique molecular marker or markedly overexpressed targets and the processes they modulate has led to new targeted molecular cancer therapies. Molecular imaging can yield valuable information such as early stage diagnosis, predicting the risk of cancer progression, rationally selecting therapy and monitoring response to therapy.<sup>23</sup> Molecular probes which target receptors involved in specific physiological processes such as cell proliferation (rate of cell division), apoptosis (programmed cell death), angiogenesis (growth of new blood vessels) and metastasis (spread of cancer) are currently the focus of much research<sup>12, 24, 25</sup> because these processes reflect tumour growth, composition and blood supply.

#### **1.1.4. Targeted therapy**

Many disease states cause cellular functions to differ from normal healthy tissue. This often means that receptors or proteins are expressed at abnormal levels. Targeted therapy exploits a recognised disease biomarker which is often conjugated to an optically active reporter to provide information about the biochemical processes as they occur within the disease.

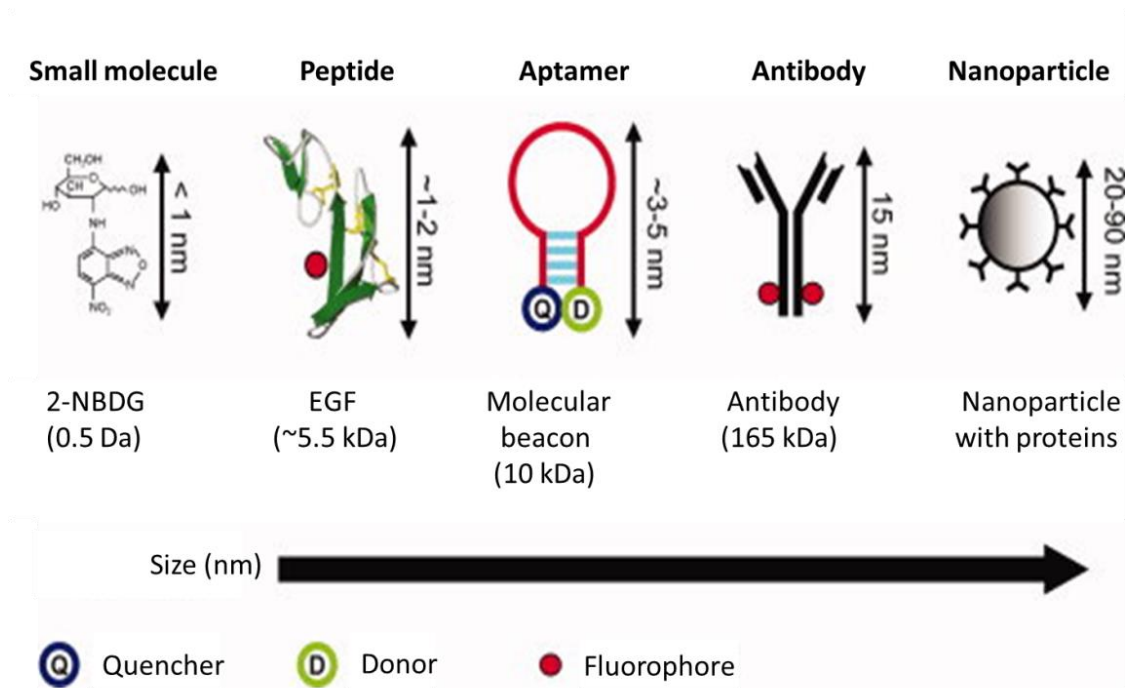


Figure 4: Examples of molecular specific contrast agents. Small molecules, peptides and antibodies need to be labelled with a fluorescent moiety for OI. (Nanoparticles include quantum dots (QD)). (Reproduced from *J. Mater. Sci: Mater. Med.*)<sup>26</sup>

This kind of therapy is ideal for treating tumours particularly when they have metastasised to other areas of the body. The targeted biomarker may be a vector specifically expressed or up-regulated in the tumour or it can be associated with an underlying biological process such as angiogenesis or metastasis. These markers can not only be used to diagnose the tumour but also to give important information about the biochemical processes of the diseased cells since proteins and receptors regulate many of these processes.

There are many examples of molecular specific agents including small molecule antagonists, peptide chains and antibodies,<sup>26</sup> see Figure 4, once conjugated to a fluorescent moiety these become molecular specific optical contrast agents. There is an equally large array of disease biomarkers, giving much scope for imaging and diagnosing many types of tumours.<sup>24, 27</sup>

#### **1.1.4.1. Quantum dots as molecular specific contrast agents.**

To give one specific example; quantum dots (QD) are a recent development for targeted therapy. They are nanoparticles with highly sensitive fluorescent profiles and have been conjugated to many different biomolecules, including peptides and antibodies which have been used to image several different disease biomarkers.<sup>28</sup> The major advantage of QD is that fluorescence emission is size dependent, different sized QD will emit light at different wavelengths and can be used to give multi-coloured images. Gao *et al.* tagged cancer cells with QD of different sizes and were able to observe multicoloured fluorescence images with as few as 10-100 cancer cells, see Figure 5.<sup>29</sup> This study demonstrated not only the enhanced optical properties but also the sensitivity of QD.

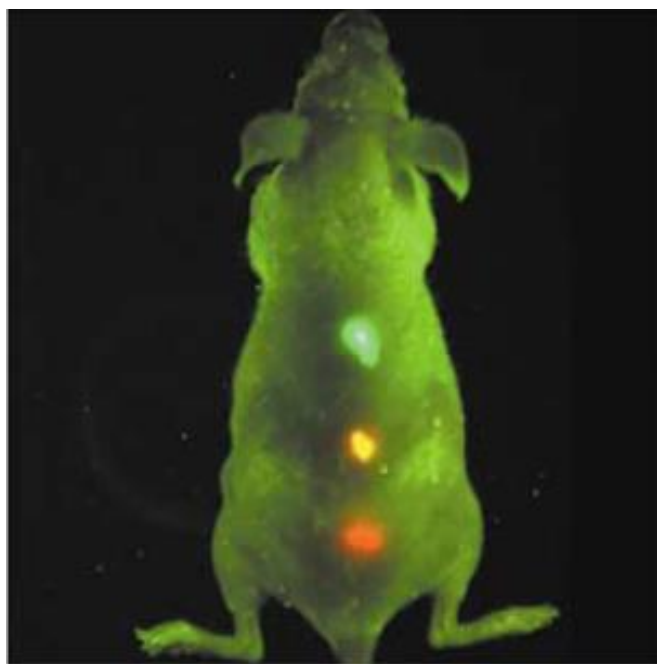


*Figure 5: Imaging of different sized QD targeting cancer cells in a mouse model.*

*(Reproduced from Methods Mol. Biol.)<sup>29</sup>*

Targeted therapy utilises the idea of targeted imaging, molecular probes selectively attach to a targeted cell surface receptor and by means of an optically active moiety generate an image which reflects the biochemistry of the tumour. This information can then be used to direct targeted therapy. The first step in developing new targeted probes is the identification of a target.

## **1.2. Chemokines and chemokine receptors**

Chemokines comprise a protein family consisting of at least forty-six distinct chemokines and around twenty chemokine receptors.<sup>30</sup> Chemokines are small, water soluble, low molecular weight proteins (8-12 kDa) which bind to their cognate G-protein coupled receptor (GPCR) and elicit a cellular response. Chemokines and their receptors are now known to be involved significantly in a wide spectrum of diseases and conditions, including cancer and HIV, as well as multiple sclerosis, rheumatoid arthritis, allergic disorders, asthma, psoriasis and inflammatory bowel disease.<sup>31</sup> Chemokines are primarily involved in the migration of cells or control of cell movement (chemotaxis) and have multiple functions in normal cells including embryogenesis, angiogenesis and wound healing<sup>10</sup> but have also been shown to have a paramount role in tumour progression.<sup>32, 33</sup>

### **1.2.1. The chemokine receptor CXCR4**

The chemokines can be classified into four groups; CXC, CC, CX3C and C (where C = cysteine) based on the positioning of the conserved two *N*-terminal cysteine residues. CXCR4 is a seven transmembrane (TM) GPCR, rich in basic amino acids with three intracellular and three extracellular connecting loops (ECL 1,2 and 3), see Figure 6. It is 352 amino acids in length and has an overall electrostatic surface charge of 9- at physiological pH.<sup>34</sup>

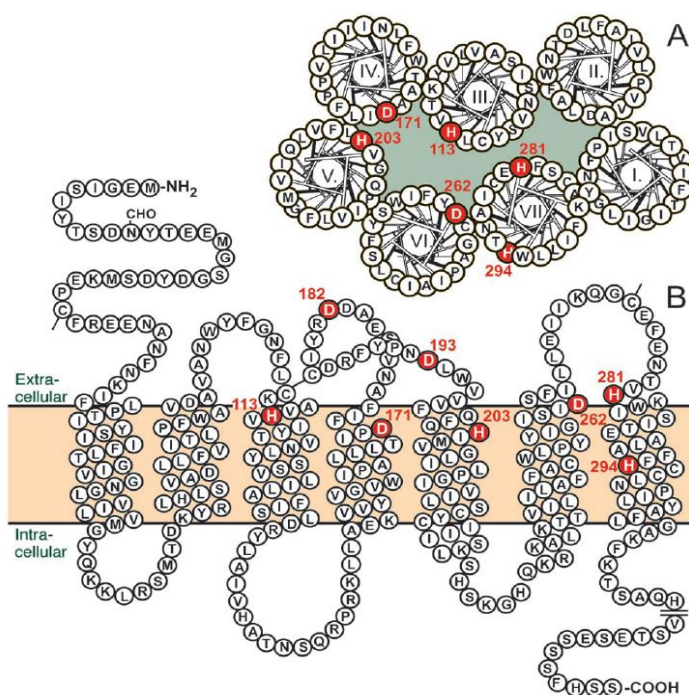


Figure 6: Helical wheel (A) and serpentine diagram (B) of the CXCR4 receptor. (Reproduced from *J. Biol. Chem.*)<sup>35</sup>

Until recently the crystal structure of CXCR4 had not been determined and calculated homology models developed from bovine rhodopsin<sup>36</sup> (a member of the same protein family) had been used as a substitute. In November 2010, Stevens and co-workers reported the first crystal structure of CXCR4.<sup>37</sup> Five independent crystal structures bound to small molecule antagonists (including IT1t, see Figure 7) were reported along with detailed information on the location and shape of the ligand binding site, see Figure 8. The crystal structures revealed new clues into binding interactions and cemented previously thought ideas.

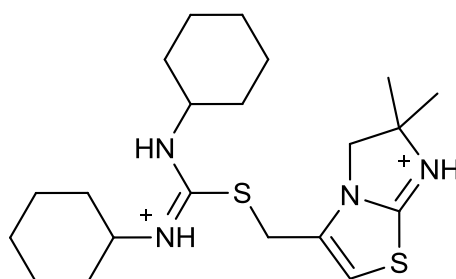


Figure 7: Structure of the small molecule antagonist IT1t.

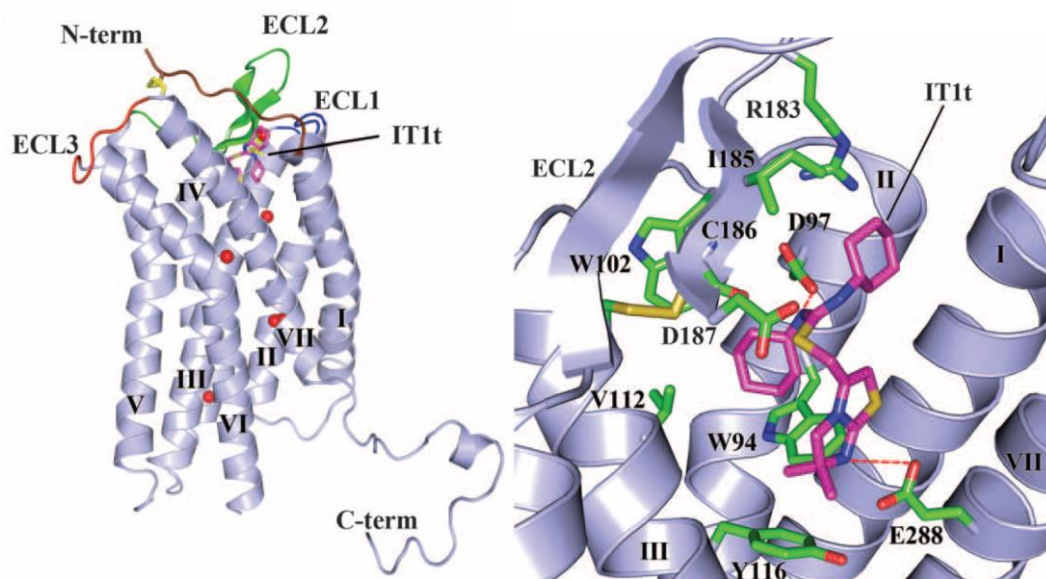


Figure 8: (Left) Overall fold of the CXCR4-IT1t complex. The receptor is coloured blue. The N-terminus, ECL1, ECL2 and ECL3 are coloured brown, blue, green and red, respectively. IT1t is shown as a stick representation in magenta with the disulfide bonds in yellow. Conserved water molecules are shown in red. (Right) CXCR4 ligand-binding cavity for IT1t (magenta) the residues of the receptor involved in ligand interactions are shown in green. Nitrogen atoms are blue, oxygen atoms are red and sulfur atoms are yellow.

(Reproduced from Science)<sup>37</sup>

CXCR4 has been shown to be an important factor in the migration, invasiveness, proliferation and metastasis of tumours.<sup>38</sup> At least twenty-three different types of human tumours<sup>39</sup> overexpress CXCR4 including non-small cell lung cancer, ovarian and prostate cancer and colorectal cancer but it is most prominent in breast cancers.<sup>33</sup> CXCR4 is overexpressed in a large percentage of breast cancers particularly in the cytoplasm suggesting an important role in tumour progression, making it an ideal biomarker for tumour imaging.<sup>38</sup> High levels of CXCR4 indicate the potential for metastatic spread and hence the need for rigorous treatment. In studies using mouse models it was found that blocking the CXCR4 receptor decreased breast cancer cell invasiveness and metastasis.<sup>40</sup>

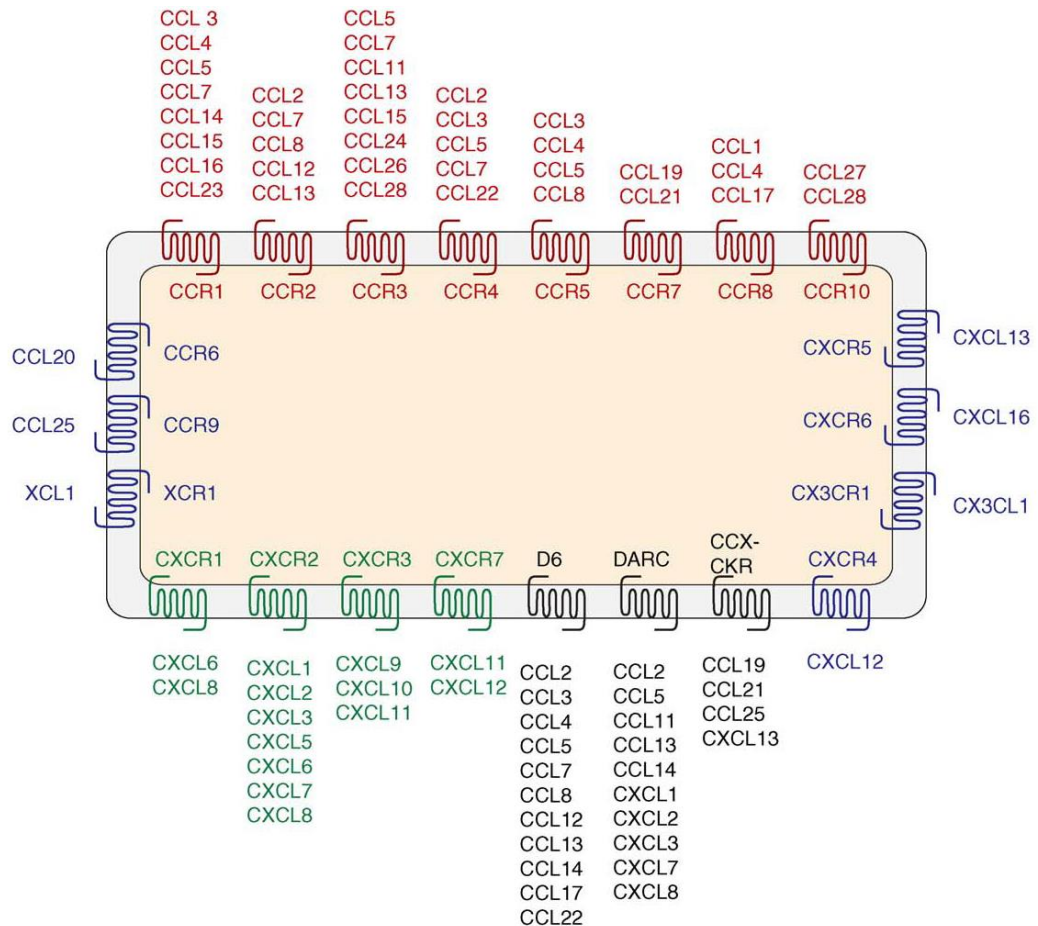


Figure 9: Chemokines and chemokine receptor families. (Reproduced from *Trends in Mol. Med.*)<sup>41</sup>

Most chemokines and chemokine receptors are promiscuous in their interactions, see Figure 9.<sup>41</sup> However, CXCR4 has a sole natural ligand CXCL12 and it is this interaction between the receptor-ligand pair which facilitates metastasis to distant organs.<sup>42</sup> It is thought that chemokines are secreted by target organs and act as attractants to metastasising cancer cells.<sup>33</sup> The CXCR4/CXCL12 gradient plays a crucial role in controlling this. CXCL12 is expressed constitutively in a number of tissues and may explain why tumours employ this receptor-ligand pair for metastasis.<sup>10</sup> Physiologically the CXCR4/CXCL12 gradient is involved in the migration of embryonic cells which controls normal growth and development.

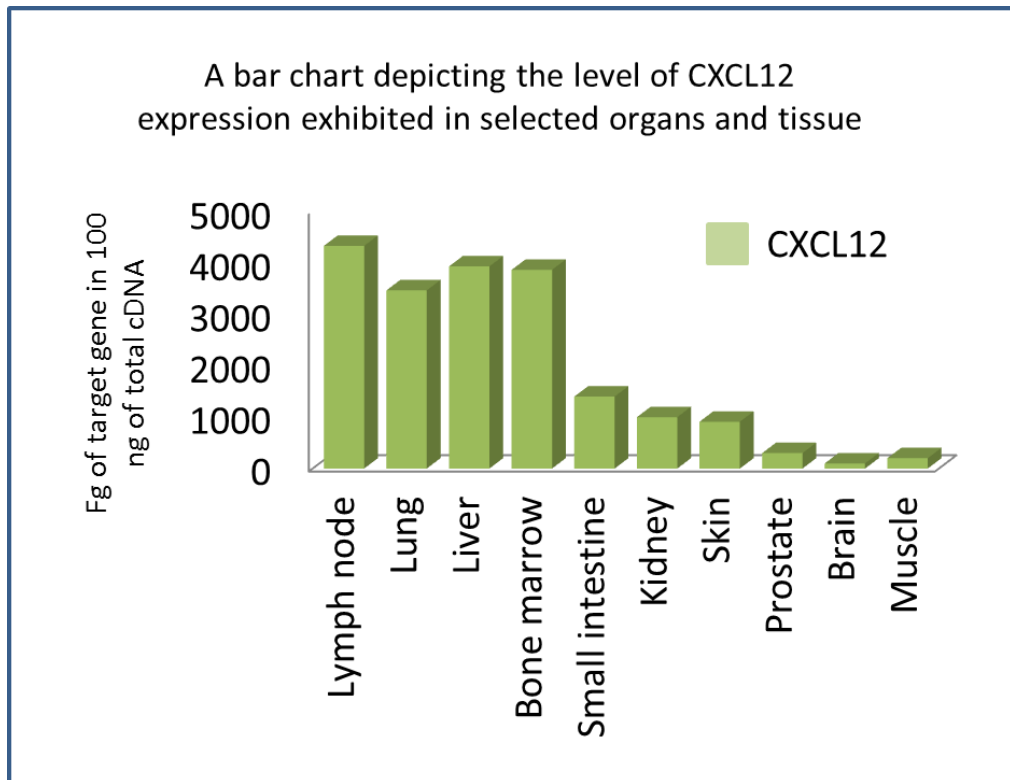


Figure 10: CXCL12 expression in normal human organs. Values are expressed as femtograms of target gene in 100 ng of total cDNA. (Adapted from Nature.)<sup>43</sup>

In 2001, Muller *et al.* published a paper which proved that the chemokines CXCR4 and CCR7 and their respective ligands play a critical role in determining the metastatic destination of breast cancer by acting directly on tumour cell migration and invasion.<sup>43</sup> They noted that CXCR4 is highly expressed in several breast cancer cell lines but also that CXCL12 is at peak levels of expression in organs representing the first destination of breast cancer metastasis. Breast cancers metastasise to lymph nodes, lung, liver and bone marrow and they were able to correlate this with the level of CXCL12 expression observed in these organs, see Figure 10.

The migrational cues employed during embryogenesis seem to be duplicated in tumour progression and metastasis. Blocking the CXCR4 receptor could not only provide a means of locating and diagnosing the cancer but also a novel way of preventing the spread of cancer with some early studies indicating that progression of cancers can be mediated by small molecule receptor antagonists.

### 1.3. Saturated tetraazamacrocycles as small molecule receptor antagonists

The term macrocycle will be used to describe the class of saturated tetraazamacrocycles based on a cyclam (14-membered) or cyclen (12-membered) backbone including their derivatives, see Figure 11.

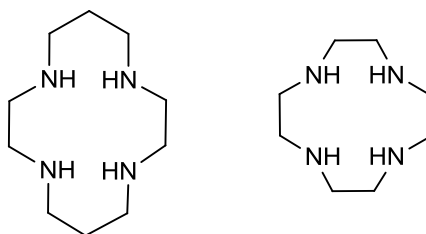


Figure 11: Structure of the tetraazamacrocycles; cyclam (left) and cyclen (right).

Now the target receptor has been identified, ligands need to be designed which have high affinity and optimum *in vivo* characteristics to target this receptor. Macrocycles are fundamental to a number of biological systems<sup>44</sup> and have shown a remarkable affinity for the CXCR4 receptor. Interest in macrocyclic structures for cancer studies began with their initial success as HIV antagonists.<sup>45, 46</sup>

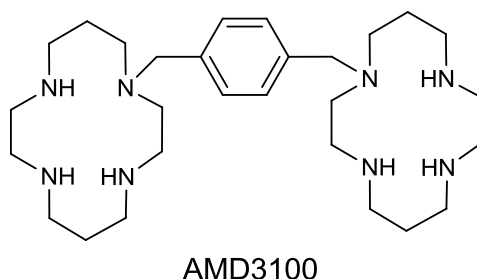


Figure 12: Molecular structure of AMD3100.

AMD3100, see Figure 12 section 1.3., was discovered as a potent HIV inhibitor by blocking the virus' entry into the cell<sup>47</sup> and was licensed for use in 2009, as a stem cell mobilising agent for patients who had recently undergone chemotherapy.<sup>48</sup> Following this many groups realised the potential of macrocyclic structures for disease control and therapy. Macrocycles show a range of properties depending on their design which leads to a host of potential applications. Macrocycles utilise both the chelate and the macrocyclic effect to enhance stability<sup>9</sup> and have been shown to have an ideal structure and cavity size for complexing d-block metal ions.<sup>49</sup>

### 1.3.1. The chelate effect

The chelate effect explains the enhanced stability of a complex containing polydentate ligands over one containing (similar) monodentate ligands. 'Free' energy is gained when a bidentate or polydentate ligand binds to a metal ion in comparison to the corresponding number of unidentate ligands leading to more stable complexes. The macrocyclic effect is a similar concept describing the property of coordinating macrocyclic molecules. It was first described in 1969 by Cabbiness and Margerum<sup>50</sup> who noted that the stability of a copper(II) complex was enhanced when coordinated to Curtis' macrocycle,<sup>51</sup> see Figure 13, in comparison to similar non-cyclic tetraamine ligands. This stability can be attributed to the preorganisation of macrocyclic ligands along with the complementarity between the metal ion and the ligand.

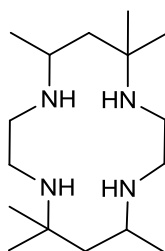


Figure 13: Curtis' macrocycle; 5,7,7,12,14,14-hexamethyl-1,4,8,11-tetraazacyclotetradecane.

### 1.3.2. Monomacrocycles

Monomacrocycles have received considerable interest from many groups<sup>52, 53</sup> they are relatively easy to synthesise and unlike their bismacrocyclic counterparts have the potential for improved pharmacological properties due to a reduced molecular charge.<sup>54</sup> The small molecule antagonist AMD3465, see Figure 14, represents such a possibility and showed a 10-fold higher affinity for the CXCR4 receptor in intracellular calcium signalling, chemotaxis, CXCR4 endocytosis and mitogen-activated protein kinase phosphorylation studies when compared to AMD3100.<sup>54</sup>

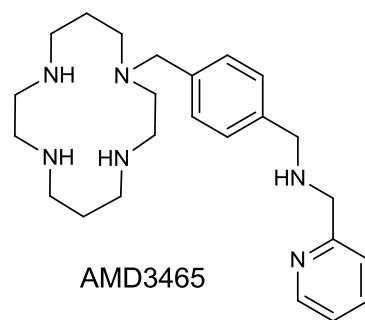


Figure 14: Molecular structure of AMD3465.

The binding mode of macrocyclic compounds with the CXCR4 receptor has been attributed to a series of specific interactions. Gerlach *et al.* have elegantly demonstrated that macrocycles are likely to form hydrogen-bond stabilised interactions with carboxylic acid groups.<sup>35</sup> Through site directed mutagenesis they established that macrocyclic compounds bind to specific aspartate (Asp) residues in TM segments in the CXCR4 receptor binding pocket. Asp171 in TM-IV and Asp262 in TM-VI have shown to be intrinsic to the binding ability of macrocycles, see Figure 15.

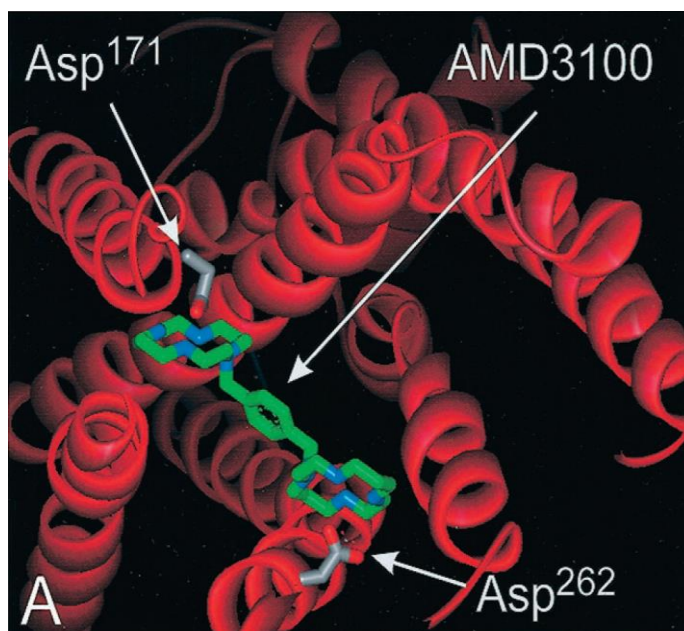


Figure 15: Molecular model of the main ligand binding pocket of the CXCR4 receptor with AMD3100 docked into favourable interactions with Asp171 and Asp262.

(Reproduced from *J. Biol. Chem.*)<sup>35</sup>

Recently, additional hydrogen-bonding to Glutamate288 (Glu) in the binding pocket *via* the secondary amines has also been realised to be an important interaction and even  $\pi$ - $\pi$  stacking interactions with tryptophan residues have been suggested to be important for binding ability.<sup>31</sup>

### 1.3.3. Metal complexes of monomacrocycles

Macrocycles are metal chelating agents and evidence has shown their ability to complex to a wide range of metal ions particularly first row transition metal ions bearing a 2+ charge. It has also been shown that a pendant arm can initiate metal complex formation by catching the metal ions and directing them into the macrocyclic cavity,<sup>44</sup> these pendant armed derivatives have gone on to show remarkable kinetic inertness *in vivo*.<sup>55</sup> Incorporation of nickel(II) or zinc(II) into the macrocyclic compound AMD3100 has shown an increase in affinity for the CXCR4 receptor in comparison to the corresponding 'free' macrocycle. The affinity of AMD3100 for the CXCR4 receptor is increased by 10-fold upon incorporation of zinc(II).<sup>56</sup> Evidence suggests that AMD3100 is actually administered as a pro-drug and once inside the body it complexes with zinc(II) ions in the blood to form the active drug;  $[\text{Zn}_2\text{AMD3100}]^{4+}$ .<sup>57</sup> This suggests metal complexes of macrocyclic compounds may provide an opportunity to optimise binding to the CXCR4 receptor and prompts the need for further study. The different electronic arrangements of the metal ions will cause different binding affinities but overall the increase in affinity is thought to be due to the formation of coordinate bonds between the metal ion and aspartate residues.

Metal containing macrocycles with a cyclam skeleton (14-membered ring) undergo marked conformational changes during binding.<sup>49, 58</sup> Upon metal coordination the four nitrogen atoms become chiral and the N-H bonds lie above or below the ligand plane, creating six possible configurations, see Figure 16. *Trans*-III is the most common configuration as it is the most stable due to lower strain energy<sup>59</sup> but there is evidence to suggest that a *cis*-V configuration is optimal for binding to the CXCR4 receptor.<sup>60, 61</sup> Therefore configurational fixing may be a route to optimise interactions with CXCR4. Indeed several cyclam derivatives which have shown high

affinity for the CXCR4 receptor adopt a *cis-V* configuration in the solid state, e.g.  $[\text{Zn}_2\text{AMD3100}]^{4+}$ , but are in equilibrium in solution.

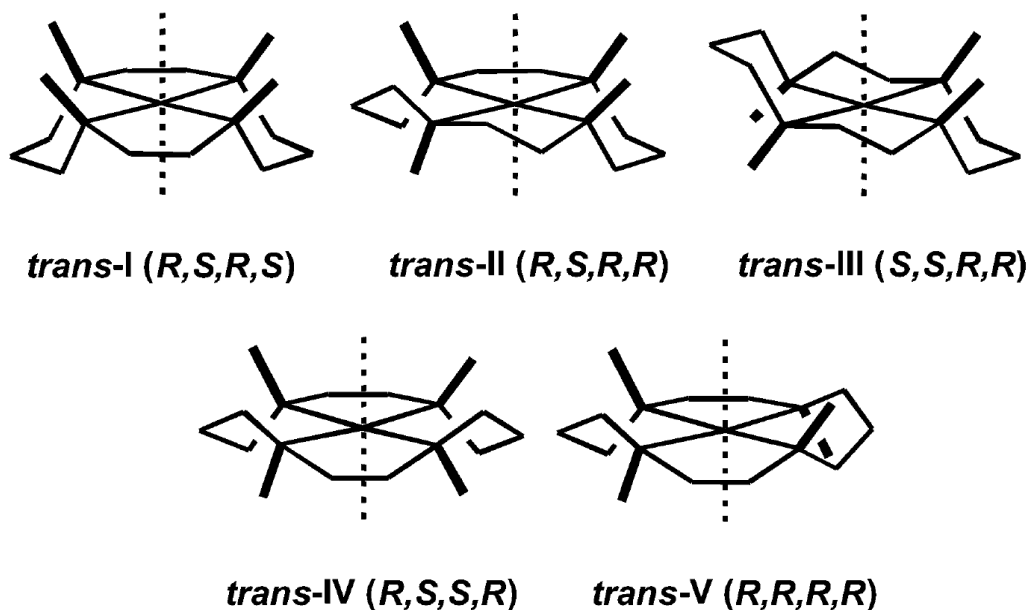


Figure 16: Representations of the six configurational arrangements cyclam derived structures containing metal ions can adopt. (Reproduced from *Chem. Soc. Rev.*)<sup>62</sup>

Metal ions allow not only stronger interactions at the CXCR4 receptor due to the formation of coordinate bonds (over weaker hydrogen-bonding interactions) but also a more stable interaction because of the geometry they cause the macrocycle to fold into. This stability has been shown to increase the residence time of macrocycles at the CXCR4 receptor. Archibald and co-workers used a highly rigid copper(II) complexed bismacrocycle and demonstrated an increased residence time at the CXCR4 receptor when compared to that of AMD3100.<sup>63</sup> If macrocycles are to be used as diagnostic and therapeutic agents targeting chemokine receptors this may be advantageous.

#### 1.3.4. Configurationally restricted macrocycles

Ethyl bridged monomacrocycles were first synthesised by Wainwright and Hancock in the 1980s<sup>64, 65</sup> followed by Weisman and Wong in the 1990s.<sup>66</sup> Structurally reinforcing the macrocyclic skeleton involves addition of an ethylene bridge either between opposite or adjacent nitrogens. Connecting opposite nitrogens forms a

cross bridge (CB) structure and connecting adjacent nitrogens forms a side bridge (SB) structure, see Figure 17.

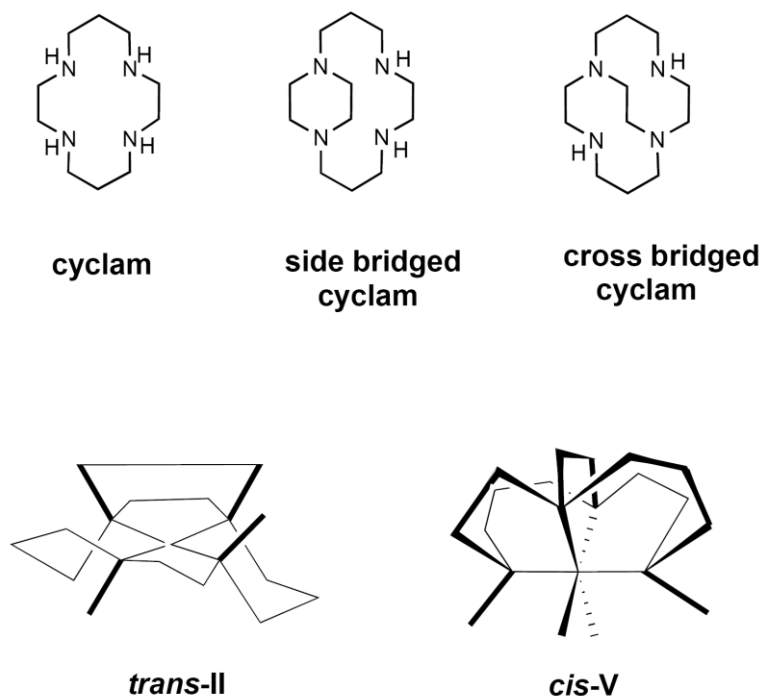


*Figure 17: With the addition of an ethylene bridge between adjacent nitrogens a trans-II configuration is adopted (when mono-N-alkylated). With the addition of an ethylene bridge between opposite nitrogens a cis-V configuration is adopted.*

*(Reproduced from Curr. Med. Chem.)<sup>31</sup>*

Structurally reinforcing the skeleton allows control of several parameters including flexibility, basicity, ring size, steric strain and importantly configuration. Addition of an ethylene bridge locks the configuration and means only one configuration is possible; SB compounds adopt a *trans-II* configuration when mono-*N*-alkylated or *trans-IV* when bis-*N*-alkylated and CB compounds are topologically constrained to a *cis-V* configuration, see Figure 17.

A few research groups<sup>67</sup> including our own<sup>68</sup> have utilised this restriction in configuration to form stable complexes for chelation to metal ions and subsequent use *in vivo*. Bismacrocycles were identified as the first class of specific small molecule CXCR4 antagonists.<sup>69</sup> They are composed of two cyclam rings linked by an

aromatic or aliphatic linker and to date only one has been licensed for clinical use (AMD3100, see Figure 12, section 1.3.) despite a range of such molecules being synthesised, see Figure 18.

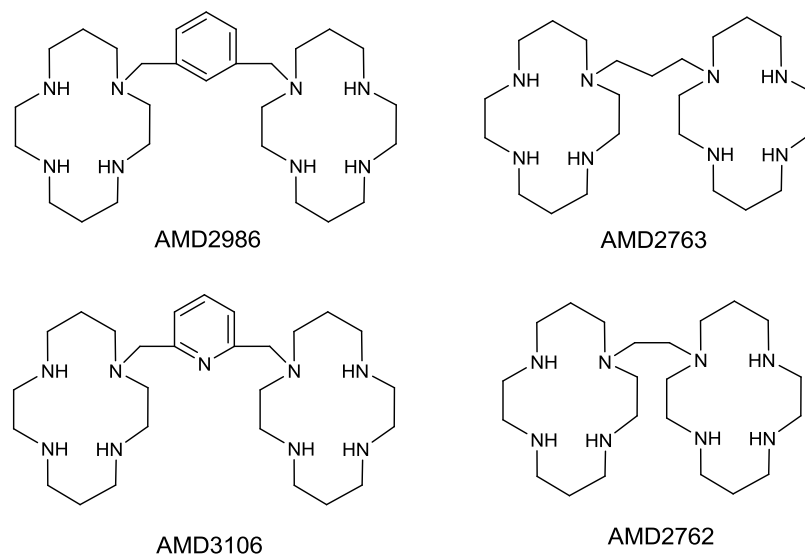


Figure 18: Molecular structures of bicyclams.

This emphasises the need for further study into bismacrocylic structures and to establish their efficacy against the CXCR4 receptor. It remains to be seen what will become of these antagonists and whether any will succeed in making it to clinical trials but what is still apparent is the potential to optimise the bismacrocylic structure by restricting the configuration to obtain ultra-stable complexes for use *in vivo*.<sup>58, 70</sup>

#### 1.4. Targeted MFCs using porphyrin bioconjugates

Macrocycles provide a means of targeting a disease biomarker as well as the potential to complex metal ions. In order to create viable MFCs capable of simultaneous diagnosis and therapy, a therapeutic moiety needs to be attached with optimal features for *in vivo* use and conjugation to the macrocycle. Porphyrins can act not only as fluorescent agents but also as photodynamic therapy (PDT) agents which can be used therapeutically. Porphyrins have shown considerable clinical efficacy with selected porphyrin and porphyrin type compounds being licensed for clinical use. However, their use is flawed by non-specific uptake as well

as generalised photosensitization suffered by patients.<sup>71</sup> Due to this porphyrins are being developed for conjugation to a targeted bifunctional chelator (BFC) (a chelating ligand with a functional group that can be used for attachment to a bio-targeting vector). The targeted BFC can be used to diagnose and locate the tumour, once located the BFC can then act as a drug delivery system and the photodynamic activity of the porphyrin can be activated (with a specific wavelength of light) to kill cancer cells.

#### 1.4.1. Photodynamic therapy

PDT is a minimally invasive procedure being developed as an alternative to traditional methods (surgery, radiotherapy and chemotherapy) for the treatment of cancers.<sup>72</sup> PDT is typically a two-step process where a selectively localised light-sensitive drug<sup>73</sup> known as a photosensitiser (PS), which is non-toxic in the absence of light, is administered, see Figure 19. Over a period of time (normally 24–96 hours) there will be an accumulation of the PS in cancerous vs. healthy tissue.<sup>74</sup> The tumour is then irradiated with light of the correct wavelength to activate the PS.

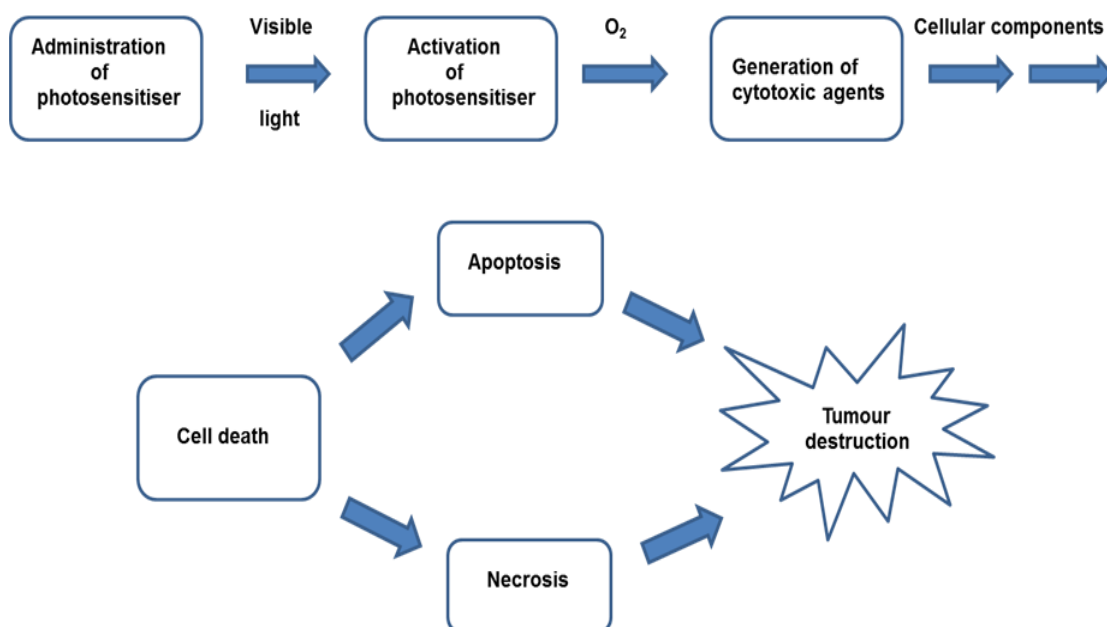


Figure 19: Photosensitiser initiated cell death. (Adapted from Metal based drugs)<sup>73</sup>

### 1.4.2. Porphyrins as photosensitisers

Porphyrins are planar, aromatic azamacrocycles, classed as tetrapyrrolic having four pyrrolic sub-units linked through methine bridges, see Figure 20.

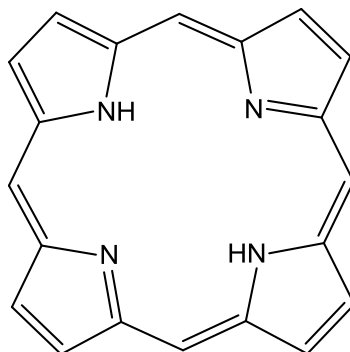


Figure 20: Structure of the porphine macrocycle.

Porphyrin derivatives are inherently similar to many naturally occurring porphyrins present in biological systems and as such many display little or no toxicity in the absence of light. The porphyrin core contains a highly conjugated  $\pi$  system, giving rise to strong absorption in the visible region.

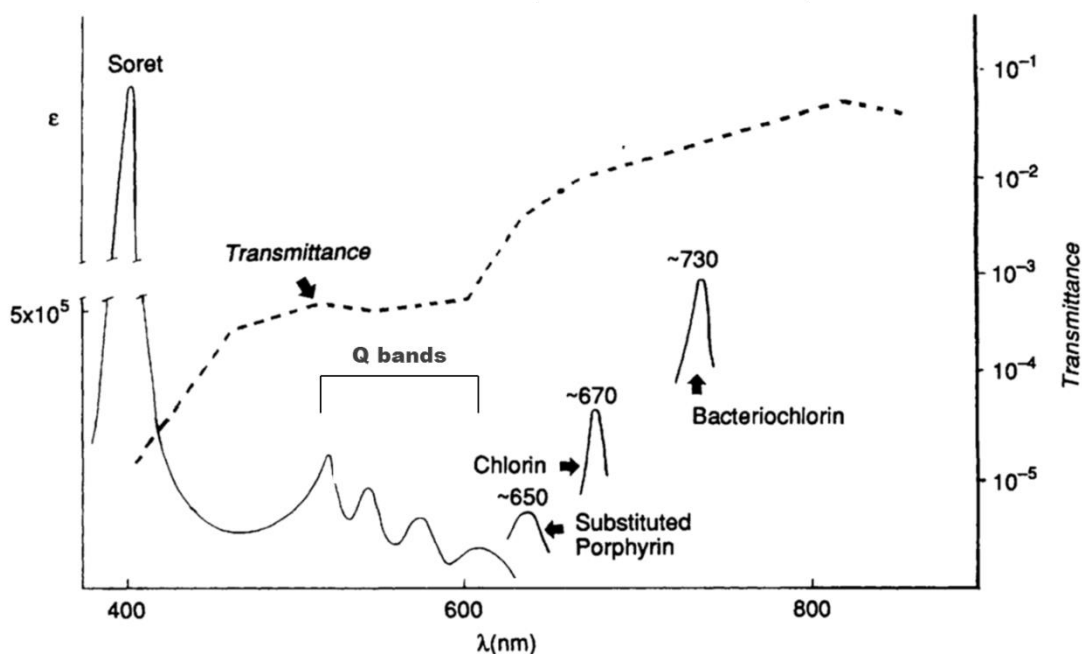
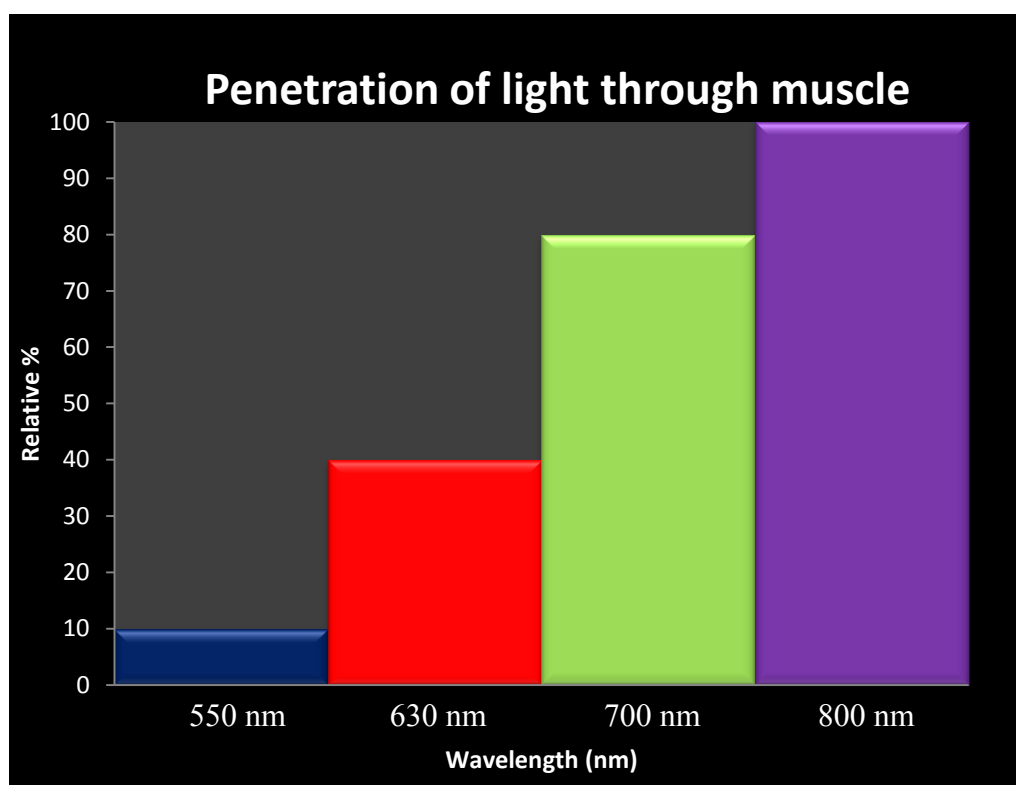


Figure 21: Relationship between the absorption profile of a porphyrin and the amount of transmitted light. The transmittance of light increases towards the red end of the spectrum.

(Adapted from Chem. Soc. Rev.)<sup>75</sup>

Porphyrins have very characteristic UV-vis spectra consisting of an intense absorption band around 400 nm known as the Soret band and four weaker absorptions between 450 – 700 nm known as the Q bands, see Figure 21.<sup>75</sup> The absorption profiles of porphyrins, and porphyrin derivatives such as chlorins and bacteriochlorins, therefore extend to the red and NIR regions of the electromagnetic spectrum (600 – 800 nm). At higher wavelengths, transmittance of light through tissue occurs to a greater degree thus allowing for deeper tissue penetration, see Figure 22.<sup>76</sup>



*Figure 22: A bar chart showing the relationship between wavelength and tissue penetration.*

The efficiency of a PS is dependent on it having suitable photophysical properties. Ideally a high quantum yield of triplet formation ( $\Phi_T \geq 0.5$ ), a high singlet oxygen quantum yield ( $\Phi_\Delta \geq 0.5$ ) a high triplet state energy ( $\geq 94$  KJ/mol) and a long triplet state lifetime (microsecond range).<sup>73</sup> The length of a porphyrin's triplet state lifetime and local oxygen concentration will then determine the probability of it interacting with molecular oxygen to produce singlet oxygen. The more chance

there is of this happening (due to a longer triplet state lifetime) the more cellular damage this will ultimately inflict.

### 1.4.3. Development of porphyrin photosensitisers

An ideal PS must display several properties; as well as having a strong absorption in the red/NIR region and a long triplet state lifetime they must also accumulate in tumour tissue more so than healthy tissue, have negligible dark toxicity, be a single, well characterised compound and show a rapid clearance from the body.<sup>77</sup>

Porphyrins display many of these properties and to date one porphyrin (photofrin) and three chlorins (temoporfin, verteporfin and MACE) are licensed for clinical use to treat cancers. Photofrin, is a first generation PS, see Figure 23, used to treat lung, genitourinary and digestive tract cancers. Despite its approval for clinical use it displays some drawbacks including long lived generalised photosensitivity and limited tissue penetration at the clinically used wavelength, 630 nm.<sup>78</sup>

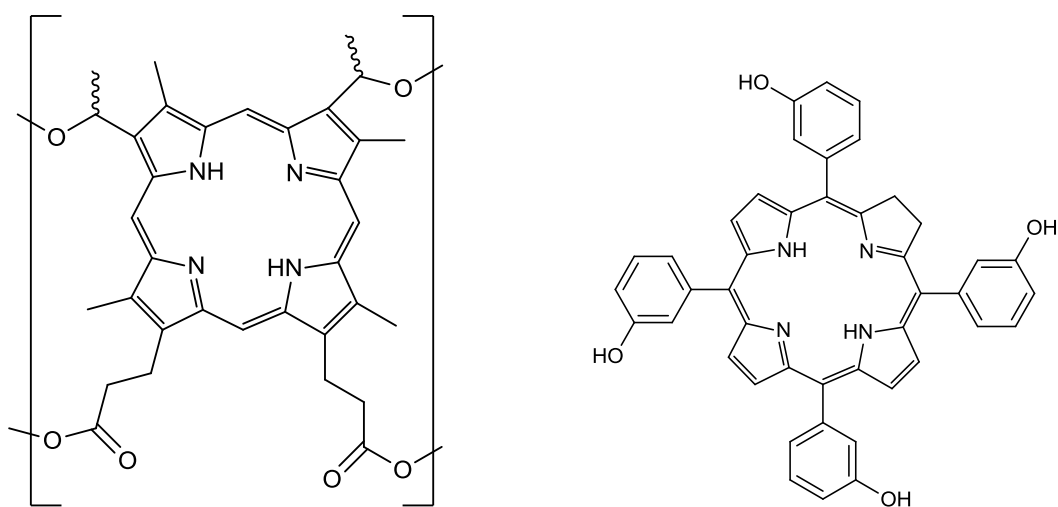


Figure 23: Clinically licensed porphyrins; photofrin (left) and temoporfin (right).

As a consequence second generation PS were developed to counter these drawbacks and improve photophysical characteristics. Temoporfin is a second generation PS, see Figure 23, used to treat head and neck cancers and benefits from having a 'red-shifted' absorption band (655 nm) compared to Photofrin.

The major problem associated with the clinical use of porphyrins is their accumulation in healthy tissue and subsequent generalised photosensitisation suffered by patients after use.<sup>74</sup> This occurs because porphyrins are not actively targeting the tumour and only accumulate there due to morphological differences between the tumour and peritumoural tissue. This has been attributed to poorer lymphatic drainage, leaky vasculature and increased proliferation rates of tumour tissue over healthy tissue.<sup>79</sup> These factors have prompted much research into the development of porphyrins conjugated to drug delivery vehicles to prevent the accumulation of porphyrin in healthy tissue; the so-called 'third generation' of PS.  
72, 76

#### **1.4.4. Third generation porphyrins – improved PDT agents**

The growing need to overcome certain drawbacks associated with the clinical use of porphyrins has led many groups to employ a drug delivery vehicle; these vehicles have some targeting property or a propensity to be taken in by the tumour tissue. Several groups have successfully conjugated porphyrins to a variety of drug delivery vehicles including sugars,<sup>80</sup> peptides,<sup>76, 81</sup> monoclonal antibodies (mAb)<sup>82, 83</sup> and mAb fragments.<sup>74</sup> The grafting of mAb is common<sup>84</sup> but have shown a slow clearance *in vivo* due to their size prompting the use of mAb fragments which have shown superior specificity and increased speed of penetration.<sup>74</sup> Peptides could arguably be the most well-used vehicle for conjugation to porphyrins corroborated by the wealth of literature regarding peptide-porphyrin conjugates.<sup>72, 76</sup> Peptides are easily synthesised and modified, show low toxicity *in vivo* and their small size makes them non-immunogenic. Indeed in 2006, Sibrian-Vazquez *et al.* concluded that the biological efficacy of porphyrins can be increased by conjugation to a peptide as it enhances their cellular uptake and delivery.<sup>81</sup> In 2008 the same group synthesised a series of porphyrin-peptide conjugates bearing a cell penetrating peptide (CPP) (and a nuclear localisation signal).<sup>85</sup> All conjugates were stable in non-enzymatic conditions (some peptide cleavage was observed in enzymatic conditions) and showed accumulation in human cancer cells in comparison to their porphyrin precursors. In the same year Sehgal *et al.* developed a porphyrin

conjugated to a CPP, see Figure 24 and demonstrated that it not only showed low dark cytotoxicity ( $IC_{50} = 38.0 \mu\text{mol}$ ) but also selective accumulation in prostate tumours.<sup>71</sup>

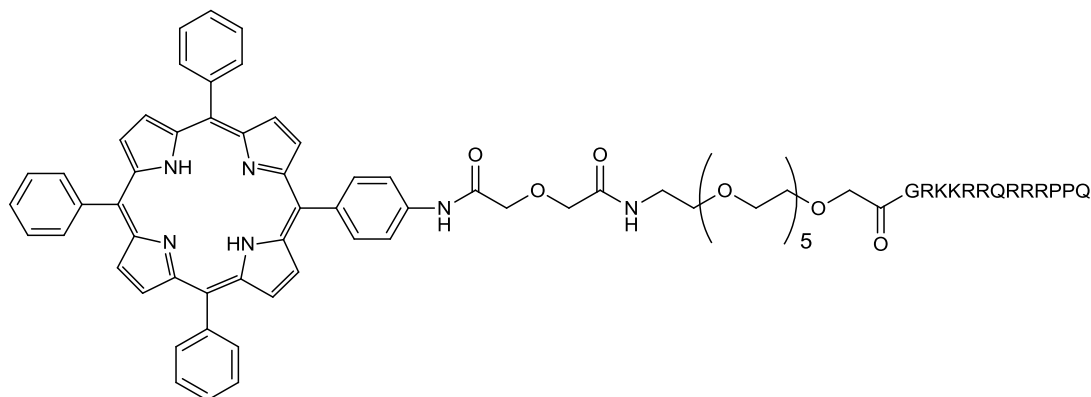
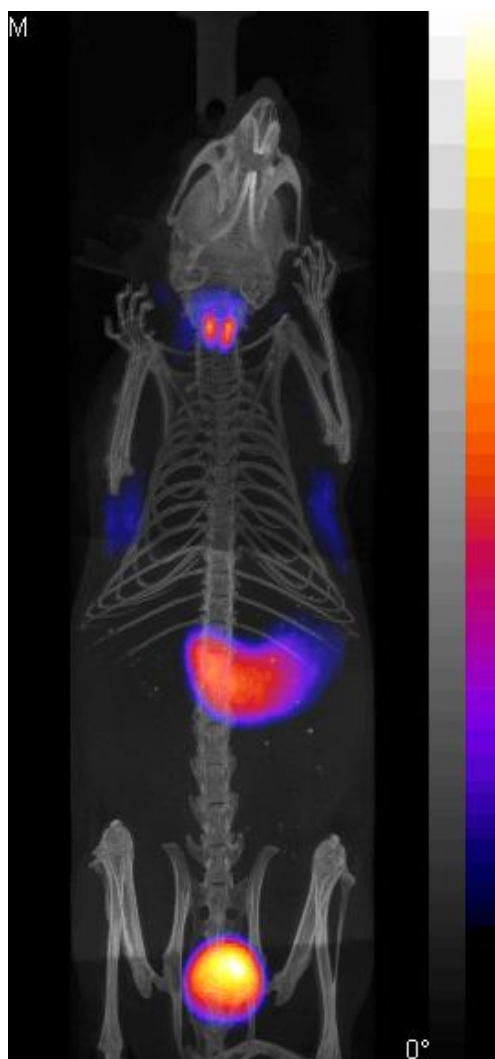


Figure 24: A porphyrin-peptide conjugate shown to selectively accumulate in prostate tumours.<sup>71</sup>

Chaloin *et al.* were able to show not only a marked improvement in cellular uptake but also greater cell growth inhibition and DNA cleavage activity using a Mn-porphyrin conjugated to a targeting chimeric peptide when compared to the nonconjugated metalloporphyrin.<sup>86</sup> Recently nanoparticles have also been employed due to their ease of synthesis and functionalisation.<sup>84, 87</sup> Zaruba *et al.* conjugated porphyrins to gold nanoparticles and demonstrated a significant improvement in PDT activity by reduction of tumour size in comparison to unconjugated porphyrin.<sup>88</sup> A Zn-phthalocyanine-gold nanoparticle conjugate has also been used to successfully target breast cancer cells whilst maintaining its photodynamic property since the group observed PDT associated cell death in *in vitro* studies.<sup>89</sup> Third generation porphyrin conjugates have demonstrated promising *in vitro* results and have ultimately improved specificity in targeting PDT drugs to tumours.<sup>72</sup> There is significant clinical potential of such conjugates and efforts to optimise synthetic procedures and improve biological efficacy remains an important area of research.

## 1.5. Imaging cancers using the nuclear imaging modality PET

Nuclear medicine is the branch of medical imaging that uses gamma or positron emitting radionuclides to generate an image of the *in vivo* distribution of a radiopharmaceutical.<sup>90</sup> Radiopharmaceuticals are incorporated into ligands which have the ability to interact with molecular targets to produce images which portray the biochemical and physiological status of the tissues concerned, see Figure 25.



*Figure 25: Thyroid imaging in a mouse model using PET. Accumulation of radioactivity can also be seen in the liver and bladder due to metabolism and excretion. Colour scale represents the amount of radioactivity accumulated; black = minimum, white = maximum.*

*Image obtained from Prof. P. Blower, Kings College, London.*

PET was first discovered in the 1960s, with the first medical scanner being developed in 1975.<sup>91</sup> Since then it has been a useful research tool but its true potential has only recently been realised<sup>90</sup> due to the rapidly expanding field of nuclear medicine coupled with the emerging discipline of molecular imaging. The use of PET has increased substantially in the last decade, with recent figures estimating that 40,000 PET scans were carried out by the NHS in England in 2011 ([www.nhs.uk/conditions/PET-scan/Pages/Introduction.aspx](http://www.nhs.uk/conditions/PET-scan/Pages/Introduction.aspx)).

PET is a highly sensitive, quantitative imaging technique providing a means to image and measure the rates of biological processes *via* the distribution and localisation of a radionuclide *in vivo*. A positron is emitted from the nucleus of the radionuclide which then travels a non-linear distance (range 1-5 mm in tissue depending on the radionuclide)<sup>92</sup> before colliding with an electron. This annihilation event causes the release of two gamma photons of equal energy (511 keV). These photons are emitted approximately 180° to each other and are detected by a PET scanner, see Figure 26.<sup>25</sup>

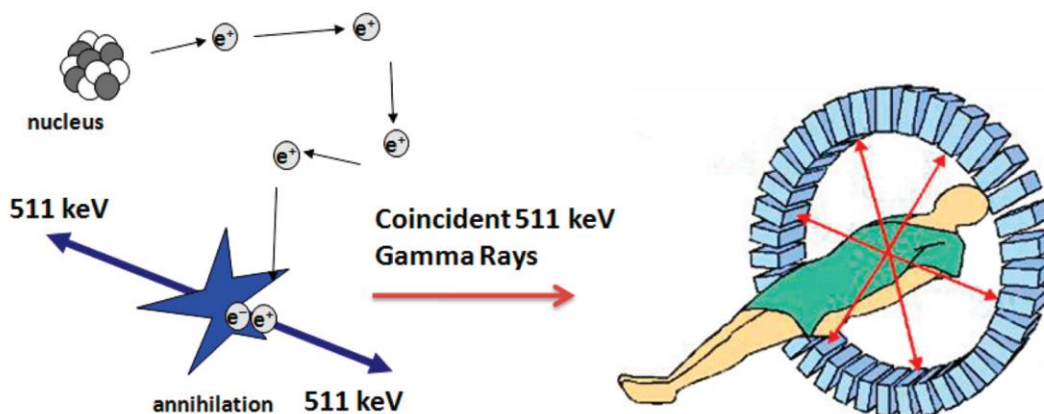
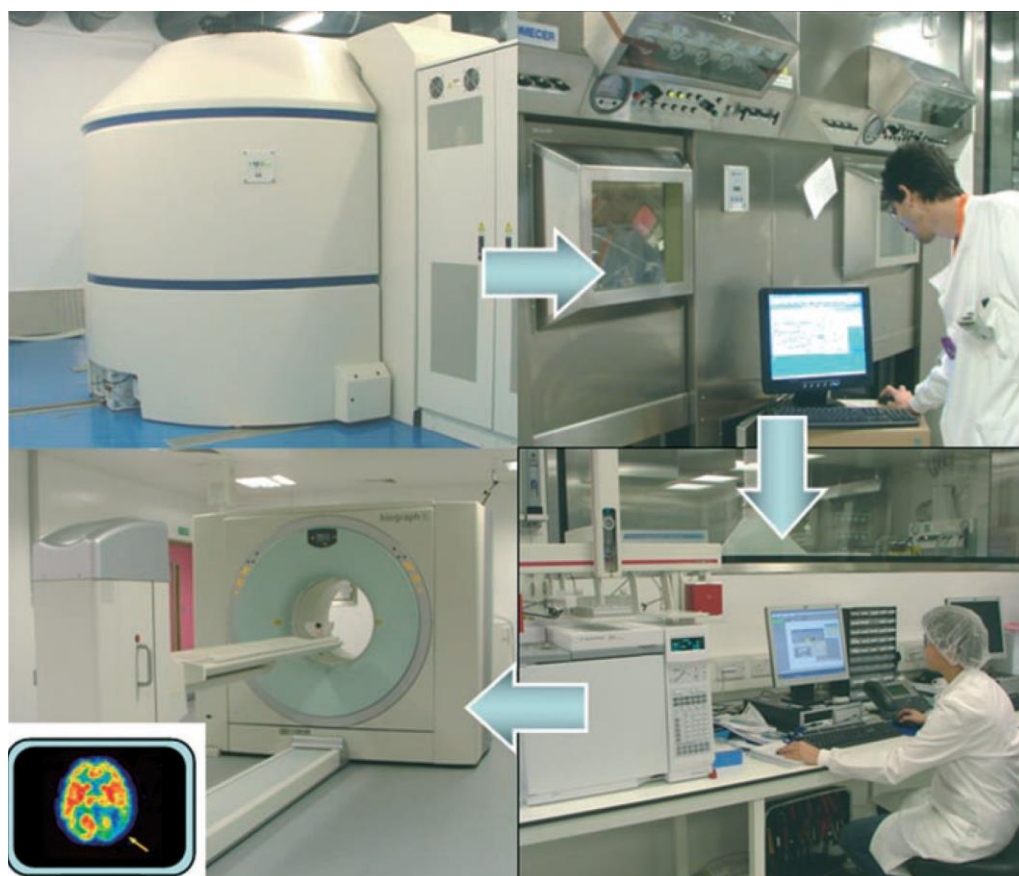


Figure 26: Schematic of imaging with a PET scanner. (Reproduced from *Acc. Chem. Res.*)<sup>9</sup>

This method is more sensitive than single photon techniques because there are two points of reference. The gamma rays are also detected directly, whereas in single photon techniques the beam passes through a “grid” to ensure lateral gammas are not detected but this results in a loss of sensitivity. The PET scanner is rotated around the patient allowing the precise position of the emitted gamma rays to be

determined. This information is then manipulated to provide a three dimensional tomographic image.

PET is a particularly advantageous technique compared to other imaging modalities, since it produces the most quantitative data of all the clinical imaging techniques available and is able to image deep tissue, see Figure 3, section 1.1.3. PET tracers can be administered at low enough concentrations ( $10^{-9} - 10^{-12}$  M) so as not to elicit a physiological response and ensures that the tracer will have little to no detrimental effect upon the patient under study, whilst still being concentrated enough in the tissue to allow for effective imaging.



*Figure 27: The process of PET radiotracer production. From top left: a commercially available biomedical cyclotron; an automated radiolabelling system controlled from outside the hot cell; analysis and quality-control laboratory; a PET scanner (Siemens); and a processed PET image (bottom left). The whole process typically takes a few hours.*

*(Reproduced from Angew. Chemie Int. Ed.)<sup>93</sup>*

The limitations of PET are associated mainly with its resolution. Physics imposes some intrinsic limits on PET scanners and means there is a definite limit of resolution.<sup>19</sup> Currently PET scanners have a limit of resolution between 1-5 mm and this places boundaries on the size of the tumour which can be accurately imaged.

A cyclotron is required to produce all the routinely used radiopharmaceuticals (except  $^{68}\text{Ga}$  which is generator produced), they are then manipulated into a radiolabelled system within a 'hot cell' before administration into a patient, see Figure 27. This means PET facilities have to be close to or within a sensible shipping distance of the cyclotron centre.

PET requires specific probes labelled with a short-lived positron emitting radioisotope to image and measure biochemical processes.<sup>20, 25</sup> Positron emitters include biologically important elements like  $^{11}\text{C}$ ,  $^{13}\text{N}$ ,  $^{15}\text{O}$ . All of these elements are found in naturally occurring compounds. The non-radioactive elements can potentially be replaced with the equivalent radioactive element to give a radiopharmaceutical which is biologically the same as the natural compound. Metals including  $^{61/62/64}\text{Cu}$ ,  $^{67/68}\text{Ga}$ ,  $^{89}\text{Zr}$  and  $^{86}\text{Y}$  are beginning to play a key role in the design of PET radiopharmaceuticals, gaining importance because of their longer lifetimes, increased production and ability to bind to a range of targeting ligands.<sup>90</sup>

### **1.5.1. Current radiopharmaceuticals**

An ideal radiopharmaceutical would, after injection, efficiently interact with the desired molecular pathway where it would be absorbed and produce a highly sensitive image with low signal-background.<sup>94</sup> Any radioligand not reaching the desired target would then be rapidly excreted from the body and not accumulate in non-target areas. Unfortunately due to the complexity of biological systems this ideal state is rarely met, however many radiopharmaceuticals are capable of imaging a variety of tissue functions and metabolic processes and have shown much promise for diagnosis and even therapy. Perhaps the best example of this and certainly the most commonly used PET radiopharmaceutical is  $^{18}\text{F}$ -

fluorodeoxyglucose ( $^{18}\text{F}$ -FDG),<sup>95, 96</sup> accounting for more than 90% of all PET studies.<sup>25</sup>

### 1.5.1.2. $^{18}\text{F}$ -Fluorodeoxyglucose

Fluorodeoxyglucose (FDG) exploits the increased rate of glycolysis seen in tumour cells.<sup>97</sup> This knowledge led to the design and use of the radio-labelled glucose molecule  $^{18}\text{F}$ -FDG, see Figure 28, for imaging this up-regulation.

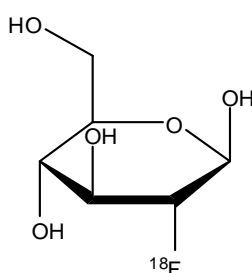
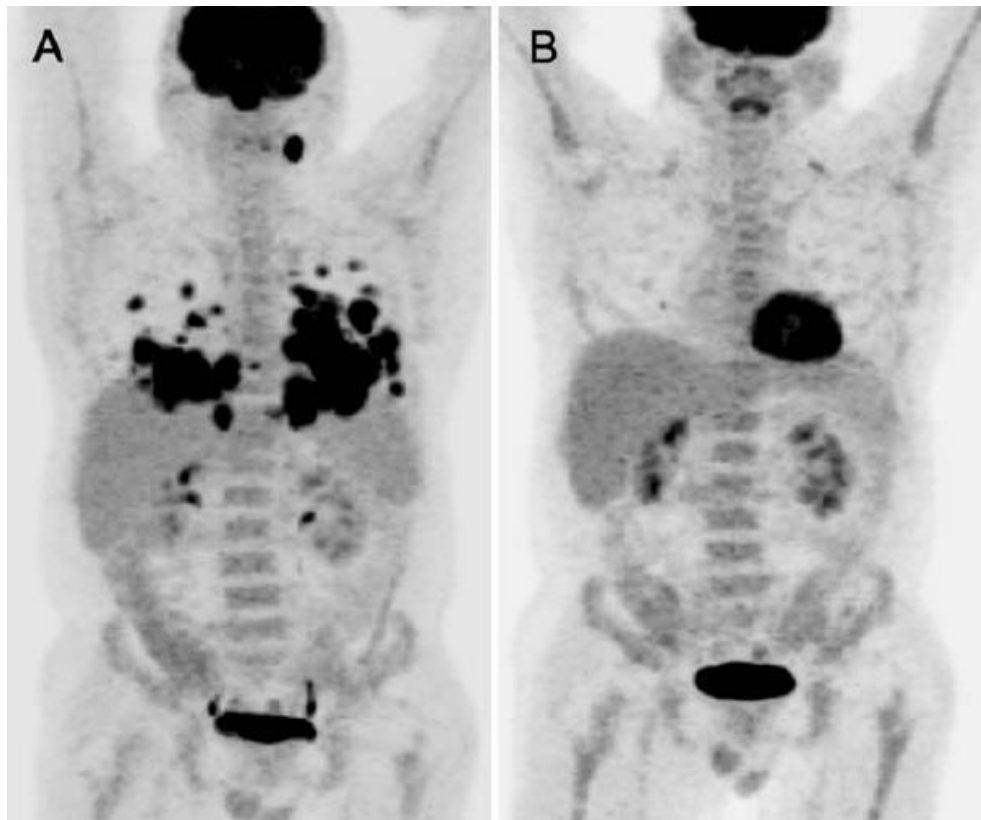


Figure 28: Structure of  $^{18}\text{F}$ -fluorodeoxyglucose ( $^{18}\text{F}$ -FDG).

$^{18}\text{F}$ -FDG is effectively trapped intracellularly because the  $^{18}\text{F}$  atom prevents the next step in glucose metabolism. There is then a gradual accumulation of  $^{18}\text{F}$ -FDG in tumour cells as opposed to healthy tissue and the concentration of tracer imaged then relates to the metabolic activity of the tumour. Schoder *et al.* and Wood *et al.* have demonstrated much clinical promise for  $^{18}\text{F}$ -FDG in many cancers including breast, lung, head and neck and non-Hodgkins lymphoma, see Figure 29.<sup>25, 96</sup>

$^{18}\text{F}$ -FDG PET scans have shown many advantages over standard CT scans. They can distinguish malignant from benign tumours with a sensitivity of 80-100% and detect distant metastases not picked up on a CT scan.<sup>15</sup> This level of information could influence the operability of a patient and future therapy.  $^{18}\text{F}$ -FDG can not only be used as a radiotracer for imaging it can also be used to assess whether treatment is working. Chemotherapy is very toxic and patients can sometimes undergo courses with little overall benefit. Avril and Weber have linked a reduction in FDG uptake after the first course of chemotherapy to an overall benefit whilst those not showing a reduction tended not to benefit from further courses of chemotherapy.<sup>98</sup>

The main limitation of using  $^{18}\text{F}$ -FDG as a radiotracer is that it has limited use for slowly growing tumours with low glucose levels because little distinction can be made between healthy tissue and tumours.  $^{18}\text{F}$ -FDG also accumulates in areas such as the kidneys and bowel which may make distinguishing tumours close to these sites difficult and is not specifically targeting the tumour, relying on metabolic differences for accumulation at the tumour site.



*Figure 29:  $^{18}\text{F}$ -FDG PET image of a patient with non-Hodgkins lymphoma before and after chemotherapy. Scan A shows disease sites in the left neck, mediastinum, lungs and lymph nodes in the upper abdomen. Scan B shows complete resolution of the disease after chemotherapy. (Reproduced from Cancer Metast. Rev.)<sup>25</sup>*

$^{18}\text{F}$ -FDG demonstrates the utility and effectiveness of PET as an imaging tool. The limitations and efficacy of current radiopharmaceuticals may lie in their intrinsic design and efforts are needed to design more targeted radiopharmaceuticals. This includes both the targeting ligand as well as the properties of the radiolabelled material. As Glasspool *et al.* noted 'the efficacy of any imaging agent depends on its specificity for the target tumour.'<sup>15</sup>

## 1.6. The advantages of $^{64}\text{Cu}$ as a radiopharmaceutical

A prerequisite to performing PET studies is the availability of a suitable radiopharmaceutical.<sup>99</sup> Traditional positron emitting radioisotopes include  $^{15}\text{O}$ ,  $^{11}\text{C}$ ,  $^{13}\text{N}$ , and  $^{18}\text{F}$  all of which are very useful because many biological molecules contain such elements or they can be easily incorporated into biological molecules in the case of  $^{18}\text{F}$ .

Radionuclide	Half life	Production	$\beta$ max (keV) maximum, range in water (mm)	Chemistry
$^{15}\text{O}$	2.03 min	Cyclotron	1732 keV, 8.0 mm	Fast on-line gas phase chemistry
$^{13}\text{N}$	9.97 min	Cyclotron	1198 keV, 5.1 mm	Fast organic chemistry
$^{11}\text{C}$	20 min	Cyclotron	960 keV, 3.9 mm	Fast organic chemistry
$^{68}\text{Ga}$	68 min	Generator	1899 keV, 8.9 mm	Chelation chemistry
$^{18}\text{F}$	109.8 min	Cyclotron	634 keV, 2.3 mm	Fast organic chemistry
$^{64}\text{Cu}$	12.7 hours	Cyclotron	653 keV, 2.4 mm	Chelation chemistry
$^{89}\text{Zr}$	78.4 hours	Cyclotron	897 keV, 3.6 mm	Chelation chemistry
$^{124}\text{I}$	4.17 days	Cyclotron	1535 keV (50%), 6.9 mm, 2138 keV (50%), 10.2 mm	Organic chemistry

Table 1: Frequently used radionuclides, their production method, positron energy and type of radiolabelling chemistry. (Adapted from Methods.)<sup>20</sup>

Therefore these radioisotopes can simply replace a naturally occurring element without changing the overall function or structure of that biologically important molecule. The disadvantage of these isotopes is that they have short half-lives, see Table 1, placing limits on their use.

PET radiotracers with longer lived half-lives are particularly attractive because they allow the study of longer lived processes within the body and do not limit PET facilities to such an extent.<sup>100</sup> A cyclotron is still required but PET facilities do not have to be situated as close allowing PET imaging to be carried out at more centres.

<sup>64</sup>Cu has particularly favourable properties for use as a radionuclide including its half-life, decay characteristics ( $\beta^+$  and  $\beta^-$ ), ability for large scale production and high specific activity.<sup>70</sup> The most common production method for <sup>64</sup>Cu utilises the <sup>64</sup>Ni(p,n)<sup>64</sup>Cu reaction using a biomedical cyclotron<sup>101</sup> but there are other reported methods in the literature.<sup>102, 103</sup> The <sup>64</sup>Ni(p,n)<sup>64</sup>Cu reaction is high yielding with reports of >1 Ci of radioactivity in three hours.<sup>101</sup> A typical dosage of 2-20 mCi would be required for a human PET scan.<sup>19</sup>

In order to be useful as a diagnostic imaging agent <sup>64</sup>Cu must be delivered as a stable complex which will not only achieve high uptake of the copper ion with little transmetallation *in vivo* but also specifically target the diseased tissue either due to its design or by conjugation to a targeting moiety.<sup>99, 103</sup>

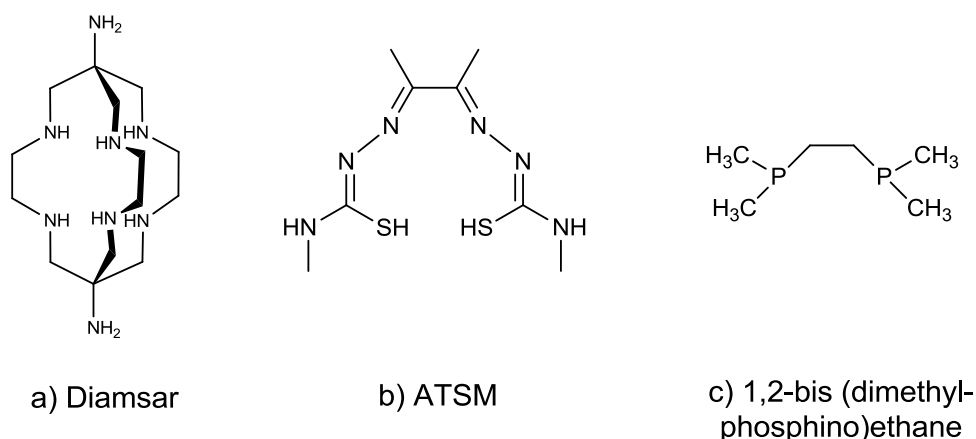


Figure 30: Examples of a) a sarcophagine, b) a bis-thiosemicarbazone and c) a diphosphine ligand.

Copper(II) has a well-established coordination chemistry making it ideal for chelation to a wide range of chelators and BFC.<sup>103</sup> Copper(II) complexes tend to be thermodynamically stable but kinetically labile. To overcome this lability the kinetics of dissociation need to be slowed down.<sup>104</sup> This can be achieved by synthesising rigid chelators prompting significant research efforts into development of stable <sup>64</sup>Cu chelators.

Several classes of chelators have been synthesised including sarcophagines,<sup>105</sup> diphosphine ligands<sup>103</sup> and bis-thiosemicarbazone ligands,<sup>106</sup> see Figure 30, but the most extensively studied class of chelators are based on cyclam and cyclen backbones due to their affinity not only for small metal ions but also for the CXCR4 receptor.

#### **1.6.1. Chelators based on cyclam and cyclen backbones**

Cyclam and cyclen based macrocycles form complexes of high kinetic and thermodynamic stability with metal ions.<sup>53</sup> This knowledge plus the well-established coordination chemistry of copper(II) has led to the development of many macrocyclic chelator ligands. Two particularly successful compounds are 1,4,8,11-tetraazacyclotetradecane-1,4,8,11-tetraacetic acid (TETA) and 1,4,7,10-tetraazacyclododecane-1,4,7,10-tetraacetic acid (DOTA), see Figure 31. The pendant carboxylic acid groups increase complex stability by forming six-coordinate copper(II) complexes; four from nitrogen donors and two from the pendant arms.<sup>53</sup> Anderson and co-workers demonstrated that <sup>64</sup>Cu-TETA conjugated to an anti-colorectal monoclonal antibody (mAb) fragment showed superior tumour uptake when compared to <sup>111</sup>In and <sup>124</sup>I conjugated to the same mAb fragments.<sup>107</sup> They also established that <sup>64</sup>Cu-DOTA conjugated to a CEA mAb fragment showed selective uptake in CEA positive tumours.<sup>108</sup> However, <sup>64</sup>Cu-DOTA was shown to be relatively unstable *in vivo* when compared to <sup>64</sup>Cu-TETA, limiting its use and even <sup>64</sup>Cu-TETA was shown not to be optimal as a BFC. Despite initial success with such ligands, Anderson and co-workers demonstrated the dissociation of <sup>64</sup>Cu from <sup>64</sup>Cu-TETA-Octreotide (a targeted probe) and subsequent binding to superoxide dismutase (SOD) in the liver.<sup>109</sup>

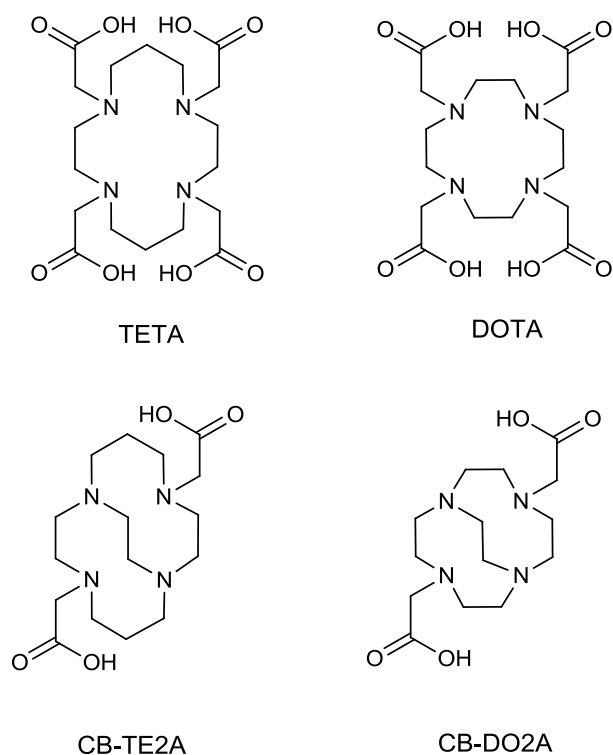


Figure 31: Structures of macrocyclic  $^{64}\text{Cu}$  chelators.

This led to the design of rigidified chelators and several new ligand systems including CB-TE2A and CB-DO2A, see Figure 31. These ligands have displayed high kinetic inertness *in vivo* and this is thought to be due to the locked *cis-V* configuration displayed by the CB compounds being an ideal geometry for copper(II).<sup>103</sup> The CB structure also completely encapsulates the copper ion reducing the potential for metal loss.<sup>110</sup> CB-TE2A has shown remarkable resistance to transmetallation and suggests the ligand may have a promising role as a BFC.

Recently two papers have been published using a radiolabelled CXCR4 antagonist  $^{64}\text{Cu}$ -AMD3100 to target CXCR4 expressing tumours.<sup>111, 112</sup> Nimmagadda and co-workers were the first to publish *in vivo* work and their results demonstrated that  $^{64}\text{Cu}$ -AMD3100 could be used as a non-invasive method for detecting metastatic spread and the metastatic potential of a lesion, see Figure 32.<sup>111</sup>

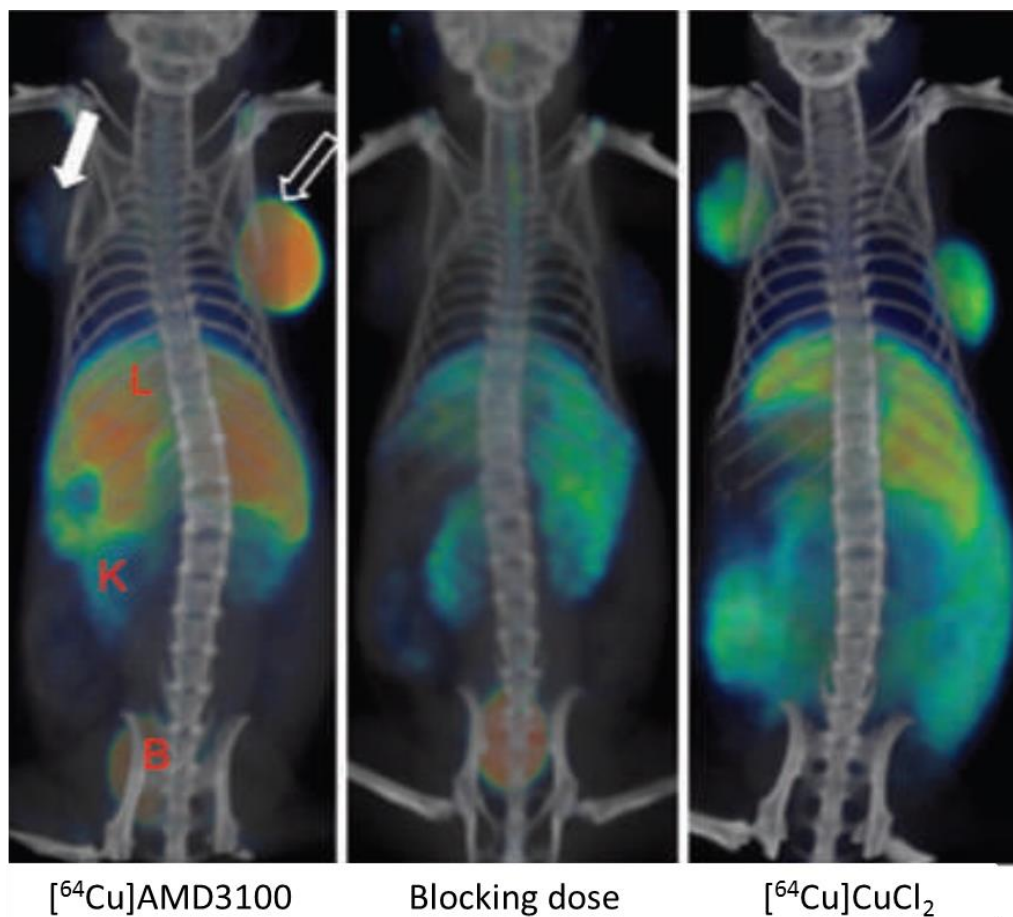


Figure 32: Whole body images of  $^{64}\text{Cu}$ -AMD3100 (left), 50 mg/kg of AMD3100 blocking dose followed by  $^{64}\text{Cu}$ -AMD3100 (middle), and  $[^{64}\text{Cu}]\text{CuCl}_2$  alone (right). All images were scaled to the same maximum threshold value. L = Liver, K= Kidney, B = Bladder. (Reproduced from *Cancer Res.*)<sup>111</sup>

Their results using breast xenograft and experimental metastatic models showed specific accumulation in lesions signifying that  $^{64}\text{Cu}$ -AMD3100 could feasibly be used to image graded levels of CXCR4 expression. The limitation of this work is that introduction of copper(II) actually reduces the affinity of AMD3100 for CXCR4 by 7-fold. This limitation could be overcome by using a more suitable macrocyclic chelator. There is significant potential to use macrocyclic ligands as targeted  $^{64}\text{Cu}$  chelators but there is also a need for further research into structurally rigidified BFC for use in targeted molecular imaging.

## 1.7. Research aims

The aim of this work is to synthesise and validate tetraazamacrocyclic compounds as CXCR4 antagonists and demonstrate their potential for attachment to biologically active groups such as porphyrins thus allowing the potential for targeted PDT to be evaluated. Methods for conjugation of such groups need to be devised and may require the use of a spacer arm to prevent unwanted interactions occurring since previous research within our group noted that when a rhodamine dye was conjugated directly to the CXCR4 antagonist, false positive results were observed *in vitro* due to the non-specific uptake of the dye by cancer cells.<sup>63</sup>

Novel tetraazamacrocyclic compounds will be synthesised whose design will be optimised to target the CXCR4 receptor and allow for further conjugation. The aim is to influence the current library of known CXCR4 antagonists by providing a novel high affinity antagonist with improved biological activity. Macrocyclic compounds can also be labelled with <sup>64</sup>Cu; a positron emitting radioisotope making the macrocycle a BFC possessing both targeting and diagnostic properties. Known photodynamically active porphyrins will be synthesised and their conjugation to macrocyclic antagonists evaluated.

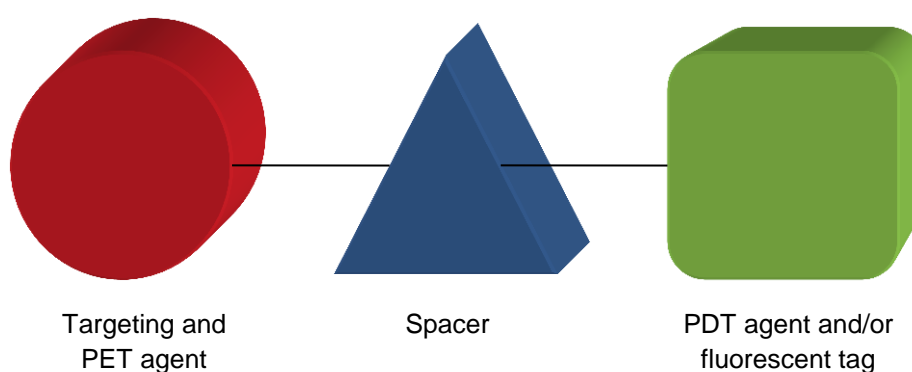


*Figure 33: Schematic representing the key components of a proposed MFC with diagnostic and therapeutic properties.*

Conjugation of tetraazamacrocyclic compounds and porphyrins would produce novel MFCs with the potential for targeted diagnosis and therapy of CXCR4 expressing tumours, see Figure 33.

## **1.8. Summary**

There are a number of advantages and a wide scope for MFCs incorporating macrocycles and porphyrins in the development of targeted diagnostic and therapeutic MFCs. In chapter 2 the synthesis of novel mono- and bismacrocycles is discussed along with their copper(II), zinc(II) and nickel(II) complexes. Chapter 3 details the conjugation of various linker groups to a novel CB biscyclen ligand. Chapter 4 provides an evaluation of the macrocyclic ligands discussed in the previous two chapters as CXCR4 antagonists. A detailed biological evaluation of a novel copper(II) containing CB biscyclen ligand is also presented. Chapter 5 outlines the synthesis of several known porphyrin compounds and details synthetic steps taken towards the formation of novel MFCs, *via* conjugation of novel macrocyclic compounds.

## **Chapter 2**

# **Synthesis of novel saturated tetraazamacrocycles and their metal complexes**

## 2.1. Synthetic strategy

The synthesis of novel macrocyclic compounds whose structure is optimised to obtain high binding affinity at the CXCR4 receptor was explored. Optimisation included restricting the configuration of the macrocycles by introducing an ethylene bridge to produce cross bridged (CB) and side bridged (SB) compounds and also complexation with transition metal ions; copper(II), nickel(II) and zinc(II).

## 2.2. Past strategies

Macrocyclic ligands play important roles in biological systems, they are easily derivatised and form stable complexes with metal ions, such factors have initiated a broad spectrum of research activities and their applications range from industry to medicine to biomedical imaging.

Cyclam; a fourteen-membered,  $N_4$ -donor macrocyclic ring and its smaller counterpart cyclen; a twelve-membered,  $N_4$ -donor macrocyclic ring have been utilised in drug design. Their carbon skeletons are rigid enough to provide strong metal binding sites and orient functional groups stereoselectively but they are flexible enough to accommodate the structural changes needed to interact with biological targets.<sup>113</sup>

Macrocyclic ligands can be functionalised through carbon or nitrogen atoms; this coupled with the wide variety of pendant arms available has led to a huge array of related but structurally different macrocyclic ligands. The addition of a pendant arm to a macrocyclic skeleton has a number of advantages. They can increase the number of donor atoms for coordination to a metal centre. In this respect pendant arms can facilitate complexation reactions, guiding the metal ion into the macrocyclic cavity. Addition of a pendant arm can also provide additional functionality to the compound for conjugation to other molecules of interest. They can also increase the stability of the overall compound. These advantages are an important aspect of macrocyclic design and the following sections give selected examples from the last twenty years of monomacrocyclic ligands with either C-functionalised or N-functionalised skeletons.

### 2.2.1. C-functionalised monomacrocycles

An early example of C-functionalised monomacrocycles was reported by Parker and co-workers who prepared macrocycles of varying ring size bearing exocyclic amino groups ( $L^1$ - $L^4$ ), see Figure 34; chosen to allow formation of an amide bond between the macrocyclic ligand and a modified protein designed to bind to a specific glycoprotein (TAP-72) target, overexpressed in colon tumours.<sup>114</sup>

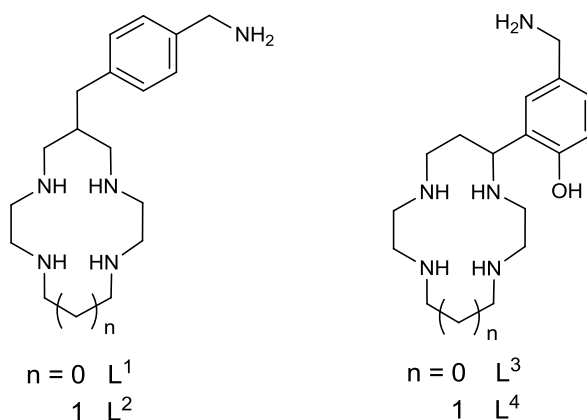


Figure 34: Structures of C-functionalised aminomethyl bearing monomacrocycles  $L^1$ - $L^4$  as reported by Parker and co-workers.<sup>114</sup>

In 2004, Archibald and co-workers noted that much of the research effort surrounding cyclam and its analogues bore N-functionalisations and as such there was a need to produce a versatile and efficient method for C-functionalised derivatives. They presented the novel synthesis for the attachment of 4-nitrobenzyl in the 6-C position utilising bisaminal intermediates as structural templates.<sup>115</sup> Despite a lengthy procedure the final C-functionalised macrocycles bearing either one benzyl arm;  $L^5$  or two benzyl arms;  $L^6$  were produced in reasonable yield, see Figure 35. The group went on to publish the efficient synthesis of a structurally reinforced C-functionalised cyclam compound;  $L^7$ , see Figure 35.<sup>116</sup> This BFC is a derivative of the clinically applicable TETA ligand and its analogue CB-TE2A, see Figure 35. The authors detailed a seven step synthesis to produce a CB ligand with two acid arms bearing an exocyclic isothiocyanate group,  $L^7$ , in an overall yield of 20%. This is the first BFC of CB-TE2A that retains both the acid groups.

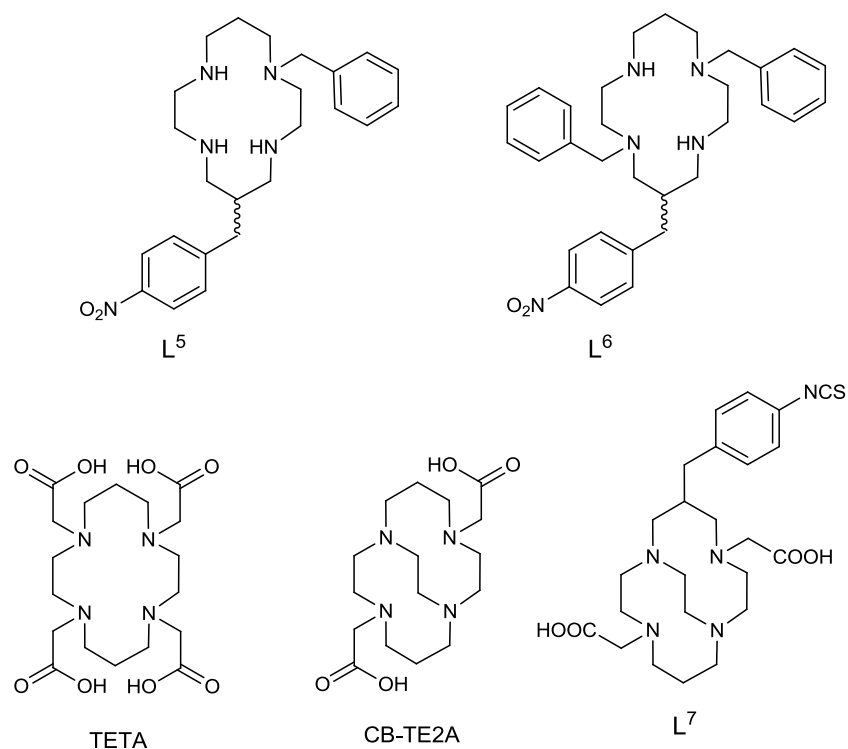


Figure 35: C-functionalised ligands L<sup>5</sup>-L<sup>7</sup> as outlined by Archibald and co-workers and the structures of TETA and CB-TE2A.<sup>115, 116</sup>

In 2004, Liang and Sadler reviewed the topic of cyclam complexes and their applications in medicine<sup>62</sup> and noted that C-functionalised dioxocyclam ligands; L<sup>8</sup>-L<sup>11</sup> were receiving considerable attention from several research groups,<sup>117-119</sup> see Figure 36. These compounds are able to bind metal ions with subsequent loss of two amide protons making metal binding highly pH sensitive.

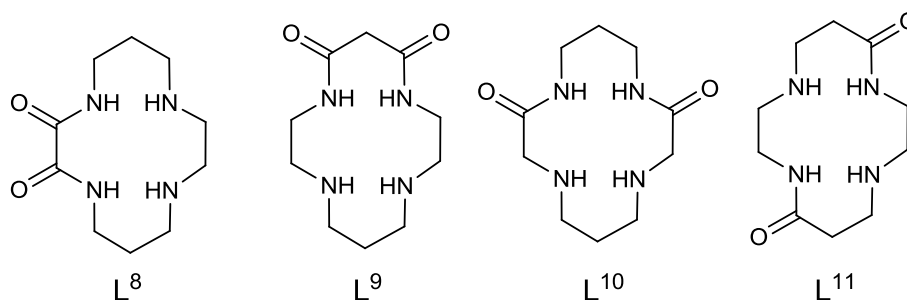


Figure 36: Structures of dioxocyclam ligands; L<sup>8</sup>-L<sup>11</sup>.<sup>62</sup>

Recently Rousselin *et al.* outlined the synthesis of C-functionalised azamacrocycles where the aminomethyl group was introduced onto the macrocyclic backbone

during a cyclisation step, see Figure 37, thus circumventing the need to prepare a C-functionalised synthon, producing  $L^{12}$  in 39% and  $L^{13}$  in 42% yield.<sup>120</sup>

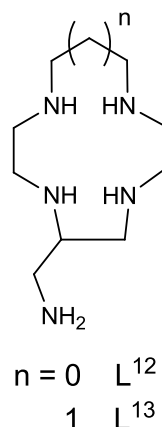


Figure 37: Structures of aminomethyl C-functionalised macrocycles;  $L^{12}$  and  $L^{13}$  as outlined by Rousselin et al.<sup>120</sup>

### 2.2.2. N-functionalised monomacrocycles

As mentioned much of the research effort into functionalised macrocycles involve N-functionalisations, some examples of structurally rigidified monomacrocycles bearing a functional pendant arm have been selected for discussion.

#### 2.2.2.1. SB monomacrocycles bearing functional pendant arms

Wainwright and Hancock were the first group to take steps to rigidify the carbon skeleton of azamacrocycles,<sup>64, 65, 121</sup> publishing the structural reinforcement of cyclen using 1,2-dibromoethene ( $L^{14}$ ) in 1982,<sup>122</sup> see Figure 38. Addition of an ethylene bridge between adjacent nitrogen atoms forms a piperazine ring which of the four conformations it can adopt (chair, boat, twist and half-boat) is most stable in the chair conformation. When dealing with SB cyclam derivatives the configurations of subsequent metal complexes are restricted to either *trans*-II (monosubstituted species) or *trans*-IV (disubstituted species).

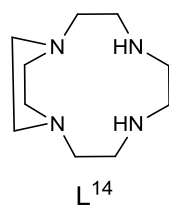


Figure 38: Structure of a SB macrocycle published by Wainwright (L<sup>14</sup>).<sup>122</sup>

Archibald and co-workers have been at the forefront of this research, synthesising three SB ligands with functional pendant arms. A nitrophenyl SB monocyclam ligand; L<sup>15</sup> was published along with an aminophenyl derivative; L<sup>16</sup>, see Figure 39.<sup>123</sup> A carboxylic acid functionalised ligand termed HSBTE1A was also published in the same year,<sup>53</sup> see Figure 39.

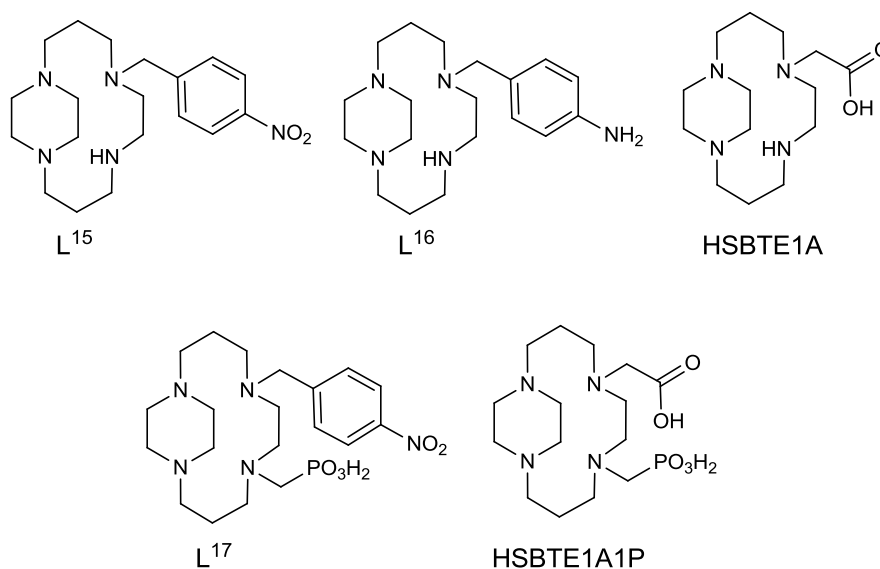


Figure 39: SB monocyclam ligands bearing functional pendant arms; L<sup>15</sup>, L<sup>16</sup>, HSBTE1A, L<sup>17</sup> and HSBTE1A1P.<sup>53, 123</sup>

Plutnar *et al.* utilised the chemistry outlined by Archibald to synthesise an unsymmetrically substituted SB ligand bearing a nitrophenyl and a phosphonate pendant arm; L<sup>17</sup>, hoping that this mixed arm species would improve complexation parameters.<sup>52</sup> A mixed arm species was also synthesised by Boswell *et al.*, who attached a phosphate arm to Archibald's HSBTE1A ligand, using a classical Kabachnik-Fields reaction to introduce the phosphonate arm, to produce HSBTE1A1P, see Figure 39, in 72% overall yield.<sup>70</sup>

### 2.2.2.2. CB monomacrocycles bearing functional pendant arms

Weisman and Wong were the first group to publish the synthesis of a CB cyclam compound ( $L^{18}$ ),<sup>66</sup> with Bencini publishing the analogous CB cyclen compound ( $L^{19}$ ) a few years later<sup>124</sup>, see Figure 40. Attachment of an ethylene bridge between opposite nitrogen atoms forces the ensuing macrocycle into a ‘clamshell’ structure and restricts the configuration of subsequent metal complexes to *cis-V*.

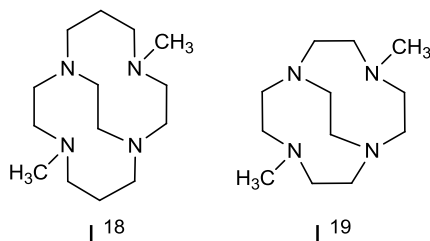


Figure 40: Structures of rigidified macrocycles published by Weisman ( $L^{18}$ ) and Bencini ( $L^{19}$ ).<sup>66, 124</sup>

There are several articles detailing the advantages of incorporating a CB into the macrocyclic framework, with Busch terming them ‘ultra rigid’ ligands<sup>125</sup> but relatively few CB compounds have been published with functional pendant arms since Wong and co-workers detailed the synthesis of CB-TE2A in 2000, along with two other CB derivatives with functional arms; a diester ( $L^{20}$ ) and a diamide ( $L^{21}$ ),<sup>126</sup> see Figure 41. An analogous CB cyclen derivative of CB-TE2A; CB-DO2A was also synthesised by Wong and co-workers,<sup>126</sup> see Figure 41. The *in vivo* stability of the <sup>64</sup>Cu complexes of CB-TE2A and CB-DO2A has been evaluated by Boswell *et al.* and found to have a higher stability constant than <sup>64</sup>Cu-TETA and <sup>64</sup>Cu-DOTA.<sup>110</sup> Wong and co-workers went on to synthesise copper(II) and zinc(II) complexes of the diamide  $L^{21}$ , along with its analogous cyclen derivative  $L^{22}$ .<sup>127</sup>

In 2007, Weisman and Wong evaluated how pendant arm length would influence kinetic inertness and resistance to reduction of subsequent copper(II) complexes,<sup>128</sup> synthesising two new CB ligands bearing propylacetate pendant arms ( $L^{23}$  and  $L^{24}$ ). Despite comparable acid inertness to CB-TE2A and CB-DO2A, the authors concluded that  $L^{23}$  and  $L^{24}$  showed poorer clearance properties *in vivo*, behaviour thought to be

a consequence of their higher reduction potentials. Recently, this same group have published the synthesis of a mixed arm species, a phosphonate/acetate species;  $L^{25}$ .<sup>129</sup> The phosphonate arm was shown to improve radio-labelling conditions while the carboxy arm provides a scaffold to facilitate further bioconjugation.

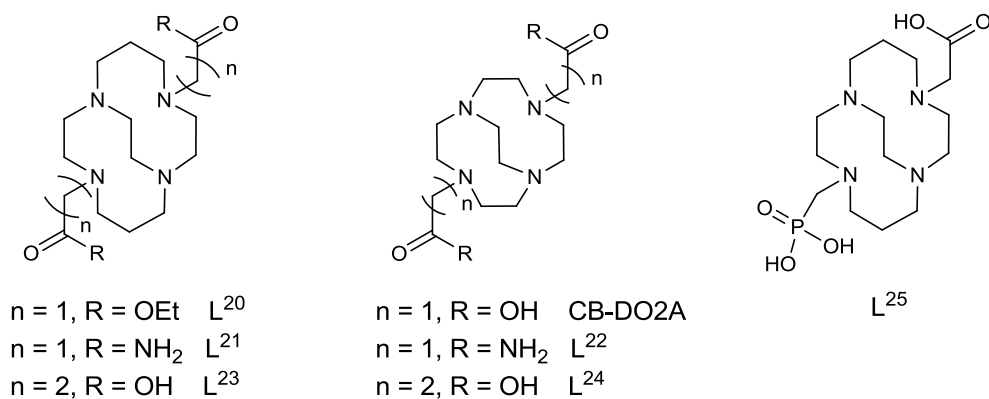


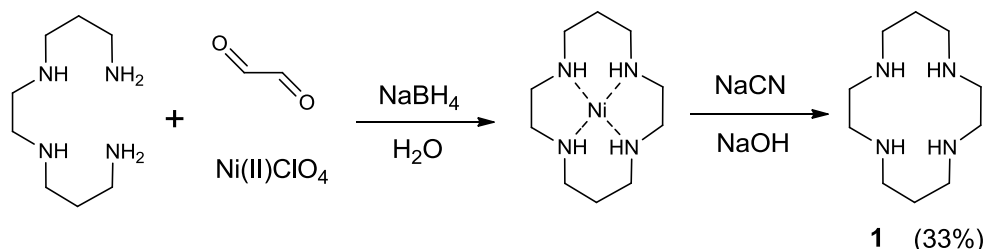
Figure 41: Structures of CB monomacrocycles bearing functional pendant arms; CB-DO2A and  $L^{20}$ - $L^{25}$ , synthesised by Weisman, Wong and co-workers.<sup>128, 129</sup>

### 2.3. Synthesis of monomacrocyclic ligands

Mono-ring azamacrocyclic compounds offer some useful properties as CXCR4 antagonists. Despite often not being as effective inhibitors as their multi-ring counterparts they are much simpler to synthesise. Azamacrocycles are not generally orally bioavailable but the monomacrocycles, with their lower molecular weight and decreased molecular charge in comparison to multi-ring macrocycles have the potential to show improved pharmacological properties such as biodistribution and clearance.

In order to produce configurationally restricted macrocycles, precursors had to be synthesised. These precursors provide the macrocyclic skeleton to which modifications can be made. 1,4,8,11-Tetraazacyclotetradecane (cyclam) (**1**) was prepared following the Barefield method<sup>130</sup> with some modifications. 1,5,8,12-Tetraazadodecane; an acyclic tetraamine was reacted with a molar equivalent of glyoxal and nickel(II) perchlorate in the presence of an excess of sodium borohydride to produce a closed nickel(II) containing macrocycle, the nickel(II) ion was then removed from the cavity with sodium cyanide, see Scheme 1.  $^1\text{H}$  NMR

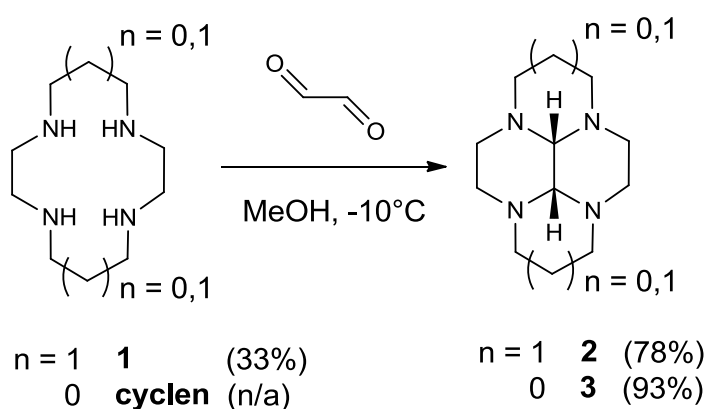
gave peaks equivalent to twenty four protons and the splitting patterns were consistent with literature data. CHN analysis confirmed the purity of compound **1**.



*Scheme 1: The synthetic pathway to produce cyclam (1).*

Cyclam has been shown to interact with the CXCR4 chemokine receptor but evidence suggests that it is not sufficiently rigid to provide specific, stable interactions. Cyclam can be bridged with glyoxal to produce the bisaminal macrocycle **2**, which can then be functionalised and derivatised to produce structurally rigidified macrocycles.

Synthesis of bridged cyclam (**2**) and bridged cyclen (**3**) was adapted from a method proposed by Handel and Le Baccon,<sup>131</sup> see Scheme 2. The reaction is temperature dependent and the reaction mixture must be kept below  $-10^{\circ}\text{C}$  over the period of time that the glyoxal is added to prevent polymerisation. The product is extracted into diethyl ether to separate it from any polymeric material formed.



*Scheme 2: Synthetic route to obtain bridged cyclam (2) and bridged cyclen (3).*

Analysis by  $^1\text{H}$  NMR spectroscopy of bridged cyclam (**2**) confirmed that there was no polymerisation of the product and showed peaks equivalent to twenty two protons, with the expected splitting patterns. An identical reaction was performed to synthesise bridged cyclen (**3**), see Scheme 2. NMR data confirmed a pure compound was obtained. Both compounds were synthesised in good yields (>60%) providing two precursors from which a range of configurationally restricted macrocycles can be synthesised.

Rigidifying the carbon skeleton allows for control of the reactivity of the amine groups this is because addition of the glyoxal bridge forces the resulting macrocycle into a *cis* configuration, see Figure 42. This configuration results in two *exo* lone pairs (which point out of the structure) and two *endo* lone pairs (which point into the structure) on the nitrogen atoms. The *exo* lone pairs are the only ones available for reaction and so only two of the nitrogen positions can be substituted.

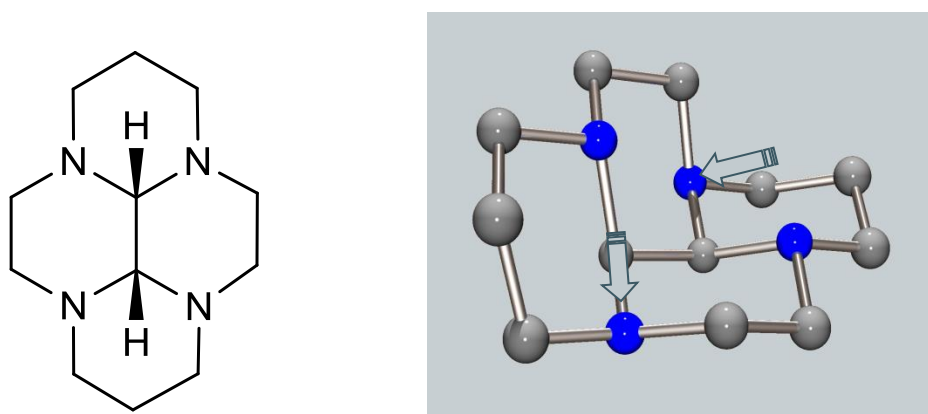
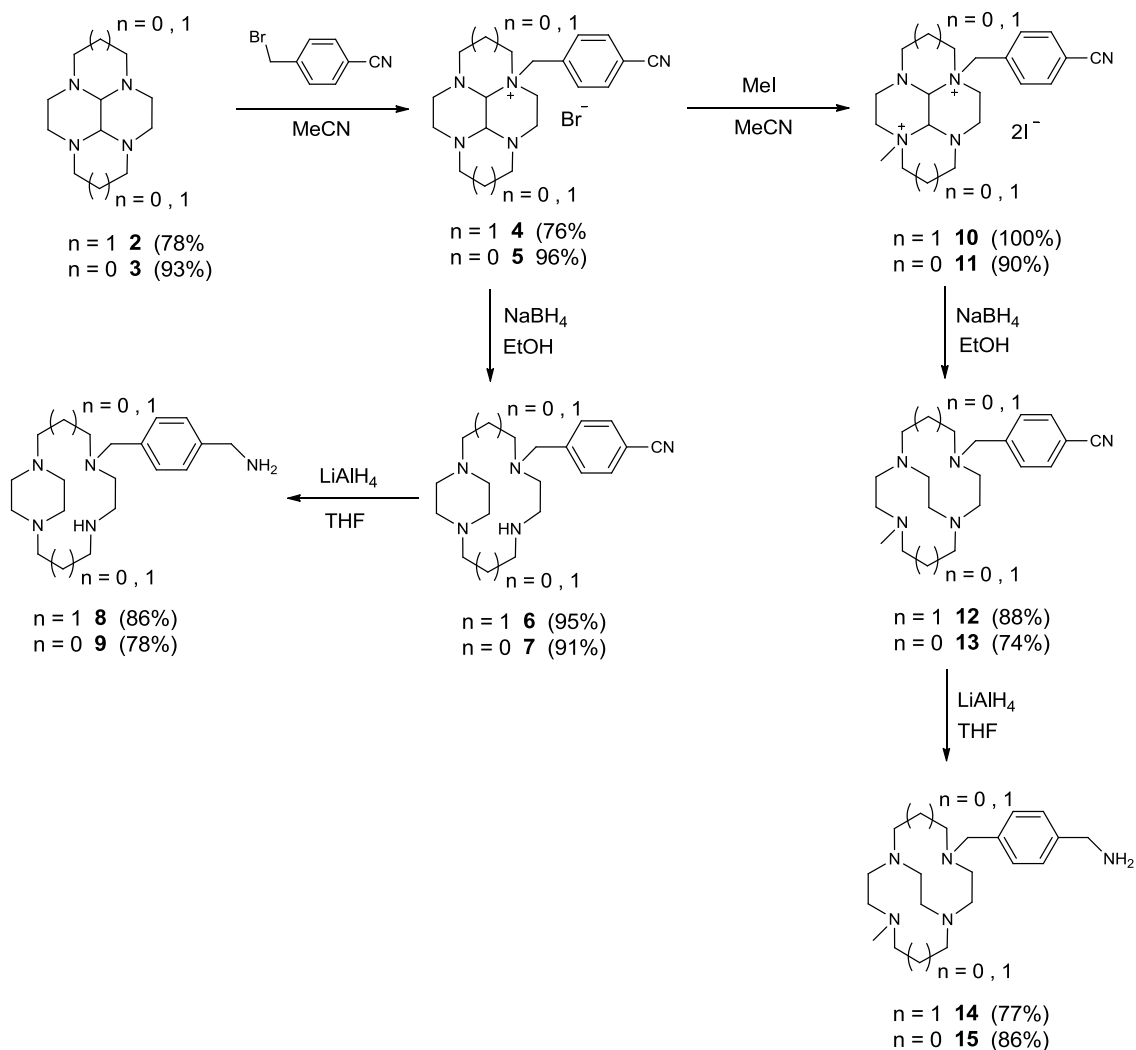


Figure 42: Molecular structure of bridged cyclam showing a *cis* configuration (left). Ball and stick representation, indicating the presence of two *exo* and two *endo* lone pairs (right). Grey = carbon atoms, blue = nitrogen atoms.  
Note hydrogen atoms have been omitted for clarity.

### 2.3.1. Configurationally restricted monomacrocycles

Rigidifying the cyclam skeleton to produce either CB or SB compounds has received considerable attention from several research groups,<sup>52, 53, 66, 132</sup> not just because they are relatively easy to synthesise but also that they have the potential for improved pharmacological properties due to their low molecular weight and

decreased molecular charge in comparison to their bismacrocylic counterparts. Bridged cyclam (**2**) and bridged cyclen (**3**) were used to synthesise analogous mono-ring SB and CB compounds, see Scheme 3. Addition of a pendant arm, methylation and reduction of the macrocyclic ligands were performed following established literature preparations.<sup>66, 133, 134</sup>



*Scheme 3: Synthetic route to produce a range of structurally related CB and SB cyclam and cyclen compounds.*

Previous work within our group included the synthesis of a number of mono-ring structures with an aniline pendant group, see L<sup>16,123</sup>. However, having the primary amine directly attached to the aromatic ring created problems in subsequent reactions that were attributed to the nitrogen lone pair being delocalised into the

aromatic ring reducing its reactivity. A pendant arm with a cyano group in the *para*-position can be reduced to a methylamine group and this extra carbon between the benzyl and primary amine will prevent any delocalisation. 4-(Bromomethyl) benzonitrile was used as a pendant arm and subsequently reduced to an (aminomethyl)phenyl group.

All compounds were produced in good yields and fully characterised. Compounds **4** and **5** gave clean NMR spectra and CHN analysis confirmed the purity of these compounds. Sodium borohydride reduction did introduce a slight impurity (<10%) into compounds **6**, **7**, **12** and **13** but  $^{13}\text{C}$  NMR data confirmed a successful reaction due to the disappearance of the aminal peaks. Subsequent reduction of the cyano group to give compounds **8**, **9**, **14** and **15** required method development, see section 2.3.2., before the compounds were successfully isolated. SB cyclam **8** and SB cyclen **9** were synthesised in 86% and 78% yields, respectively from their cyano derivatives and CB cyclam **14** and CB cyclen **15** were synthesised in 77% and 86% yields respectively from their cyano derivatives, using  $\text{LiAlH}_4$  as a reducing agent.

### 2.3.2. Reduction methods

The literature offers a wealth of methods for reduction of cyano groups. Methods for using borane-tetrahydrofuran (borane-THF) complex<sup>114, 135</sup> and Raney nickel<sup>136</sup> were attempted first due to their availability in the lab. The borane-THF complex in THF (1 M) solution was used in an attempt to reduce compound **8**. Analysis of  $^{13}\text{C}$  NMR spectroscopic data showed that the cyano peak was still present and the  $^1\text{H}$  NMR spectrum only showed peaks equivalent to thirty one protons, indicating that the reduction had not occurred. Raney nickel was used to reduce a portion of compound **9**.  $^{13}\text{C}$  NMR showed a successful reduction had occurred due to the disappearance of the cyano peak but also the presence of impurities, a low yield was also obtained (45%).

Since these reagents seemed not to be giving the desired product in high yield,  $\text{LiAlH}_4$  was employed. Following a literature method<sup>137</sup> initial attempts to reduce SB compounds **8** and **9** with  $\text{LiAlH}_4$  were successful but produced low yields. This arose

because a sticky precipitate formed on decomposition of the excess  $\text{LiAlH}_4$  with ammonium chloride. Attempts to dry out the precipitate or wash out the product with different solvents proved futile and subsequently a maximum yield of 50% was achieved.  $^{13}\text{C}$  NMR and mass spectrometry (MS) data of **8** and **9** confirmed that the products had formed due to the disappearance of the cyano peak leaving just four aromatic carbons and mass ions of 346 and 318, respectively. An improvement was required for the method used to decompose the excess  $\text{LiAlH}_4$ . Water and sodium hydroxide were used to decompose the excess  $\text{LiAlH}_4$  in amounts dictated by the amount of starting material, as described in Procter's Advanced Practical Organic Chemistry.<sup>138</sup> This produced a granular precipitate which subsequently improved yields (>75%). Analytical data supported the conclusion that these high yielding reductions had been successful, although some minor impurities were noted in the NMR spectra (< 10%). These methylamine bearing pendant arms permit the formation of stable amide bonds or easy conversion to other functionalities such as isothiocyanates.

### **2.3.3. Novel metal-containing monomacrocycles**

Tetraazamacrocycles are ideally set up to complex metal ions, in particular transition metal ions with a 2+ charge. The chemistry in sections 2.3.1-2.3.3., describes a novel series of configurationally restricted monomacrocyclic compounds, complex formation with various metal ions produced a novel series of metal containing monomacrocycles.

Copper(II), nickel(II) and zinc(II) were the transition metal ions of choice since previous studies have shown improved binding affinities for CXCR4 when macrocycles have been complexed with these metals (*ca.* AMD3100, section 1.3.). Copper can adopt various oxidation states and coordination geometries. Its radioisotopes also make it a metal of interest since such compounds would be useful diagnostic probes. Nickel(II) also displays some interesting coordination properties. It can either form diamagnetic square planar complexes or expand its coordination sphere to octahedral through incorporation of additional donors. The concentration of zinc(II) ions in the blood is *ca.*  $19\ \mu\text{M}$ <sup>139</sup> which has been calculated

to be high enough that, at physiological pH, AMD3100 would exist as its zinc(II) complex;  $[\text{Zn}_2\text{AMD3100}]^{4+}$ , which shows a higher affinity for CXCR4 than the free ligand. Also zinc(II) does not undergo redox chemistry in biological systems due to its full shell of d-electrons.

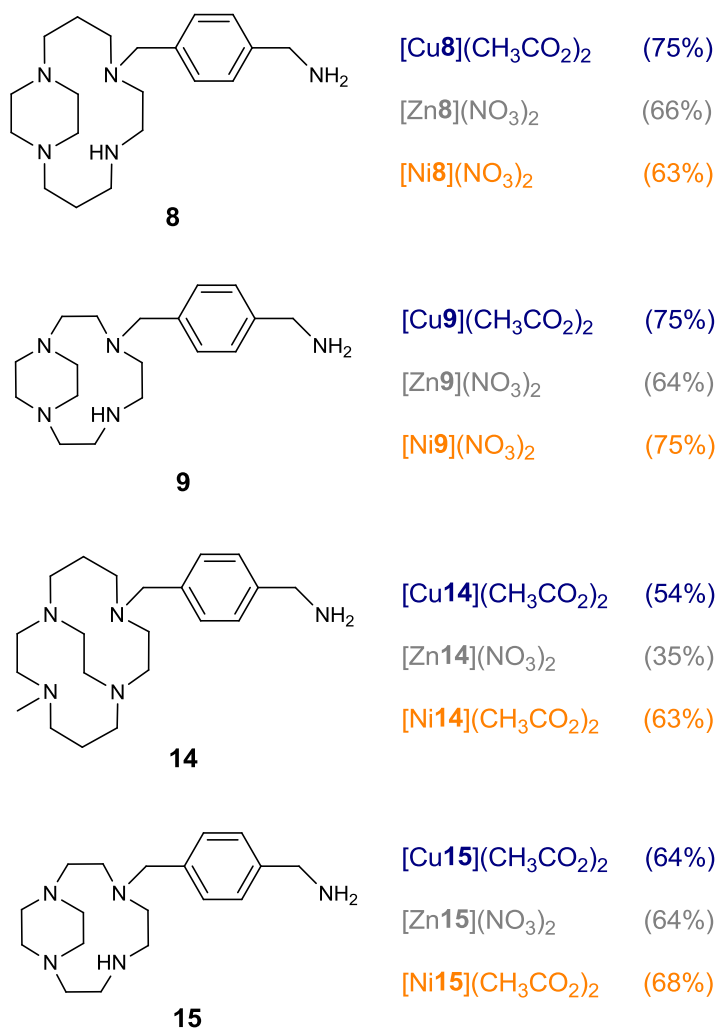


Figure 43: Representative structures of copper(II), zinc(II) and nickel(II) complexes of monomacrocyclic ligands **8**, **9**, **14** and **15**. Note in some cases anions and/or solvent molecules may coordinate to the metal centre.

Copper(II) acetate monohydrate, nickel(II) nitrate hexahydrate, nickel(II) acetate and zinc(II) nitrate hexahydrate were used to make a novel series of such compounds, see Figure 43. Standard preparations were followed for all the complexation reactions.<sup>58, 126</sup> All complexes were purified *via* size exclusion chromatography (sephadex LH20) which can give up to a 30% loss in product

resulting in a wide range of yields (35% – 92%). Complexes were characterised by MS, CHN analysis and where applicable UV-vis spectroscopy.

The choice of anion, acetate or nitrate, was used interchangeably depending on availability of metal salt. The anion has no effect on the subsequent affinity of the macrocycle for CXCR4 so it could be argued that the choice of anion does not matter. However, the properties of the anion do have an effect on solubility and toxicity. Hexafluorophosphate salts are less soluble in water than acetate, nitrate and halide salts. They also show a strong toxicological effect *in vivo*. A previous study in our group tested a metal containing macrocyclic compound with associated hexafluorophosphate anions in mice. This compound showed high toxicity that was attributed to the low solubility of the complex. However, the acetate, chloride and nitrate containing compounds have not shown any toxicological effects in our *in vivo* studies with macrocyclic compounds. Acetate ions are particularly useful in the formation of model compounds because they have the same structure as aspartate residues (the residues responsible for receptor binding).

It is much harder to insert a metal ion into a CB cavity rather than a SB cavity due to the decreased structural flexibility, as can be seen from the reaction conditions employed. Nickel(II) and zinc(II) CB complexes are more difficult to synthesise because protons abstracted from water or solvent molecules compete effectively with metal ions to be in the CB cavity. The same issue occurs for the copper(II) complexes but they are able to compete more effectively. However, appropriate reaction conditions were determined and CHN data for each of the twelve metal complexes described shows successful insertion of the metal ion into the cavity to form pure compounds, solvent molecules (water and methanol (MeOH)) were noted but crystallography data often shows that solvent molecules are incorporated in the unit cell.

## 2.4. Design and synthesis of novel high affinity bismacrocycles and their metal complexes.

### 2.4.1. Past strategies – bismacrocycles

The isolation of a biscyclam compound, see Figure 12 section 1.3., by the Johnson Matthey Technology centre in 1994 began the AMD3100 story.<sup>140</sup> In 1995, De Clercq and co-workers went on to synthesise a range of biscyclams and assess their activity against selected strains of HIV (HIV 1 (IIB) and HIV-2 (ROD)).<sup>141</sup> Ring size varied between 12 and 16 atoms and alkyl and aryl linkers in *meta*- and *para*-positions (L<sup>26</sup>-L<sup>31</sup>) were tested, see Figure 44 for selected structures. Their systematic variation to ascertain the structural features needed for potent activity concluded that 12-14 membered macrocycles joined by aryl rather than alkyl linkers showed higher potency. A similar study a year later looking into the activity of biscyclams linked by pyridine or pyrazine linkers found that 2,6- and 3,5-pyridine linked biscyclams were potent inhibitors of HIV-1 and HIV-2 but analogous 2,5- and 2,4-substituted biscyclams showed dramatically reduced activity.<sup>142</sup> This was attributed to the availability of the pyridine nitrogen to form coordinate bonds with the metal ions.

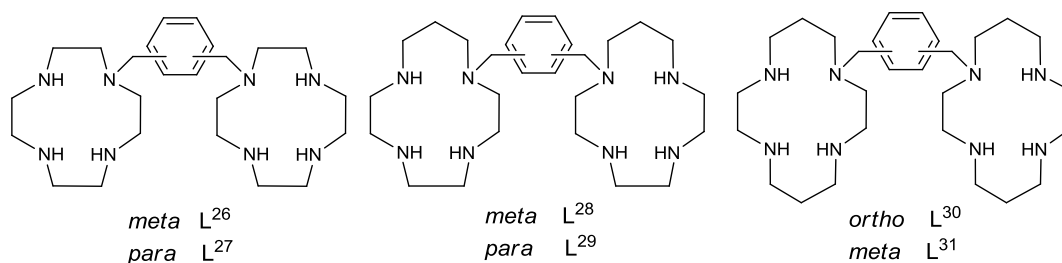


Figure 44: *ortho*-, *meta*- and *para*-substituted 12-14-membered azamacrocycles; L<sup>26</sup>-L<sup>31</sup> as outlined by De Clercq and co-workers.<sup>141</sup>

All of the biscyclams synthesised by De Clercq and co-workers were non-restricted in the sense that they did not contain any features of structural reinforcement; a factor known to facilitate the formation of stable metal complexes. Archibald and co-workers synthesised a xylyl linked SB biscyclam compound L<sup>32</sup>,<sup>58</sup> see Figure 45. They noted that its zinc(II) complex has only one configurational isomer and shows high activity against strains of HIV.

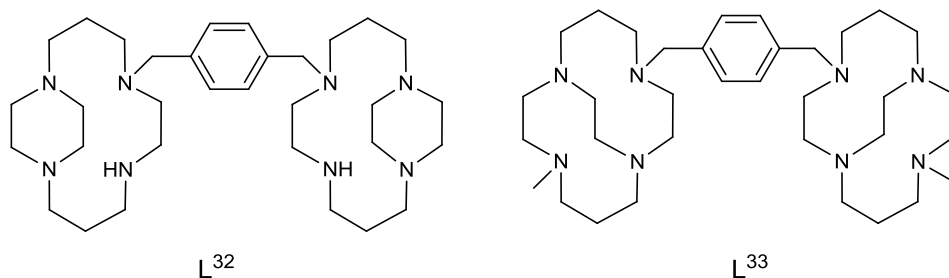


Figure 45: Structures of configurationally restricted biscyclams  $L^{32}$  and  $L^{33}$ .<sup>58, 63</sup>

This same group went on to synthesise an analogous CB biscyclam ligand;  $L^{33}$  and demonstrated that its copper(II) complex not only showed high affinity for the CXCR4 receptor in cellular assays, in comparison to AMD3100, but also an increased residence time at the receptor.<sup>63</sup> This observation was attributed to the ability of  $[\text{Cu}_2\text{L}^{33}]^{4+}$  to form coordination bonds with aspartate residues in the receptor binding pocket rather than the dominant H-bonding interactions for AMD3100.

Lindoy and co-workers synthesised novel biscyclams in a linear array bearing a nitro ( $L^{34}$ ) or an amino ( $L^{35}$ ) functional group, to radiolabel with  $^{64}\text{Cu}$ , see Figure 46, these novel compounds incorporated a reactive handle for subsequent conjugation to antibodies but did not possess any configurational restraint and the authors noted sluggish radiolabeling for some of their compounds.<sup>143</sup>

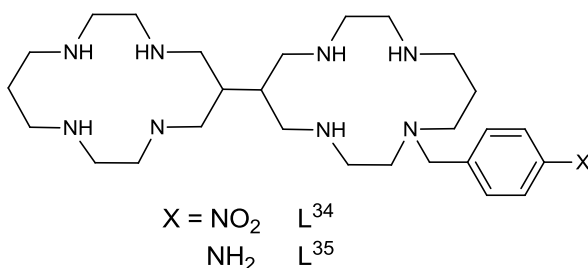
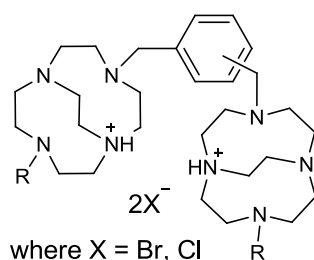


Figure 46: Structures of linear biscyclams;  $L^{34}$  and  $L^{35}$  as outlined by Lindoy and co-workers.<sup>143</sup>

Bernier *et al.* reported a facile route to synthesising CB bicyclen compounds bearing pendant arms in three steps.<sup>144</sup> They evaluated the properties and characteristics of this small family of bicyclens;  $L^{36}$ - $L^{39}$ , see Figure 47, noting that

metal complexes of such configurationally restricted ligands would produce interesting thermodynamic and kinetic properties.



*meta*, R = CH<sub>2</sub>CO<sub>2</sub>Et L<sup>36</sup>  
*para*, R = CH<sub>2</sub>CO<sub>2</sub>Et L<sup>37</sup>  
*meta*, R = CH<sub>2</sub>CH<sub>2</sub>OH L<sup>38</sup>  
*para*, R = CH<sub>2</sub>CH<sub>2</sub>OH L<sup>39</sup>

Figure 47: Structures of a family of configurationally restricted bicyclens; L<sup>36</sup>-L<sup>39</sup>, linked by a *para*- or *meta*-substituted xylyl bridge synthesised by Bernier *et al.*<sup>144</sup>

One important strategy adopted by several research groups is the use of protecting groups to facilitate the formation of structurally diverse bicyclen ligands. Xylyl bridged hexaacetate bicyclen ligands were reported by Costa *et al.*<sup>145</sup> Linkage of the *para*- or *meta*-substituted xylyl group using the glyoxal derivative of cyclen followed by treatment with an excess of ethyl bromoacetate afforded the hexaesters. Hydrolysis with HCl affords bicyclens L<sup>40</sup> and L<sup>41</sup>, see Figure 48. Other groups such as those of Gunnlaugsson<sup>146</sup> and Faulkner<sup>147</sup> synthesised their triprotected cyclen ligand first then used a xylyl linker to form the hexa protected bicyclen structure.

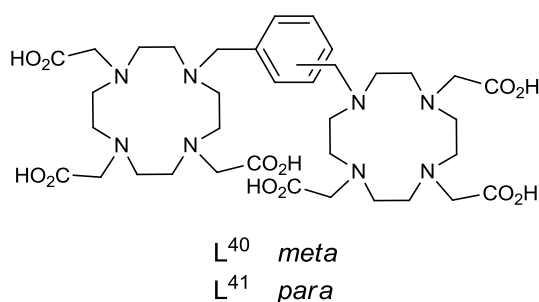


Figure 48: Structure of *meta*- and *para*-substituted bicyclen ligands; L<sup>40</sup> and L<sup>41</sup> bearing protecting groups outlined by Costa *et al.*<sup>145</sup>

Delevay *et al.* synthesised four biscyclen compounds bearing a *meta*- or *para*-phenyl linker previously synthesised by De Clercq and co-workers<sup>141</sup> as well as an *ortho*-derivative (L<sup>42</sup>) and a 2,6-pyridine derivative (L<sup>43</sup>),<sup>148</sup> see Figure 49. The aim of their study was to assess the binding features of the two cyclen moieties and evaluate the factors governing their interaction with anionic phosphate substrates. Their results revealed that all four ligands were good receptors for organic polyphosphate anions.

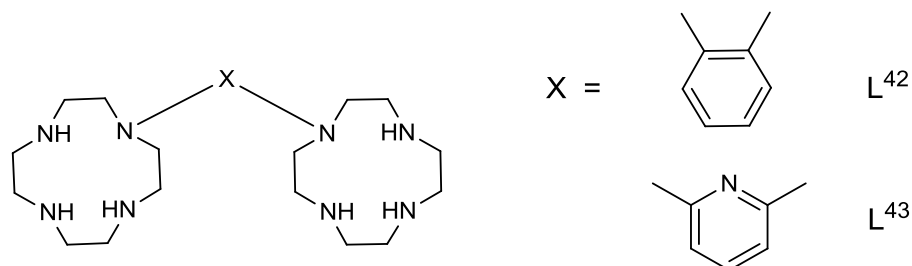


Figure 49: Structures of the *ortho*- and 2,6-pyridyl substituted biscyclen ligands; L<sup>42</sup> and L<sup>43</sup> outlined by Delevay *et al.*<sup>148</sup>

Recently Tanaka *et al.* described the synthesis of a series of *meta*- and *para*-substituted bismacrocycles<sup>149</sup> including L<sup>26</sup>, L<sup>27</sup>, AMD3100 and L<sup>31</sup>; ligands previously synthesised by De Clercq and co-workers.<sup>141</sup> New ligands included a *meta*-substituted cyclal bismacrocycle (L<sup>44</sup>); the *para*-analogue (L<sup>45</sup>) had previously been reported by De Clercq<sup>142</sup> and an unsymmetrical bismacrocycle bearing a cyclam and a cyclen ring in both *meta*- and *para*-substitution patterns (L<sup>46</sup> and L<sup>47</sup>), see Figure 50.

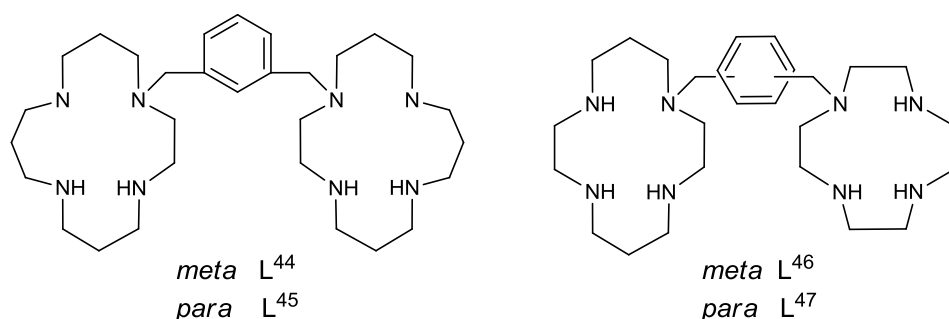


Figure 50: Structures of *meta*- and *para*-substituted bismacrocycles L<sup>44</sup>-L<sup>47</sup>.<sup>149</sup>

#### 2.4.2. Synthesis of a novel CB bicyclen ligand; 1,1'-[3,5-dimethylaminobenzyl]-7,7'-[methyl]-bis(1,4,7,10-tetraazabicyclo[5.5.2]dodecane) (**20**)

A screening of various *ortho*-, *meta*- and *para*-substituted bismacrocyclic compounds was carried out between ourselves and collaborators Tim Hubin (USA) and Erik De Clercq (Belgium). Metal complexes of a *meta*-substituted CB bicyclen compound  $L^{48}$ , see Figure 51, were found to have a very high affinity for the CXCR4 receptor in cellular studies ( $IC_{50}$ ;  $[Cu_2L^{48}]^{4+} = 3.6$  nM,  $[Zn_2L^{48}]^{4+} = 3.4$  nM), see section 4.2.

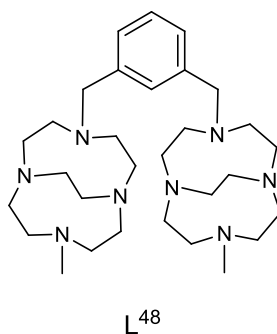
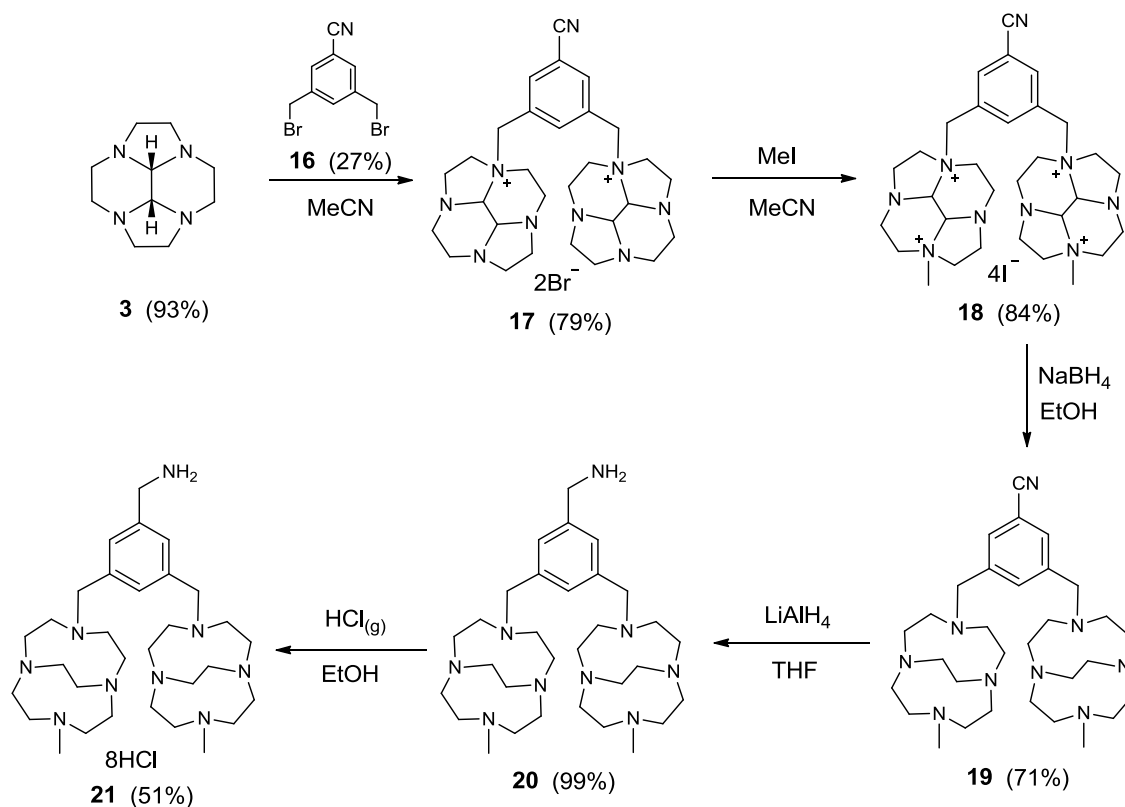


Figure 51: Structure of a high affinity CXCR4 antagonist  $L^{48}$ .

This compound does not include a reactive functional group to allow for further conjugation so research into a full synthetic route for such a compound was devised, see Scheme 4.

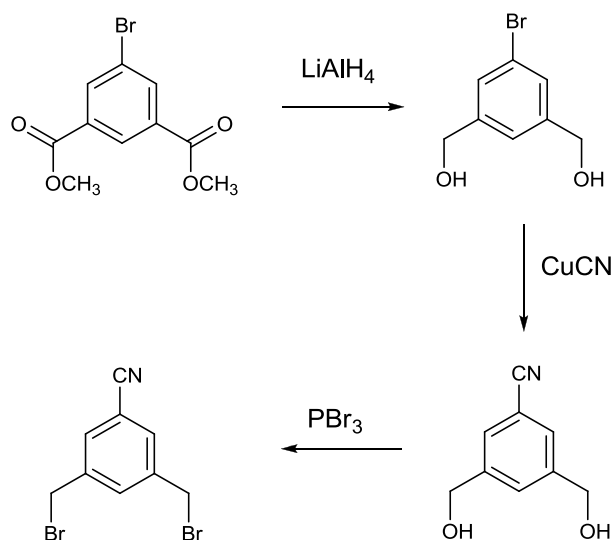
My previous work had determined an effective and robust method for the reduction of a cyano functionality on an azamacrocyclic derivative to a methylamine group and so this chemistry was utilised. Synthesis of the *meta*-linking group (**16**) proved challenging but once optimised all subsequent steps were achieved in high yield (*ca.* 71-99%). Initially this synthetic route was tried on a small scale and produced 120 mg of **20** however, the reaction was scaled-up and synthesis of 1.80 g (99%) of bismacrocycle **20** has been achieved. The  $LiAlH_4$  reduction step was optimised from previous reactions see section 2.3.2. A HCl salt of **20** was also obtained, **21**. HCl salts are solid thus allowing CHN analysis to be obtained, further proof for successful isolation of this novel compound.



Scheme 4: Synthetic route to obtain a novel amine terminating CB bicyclic compound **20**.

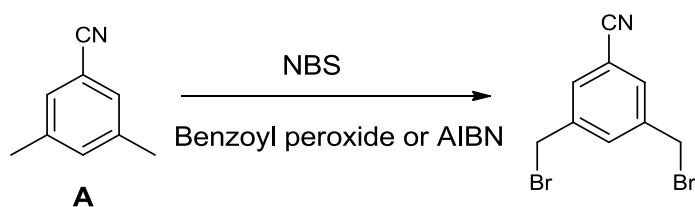
#### 2.4.2.1. Synthesis of 3,5-di(bromomethyl)benzonitrile

3,5-Di(bromomethyl)benzonitrile not only provides a *meta*-substituted linking group but also a cyano group which can go on to be reduced to a methylamine group and reacted further. A number of routes could be used to synthesise 3,5-di(bromomethyl)benzonitrile, one such possible route is outlined in Scheme 5. This method would take several days to complete and the multi-step nature means the overall yield could be low.



Scheme 5: A possible route to obtain 3,5-di(bromomethyl)benzonitrile.

A search of the literature gave several methods outlining the synthesis of 3,5-di(bromomethyl)benzonitrile from 3,5-dimethylbenzonitrile (**A**). A one-step process to access the di-brominated product would reduce overall synthesis time. The methods used chlorinated solvents ( $\text{CCl}_4$  or DCM) and either benzoyl peroxide or azobisisobutyronitrile (AIBN) as a radical initiator with *N*-bromosuccinimide (NBS) as the brominating agent, see Scheme 6, with moderate to high yields (*ca.* 37- 72%) reported.



Scheme 6: Bromination of 3,5-dimethylbenzonitrile using NBS and a radical initiator.

#### 2.4.2.1.1. Using benzoyl peroxide as the initiator

Xi *et al.* used dry  $\text{CCl}_4$ , a slight excess of NBS (2.06 equivalents) and benzoyl peroxide as a radical initiator, refluxing the reagents for two days without the use of an external light source.<sup>150</sup> An extraction was performed followed by chromatographic purification to afford a colourless solid in 72% yield. Easson *et al.* opted to use DCM with 2.2 equivalents of NBS using benzoyl peroxide as the initiator.<sup>151</sup> An external

light source (200 W) was used during the 1 hour reflux followed by an extractive and chromatographic purification to give a white solid in 40% yield. Karlin *et al.* also used  $\text{CCl}_4$  but used two equivalents of NBS with benzoyl peroxide as the radical initiator. After a 24 hour reflux using an external light source, the reaction mixture was filtered and recrystallised to afford a 37% yield.<sup>152</sup>

Initially conditions outlined by Easson *et al.* were trialled due to the less toxic effects of DCM in comparison to  $\text{CCl}_4$  on the environment. The fast reaction time would also be advantageous. After 1 hour of reflux, TLC of the reaction mixture revealed large amounts of starting material was still present but a faint second spot could be observed. After a further hour at reflux the presence of starting material was still apparent but the second spot had increased in intensity. Chromatographic purification using 20% ethyl acetate in hexane, as outlined by the authors, did not separate the spots. It was concluded that the reaction time was not long enough to drive the bromination reaction to completion and the solvent system used for chromatographic purification was not ideal. Karlin *et al.* obtained a pure product though recrystallisation of the crude mixture but attempts to reproduce their method proved unsuccessful. After a much longer reaction time of 24 hours, TLC revealed the presence of three spots of equal intensity, one spot was determined to be starting material leaving two new spots – possibly the desired product and a mono-brominated product. Recrystallization of the crude material afforded white solid but TLC and NMR data showed the presence of three products. MS data confirmed a mixture of products was present.

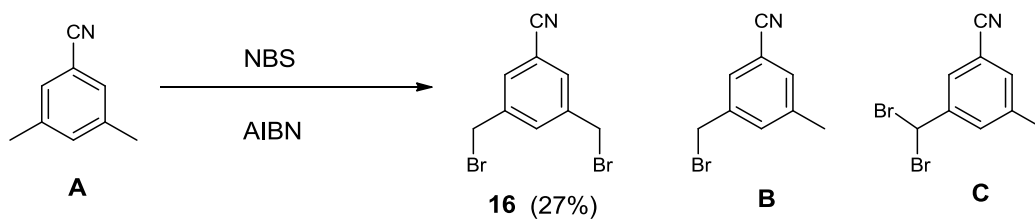
Initial attempts to synthesise 3,5-di(bromomethyl)benzotrile using benzoyl peroxide as the initiator were encouraging. Attempts to obtain the desired product identified the need for a long reaction time (*ca.* 24 hours) but the attempted purification methods were inadequate. Other reports in the literature suggested using AIBN as the initiator.

#### 2.4.2.1.2. Using AIBN as the initiator

Bodwell *et al.* used AIBN as the initiator with NBS in CCl<sub>4</sub> in the presence of an external light source.<sup>153</sup> After a 2 hour reaction they obtained a 40% yield of the desired product. Segura *et al.* opted to use DCM as solvent for their bromination reaction using analogous conditions to those outlined by Boswell *et al.* but did not report the yield obtained.<sup>154</sup> Fisher *et al.* brominated a variety of cyanotoluene derivatives employing similar conditions to those outlined by Easson *et al.*<sup>155</sup> An overnight reflux with equimolar amounts of NBS in CCl<sub>4</sub> with AIBN as the initiator followed by recrystallisation or chromatographic purification allowed them to obtain the desired products.

As radical initiators; benzoyl peroxide and AIBN are by nature unstable, decaying readily if not stored under the correct conditions. At this point it became clear that the reaction conditions previously employed were not taking into account the unstable nature of the initiator and attempts were made to minimise water content by using anhydrous, degassed solvents and performing the reaction under an argon atmosphere.

Using an adapted method, combining aspects of previous attempts; two equivalents of NBS in anhydrous CCl<sub>4</sub> were refluxed for 24 hours under an argon atmosphere with 3,5-dimethylbenzotrile, using AIBN as the initiator and an external light source. After extraction a crude orange oil was obtained. TLC again showed the presence of three spots but none were the starting material indicating that the three spots were bromination products. Previous attempts at chromatographic purification indicated that the polarity of the eluent was not ideal for separation. Testing various polarities of eluent, ranging from 0-20% ethyl acetate in hexane, concluded that 10% ethyl acetate in hexane gave better separation of products. The three products were successfully separated with the desired product; 3,5-di(bromomethyl)benzotrile (**16**) isolated in 27% yield. A monobrominated product (**B**) and a second dibrominated product (**C**) were also isolated, see Scheme 7, and identified using NMR and MS analysis.



*Scheme 7: The bromination products of the synthesis of 3,5-di(bromomethyl)benzonitrile (16) using NBS and AIBN as the initiator. Products include the desired 3,5-di(bromomethyl)benzonitrile (16) and two further brominated products B and C.*

These reaction conditions have been repeated several times and the method is reproducible, always obtaining between 20-27% of 3,5-di(bromomethyl)benzonitrile (16). Although this method has now provided appreciable yields there is the possibility that the maximum yield for this reaction is 33% due to the presence of the two other bromination products, which are always present and always of equal intensity. However, gram quantities of 3,5-di(bromomethyl)benzonitrile can now be synthesised in a two day time frame in high purity. This small organic moiety is part of a much larger synthetic scheme and so efforts to find the highest yielding reaction were not a priority.

#### **2.4.2.2. Configurational restriction**

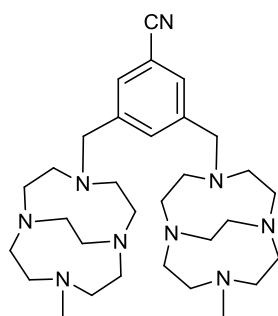
Rigidifying the cyclam skeleton has received considerable attention from many research groups<sup>66, 156</sup> not just because they are relatively easy to synthesise but they have also displayed promising results *in vitro*.<sup>68</sup> Formation of the bismacrocycle **17** is performed in dry acetonitrile (MeCN) and yields depend on the ability of the product to precipitate out of solution. The amount of solvent used is therefore an important factor, if too much solvent is used precipitation of the product is hindered. Removal of some of the solvent and addition of ether has been found to precipitate the solid product but impurities have been noted. After several attempts at this reaction using various amounts of solvent and obtaining variable yields optimum conditions were determined. The ideal reaction conditions are 40 ml of dry MeCN per gram of bridged cyclen (**3**). Methylation of **17** to produce the tetraiodo salt **18** is again solvent dependent but due to a greater positive charge the product precipitates out more readily and less variation in yield has been observed

(average 77%) but a similar rule for the amount of solvent used should be applied (40 ml of solvent per gram of starting material).

Reduction of compound **18** to the configurationally restricted CB biscyclen **19** uses sodium borohydride.<sup>126</sup> The reaction requires a lengthy synthesis time and mild conditions (14 days, RT) in order to produce the desired compound. The product is obtained *via* an extractive work-up with quantitative yields obtained due to the basification of the aqueous layer which deprotonates to give a neutral macrocyclic compound that is highly soluble in organic solvent. The cyano functionality was then reduced to a methylamine group using LiAlH<sub>4</sub> under conditions previously outlined in section 2.3.2., to produce the novel CB biscyclen ligand **20**. This compound is a viscous oil so CHN analysis is challenging, this problem is easily overcome by formation of a HCl salt. HCl gas was bubbled through an ethanolic solution of bismacrocycle **20** and the resulting precipitate was collected and dried. CHN analysis confirms presence of an octahydrochloride salt **21**.

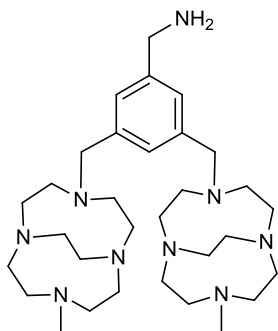
#### **2.4.2.3. Metal complexes of CB biscyclen ligand 20**

Copper(II) complexes of bismacrocycles **19** and **20**; [Cu<sub>2</sub>**19**]<sup>4+</sup> and [Cu<sub>2</sub>**20**]<sup>4+</sup> were successfully synthesised, see Figure 52, using a standard prep, see section 2.3.3.. A copper(II) complex of the cyano bearing bismacrocycle (**19**) was made because it will be interesting to see whether different functional groups on the *meta*-position have any effect on the binding affinity of these bismacrocycles to the CXCR4 chemokine receptor. Copper(II) complexes are particularly pertinent to this body of work because azamacrocyclic copper(II) complexes form much more rapidly than other metal complexes and the 'cold' <sup>63/65</sup>Cu could be replaced with <sup>64</sup>Cu for subsequent use as a PET imaging agent. Zinc(II) and nickel(II) complexes of bismacrocycle **20**; [Zn<sub>2</sub>**20**]<sup>4+</sup> and [Ni<sub>2</sub>**20**]<sup>4+</sup> were also successfully synthesised, see Figure 52. It is hoped that the two ring conformation coupled with configurational restraint and the inclusion of metal centres will mean these compounds will show high binding affinity for the CXCR4 receptor.



**19**

[Cu**19**](CH<sub>3</sub>CO<sub>2</sub>)<sub>2</sub> (44%)



**20**

[Cu**20**](CH<sub>3</sub>CO<sub>2</sub>)<sub>2</sub> (77%)

[Zn**20**](CH<sub>3</sub>CO<sub>2</sub>)<sub>2</sub> (88%)

[Ni**20**](CH<sub>3</sub>CO<sub>2</sub>)<sub>2</sub> (90%)

Figure 52: Representative structures of metal complexes of bismacrocycles **19** and **20**. Note in some cases anions and/or solvent molecules may coordinate to the metal centres.

## 2.5. Bismacrocycles as CXCR4 antagonists?

A paper published by Oltmanns and co-workers stated that a bis[Zn(cyclen)]<sup>4+</sup> complex, see Figure 53, showed a 'lack of measurable CXCR4 interaction' when competed with a *meta* derivative of the clinically licensed drug AMD3100.<sup>157</sup>

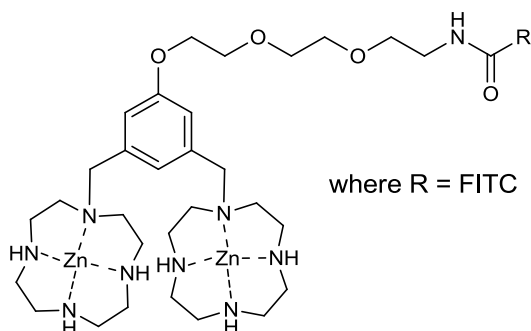


Figure 53: A bis[Zn(cyclen)]<sup>4+</sup> compound synthesised by Oltmanns et al.<sup>157</sup>

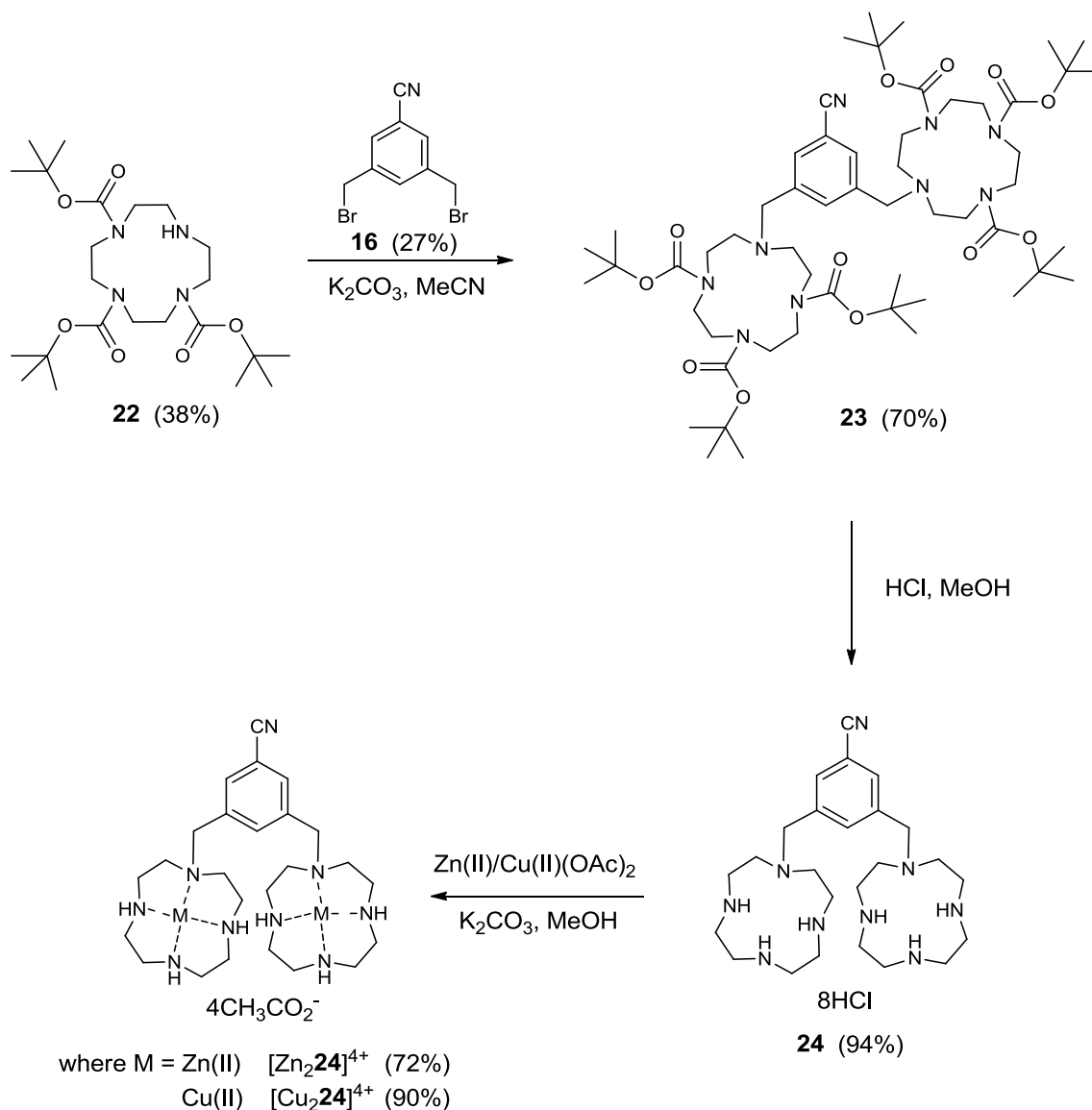
They used apoptotic Jurkat cells, competing a 100 times excess of *meta* AMD3100 with their bis[Zn(cyclen)]<sup>4+</sup> complex and concluded that their study showed no

measurable interaction with CXCR4, using flow cytometry. Based on our own studies it is unlikely that such tetraazamacrocyclic compounds have no interaction with CXCR4.

### 2.5.1. Synthesis of metal complexes of a *meta*-substituted biscyclen ligand; **24**.

To ascertain whether the observations by Oltmanns *et al.* are correct an analogous *meta*-substituted biscyclen ligand (**24**) and both its zinc(II)  $[\text{Zn}_2\mathbf{24}]^{4+}$  and copper(II)  $[\text{Cu}_2\mathbf{24}]^{4+}$  complexes were synthesised, see Scheme 8, and tested *in vitro* against a CXCR4 expressing cell line (Jurkat) in a competition binding assay, the results of which are discussed in Chapter 4.

Di-*tert*-butyl dicarbonate was chosen as the protecting group for its well-known reactivity. Dessolin *et al.* have previously demonstrated good results using this protecting group for cyclam derivatives.<sup>158</sup> The limitation of this method is that mono- and di- protected compounds can form, limiting the amount of the desired tri-protected compound, after purification *via* flash chromatography a 38% yield was obtained which was deemed reasonable for this synthesis and no further method development was attempted. Subsequent formation of the biscyclen using 3,5-di(bromomethyl)benzotrile (**16**), whose synthesis has been described previously, see section 2.4.2.1., required the use of potassium carbonate to deprotect the secondary amine and allow for alkylation. TLC showed presence of starting material but this was easily separated from the product *via* flash chromatography producing **24** in 70% yield. Deprotection *via* an overnight reflux in HCl resulted in complete deprotection of all six Boc groups confirmed by <sup>1</sup>H and <sup>13</sup>C NMR and yielded an octa- HCl salt. Copper(II) and zinc(II) acetate complexes of this macrocyclic ligand were made.  $[\text{Zn}_2\mathbf{24}]^{4+}$  and  $[\text{Cu}_2\mathbf{24}]^{4+}$  were purified *via* size exclusion chromatography yielding pure complexes confirmed by MS and CHN analysis.

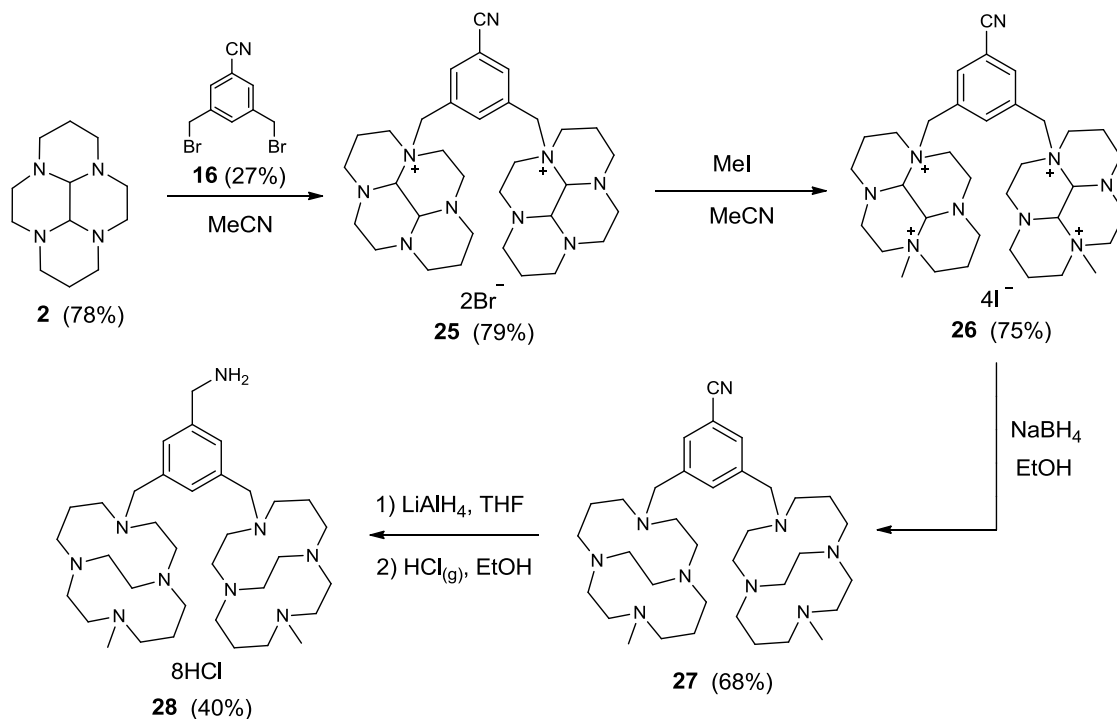


*Scheme 8: Synthetic route to **24**; a meta-substituted biscyclam ligand and its metal complexes  $[\text{Zn}_2\text{24}]^{4+}$  and  $[\text{Cu}_2\text{24}]^{4+}$ . Note in the case of metal complexes anions and/or solvent molecules may coordinate to the metal centres.*

## 2.6. Synthesis of a novel CB biscyclam ligand; 1,1'-[3,5-dimethylamino benzyl]-8, 8'-[methyl]-bis-1,4,8,11-tetraazabicyclo [10.2.2]hexadecane octahydrochloride (**28**)

An analogous synthetic route to that devised to obtain bismacrocycle **20** was performed using bridged cyclam (**2**) to give a *meta*-substituted configurationally restricted biscyclam compound **28**, which was isolated as an octahydrochloride salt,

see Scheme 9. Yields for each step are comparable to the corresponding steps in the synthesis of **21**. NMR, CHN and MS analysis of this compound confirm both the presence and purity of the final product (inclusion of solvent molecules was noted).



Scheme 9: Synthetic route to obtain a meta-substituted CB bicyclam compound, isolated as a hydrochloride salt (**28**).

*Para*-substituted bicyclam structures, such as AMD3100, have been shown to have high affinity for the CXCR4 receptor, there are fewer examples of *meta*-substituted bicyclam compounds. Intuitively, the steric hindrance induced by having two 14 membered rings in a *meta*-substitution pattern may conceivably hinder binding at the CXCR4 receptor but this may not be the case and so biological studies are required to investigate this further, see Chapter 4.

### 2.6.1. Metal complexes of CB bicyclam ligand **28**

To provide a comparative study to the metal complexes of bicyclen **20**, the copper(II), zinc(II) and nickel(II) complexes of bicyclam **28** were synthesised in 74%, 58% and 46% yields respectively, see Figure 54. This variation in yield has been observed previously when complexing metals in macrocyclic cavities and is put down to the purification procedure which can carry up to a 30% loss.

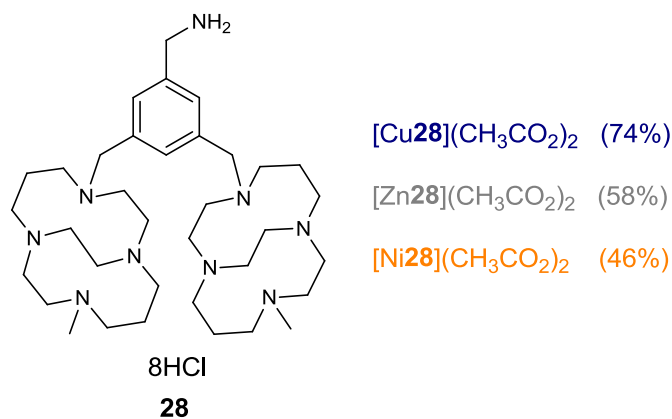


Figure 54: Representative structures of copper(II), zinc(II) and nickel(II) complexes of the CB biscyclam ligand **28**. Note in some cases anions and/or solvent molecules may coordinate to the metal centres.

## 2.7. Conclusions

This section of work outlines the successful synthesis of a series of novel CB and SB N-functionalised macrocycles. CB and SB monomacrocycles bearing methylamine pendant arms were synthesised, their copper(II), zinc(II) and nickel(II) complexes have also been synthesised. Monomacrocycles offer potentially improved pharmacological properties and an evaluation of their binding affinities for CXCR4 is discussed in Chapter 4. A multi-step synthetic route to obtain a *meta*-substituted CB biscyclam compound bearing a methylamine pendant arm (**20**) has been completed. Copper(II), zinc(II) and nickel(II) complexes of this novel configurationally restricted bismacrocycle have been synthesised, their affinities for CXCR4 are also reported in Chapter 4. To provide a comparative study the multi-step synthesis of an analogous *meta*-substituted CB biscyclam compound bearing a methylamine pendant arm (**28**) was attempted and the final compound was successfully isolated as an octahydrochloride salt. The copper(II), zinc(II) and nickel(II) complexes of this novel bismacrocylic species have been synthesised for evaluation as CXCR4 antagonists. A non-restricted biscyclam compound **24** and its zinc(II) and copper(II) complexes have also been synthesised to assess whether these ligands have a measurable interaction with the CXCR4 receptor.

## **Chapter 3**

### **Development of a spacer arm**

### 3.1. Introduction

As previously mentioned the design of MFCs will require the use of a spacer arm to link distinct parts together preventing any interactions between the diagnostic and therapeutic groups and offering the opportunity to tune properties such as pharmacokinetics. It will be necessary to attach spacer groups of different lengths and solubilities since the optimum characteristics are as yet unknown but properties such as water solubility and bioavailability would be useful. Ideally the spacer arm needs to be long enough to allow the macrocyclic component to interact with the CXCR4 receptor without interference from the bulky porphyrin but not so long that it will compromise the targeting properties of the macrocycle by interacting with other cell surface proteins. The use of a spacer arm has been employed in the design of MFCs by many groups and there are a significant number of reactions from which to draw appropriate methodology.

#### 3.1.1. Synthetic strategy

To attach spacer groups of varied molecular structure to bismacrocycle **20**. This will produce functionalised ligands with targeting and diagnostic properties with reactive handles for further conjugation. Methods will focus on the formation of amide bonds, a widely used functionality, utilising activating groups.

### 3.2. The formation of amide bonds

The formation of an amide bond by reacting an amine and a carboxylic acid (initially forming a salt) is a common feature in both small or complex and synthetic or natural molecules. This reaction has been used in many areas of organic, bioinorganic and medicinal chemistry but most notably in peptide synthesis. The formation of amide bonds usually relies on activation of the acidic moiety, achieved with a wide variety of coupling reagents, followed by aminolysis with the amine functionality, see Figure 55. The scope of methods involving amide bond formation is large and a thorough review of the topic was carried out by Montalbetti *et al.*<sup>159</sup>

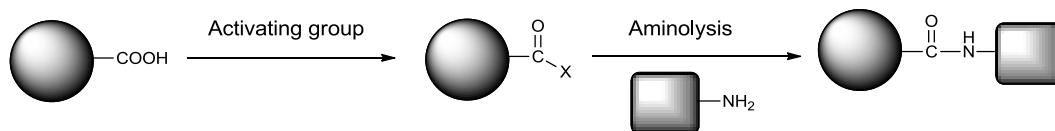


Figure 55: General scheme outlining the formation of an amide bond using an activated acid species. (Adapted from *Tetrahedron*)<sup>159</sup>

### 3.2.1. *N*-hydroxysuccinimide ester functionalities

As mentioned, there are a wide variety of coupling reagents available to activate the acidic moiety. This section focuses on one such activating group; NHS esters, highlighting a specific example of how it has been utilised to conjugate components to form a MFC.

Kuril *et al.* labelled a DTPA chelate with a fluorescent dye (Cy 5.5), incorporating an acidic handle for further conjugation, see Figure 56.<sup>160</sup> This acidic handle was activated with a disuccinimidyl group producing an activated NHS ester compound. The DTPA chelate with fluorescent properties was then conjugated to a lysine residue on an antagonistic peptide, known to bind to the CXCR4 receptor producing a MFC targeted to the CXCR4 receptor with dual modality imaging properties.

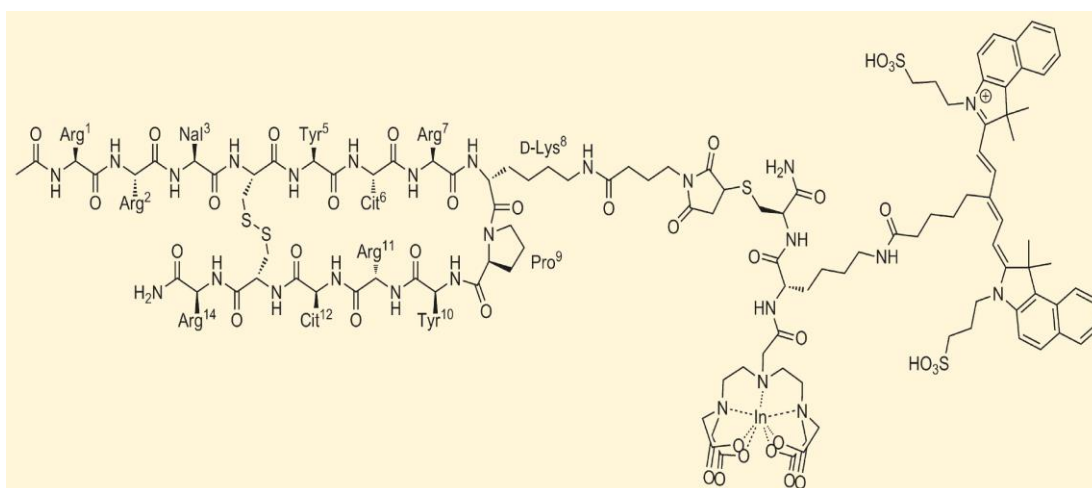
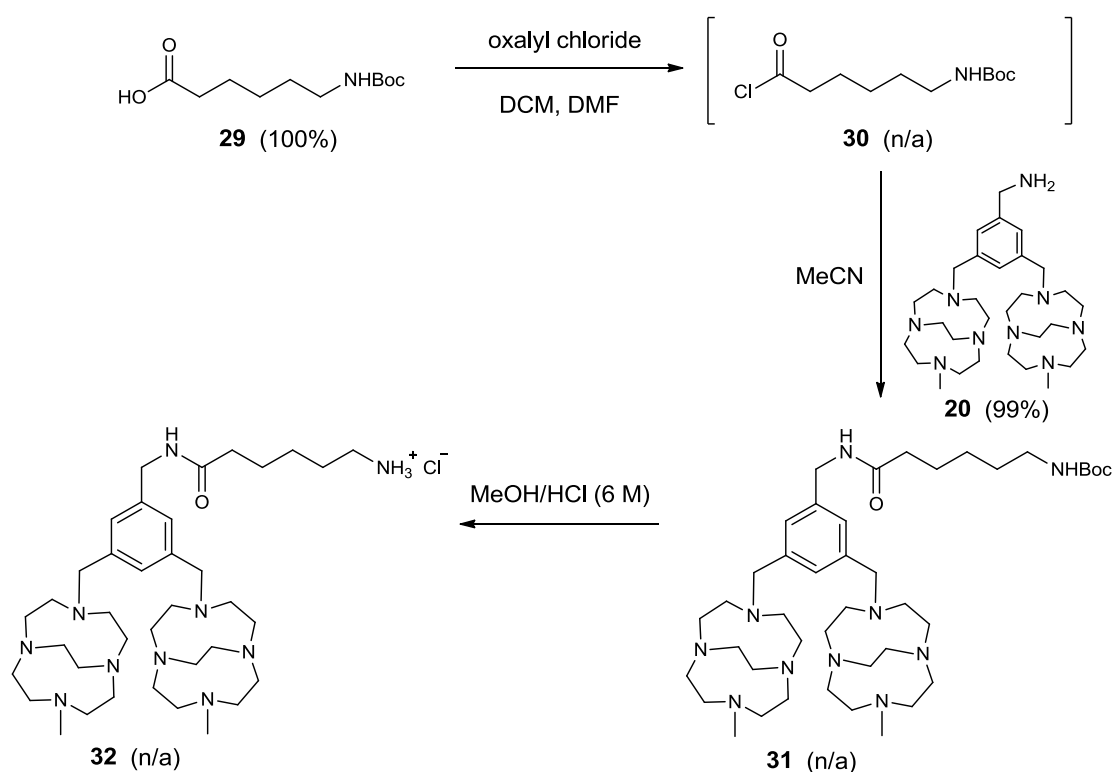


Figure 56: Utilising the NHS ester functionality to conjugate a targeted antagonistic peptide to a DTPA chelate bearing a fluorescent dye. (Reproduced from *Bioconj. Chem.*)<sup>160</sup>

### 3.3. Formation of an acid chloride

Acid chlorides, an activated form of a carboxylic acid, are a widely used functional group in amide coupling reactions. One idea was to protect the amine end of an organic acid, 6-aminohexanoic acid, make an acid chloride *in situ* by addition of oxalyl chloride followed by addition of bismacrocycle **20**, see Scheme 10. Deprotection of the Boc group with acid would then afford bismacrocycle **32**; a linking group terminating in a primary amine group.



Scheme 10: Attempted synthetic route to append an *in situ* generated acid chloride; **29** to bismacrocycle **20** to produce bismacrocycle **32**.

Boc protection of 6-aminohexanoic acid to produce compound **29** was quantitative as described in the literature<sup>161</sup>, the addition of the Boc group confirmed by analysis of <sup>1</sup>H NMR and <sup>13</sup>C NMR spectra. MS analysis also confirmed the presence of the product ( $m/z$  254  $[M + Na]^+$ ). A search of the literature provides a wealth of methods to form an acid chloride *in situ* dating back to the early 1980s. Carpino *et al.* outlined the synthesis of Fmoc amino acid chlorides describing them as facile, stable coupling agents and used them to rapidly synthesise peptide sequences.<sup>162</sup>

Their simple method of reacting an acid with a 10-fold excess of SOCl<sub>2</sub> with 0.1 equivalents of DMF as a catalyst afforded high yields (ca. 79-96%) across a range of Fmoc protected amino acids. Buckley *et al.* used oxalyl chloride together with DMF as a catalyst to produce high yields of acid chlorides (>85%) from a range of acidic compounds bearing amine functionalities.<sup>163</sup>

Synthesis of the Boc protected bismacrocycle **30** involved *in situ* formation of the acid chloride **30**, using conditions outlined by Buckley *et al.*<sup>163</sup> The acid chloride was not isolated but a change of solvent was required to dissolve bismacrocycle **20**, after 24 hour period of stirring, bismacrocycle **31** was isolated, see Scheme 10. MS showed a peak at  $m/z$  769  $[M + H]^+$  indicating that the product was forming but the NMR data was swamped by peaks associated with the linker group. A low integral aromatic region was observed in both the <sup>1</sup>H NMR and <sup>13</sup>C NMR spectra, indicating that the desired product may well be forming but in very low yield. This could be due to the acid chloride not forming *in situ* or once formed it is not then reacting efficiently with bismacrocycle **20**. A portion of the orange oil obtained was refluxed in HCl (6 M) overnight to deprotect the amine group producing bismacrocycle **32**. NMR spectra confirmed the Boc peak had been removed but again only a very small aromatic region (with low integration) was obtained. MS analysis showed presence of a peak at  $m/z$  279  $[20 + H]^{2+}$ , this could well be a fragment of the product but it could also suggest that the spacer group was not attached to the macrocycle since no higher mass peaks of relevance were observed. This deprotection step was attempted again with TFA using DCM as the solvent. The crude product was purified *via* an extractive organic work up to yield orange oil. MS showed none of the expected ions and <sup>13</sup>C NMR was missing aromatic peaks and the carbonyl peak indicating that the spacer group may well have been cleaved.

As mentioned, the low yield obtained for compound **31** could be due to the acid chloride not forming *in situ*, attempts were therefore made to isolate **30**. MS analysis showed a peak for the fragment shown in Figure 57, but there was no evidence of a chlorine containing isotope pattern so this fragment could have simply been due to the starting material. NMR data also implies that the reaction

was unsuccessful. The OH proton can still be observed in the  $^1\text{H}$  NMR and there are too many peaks in the  $^{13}\text{C}$  NMR to account for the product alone. The analysis is somewhat inconclusive and the decision was taken to investigate alternative reactions for amide bond coupling.

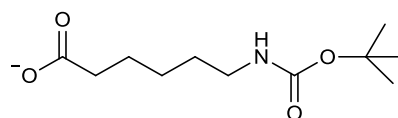
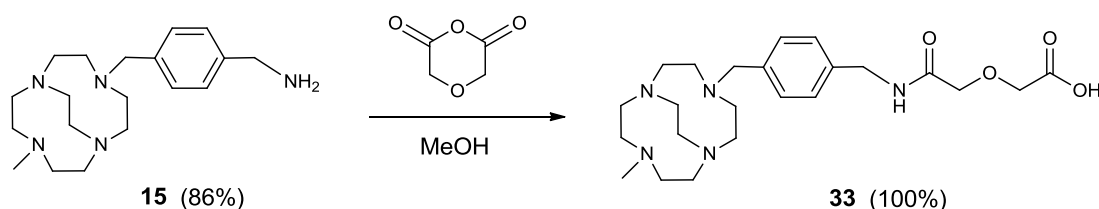


Figure 57: Structure of the fragment observed in the MS analysis in an attempt to isolate acid chloride **30**.

### 3.4. Ring-opening of diglycolic anhydride

Alternative reactions were investigated to find a successful, high yielding reaction for the addition of a spacer arm. One alternative is the ring opening of diglycolic anhydride, which is a standard reaction to test the reactivity of amines.<sup>164, 165</sup> If successful the macrocycle would then have a spacer terminating in an acidic group with an ether oxygen in the chain, which should improve biocompatibility (cf. PEG chains). This acidic group could then be activated by means of various coupling reagents for reaction with primary amines.

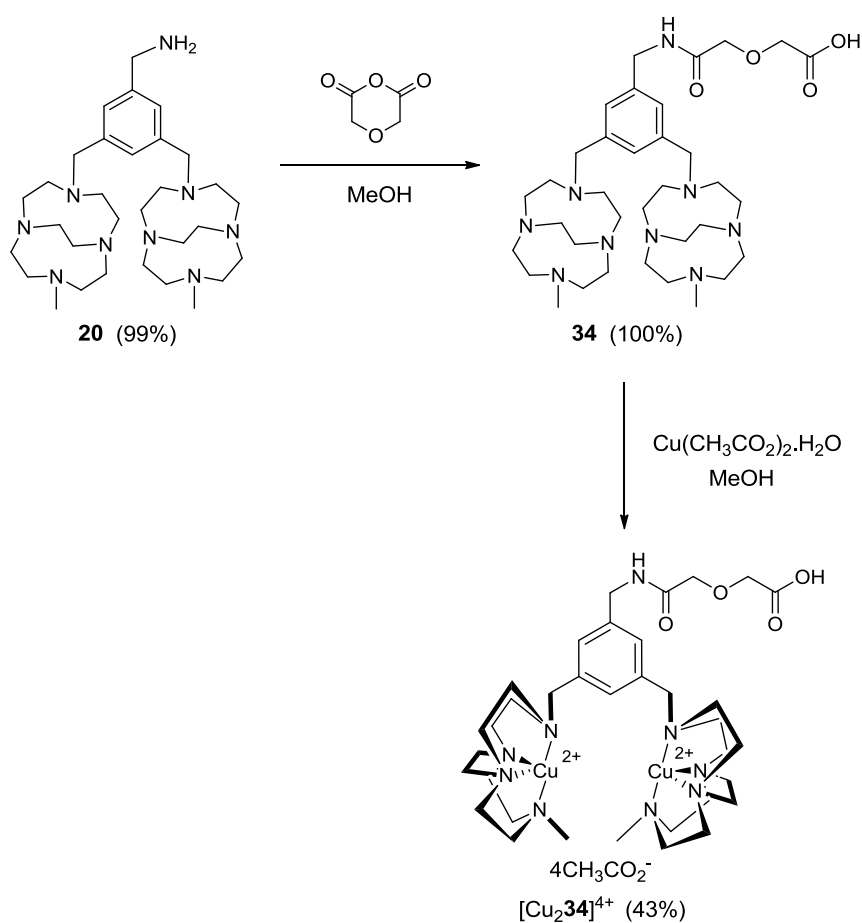


Scheme 11: Ring-opening of diglycolic anhydride to produce an acid terminating monomacrocycle **33**.

Monocycle **15** (used for test reactions instead of the more challenging to synthesise bismacrocycle **20**) successfully ring opened diglycolic anhydride to produce compound **33**, see Scheme 11, confirmed by MS ( $m/z$  448  $[\text{M} + \text{H}]^+$ ) and  $^{13}\text{C}$  NMR data. Some peaks in the  $^1\text{H}$  NMR spectrum were poorly resolved but did

integrate to the correct number of protons. The  $^{13}\text{C}$  NMR spectrum clearly shows the expected number of carbonyl peaks.

An analogous reaction was performed with biscyclen **20** to produce compound **34**, see Scheme 12.  $^{13}\text{C}$  NMR is conclusive for the formation of the desired product and MS shows the mass ion at  $m/z$  672  $[\text{M} + \text{H}]^+$ . This reaction has been attempted on four separate occasions and is not only reproducible but goes to completion even with a 1:1 ratio and hence does not require a purification step.



*Scheme 12: Ring-opening of diglycolic anhydride and subsequent copper(II) complexation of macrocycle **34**. Note in the case of the metal complex anions and/or solvent molecules may coordinate to the metal centres.*

Complexation of copper(II) into the macrocyclic cavities to give  $[\text{Cu}_2\mathbf{34}]^{4+}$  was then attempted, see Scheme 12. MS and CHN analysis show that the reaction was successful and a pure product was obtained. The low yield was a little disappointing

(43%) but size exclusion chromatography purification can carry up to a 30% loss. This section of work describes the successful addition of an acid terminating spacer arm to bismacrocycle **20** and isolation of its pure copper complex  $[\text{Cu}_2\mathbf{34}]^{4+}$ .

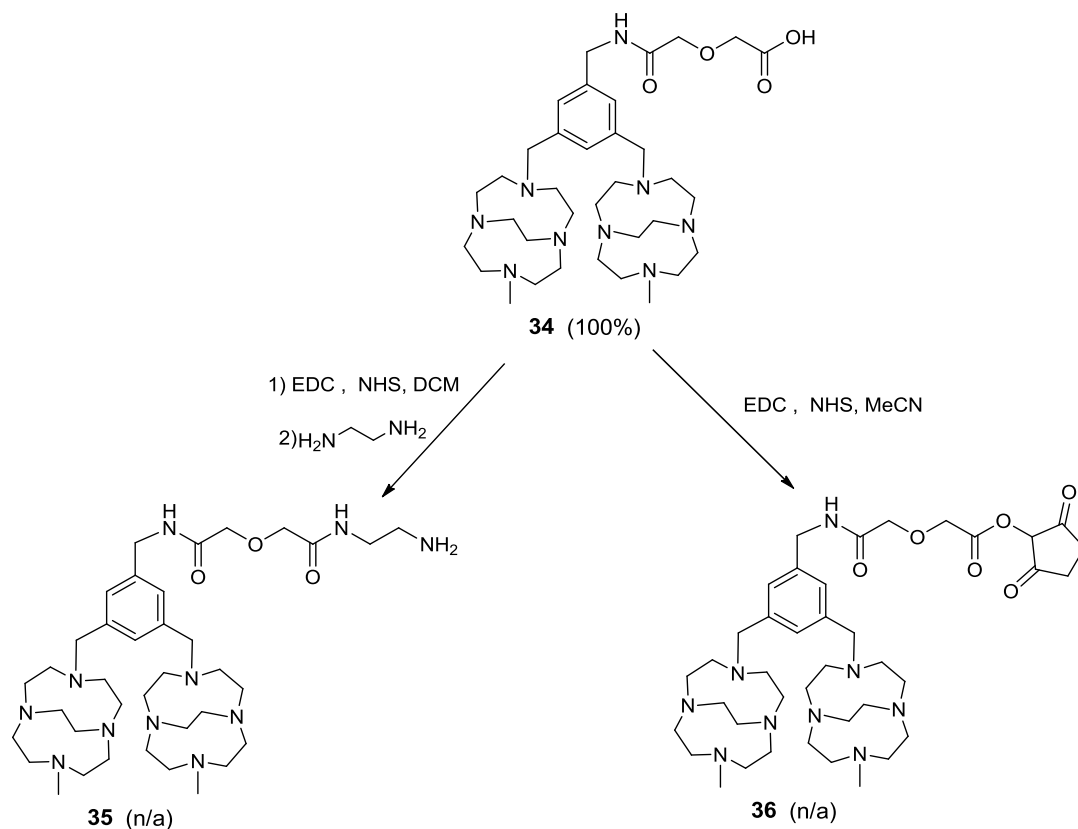
#### 3.4.1. Activation of bismacrocycle **34**

Amide bond formation is a widely used reaction in several fields, most notably peptide synthesis and requires an amine and an acid group. Usually, but not always, coupling reagents are used to facilitate such a reaction, usually by activation of the acidic functionality, as discussed in section 3.3. with acid chlorides.

Reactions to activate the acidic end of bismacrocycle **34** were attempted. There are several ways to activate the acidic functionality, NHS ester groups are commonly employed as they are relatively stable, therefore easy to isolate and store. One attempt involved employing EDC and NHS as coupling reagents following a patent submitted by Diiachi Pure Chemicals.<sup>166</sup> The coupling reagents and bismacrocycle **34** were stirred together for 4 hours to form an activated NHS ester *in situ*; a large excess of ethylenediamine was then added to form compound **35**; an amine terminating bismacrocycle. MS analysis gave a product peak at  $m/z$  714  $[\text{M} + \text{H}]^+$  but NMR data suggested a mixture of products, also evident by the high calculated yield (>100%) and the peaks relating to the macrocycle were relatively small. A purification step is necessary for this reaction but difficult to achieve since EDC is soluble in water (as is the product), and ethylenediamine is basic (as is the product) so an extraction into organic solvent under basic conditions would not separate these components.

The data obtained for compound **35** seemed to suggest the desired product was forming but in low yield, an observation previously seen when trying to form compound **31**. In order to assess why the compound was forming in low yield, isolation of the NHS ester was attempted, this would at least conclude whether the activated acid was forming. Following an adapted procedure outlined by Boswell *et al.*, bismacrocycle **34** was reacted with NHS in the presence of EDC, see Scheme 13.<sup>167</sup> Purification involved removal of the excess EDC by washing with water to give compound **36**. NMR data again suggested a mixture of products but MS analysis did

not show any of the expected ions. This data suggests that the activated NHS ester was not forming or is very difficult to isolate. Since there are a wealth of other coupling reagents to choose from new methods were sought.

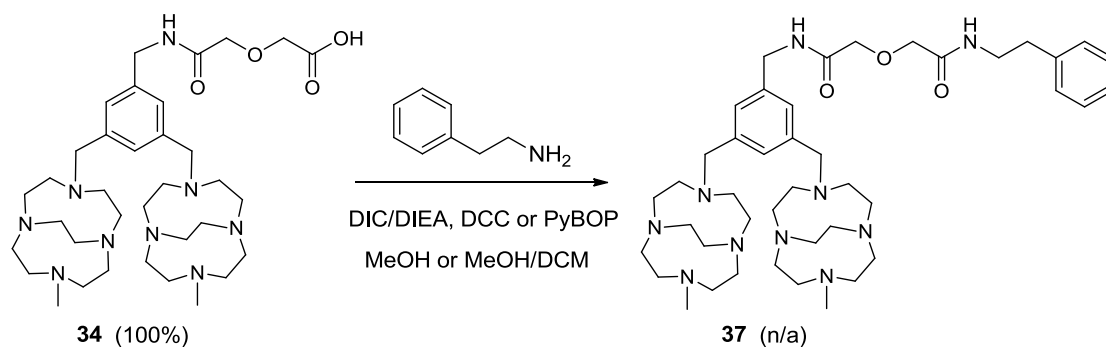


*Scheme 13: Attempted reactions to activate bismacrocycle **34** by means of an NHS ester.*

Dicyclohexylcarbodiimide (DCC) and diisopropylcarbodiimide (DIC) are commonly used reagents to form amides, esters and acid anhydrides and are widely employed in peptide synthesis.<sup>76</sup> DCC tends to be used in solution phase reactions and DIC for solid supported reactions. Carbodiimides hydrolyse to form ureas and these by-products need to be removed from reaction mixtures. DCU, the urea by-product of DCC is insoluble in a lot of organic solvents and so is easily filtered out of a reaction mixture. Whereas DIU, the urea by-product of DIC is soluble in most organic solvents meaning it can be extracted out of the reaction mixture.

Both coupling reagents were used in separate attempts to activate bismacrocycle **34**, following an adapted procedure outline by Sprague *et al.*<sup>168</sup> Phenylethylamine was used as the amine counterpart to produce bismacrocycle **37**, as the aromatic

region is distinct in the NMR spectra and can be easily identified. DIPEA was used alongside DIC because literature methods show the basicity of DIPEA can help to progress coupling reactions.<sup>76</sup> Bismacrocycle **34** was allowed to stir with the coupling reagents in DMF for 30 min to facilitate activation of the acid, followed by addition of a large excess of phenylethylamine, see Scheme 14. After removal of DMF, the crude oil was redissolved in water and extracted with DCM to remove the urea by-product. Removal of DIPEA was more challenging since the product is also basic, since DIPEA is a liquid high vacuum drying was attempted to remove any traces but the high yield (>100%) indicated that this may not have been successful. NMR data indicated impurities were present and peaks were not well-defined and therefore hard to integrate accurately. Despite not being well-defined, expected peaks in the alkyl, aromatic and carbonyl regions were present indicated that, although impure, the product may have formed. However, MS analysis showed none of the expected ions for the product.



*Scheme 14: Proposed synthetic route to attach phenylethylamine to bismacrocycle **34** using various coupling reagents.*

Using an analogous method, DCC was used in an attempt to activate bismacrocycle **34** with MeOH as the solvent, followed by addition of phenylethylamine in excess. After filtering and removal of solvent a crude orange oil was obtained. At this stage the crude product was analysed to determine whether reaction had occurred to form bismacrocycle **37**. The <sup>13</sup>C NMR spectrum showed too few peaks for the desired product and none of the expected ions were observed in the MS. The <sup>1</sup>H NMR spectrum was however more promising integrating to the correct number of

protons. This promising data led to a repeat of the reaction using an excess of bismacrocycle **33** instead of phenylethylamine to see if this would help drive the reaction. The NMR data obtained was much more indicative of a successful reaction. The  $^1\text{H}$  NMR integrates correctly, the  $\text{CH}_2$  protons for the acid appended spacer arm are observed and the aromatic region has additional peaks compared to that of the starting macrocycle (**34**). The  $^{13}\text{C}$  NMR shows peaks in the alkyl, aromatic and carbonyl region, twenty peaks were observed rather than the expected seventeen, this is most likely due to the excess of compound **34** used, also evident from the calculated yield (>100%). However, despite the promising NMR data, MS did not show the mass ion for the product. A peak corresponding to bismacrocycle **20** was observed at  $m/z$  556 [**20** + H] $^+$ . This peak does not necessarily indicate that the reaction did not work however as this could be a fragment of the product. The conflicting data makes it difficult to conclude whether this reaction was successful or not.

PyBOP ((benzotriazol-1-yloxy)tripyrrolidino phosphonium hexafluorophosphate) a less hazardous analogue of BOP ((benzotriazol-1-yloxy)tris(dimethylamino) phosphonium hexafluorophosphate) has been used by several groups to successfully couple porphyrins to peptides.<sup>169, 170</sup> Since ultimately a porphyrin will replace the current model amine; phenylethylamine, this coupling reagent may prove very useful for future reactions. Analogous reaction conditions were used to those outlined when using DCC with an excess of bismacrocycle **34**. MS showed the mass ion of the coupled product (**37**) to be present  $m/z$  775 [M + H] $^+$  and a HRMS was also obtained. The  $^1\text{H}$  NMR spectrum integrates to seventy three protons instead of the expected seventy but some of the peaks are broad so this may account for the slight discrepancy. Broad peaks were observed in the alkyl region characteristic of a macrocycle as well as a busier aromatic region than the starting macrocycle (**34**).

This series of reactions demonstrates that amide bond formation when a macrocyclic species is present is challenging even with 'standard' peptide coupling reagents. Some promising leads have been identified; using PyBOP as a coupling

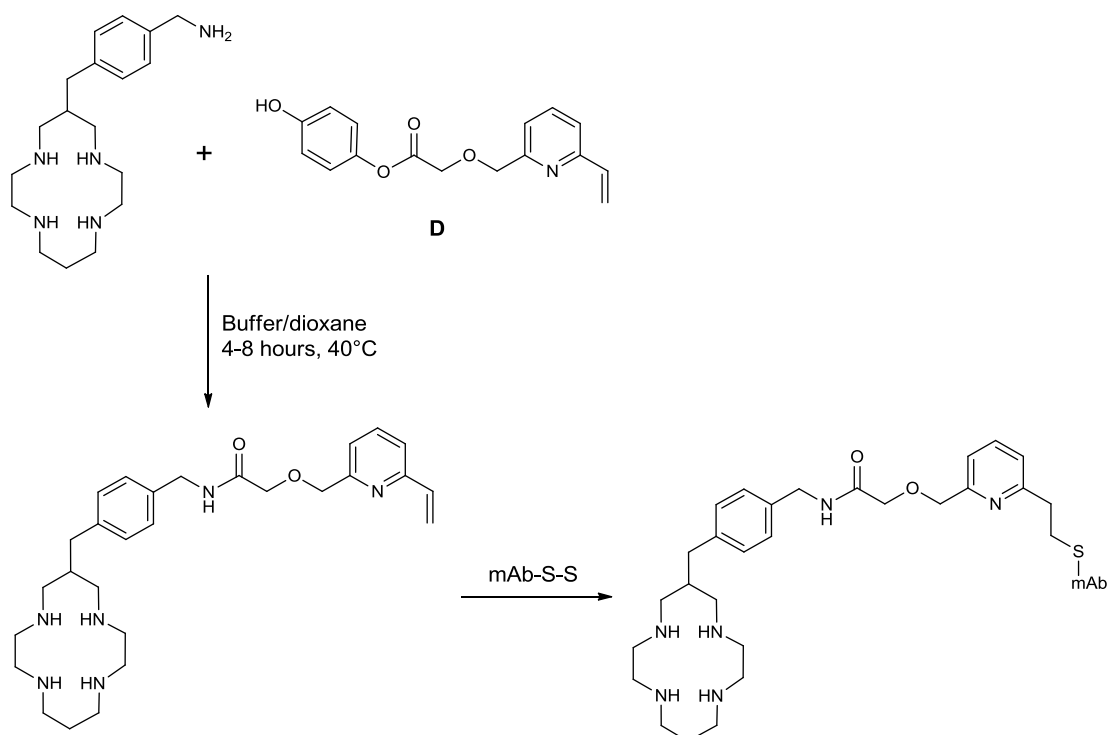
reagent seems to give the best results of the compounds tested but compound purity remains the key issue.

### 3.4.2. Activation using *p*-nitrophenol

Despite their wide use in peptide synthesis, the use of coupling reagents when a macrocyclic species is involved is less widely published. The group of Parker however,<sup>114</sup> have successfully used activated ester compounds to attach a variety of peptides to macrocyclic species utilising *p*-nitrophenol as an activating agent.

#### 3.4.2.1. Previous strategy

Parker and co-workers synthesised four C-functionalised monomacrocycles bearing alkylamine pendant arms, see Figure 34 section 2.2.1.<sup>114</sup> These monomacrocycles were then attached to a *p*-nitrophenol activated heterobifunctional vinylpyridine linker (**D**), this linker allowed subsequent attachment to a mAb, see Scheme 15.



*Scheme 15: Synthetic scheme to attach a *p*-nitrophenol activated vinylpyridine linker (**D**) to a C-functionalised macrocycle and subsequent conjugation to a mAb as outlined by Parker and co-workers.<sup>114</sup>*

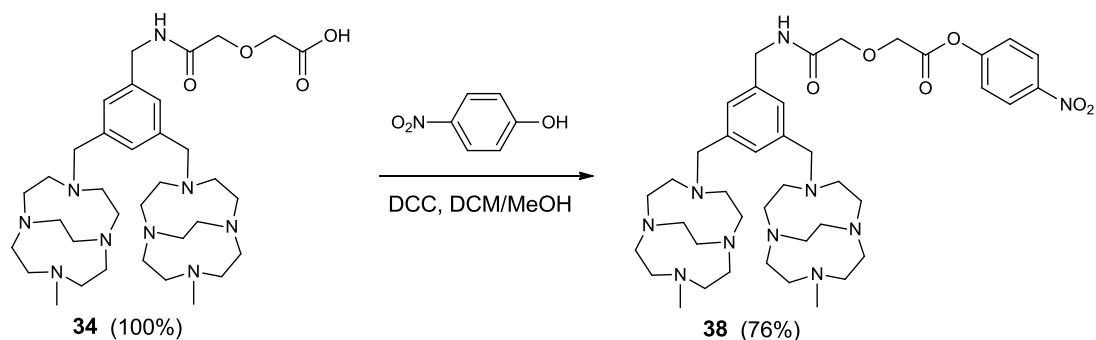
They were able to efficiently radiolabel these antibody conjugates with either  $^{64}\text{Cu}$  or  $^{67}\text{Cu}$  and were able to demonstrate that these complexes were stable with respect to copper(II) loss *in vivo* during kinetic studies. Their method for attaching the aminomethyl bearing macrocycles to heterobifunctional vinylpyridine linkers activated by *p*-nitrophenol involved an extraction method for isolating the pure macrocyclic product, despite only obtaining a 55% yield this method may solve previous issues found when trying to remove coupling reagents and isolate a pure macrocyclic species.

#### **3.4.2.2. Activation of bismacrocycle 33 with *p*-nitrophenol**

Previous attempts to activate the acidic end of bismacrocycle **34** proved challenging, see section 3.4.1. However, an activated compound would be very useful for subsequent conjugation reactions. Formation of an activated ester bisazamacrocycle using *p*-nitrophenol was not something that Parker and co-workers tried but they did successfully react activated ester linkers with azamacrocycles. Hence isolation of such an activated macrocycle should be possible.

Parker and co-workers attached *p*-nitrophenol to their vinylpyridine linker by means of DCC, utilising the fact that the by-product; DCU can be filtered out of the reaction.<sup>114</sup> An adapted method was attempted to activate bismacrocycle **34** with *p*-nitrophenol and the resulting activated ester; **38** was isolated *via* an extractive work-up procedure obtaining yields in the range of 54 to 76%, see Scheme 16.

One observation made during the extractive work up is that successive washing is needed to remove all traces of *p*-nitrophenol, which is bright yellow. A *p*-nitrophenol impurity equating to ~5-10% of the sample was noted in the NMR spectra by characteristic doublets at  $\delta$  6.24 and 7.35 in the aromatic region of the  $^1\text{H}$  NMR spectra.

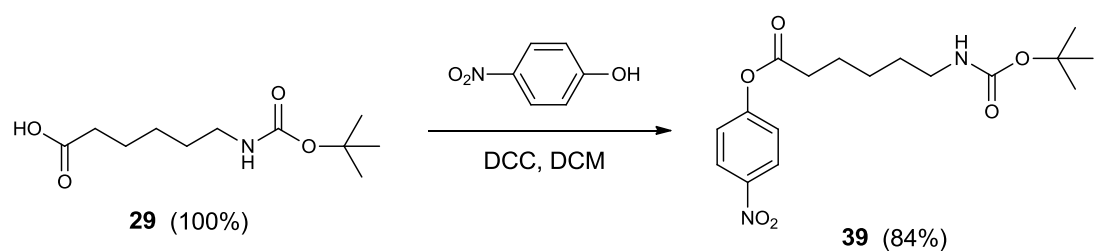


Scheme 16: Activation of bismacrocycle **34** with *p*-nitrophenol to give an activated ester **38**.

Despite carrying an impurity (~5-10%) of *p*-nitrophenol the activated ester **38** was felt to be sufficiently pure for future reactions and the most successful attempt at forming an activated bismacrocycle for further conjugation reactions.

#### 3.4.2.3. Synthesis to attach amine terminating spacer arms to macrocycles utilising *p*-nitrophenol chemistry

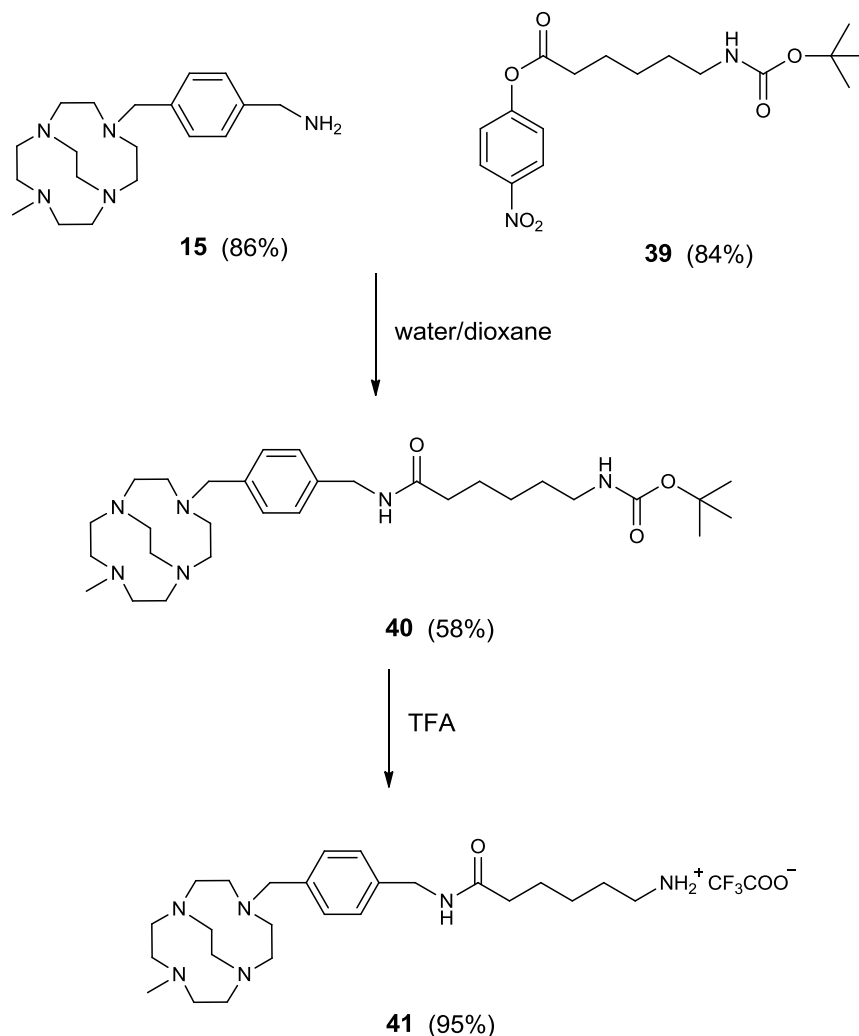
Previous attempts to form an acid chloride with compound **29** had proved challenging but the progress of reactions when utilising *p*-nitrophenol inspired an attempt to form 4-nitrophenyl 6-((*tert*-butoxycarbonyl)amino)hexanoate (**39**), the activated ester of **29**, see Scheme 17.



Scheme 17: Formation of 4-nitrophenyl 6-((*tert*-butoxycarbonyl)amino)hexanoate (**39**).

DCC was again utilised due to the ease of filtering out the by-product DCU using a method similar to that used to obtain bismacrocycle **38**. NMR data of this crude revealed a large *p*-nitrophenol impurity. This was successfully removed from the desired product by chromatographic purification using 2% MeOH in DCM as eluent. CHN analysis along with NMR data confirmed the purity of the desired product **39**.

Successful isolation of the activated ester **39** led to a revival of the synthetic route to isolate the amine terminating bismacrocycle **32**. To retain stocks of the more valuable bismacrocycle **20**, this scheme was initially tested with monomacrocycle **15**.

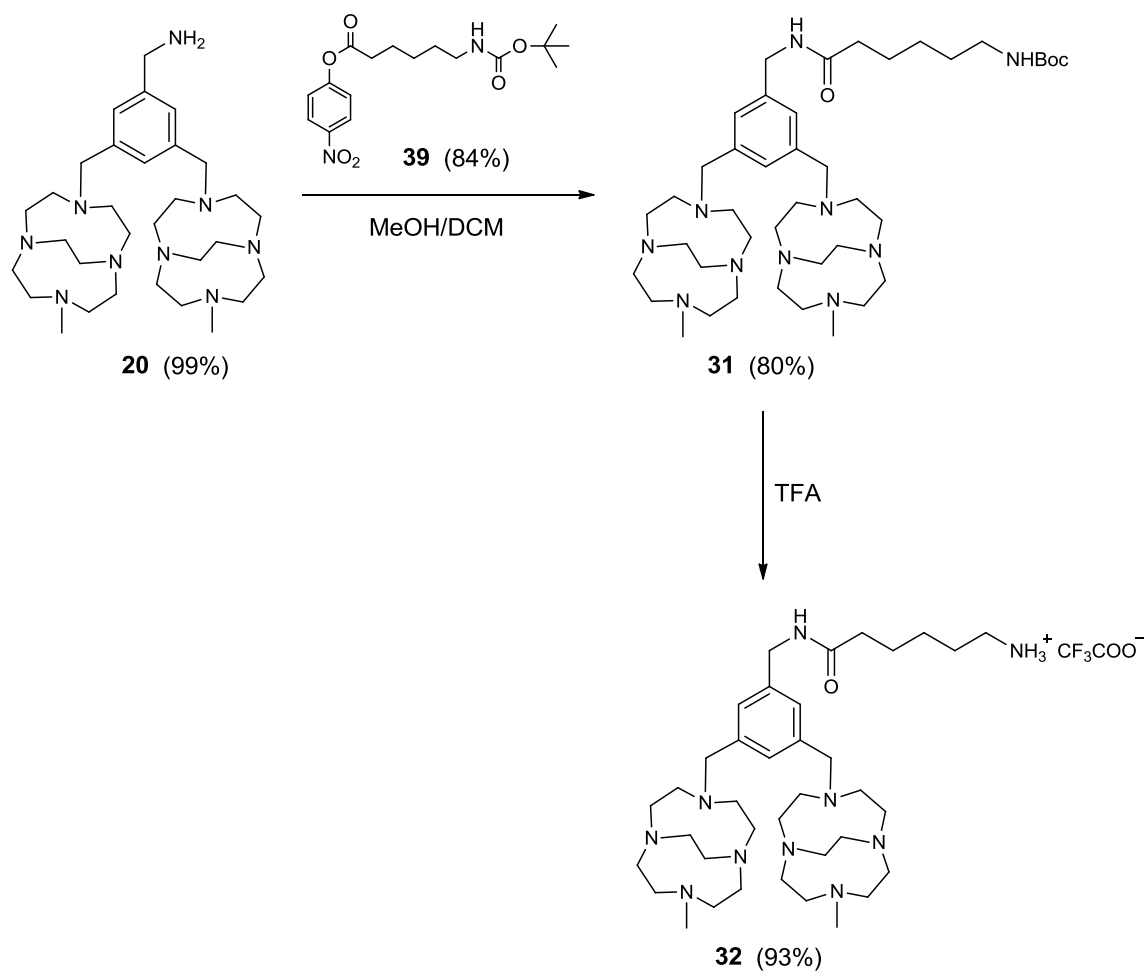


*Scheme 18: Synthetic route to obtain an amine terminating monomacrocycle (**41**) utilising p-nitrophenol chemistry.*

Monomacrocycle **15** was reacted with the activated ester **39**, using an adaption of the method outlined by Parker and co-workers, see Scheme 18. The work up afforded compound **40** in 58% yield. NMR data confirms successful attachment of the linker group due to the characteristic Boc peak, MS also confirms presence of

the product. Deprotection of compound **40** with TFA afforded the amine terminating macrocycle **41**, in 95% yield.

These encouraging results prompted monomacrocycle **15** to be substituted by bismacrocycle **20**. In an analogous synthetic route, bismacrocycle **31** was obtained *via* addition of the activated ester **39** to bismacrocycle **20** in 80% yield, see Scheme 19.



*Scheme 19: Synthetic route to obtain an amine terminating bismacrocycle (**32**) utilising *p*-nitrophenol chemistry.*

Analytical data confirmed presence of the product again using the distinctive peak associated with the Boc group to confirm attachment along with MS analysis. Subsequent deprotection of the amine group afforded bismacrocycle **32** in 79% yield. NMR confirmed the loss of the Boc peak. A test with ninhydrin also showed a

positive test for the presence of a primary amine (presence of a bold purple spot) further confirming successful deprotection of the Boc group.

### 3.4.3. A biotin activated ester; towards the synthesis of an *in vitro* evaluation probe.

The biotin-streptavidin pairing is one of the strongest known non-covalent interactions ( $K_d$  in the order of  $4 \times 10^{-14} \text{ M}^{-1}$ )<sup>171</sup> and has been widely utilised in the biochemical industry for use in biochemical assays,<sup>172-175</sup> Biotin or vitamin H is a low molecular weight organic compound essential for fatty acid production. Streptavidin is a 60 kDa protein comprising of four subunits each of which can bind to a biotin molecule.

Although a biotin-streptavidin construct will not provide a clinically relevant MFC because of immunogenic responses and the possibility of side reactions since it is a common system used by the body,<sup>176</sup> it would provide a useful *in vitro* evaluation tool. The initial idea was to attach a streptavidin-FITC conjugate to an activated ester biotin bismacrocylic compound, see Figure 58.

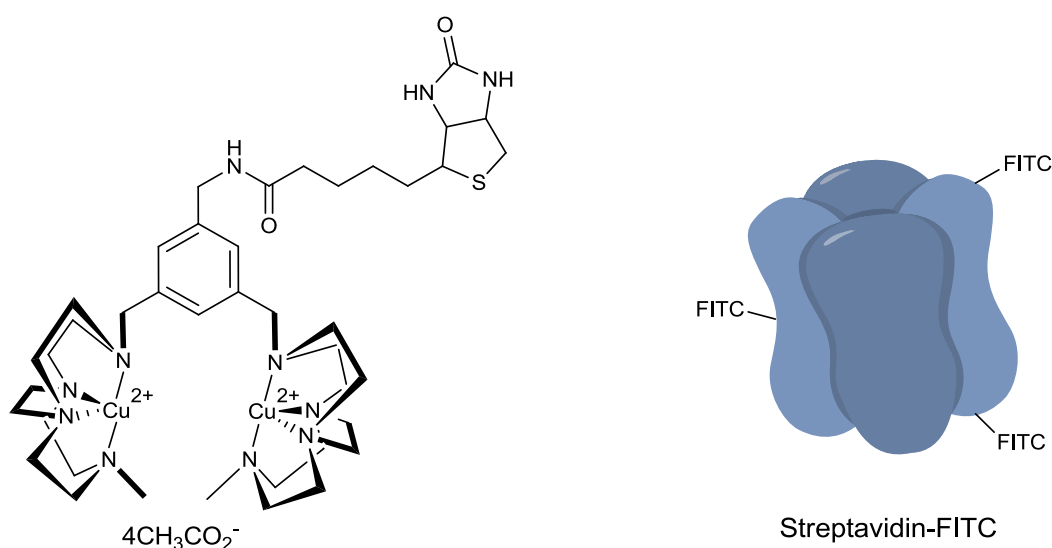
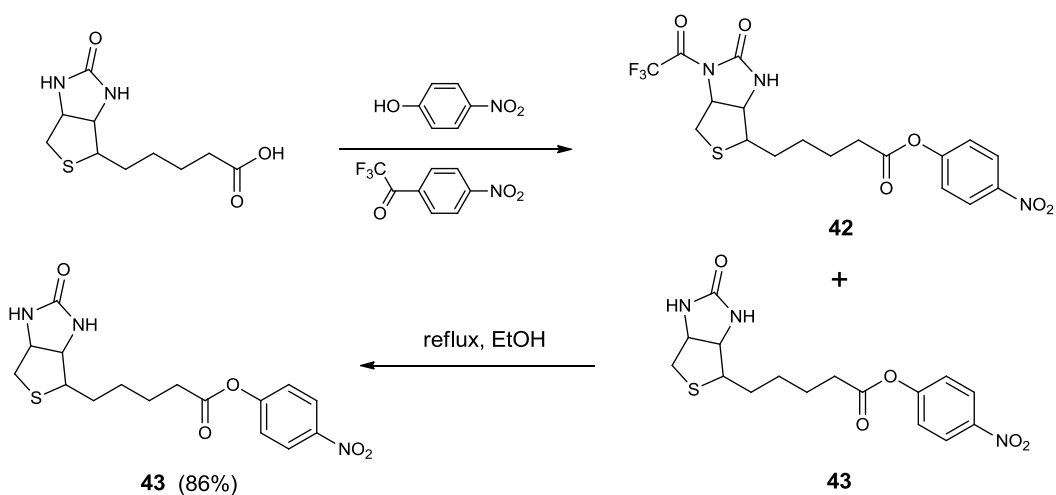


Figure 58: Components to produce a targeted multimodal *in vitro* evaluation probe. Note in the case of the copper(II) complex some anions and/or solvent molecules may be bound to the metal centres.

This MFC will have both targeting properties for the CXCR4 receptor with the potential to be a multimodal imaging probe by utilising the chelating abilities of the macrocycle for  $^{64}\text{Cu}$  and the fluorescent properties of the organic dye. This type of probe would provide a useful construct for cellular studies and demonstrate the potential of macrocyclic conjugates for use in living systems.

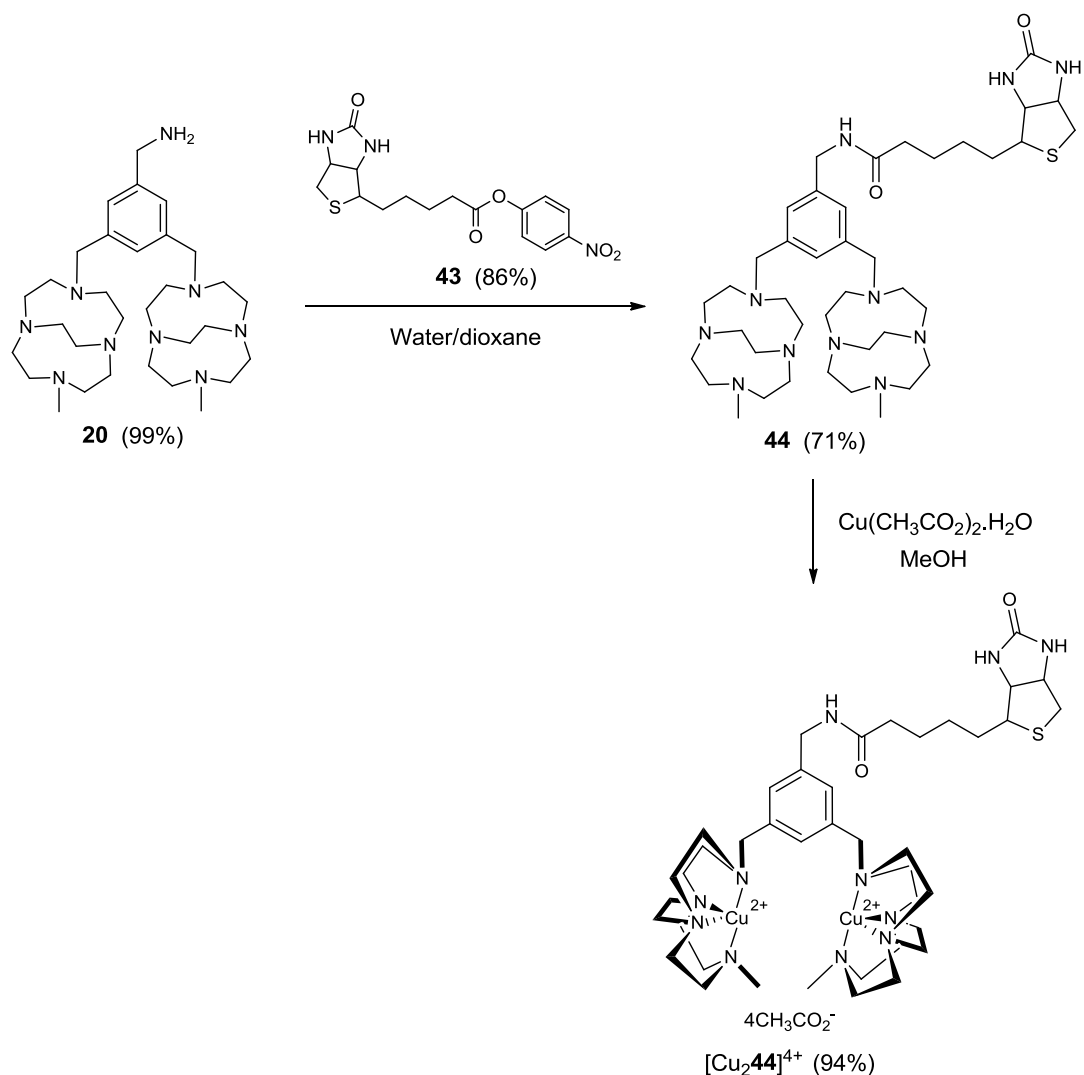
A search of the literature only gave one example of a group using *p*-nitrophenol to activate biotin to form an activated ester.<sup>177</sup> The synthesis of which is outlined in Scheme 20. The authors observed a mixture of biotin products in their initial reaction which they were subsequently able to purify to give the desired product by recrystallisation. Similar observations were made when repeating this reaction and recrystallisation gave the desired activated biotin (**43**) compound confirmed by  $^1\text{H}$  NMR,  $^{13}\text{C}$  NMR, MS and CHN analysis in 86% yield.



Scheme 20: Formation of an activated ester analogue of biotin (**43**) following conditions outlined by Bodanszky et al.<sup>177</sup>

This activated biotin compound (**43**) was successfully conjugated to bismacrocycle **20**, to give the biotin tagged bismacrocycle **44**, by the same method as that used to form bismacrocycle **37**. Followed by subsequent copper(II) complexation, see Scheme 21, using a standard preparation. Analytical data confirms the presence and purity of the final copper(II) containing compound  $[\text{Cu}_2\mathbf{44}]^{4+}$ . Observations within our own group have observed a series of side reactions when trying to attach

organic moieties to copper(II) containing macrocycles and so attachment to the free chelator was preferred.



*Scheme 21: Conjugation of biotin-p-nitrophenyl ester **43** to bismacrocycle **20** and subsequent complexation of copper(II) acetate to form  $[\text{Cu}_2\mathbf{44}]^{4+}$ . Note in the case of  $[\text{Cu}_2\mathbf{44}]^{4+}$ , anions and/or solvent molecules may coordinate to the metal centres.*

### 3.5. Conclusions

This chapter outlines the successful attachment of various spacer arms to the aminomethyl terminating bismacrocycle **20**, see Figure 59, utilising various synthetic pathways, such as ring opening of diglycolic anhydride and *p*-nitrophenol activation of an acidic group. These bismacrocylic compounds have the potential to conjugate to complementary porphyrin compounds to produce novel MFCs with diagnostic

and therapeutic capabilities. Further a *p*-nitrophenol activated biotin tag (**43**) has been successfully attached to bismacrocycle **20** and isolation of its copper(II) complex has been achieved  $[\text{Cu}_2\mathbf{44}]^{4+}$ . This compound has the potential for attachment to streptavidin-FITC to produce a useful *in vitro* evaluation probe.

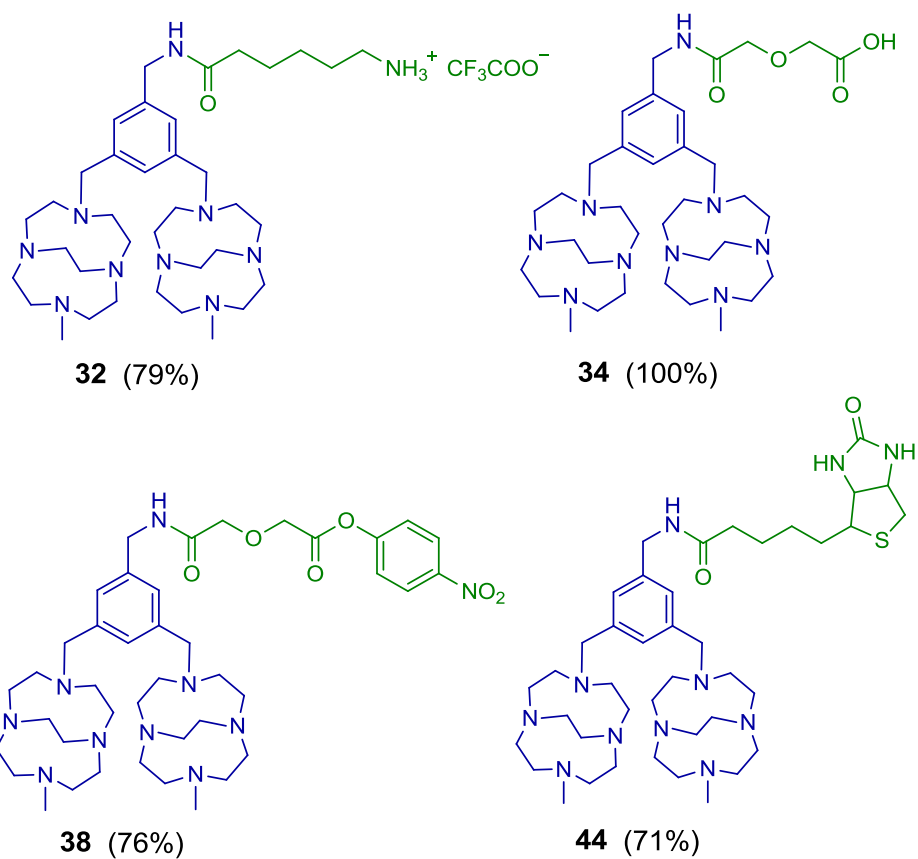


Figure 59: Structures of successfully isolated bismacrocycles bearing spacer arms.

## **Chapter 4**

# **Biological evaluation of mono and bismacrocycles as CXCR4 antagonists**

## **4.1. Introduction**

CXCR4 is a seven transmembrane (TM) G-protein coupled receptor (GPCR) with a surface rich in aspartate, histidine and tyrosine residues and has a negative electrostatic surface charge at physiological pH. It is found in the membrane of a range of cells including pre B cells, mast cells, adult CD34+ bone marrow progenitor cells, epithelial cells (intestinal and alveolar) and neurons.<sup>178, 179</sup> CXCR4 has a sole natural ligand; CXCL12, a 67 residue polypeptide with a positive electrostatic surface charge at physiological pH, mainly produced by stromal cells e.g. osteoblasts and fibroblasts in the bone marrow.<sup>43</sup> It was accepted that CXCR4 and CXCL12 have a monogamous relationship although there is now some evidence to suggest that CXCR4 also interacts with ubiquitin<sup>180</sup> and that CXCL12 causes a migrational response in specific cells when bound to CXCR7.<sup>181</sup>

CXCR4 is a signalling receptor and its interactions with its ligand CXCL12 are responsible for the proliferation, survival and chemotaxis of haematopoietic CD34+ progenitor cells in the bone marrow<sup>182</sup> as well as the migration and positioning of B-lymphocytes to secondary lymphoid organs<sup>183</sup> and the migration of antibody-secreting plasma blasts from the spleen in the bone marrow during an immune response.<sup>184</sup> CXCR4 also has an essential developmental role being responsible for organogenesis at the embryonic stage. A recent study examining human foetal tissue samples confirmed the widespread importance of CXCR4 in the bone marrow, heart, liver, kidney, brain and intestine during development.<sup>185</sup>

### **4.1.1. CXCR4 – role in cancer and HIV**

Chemokines and their receptors have been implicated in a wide spectrum of diseases, particularly inflammatory conditions such as asthma and rheumatoid arthritis. CXCR4 specifically has been shown to play a role in a number of diseases, most notably HIV and cancer.

In the 1990s, chemokines CCR5 and CXCR4 were shown to be co-receptors for HIV-1 cell entry. HIV enters target cells by fusion of the viral and target cell membranes,

this fusion is mediated by the viral envelope glycoproteins gp120 and gp41 and CD4 receptors on the target cell surface. Experiments showed that co-receptors were also required for this fusion to occur,<sup>186</sup> see Figure 60.

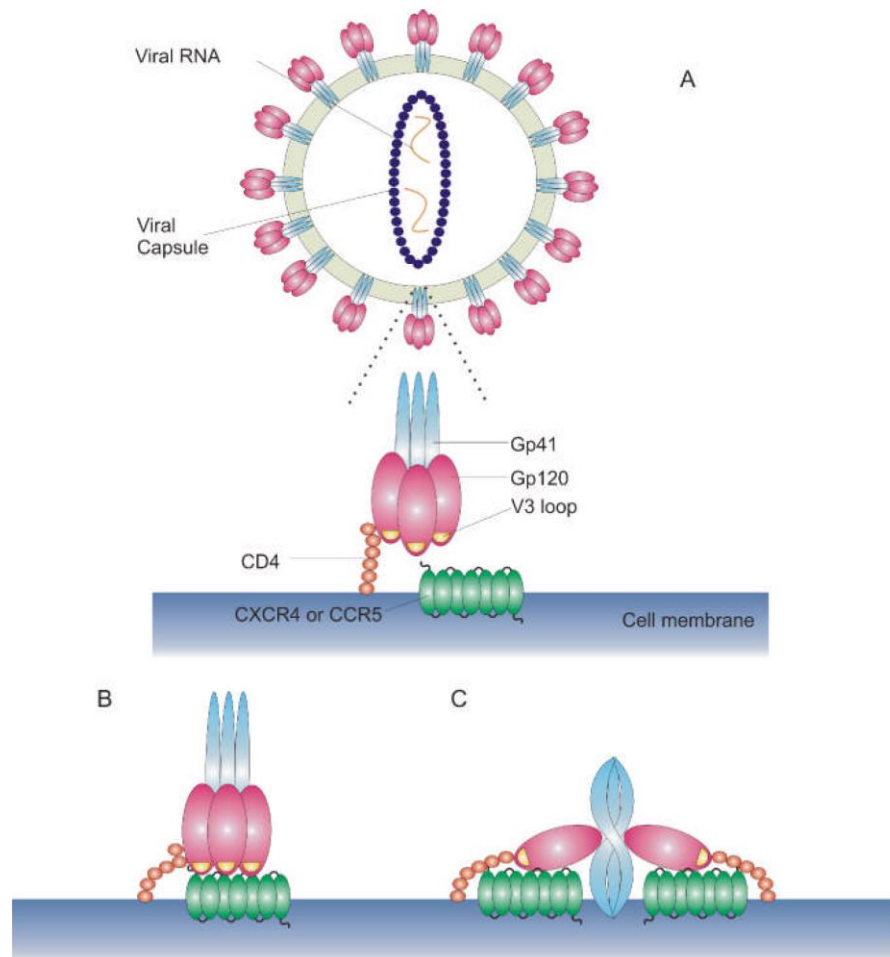


*Figure 60: HIV cell entry: A) interaction of gp120 with CD4, B) interaction of gp120 with CXCR4 or CCR5, C) conformational change in gp41 followed by fusion. (Reproduced from Curr. Med. Chem.)<sup>31</sup>*

CXCR4 has also been shown to have a role in the growth, survival and metastasis (spread) of tumours<sup>179, 187</sup> and is overexpressed on many different tumour types, see Chapter 1 section 1.2.1. The CXCR4/CXCL12 gradient has been shown to play a critical role in determining the metastatic destination of breast cancer by acting directly on tumour cell migration and invasion.<sup>43</sup>

#### **4.1.2. CXCR4 antagonists**

The role of CXCR4 in these widespread diseases has led to a huge effort in the design and implementation of CXCR4 antagonists to block the receptors ability to either be involved in HIV cell entry or along with its ligand CXCL12 be involved in the metastatic spread of cancer cells. Initially, the therapeutic potential of targeting CXCR4 was focused on the development of anti-HIV drugs and several peptidic compounds and non-macrocyclic small molecules have been developed as 'HIV entry inhibitors'.<sup>31</sup> T22; a cationic peptide was one of the first developed<sup>188</sup> but its analogue T140 proved to be a stronger inhibitor against HIV-1 cell entry,<sup>189</sup> ALX40-4C; a polypeptide gave an IC<sub>50</sub> of 3 nM in an MT-4 assay against X4 strains of HIV,<sup>190</sup> a less potent peptide CGP64222 demonstrated a potency of 3-9 μM in the same assay but over a wide range of HIV strains.<sup>191</sup> A small molecule antagonist KRH-1636 was developed in Japan and showed an EC<sub>50</sub> of 19 nM in at MT-4 assay against X4 strains.<sup>192</sup> The small molecule antagonists AMD070 and AMD3465 were developed in the USA,<sup>193, 194</sup> AMD070 boasts oral availability whilst AMD3465 inhibits binding of CXCL12 in the nanomolar range.

##### **4.1.2.1. AMD3100**

Arguably the most successful CXCR4 antagonist is the bismacrocycle AMD3100 (1,1'-[1,4-phenylenebis(methylene)]-bis-[1,4,8,11-tetraazacyclotetradecane]), see Figure 12, section 1.3, showing potency at sub-micromolar concentrations against HIV-1 and HIV-2.<sup>69</sup> AMD3100 was licensed for clinical use in 2008 as a stem cell mobilising agent under the brand name Plerixafor for use in non-Hodgkin's lymphoma and multiple myeloma patients.<sup>195</sup> As previously mentioned AMD3100 is actually thought to be a prodrug and in fact [Zn<sub>2</sub>AMD3100]<sup>4+</sup> is the active species at physiological pH, with the zinc(II) ions being sequestered from the blood.<sup>139</sup> [Zn<sub>2</sub>AMD3100]<sup>4+</sup> shows a 50-fold increase in binding to CXCR4 and evidence suggests that this is due to the formation of coordinate bonds between the metal ion and aspartate residues in the binding cleft of CXCR4.<sup>196</sup>

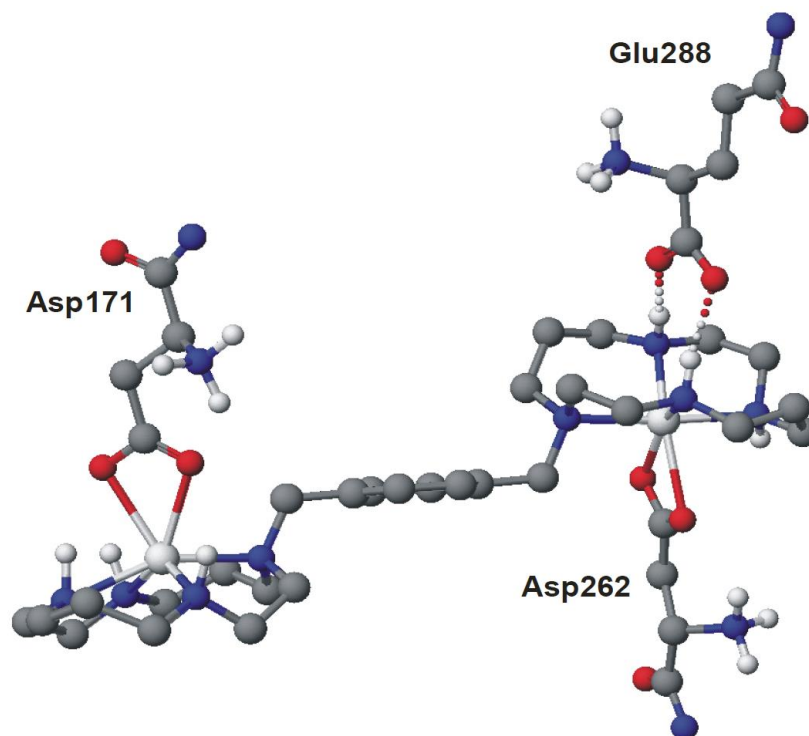


Figure 61: Ball and stick representation of the interactions of  $[Zn_2AMD3100]^{4+}$  with Asp262, Asp171 and Glu288 of CXCR4. (Reproduced from *J. Am. Chem. Soc.*)<sup>113</sup>

Gerlach *et al.* identified Asp262 and Asp171 as the most important amino acids for AMD3100 receptor binding, with Glu288 also potentially forming H-bonding interactions, see Figure 61.<sup>113, 197</sup>

## 4.2. Previous studies

The amount of literature outlining the efficacy and affinity of macrocyclic ligands as CXCR4 antagonists is somewhat limited, particularly in comparison to the wealth of literature regarding the design and synthesis of macrocyclic ligands.

De Clercq and co-workers were the first group to evaluate a large array of bismacrocyclic compounds for anti-HIV activity in MT-4 cells, see Table 2 and Figure 62 for select examples.<sup>141</sup> Their studies concluded that potent anti-HIV activity and low cytotoxicity was dependent on the substitution pattern connecting macrocycles having 12-14 members. A *meta*-substitution pattern gave the highest potency for 12

and 13-membered rings whereas *para*-substitution gave the highest potency for 14-membered rings.

Bismacrocyclic	EC <sub>50</sub> (μM)		CC <sub>50</sub> (μM)
	HIV-1 (III-B)	HIV-2 (III-B)	
L <sup>26</sup>	0.075	0.536	55
L <sup>27</sup>	0.322	2.360	20
L <sup>28</sup>	0.041	0.062	>184
L <sup>29</sup>	0.167	0.234	>208
L <sup>30</sup>	1.357	3.128	>168
L <sup>31</sup>	0.034	0.042	>421
AMD3100	0.004	0.006	>421

Table 2: Anti-HIV activity of bismacrocyclics with varying ring size. (Adapted from *J. Med. Chem.*)<sup>141</sup>

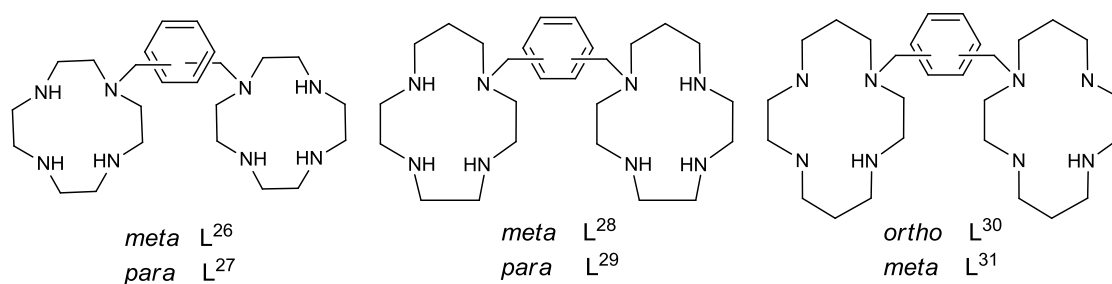


Figure 62: *ortho*-, *meta*- and *para*-substituted 12-14-membered azamacrocyclics; L<sup>26</sup>-L<sup>31</sup> as outlined by De Clercq and co-workers.<sup>141</sup>

A similar study looking into the activity of pyridine and pyrazine linked biscyclams found that activity was dependent on the substitution of the heteroaromatic linker. Pyridine linkers in a 2,6- or 3,5- substitution patterns were found to be potent inhibitors of HIV-1 and HIV-2 in MT-4 cells whereas 2,4- and 2,5- substitution patterns not only showed reduced potency but were also very toxic to MT-4 cells.<sup>142</sup> De Clercq and co-workers have recently demonstrated that not all eight nitrogen atoms in the structure of AMD3100 are necessary for high potency, see Figure 63.<sup>198</sup> Accordingly they synthesised a range of monomacrocyclic compounds including

AMD3465, L<sup>49</sup> and L<sup>50</sup>, see Figure 63, which showed EC<sub>50</sub>'s against the cytopathic effects of HIV-1 of 9, 1 and 4 nM, respectively, comparable to AMD3100 (EC<sub>50</sub> = 4 nM against HIV-1). These monomacrocyclic compounds represent antagonists which have the properties suitable for HIV treatment *via* oral administration.

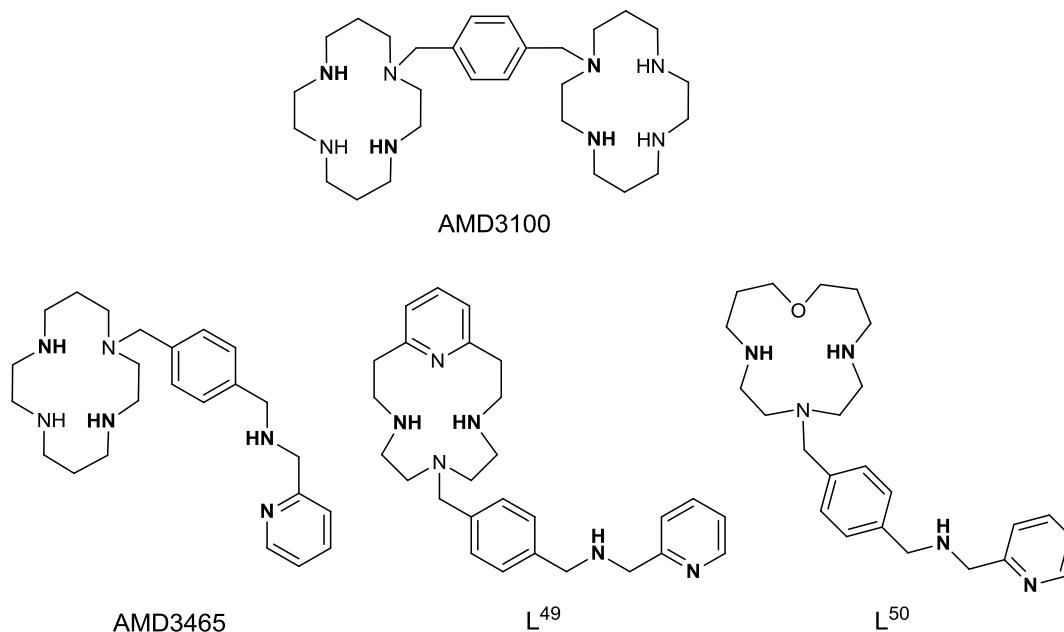


Figure 63: Key nitrogen atoms required for potency are highlighted in the structure of AMD3100 along with the structures of AMD3465, L<sup>49</sup> and L<sup>50</sup>.<sup>198</sup>

Archibald and co-workers have evaluated the potential of their configurationally restricted bismacrocycles as CXCR4 antagonists. The cytopathic and cytotoxic properties of the SB bicyclam ligand L<sup>32</sup>, see Figure 64, and its zinc(II)<sup>58</sup> and copper(II) complex<sup>199</sup> have been evaluated, see Table 3, along with the copper(II) complex of the CB bicyclam ligand L<sup>33</sup>,<sup>63</sup> see Figure 64, using AMD3100 and [Zn<sub>2</sub>AMD3100]<sup>4+</sup> as controls. Their results show that the 'free' ligand L<sup>32</sup> is considerably less active than AMD3100 which can be rationalised by the reduced number of possible H-bonding interactions which can occur (6 for AMD3100, 2 for L<sup>32</sup>).<sup>58</sup> They noted that incorporation of a metal centre had a dramatic effect on the anti-viral activity, more so when zinc(II) was involved. [Zn<sub>2</sub>L<sup>32</sup>]<sup>4+</sup> is three orders of magnitude more potent than its corresponding 'free' ligand L<sup>32</sup>, demonstrating the importance of the coordination interaction to chemokine receptor binding. [Zn<sub>2</sub>L<sup>32</sup>]<sup>4+</sup> also shows higher anti-HIV activity than AMD3100 and [Zn<sub>2</sub>AMD3100]<sup>4+</sup>

validating the strategy of configurational restriction. Following on from this both copper(II) complexes ( $[\text{Cu}_2\text{L}^{32}]^{4+}$  and  $[\text{Cu}_2\text{L}^{33}]^{4+}$ ) showed sub-micromolar anti-HIV activities but the CB complex ( $[\text{Cu}_2\text{L}^{33}]^{4+}$ ) superseded the SB complex ( $[\text{Cu}_2\text{L}^{32}]^{4+}$ ). CB complexes are restricted to a *cis-V* configuration whereas the SB complex is restricted to a *trans-II* configuration. These results suggest that a *cis-V* configuration may be an ideal property for high binding affinity to be achieved. This is because configurationally restricting the macrocycle provides a pre-organised, rigid chelator which can only adopt one 'shape' for binding.<sup>63</sup> These effects optimise coordinate bond formation with the CXCR4 receptor to give improved potency.

Compound	HIV strain	Av EC <sub>50</sub> <sup>a</sup> ( $\mu\text{M}$ )	Av CC <sub>50</sub> <sup>b</sup> ( $\mu\text{M}$ )	SI <sup>c</sup>
$\text{L}^{32}$	HIV-1 (III <sub>B</sub> )	6.980	>225.0	>32
	HIV-2 (ROD)	23.200	>225.0	>10
$[\text{Zn}_2\text{L}^{32}]^{4+}$	HIV-1 (III <sub>B</sub> )	0.003	60.6	24225
	HIV-2 (ROD)	0.004	60.6	15140
$[\text{Cu}_2\text{L}^{32}]^{4+}$	HIV-1 (III <sub>B</sub> )	0.026	>150.0	>5770
	HIV-2 (ROD)	0.056	>150.0	>2680
$[\text{Cu}_2\text{L}^{33}]^{4+}$	HIV-1 (III <sub>B</sub> )	0.004	>115.0	>26744
AMD3100	HIV-1 (III <sub>B</sub> )	0.011	>225.0	20455
$[\text{Zn}_2\text{AMD3100}]^{4+}$	HIV-1 (III <sub>B</sub> )	0.008	>225.0	28125

Table 3: Anti-HIV activity, cytotoxicity (CC<sub>50</sub>) and selectivity index (SI) for  $\text{L}^{32}$ ,  $\text{L}^{33}$  and their metal complexes. <sup>a</sup> Average effective concentration (EC) to reduce the HIV-induced cytopathic effect by 50% in MT-4 cells. <sup>b</sup> Concentration required to have a cytotoxic effect reducing MT-4 cell viability by 50%. <sup>c</sup>  $SI = CC_{50}/IC_{50}$ .

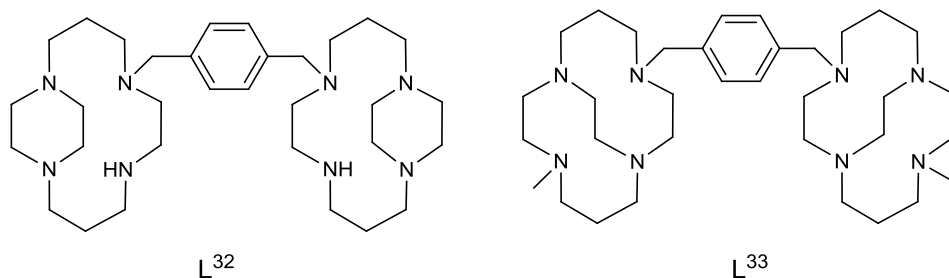


Figure 64: Structures of configurationally restricted biscyclams  $L^{32}$  and  $L^{33, 58, 63}$ .

Recently Archibald and co-workers have also evaluated the affinity of *meta*-substituted bismacrocycles. Evaluating the copper(II) and zinc(II) complexes of  $L^{48}$  and the copper(II), zinc(II) and nickel(II)<sup>132</sup> complexes of  $L^{51}$ , see Figure 65. Calcium signalling studies were carried out to establish the concentration of ligand needed to reduce the 'normal' signalling of CXCR4, that is triggered by CXCL12, by 50% ( $IC_{50}$ ) as well as anti-HIV activity, see Table 4.

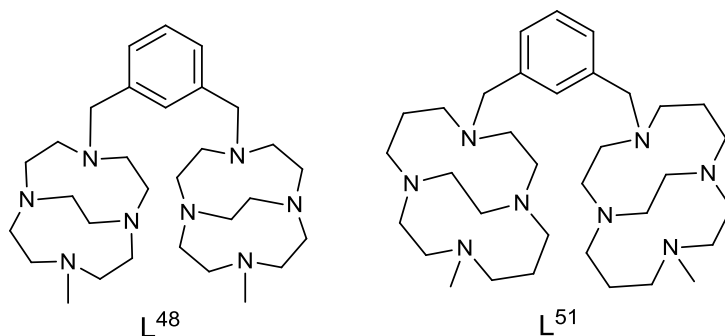


Figure 65: Structures of the *meta*-substituted bismacrocycles  $L^{48}$  and  $L^{51}$ .

Metal complexes of  $L^{48}$  were noted as particularly potent CXCR4 antagonists, demonstrating low  $EC_{50}$  values indicating high anti-HIV activity.  $[Cu_2L^{48}]^{4+}$  showed comparable affinity to AMD3100 (*ca.*  $IC_{50}$  10.4 nM vs. 11 nM, respectively) but the analogous zinc(II) complex  $[Zn_2L^{48}]^{4+}$  showed over a 3-fold higher affinity for CXCR4. One explanation for the potent activity of these complexes could be that the metal substitution pattern of the cyclen rings allows for an ideal shape for binding, allowing the metal ions to bind strongly to the aspartate residues in the binding pocket of CXCR4.

Compound	Ca <sup>2+</sup> flux <sup>a</sup> IC <sub>50</sub> (nM)	Anti-HIV-1 <sup>b</sup> EC <sub>50</sub> <sup>c</sup> (nM)
[Cu <sub>2</sub> L <sup>48</sup> ] <sup>4+</sup>	10.4	3.6
[Zn <sub>2</sub> L <sup>48</sup> ] <sup>4+</sup>	3.3	3.4
[Cu <sub>2</sub> L <sup>51</sup> ] <sup>4+</sup>	63.0	24.9
[Zn <sub>2</sub> L <sup>51</sup> ] <sup>4+</sup>	874.0	398.0
[Ni <sub>2</sub> L <sup>51</sup> ] <sup>4+</sup>	194.0	398.0
AMD3100	11.0	180.0

Table 4: Calcium signalling and anti-HIV data for metal-containing meta-substituted bismacrocycles using AMD3100 as a control. <sup>a</sup> U87.CXCR4 cell line. IC<sub>50</sub> is the concentration of the compound required to inhibit 50% of the CXCL12 induced Ca<sup>2+</sup> signal. <sup>b</sup> CD4+CXCR4+T cell line, MT-4 cells, using the HIV-1 X4 strain III<sub>B</sub>. <sup>c</sup> Average EC<sub>50</sub> to reduce the HIV-induced cytopathic effect by 50% in MT-4 cells.

The metal complexes of L<sup>51</sup> showed lower affinity for CXCR4 in comparison to the metal complexes of L<sup>48</sup> by two orders of magnitude, but it should be noted that they are still active at sub μM levels. The detrimental effect on affinity could be because of the larger ring size of cyclam rings as opposed to cyclen rings, indicating that a *meta*-substitution pattern may not be ideal for 14-membered rings.

Tanaka *et al.* have also evaluated the anti-HIV activity, cytotoxicity and binding activity of bismacrocycles.<sup>149</sup> They focused on spatial positioning looking at various *meta*- and *para*-substituted bismacrocycles, several of which had been previously synthesised by De Clercq and co-workers.<sup>141, 142</sup> Zinc(II) and copper(II) complexes of all of their bismacrocyclic ligands were made and several demonstrated high binding affinity for CXCR4 based on the inhibition of [<sup>125</sup>I]CXCL12 in Jurkat cells.

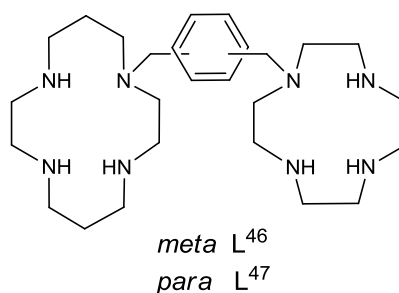


Figure 66: Structure of unsymmetrical bismacrocycles L<sup>46</sup> and L<sup>47</sup>.<sup>149</sup>

Zinc(II) complexes of L<sup>46</sup> and L<sup>47</sup>, see Figure 66, were their two most active compounds (IC<sub>50</sub> = 11 and 8 nM, respectively), comparable to the binding affinities of AMD3100 and [Zn<sub>2</sub>AMD3100]<sup>4+</sup> (IC<sub>50</sub> = 11 and 8 nM, respectively). These zinc(II) complexes also showed slightly higher anti-HIV activity against X4-HIV-1 in MT-4 cells (EC<sub>50</sub> = 39 and 36 nM, respectively) but showed high cytotoxicity in comparison to similar compounds.<sup>58, 141</sup>

#### 4.2.1. Strategy

This chapter aims to explore the binding affinity of all the mono- and bismacrocylic compounds outlined in Chapter 2 using competition binding assays and calcium flux studies (using AMD3100 as a control). Anti-HIV activity will also be presented for bismacrocylic compounds and compared to the clinically licensed drug AMD3100. A detailed biological study of the lead compound [Cu<sub>2</sub>**20**]<sup>4+</sup> is presented. The effect on affinity of spacer arms attached to bicyclic compounds has also been evaluated using two specific examples.

### 4.3. Biological assays

Biological assays were used to determine the affinity and potency of macrocylic compounds for CXCR4 in cell lines known to overexpress the receptor.

#### 4.3.1. Antibody competition binding assay

This process involves competing each macrocycle with a mAb specific to CXCR4 in a competition binding assay to allow a % of inhibition to be determined. These studies were carried out in Jurkat cells, a human leukaemia cell line known to overexpress the CXCR4 receptor ('normal' cell = 10,000 copies of CXCR4, Jurkat cell

= 140,000 copies of CXCR4). The ligand under study was incubated with the Jurkat cells in a large excess to saturate all of the CXCR4 receptors on the cell surface followed by incubation with a mAb specific to the CXCR4 receptor. The amount of anti-CXCR4 antibody bound can be assessed using a secondary fluorescently tagged antibody to bind to the primary mAb.

Flow cytometry was used to detect how much CXCR4 specific mAb is attached to the receptors (using the fluorescent property of the secondary Ab) and consequently how much of the ligand under study is bound to the receptor. Flow cytometry works on the principle of detecting the properties of individual cells (in this case whether they are fluorescently tagged or not). If fluorescence is observed this means the mAb is bound to the CXCR4 receptors, conversely if no fluorescence is observed then the ligand under study must be bound to the receptor. The amount of fluorescence can then be quantified through the use of controls. A negative control contains only Jurkat cells suspended in PBS and measures the background level fluorescence. The positive control contains the cells incubated with the antibody specific to the CXCR4 receptor and the secondary fluorescently tagged antibody giving the maximum amount of fluorescence that could be observed i.e. the fluorescence when all the receptors are occupied by the mAb specific to the CXCR4 receptor.

#### **4.3.2. Calcium(II) flux studies**

Intracellular calcium(II) flux studies probe the blocking of the natural signalling process between CXCR4 and the small protein that activates it, CXCL12. CXCL12 is the sole natural ligand for the CXCR4 receptor and upon binding a host of downstream effects occur, see Figure 67, one of which is the intracellular release of calcium(II) ions.

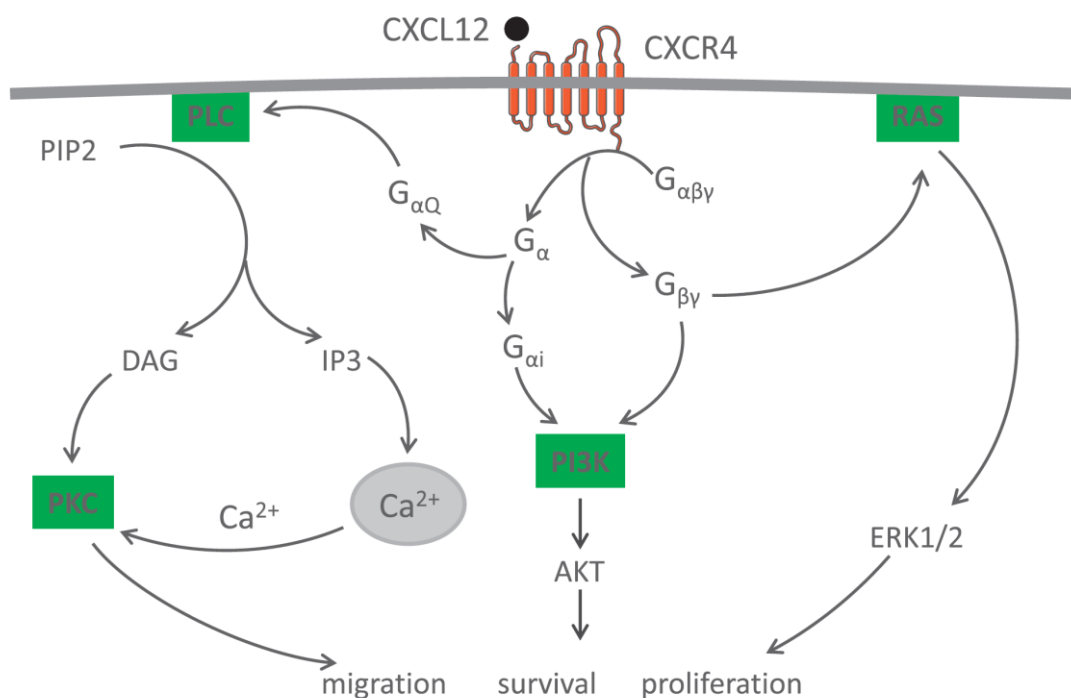


Figure 67: Downstream pathways caused by the stimulation of CXCR4 by its sole natural ligand CXCL12/SDF1 $\alpha$ .<sup>200</sup>

Different concentrations of the antagonist are incubated with the CXCR4 expressing cells to block the signalling between CXCR4 and CXCL12; hence reducing the calcium(II) ions released in the presence of CXCL12. The intracellular release of calcium(II) ions is detected with a calcium(II) sensitive dye, which fluoresces on binding to a calcium(II) ion. Therefore if the antagonist blocks CXCL12 from binding the number of calcium(II) ions released will decrease resulting in a decrease in the observed fluorescence. The abrogation of this flux was recorded at a series of antagonist concentrations to give a value whereby a 50% reduction in signal was observed (IC<sub>50</sub>). These studies were carried out in U87.CD4.CXCR4 cells, a human glioblastoma cell line which has been transfected to express high levels of CXCR4.<sup>201</sup>

#### 4.4. Monomacrocycles as CXCR4 antagonists

The series of monomacrocyclic metal complexes outlined in Chapter 2, see Figure 43 were evaluated as antagonists for CXCR4 using a competition binding assay and the signal blocking calcium flux study.

The results for both assays are presented in Table 5, using the clinically licensed drug AMD3100 as a comparator. As well as establishing the IC<sub>50</sub> values of these complexes, cytotoxic effects were also probed. CC<sub>50</sub> values are presented, which is the concentration needed to reduce cell viability by 50%. Selectivity indices (SI) are also presented as an indication of the toxicity verses the antagonist potency for each of the metal complexes.

Cell line	U87.CD4.CXCR4			Jurkat
Complex	Av <sup>a</sup> IC <sub>50</sub> <sup>b</sup> (μM)	Av <sup>a</sup> CC <sub>50</sub> <sup>c</sup> (μM)	SI <sup>d</sup>	Av <sup>a</sup> % inhibition
[Cu8] <sup>2+</sup>	2.200	93.71	45	42
[Zn8] <sup>2+</sup>	0.034	186.94	623	45
[Ni8] <sup>2+</sup>	8.330	189.31	23	32
[Cu9] <sup>2+</sup>	3.556	200.63	56	19
[Zn9] <sup>2+</sup>	0.012	14.30	1430	38
[Ni9] <sup>2+</sup>	0.660	106.16	161	42
[Cu14] <sup>2+</sup>	0.222	53.59	244	19
[Zn14] <sup>2+</sup>	0.273	182.17	675	52
[Ni14] <sup>2+</sup>	7.850	35.99	5	51
[Cu15] <sup>2+</sup>	0.468	88.48	188	26
[Zn15] <sup>2+</sup>	0.259	191.98	738	37
[Ni15] <sup>2+</sup>	0.453	106.16	161	40
AMD3100	0.031	>125.00	>4032	72

Table 5: The IC<sub>50</sub> (calcium signalling), CC<sub>50</sub> and SI of a series of novel metal containing monomacrocycles in the cell line U87.CD4.CXCR4 are presented along with their % of inhibition of anti-CXCR4 mAb binding in Jurkat cells. <sup>a</sup> Experiments were run in either duplicate or triplicate and the results averaged. <sup>b</sup> Concentration required to reduce the level of Ca<sup>2+</sup> ions observed during a 'normal' signalling process by 50% (IC<sub>50</sub>) in U87.CD4.CXCR4 cells. <sup>c</sup> Concentration required to reduce cell viability by 50% (CC<sub>50</sub>) in U87.CD4.CXCR4 cells. <sup>d</sup>

$$SI = CC_{50}/IC_{50}$$

The first thing to note is that none of the metal containing monomacrocycles show high % mAb inhibition in Jurkat cells in comparison to AMD3100. This does not necessarily mean they do not act as antagonists just that they cannot compete effectively with the anti-CXCR4 mAb, due to the fact that only one coordinate bond

can form with a single metal centre. This trend has been observed previously within our group and so was not unexpected. However, what monomacrocyclic ligands possess is the potential for improved pharmacological properties such as oral bioavailability due to their reduced molecular charge and lower molecular weight in comparison to their bismacrocyclic counterparts. This study was not aimed at finding a high affinity antagonist but to assess whether there were any standout candidates for further investigation.

[Zn9]<sup>2+</sup> was the most potent metal complex, showing a 2.5-fold increase in affinity for CXCR4 in comparison to AMD3100 (IC<sub>50</sub> = 12 nM vs. 31 nM) but was more cytotoxic. Looking at the SI, zinc(II) complexes regardless of ring size (12 or 14 membered) and configuration (SB or CB) showed higher activity than their analogous copper(II) and nickel(II) complexes. In fact looking solely at which metal ion is involved the trend appears to be zinc(II)>copper(II)=nickel(II). This trend has been previously observed in our group with metal complexes of bismacrocyclic L<sup>32,199</sup> see section 4.2. Explanations for the high activity observed when zinc(II) is present could be that relative to copper(II) and nickel(II) the zinc(II) ion forms stronger binding interactions with the protein. This may be attributed to the greater flexibility in coordination geometry preferences of a d<sup>10</sup> metal ion. On the whole CB complexes showed higher affinity for CXCR4 than SB complexes, with the increase in potency accompanied by a slight increase in cytotoxicity. This trend has also been previously observed<sup>63</sup> and can be attributed to the restricted *cis*-V configuration of CB complexes, there is some evidence to suggest that a *cis*-V configuration is the optimum configuration for binding to the aspartate residues in the binding cleft of CXCR4.<sup>202</sup>

In conclusion zinc(II) monomacrocycles offer the most potential for improved pharmacological properties of all the monomacrocycles tested. [Zn9]<sup>2+</sup> showed the highest affinity for CXCR4 over a 2.5-fold better affinity than AMD3100 but did have higher cytotoxicity in the cells. A study into the binding profile of [Zn9]<sup>2+</sup> could reveal why and improvements could be made, for example a study into whether anions have any effect on toxicity could provide some very useful information.

## **4.5. Bismacrocycles as CXCR4 antagonists**

Metal containing bismacrocycles were evaluated along with their 'free' ligand counterparts using mAb competition binding assays and CXCL12 signal blocking calcium flux studies. The anti-HIV activities of these macrocycles were also evaluated.

### **4.5.1. Evaluation of binding affinity**

Bismacrocyclic compounds have the potential to be high affinity antagonists for CXCR4 due to the potential of each of the metal centres to form a coordinate bond with Asp262 and Asp171 respectively in the binding cleft of CXCR4. This has been established for AMD3100 using site directed mutagenesis studies. This arrangement is possible due to the high flexibility of the CXCR4 receptor. Stevens and co-workers published the crystal structure of CXCR4 in 2010, and docking studies could potentially provide the 'real' location of residues key for receptor binding.<sup>37</sup> However, the high flexibility may be problematic when correlating the crystal structure with other data. A distance of 16 Å between Asp262 and Asp171 is observed in the X-ray structure, see Figure 68.

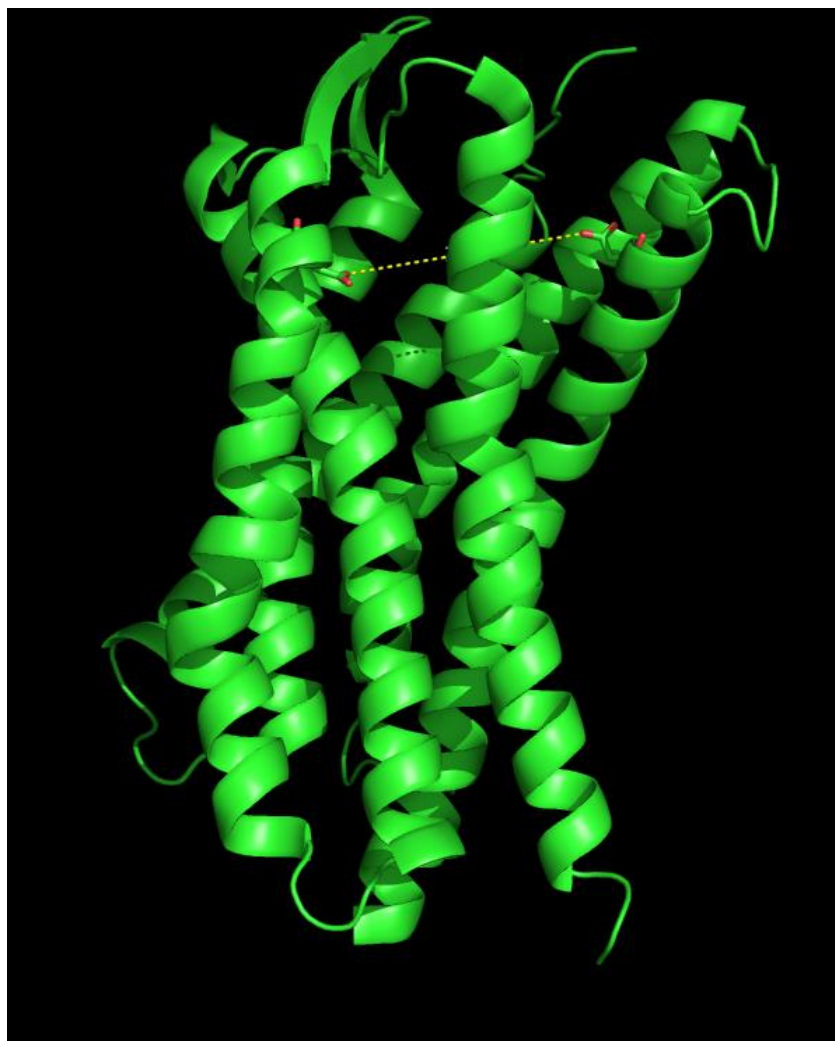


*Figure 68: A representation of the crystal structure of CXCR4 showing the distance between Asp262 and Asp171 (the residues key for binding to AMD3100) ca. 16 Å. (Pymol using pdb data file).*

Interestingly a distance of ca. 12 Å is an averaged value between the two metal centres of AMD3100, see Figure 69, leading to the conclusion that the receptor must flex in order to accommodate the antagonist. Hence the protein conformation can change significantly. This high flexibility means that to give an accurate picture of the interaction between a bicyclam type antagonist and the protein, the CXCR4 receptor would need to be crystallised with the antagonist bound. The crystal structure is valuable but only provides a snapshot of protein configuration and so is not useful for docking studies but it can be used as the starting point for more

accurate modelling studies to understand the binding modes of macrocyclic antagonists.

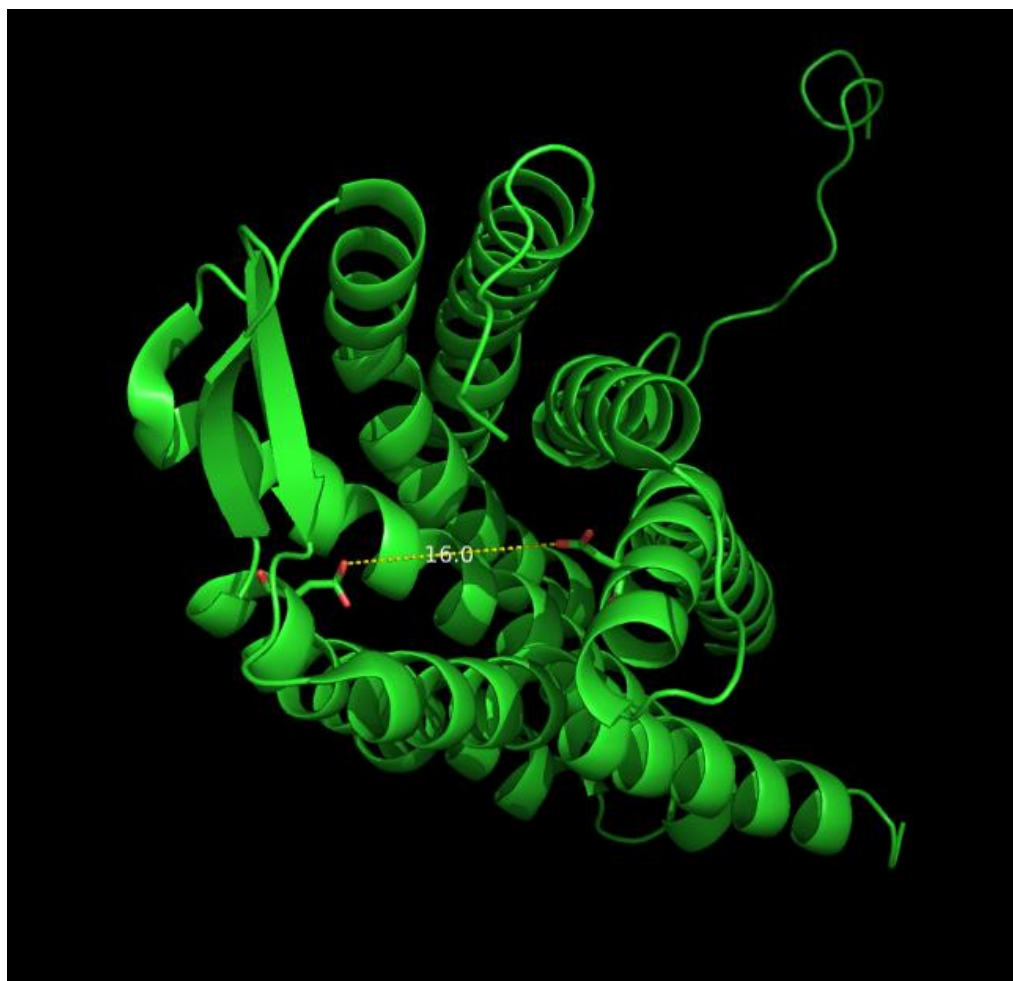


*Figure 69: A homology model of the crystal structure of CXCR4 outlining the distance between the two metal centres in AMD3100 ca. 12 Å. (pymol using the pdb data file).*

#### **4.5.2. Antibody competition and signal blocking assays**

Antibody competition binding assays as well as CXCL12 signal blocking calcium flux studies were performed, see Table 6, to assess the binding affinity of a series of bismacrocycles whose synthesis was presented in Chapter 2.

Cell line	U87.CD4.CXCR4			Jurkat
	Av <sup>a</sup> IC <sub>50</sub> <sup>b</sup> (nM)	Av <sup>a</sup> CC <sub>50</sub> <sup>c</sup> (μM)	SI <sup>d</sup>	Av <sup>a</sup> % inhibition
<b>19</b>	8520	81.55	10	85
[Cu <sub>2</sub> <b>19</b> ] <sup>4+</sup>	14	AD	-	97
<b>20</b>	2210	89.67	41	87
[Cu <sub>2</sub> <b>20</b> ] <sup>4+</sup>	39	AD	-	96
[Zn <sub>2</sub> <b>20</b> ] <sup>4+</sup>	98	44.65	456	88
[Ni <sub>2</sub> <b>20</b> ] <sup>4+</sup>	143	53.88	377	90
<b>24</b>	26	60.26	2318	69
[Zn <sub>2</sub> <b>24</b> ] <sup>4+</sup>	7	120.11	17159	18
[Cu <sub>2</sub> <b>24</b> ] <sup>4+</sup>	AD	AD	-	25
<b>27</b>	27000	98.37	4	48
[Cu <sub>2</sub> <b>27</b> ] <sup>4+</sup>	21	46.23	2201	89
<b>28</b>	22000	52.91	2	85
[Cu <sub>2</sub> <b>28</b> ] <sup>4+</sup>	11	39.99	3635	96
[Zn <sub>2</sub> <b>28</b> ] <sup>4+</sup>	51	49.44	969	60
[Ni <sub>2</sub> <b>28</b> ] <sup>4+</sup>	93	22.06	237	34
AMD3100	31	>125.00	4032	72

Table 6: The IC<sub>50</sub> (calcium signalling), CC<sub>50</sub> and SI of a series of novel bismacrocyces and their metal complexes in the cell line U87.CD4.CXCR4 are presented along with their % of inhibition of anti-CXCR4 mAb binding in Jurkat cells. <sup>a</sup> Experiments were run in either duplicate or triplicate and the results averaged. <sup>b</sup> Concentration required to reduce the level of Ca<sup>2+</sup> ions observed during a 'normal' signalling process by 50% (IC<sub>50</sub>) in U87.CD4.CXCR4 cells. <sup>c</sup> Concentration required to reduce cell viability by 50% (CC<sub>50</sub>) in U87.CD4.CXCR4 cells. <sup>d</sup>  $SI = CC_{50}/IC_{50}$ . AD = Awaiting data.

All bismacrocyces (free ligands and metal complexes) were confirmed to bind to the CXCR4 receptor by flow cytometry displacement studies with an anti-CXCR4 antibody, with the exception of [Zn<sub>2</sub>**24**]<sup>4+</sup>, [Cu<sub>2</sub>**24**]<sup>4+</sup>, **27** and [Ni<sub>2</sub>**28**]<sup>4+</sup>, all bismacrocyces showed >60% inhibition. CXCL12 signal blocking calcium flux studies showed that all the 'free' ligands; **19**, **20**, **27** and **28** with the exception of **24** were considerably less active than AMD3100, which showed IC<sub>50</sub> values three orders of magnitude higher. This can be rationalised by looking at the potential for H-bonding interactions. AMD3100 has six secondary amines available to hydrogen bond and

the flexibility to find the optimal arrangement for binding whereas ligands **19**, **20**, **27** and **28** are configurationally restricted macrocycles with limited potential to form N-H donor hydrogen bonds. Free ligand **24**, like AMD3100 has six secondary amines in its structure and is not configurationally restricted so has the potential to adopt an optimal arrangement for H-bonding interactions to occur and explains why this free ligand and not any of the others shows an activity comparable to that of AMD3100.

Despite the configurationally restricted free ligands showing low activity towards blocking the CXCL12 induced signalling of CXCR4 this is overcome when metal ions are present. All metal-containing macrocycles of ligands **19**, **20**, **27** and **28** show affinities one or two orders of magnitude greater than their respective free ligands, the gain from having a metal ion present more than outweighs the decrease in H-bonding potential. Configurationally restricted ligands have a more rigid shape which can slow the kinetics of complex formation and dissociation; such properties are important when these complexes are to be used *in vivo*.<sup>110</sup> As previously mentioned CB complexes are restricted to a *cis-V* configuration and there is evidence to suggest that this is the optimum configuration for high affinity binding due to an optimised coordination geometry for coordinate bond formation between the metal centre and an amino acid side chain.<sup>58</sup>

$[\text{Cu}_2\mathbf{19}]^{4+}$  and the lead complex  $[\text{Cu}_2\mathbf{20}]^{4+}$  both demonstrated the same high affinity for binding to CXCR4 in the mAb competition binding assay but results differed somewhat in the CXCL12 signal blocking calcium flux study.  $[\text{Cu}_2\mathbf{19}]^{4+}$  shows a lower  $\text{IC}_{50}$  value than  $[\text{Cu}_2\mathbf{20}]^{4+}$  indicating slightly higher potency, this is somewhat unexpected since  $[\text{Cu}_2\mathbf{20}]^{4+}$  has a primary amine in its structure which has the potential to hydrogen bond and therefore could potentially improve binding to the CXCR4 receptor. However, both complexes are active on the nanomolar scale and are therefore high affinity antagonists. The observation of binding affinity *cyano* > *methylamine* is not observed when comparing  $[\text{Cu}_2\mathbf{27}]^{4+}$  and  $[\text{Cu}_2\mathbf{28}]^{4+}$  complexes so the origin of this trend is not immediately obvious.

The copper(II), zinc(II) and nickel(II) complexes for ligands **20** and **28** show that in terms of the metal ion, the receptor affinity is copper(II)>zinc(II)>nickel(II). This observation is however, in contrast to results previously obtained in our group for the SB ligand **L**<sup>32</sup> where the receptor affinity was zinc(II)>nickel(II)>copper(II)<sup>58, 199</sup> and observations of Tanaka *et al.* who observed higher binding affinities for zinc(II) complexes over copper(II) complexes.<sup>149</sup> Weisman, Wong and co-workers have noted that complexation of copper(II) into CB macrocycles reduces the lability of the copper(II) ion and results in very inert complexes.<sup>104</sup> This could explain the trend observed since Archibald's observations were based on a SB ligand and Tanaka's macrocycles were not configurationally restricted. Another explanation for the lability of copper(II) ions could be due to binding preferences in the coordination sphere (axial vs. equatorial).

[Cu<sub>2</sub>**20**]<sup>4+</sup>, [Zn<sub>2</sub>**20**]<sup>4+</sup> and [Ni<sub>2</sub>**20**]<sup>4+</sup> all showed efficient antagonism for CXCR4, requiring sub-micromolar concentrations to reduce the normal signalling of CXCR4 by 50%, with [Cu<sub>2</sub>**20**]<sup>4+</sup> showing comparable affinity to AMD3100 (IC<sub>50</sub> = 39 nM vs. 31 nM). [Cu<sub>2</sub>**20**]<sup>4+</sup> has the potential to be a targeted PET probe, if radiolabelled with <sup>64</sup>Cu and so this result is particularly encouraging for progressing this ligand as a biological probe. [Cu<sub>2</sub>**28**]<sup>4+</sup>, [Zn<sub>2</sub>**28**]<sup>4+</sup> and [Ni<sub>2</sub>**28**]<sup>4+</sup> showed unexpectedly high affinity for CXCR4 (IC<sub>50</sub> < 0.1 μM). Intuitively it might be thought that the *meta*-substitution pattern would create steric hindrance between the larger cyclam rings possibly leading to a poor fit in the receptor cavity but this does not appear to be the case. [Cu<sub>2</sub>**28**]<sup>4+</sup> demonstrated almost a 3-fold higher affinity than AMD3100 (IC<sub>50</sub> = 11 nM vs. 31 nM) and its potential as a PET probe should not be overlooked.

Ligand **24** and its metal complexes [Zn<sub>2</sub>**24**]<sup>4+</sup> and [Cu<sub>2</sub>**24**]<sup>4+</sup> all showed a measurable interaction with CXCR4 in flow cell cytometry mAb displacement studies with an anti-CXCR4 antibody. Only 26 nM of ligand **24** was required to reduce the 'normal' signalling of CXCR4 with CXCL12 by 50%, a higher concentration of AMD3100 was required to illicit the same result. This is rather surprising since there is no metal ion to form coordinate bonds but may be due to the high number of H-bonding interactions that are possible. Its zinc(II) complex; [Zn<sub>2</sub>**24**]<sup>4+</sup> showed extremely high

affinity for CXCR4 in the CXCL12 signal blocking calcium flux study ( $IC_{50} = 7$  nM), over 4-fold higher than AMD3100, coupled with very low cytotoxicity ( $CC_{50} = 120.11$   $\mu$ M) this compound has the highest SI of the compounds tested, in stark contrast to findings published by Oltmanns *et al.*<sup>157</sup>

#### 4.5.2.1. Anti-HIV activity

The series of bismacrocylic compounds described in Chapter 2 were also tested for anti-HIV activity (against an X4 HIV-1 viral strain) in MT-4 cells using AMD3100 and its zinc(II) complex for comparison, see Table 7. MT-4 NL4.3WT is a standard immune system cell which has been transfected with HTLV-1 (a viral strain).

This study revealed that all metal complexes show a more potent anti-HIV activity than their respective 'free' ligands, except **24** and  $[Zn_2\mathbf{24}]^{4+}$  and  $[Cu_2\mathbf{24}]^{4+}$  ( $IC_{50} = 65$  nM vs. 73 nM and 45460 nM), indicating the general importance of a metal ion for binding and thus potent activity. Despite its potent activity in comparison to its metal complexes ligand **24** showed relatively high cytotoxicity ( $CC_{50} = 21.22$   $\mu$ M) towards the cells in comparison to similar complexes. The *meta*-substituted biscyclam derivatives  $[Cu_2\mathbf{27}]^{4+}$  and  $[Cu_2\mathbf{28}]^{4+}$  showed potent anti-HIV activity;  $IC_{50} = 8$  nM and 14 nM respectively, comparable to  $Zn_2$ AMD3100 ( $IC_{50} = 8$  nM) and AMD3100 ( $IC_{50} = 11$  nM). Indeed  $[Cu_2\mathbf{27}]^{4+}$  showed the highest SI of the class of bismacrocylics tested.

One interesting trend is that the copper(II) containing cyano derivatives of ligands **20** and **28**;  $[Cu_2\mathbf{19}]^{4+}$  and  $[Cu_2\mathbf{27}]^{4+}$  show higher anti-HIV activity than the copper(II) containing methylamine derivatives;  $[Cu_2\mathbf{20}]^{4+}$  and  $[Cu_2\mathbf{28}]^{4+}$ .

Cell line	MT-4 (NL4.3WT)	MT-4 (NL4.3WT)	MT-4 (NL4.3WT)
Complex	Av <sup>a</sup> IC <sub>50</sub> <sup>b</sup> (μM)	Av <sup>a</sup> CC <sub>50</sub> <sup>c</sup> (μM)	SI <sup>d</sup>
<b>19</b>	0.850	85.72	101
[Cu <sub>2</sub> 19] <sup>4+</sup>	0.030	>109.28	>3643
<b>20</b>	0.610	85.54	140
[Cu <sub>2</sub> 20] <sup>4+</sup>	0.185	>108.77	>588
[Zn <sub>2</sub> 20] <sup>4+</sup>	0.380	54.62	144
[Ni <sub>2</sub> 20] <sup>4+</sup>	0.220	54.98	250
<b>24</b>	0.065	21.22	326
[Zn <sub>2</sub> 24] <sup>4+</sup>	0.073	>120.11	>1645
[Cu <sub>2</sub> 24] <sup>4+</sup>	45.460	>121.23	>3
<b>27</b>	8.550	87.51	10
[Cu <sub>2</sub> 27] <sup>4+</sup>	0.008	>102.97	>13729
<b>28</b>	9.960	>110.66	>11
[Cu <sub>2</sub> 28] <sup>4+</sup>	0.014	52.60	3757
[Zn <sub>2</sub> 28] <sup>4+</sup>	0.027	89.90	3380
[Ni <sub>2</sub> 28] <sup>4+</sup>	0.414	35.84	87
AMD3100	0.011	>225.00	>20455
[Zn <sub>2</sub> AMD3100] <sup>4+</sup>	0.008	>225.00	>28125

Table 7: Anti-HIV data; IC<sub>50</sub>, CC<sub>50</sub> and SI of a series of bismacrocycles tested in MT-4 cells.<sup>a</sup>

Experiments were run in either duplicate or triplicate and the results averaged.<sup>b</sup>

Concentration required to reduce the level of Ca<sup>2+</sup> ions observed during a 'normal' signalling process by 50% (IC<sub>50</sub>) in MT-4 cells.<sup>c</sup> Concentration required to reduce cell viability by 50%

(CC<sub>50</sub>) in MT-4 cells.<sup>d</sup> SI = CC<sub>50</sub>/IC<sub>50</sub>.

#### 4.5.3. Detailed biological evaluation of [Cu<sub>2</sub>20]<sup>4+</sup>

The potency and activity of the antagonist [Cu<sub>2</sub>20]<sup>4+</sup> has been established, mAb competition binding assays and CXCL12 signal blocking calcium flux studies have shown it to be active in the nanomolar range in line with some of our most potent antagonists.<sup>63</sup> An in depth evaluation of this copper(II) complex revealed how this complex acts as a high affinity antagonist for the CXCR4 receptor. The novel aspect of [Cu<sub>2</sub>20]<sup>4+</sup> is that it has a reactive handle for further conjugation and these biological tests show this group is not significantly interfering with the antagonist's ability to bind to the CXCR4 receptor.

#### **4.5.3.1. Downstream signalling: Does an antagonist inhibit the co-localisation of CXCR4 with early endosome antigen 1 (EEA1) upon CXCL12 stimulation?**

As previously mentioned CXCL12/SDF1 $\alpha$  is the sole natural ligand of the CXCR4 receptor, stimulation with CXCL12 not only causes the downstream effects seen in Figure 67 but also causes the receptor to be internalised into the cell *via* endosomal compartments (as observed by FRET). Within the endosomal compartment is the antigen EEA1, involved in the internalisation process so it can be used to quantify the level of receptor internalisation. Cells stably expressing CXCR4 receptors with a GFP tag were used to see whether, upon CXCL12 stimulation, they were internalised into the cell. Staining of EEA1 also allows its position to be located in the cell to see if this matches that of the CXCR4 receptor; if the process is endosomal they should be co-localised. If [Cu<sub>2</sub>20]<sup>4+</sup> is acting as an antagonist, incubation with this complex should decrease the amount of fluorescence observed in the cell due to it preventing internalisation of the CXCR4 receptor by blocking its interaction with CXCL12.

The top row of results in Figure 70, show where the GFP tagged CXCR4 receptors are located in the cell in the presence and absence of CXCL12 and also when increasing concentrations of [Cu<sub>2</sub>20]<sup>4+</sup> are added in the presence of CXCL12. The second row of results shows the position of EEA1 in the cells using a fluorescent antibody specific to EEA1 (anti-EEA1) in the absence/presence of CXCL12 and when the antagonist is added in the presence of CXCL12. The final row of results is then a fusion of this information. An agent was used to stain the nucleus of each cell to define regions ('merge + Nuc' (blue)). The fluorescence of both CXCR4 and the EEA1 antigen can then be seen. Once stimulated with CXCL12 co-localisation can be seen, a fusion of green and red leads to bright yellow spots. As increasing concentrations (nanomolar scale) of the antagonist are introduced the fluorescence reverts back to that of the control i.e. when there was no CXCL12 stimulation (bottom left). The lack of co-localisation observed when 750 nM of the antagonist is introduced proves that the antagonist is blocking the CXCR4 receptor, preventing its internalisation into the cell from CXCL12 stimulation. To enable a proper quantification of these

results, the same tests were performed with 75 nM and 750 nM of the antagonist AMD3100 in the presence of CXCL12, see Figure 71. A similar observation to that of the  $[Cu_220]^{4+}$  can be made; as the concentration of antagonist increases the amount of co-localisation decreases this is due to the antagonist blocking CXCL12 from binding, preventing internalisation.

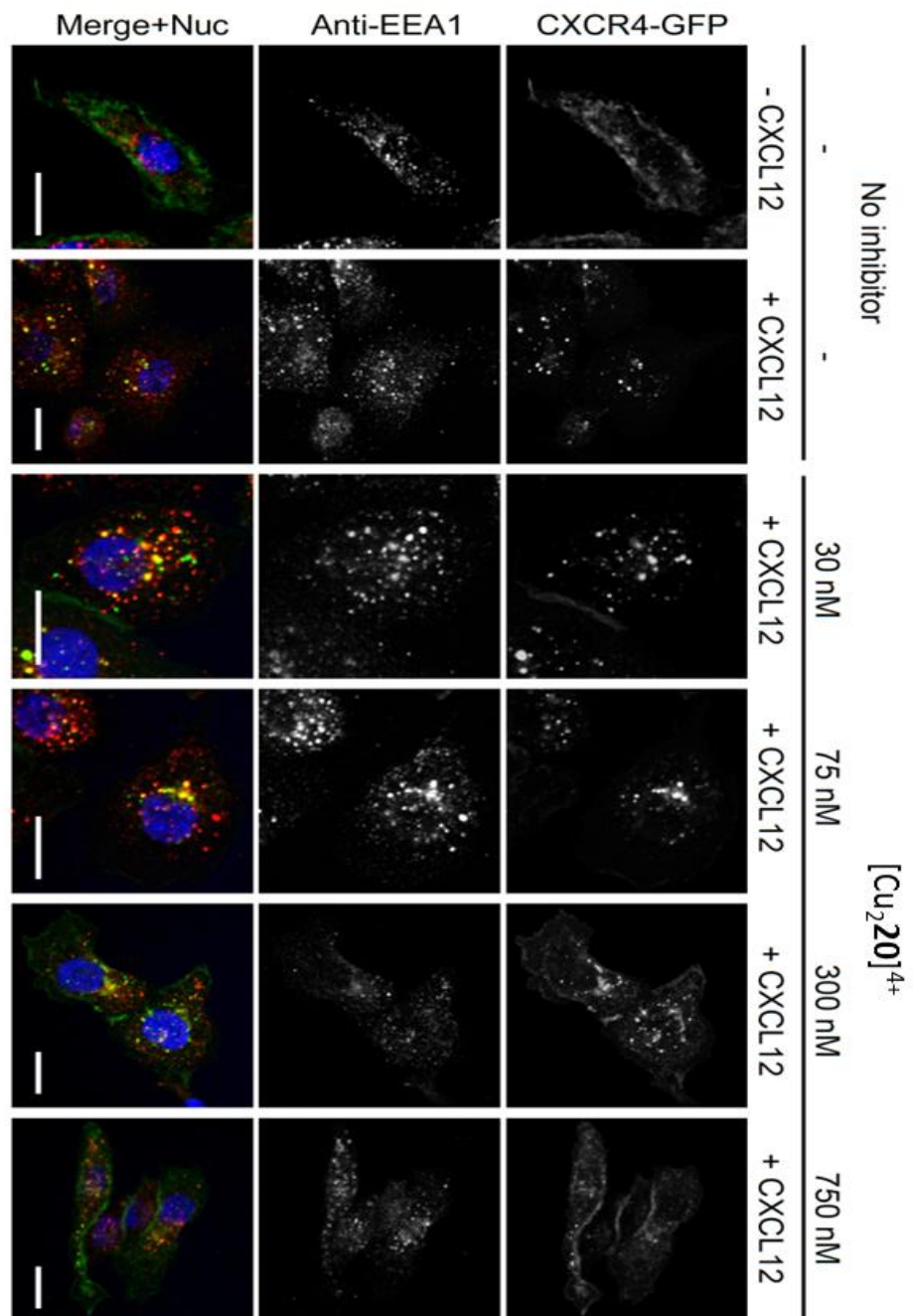


Figure 70: Microscope images showing the co-localisation of CXCR4 and EEA-1 in the presence of CXCL12 and how this co-localisation is affected upon addition of increasing concentrations of  $[Cu_220]^{4+}$ .

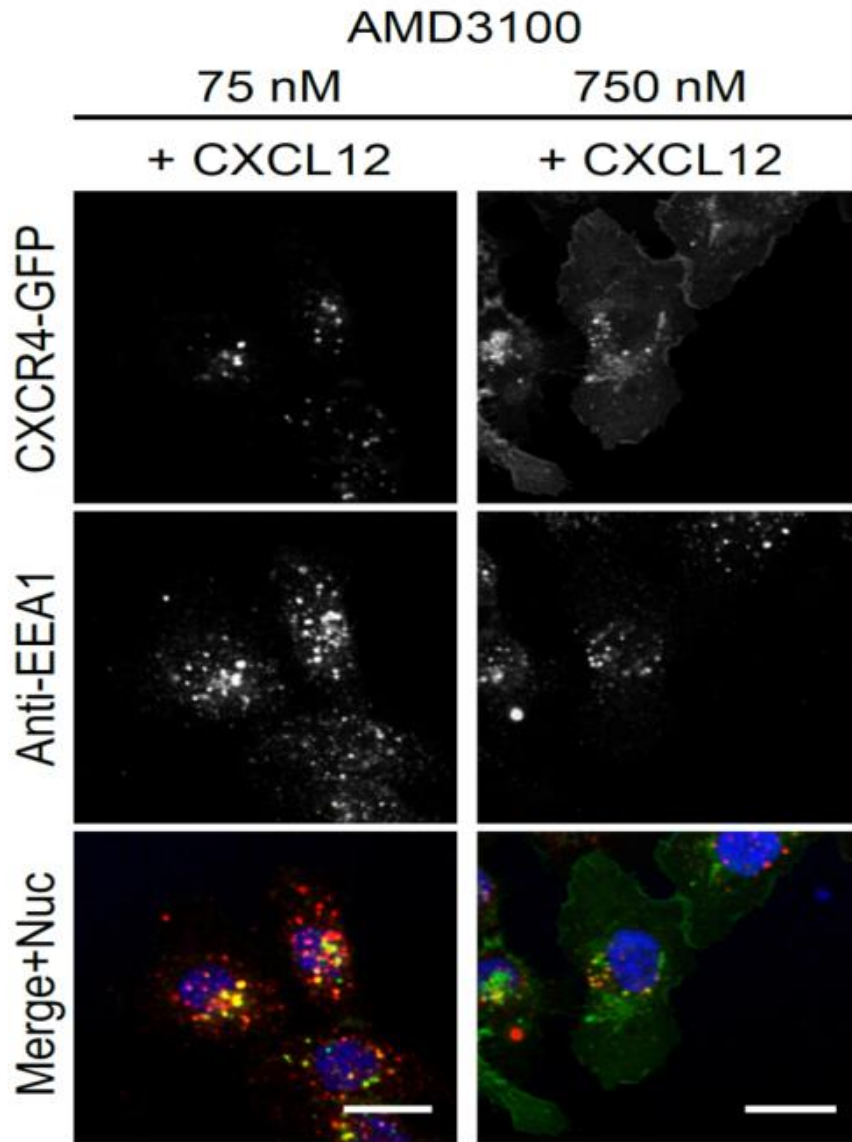


Figure 71: Microscope images showing how the co-localisation of CXCR4 and EEA-1 with CXCL12 stimulation is affected in the presence of AMD3100.

These observations can be represented as a bar chart, see Figure 72. It can be seen that  $[\text{Cu}_2\mathbf{20}]^{4+}$  is preventing the same fraction of co-localisation as AMD3100 at a concentration of 75 nM with  $[\text{Cu}_2\mathbf{20}]^{4+}$  performing better at 750 nM.

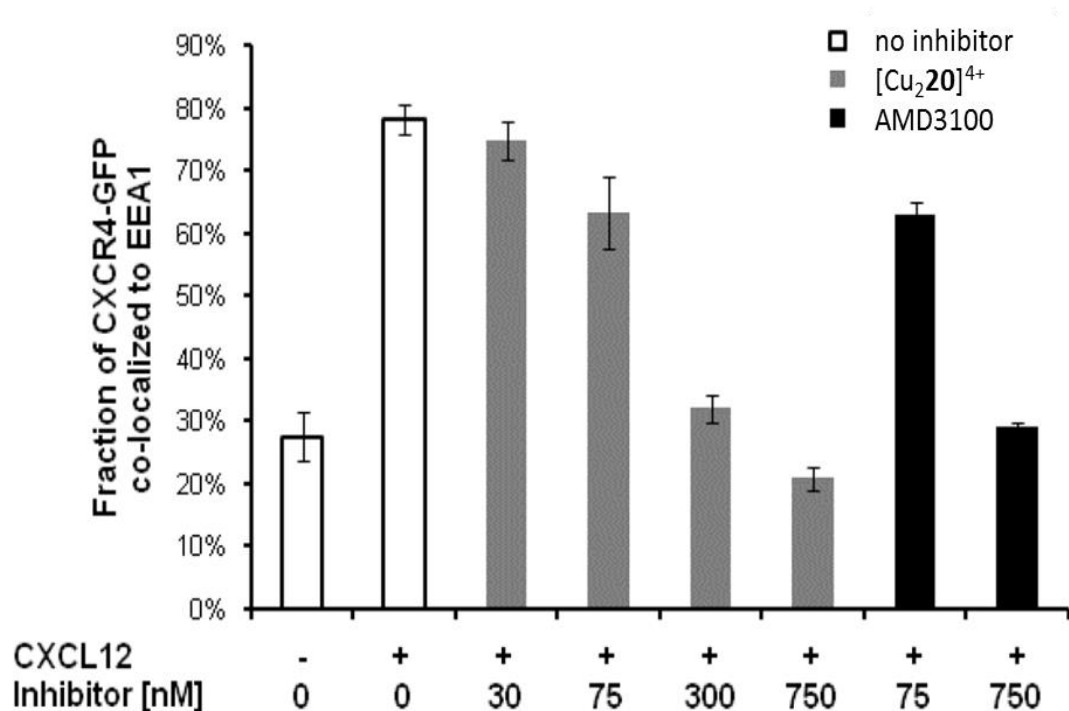


Figure 72: A bar chart comparing the effectiveness of antagonists [Cu<sub>2</sub>20]<sup>4+</sup> and AMD3100 to interfere with an internalisation process with increasing concentration.

#### 4.5.3.2. CXCR4 phosphorylation and downstream signalling events

In an analogous study, phosphorylation enzymes were considered, as part of the internalisation process involves phosphorylation of the CXCR4 receptor. Upon stimulation with CXCL12 the CXCR4 receptor is phosphorylated and internalised in the cell. Several kinases are involved in this process including ERK 1/2 and p38MAPK. Hsp27 is a signalling molecule and a direct target of p38MAPK. In this test the amount of phosphorylated CXCR4 (p324/5-CXCR4) was analysed against the amount of phosphorylation enzymes when in the presence of CXCL12. As part of the internalisation process for CXCR4 an up-regulation of the expression of these phosphorylation enzymes occurs.

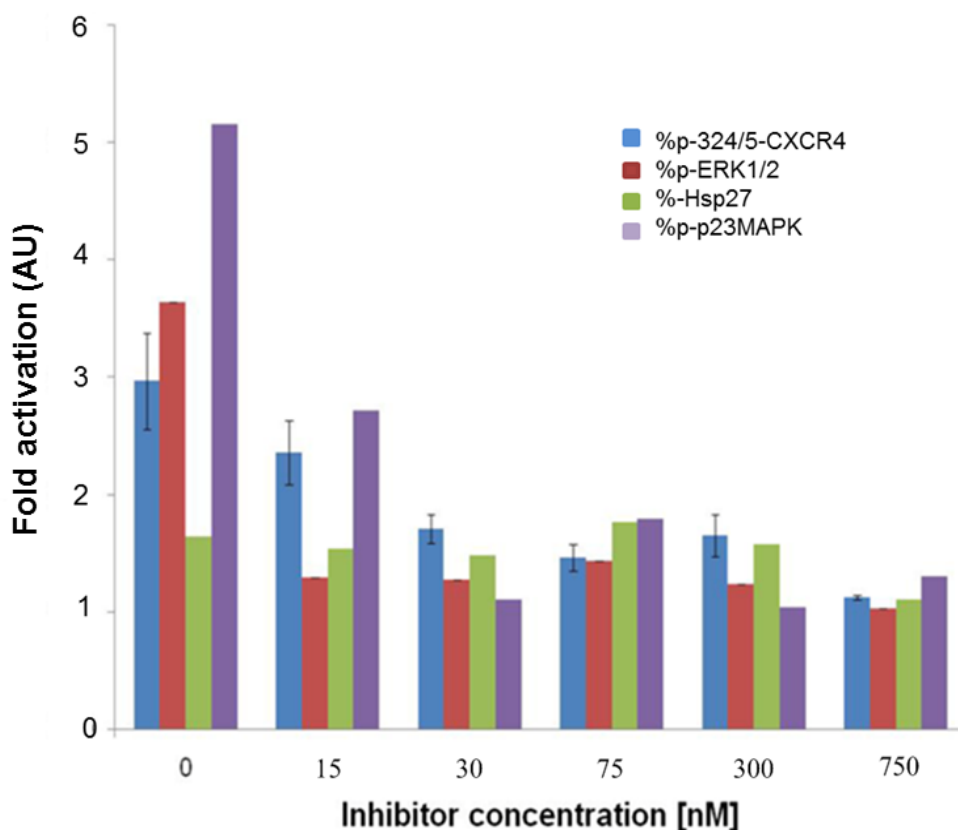


Figure 73: A bar chart depicting the levels of phosphorylation enzymes present upon addition of increasing concentrations of  $[Cu_220]^{4+}$ . Note 1 AU on the y-axis is the normal activation level.

The amount of phosphorylated CXCR4 (p324/5-CXCR4) decreases as the concentration of antagonist increases, see Figure 73. The amount of p38MAPK decreases sharply with introduction of the antagonist then further decreases as the concentration of the antagonist is increased. The amount of ERK1/2 decreases sharply with introduction of the antagonist but then remains at a constant level despite increasing the concentration of the antagonist. As expected, the amount of Hsp27 remains constant throughout the experiment, since this is a signalling molecule. These results suggest that antagonist  $[Cu_220]^{4+}$  is affecting the phosphorylation process due to it blocking the binding pocket of the CXCR4 receptor, preventing CXCL12 from binding. This is confirmed by the decrease in expression of the phosphorylation enzymes.

#### 4.5.3.3. Reduced CXCR4 receptor degradation in the presence of [Cu<sub>2</sub>20]<sup>4+</sup>

Once a CXCR4 receptor has been internalised into the cell, it is often degraded by a series of 'housekeeping' proteins, one such protein being GAPDH. The cell will then synthesise a new CXCR4 receptor and send it up to the cell membrane. To test for receptor degradation cycloheximide (an inhibitor of protein biosynthesis) was employed to prevent new protein synthesis. The amount of degradation in the presence of CXCL12 with increasing concentrations of the antagonist [Cu<sub>2</sub>20]<sup>4+</sup> was then determined using western blot assays, see Figure 74.

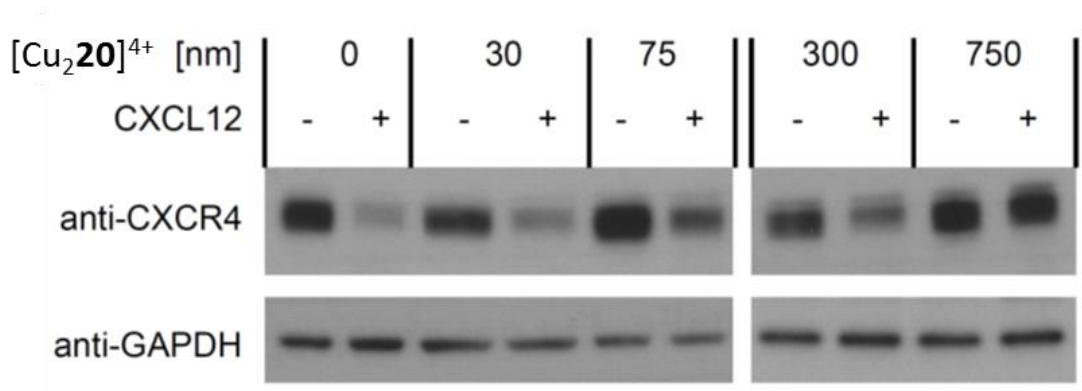


Figure 74: Western blot assay depicting the level of degradation observed with and without the presence of CXCL12 with increasing concentration of the antagonist [Cu<sub>2</sub>20]<sup>4+</sup>.

It can be seen that as the concentration of [Cu<sub>2</sub>20]<sup>4+</sup> increases the % of CXCR4 degradation decreases, see Figure 75. These results coincide with the previous tests performed. If the antagonist is blocking the CXCR4 receptor it cannot be stimulated by its ligand CXCL12 so it will not be internalised into the cell and therefore cannot be degraded.

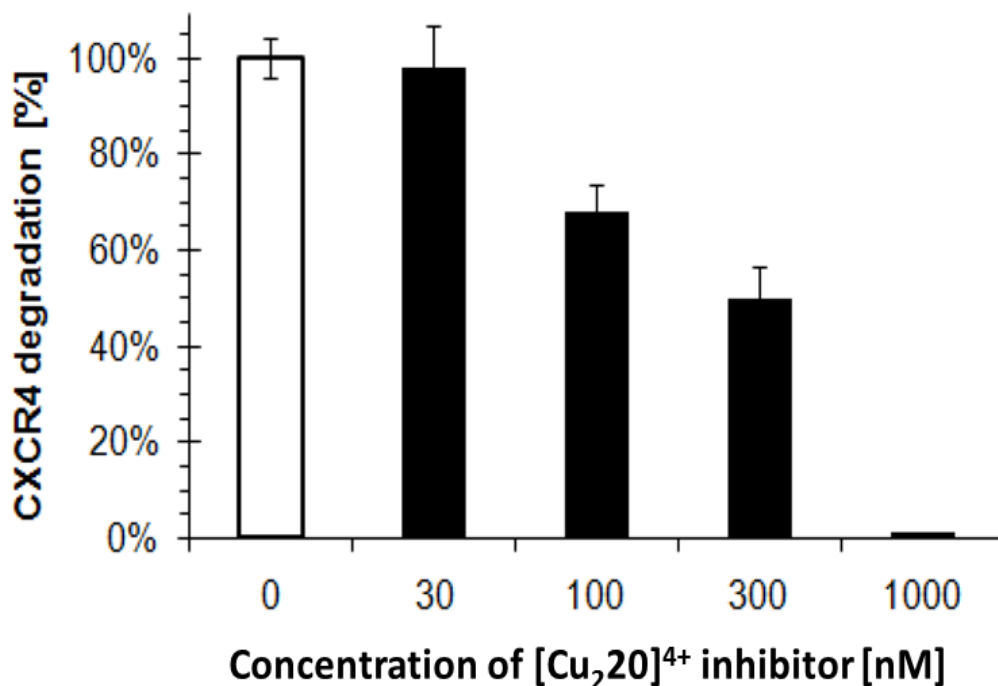


Figure 75: A bar chart showing the decrease in degradation observed with increasing concentrations of antagonist  $[\text{Cu}_2\mathbf{20}]^{4+}$ .

In conclusion this series of biological assays proves that  $[\text{Cu}_2\mathbf{20}]^{4+}$  is an antagonist for CXCR4 and can effectively block or disrupt the ‘normal’ downstream effects of the receptor upon stimulation with its natural ligand CXCL12.  $[\text{Cu}_2\mathbf{20}]^{4+}$  is not just blocking the receptor from signalling however, these results reveal that  $[\text{Cu}_2\mathbf{20}]^{4+}$  is locking the receptor on the surface of the cell, stopping the internalisation and recycling processes which would result in formation of a new receptor.

#### 4.6. Addition of spacer arms – acidic and a biotin tag

Various spacer arms were attached to bismacrocycle  $[\text{Cu}_2\mathbf{20}]^{4+}$ , presented in Chapter 3. These spacer arms provide a means to conjugate other molecules of interest such as porphyrins whilst providing the necessary distance to prevent unwanted interactions.  $[\text{Cu}_2\mathbf{20}]^{4+}$  has been shown to be a high affinity antagonist for CXCR4 with low cytotoxicity so it is necessary to establish whether the addition of a spacer arm has an effect on this binding affinity. Two specific examples were evaluated,  $[\text{Cu}_2\mathbf{34}]^{4+}$ ; terminating in an acidic group and  $[\text{Cu}_2\mathbf{44}]^{4+}$  terminating in a biotin molecule, see Table 8.

CXCR4 has an overall surface charge of 9<sup>-</sup>, [Cu<sub>2</sub>20]<sup>4+</sup> has an associated charge of 4<sup>+</sup>, introduction of an acidic group into the structure of [Cu<sub>2</sub>20]<sup>4+</sup> could decrease this positive charge and have a detrimental effect on the electrostatic interactions between the macrocycle and the receptor. Biotin is a naturally occurring organic molecule used extensively in biochemical assays and it is therefore not likely to have an effect on cytotoxicity but the steric bulk of biotin with its fused tetrahydroimidazole and tetrahydrothiophene rings, may have an effect on the binding affinity.

Cell line	U87.CD4.CXCR4			Jurkat
	IC <sub>50</sub> <sup>a</sup> (nM)	CC <sub>50</sub> <sup>b</sup> (μM)	SI <sup>c</sup>	% inhibition
[Cu <sub>2</sub> 20] <sup>4+</sup>	39	-	-	96
[Cu <sub>2</sub> 34] <sup>4+</sup>	135	22.89	170	88
[Cu <sub>2</sub> 44] <sup>4+</sup>	393	79.45	202	89
AMD3100	11	>225.00	20455	72

*Table 8: The IC<sub>50</sub> (calcium signalling), CC<sub>50</sub> and SI of a series of novel metal containing bismacrocycles bearing spacer arms in the cell line U87.CD4.CXCR4 are presented along with their % of inhibition of anti-CXCR4 mAb binding in Jurkat cells. <sup>a</sup> Experiments were run in either duplicate or triplicate and the results averaged. <sup>b</sup> Concentration required to reduce the level of Ca<sup>2+</sup> ions observed during a 'normal' signalling process by 50% (IC<sub>50</sub>) in U87.CD4.CXCR4 cells. <sup>c</sup> Concentration required to reduce cell viability by 50% (CC<sub>50</sub>) in U87.CD4.CXCR4 cells. <sup>d</sup> SI = CC<sub>50</sub>/IC<sub>50</sub>.*

Flow cell cytometry displacement studies with an anti-CXCR4 antibody confirmed that both [Cu<sub>2</sub>34]<sup>4+</sup> and [Cu<sub>2</sub>44]<sup>4+</sup> bind to CXCR4 with a high % of inhibition observed for both complexes. CXCL12 signal blocking calcium(II) flux studies show that both the acidic terminating and biotin tagged bismacrocycles have lower potencies than [Cu<sub>2</sub>20]<sup>4+</sup> (IC<sub>50</sub> = 135 and 393 nM, respectively) but are still active at sub-micromolar levels. [Cu<sub>2</sub>34]<sup>4+</sup> also showed a higher cytotoxicity in the cells.

In conclusion whilst the addition of a spacer arm, be it acidic or a biotin tag, has a slightly detrimental effect on binding affinity and cytotoxicity in comparison to bismacrocycle [Cu<sub>2</sub>20]<sup>4+</sup>, [Cu<sub>2</sub>34]<sup>4+</sup> and [Cu<sub>2</sub>44]<sup>4+</sup> are still active at sub micromolar levels and as such can be termed high affinity antagonists.

## 4.7. Conclusions

Synthesising a range of macrocyclic compounds provides a systematic approach to establishing structure affinity relationships for CXCR4 antagonists. Thus allowing binding profiles to be established which can be tuned to achieve desired properties. The macrocycles presented in Chapter 2 along with  $[\text{Cu}_2\mathbf{34}]^{4+}$  and  $[\text{Cu}_2\mathbf{44}]^{4+}$  were tested for their affinity and potency for CXCR4 through competition binding assays and CXCL12 signal blocking calcium flux studies.

Monomacrocycles have the potential for improved pharmacological properties and are easier to synthesise than their bismacrocyclic counterparts and some interesting trends were observed. Zinc(II) complexes showed higher activity than their analogous copper(II) and nickel(II) derivatives.  $[\text{Zn}\mathbf{9}]^{2+}$  showed a 2.5-fold higher affinity for CXCR4 than the clinically licensed drug AMD3100.

The novel set of *meta*-substituted biscyclen complexes;  $[\text{Cu}_2\mathbf{20}]^{4+}$ ,  $[\text{Zn}_2\mathbf{20}]^{4+}$  and  $[\text{Ni}_2\mathbf{20}]^{4+}$  all demonstrated high activity for CXCR4, requiring sub-micromolar concentrations to reduce the CXCL12 induced signalling with CXCR4 by 50%,  $[\text{Cu}_2\mathbf{20}]^{4+}$  showing comparable affinity to AMD3100 ( $\text{IC}_{50} = 39 \text{ nM}$  vs.  $31 \text{ nM}$ ).  $[\text{Cu}_2\mathbf{20}]^{4+}$  has the potential to be a targeted PET probe, if radiolabelled with  $^{64}\text{Cu}$ , a detailed evaluation of its binding properties concluded that it exerts its antagonistic effects by locking the receptor on the surface of the cell, stopping the internalisation and recycling processes which would result in formation of a new receptor. The analogous set of *meta*-substituted biscyclam complexes;  $[\text{Cu}_2\mathbf{28}]^{4+}$ ,  $[\text{Zn}_2\mathbf{28}]^{4+}$  and  $[\text{Ni}_2\mathbf{28}]^{4+}$  showed unexpectedly high affinity for CXCR4 ( $\text{IC}_{50} < 0.1 \mu\text{M}$ ). Intuitively it might be thought that the *meta*-substitution pattern would create steric hindrance between the larger cyclam rings in the receptor cavity but this does not appear to be the case.  $[\text{Cu}_2\mathbf{28}]^{4+}$  demonstrated a 3-fold higher affinity than AMD3100 ( $\text{IC}_{50} = 11 \text{ nM}$  vs.  $31 \text{ nM}$ ) and its potential as a PET probe should not be overlooked.

The non-restricted biscyclen ligand **24** and its zinc(II) and copper(II) complexes;  $[\text{Zn}_2\mathbf{24}]^{4+}$  and  $[\text{Cu}_2\mathbf{24}]^{4+}$ , all showed a measurable interaction with CXCR4 in contrary

to Oltmanns results.<sup>157</sup> The 'free' ligand **24** has comparable affinity to AMD3100 ( $IC_{50} = 26$  nM vs. 31 nM) which can be rationalised by considering the large number of potential H-bonding interactions these ligands possess.  $[Zn_2\mathbf{24}]^{4+}$  shows a 4-fold improvement in affinity compared to AMD3100, showing the highest SI of the class of bismacrocycles tested. The presence of zinc(II) for high affinity was also observed with the monomacrocyclic ligands. Anti-HIV activity was assessed, copper(II) complexes of the cyano terminating ligands **19** and **27** were highlighted as particularly potent ligands in MT-4 cells.

The successful attachment of organic spacer arms to bismacrocycle **20** have been presented in Chapter 3.  $[Cu_2\mathbf{34}]^{4+}$  an acidic terminating derivative of  $[Cu_2\mathbf{20}]^{4+}$  and  $[Cu_2\mathbf{44}]^{4+}$  a biotin tagged derivative were tested to assess whether the attachment of a spacer arm had any effect on binding affinity in comparison to  $[Cu_2\mathbf{20}]^{4+}$ . Although a slight decrease in affinity was observed in both the competition assays and the CXCL12 signal blocking calcium flux studies, both  $[Cu_2\mathbf{34}]^{4+}$  and  $[Cu_2\mathbf{44}]^{4+}$  were still active at sub micromolar levels and so it was concluded that these spacer arms were having no significant detrimental effect on the affinity of the macrocycle for the CXCR4 receptor.

## **Chapter 5**

### **Synthesis of porphyrin compounds; towards the formation of novel MFCs**

## 5.1. Introduction

The successful synthesis of bismacrocylic compounds bearing functional spacer arms is presented in Chapter 3. Porphyrin compounds bearing complementary functionalities needed to be synthesised in order to obtain all of the building blocks to assemble a potentially diagnostic and therapeutic MFC. Saturated tetraazamacrocycles and porphyrins have very different properties in terms of solubility and basicity and the challenge is to ascertain conditions which suit both types of compound and allow a conjugation product to be prepared and successfully isolated.

## 5.2. Synthetic strategy

The strategy adopted was to synthesise water soluble porphyrin compounds and determine the necessary conditions to attach these porphyrins to bismacrocylic compounds bearing spacer arms producing novel MFCs with possible diagnostic and therapeutic properties.

### 5.2.1. Previous strategies

The clinical potential for conjugating PDT active porphyrins to targeted biomolecules is considerable and some examples have previously been highlighted, see Chapter 1, section 1.4.4. This section describes some synthetic strategies adopted to attach biomolecules to various porphyrin derivatives focusing on reactions involving amino and carboxy groups, see Figure 76.

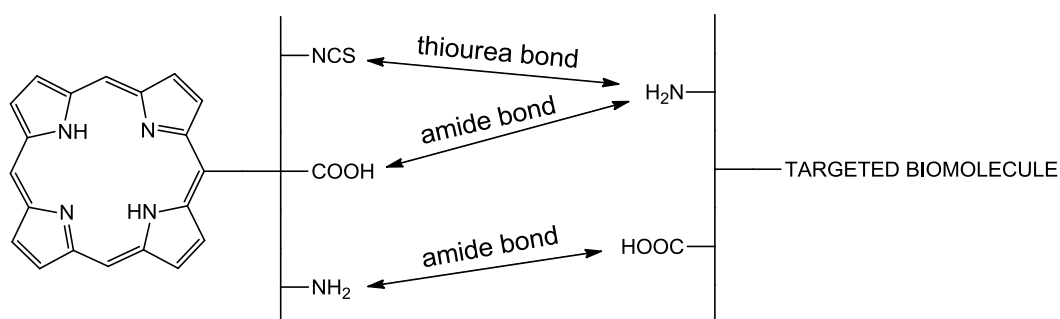


Figure 76: Strategies to form either thiourea or amide bonds between porphyrins and targeted biomolecules. (Adapted from *Photochem. Photobiol. Sci.*)<sup>76</sup>

One class of biomolecules, peptides, have received considerable attention<sup>76</sup> because their structure dictates that at least one amine group will be present, formation of a thiourea or amide bond is then dictated by the functionality of the coupling porphyrin. A popular approach for porphyrin derivatives bearing a carboxy group is activation with NHS to form an activated NHS ester species. Tome and co-workers activated carboxy functionalised porphyrins with NHS to form an NHS ester species which they reacted with poly-(L-lysine).<sup>203</sup> An alternative strategy is to use carbodiimide activation. Boisbrun *et al.* activated a carboxy functionalised porphyrin using DCC/HOBT and coupled an RDG peptide to this activated species to produce L<sup>52</sup>, see Figure 77.<sup>204</sup>

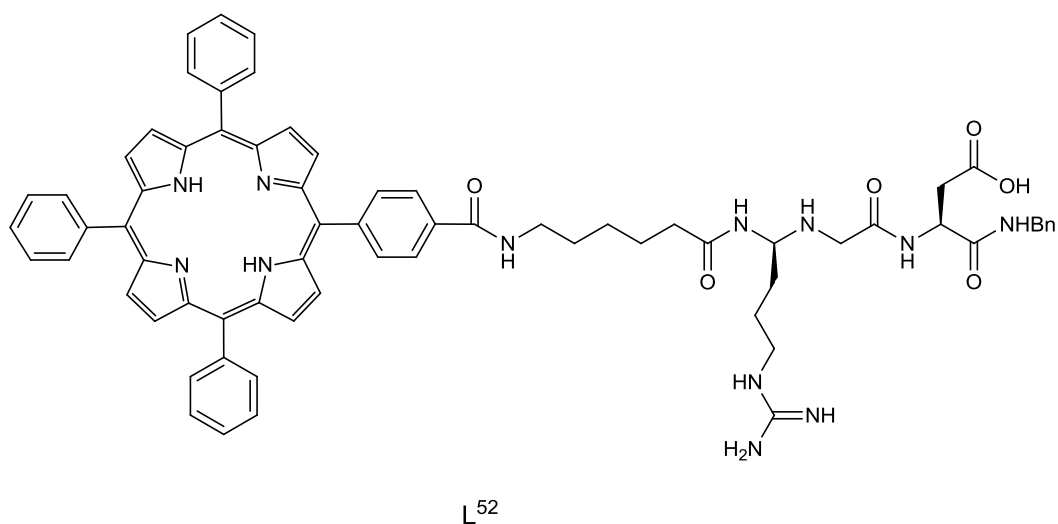


Figure 77: Conjugation of an RDG peptide to a carboxy functionalised porphyrin to give L<sup>52</sup> outlined by Boisbrun *et al.*<sup>204</sup>

Starkey *et al.* chose a similar method activating their bis-carboxy functionalised porphyrin with DCC/DMAP for subsequent conjugation of two cyclic peptides, this conjugate (L<sup>53</sup>) showed potential to target ‘deep-seated’ tumours,<sup>205</sup> see Figure 78. The use of ‘non-standard’ coupling reagents has also been exploited; Choi *et al.* conjugated a carboxy-functionalised dihydroxychlorin to a cell-penetrating arginine heptamer using HBTU, showing improved cellular uptake compared to the non-conjugated chlorin.<sup>206</sup> PyBOP mediated couplings have also found use for activating

carboxy functionalised porphyrins for subsequent conjugation to cell targeting peptides<sup>207</sup> with Rahimpour *et al.* noting better yields and purity when using PyBOP as opposed to carbodiimide activation.<sup>170</sup>

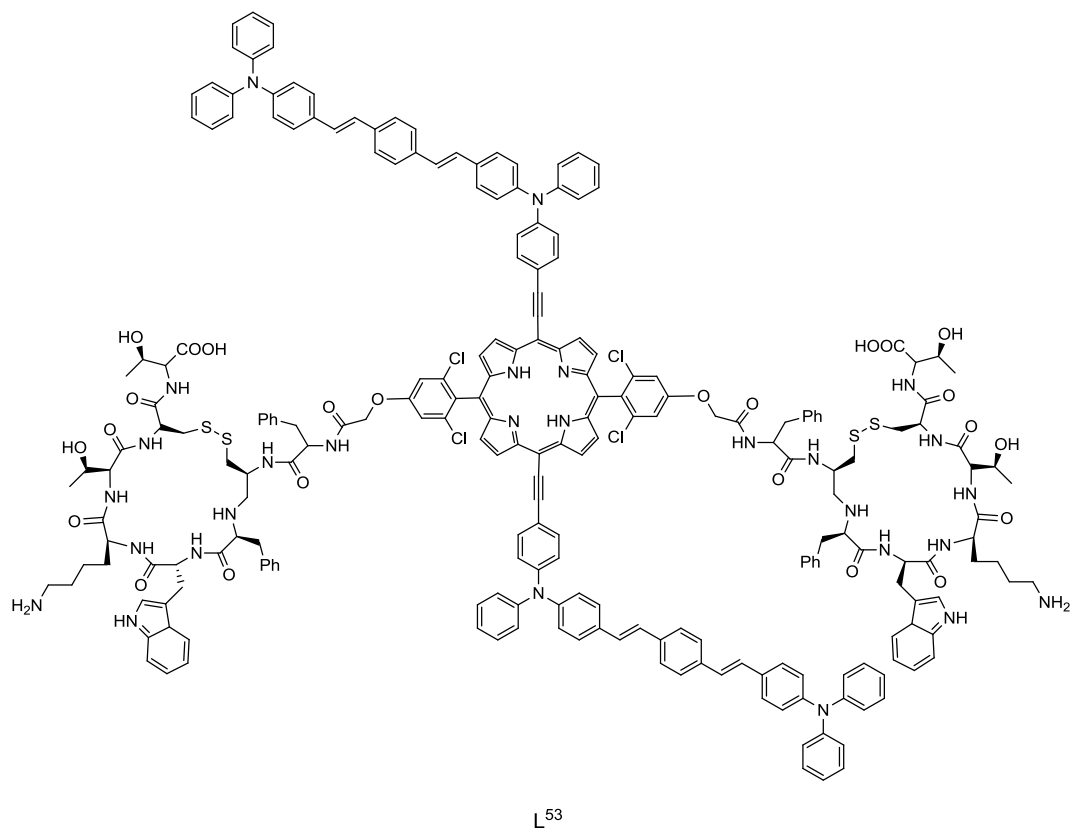


Figure 78: A bis-carboxy functionalised porphyrin conjugated to two cyclic peptides (L<sup>53</sup>) outlined by Starkey *et al.*<sup>205</sup>

Shi *et al.* developed a porphyrin PET probe targeted to the folate receptor utilising the amine reactive ends of a peptide.<sup>208</sup> They attached pyropheophorbide (commercially available) which terminates in a carboxylic acid to the N-terminus of a peptide linker (GDEVDSGK) attaching the other amine end to a folate targeted biomolecule. This was then radiolabelled with <sup>64</sup>Cu, non-invasive PET imaging showed good biodistribution, favourable pharmacokinetics and selectivity towards folate-receptor positive tumours.

Sibrian-Vazquez *et al.* took the amine functionalised porphyrin L<sup>54</sup> converting to two different amine reactive groups; the isothiocyanate L<sup>55</sup> (using 1,1'-thiocarbonyldi-2(1H)-pyridone (TCP)) and the carboxylic acid L<sup>56</sup> (*via* reaction with glutaric acid),<sup>209</sup>

see Figure 79. Various peptides bearing one or more lysine residues were then attached, the isothiocyanate derivative in the presence of TEA and the carboxy derivative in the presence of TBTU, to produce a series of porphyrin-peptide conjugates formed through a thiourea or amide bond.

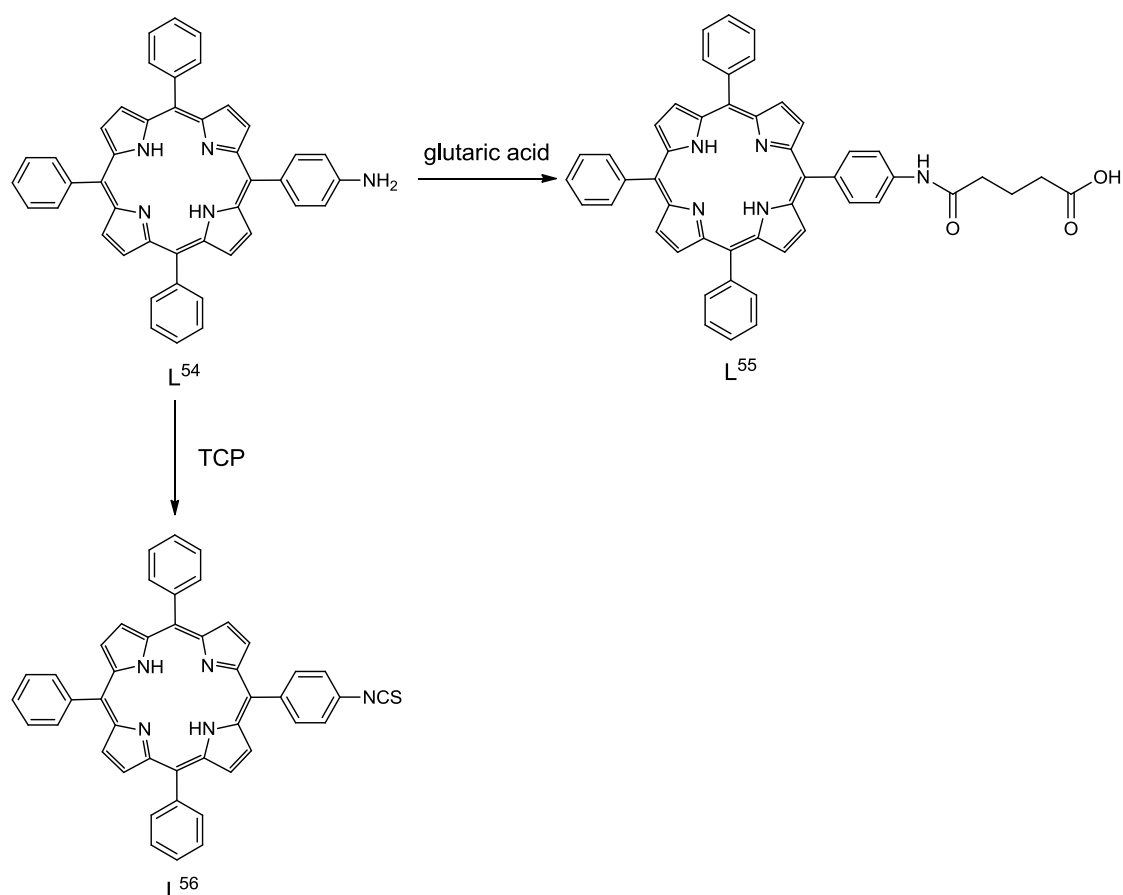


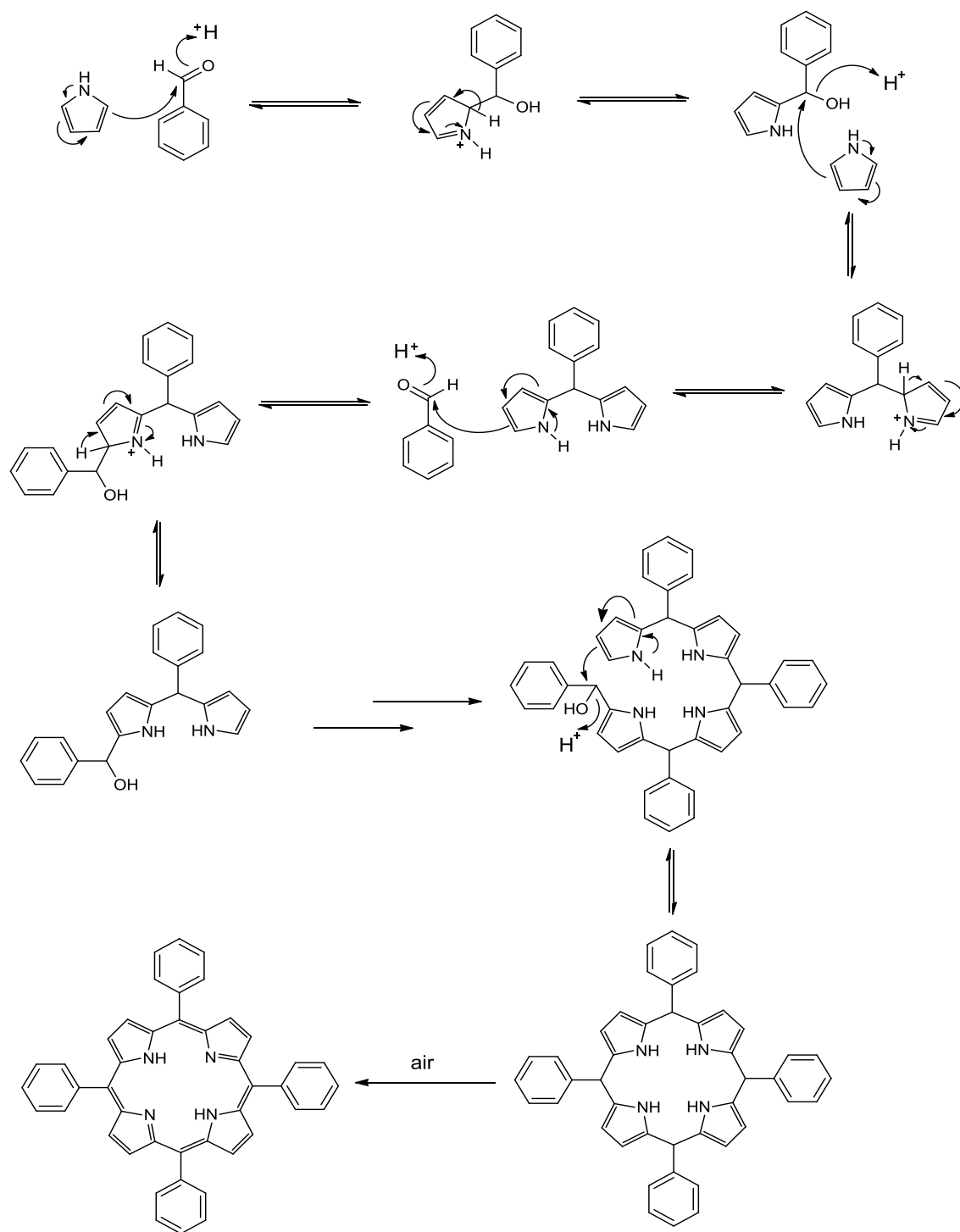
Figure 79: Conversion of  $L^{54}$  to different amine-reactive groups; carboxy ( $L^{55}$ ) and isothiocyanate ( $L^{56}$ ) outlined by Sibrian-Vasquez *et al.*<sup>209</sup>

Biron and Voyer utilised an amino functionalised tri-pyridyl porphyrin and attached carboxy terminating amino acids containing a glutamic acid side chain using DCC as a coupling reagent.<sup>210</sup> These porphyrin-amino acid derivatives display DNA binding properties. Weimin *et al.* also used DCC to attach L-phenylalanine or 1-carboxymethyl-5-fluorouracil (5-Fu acid) to 5,10-bis-NH<sub>2</sub>-TPP in either one or two equivalents.<sup>211</sup> These amino acid modified porphyrins showed improved

photocytotoxicities in comparison to their precursors in a human oesophageal cell line (Ec9706).

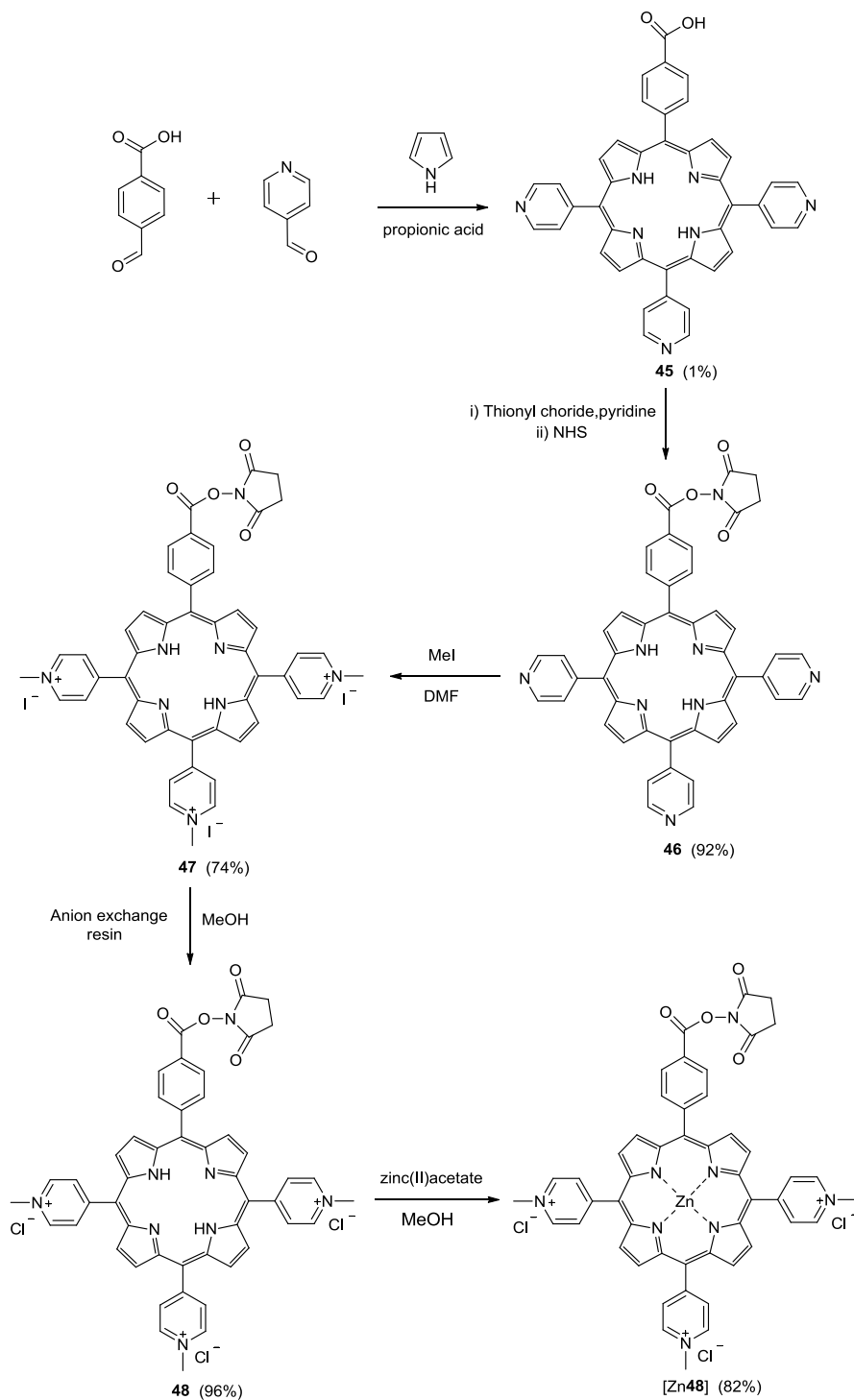
### **5.3. Synthesis of water soluble porphyrins**

One of the oldest and still most commonly used methods for the synthesis of symmetrical tetraarylporphyrins is the Rothmund synthesis<sup>212</sup> using Adler–Longo conditions.<sup>213</sup> Freshly distilled pyrrole along with a molar equivalent of the benzaldehyde are added to refluxing propionic acid open to the air; the mechanism is outlined in Scheme 22. Many porphyrins are also amenable to Lindsey conditions,<sup>214</sup> a complementary method to the one set out by Adler and Longo. However, there are significant problems when benzaldehydes bearing heterocyclic moieties are used. Whilst Adler-Longo conditions typically give low yields, Lindsey conditions can fail all together, this has been attributed to the poor solubility of intermediates in the acidified solvent.<sup>215</sup>

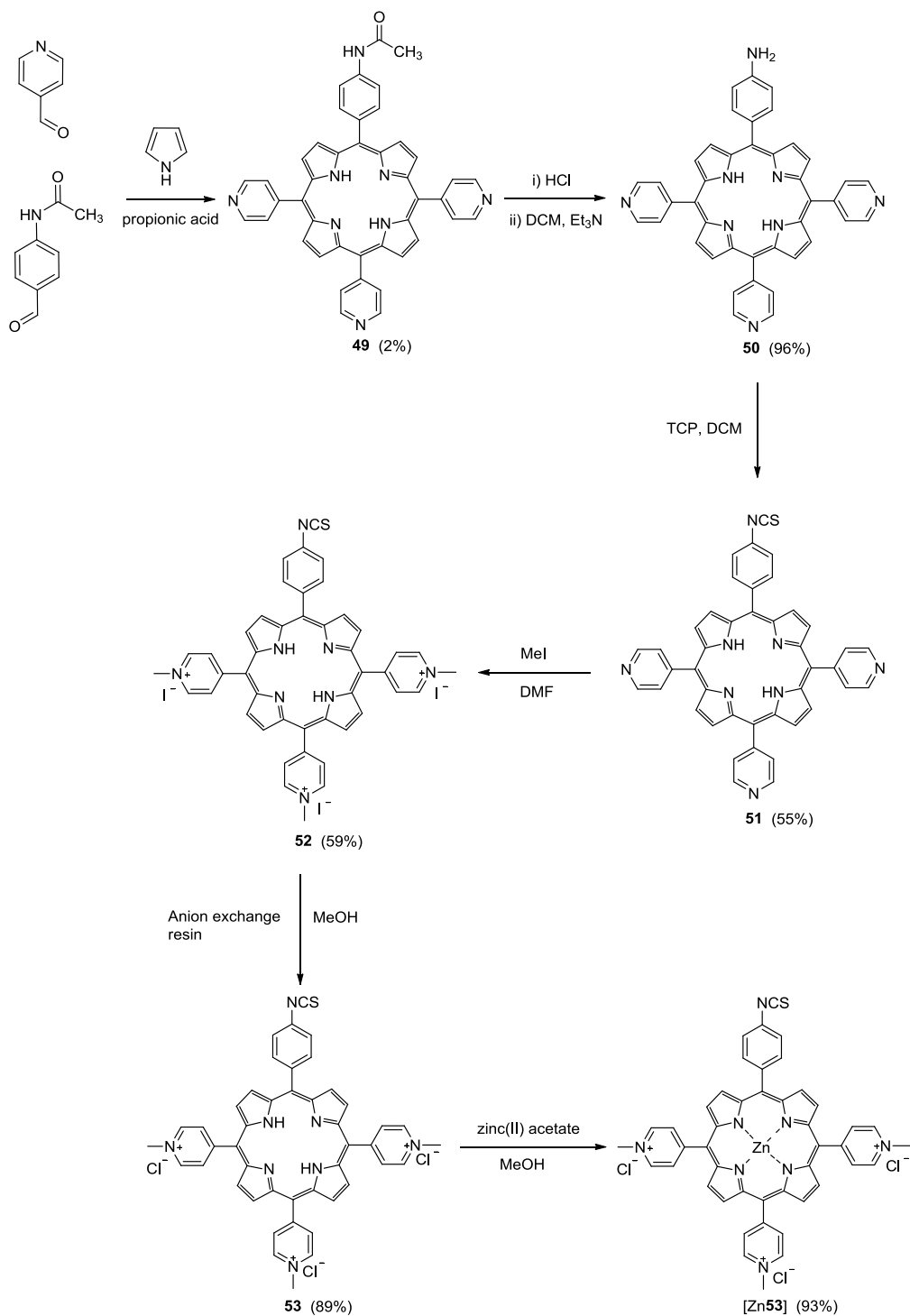


Scheme 22: Mechanism for the formation of tetraphenyl porphyrin (TPP) using Adler-Longo conditions. (Reproduced from *J. Hetero. Chem.*)<sup>216</sup>

Unsymmetrically substituted porphyrins can also be formed using Adler-Longo conditions. The synthesis of porphyrins **45** and **49** was carried out *via* a [3 + 1] condensation reaction under Adler-Longo conditions, see Schemes 23 and 24.



Scheme 23: Synthetic route to produce zinc-5-[4-(succinimide-N-oxycarbonyl)phenyl]-10,15,20-tris-(4-N-methylpyridinium)porphyrin trichloride [**Zn48**].



*Scheme 24: Synthetic route to produce zinc-5-(4-isothiocyanatophenyl)-10,15,20-tris(4-N-methylpyridiniumyl) porphyrin trichloride [Zn53].*

These [3 + 1] condensation reactions produce a mixture of six products, see Figure 80, the desired product making up a fraction of the overall mixture. Extensive

purification *via* column chromatography was required to separate these porphyrin products resulting in low yields of the desired product (*ca.* 1% for **45** and 2% for **49**).

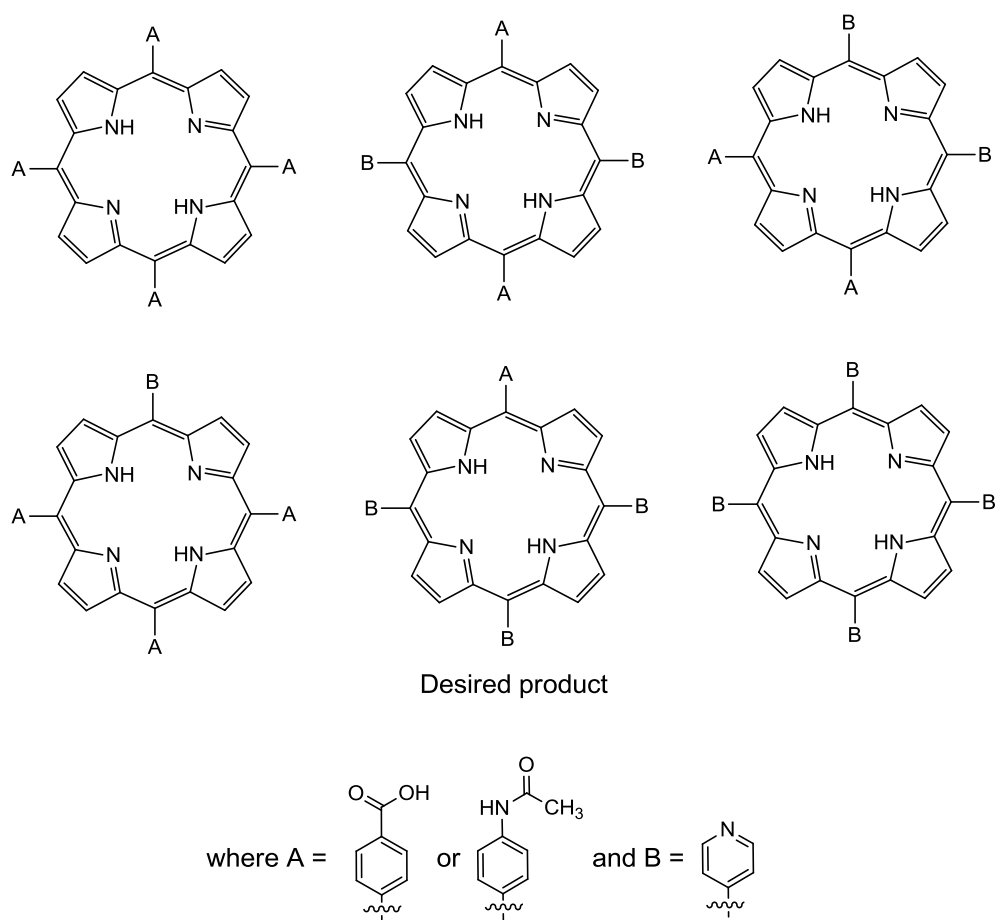


Figure 80: The six possible porphyrin products from [3 + 1] condensation reactions.

Fortunately subsequent steps are much higher yielding. Activation of the acidic group on porphyrin **45** was achieved *via in situ* generation of an acid chloride, addition of NHS produced an NHS ester species, recrystallisation afforded the desired product (**46**) in 92% yield. The triiodo species **47** was obtained *via* methylation of each of the pyridyl nitrogen atoms, the product was isolated in 74% yield. Anion exchange to give the more water soluble trichloro species **48**, gave 66% of the desired product and protection of the tetrapyrrolic cavity using zinc(II) gave the final product [Zn**48**] in 82% yield, following a standard complexation procedure;<sup>217</sup> zinc(II) acetate/RT/1 hour.

Protection of the porphyrin cavity with zinc(II) was necessary because steps to form novel MFCs will ultimately require the use of copper(II) salts. Porphyrins, like saturated tetraazamacrocycles, have an ideal cavity size to complex with transition metal ions and will readily complex copper(II) into their cavities rendering them inactive as PDT agents due to the paramagnetic nature of the resulting complex. Retrieval of the free-base porphyrin requires strongly acidic conditions. This problem is easily overcome by pre-coordination of the porphyrin cavity with zinc(II). This is not only a simple and high yielding procedure but the resulting zinc(II) porphyrin retains its fluorescent and singlet oxygen producing capability. They can also undergo NMR analysis since zinc(II) has a full shell of d-electrons ( $d^{10}$ ) and is therefore diamagnetic. If necessary the zinc(II) ion can also be removed from the cavity by stirring in TFA.

Formation of the zinc(II) protected cationic porphyrin [Zn**53**] requires a slightly longer synthetic route. Refluxing porphyrin **49** in acid unmasks the primary amine group, a chromatographic purification step is required to remove any unreacted starting material to give porphyrin **50** in 96% yield. This is easily converted to an isothiocyanate group using TCP, as opposed to the more widely adopted but more toxic and volatile thiophosgene, following conditions outlined by Boyle and co-workers.<sup>218</sup> A chromatographic step to remove excess pyridone and unreacted starting material reduces the high yield seen in previous steps to 55% of porphyrin **51**. Methylation to form the triiodo species and anion exchange to give the water soluble trichloro species gave 59% and 89% yields of porphyrins **52** and **53**, respectively. The porphyrin cavity was protected with zinc(II) to give afford [Zn**53**] in 93% yield.

### **5.3.1. Characterisation of porphyrin products.**

Porphyrins **45-53** inclusive of the zinc(II) complexes; [Zn**48**] and [Zn**53**], were characterised by  $^1\text{H}$  NMR data. Mass spectrometry was also an important analytical tool since many steps involved a functional group change that was not always indicative in the NMR spectra. MS data were collected for all porphyrins (free-base and complexes).

Porphyrins are aromatic systems which obey Hückel's rule of aromaticity ( $(4n + 2) \pi$  electrons, where  $n = 5$ ), this aromaticity can be observed through  $^1\text{H-NMR}$  spectroscopy causing distinct and characteristic features to arise in the acquired spectra. For free-base porphyrins the most notable feature is the presence of a signal with a negative chemical shift (around  $\delta -2$  ppm). This high-field signal is a singlet integrating to two and represents the two inner macrocyclic protons termed internal protons. These internal protons are attached to two inner pyrroline nitrogen atoms and are highly shielded due to the powerful aromatic ring current observed within the system; a result of  $\pi$ -delocalisation. At the other end of the scale distinctive features arise at  $\delta 9$  and  $10$  ppm. These low field signals are caused by significant deshielding of the external  $\beta$ - and *meso*-protons; the *meso*-protons are affected to a greater extent than the  $\beta$ -protons.

The free-base porphyrins **45-53** all showed a distinct singlet around  $\delta -2$  ppm in their  $^1\text{H NMR}$  spectra along with distinct peaks at low field values indicative of the  $\beta$ - and *meso*-protons. The metalloporphyrins [Zn**48**] and [Zn**53**] displayed very similar spectra to their free-base counterparts but without the peak at a negative chemical shift value indicating that the internal protons are no longer present.

#### **5.3.1.1. UV-vis analysis**

Porphyrins, due to their highly conjugated skeleton, produce very distinct electronic absorption spectra. Consisting of a sharp, intense transition around  $400$  nm; the Soret band, caused by a transition from the ground state to the second excited state ( $S_0 - S_2$ ) and four broader transitions of weaker intensity; the Q bands, the first of which, around  $550$  nm, is caused by a transition from the ground state to the first excited state ( $S_0 - S_1$ ), see Figure 21, section 1.4.2.<sup>219, 220</sup> Metalloporphyrins display different absorption spectra to their free-base counterparts, making UV-vis analysis a characteristic way of ascertaining whether a metal ion has been inserted into the porphyrin cavity. The UV-vis spectrum of a metalloporphyrin consists of the typical intense Soret band around  $400$  nm but only two other bands termed  $\alpha$  and  $\beta$  usually between  $500$  and  $600$  nm. The energy gap separating the Q bands is attributed to different vibrational components of the same electronic transition. The transition

dipole moments experienced by free-base porphyrins in the x and y directions are different whereas those for more symmetric porphyrins i.e metalloporphyrins are the same.<sup>220</sup> This means that the dipole transitions of metalloporphyrins have the same energy and overlap, reducing the number of bands observed, this results in a change in the conjugated ring symmetry from  $D_{4h}$  to  $D_{2h}$ .<sup>221</sup>

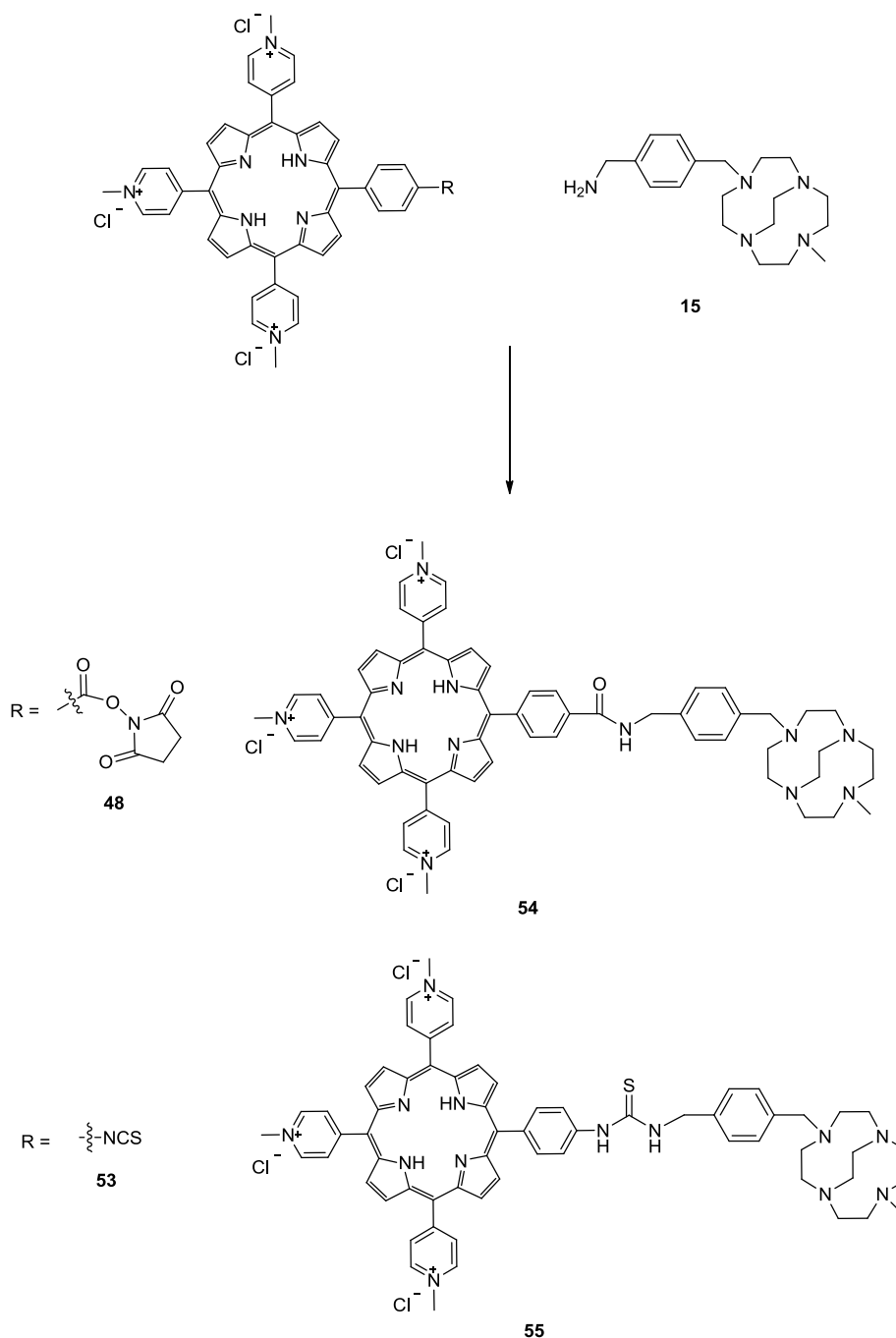
All free-base porphyrins (**45-53**) produced the characteristic UV-vis spectrum described above. Both [Zn**48**] and [Zn**53**] showed only two bands along with the Soret band in their electronic absorption spectra confirming that a zinc(II) ion is occupying the porphyrin cavity. The wavelength and intensity of transitions varies slightly in the series synthesised due to solvent choice and the identity of substituents on the porphyrin ring as these factors affect the relative energies of transitions also causing slight shifts in the wavelengths of peaks.

The design features employed (methylation and anion exchange) to obtain [Zn**48**] and [Zn**53**] are intrinsic to the overall design of the MFC. Methylation produces cationic porphyrins which are useful because the CXCR4 receptor is negatively charged and this may aid or at least not hinder binding of the bismacrocylic species at the CXCR4 receptor. Anion exchange from iodide to chloride improves water solubility; a valuable property for drug candidates. Two water soluble zinc containing porphyrins; [Zn**48**] and [Zn**53**], bearing an NHS ester and an NCS functionality, respectively, were successfully synthesised.

#### **5.4. Towards the synthesis of water soluble MFCs**

Conjugating a targeting group to the porphyrin can reduce the systemic effects associated with their clinical use as PDT agents. Therefore initial attempts to conjugate these water soluble porphyrins to CXCR4 targeted macrocycles were made. Two small scale conjugations were attempted between porphyrins **48** and **53** and methylamine bearing CB monocyclen **15** to produce conjugates **54** and **55** respectively, see Scheme 25. Metal-free starting materials were chosen to aid in the interpretation of analytical data. Despite this,  $^1\text{H}$  NMR spectra of both conjugation attempts were not easy to interpret due to a series of broad overlapping multiplets.

MS data for conjugate **54** showed a peak corresponding to a porphyrin fragment at 874 [**48** – Cl]<sup>+</sup>. No peaks were observed for the starting macrocycle or for the conjugation product (**54**). MS data for conjugate **55** showed a peak for macrocycle **15** at 332 [**15** + H]<sup>+</sup> and a peak corresponding to a porphyrin fragment at 755 [**53** – 2Cl]<sup>+</sup>. A peak for the conjugation product was not observed.



*Scheme 25: Attempted conjugation reactions between porphyrins **48** and **53** and monomacrocycle **15** to produce conjugated products; **54** and **55**.*

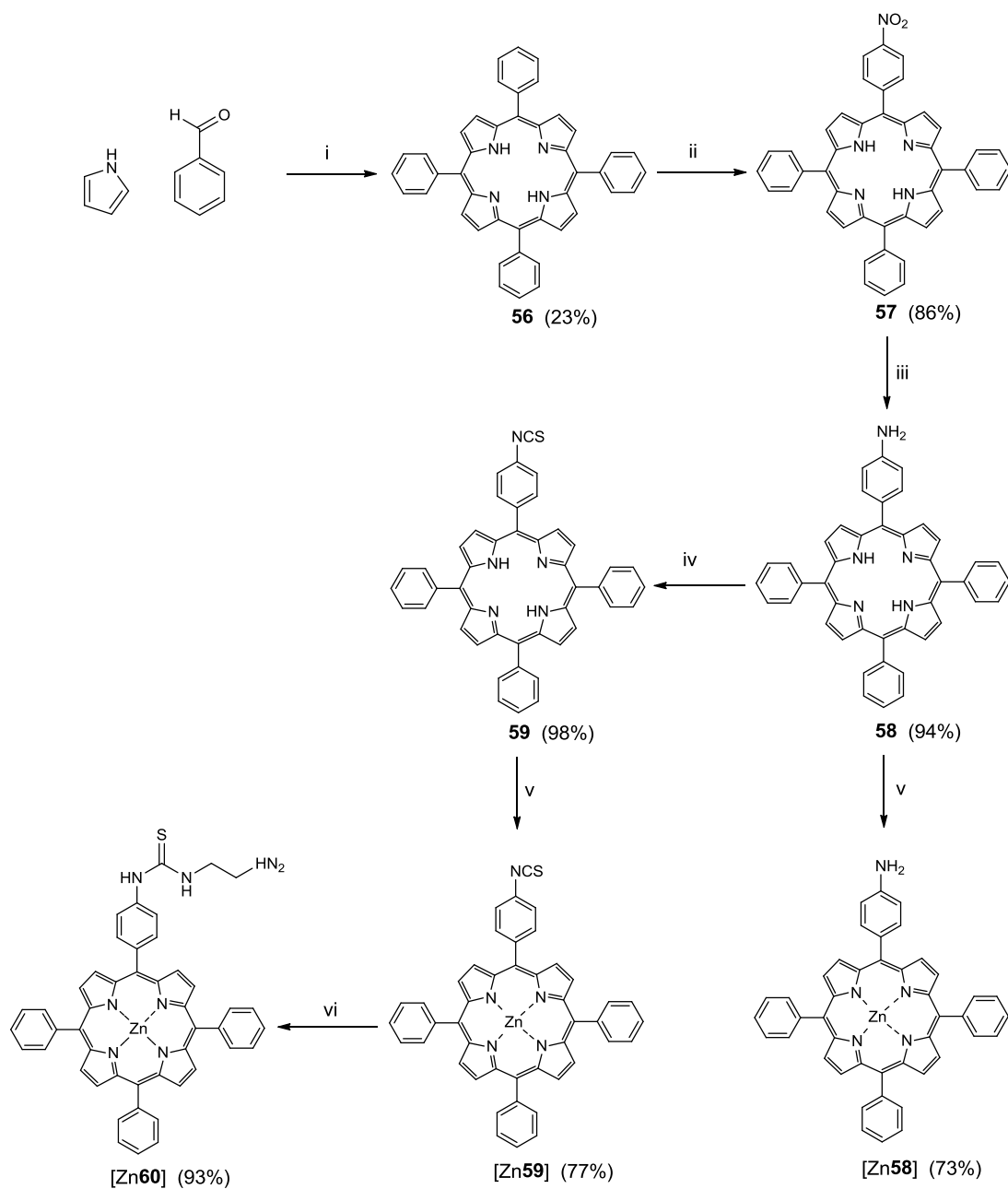
Size exclusion chromatography was used to purify the reaction mixtures and would separate any unconjugated macrocycle from a porphyrin conjugate. The lack of macrocyclic peaks in the MS data for conjugate **54** suggests that the starting materials have been separated on the column and the reaction was not successful, this would explain why only peaks pertaining to the porphyrin were observed. It is encouraging to see peaks associated with macrocycle **15** in the MS analysis of conjugate **55** but the lack of a peak for the conjugated product makes it hard to verify whether the reaction was successful. Since water soluble porphyrins have a lengthy synthesis time it was decided that organic soluble porphyrins bearing functional groups would be synthesised and used to optimise reaction conditions before any further attempts were made with the water soluble porphyrins. Organic soluble porphyrins can be made in a much shorter synthesis time and in higher yields.

## **5.5. Organic soluble porphyrins; useful models**

### **5.5.1. Tetraphenylporphyrin and its derivatives**

The synthesis of tetraphenylporphyrin (TPP) (**56**) using Adler-Longo conditions is well established. The symmetrical nature of the porphyrin makes it easier to isolate from the reaction mixture than unsymmetrical porphyrins and so improved yields are observed. TPP was synthesised in 23% yield comparable to that achieved by Adler-Longo<sup>213</sup> and used to synthesise a range of derivatives bearing functional groups, see Scheme 26.

The mono-nitration of TPP to obtain TPP-NO<sub>2</sub> (**57**) is a desirable procedure due to the ease of converting the nitro group into other useful functionalities such as a primary amine or a diazonium group and the insensitivity of nitration reactions to peripheral crowding.<sup>222</sup>



*Scheme 26: Synthetic route to synthesise organic soluble porphyrins and their zinc complexes. Conditions: i) propionic acid, 1 hour reflux, ii)  $[\text{NO}_2][\text{BF}_4]$ , DCM, RT, iii) HCl and  $\text{SnCl}_2 \cdot 2\text{H}_2\text{O}$  at  $60^\circ\text{C}$  for 1 hour, iv) TCP in DCM for 6 hours at RT, v) zinc(II) acetate in MeOH, 15 min at RT, vi) ethylenediamine for 18 hours at RT.*

#### 5.5.1.1. Mono-nitration of TPP

Nitration of various porphyrins have been investigated by a number of groups using a variety of nitrating agents including  $\text{N}_2\text{O}_4$ ,<sup>223, 224</sup>  $\text{AgNO}_2/\text{I}_2$ <sup>225</sup> and  $\text{Cu}(\text{NO}_3)_2/\text{AcOH}/\text{Ac}_2\text{O}$ <sup>226, 227</sup> on free-base and metalloporphyrins. Wickramasinghe *et al.* evaluated all

of these nitrating agents for the  $\beta$  nitration of zinc(II) and nickel(II) pentasubstituted porphyrins ( $L^{57}$  and  $L^{58}$ ), see Figure 81.<sup>222</sup> Nitration of zinc(II) porphyrin  $L^{57}$ , with  $\text{AgNO}_2/\text{I}_2$  produced a mixture of mono- ( $L^{59}$ ) and bis-nitrated ( $L^{61}$ ) products as well as starting material, see Figure 81. Reaction of the nickel(II) porphyrin  $L^{58}$ , with  $\text{AgNO}_2/\text{I}_2$ ,  $\text{N}_2\text{O}_4$  or  $\text{Cu}(\text{NO}_3)_2$  produced mixtures of mono- ( $L^{60}$ ) and regioisomeric bis-nitrated ( $L^{62}$ ) products, see Figure 81. Their results suggest that control of the nitration reaction is difficult to achieve and can vary depending on the nature of the porphyrin. Wyrebek *et al.* reported the mono-nitration of copper(II)-TPP using  $\text{HNO}_3$  at RT reporting 74-93% yields but harsh conditions ( $\text{TFA}/\text{H}_2\text{SO}_4$ , reflux) were required to obtain the free-base porphyrin.<sup>228</sup>

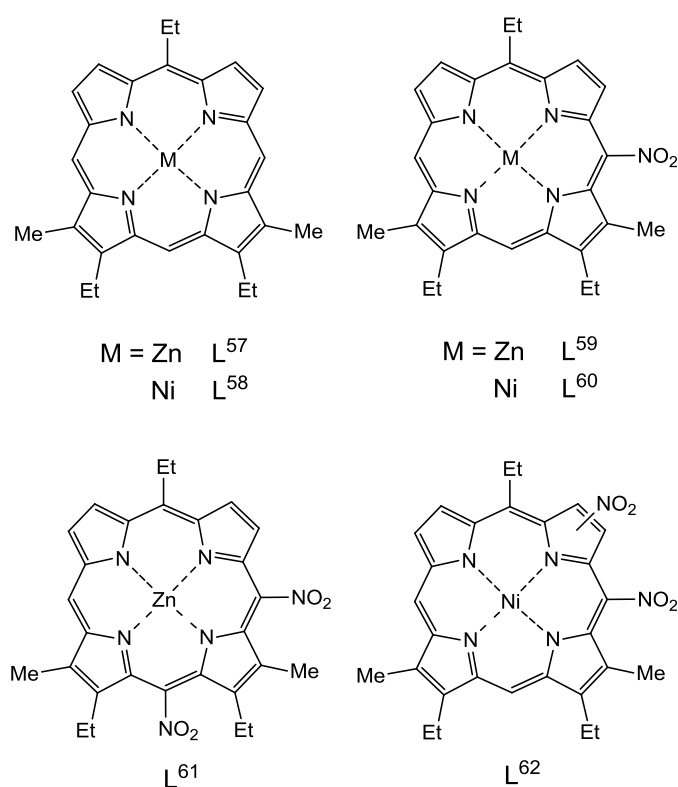


Figure 81: The nitration products ( $L^{59}$ - $L^{62}$ ) observed from nitration of metalloporphyrins  $L^{57}$  and  $L^{58}$  using various nitrating agents outlined by Wickramasinghe *et al.*<sup>222</sup>

Nitric acid (fuming red or yellow) has been utilised by several groups to nitrate TPP. Kruper *et al.* demonstrated mono-nitration of TPP at the *para*-phenyl position using fuming nitric acid obtaining 46-56% yields,<sup>229</sup> similar to that published by Weimin *et al.* (*ca.* 55% yield).<sup>211</sup> Meng *et al.* reported higher yields (74%) for this nitration

reaction by using a mixture of HNO<sub>3</sub> with either H<sub>2</sub>SO<sub>4</sub> or acetic acid.<sup>230</sup> The group of Ostrowski has also used HNO<sub>3</sub> as a nitrating agent obtaining various degrees of nitration on the *para*-phenyl positions of TPP depending on the reaction temperature, amount of acid used and the reaction time employed.<sup>231</sup> Luguva *et al.* opted to use NaNO<sub>2</sub>/TFA as nitrating reagents and were able to control the degree of nitration with the amount of NaNO<sub>2</sub> used and the reaction time employed but did note that a mixture of bis-nitrophenyl porphyrins formed when trying to isolate the mono-nitrated product.<sup>232</sup> Recently Smith and Dzyuba have presented the nitration of TPP using nitronium tetrafluoroborate ([NO<sub>2</sub>]<sup>+</sup>BF<sub>4</sub><sup>-</sup>), which has received limited attention as a nitrating agent of porphyrins but the authors describe as a 'mild, easy to handle and selective nitrating agent'.<sup>233</sup> They determined that slow, sequential addition of molar equivalents of [NO<sub>2</sub>]<sup>+</sup>BF<sub>4</sub><sup>-</sup> in 0.5 M sulfolane solution produced clean, high yielding conversions. The authors stress that it is this sequential addition of specific molar equivalents of [NO<sub>2</sub>]<sup>+</sup>BF<sub>4</sub><sup>-</sup> which is essential to the degree of nitration introduced into TPP, see Figure 82. Bis- (exclusively 5,10-bis-NO<sub>2</sub>-TPP) and tris-nitrated species were also cleanly isolated from sequential addition reactions.

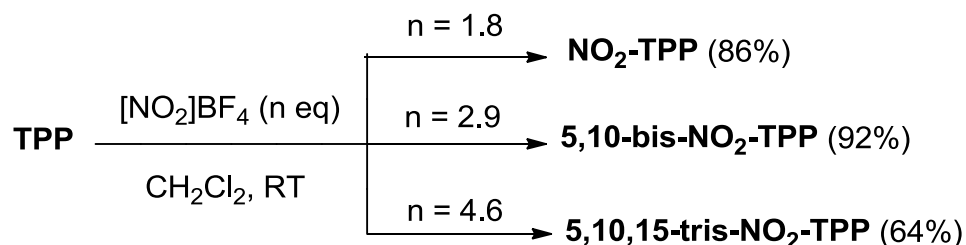


Figure 82: Addition of specific equivalents of [NO<sub>2</sub>]<sup>+</sup>BF<sub>4</sub><sup>-</sup> to TPP allows the clean isolation of mono, bis- and tris-nitration products. (Reproduced from Arkivoc)<sup>233</sup>

Following conditions set out by Smith and Dzyuba,<sup>233</sup> the isolation of TPP-NO<sub>2</sub> (**57**) was successfully achieved in 86% yield, comparable to the published yield. It was noted, similar to the authors' observations, that after the sequential addition of 1.8 molar equivalents of [NO<sub>2</sub>]<sup>+</sup>BF<sub>4</sub><sup>-</sup> and the allocated stirring time, unreacted TPP was still visible on the TLC plate. Addition of a further 0.5 molar equivalents of [NO<sub>2</sub>]<sup>+</sup>BF<sub>4</sub><sup>-</sup> was performed sequentially and whilst TLC indicated the amount of starting material was decreasing a second spot lower in R<sub>f</sub> than the mono-nitrated product

was noted; thought to be a bis-nitrated product. Although the reaction had not gone to completion at this point it was deemed better to stop the reaction and recover TPP, which could be recycled and used in a successive reaction, rather than drive the reaction further since a bis-nitrated product was not desirable for this work. The presence of small amounts of TPP and a bis-nitrated product may explain why a slightly lower yield to that described by Smith and Dzyuba was obtained.

TPP-NO<sub>2</sub> (**57**) was easily converted to TPP-NH<sub>2</sub> (**58**) following standard reaction conditions<sup>234</sup>; SnCl<sub>2</sub>/HCl to afford a 94% yield, comparable to (or better than) published yields.<sup>230, 232</sup> The amino functionality was readily converted to an isothiocyanate group utilising TCP. A facile chromatographic purification step to remove trace amounts of unreacted starting material observed using TLC, afforded TPP-NCS (**59**) in near quantitative yield (*ca.* 98%). Porphyrins **58** and **59** were then coordinated with zinc(II) to afford metalloporphyrins [Zn**58**] and [Zn**59**] in 73% and 77% yields, respectively, using conditions outlined previously;<sup>217</sup> zinc(II) acetate/RT/1 hour. [Zn**60**] was synthesised by stirring Zn-TPP-NCS ([Zn**59**]) with ethylenediamine at RT affording a 94% yield.

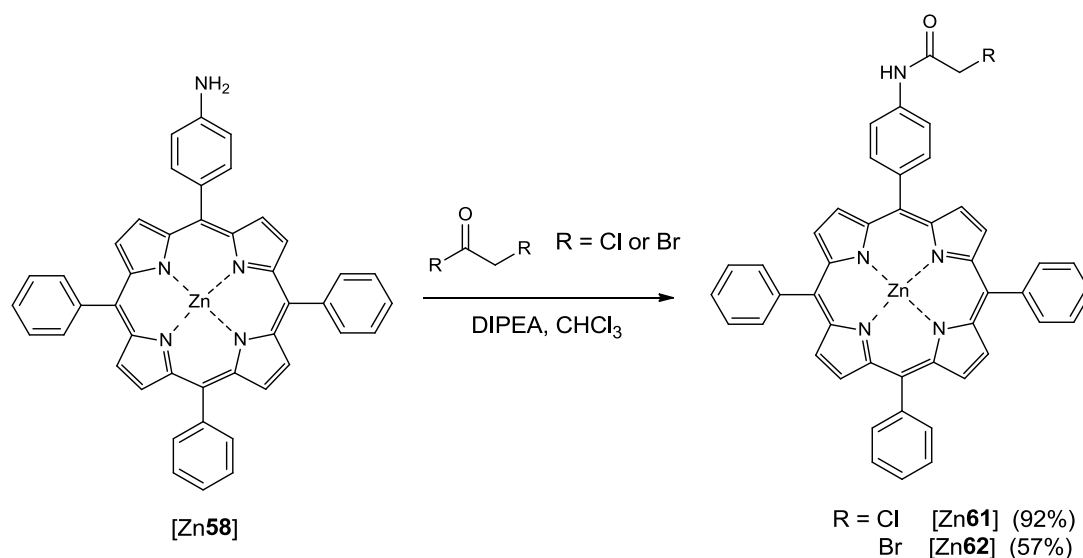
Free base porphyrins **56-60** and metalloporphyrins [Zn**58**], [Zn**59**] and [Zn**60**] were fully characterised by <sup>1</sup>H NMR, MS and UV-vis analysis, details for which have been previously described, see section 5.3.1.1.

At this stage it should be noted that metalloporphyrins [Zn**58**] and [Zn**60**] both terminate in an amine group so will react with acid or activated acid functionalities to form amide bonds. [Zn**59**] bears an isothiocyanate group so will react with an amine group to produce thiourea linkages. Bismacrocycles terminating in acid, activated acid and amine groups have been previously described, see Chapter 3. The range of amine reactive porphyrins was expanded to improve the probability of ascertaining successful reaction conditions.

#### **5.5.1.2. Formation of acyl halide derivatives**

Acyl halide compounds were reacted with Zn-TPP-NH<sub>2</sub> [Zn**58**] to form metalloporphyrins [Zn**61**] and [Zn**62**], see Scheme 27, utilising the basicity of DIPEA.

These halide bearing derivatives will readily react with amine functionalities in  $S_N2$  type reactions. Chromatographic purification afforded the chloro derivative [Zn61] in high yield (ca. 92%) with the bromo derivative [Zn62] isolated in moderate yield (ca. 57%), this was caused by poor separation from the amine bearing starting material; [Zn58]. Both metalloporphyrins were characterised by  $^1\text{H}$  NMR, MS and UV-vis showing the characteristic features described previously, see sections 5.3.1 and 5.3.1.1.



*Scheme 27: Addition of acyl halides to Zn-TPP-NH<sub>2</sub> to produce [Zn61] and [Zn62].*

This idea has been tested by Denat and co-workers who synthesised a chloro bearing porphyrin derivative for subsequent reaction with a secondary amine bearing compound.<sup>235</sup> It should be noted that a mixture of products was obtained using their reaction conditions.

The previous sections detail the successful synthesis of several organic soluble metalloporphyrins bearing various functional groups for subsequent conjugation to complementary bismacrocylic compounds were successfully synthesised.

## 5.6. Towards the synthesis of organic soluble MFCs

The necessary building blocks to produce novel MFCs with diagnostic and therapeutic properties have been synthesised, see Figure 83. The PDT active

metalloporphyrins described in section 5.5. have complementary functionalities to react with the CXCR4 targeted bismacrocylic compounds bearing spacer arms outlined in Chapter 3.

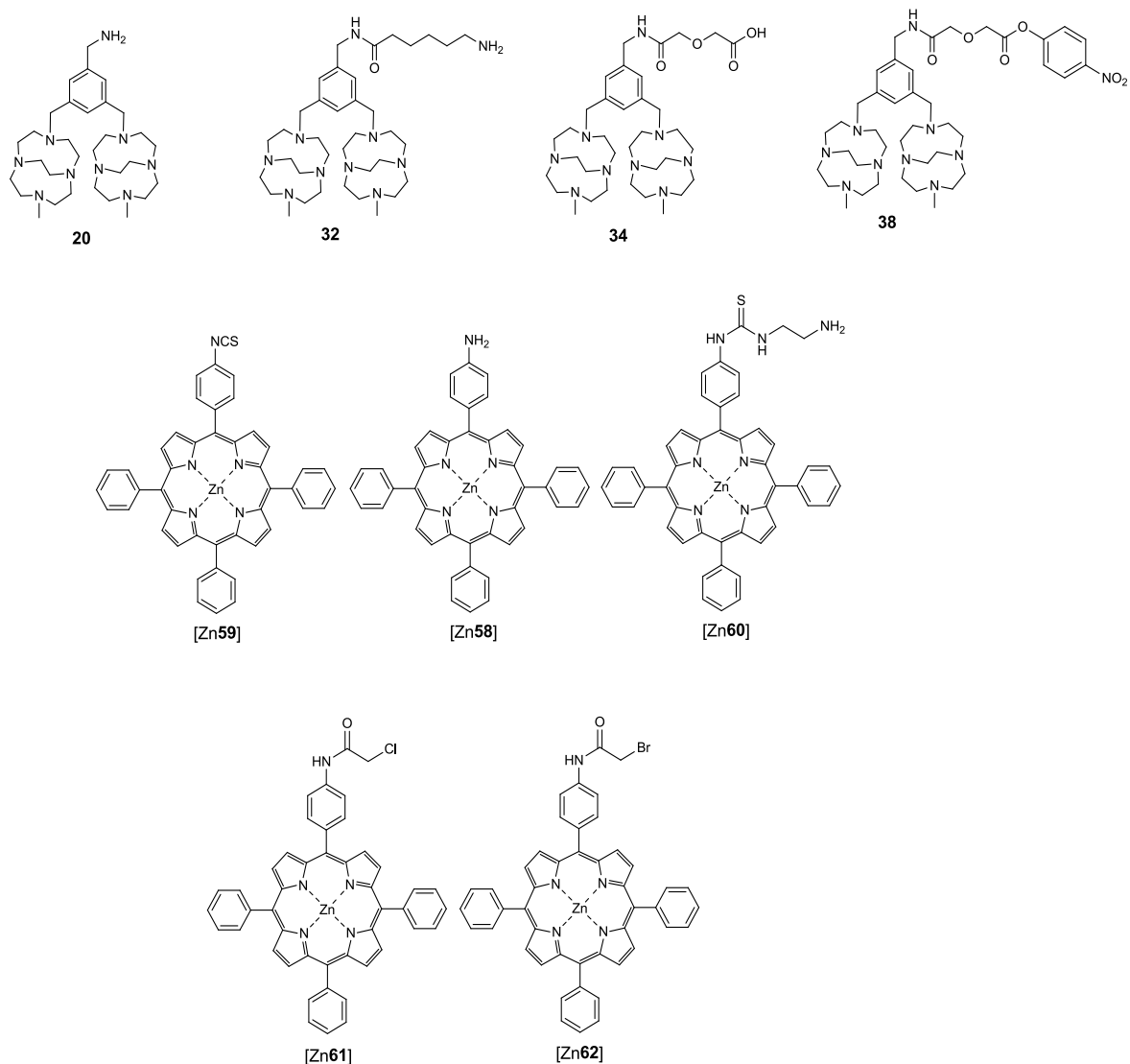


Figure 83: Structures of the 'building blocks' synthesised to make novel MFCs.

Due to time constraints several conjugation reactions were attempted in parallel. All reactions were monitored *via* TLC to follow consumption of the starting porphyrin. Once the reaction was deemed finished solvents were removed *in vacuo*. Reaction mixtures were then sent for MS analysis to ascertain whether a conjugation product was present. Any reactions showing presence of the desired product would be subject to a purification procedure, in this way time would not be

wasted on developing a purification method for reactions which were not indicating the presence of the desired product. Ten reactions were set up using the bismacroyclic species outlined in Chapter 3; **20**, **32**, **34** or **38** along with the complementary metalloporphyrin.

Reaction conditions employed to obtain conjugates **63** and **65**, see Table 9, were obtained from Denat and co-workers,<sup>235</sup> who had used similar conditions to conjugate a secondary amine bearing macrocyclic ligand to acyl halide bearing porphyrins. All four reaction pathways were monitored *via* TLC and after 24 hours all showed the presence of two new porphyrin spots of lower  $R_f$  value, one at  $R_f$  0.22 and one on the baseline. The baseline spot had the potential to be a conjugated product and so reactions were stopped and sent for MS analysis. Spectra obtained for all four attempts were very similar, none displayed peaks relating to the desired conjugated product but all contained a peak a  $m/z = 692$  with a zinc(II) isotope pattern identified as Zn-TPP-NH<sub>2</sub> [Zn**58**] and relates to the spot observed at  $R_f$  0.22 on the TLC plate, indicating that the starting material [Zn**61**] or [Zn**62**] is degrading during the reaction. This degradation suggested that the reaction conditions employed were too harsh. Therefore milder conditions were used to obtain conjugates **64** and **66**. After 2 hours TLC indicated that both reactions were complete due to complete consumption of the porphyrin starting material. Intuitively, the longer spacer chain of bismacrocycle **32** may have a better chance of conjugating to Zn-TPP-NCS [Zn**59**] as there will be less steric hindrance around the reactive functional groups but MS analysis showed no peaks for conjugate **66** only a peak for the starting porphyrin Zn-TPP-NCS [Zn**59**] at  $m/z = 734$ . However, MS analysis for reaction of the methylamine terminating bismacrocycle **20** with Zn-TPP-NCS [Zn**59**] showed two peaks pertaining to the conjugation product **64**; one at 1293 [**64** + H]<sup>+</sup> and a doubly charged peak at  $m/z = 647$  [**64** + 2H]<sup>2+</sup>.

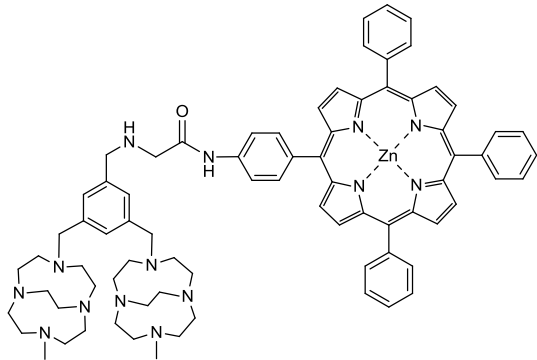
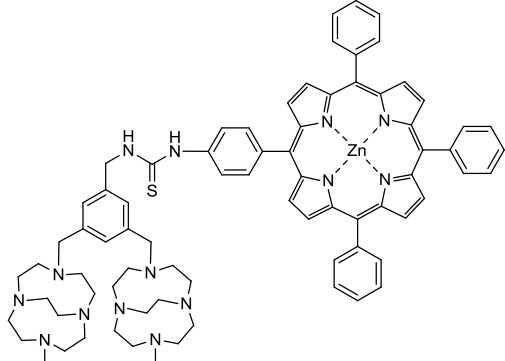
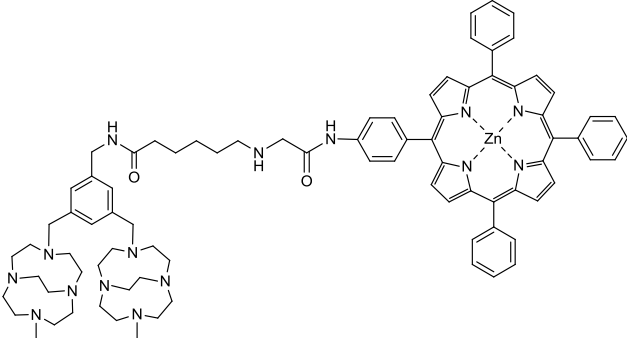
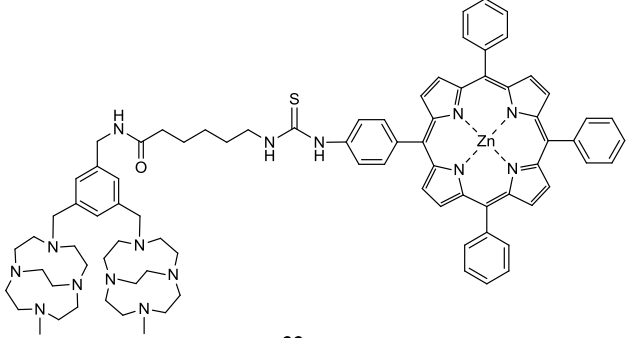
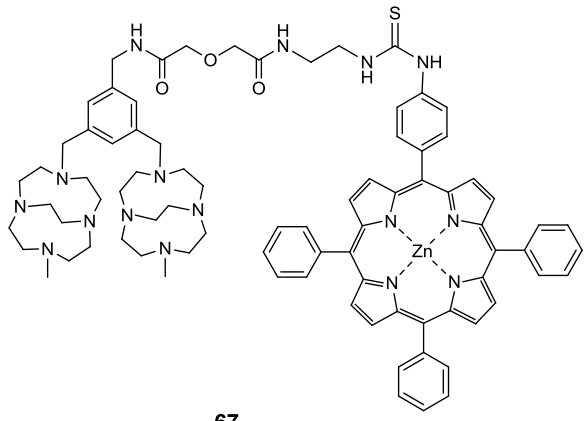
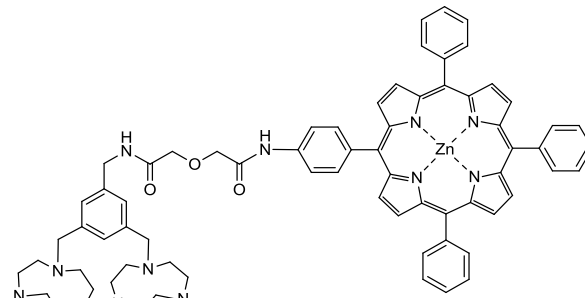
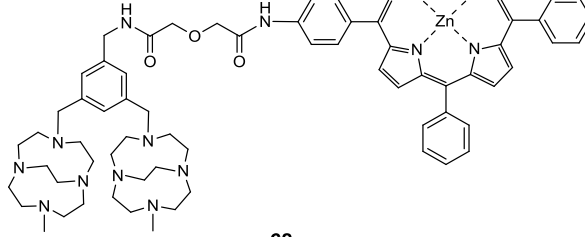
Macrocyclic	Metalloporphyrin	Reaction conditions	Potential conjugation product
20	[Zn61]	K <sub>2</sub> CO <sub>3</sub> , MeOH reflux, 24 h	 <p style="text-align: center;"><b>63</b></p>
20	[Zn62]		
20	[Zn59]	Stir, MeOH RT, 2 h,	 <p style="text-align: center;"><b>64</b></p>
32	[Zn61]	K <sub>2</sub> CO <sub>3</sub> , MeOH reflux, 24 h,	 <p style="text-align: center;"><b>65</b></p>
32	[Zn62]		
32	[Zn59]	Stir, MeOH, RT, 2h	 <p style="text-align: center;"><b>66</b></p>

Table 9: Structures of the expected conjugation products obtained from reacting amine terminating bismacrocylic species with metalloporphyrins.

UV-vis confirms that a zinc porphyrin is still present; all three bands are slightly shifted (Soret and alpha red shifted, beta blue shifted) in comparison to the starting porphyrin ([Zn-TPP-NCS]). As previously mentioned the position of the peaks can be affected by the nature of the substituents attached to the porphyrin so this may be an indication of a successful conjugation reaction.  $^1\text{H}$  NMR shows two distinct regions in the spectra, a broad, undefined multiplet between  $\delta$  4.5-6; characteristic of a bismacrocylic species with sharper peaks between  $\delta$  9-11; characteristic of a porphyrin species. The spectrum is hard to integrate with any accuracy and so it is difficult to conclude if a successful conjugation reaction has occurred from this data.

Reactions involving an acidic terminating or activated acid type bismacrocycle were also attempted, see Table 10. Reaction of the activated ester bismacrocycle **38** with the metalloporphyrin [Zn**60**] showed presence of new porphyrin spots after 4 hours at 40°C, using TLC. However, MS analysis did not show the presence of any peaks relating to the conjugation product **67** or the starting materials, indicating that there was some possible degradation of material. An analogous reaction using [Zn**58**] instead of [Zn**60**] to form conjugate **68** was attempted, the reaction was monitored *via* TLC for 24 hours after which time no new spots were observed and the reaction was abandoned.

Previous reactions described in Chapter 3, section 3.4.1., have identified PyBOP and DCC as useful coupling reagents when bismacrocylic species are involved. Two reactions were attempted between acid terminating bismacrocycle **34** and Zn-TPP-NH<sub>2</sub> [Zn**58**] to make conjugate **68**, one using PyBOP/DIPEA as the coupling reagents and the other DCC/DIPEA. As previously observed TLC showed presence of new porphyrin spots after 4 hours at 40°C but MS analysis did not show any peaks pertaining to conjugate **68** and only a peak for the starting porphyrin ([Zn**58**]) could be identified.

Macrocycle	Metallo-porphyrin	Reaction conditions	Potential conjugation product
<b>38</b>	[Zn <b>60</b> ]	Stir, 4 h, 40°C, DCM/MeOH	 <p style="text-align: center;"><b>67</b></p>
<b>38</b>	[Zn <b>58</b> ]	Stir, 24 h, 40°C, MeOH	 <p style="text-align: center;"><b>68</b></p>
<b>34</b>	[Zn <b>58</b> ]	PyBOP, DIPEA, stir, 4 h, 40°C, DCM/MeOH DCC, DIPEA, stir, 4 h, 40°C, DCM/MeOH	 <p style="text-align: center;"><b>68</b></p>

*Table 10: Structures of the expected conjugation products obtained from reacting an acid or an activated ester terminating bismacrocylic species with metalloporphyrins.*

The series of reactions to form novel MFCs, see Table 9 and 10, has highlighted one potentially successful conjugation; the reaction of bismacrocycle **20** with metalloporphyrin [Zn**59**] to form conjugate **64**. An appropriate purification method is now required.

The 'proton sponge' nature of bismacrocylic compounds prevents the use of silica as a chromatography material. Size exclusion chromatography using sephadex LH20 would separate a conjugated product from starting materials. A 'test' purification

with [Zn59] indicated that this might not be possible however as the metalloporphyrin streaked down the column resulting in poor recovery of the product. Semi-prep HPLC could be a viable method for purifying such conjugation attempts since columns can be purchased which are suitable for the separation of highly basic compounds (phenomenex, Gemini) but due to time constraints this was not investigated further.

## 5.7. Conclusions

The successful synthesis of two water soluble porphyrins **48** and **53** and their zinc(II) complexes [Zn**48**] and [Zn**53**] has been carried out. Isolation of the free-base porphyrins was achieved through extensive chromatographic purification resulting in low yields making these water soluble porphyrins a valuable commodity. Initial attempts to conjugate porphyrins **48** and **53** to monomacrocycle **15** were trialled and analytical data for each attempt, whilst encouraging, was not conclusive of a successful conjugation, highlighting the need to ascertain reaction conditions before using valuable stocks of material. Subsequently, a series of organic soluble metalloporphyrins were successfully synthesised; [Zn**58**], [Zn**59**], [Zn**60**], [Zn**61**] and [Zn**62**], in yields comparable to published values. Test reactions were then performed to ascertain the reaction conditions required to conjugate these metalloporphyrins to various bismacrocylic compounds bearing spacer arms. Spectroscopic data indicates that the conjugation of isothiocyanate terminating metalloporphyrin [Zn**59**] and the amine terminating bismacrocycle **20** to produce conjugate **64** was successful. Work continues to ascertain a purification method for this conjugate with semi-prep HPLC identified as a viable option.

## **Chapter 6**

### **Conclusions and future work**

## 6.1. Conclusions

### 6.1.1. Overview

The design and synthesis of clinically useful compounds to diagnose and/or treat cancers is a challenging task. The improvement in the design of chelating ligands along with PET technologies has led to a surge in the production of clinically relevant PET probes. PET radiotracers with longer-lived half-lives such as  $^{64}\text{Cu}$  are particularly attractive because they allow the study of longer-lived processes within the body. The use of tetraazamacrocyclic ligands as chelating agents has been well documented in the literature but their use in a clinical setting has often been hampered by transmetallation and associated toxicity. This work demonstrates the development of several novel macrocyclic ligands through structural rigidification and functional group modification, as improved chelating ligands. The propensity of macrocyclic ligands to bind to the chemokine receptor CXCR4, which is known to be overexpressed on at least 23 different human cancers means these ligands have the potential to be targeted probes. Porphyrins are therapeutically active PDT agents examples of which have been licensed for clinical use. Their conjugation to macrocyclic ligands would produce a probe with multifunctional capabilities namely the diagnosis and treatment of CXCR4 expressing tumours. This work outlines steps towards producing such a complex probe for use in a clinical setting.

### 6.1.2. Main achievements

The successful synthesis of a series of novel, configurationally restricted, N-functionalised monomacrocyclic compounds bearing a methylamine pendant arm (**8**, **9**, **14**, **15**) and their copper(II), zinc(II) and nickel(II) complexes have been described. Configurational restriction was achieved through addition of an ethylene bridge between opposite or adjacent nitrogen atoms to form cross bridged (CB) or side bridged (SB) compounds, respectively. A pendant arm; 4(bromomethyl) benzonitrile was attached to one of the nitrogen atoms on the macrocyclic skeleton and  $\text{LiAlH}_4$  was found to reduce the cyano group to a methylamine group in high yield (*ca.* >77%).  $[\text{Zn}9]^{2+}$ , a SB cyclen ligand, showed the highest affinity for CXCR4 of the series tested ( $\text{IC}_{50} = 0.012 \mu\text{M}$ ), over 2.5-fold higher than AMD3100 ( $\text{IC}_{50} = 0.031$

$\mu\text{M}$ ) and a SB monocyclam complex  $[\text{Zn}\mathbf{8}]^{2+}$  ( $\text{IC}_{50} = 0.034 \mu\text{M}$ ) showed comparable affinity to that of AMD3100.

The completion of a multi-step synthetic route to obtain a novel biscyclen compound bearing a methylamine pendant arm has been outlined. Copper(II), zinc(II) and nickel(II) complexes of this novel configurationally restricted bismacrocycle have been synthesised. With the copper(II) complex being an important ligand for potential use as a PET agent. These metal containing compounds were designed to be high affinity antagonists for CXCR4, incorporation of two cyclen rings in a *meta*-substitution pattern coupled with configurational restriction were the design features employed to obtain high affinity. A methylamine pendant arm also allowed for further reaction of this bismacrocycle through formation of amide bonds. The non-complexed ligand (**20**) showed high binding for the CXCR4 receptor (% inhibition = 87%) but as expected its analogous metal complexes;  $[\text{Cu}_2\mathbf{20}]^{4+}$ ,  $[\text{Zn}_2\mathbf{20}]^{4+}$ ,  $[\text{Ni}_2\mathbf{20}]^{4+}$ , all showed higher affinity for CXCR4 (% inhibition = 88%, 90% and 96%, respectively), sub-micromolar concentrations were required to reduce the normal signalling of CXCR4 by 50% with  $[\text{Cu}_2\mathbf{20}]^{4+}$  showing comparable affinity to ADM3100 ( $\text{IC}_{50} = 39 \text{ nM}$  vs.  $31 \text{ nM}$ ). These results can be rationalised by the formation of coordinate bonds between the metal ions and the aspartate residues as opposed to the weaker H-bonding interactions formed when a metal ion is not present.  $[\text{Cu}_2\mathbf{20}]^{4+}$  has the potential to be a targeted PET probe, if radiolabelled with  $^{64}\text{Cu}$  so a detailed evaluation of its binding properties were undertaken and concluded that it exerts its antagonistic effects by locking the receptor on the surface of the cell, stopping the internalisation and recycling processes which would result in formation of a new receptor.

To provide a comparative study the multi-step synthesis of an analogous CB biscyclam compound bearing a methylamine pendant arm was attempted and the final compound was successfully isolated as an octahydrochloride salt (**28**). The copper(II), zinc(II) and nickel(II) complexes of this novel bismacrocylic species have also been synthesised for evaluation as CXCR4 antagonists.  $[\text{Cu}_2\mathbf{28}]^{4+}$ ,  $[\text{Zn}_2\mathbf{28}]^{4+}$  and  $[\text{Ni}_2\mathbf{28}]^{4+}$  showed unexpectedly high affinity for CXCR4 ( $\text{IC}_{50} > 0.1 \mu\text{M}$ ). Intuitively it

might be thought that the *meta*-substitution pattern would create steric hinderance between the larger cyclam rings possibly leading to a poor fit in the receptor cavity but this does not appear to be the case.  $[\text{Cu}_2\mathbf{28}]^{4+}$  demonstrated a 3-fold higher affinity than AMD3100 ( $\text{IC}_{50} = 11 \text{ nM}$  vs.  $31 \text{ nM}$ ) and its potential as a PET probe should not be overlooked.

The synthesis of a non-configurationally restricted *meta*-substituted biscyclen (**24**) was synthesised through tris-protection of cyclen rings followed by cleavage of these groups. Its copper(II) and zinc(II) complexes were also synthesised in high yield (72% and 90%, respectively). All three compounds showed a measurable interaction with CXCR4 in contrast to Oltmanns results.<sup>157</sup> The 'free' ligand **24** has comparable affinity to AMD3100 ( $\text{IC}_{50} = 26 \text{ nM}$  vs.  $31 \text{ nM}$ ) whilst the zinc(II) complex;  $[\text{Zn}_2\mathbf{24}]^{4+}$  showed a 4-fold improvement in affinity compared to AMD3100. Anti-HIV activity was also assessed and copper(II) complexes of the cyano terminating ligands **19** and **27** were highlighted as particularly potent ligands in MT-4 cells.

Various spacer arms were attached to bismacrocycle **20** *via* amide bond formation for subsequent conjugation to a porphyrin. The spacer arm provides a means of reducing steric hindrance and preventing any unwanted interactions between the bismacrocycle and the porphyrin. The optimum requirements of the spacer arm are unknown so it was necessary to synthesise several compounds to ascertain useful features. An acidic terminating spacer arm was successfully attached to bismacrocycle **20** to form compound **34**, *via* ring opening of diglycolic anhydride, its copper(II) complex;  $[\text{Cu}_2\mathbf{34}]^{4+}$ , was also successfully isolated in 43% yield. Attempts to activate the acidic terminating bismacrocycle (**34**) proved challenging but DIC and PyBOP were established as useful coupling reagents for amide bond formation. *p*-Nitrophenol was established as a useful activating agent and was successfully used to form an activated ester species (**38**) of bismacrocycle **34**. 4-Nitrophenyl 6-((*tert*-butoxycarbonyl)amino)hexanoate was also successfully synthesised and attached to bismacrocycle **20**, after deprotection of the Boc group, an amine terminating bismacrocycle (**32**) was isolated. A biotin tagged bismacrocycle (**44**) and its

copper(II) complex;  $[\text{Cu}_2\mathbf{44}]^{4+}$  were also successfully isolated in 71% and 94% yields, respectively, through attachment of a *p*-nitrophenol activated biotin species (**43**).

$[\text{Cu}_2\mathbf{20}]^{4+}$  has demonstrated high binding affinity for CXCR4 and its antagonistic properties arise from its ability to lock the receptor on the surface of the cell preventing it from signalling. It was necessary to evaluate the effects on affinity that addition of a spacer arm may have. Two copper(II) containing bismacrocyces bearing an acidic and a biotin tag;  $[\text{Cu}_2\mathbf{34}]^{4+}$  and  $[\text{Cu}_2\mathbf{44}]^{4+}$  were evaluated against  $[\text{Cu}_2\mathbf{20}]^{4+}$ . Both  $[\text{Cu}_2\mathbf{34}]^{4+}$  and  $[\text{Cu}_2\mathbf{44}]^{4+}$  showed high % of inhibition in a competition binding assay (% inhibition = 88% and 89%, respectively) but showed lower binding affinities for CXCR4 ( $\text{IC}_{50}$  = 135 nM and 393 nM, respectively) compared to  $[\text{Cu}_2\mathbf{20}]^{4+}$  ( $\text{IC}_{50}$  = 39 nM) in calcium flux studies. Both were still active at sub-micromolar concentrations however. The acidic terminating bismacrocycle  $[\text{Cu}_2\mathbf{34}]^{4+}$  also showed a higher toxicity than both the biotin tagged bismacrocycle;  $[\text{Cu}_2\mathbf{44}]^{4+}$  and  $[\text{Cu}_2\mathbf{20}]^{4+}$ .  $[\text{Cu}_2\mathbf{44}]^{4+}$  represents the potential to form a useful *in vitro* evaluation tool with multifunctional properties through exploitation of the known avidin-biotin interaction. Work to establish a suitable biological assay to demonstrate this interaction continues.

A series of water soluble and organic soluble porphyrins and their zinc(II) complexes were synthesised, attempts to conjugate these to various macrocyclic ligands proved challenging. One conjugation between the metalloporphyrin  $[\text{Zn}\mathbf{59}]$  bearing an isothiocyanate group and bismacrocycle **20** bearing an amino group showed promising analytical data for formation of the desired conjugate (**64**). Work continues to establish a purification method for such conjugates.

### 6.1.3. Overall achievements in relation to the field

This research has been focused on the design and synthesis of tetraazamacrocyclic species for biological applications. Novel configurationally restricted mono and bis macrocyces have been synthesised bearing functional pendant arms. These ligands are designed to have improved stability and adopt an ideal configuration for binding to the target receptor.

This work details efficient and reproducible multi-step synthetic routes to obtain novel CB and SB monomacrocycles as well as novel CB *meta*-substituted bismacrocycles. The chelation properties of macrocycles have been utilised to make copper(II), zinc(II) and nickel(II) complexes with copper(II) complexes having the potential to be turned into PET probes by radiolabelling with  $^{64}\text{Cu}$ . Several of these metal complexes displayed greater affinity for CXCR4 than the clinically licensed drug AMD3100 also showing low cytotoxicity indicating the potential of these ligands for use in a clinical setting. Addition of various organic spacer arms to a CB bicyclic ligand did not have any significantly detrimental effect on binding affinity. These spacer arms can be used to tune the properties of the macrocycle, such as overall charge and biocompatibility as well as introducing functionality to the macrocyclic core. Conjugations to therapeutically active porphyrin molecules proved challenging but important steps have been made towards the synthesis of tetraazamacrocyclic-porphyrin conjugates to produce targeted MFCs.

This work enriches the current range of known macrocyclic ligands for biological use, highlighting the importance of configurational restriction and chelation of metal ions. Expanding the functionality of the macrocyclic core through attachment of organic spacer arms demonstrates the wide scope of potential uses for macrocyclic ligands. The design and use of MFCs is a relatively new field and so steps towards the synthesis of tetraazamacrocyclic-porphyrin conjugates as targeted MFCs presents novel ideas for this field.

## 6.2. Future work

### 6.2.1. Short-term goals

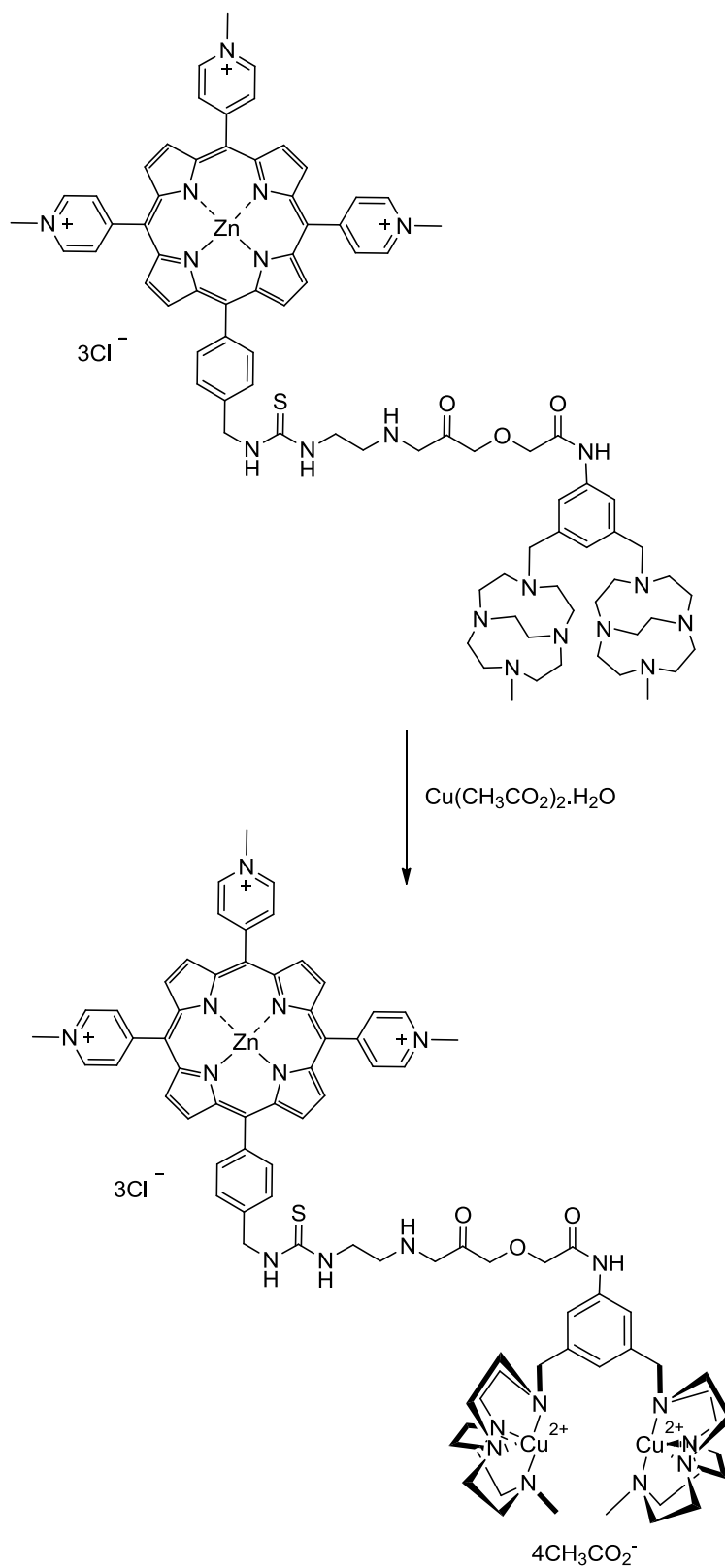
- A more detailed evaluation of monomacrocyclic zinc complexes is necessary to establish how they are acting as high affinity antagonists. It would be useful to perform the same set of biological assays on  $[\text{Zn}9]^{2+}$  as was performed  $[\text{Cu}_220]^{4+}$  to establish its mode of action for CXCR4. Computer modelling may also provide a way to establish how the zinc(II) mono-ring

complexes bind to CXCR4 and explain their high affinity since the crystal structure of CXCR4 is now known.

- Analytical data confirms the successful isolation of the biotin tagged bismacrocycle [Cu<sub>2</sub>**44**]<sup>4+</sup>. A suitable biological assay to demonstrate its interaction with streptavidin-FITC is required.
- Assess why many of the conjugation attempts between bismacrocylic species and porphyrins did not give the desired conjugation product in the MS analysis; did the experiment not work or are the compounds difficult to ionise? i.e. is there a problem with analysing these compounds due to their complex nature.
- Establish a purification method for conjugate **64** which could be extrapolated to other bismacrocycle-porphyrin conjugates. HPLC would be a sensible method to try initially.

#### 6.2.2. Long-term goals

- Once conditions have been optimised and a purification method established for azamacrocyclic-porphyrin conjugates. Copper(II) needs inserting into the bismacrocylic cavities, see Scheme 28, removal of zinc(II) is optional as PDT activity is not lost with it in the porphyrin cavity. Addition of copper(II) as the final synthetic step also suits a radiochemical synthesis where the addition of the radioactive moiety is ideally the final step of a synthetic route.
- These conditions could then be extrapolated to a water soluble porphyrin to produce a water soluble MFC with targeting properties. A biological evaluation of these water soluble MFCs would be needed to assess the cytotoxicity, PDT activity and affinity for the CXCR4 receptor.
- Radiolabelling with <sup>64</sup>Cu could then begin to establish the conditions required to produce a radiolabelled water soluble MFC suitable for PET imaging with therapeutic and targeting properties for CXCR4 expressing tumours.



*Scheme 28: An example of copper(II) insertion into saturated azamacrocyclic cavities producing a novel MFC. Note anions and/or solvent molecules may coordinate to the copper(II) centres.*

# **Chapter 7**

## **Experimental**

## 7.1. General methods

Unless indicated otherwise,  $^1\text{H}$  NMR and  $^{13}\text{C}$  NMR spectra were obtained using a Jeol JNM-LA400 spectrometer at 400 MHz for  $^1\text{H}$  and 100 MHz for  $^{13}\text{C}$  in the solvents indicated, referenced against standard internal TMS or residual non deuterated solvent signal. Chemical shifts ( $\delta$ ) are quoted in parts per million (ppm) and coupling constants ( $J$ ) are quoted in hertz (Hz). Splitting patterns are designated as s (singlet), d (doublet), t (triplet), q (quartet), quin (quintet), m (multiplet) and br (broad). MS was performed using a Finnegan MAT 900 XLT system using electrospray ionisation (ESI). Accurate mass spectrometry measurements (HRMS) were obtained using a LQT Orbitrap XL. UV-vis spectra were obtained using an Agilent 8453E UV-vis diode array spectrometer using quartz cells. CHN analysis was performed using a CHN analyser EA1108 (Carlo Erba).

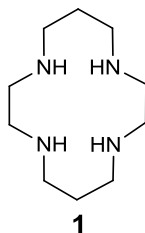
Bulk solvent was removed by rotary evaporation on a Buchi RE 111 evaporator equipped with a diaphragm vacuum pump, trace solvent was removed on a Schlenk line equipped with an oil pump. Reactions were performed at room temperature (RT) unless otherwise stated. All metal containing compounds were purified *via* size exclusion chromatography using sephadex LH20, which was pre-soaked in MeOH for three hours before use.

### 7.1.1. Materials

Materials for chemical reactions were purchased from Aldrich Chemical co., Fisher, Acros, Novabiochem, Goss and Strem. Solvents used were either general purpose or HPLC grade and were used as received. MeCN, dichloromethane (DCM) and tetrahydrofuran (THF) were dried over molecular sieves according to methods outlined by Bradley and co-workers.<sup>236</sup> Dry MeOH was purchased from Acros Chemicals and was used as purchased.

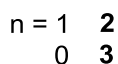
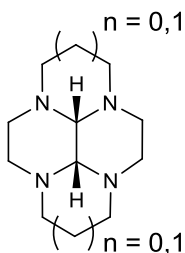
## 7.2. Synthetic procedures

### 7.2.1. Synthesis of 1,4,8,11-tetraazacyclotetradecane (1)



1,5,8,12-Tetraazadodecane (26.0 g, 0.15 mol) was added to a solution of nickel(II) perchlorate (54.7 g, 0.15 mol) in water (400 ml). The resulting red/brown solution was cooled to  $\sim 5^{\circ}\text{C}$  and an aqueous solution of glyoxal (40% w/w, 25 ml, 0.15 mol) was added, the resulting solution was left to stand for 4 hours. The mixture was again cooled to  $\sim 5^{\circ}\text{C}$  and treated with sodium borohydride (11.0 g, 0.30 mol) in small portions. The solution was heated to  $90^{\circ}\text{C}$  for 20 min and filtered whilst hot. Sodium cyanide (29.0 g, 0.60 mol) was added to the filtrate which was heated to the point of reflux then left to cool overnight. Sodium hydroxide (15.0 g, 0.38 mol) was added and the resulting yellow-brown mixture was filtered through a pad of hyflo super cel. The solid was washed with chloroform (3 x 100 ml) and the aqueous layer was then extracted with chloroform (5 x 100 ml). The organic phases were dried ( $\text{Na}_2\text{SO}_4$ ), filtered and the solvent removed *in vacuo*. The resulting yellow solid was recrystallised from chlorobenzene (150 ml), filtered and washed with ether (50 ml) to yield white needles (9.78 g, 33%).  $^1\text{H}$  NMR (400 MHz,  $\text{CDCl}_3$ ,  $\delta$ ): 1.72 (m, N- $\beta$ - $\text{CH}_2$ , 4H), 2.19 (br s, NH, 4H), 2.68 (s, N- $\alpha$ - $\text{CH}_2$ , 8H), 2.74 (m, N- $\alpha$ - $\text{CH}_2$ , 8H).  $^{13}\text{C}$  NMR (100 MHz,  $\text{CDCl}_3$ ,  $\delta$ ):  $\delta$  29.47 (N- $\beta$ - $\text{CH}_2$ ), 49.39 (N- $\alpha$ - $\text{CH}_2$ ), 50.71 (N- $\alpha$ - $\text{CH}_2$ ). HRMS ( $m/z$ ):  $[\text{M} + \text{H}]^+$  calcd for  $\text{C}_{10}\text{H}_{19}\text{N}_4$ , 201.2081; found, 201.2074. Anal. calcd for  $\text{C}_{10}\text{H}_{25}\text{N}_4$ : C, 59.96; H, 12.08; N, 27.97. Found: C, 59.99; H, 12.42; N, 27.59.

**7.2.2. Synthesis of *cis*-3a,5a,8a,10a-tetraazaperhydropyrene (2) and *cis*-13-1,4,7,10-tetraazatetracyclo[5.5.1.0<sup>4,14</sup>.0<sup>10,13</sup>]tetradecane (3)**



**General procedure A**

The macrocycle was dissolved in MeOH and cooled to  $-10^{\circ}\text{C}$ . A cold ( $0^{\circ}\text{C}$ ) aqueous solution of glyoxal was added dropwise over 90 min. The clear solution was stirred at  $-10^{\circ}\text{C}$  for 30 min then at RT for 3 hours. The solvent was removed *in vacuo* and the crude solid was redissolved in diethyl ether. The filtrate was dried ( $\text{MgSO}_4$ ), filtered and solvent removed *in vacuo*.

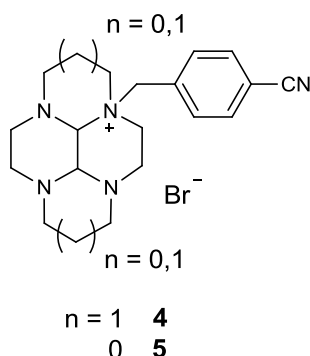
***cis*-3a,5a,8a,10a-Tetraazaperhydropyrene (2)**

Amounts: 1,4,8,11-Tetraazacyclotetradodecane (**1**) (8.13 g, 40.6 mmol), MeOH (200 ml), glyoxal (40% w/w, 5.89 g, 101.8 mmol), diethyl ether (200 ml). To yield a white solid (7.00 g, 78%).  $^1\text{H}$  NMR (400 MHz,  $\text{CDCl}_3$ ,  $\delta$ ): 1.23 (m, N- $\beta$ - $\text{CH}_2$ , 2H), 2.09-2.34 (m, N- $\alpha$ - $\text{CH}_2$ , 8H), 2.72 (d,  $J = 10.6$  Hz, N- $\beta$ - $\text{CH}_2$ , 2H), 2.90-2.97 (m, N- $\alpha$ - $\text{CH}_2$ , 6H), 3.08 (s, CH, 2H), 3.53 (t,  $J = 10.5$  Hz, N- $\alpha$ - $\text{CH}_2$ , 2H).  $^{13}\text{C}$  NMR (100 MHz,  $\text{CDCl}_3$ ,  $\delta$ ): 19.29 (N- $\beta$ - $\text{CH}_2$ ), 44.47 (N- $\alpha$ - $\text{CH}_2$ ), 52.20 (N- $\alpha$ - $\text{CH}_2$ ), 54.07 (N- $\alpha$ - $\text{CH}_2$ ), 55.76 (CH). HRMS ( $m/z$ ):  $[\text{M} + \text{H}]^+$  calcd for  $\text{C}_{12}\text{H}_{23}\text{N}_4$ , 223.1916; found, 223.1917. Anal. calcd for  $\text{C}_{12}\text{H}_{22}\text{N}_4$ : C, 64.83; H, 9.97; N, 25.20. Found: C, 64.63; H, 10.22; N, 25.18.

***cis*-13-1,4,7,10-Tetraazatetracyclo[5.5.1.0<sup>4,14</sup>.0<sup>10,13</sup>]tetradecane (3)**

Amounts: 1,4,7,10-Tetraazacyclododecane (cyclen) (4.18 g, 24.3 mmol), MeOH (150 ml), glyoxal (40% w/w, 3.52 g, 60.7 mmol), diethyl ether (150 ml). To yield a cream solid (4.40 g, 93%). <sup>1</sup>H NMR (400 MHz, CDCl<sub>3</sub>, δ): 2.49 (m, N-CH<sub>2</sub>, 4H), 2.63 (br s, N-CH<sub>2</sub>, 4H), 2.88-2.96 (m, N-CH<sub>2</sub>, 8H), 3.07 (s, CH, 2H). <sup>13</sup>C NMR (100 MHz, CDCl<sub>3</sub>, δ): 50.27 (N-CH<sub>2</sub>), 51.05 (N-CH<sub>2</sub>), 77.44 (CH). HRMS (*m/z*): [M + H]<sup>+</sup> calcd for C<sub>10</sub>H<sub>19</sub>N<sub>4</sub>, 195.1607; found, 195.1604. Anal. calcd for C<sub>10</sub>H<sub>18</sub>N<sub>4</sub>: C, 61.82; H, 9.34; N, 28.84. Found: C, 61.96; H, 9.50; N, 28.67.

### 7.2.3. Synthesis of 3a-[4-cyanobenzyl]-decahydro-3a,5a,8a,10a-tetraaza-pyrenium bromide (4) and 2a-[4-cyanobenzyl]-decahydro-2a,4a,6a,8a-tetraaza-pyrenium bromide (5)



#### General procedure B

The macrocycle was dissolved in dry MeCN, 4-(bromomethyl)benzotrile was added and the solution was stirred under argon for 2 days. The resulting precipitate was filtered and washed with diethyl ether.

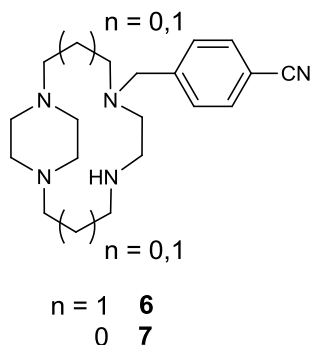
#### 3a-[4-Cyanobenzyl]-decahydro-3a,5a,8a,10a-tetraaza-pyrenium bromide (4)

Amounts: *cis*-3a,5a,8a,10a-Tetraazaperhydropyrene (**2**) (3.50 g, 15.7 mmol), MeCN (150 ml), 4-(bromomethyl)benzotrile (7.72 g, 39.4 mmol) diethyl ether (2 x 25 ml). To yield a white solid (5.00 g, 76%).  $^1\text{H}$  NMR (400 MHz,  $\text{D}_2\text{O}$ ,  $\delta$ ): 1.30 (d,  $J = 13.4$  Hz, N- $\beta$ - $\text{CH}_2$ , 1H), 1.63 (d,  $J = 13.4$  Hz, N- $\beta$ - $\text{CH}_2$ , 1H), 1.98-2.19 (m, N- $\alpha$ - $\text{CH}_2$ , 3H), 2.31-2.37 (m, N- $\beta$ - $\text{CH}_2$ , 2H), 2.48 (t,  $J = 12.4$  Hz, N- $\alpha$ - $\text{CH}_2$ , 1H), 2.87-2.99 (m, N- $\alpha$ - $\text{CH}_2$ , 8H), 3.06-3.20 (m, N- $\alpha$ - $\text{CH}_2$ , 2H), 3.31-3.46 (m, N- $\alpha$ - $\text{CH}_2$ , 2H), 3.55 (s, CH, 1H), 4.08 (t,  $J = 13.0$  Hz, Ar  $\text{CH}_2$ , 1H), 4.18 (s, CH, 1H), 5.06 (d,  $J = 13.4$  Hz, Ar  $\text{CH}_2$ , 1H), 7.56 (d,  $J = 7.2$  Hz, Ar H, 2H), 7.75 (d,  $J = 7.2$  Hz, Ar H, 2H).  $^{13}\text{C}$  NMR (100 MHz,  $\text{D}_2\text{O}$ ,  $\delta$ ): 17.98 (N- $\beta$ - $\text{CH}_2$ ), 18.39 (N- $\beta$ - $\text{CH}_2$ ), 41.94 (N- $\alpha$ - $\text{CH}_2$ ), 46.55 (N- $\alpha$ - $\text{CH}_2$ ), 48.62 (N- $\alpha$ - $\text{CH}_2$ ), 51.34 (N- $\alpha$ - $\text{CH}_2$ ), 51.92 (N- $\alpha$ - $\text{CH}_2$ ), 53.32 (N- $\alpha$ - $\text{CH}_2$ ), 53.94 (N- $\alpha$ - $\text{CH}_2$ ), 60.22 (N- $\alpha$ - $\text{CH}_2$ ), 61.54 (Ar  $\text{CH}_2$ ), 69.54 (CH), 82.56 (CH), 113.79 (Ar C), 118.61 (CN), 131.05 (Ar CH), 133.21 (Ar CH), 133.97 (Ar C). HRMS ( $m/z$ ):  $[\text{M} - \text{Br}]^+$  calcd for  $\text{C}_{20}\text{H}_{28}\text{N}_5$ , 338.2340; found, 338.2339. Anal. calcd for  $\text{C}_{20}\text{H}_{28}^{79}\text{BrN}_5$ : C, 57.42; H, 6.75; N, 16.74. Found: C, 57.88; H, 6.74; N, 16.49.

### 2a-[4-Cyanobenzyl]-decahydro-2a,4a,6a,8a-tetraaza-pyrenium bromide (5)

Amounts: *cis*-13-1,4,7,10-Tetraazatetracyclo[5.5.1.0<sup>4,14</sup>.0<sup>10,13</sup>]tetradecane (**3**) (3.15 g, 16.2 mmol), MeCN (150 ml), 4-(bromomethyl)benzotrile (7.95 g, 40.5 mmol), diethyl ether (2 x 50 ml). To yield a white solid (6.10 g, 96%). <sup>1</sup>H NMR (400 MHz, D<sub>2</sub>O, δ): 2.35-2.43 (m, N-CH<sub>2</sub>, 2H), 2.64-2.83 (br m, N-CH<sub>2</sub>, 4H), 2.94-3.19 (br m, N-CH<sub>2</sub>, 5H), 3.32-3.47 (m, N-CH<sub>2</sub>, 4H), 3.63 (d, *J* = 2.6 Hz, N-CH<sub>2</sub>, 1H), 3.92 (d, *J* = 2.6 Hz, CH, 2H), 4.06 (m, Ar CH<sub>2</sub>, 1H), 4.83 (d, *J* = 12.1 Hz, Ar CH<sub>2</sub>, 1H), 7.61 (d, *J* = 8.6 Hz, Ar H, 2H), 7.76 (d, *J* = 8.6 Hz, Ar H, 2H). <sup>13</sup>C NMR (100 MHz, D<sub>2</sub>O, δ): 43.77 (N-CH<sub>2</sub>), 47.57 (N-CH<sub>2</sub>), 47.62 (N-CH<sub>2</sub>), 48.21 (N-CH<sub>2</sub>), 48.31 (N-CH<sub>2</sub>), 51.33 (N-CH<sub>2</sub>), 57.24 (N-CH<sub>2</sub>), 60.63 (N-CH<sub>2</sub>), 61.63 (Ar CH<sub>2</sub>), 71.66 (CH), 83.28 (CH), 113.81 (Ar C), 118.63 (CN), 132.12 (Ar CH), 133.23 (Ar CH), 133.54 (Ar C). HRMS (*m/z*): [M – Br]<sup>+</sup> calcd for C<sub>18</sub>H<sub>24</sub>N<sub>5</sub>, 310.2029; found, 310.2026. Anal. calcd for C<sub>18</sub>H<sub>24</sub><sup>79</sup>BrN<sub>5</sub>: C, 55.39; H, 6.20; N, 17.94. Found: C, 55.39; H, 6.35; N, 17.75.

**7.2.4. Synthesis of 1-[4-cyanobenzyl]-1,4,8,11-tetraazabicyclo[10.2.2]hexadecane (6) and 1-[4-cyanobenzyl]-1,4,7,10-tetraazabicyclo[8.2.2]dodecane (7)**



**General procedure C**

The macrocycle was dissolved in ethanol and sodium borohydride was added in small portions. The mixture was stirred for 30 min then heated to reflux for 2 hours. Water was added to decompose excess sodium borohydride and the solvents were removed *in vacuo*. The residue was taken up into water and made strongly basic (pH 14, KOH). The basic solution was extracted with DCM, the combined organic extracts were dried (Na<sub>2</sub>SO<sub>4</sub>), filtered and solvent removed *in vacuo*.

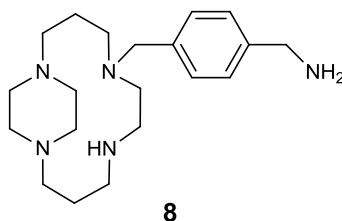
**1-[4-Cyanobenzyl]-1,4,8,11-tetraazabicyclo[10.2.2]hexadecane (6)**

Amounts: 3a-[4-cyanobenzyl]-decahydro-3a,5a,8a,10a-tetraaza-pyrenium bromide (**4**) (2.50 g, 6.0 mmol), ethanol (150 ml), sodium borohydride (5.65 g, 149 mmol), water (100ml, 150 ml), DCM (5 x 50 ml). To yield a colourless oil (1.94 g, 95%).  
<sup>1</sup>H NMR (400 MHz, CDCl<sub>3</sub>, δ): 1.68-1.77 (m, N-β-CH<sub>2</sub>, 4H), 2.22-2.29 (m, N-α-CH<sub>2</sub>, 2H), 2.51-2.68 (m, N-α-CH<sub>2</sub>, 12H), 2.90 (m, N-α-CH<sub>2</sub>, 2H), 2.98-3.03 (m, N-α-CH<sub>2</sub>, 2H), 3.15-3.22 (m, N-α-CH<sub>2</sub>, 2H), 3.67 (s, Ar CH<sub>2</sub> + NH, 3H), 7.42 (d, J = 8.1 Hz, Ar H, 2H), 7.61 (d, J = 8.1 Hz, Ar H, 2H). <sup>13</sup>C NMR (100 MHz, CDCl<sub>3</sub>, δ): 23.52 (N-β-CH<sub>2</sub>), 26.05 (N-β-CH<sub>2</sub>), 48.06 (N-α-CH<sub>2</sub>), 48.29 (N-α-CH<sub>2</sub>), 50.09 (N-α-CH<sub>2</sub>), 51.24 (N-α-CH<sub>2</sub>), 54.56 (N-α-CH<sub>2</sub>), 54.81 (N-α-CH<sub>2</sub>), 55.50 (N-α-CH<sub>2</sub>), 56.87 (N-α-CH<sub>2</sub>), 57.56 (Ar CH<sub>2</sub>), 110.66 (Ar C), 118.85 (CN), 129.73 (Ar CH), 131.80 (Ar CH), 144.50 (Ar C). HRMS (m/z): [M + H]<sup>+</sup> calcd for C<sub>20</sub>H<sub>31</sub>N<sub>5</sub>, 342.2658; found, 342.2652.

### 1-[4-Cyanobenzyl]-1,4,7,10-tetraazabicyclo[8.2.2]dodecane (7)

Amounts: 2a-[4-Cyanobenzyl]-decahydro-2a,4a,6a,8a,tetraaza-pyrenium bromide (5) (3.00 g, 7.7 mmol), ethanol (150 ml), sodium borohydride (7.27 g, 192.0 mmol), water (100 ml, 150 ml), DCM (5 x 50 ml). To yield an orange oil (2.20 g, 91%). <sup>1</sup>H NMR (400 MHz, CDCl<sub>3</sub>, δ): 2.06-3.51 (br m, N-CH<sub>2</sub>, 20H), 3.59-3.91 (m, Ar CH<sub>2</sub> + NH, 3H), 7.40-7.68 (br ov, Ar H, 4H). <sup>13</sup>C NMR (100 MHz, CDCl<sub>3</sub>, δ): 41.26 (N-CH<sub>2</sub>), 47.82 (N-CH<sub>2</sub>), 47.86 (N-CH<sub>2</sub>), 48.22 (N-CH<sub>2</sub>), 49.41 (N-CH<sub>2</sub>), 51.91 (N-CH<sub>2</sub>), 55.09 (N-CH<sub>2</sub>), 55.30 (N-CH<sub>2</sub>), 55.79 (N-CH<sub>2</sub>), 57.13 (N-CH<sub>2</sub>), 59.50 (Ar CH<sub>2</sub>), 109.67 (Ar C), 117.36 (CN), 128.52 (Ar CH), 130.54 (Ar CH), 143.24 (Ar C). HRMS (*m/z*): [M + H]<sup>+</sup> calcd for C<sub>18</sub>H<sub>28</sub>N<sub>5</sub>, 314.2245; found, 314.2339.

### 7.2.5. Synthesis of 1-[4-aminomethylbenzyl]-1,4,8,11-tetraazabicyclo[10.2.2]hexadecane (8)



#### Method 1 – Attempted synthesis

1-[4-Cyanobenzyl]-1,4,8,11-tetraazabicyclo[10.2.2]hexadecane (**6**) (1.35 g, 3.95 mmol) was treated with borane-THF (45 ml, 45.00 mmol) and the solution was refluxed under nitrogen for 18 hours. After quenching the excess borane with MeOH (10 ml), solvents were removed *in vacuo*. The residue was treated with boiling 6M HCl (120 ml) and refluxed for 3 hours. After removal of solvents *in vacuo* the residue was taken up into water (50 ml) and made strongly basic (pH > 12, KOH). The aqueous phase was extracted with DCM (5 x 50 ml). The organic layers were dried (Na<sub>2</sub>SO<sub>4</sub>), filtered and removed *in vacuo* to yield a pale, yellow oil (1.36 g, 100%). <sup>1</sup>H NMR (400 MHz, CDCl<sub>3</sub>, δ): 1.62-1.69 (m, N-β-CH<sub>2</sub>, 4H), 2.46-2.59 (br m, N-α-CH<sub>2</sub> + NH, 15H), 2.82-2.93 (m, N-α-CH<sub>2</sub>, 4H), 3.11-3.15 (m, N-α-CH<sub>2</sub>, 2H), 3.57 (s, Ar CH<sub>2</sub>, 2H), 7.34 (d, *J* = 8.1 Hz, Ar H, 2H), 7.54 (d, *J* = 8.1 Hz, Ar H, 2H). <sup>13</sup>C-NMR (CDCl<sub>3</sub>): δ 23.59 (N-β-CH<sub>2</sub>), 26.15 (N-β-CH<sub>2</sub>), 48.01 (N-α-CH<sub>2</sub>), 50.17 (N-α-CH<sub>2</sub>), 51.74 (N-α-CH<sub>2</sub>), 54.62 (N-α-CH<sub>2</sub>), 54.85 (N-α-CH<sub>2</sub>), 56.95 (N-α-CH<sub>2</sub>), 57.62 (Ar CH<sub>2</sub>), 110.72 (Ar C), 110.89 (CN), 129.76 (Ar CH), 131.84 (Ar CH), 144.45 (Ar C).

#### Method 2

##### General procedure D

LiAlH<sub>4</sub> was dissolved in anhydrous THF. The macrocycle in anhydrous THF was added dropwise under ice-cooling. After complete addition the mixture was stirred for 30 min and then heated to reflux for 3 hours. After cooling, aqueous ammonium chloride was added dropwise. The resulting precipitate was filtered, washed with THF and the solvents were removed *in vacuo*.

Amounts: LiAlH<sub>4</sub> (0.53 g, 14.10 mmol), THF (20 ml), 1-[4-cyanobenzyl]-1,4,8,11-tetraazabicyclo[10.2.2]hexadecane (**6**) (1.20 g, 3.50 mmol), THF (20 ml), aqueous ammonium chloride (5 ml), THF (2 x 50 ml). To yield a yellow oil (0.60 g, 50%).  
<sup>1</sup>H NMR (400 MHz, CDCl<sub>3</sub>, δ): 2.21-2.29 (m, N-β-CH<sub>2</sub>, 4H), 2.52-2.71 (m, N-α-CH<sub>2</sub>, 20H), 2.94-3.20 (m, NH<sub>2</sub> + NH, 3H), 3.23-3.33 (m, Ar CH<sub>2</sub>, 2H), 3.66 (s, CH<sub>2</sub>-NH<sub>2</sub>, 2H), 7.22 (d, *J* = 7.9 Hz, Ar H, 2H), 7.27 (d, *J* = 7.9 Hz, Ar H, 2H). <sup>13</sup>C NMR (100 MHz, CDCl<sub>3</sub>, δ): 23.33 (N-β-CH<sub>2</sub>), 26.08 (N-β-CH<sub>2</sub>), 46.05 (N-α-CH<sub>2</sub>), 47.96 (N-α-CH<sub>2</sub>), 50.40 (N-α-CH<sub>2</sub>), 51.00 (N-α-CH<sub>2</sub>), 54.55 (N-α-CH<sub>2</sub>), 54.89 (N-α-CH<sub>2</sub>), 55.27 (N-α-CH<sub>2</sub>), 56.14 (Ar CH<sub>2</sub>), 56.80 (CH<sub>2</sub>-NH<sub>2</sub>), 126.59 (Ar C), 129.66 (Ar CH), 136.15 (Ar CH), 141.83 (Ar C). HRMS (*m/z*): [M + H]<sup>+</sup> calcd for C<sub>20</sub>H<sub>36</sub>N<sub>5</sub>, 346.2971; found, 346.2965.

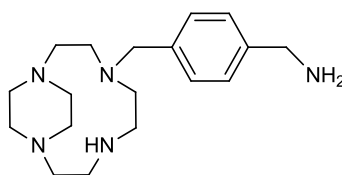
### Method 3-Preferred route

#### General procedure E

LiAlH<sub>4</sub> was dissolved in anhydrous THF. The macrocycle in anhydrous THF was added dropwise under ice-cooling. After complete addition the mixture was stirred for 30 min and then heated to reflux for 3 hours. The reaction was cooled in an ice-bath, water was added dropwise followed by 15% sodium hydroxide solution followed by a second portion of water. The resulting white precipitate was filtered and washed with THF then water. The aqueous layer was made strongly basic (pH > 12, KOH) and extracted with THF. The organic phases were dried (Na<sub>2</sub>SO<sub>4</sub>), filtered and solvents removed *in vacuo*.

Amounts: LiAlH<sub>4</sub> (0.63 g, 16.70 mmol), THF (20 ml), 1-[4-cyanobenzyl]-1,4,8,11-tetraazabicyclo[10.2.2]hexadecane (**6**) (1.90 g, 5.50 mmol), THF (30 ml), water (0.40 ml), 15% sodium hydroxide (0.40 ml), water (1.20 ml), THF (2 x 20), water (2 x 10 ml), THF (5 x 25 ml). To yield a yellow oil (1.66 g, 86%). <sup>1</sup>H NMR (400 MHz, CDCl<sub>3</sub>, δ): 1.74-1.86 (m, N-β-CH<sub>2</sub>, 4H), 2.23-2.27 (m, N-α-CH<sub>2</sub>, 2H), 2.52-2.62 (br m, N-α-CH<sub>2</sub> + NH + NH<sub>2</sub>, 14H), 2.92-3.00 (m, N-α-CH<sub>2</sub>, 3H), 3.25-3.28 (m, N-α-CH<sub>2</sub>, 2H), 3.65 (s, N-α-CH<sub>2</sub>, 1H), 3.73-3.76 (m, CH<sub>2</sub>-NH<sub>2</sub>, 2H), 3.86 (s, Ar CH<sub>2</sub>, 2H), 7.23-7.29 (br ov, Ar H, 4H). <sup>13</sup>C NMR (100 MHz, CDCl<sub>3</sub>, δ): 23.37 (N-β-CH<sub>2</sub>), 25.51 (N-β-CH<sub>2</sub>), 26.07 (N-α-CH<sub>2</sub>), 30.22 (N-α-CH<sub>2</sub>), 46.11 (N-α-CH<sub>2</sub>), 48.02 (N-α-CH<sub>2</sub>), 50.45 (N-α-CH<sub>2</sub>), 51.03 (N-α-CH<sub>2</sub>), 54.59 (N-α-CH<sub>2</sub>), 54.90 (N-α-CH<sub>2</sub>), 55.32 (N-α-CH<sub>2</sub>), 56.21 (N-α-CH<sub>2</sub>), 56.85 (Ar CH<sub>2</sub>), 60.87 (CH<sub>2</sub>-NH<sub>2</sub>), 126.59 (Ar C), 129.66 (Ar CH), 136.15 (Ar CH), 141.83 (Ar C). HRMS (*m/z*): [M + H]<sup>+</sup> calcd for C<sub>20</sub>H<sub>36</sub>N<sub>5</sub>, 346.2971; found, 346.2969.

### 7.2.6. Synthesis of 1-[4-aminomethylbenzyl]-1,4,7,10-tetraazabicyclo[8.2.2]dodecane (9)



9

#### Method 1- Attempted synthesis

1-[4-Cyanobenzyl]-1,4,7,10-tetraazabicyclo[8.2.2]dodecane (**7**) (1.30 g, 3.9 mmol) was dissolved in THF (100 ml). Aqueous ammonia (30%, 20 ml) was added and the flask was evacuated then flushed with argon three times. Raney 2800 nickel (50 wt% slurry in water, 20 ml) was added. The flask was evacuated and flushed with hydrogen three times then left to stir for 18 hours. The mixture was filtered through hyflo super cel and washed with THF (20 ml) then MeOH (20 ml). Solvents were removed *in vacuo* and the resulting solid was taken up in DCM (50 ml). The organic layer was partitioned between an aqueous layer of ammonia (30%, 25 ml) and 4M KOH (10 ml). The aqueous layer was extracted with DCM (3 x 50 ml). The combined organic layers were dried (MgSO<sub>4</sub>), filtered and the solvents removed *in vacuo* to yield an orange oil (0.38 g, 29%). <sup>1</sup>H NMR (400 MHz, CDCl<sub>3</sub>, δ): 1.99 (m, N-CH<sub>2</sub>, 2H), 2.25 (m, N-CH<sub>2</sub>, 3H), 2.37-2.47 (m, N-CH<sub>2</sub>, 4H), 2.60-3.06 (br m, N-CH<sub>2</sub>, 7H), 3.23 (m, N-CH<sub>2</sub> + NH, 3H), 3.42-3.77 (m, N-CH<sub>2</sub> + Ar CH<sub>2</sub>, 4H) 7.16-7.24 (br ov, Ar H, 4H). <sup>13</sup>C NMR (100 MHz, CDCl<sub>3</sub>, δ): 44.18 (N-CH<sub>2</sub>), 46.14 (N-CH<sub>2</sub>), 56.26 (N-CH<sub>2</sub>), 56.92 (N-CH<sub>2</sub>), 57.34 (N-CH<sub>2</sub>), 57.44 (N-CH<sub>2</sub>), 57.55 (N-CH<sub>2</sub>), 59.23 (N-CH<sub>2</sub>), 60.83 (Ar CH<sub>2</sub>), 110.53 (Ar C), 118.98 (CN), 129.27 (Ar CH), 132.04 (Ar CH), 146.17 (Ar C).

## Method 2

### General procedure D was followed

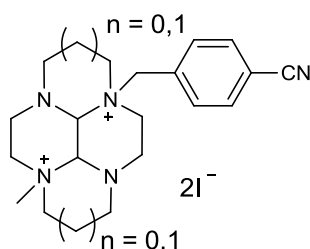
Amounts: LiAlH<sub>4</sub> (0.63 g, 16.60 mmol), THF (20 ml), 1-[4-cyanobenzyl-1,4,7,10-tetraazabicyclo[8.2.2]dodecane (**7**) (1.30 g, 4.15 mmol), THF (20 ml), aqueous ammonium chloride (5 ml), THF (2 x 50 ml). To yield a yellow/orange oil (0.40 g, 30%). <sup>1</sup>H NMR (400 MHz, CDCl<sub>3</sub>, δ): 1.92-2.10 (m, N-CH<sub>2</sub>, 2H), 2.14-2.29 (br m, NH<sub>2</sub>, 2H), 2.43-2.61 (m, N-CH<sub>2</sub>, 8H), 2.76-3.18 (m, N-CH<sub>2</sub>, 10H), 3.29-3.38 (m, Ar CH<sub>2</sub>, 1H), 3.51-3.55 (d, Ar CH<sub>2</sub>, 1H), 3.65-3.83 (m, CH<sub>2</sub>-NH<sub>2</sub>, 2H), 7.19-7.21 (d, J = 8.1 Hz, Ar H, 2H), 7.26-7.28 (d, J = 8.1 Hz, Ar H, 2H), 7.57 (br s, NH, 1H). <sup>13</sup>C NMR (100 MHz, CDCl<sub>3</sub>, δ): 43.06 (N-CH<sub>2</sub>), 46.08 (N-CH<sub>2</sub>), 48.87 (N-CH<sub>2</sub>), 49.00 (N-CH<sub>2</sub>), 49.64 (N-CH<sub>2</sub>), 50.47 (N-CH<sub>2</sub>), 51.35 (N-CH<sub>2</sub>), 53.51 (N-CH<sub>2</sub>), 55.99 (N-CH<sub>2</sub>), 57.15 (N-CH<sub>2</sub>), 58.27 (Ar CH<sub>2</sub>), 60.67 (CH<sub>2</sub>-NH<sub>2</sub>), 126.99 (Ar C), 129.67 (Ar CH), 137.36 (Ar CH), 142.06 (Ar C). HRMS (*m/z*): [M + H]<sup>+</sup> calcd for C<sub>18</sub>H<sub>32</sub>N<sub>5</sub>, 318.2657; found, 318.2652.

## Method 3-Preferred route

### General procedure E was followed

Amounts: LiAlH<sub>4</sub> (0.80 g, 21.0 mmol), THF (40 ml), 1-[4-cyanobenzyl-1,4,7,10-tetraazabicyclo[8.2.2]dodecane (**7**) (2.20 g, 7.0 mmol), THF (40 ml), water (0.50 ml), 15% sodium hydroxide (0.50 ml), water (1.50 ml), THF (2 x 30 ml), water (2 x 10 ml), THF (5 x 25 ml). To yield a yellow oil (1.73 g, 78%). <sup>1</sup>H NMR (400 MHz, CDCl<sub>3</sub>, δ): 2.19-3.14 (br m, N-CH<sub>2</sub> + NH, 23H), 3.50-3.84 (m, Ar CH<sub>2</sub> + CH<sub>2</sub>-NH<sub>2</sub>, 4H), 7.17-7.28 (br ov, Ar H, 4H). <sup>13</sup>C NMR (100 MHz, CDCl<sub>3</sub>, δ): 40.57 (N-CH<sub>2</sub>), 43.74 (N-CH<sub>2</sub>), 46.34 (N-CH<sub>2</sub>), 46.55 (N-CH<sub>2</sub>), 47.14 (N-CH<sub>2</sub>), 47.98 (N-CH<sub>2</sub>), 51.04 (N-CH<sub>2</sub>), 54.95 (N-CH<sub>2</sub>), 55.03 (N-CH<sub>2</sub>), 55.81 (N-CH<sub>2</sub>), 58.21 (Ar CH<sub>2</sub>), 65.47 (CH<sub>2</sub>-NH<sub>2</sub>), 126.99 (Ar C), 129.67 (Ar CH), 137.36 (Ar CH), 142.06 (Ar C). HRMS (*m/z*): [M + H]<sup>+</sup> calcd for C<sub>18</sub>H<sub>32</sub>N<sub>5</sub>, 318.2655; found, 318.2650.

**7.2.7. Synthesis of 3a-[4-cyanobenzyl]-8a-[methyl]-decahydro-3a,5a,8a,10a-tetraaza-pyrenium diiodide (10) and 2a-[4-cyanobenzyl]-6a-[methyl]-decahydro-2a,4a,6a,8a-tetraaza-pyrenium diiodide (11)**



n = 1    **10**  
           **0    11**

**General procedure F**

The macrocycle was suspended in anhydrous MeCN under nitrogen. Iodomethane was added dropwise. The white suspension was left to stir for 10 days. A second portion of iodomethane was added after 5 days. Excess iodomethane was removed by flowing nitrogen through the suspension for 30 min. The solid was collected by filtration, washed with ether and dried.

**3a-[4-Cyanobenzyl]-8a-[methyl]-decahydro-3a,5a,8a,10a-tetraaza-pyrenium diiodide (10)**

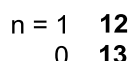
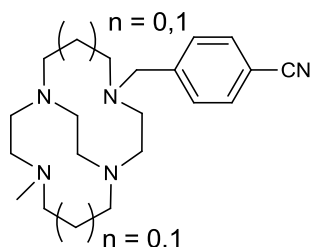
Amounts: 3a-[4-cyanobenzyl]-decahydro-3a,5a,8a,10a-tetraaza-pyrenium bromide (**4**) (2.00 g, 4.8 mmol), MeCN (100 ml), iodomethane (25 ml, 415.0 mmol then 13 ml, 208.0 mmol), diethyl ether (2 x 50 ml). To yield a white powder (2.90 g, 100%).  
<sup>1</sup>H NMR (400 MHz, DMSO, δ): 1.74 (d, *J* = 14.4 Hz, N-β-CH<sub>2</sub>, 1H), 1.85 (d, *J* = 14.4 Hz, N-β-CH<sub>2</sub>, 1H), 2.15 (s, CH<sub>3</sub>, 3H), 2.25-2.28 (m, N-β-CH<sub>2</sub>, 1H), 2.48 (m, N-β-CH<sub>2</sub>, 1H), 2.63 (m, N-α-CH<sub>2</sub>, 1H), 2.87 (m, N-α-CH<sub>2</sub>, 2H), 3.05 (m, N-α-CH<sub>2</sub>, 2H), 3.17 (m, N-α-CH<sub>2</sub>, 2H), 3.27-3.28 (m, N-α-CH<sub>2</sub>, 2H), 3.51 (m, N-α-CH<sub>2</sub>, 2H), 3.39-3.53 (m, N-α-CH<sub>2</sub>, 2H), 3.81 (d, *J* = 12.4 Hz, N-α-CH<sub>2</sub>, 1H), 4.28 (m, N-α-CH<sub>2</sub>, 2H), 4.96 (m, CH, 2H), 5.16 (m, Ar CH<sub>2</sub>, 2H), 7.82 (d, *J* = 8.2 Hz, Ar H, 2H), 8.02 (d, *J* = 8.2 Hz, Ar H, 2H). <sup>13</sup>C NMR (100 MHz, DMSO, δ): 18.00 (N-β-CH<sub>2</sub>), 18.25 (N-β-CH<sub>2</sub>), 20.45 (CH<sub>3</sub>), 45.72 (N-α-CH<sub>2</sub>), 45.90 (N-α-CH<sub>2</sub>), 46.54 (N-α-CH<sub>2</sub>), 47.38 (N-α-CH<sub>2</sub>), 48.89 (N-α-CH<sub>2</sub>), 50.17 (N-α-CH<sub>2</sub>), 50.33 (N-α-CH<sub>2</sub>), 59.54 (N-α-CH<sub>2</sub>), 59.82 (N-α-CH<sub>2</sub>), 63.91 (Ar CH<sub>2</sub>), 75.16

(CH), 113.41 (Ar C), 118.09 (CN), 131.12 (Ar CH), 132.90 (Ar CH), 134.38 (Ar C). HRMS ( $m/z$ ):  $[M - 2I]^{2+}$  calcd for  $C_{21}H_{31}N_5$ , 176.6280; found, 176.6284. Anal. calcd for  $C_{21}H_{31}N_5I_2 \cdot 3H_2O$ : C, 38.14; H, 5.64; N, 10.59. Found: C, 38.18; H, 4.83; N, 10.17.

**2a-[4-Cyanobenzyl]-6a-[methyl]-decahydro-2a,4a,6a,8a-tetraaza-pyrenium diiodide (11)**

Amounts: 2a-[4-cyanobenzyl]-decahydro-2a,4a,6a,8a,tetraaza-pyrenium bromide (**5**) (3.00 g, 7.7 mmol), MeCN (150 ml), iodomethane (39 ml, 630.0 mmol then 19.5 ml, 315 mmol), diethyl ether (2 x 50 ml). To yield a white powder (4.03 g, 90%).  $^1H$  NMR (400 MHz, DMSO,  $\delta$ ): 2.07 (s,  $CH_3$ , 3H), 2.89 (m, N- $CH_2$ , 1H), 3.02 (m, N- $CH_2$ , 2H), 3.46-3.50 (m, N- $CH_2$ , 6H), 3.60-3.76 (m, N- $CH_2$ , 4H), 3.83-3.89 (m, N- $CH_2$ , 1H), 3.95-4.04 (m, N- $CH_2$ , 1H), 4.21 (m, N- $CH_2$ , 1H), 4.62 (m, CH, 1H), 4.78 (m, CH, 1H), 4.86 (d,  $J = 13.4$  Hz, Ar  $CH_2$ , 1H), 5.08 (d,  $J = 13.4$  Hz, Ar  $CH_2$ , 1H), 7.89 (d,  $J = 8.4$  Hz, Ar H, 2H), 8.05 (d,  $J = 8.4$  Hz, Ar H, 2H).  $^{13}C$  NMR (100 MHz, DMSO,  $\delta$ ): 1.18 ( $CH_3$ ), 42.25 (N- $CH_2$ ), 42.72 (N- $CH_2$ ), 46.37 (N- $CH_2$ ), 55.53 (N- $CH_2$ ), 58.31 (N- $CH_2$ ), 58.99 (N- $CH_2$ ), 60.47 (N- $CH_2$ ), 64.44 (Ar  $CH_2$ ), 76.87 (CH), 77.12 (CH), 113.43 (Ar C), 118.07 (CN), 132.29 (Ar CH), 133.14 (Ar CH), 133.53 (Ar C). HRMS ( $m/z$ ):  $[M-I]^+$  calcd for  $C_{19}H_{27}N_5I$ , 452.1323; found, 452.1306. Anal. calcd for  $C_{19}H_{27}N_5I_2 \cdot 0.5H_2O$ : C, 38.79; H, 4.80; N, 11.91. Found: C, 38.80; H, 4.92; N, 11.79.

**7.2.8. Synthesis of 1-[4-cyanobenzyl]-8-[methyl]-1,4,8,11-tetraazabicyclo[6.6.2]hexadecane (12) and 1-[4-cyanobenzyl]-7-[methyl]-1,4,7,10-tetraazabicyclo[5.5.2]dodecane (13)**



**General procedure G**

The macrocycle was dissolved in ethanol and sodium borohydride was added in small portions. The mixture was stirred for 14 days at RT. Water was added to decompose excess sodium borohydride and the solvents were removed *in vacuo*. The residue was taken up into water and made strongly basic (pH 14, KOH). The basic solution was extracted with DCM, the combined organic extracts were dried ( $\text{Na}_2\text{SO}_4$ ), filtered and solvent removed *in vacuo*.

**1-[4-Cyanobenzyl]-8-[methyl]-1,4,8,11-tetraazabicyclo[6.6.2]hexadecane (12)**

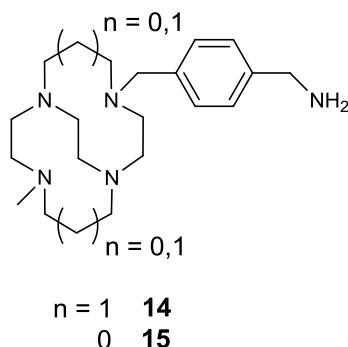
Amounts: 3a-[4-cyanobenzyl]-8a-[methyl]-decahydro-3a,5a,8a,10a-tetraazapyrenium diiodide (**10**) (2.50 g, 4.2 mmol), ethanol (120 ml), sodium borohydride (6.29 g, 166.0 mmol), water (80 ml, 100 ml), DCM (4 x 100 ml). To yield a yellow/cream oil (1.31 g, 88%).  $^1\text{H}$  NMR (400 MHz,  $\text{CDCl}_3$ ,  $\delta$ ): 1.32-1.49 (m, N- $\beta$ - $\text{CH}_2$ , 4H), 2.15-2.41 (br m, N- $\alpha$ - $\text{CH}_2$ , 16H), 2.55-2.68 (m,  $\text{CH}_3$ , 3H), 2.76 (m, N- $\alpha$ - $\text{CH}_2$ , 1H), 3.00 (d,  $J = 8.1$  Hz, N- $\alpha$ - $\text{CH}_2$ , 1H), 3.18 (d,  $J = 14.4$  Hz, N- $\alpha$ - $\text{CH}_2$ , 1H), 3.60-3.75 (m, Ar  $\text{CH}_2$ , 2H), 4.02 (m, N- $\alpha$ - $\text{CH}_2$ , 1H), 7.38 (d,  $J = 8.1$  Hz, Ar H, 2H), 7.52 (d,  $J = 8.1$  Hz, Ar H, 2H).  $^{13}\text{C}$  NMR (100 MHz,  $\text{CDCl}_3$ ,  $\delta$ ): 26.87 (N- $\beta$ - $\text{CH}_2$ ), 27.91 (N- $\beta$ - $\text{CH}_2$ ), 42.73 ( $\text{CH}_3$ ), 51.89 (N- $\alpha$ - $\text{CH}_2$ ), 52.14 (N- $\alpha$ - $\text{CH}_2$ ), 53.91 (N- $\alpha$ - $\text{CH}_2$ ), 54.07 (N- $\alpha$ - $\text{CH}_2$ ), 54.98 (N- $\alpha$ - $\text{CH}_2$ ), 55.89 (N- $\alpha$ - $\text{CH}_2$ ), 56.71 (N- $\alpha$ - $\text{CH}_2$ ), 56.93 (N- $\alpha$ - $\text{CH}_2$ ), 57.84 (N- $\alpha$ - $\text{CH}_2$ ), 59.41 (N- $\alpha$ - $\text{CH}_2$ ), 59.92 (Ar  $\text{CH}_2$ ), 110.28 (Ar C), 119.08 (CN), 129.35

(Ar CH), 131.88 (Ar CH), 146.96 (Ar C). HRMS ( $m/z$ ):  $[M + H]^+$  calcd for  $C_{21}H_{43}N_5$ , 356.2811; found, 356.2809.

### **1-[4-Cyanobenzyl]-7-[methyl]-1,4,7,10-tetraazabicyclo[5.5.2]dodecane (13)**

Amounts: 2a-[4-cyanobenzyl]-6a-[methyl]-decahydro-2a,4a,6a,8a-tetraazapyrenium diiodide (**11**) (3.00 g, 6.7 mmol), ethanol (150 ml), sodium borohydride (10.10 g, 267.0 mmol), water (100 ml, 100 ml), DCM (4 x 150 ml). To yield a yellow oil (1.63 g, 74%).  $^1H$  NMR (400 MHz, DMSO,  $\delta$ ): 2.30 (s,  $CH_3$ , 3H), 2.46-3.04 (m, N- $CH_2$ , 20H), 3.61-3.80 (m, Ar  $CH_2$ , 2H), 7.32-7.36 (m, Ar H, 2H), 7.52-7.54 (m, Ar H, 2H).  $^{13}C$  NMR (100 MHz, DMSO,  $\delta$ ): 44.07 ( $CH_3$ ), 56.21 (N- $CH_2$ ), 56.27 (N- $CH_2$ ), 56.76 (N- $CH_2$ ), 57.14 (N- $CH_2$ ), 57.25 (N- $CH_2$ ), 57.70 (N- $CH_2$ ), 57.91 (N- $CH_2$ ), 59.20 (N- $CH_2$ ), 60.49 (N- $CH_2$ ), 60.63 (Ar  $CH_2$ ), 110.46 (Ar C), 118.94 (CN), 129.22 (Ar CH), 131.99 (Ar CH), 146.13 (Ar C). MS ( $m/z$ ): 328  $[M]^+$ .

**7.2.9. Synthesis of 1-[4-aminomethylbenzyl]-8-[methyl]-1,4,8,11-tetraazabicyclo[6.6.2]hexadecane (14) and 1-[4-aminomethylbenzyl]-7-[methyl]-1,4,7,10-tetraaza bicyclo[5.5.2]dodecane (15)**



**General procedure E was followed**

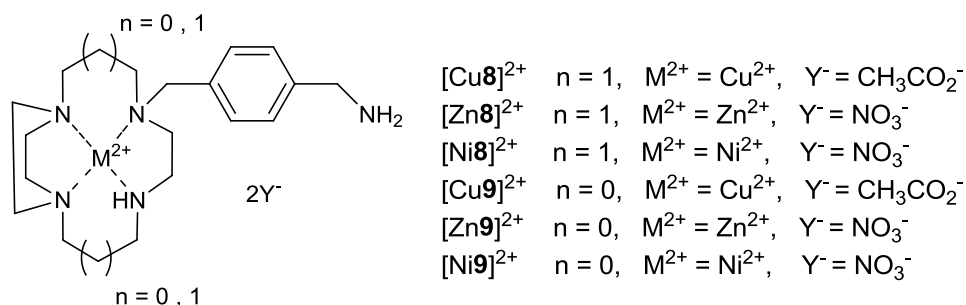
**1-[4-Aminomethylbenzyl]-8-[methyl]-1,4,8,11-tetraazabicyclo[6.6.2]hexadecane (14)**

Amounts: LiAlH<sub>4</sub> (0.19 g, 5.0 mmol), THF (20 ml), 1-[4-cyanobenzyl]-8-[methyl]-1,4,8,11-tetraaza-bicyclo[6.6.2]hexadecane (**12**) (1.45 g, 4.1 mmol), THF (20 ml), water (0.21 ml), 15% sodium hydroxide (0.21 ml), water (0.62 ml), THF (2 x 10 ml), water (2 x 5 ml), THF (5 x 25 ml). To yield a yellow oil (1.13 g, 77%). <sup>1</sup>H NMR (400 MHz, CDCl<sub>3</sub>, δ): 1.41 (m, N-β-CH<sub>2</sub> + N-α-CH<sub>2</sub>, 7H), 1.85-1.86 (m, CH<sub>3</sub>, 3H), 2.16-2.30 (m, N-α-CH<sub>2</sub> + NH<sub>2</sub>, 6H), 2.31-2.57 (m, N-α-CH<sub>2</sub>, 6H), 2.59-2.73 (m, N-α-CH<sub>2</sub>, 3H), 3.05-3.19 (m, N-α-CH<sub>2</sub>, 4H), 3.73-3.88 (m, CH<sub>2</sub>-NH<sub>2</sub> + Ar CH<sub>2</sub>, 4H), 7.22-7.33 (br ov, Ar H, 4H). <sup>13</sup>C NMR (100 MHz, CDCl<sub>3</sub>, δ): 26.82 (N-β-CH<sub>2</sub>), 30.29 (N-β-CH<sub>2</sub>), 42.96 (CH<sub>3</sub>), 52.06 (N-α-CH<sub>2</sub>), 52.27 (N-α-CH<sub>2</sub>), 53.93 (N-α-CH<sub>2</sub>), 54.84 (N-α-CH<sub>2</sub>), 55.92 (N-α-CH<sub>2</sub>), 56.25 (N-α-CH<sub>2</sub>), 56.46 (N-α-CH<sub>2</sub>), 56.52 (N-α-CH<sub>2</sub>), 57.90 (N-α-CH<sub>2</sub>), 59.15 (N-α-CH<sub>2</sub>), 59.63 (Ar CH<sub>2</sub>), 67.95 (CH<sub>2</sub>-NH<sub>2</sub>), 125.49 (Ar C), 126.72 (Ar CH), 127.65 (Ar CH), 129.07 (Ar C). HRMS (*m/z*): [M + H]<sup>+</sup> calcd for C<sub>21</sub>H<sub>38</sub>N<sub>5</sub>, 360.3124; found, 360.3122.

**1-[4-Aminomethylbenzyl]-7-[methyl]-1,4,7,10-tetraazabicyclo[5.5.2]dodecane (15)**

Amounts: LiAlH<sub>4</sub> (0.21 g, 5.6 mmol), THF (20 ml), 1-[4-cyanobenzyl]-7-[methyl]-1,4,7,10-tetraazabicyclo[5.5.2]dodecane (**13**) (1.50 g, 4.6 mmol), THF (20 ml), water (0.25 ml), 15% sodium hydroxide (0.25 ml), water (0.75 ml), THF (2 x 10 ml), water (2 x 5 ml), THF (5 x 25 ml). To yield a yellow oil (1.30 g, 86%). <sup>1</sup>H NMR (400 MHz, CDCl<sub>3</sub>, δ): 2.34-2.40 (m, CH<sub>3</sub>, 3H), 2.53-2.91 (m, N-α-CH<sub>2</sub> + NH<sub>2</sub>, 18H), 2.96-3.13 (m, N-α-CH<sub>2</sub>, 4H), 3.68-3.86 (m, CH<sub>2</sub>-NH<sub>2</sub> + Ar CH<sub>2</sub>, 4H), 7.24-7.29 (br ov, Ar H, 4H). <sup>13</sup>C NMR (100 MHz, CDCl<sub>3</sub>, δ): 25.53 (CH<sub>3</sub>), 30.25 (N-CH<sub>2</sub>), 44.17 (N-CH<sub>2</sub>), 46.10 (N-CH<sub>2</sub>), 56.22 (N-CH<sub>2</sub>), 56.86 (N-CH<sub>2</sub>), 57.28 (N-CH<sub>2</sub>), 57.42 (N-CH<sub>2</sub>), 59.15 (N-CH<sub>2</sub>), 60.80 (Ar CH<sub>2</sub>), 67.88 (CH<sub>2</sub>-NH<sub>2</sub>), 126.80 (Ar CH), 129.01 (Ar CH), 138.87 (Ar C), 141.64 (Ar C). HRMS (*m/z*): [M + H]<sup>+</sup> calcd for C<sub>19</sub>H<sub>34</sub>N<sub>5</sub>, 332.2813; found, 332.2809.

**7.2.10. Synthesis of metal complexes of ligands 1-[4-aminomethylbenzyl]-1,4,8,11-tetraazabicyclo[10.2.2]hexadecane (8) and 1-[4-aminomethylbenzyl]-1,4,7,10-tetraazabicyclo[8.2.2]dodecane (9)**



**General procedure H**

The macrocycle was dissolved in MeOH (10 ml), a methanolic (5 ml) solution of the metal salt was added dropwise. The mixture was heated to 60°C for 30 min under argon and then stirred at RT for 2 hours under argon. Solvent was removed *in vacuo* to ~5 ml then purified *via* size exclusion chromatography (sephadex LH20).

**1-[4-Aminomethylbenzyl]-1,4,8,11-tetraazabicyclo[10.2.2]hexadecane copper(II) acetate [Cu8]<sup>2+</sup>**

Amounts: 1-[4-aminomethylbenzyl]-1,4,8,11-tetraazabicyclo[10.2.2]hexadecane (**8**) (61 mg, 0.12 mmol), copper(II) acetate monohydrate (27 mg, 0.14 mmol). To yield a blue solid (114 mg, 75%). HRMS (*m/z*): [M – CH<sub>3</sub>CO<sub>2</sub>]<sup>+</sup> calcd for C<sub>22</sub>H<sub>38</sub>N<sub>5</sub>CuO<sub>2</sub>, 467.2306; found, 467.2316. Anal. calcd for C<sub>20</sub>H<sub>34</sub>N<sub>5</sub>Cu.2CH<sub>3</sub>CO<sub>2</sub>.3CH<sub>3</sub>OH.H<sub>2</sub>O: C, 50.57; H, 8.64; N, 10.92. Found: C, 50.76; H, 8.61; N, 10.86. UV-vis (MeOH) λ<sub>max</sub>, nm (ε): 642 (265 M<sup>-1</sup> cm<sup>-1</sup>).

**1-[4-Aminomethylbenzyl]-1,4,8,11-tetraazabicyclo[10.2.2]hexadecane zinc(II) nitrate [Zn8]<sup>2+</sup>**

Amounts: 1-[4-aminomethylbenzyl]-1,4,8,11-tetraazabicyclo[10.2.2]hexadecane (**8**) (110 mg, 0.32 mmol), zinc(II) nitrate hexahydrate (104 mg, 0.35 mmol). To yield a cream solid (113 mg, 66%). <sup>1</sup>H NMR (400 MHz, CD<sub>3</sub>OD, δ): 2.33-3.10 (br m, N-β-CH<sub>2</sub> + N-α-CH<sub>2</sub> + NH + NH<sub>2</sub>, 27H), 3.90 (m, Ar CH<sub>2</sub> + CH<sub>2</sub>NH<sub>2</sub>, 4H), 7.33-7.38 (m, Ar H, 4H). HRMS (*m/z*): [M - 2NO<sub>3</sub>]<sup>2+</sup> calcd for C<sub>20</sub>H<sub>35</sub>N<sub>5</sub>Zn, 204.6090; found, 204.6086. Anal. calcd for C<sub>20</sub>H<sub>34</sub>N<sub>5</sub>Zn.2NO<sub>3</sub>.3H<sub>2</sub>O: C, 40.85; H, 6.86; N, 16.68. Found: C, 40.81; H, 6.59; N, 16.59.

**1-[4-Aminomethylbenzyl]-1,4,8,11-tetraazabicyclo[10.2.2]hexadecane nickel(II) nitrate [Ni8]<sup>2+</sup>**

Amounts: 1-[4-aminomethylbenzyl]-1,4,8,11-tetraazabicyclo[10.2.2]hexadecane (**8**) (110 mg, 0.32 mmol), nickel(II) nitrate hexahydrate (102 mg, 0.35 mmol). To yield an orange solid (106 mg, 63%). HRMS (*m/z*): [M - NO<sub>3</sub><sup>-</sup> + H]<sup>+</sup> calcd for C<sub>20</sub>H<sub>35</sub>N<sub>6</sub>NiO<sub>3</sub>, 465.2110; found, 465.2119. Anal. calcd for C<sub>20</sub>H<sub>34</sub>N<sub>5</sub>Ni.2NO<sub>3</sub>: C, 42.37; H, 7.11; N, 16.47. Found: C, 42.51; H, 6.88; N, 16.64. UV-vis (H<sub>2</sub>O) λ<sub>max</sub>, nm (ε): 476 (174 M<sup>-1</sup> cm<sup>-1</sup>).

**1-[4-Aminomethylbenzyl]-1,4,7,10-tetraazabicyclo[8.2.2]dodecane copper(II) acetate [Cu9]<sup>2+</sup>**

Amounts: 1-[4-aminomethylbenzyl]-1,4,7,10-tetraazabicyclo[8.2.2]dodecane (**9**) (75 mg, 0.16 mmol), copper(II) acetate monohydrate (36 mg, 0.18 mmol). To yield a blue solid (60 mg, 75%). HRMS (*m/z*): [M - 2CH<sub>3</sub>CO<sub>2</sub>]<sup>2+</sup> calcd for C<sub>18</sub>H<sub>31</sub>N<sub>5</sub>Cu, 190.0927; found, 190.0932. Anal. calcd for C<sub>18</sub>H<sub>31</sub>CuN<sub>5</sub>.2CH<sub>3</sub>CO<sub>2</sub>.CH<sub>3</sub>OH.2H<sub>2</sub>O: C, 48.79; H, 7.83; N, 12.37. Found: C, 48.53; H, 7.71; N, 12.14. UV-vis (H<sub>2</sub>O) λ<sub>max</sub>, nm (ε): 599 (246 M<sup>-1</sup> cm<sup>-1</sup>).

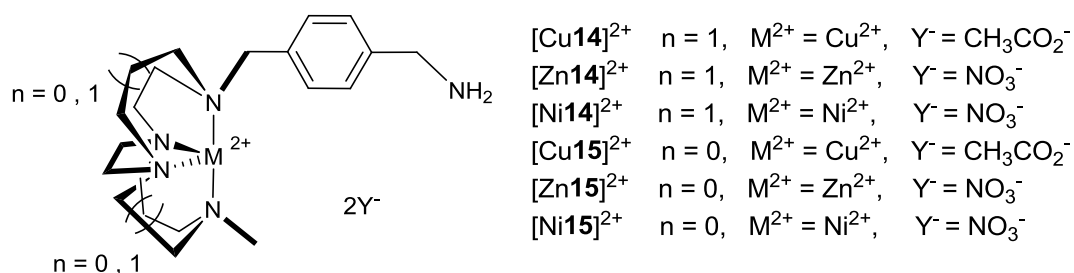
**1-[4-Aminomethylbenzyl]-1,4,7,10-tetraazabicyclo[8.2.2]dodecane zinc(II) nitrate [Zn9]<sup>2+</sup>**

Amounts: 1-[4-aminomethylbenzyl]-1,4,7,10-tetraazabicyclo[8.2.2]dodecane (**9**) (100 mg, 0.31 mmol), zinc(II) nitrate hexahydrate (103 mg, 0.35 mmol). To yield a cream solid (101 mg, 64%). <sup>1</sup>H NMR (400 MHz, CD<sub>3</sub>OD, δ): 2.38 (br s, N-CH<sub>2</sub>, 2H), 2.59-2.66 (m, N-CH<sub>2</sub>, 4H), 3.79 (br s, N-CH<sub>2</sub>, 2H), 2.92 (br s, N-CH<sub>2</sub>, 2H), 3.06-3.17 (br m, N-CH<sub>2</sub> + NH, 11H), 3.78 (br s, NH<sub>2</sub>, 2H), 4.11-4.14 (m, Ar CH<sub>2</sub> + CH<sub>2</sub>NH<sub>2</sub>, 4H), 7.44 (m, Ar H, 4H). MS: (*m/z*) 483 [M - NO<sub>3</sub>]<sup>+</sup>. Anal. calcd for C<sub>18</sub>H<sub>31</sub>ZnN<sub>5</sub>·2NO<sub>3</sub>·2CH<sub>3</sub>OH·0.5H<sub>2</sub>O: C, 41.48; H, 6.95; N, 16.91. Found: C, 41.88; H, 6.76; N, 16.82.

**1-[4-Aminomethylbenzyl]-1,4,7,10-tetraazabicyclo[8.2.2]dodecane nickel(II) nitrate [Ni9]<sup>2+</sup>**

Amounts: 1-[4-aminomethylbenzyl]-1,4,7,10-tetraazabicyclo[8.2.2]dodecane (**9**) (75 mg, 0.16 mmol), nickel(II) nitrate hexahydrate (52 mg, 0.18 mmol). To yield an orange solid (60 mg, 75%). HRMS (*m/z*): [M - 2NO<sub>3</sub><sup>-</sup> - H]<sup>+</sup> calcd for C<sub>18</sub>H<sub>30</sub>N<sub>5</sub>Ni, 374.1849; found, 374.1849. Anal. calcd for C<sub>18</sub>H<sub>30</sub>NiN<sub>5</sub>·2NO<sub>3</sub>·CH<sub>3</sub>OH·2.5H<sub>2</sub>O: C, 39.53; H, 6.98; N, 16.98. Found: C, 39.60; H, 6.58; N, 16.68. UV-vis (H<sub>2</sub>O) λ<sub>max</sub>, nm (ε): 398 (198 M<sup>-1</sup> cm<sup>-1</sup>).

**7.2.11. Synthesis of metal complexes of ligands 1-[4-aminomethylbenzyl]-8-[methyl]-1,4,8,11-tetraazabicyclo[6.6.2]hexadecane (14) and 1-[4-aminomethylbenzyl]-7-[methyl]-1,4,7,10-tetraazabicyclo[5.5.2]dodecane (15)**



**General procedure I**

The macrocycle was dissolved in degassed anhydrous MeOH (10 ml), an anhydrous methanolic (5 ml) solution of the metal salt was added dropwise and the mixture was refluxed under argon for 24 hours. Solvent was removed *in vacuo* to ~5 ml then purified *via* size exclusion chromatography (sephadex LH20).

**1-[4-Aminomethylbenzyl]-8-[methyl]-1,4,8,11-tetraazabicyclo[6.6.2]hexadecane copper(II) acetate [Cu14]<sup>2+</sup>**

Amounts: 1-[4-aminomethylbenzyl]-8-[methyl]-1,4,8,11-tetraazabicyclo[6.6.2]hexadecane (**14**) (150 mg, 0.42 mmol), copper(II) acetate monohydrate (93 mg, 0.46 mmol). To yield a blue solid (123 mg, 54%). HRMS (*m/z*): [M - 2CH<sub>3</sub>CO<sub>2</sub>]<sup>2+</sup> calcd for C<sub>21</sub>H<sub>37</sub>N<sub>5</sub>Cu, 211.1163; found, 211.1167. Anal. calcd for C<sub>21</sub>H<sub>37</sub>N<sub>5</sub>Cu.2CH<sub>3</sub>CO<sub>2</sub>.3CH<sub>3</sub>OH.0.5H<sub>2</sub>O: C, 52.03; H, 8.73; N, 10.84. Found: C, 52.06; H, 8.23; N, 10.34. UV-vis (MeOH) λ<sub>max</sub>, nm (ε): 645 (215 M<sup>-1</sup> cm<sup>-1</sup>).

**1-[4-Aminomethylbenzyl]-8-[methyl]-1,4,8,11-tetraazabicyclo[6.6.2]hexadecane zinc(II) nitrate [Zn14]<sup>2+</sup>**

Amounts: 1-[4-aminomethylbenzyl]-8-[methyl]-1,4,8,11-tetraazabicyclo[6.6.2]hexadecane (**14**) (150 mg, 0.42 mmol), zinc(II) nitrate hexahydrate (138 mg, 0.46 mmol). To yield an orange solid (81 mg, 35%). <sup>1</sup>H NMR (400 MHz, CD<sub>3</sub>OD, δ): 2.71-3.90 (br m, N-β-CH<sub>2</sub> + N-α-CH<sub>2</sub> + CH<sub>3</sub> + CH<sub>2</sub>NH<sub>2</sub>, 31H), 4.16 (m, Ar CH<sub>2</sub>, 2H), 7.41-7.49 (m, Ar H, 4H). HRMS (*m/z*): [M – 2NO<sub>3</sub>]<sup>2+</sup> calcd for C<sub>21</sub>H<sub>37</sub>N<sub>5</sub>Zn, 211.6158; found, 211.6165. Anal. calcd for C<sub>21</sub>H<sub>37</sub>N<sub>5</sub>Zn.2NO<sub>3</sub>.CH<sub>3</sub>OH.2H<sub>2</sub>O: C, 42.82; H, 7.35; N, 15.89. Found: C, 42.97; H, 6.95; N, 15.51.

**1-[4-Aminomethylbenzyl]-8-[methyl]-1,4,8,11-tetraazabicyclo[6.6.2]hexadecane nickel(II) acetate [Ni14]<sup>2+</sup>**

Amounts: 1-[4-aminomethylbenzyl]-7-[methyl]-1,4,7,10-tetraazabicyclo[5.5.2]dodecane (**15**) (200 mg, 0.56 mmol); nickel(II) acetate (108 mg, 0.61 mmol). To yield a green solid (187 mg, 63%). HRMS (*m/z*): [M – CH<sub>3</sub>CO<sub>2</sub>]<sup>+</sup> calcd for C<sub>23</sub>H<sub>40</sub>N<sub>5</sub>NiO<sub>2</sub>, 476.2532; found, 476.2530. Anal. calcd for C<sub>21</sub>H<sub>37</sub>N<sub>5</sub>Ni.2CH<sub>3</sub>CO<sub>2</sub>.CH<sub>3</sub>OH.H<sub>2</sub>O: C, 53.25; H, 8.42; N, 11.94. Found: C, 52.98; H, 8.80; N, 12.10. UV-vis (MeOH) λ<sub>max</sub>, nm (ε): 623 (194 M<sup>-1</sup> cm<sup>-1</sup>).

**1-[4-Aminomethylbenzyl]-7-[methyl]-1,4,7,10-tetraazabicyclo[5.5.2]dodecane copper(II) acetate [Cu15]<sup>2+</sup>**

Amounts: 1-[4-aminomethylbenzyl]-7-[methyl]-1,4,7,10-tetraazabicyclo[5.5.2]dodecane (**15**) (160 mg, 0.49 mmol); copper(II) acetate monohydrate (107 mg, 0.54 mmol). To yield a blue solid (160 mg, 64%). HRMS (*m/z*): [M – 2CH<sub>3</sub>CO<sub>2</sub>]<sup>2+</sup> calcd for C<sub>19</sub>H<sub>33</sub>N<sub>5</sub>Cu, 197.1015; found, 197.1015. Anal. calcd for C<sub>19</sub>H<sub>33</sub>N<sub>5</sub>Cu.2CH<sub>3</sub>CO<sub>2</sub>.2CH<sub>3</sub>OH: C, 52.02; H, 8.21; N, 12.13. Found: C, 52.28; H, 8.27; N, 11.77. UV-vis (H<sub>2</sub>O) λ<sub>max</sub>, nm (ε): 655 (108 M<sup>-1</sup> cm<sup>-1</sup>).

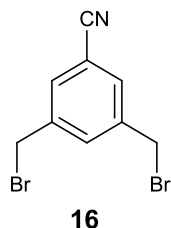
**1-[4-Aminomethylbenzyl]-7-[methyl]-1,4,7,10-tetraazabicyclo[5.5.2]dodecane  
zinc(II) nitrate [Zn15]<sup>2+</sup>**

Amounts: 1-[4-aminomethylbenzyl]-7-[methyl]-1,4,7,10-tetraazabicyclo[5.5.2]dodecane (**15**) (100 mg, 0.30 mmol); zinc(II) nitrate hexahydrate (99 mg, 0.33 mmol). To yield an orange solid (100 mg, 64%). <sup>1</sup>H NMR (400 MHz, CD<sub>3</sub>OD, δ): 2.59 (br m, 25H, CH<sub>3</sub> + N-CH<sub>2</sub> + NH<sub>2</sub>), 4.05-4.14 (m, Ar CH<sub>2</sub> + CH<sub>2</sub>NH<sub>2</sub>, 4H), 7.48-7.54 (m, Ar H, 4H). HRMS (*m/z*): [M – 2NO<sub>3</sub>]<sup>2+</sup> calcd for C<sub>19</sub>H<sub>33</sub>N<sub>5</sub>Zn, 197.6015; found, 197.6008. Anal. calcd for C<sub>19</sub>H<sub>33</sub>N<sub>5</sub>Zn.2NO<sub>3</sub>: C, 43.81; H, 6.39; N, 18.82. Found: C, 43.74; H, 6.33; N, 18.88.

**1-[4-Aminomethylbenzyl]-7-[methyl]-1,4,7,10-tetraazabicyclo[5.5.2]dodecane  
nickel(II) acetate [Ni15]<sup>2+</sup>**

Amounts: 1-[4-aminomethylbenzyl]-7-[methyl]-1,4,7,10-tetraazabicyclo[5.5.2]dodecane (**15**) (200 mg, 0.60 mmol); nickel(II) acetate (117 mg, 0.66 mmol). To yield a green solid (209 mg, 68%). HRMS (*m/z*): [M – CH<sub>3</sub>CO<sub>2</sub>]<sup>+</sup> calcd for C<sub>21</sub>H<sub>36</sub>N<sub>5</sub>NiO<sub>2</sub>, 448.2214; found, 448.2217. Anal. calcd for C<sub>19</sub>H<sub>33</sub>N<sub>5</sub>Ni.2CH<sub>3</sub>CO<sub>2</sub>.1.5CH<sub>3</sub>OH.2.5H<sub>2</sub>O: C, 48.93; H, 8.38; N, 11.65. Found: C, 48.97; H, 7.99; N, 11.33. UV-vis (MeOH) λ<sub>max</sub>, nm (ε): 623 (186 M<sup>-1</sup> cm<sup>-1</sup>).

### 7.2.12. Synthesis of 3,5-bis(bromomethyl) benzonitrile (16)



#### Method 1-Attempted synthesis

3,5-Dimethylbenzonitrile (1.00 g, 7.60 mmol) was dissolved in DCM (50 ml), NBS (2.99 g, 16.80 mmol) and benzoyl peroxide (10 mg, 0.04 mmol) were added and the mixture was refluxed under argon, upon reaching reflux a 200 W lamp was placed 10 cm from the flask. The illuminated mixture was refluxed for 1 hour, after cooling, water (20 ml) was added to quench the reaction. The organic phase was washed once with water (50 ml), once with brine (50 ml) then again with water (50 ml). The organic phase was dried ( $\text{Na}_2\text{SO}_4$ ), filtered and concentrated to yield crude orange oil. The crude was dried onto silica and purified *via* flash chromatography (eluent, ethyl acetate:hexane, 1:4) to yield a white/cream solid. The desired product was not isolated using this synthetic procedure.

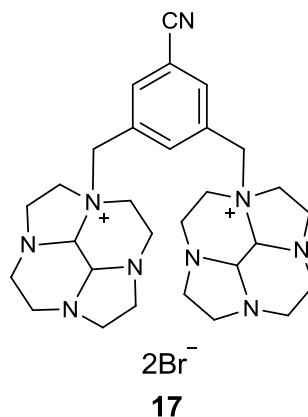
#### Method 2-Attempted synthesis

3,5-Dimethylbenzonitrile (1.00 g, 7.6 mmol) was dissolved in  $\text{CCl}_4$  (50 ml), NBS (2.71 g, 15.2 mmol), was added along with benzoyl peroxide (10 mg, 0.04 mmol). The mixture was refluxed under argon, upon reaching reflux a 200W lamp was placed 10 cm away from the flask. The illuminated mixture was refluxed for 24 hours. The mixture was filtered and solvents concentrated *in vacuo*. The resulting orange oil was recrystallized from  $\text{CCl}_4$ :hexane (80 ml, 3:5) after 2 days at 0°C a white solid was obtained. The desired product was not isolated using this synthetic procedure.

### Method 3-Preferred method

3,5-Dimethylbenzotrile (3.00 g, 23 mmol) was dissolved in degassed CCl<sub>4</sub> (80 ml). NBS (8.14 g, 46 mmol) and a trace amount of AIBN were added. The mixture was brought to reflux under an argon atmosphere. Upon reaching reflux a 200 W lamp was placed in close proximity. The mixture was then refluxed for 24 hours. Upon cooling, water (20 ml) was added to quench the reaction. The organic phase was washed with water (50 ml) then with brine (50 ml), dried (Na<sub>2</sub>SO<sub>4</sub>), filtered and the solvents removed *in vacuo* to yield an orange oil (5.79 g). The crude material was dried onto silica and purified *via* flash chromatography (eluant, ethyl acetate:hexane, 1:9) to yield a white solid (1.79 g, 27%). <sup>1</sup>H NMR (400 MHz, CDCl<sub>3</sub>, δ): 4.46 (s, CH<sub>2</sub>-Br, 4H), 7.62 (s, Ar H, 2H), 7.65 (s, Ar H, 1H). <sup>13</sup>C NMR (100 MHz, CDCl<sub>3</sub>, δ): 30.64 (CH<sub>2</sub>-Br), 113.53, (Ar C), 117.62 (CN), 132.17 (Ar CH), 133.76 (Ar CH), 139.93 (Ar C). HRMS (*m/z*): [M + H]<sup>+</sup> calcd for C<sub>9</sub>H<sub>7</sub><sup>79</sup>BrN, 286.8943; found, 286.8943. Anal. calcd for C<sub>9</sub>H<sub>7</sub><sup>79</sup>Br<sub>2</sub>N: C, 37.41; H, 2.44; N, 4.85. Found: C, 37.61; H, 2.18; N, 4.74. R<sub>f</sub> = 0.19 (silica, ethyl acetate:hexane, 1:9).

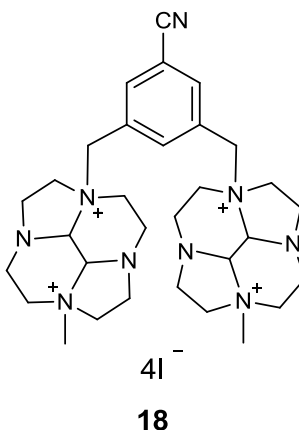
**7.2.13. Synthesis of 2a,2a'-[3,5-dimethylbenzonitrile]-bis(decahydro-2a,4a,6a,8a-tetraaza pyrenium) dibromide (17)**



**General procedure B was followed**

Amounts: Bridged cyclen (**3**) (4.25 g, 21.90 mmol), MeCN (150 ml), 3,5-dibromomethyl benzonitrile (**16**) (2.53 g, 8.80 mmol), diethyl ether (2 x 10 ml). To yield a white solid (4.71 g, 79%).  $^1\text{H}$  NMR (400 MHz,  $\text{D}_2\text{O}$ ,  $\delta$ ): 2.38-2.44 (m, N- $\text{CH}_2$ , 4H), 2.61-2.81 (m, N- $\text{CH}_2$ , 8H), 2.98-3.17 (m, N- $\text{CH}_2$ , 10H), 3.36-3.52 (m, N- $\text{CH}_2$ , 8H), 3.64 (s, N- $\text{CH}_2$ , 2H), 3.96 (s, CH, 2H), 4.07 (t,  $J = 11.4$  Hz, CH, 2H), 4.68 (m, Ar  $\text{CH}_2$ , 2H), 4.92 (d,  $J = 13.6$  Hz, Ar  $\text{CH}_2$ , 2H), 7.96 (s, Ar H, 1H), 8.06 (s, Ar H, 2H).  $^{13}\text{C}$  NMR (100 MHz,  $\text{D}_2\text{O}$ ,  $\delta$ ): 43.66 (N- $\text{CH}_2$ ), 47.58 (N- $\text{CH}_2$ ), 48.18 (N- $\text{CH}_2$ ), 51.33 (N- $\text{CH}_2$ ), 57.00 (N- $\text{CH}_2$ ), 59.62 (N- $\text{CH}_2$ ), 61.49 (N- $\text{CH}_2$ ), 71.57 (N- $\text{CH}_2$ ), 76.06 (Ar  $\text{CH}_2$ ), 83.62 (CH), 114.63 (Ar C), 117.30 (CN), 130.07 (Ar CH), 138.49 (Ar CH), 140.64 (Ar C). HRMS ( $m/z$ ):  $[\text{M} + \text{H}]^+$  calcd for  $\text{C}_{29}\text{H}_{43}\text{N}_9$ , 258.6817; found, 258.6815. Anal. calcd for  $\text{C}_{29}\text{H}_{43}^{79}\text{Br}_2\text{N}_9 \cdot 3\text{H}_2\text{O}$ : C, 47.61; H, 6.75; N, 17.23. Found: C, 47.91; H, 7.03; N, 17.15.

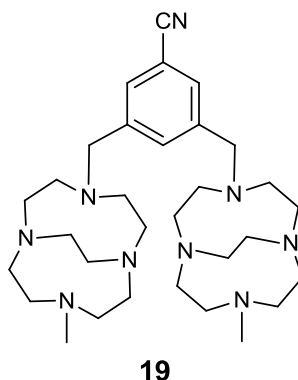
**7.2.14. Synthesis of 2a,2a'-[3,5-dimethylbenzonitrile]-6a,6a'-[methyl]-bis (decahydro-2a,4a,6a,8a-tetraazapyrenium) tetraiodide (18)**



**General procedure F was followed**

Amounts: 2a,2a'-[3,5-Dimethylbenzonitrile]-bis(decahydro-2a,4a,6a,8a-tetraaza pyrenium)dibromide (**17**) (2.66 g, 3.93 mmol), MeCN (120 ml), iodomethane (20 ml, 314.00 mmol then 10 ml, 157.00 mmol), diethyl ether (2 x 30 ml). To yield a white solid (3.46 g, 84%). <sup>1</sup>H NMR (400 MHz, DMSO, δ): 2.49 (m, CH<sub>3</sub>, 6H), 2.94-3.17 (br m, N-CH<sub>2</sub>, 7H), 3.38 (s, N-CH<sub>2</sub>, 5H), 3.44-3.53 (m, N-CH<sub>2</sub>, 5H), 3.61-3.77 (br m, N-CH<sub>2</sub>, 9H), 3.88 (m, N-CH<sub>2</sub>, 2H), 4.01 (m, N-CH<sub>2</sub>, 2H), 4.35 (m, N-CH<sub>2</sub>, 2H), 4.73 (d, *J* = 6.2 Hz, CH, 2H), 4.83-4.91 (m, Ar CH<sub>2</sub>, 4H), 5.16 (t, *J* = 13.2 Hz, CH, 2H), 8.33 (s, Ar H, 1H), 8.38 (s, Ar H, 2H). <sup>13</sup>C NMR (100 MHz, DMSO, δ): 42.36 (CH<sub>3</sub>), 42.67 (CH<sub>3</sub>), 46.46 (N-CH<sub>2</sub>), 46.47 (N-CH<sub>2</sub>), 55.33 (N-CH<sub>2</sub>), 58.37 (N-CH<sub>2</sub>), 60.66 (N-CH<sub>2</sub>), 64.43 (N-CH<sub>2</sub>), 77.12 (Ar CH<sub>2</sub>), 113.82 (Ar C), 117.56 (CN), 129.83 (Ar CH), 138.24 (Ar CH), 140.60 (Ar C). HRMS (*m/z*): [M + H]<sup>+</sup> calcd for C<sub>31</sub>H<sub>49</sub>N<sub>9</sub>I<sub>2</sub>, 400.6094; found, 400.6095. Anal. calcd for C<sub>31</sub>H<sub>49</sub>N<sub>9</sub>I<sub>2</sub>·3H<sub>2</sub>O: C, 34.69; H, 4.79; N, 11.74. Found: C, 34.57; H, 4.98; N, 11.37.

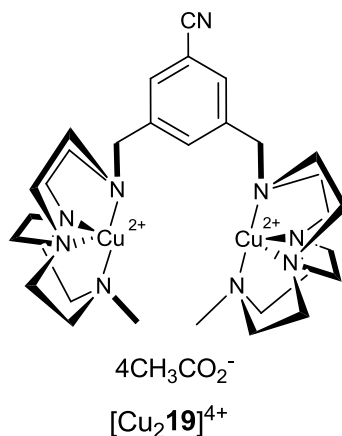
**7.2.15. Synthesis of 1,1'-[3,5-dimethylbenzonitrile]-7,7'-[methyl]-bis(1,4,7,10-tetraazabicyclo[5.5.2]dodecane) (19)**



**General procedure G was followed**

Amounts: 2a,2a'-[3,5-Dimethylbenzonitrile]-6a,6a'-[methyl]-bis(decahydro-2a,4a,6a,8a-tetraazapyrenium) tetraiodide (**18**) (7.81 g, 7.4 mmol), ethanol (300 ml), sodium borohydride (7.00 g, 185 mmol), water (150 ml, 150 ml), DCM (5 x 50 ml). To yield an orange/yellow oil (2.90 g, 71%). <sup>1</sup>H NMR (400 MHz, CDCl<sub>3</sub>, δ): 2.30 (s, CH<sub>3</sub>, 6H), 2.48-2.89 (br m, N-CH<sub>2</sub>, 40H), 2.96 (s, Ar CH<sub>2</sub>, 4H), 7.37 (s, Ar H, 2H), 7.43 (s, Ar H, 1H). <sup>13</sup>C NMR (100 MHz, CDCl<sub>3</sub>, δ): 44.22 (CH<sub>3</sub>), 56.32 (N-CH<sub>2</sub>), 56.88 (N-CH<sub>2</sub>), 57.21 (N-CH<sub>2</sub>), 57.62 (N-CH<sub>2</sub>), 59.29 (N-CH<sub>2</sub>), 60.10 (Ar CH<sub>2</sub>), 111.92 (Ar C), 119.32 (CN), 130.64 (Ar CH), 133.67 (Ar CH), 141.97 (Ar C). HRMS (*m/z*): [M + H]<sup>+</sup> calcd for C<sub>31</sub>H<sub>54</sub>N<sub>9</sub>, 552.4488; found, 552.4497.

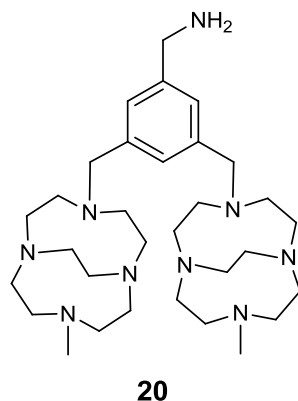
**7.2.16. Synthesis of 1,1'-[3,5-dimethylbenzonitrile]-7,7'-[methyl]-bis(1,4,7,10-tetraazabicyclo[5.5.2]dodecane) copper acetate [Cu<sub>2</sub>19]<sup>4+</sup>**



**General procedure I was followed**

Amounts: 1,1'-[3,5-Dimethylbenzonitrile]-7,7'-[methyl]-bis(1,4,7,10-tetraazabicyclo[5.5.2]dodecane) (**19**) (200 mg, 0.36 mmol), copper(II) acetate monohydrate (79 mg, 0.40 mmol). To yield a blue solid (146 mg, 44%). HRMS (*m/z*): [M - 2CH<sub>3</sub>CO<sub>2</sub>]<sup>2+</sup> calcd for C<sub>35</sub>H<sub>59</sub>Cu<sub>2</sub>N<sub>9</sub>O<sub>4</sub>, 397.6634; found, 397.6636. Anal. calcd for C<sub>31</sub>H<sub>53</sub>N<sub>9</sub>Cu<sub>2</sub>.4CH<sub>3</sub>CO<sub>2</sub>.1.5CH<sub>3</sub>OH.2H<sub>2</sub>O: C, 48.68; H, 7.57; N, 12.62; Found: C, 49.15; H, 7.26; N, 12.63. UV-vis (CH<sub>3</sub>OH) λ<sub>max</sub>, nm (ε): 655 (157 M<sup>-1</sup> cm<sup>-1</sup>).

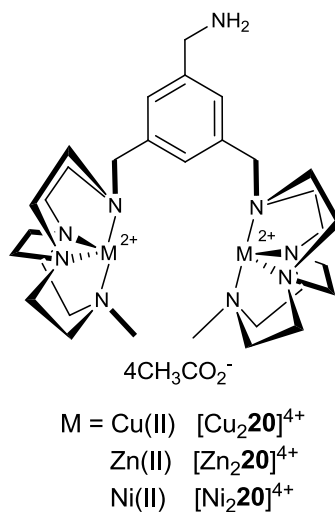
**7.2.17. Synthesis of 1,1'-[3,5-dimethylaminobenzyl]-7,7'-[methyl]-bis(1,4,7,10-tetraazabicyclo[5.5.2]dodecane) (20)**



**General procedure E was followed**

Amounts: Lithium aluminium hydride (0.37 g, 9.8 mmol), THF (50 ml), 1,1'-[3,5-dimethylbenzyl]-7,7'-[methyl]-bis(1,4,7,10-tetraazabicyclo[5.5.2]dodecane) (**19**) (1.81 g, 3.3 mmol), THF (50 ml), water (0.30 ml), 15% sodium hydroxide (0.30 ml), water (0.90 ml), THF (2 x 20 ml), water (2 x 10 ml), THF (5 x 50 ml). To yield a yellow oil (1.80 g, 99%). <sup>1</sup>H NMR (400 MHz, CDCl<sub>3</sub>, δ): 1.85 (m, N-CH<sub>2</sub>, 2H), 2.37 (s, CH<sub>3</sub>, 6H), 2.54-2.59 (m, N-CH<sub>2</sub>, 4H), 2.64-2.77 (br m, N-CH<sub>2</sub>, 11H), 2.81-2.91 (br m, N-CH<sub>2</sub>, 16H), 2.97-3.04 (m, N-CH<sub>2</sub>, 3H), 3.06-3.13 (m, N-CH<sub>2</sub>, 4H), 3.70 (br s, Ar CH<sub>2</sub>, 4H), 3.74 (m, CH<sub>2</sub>-NH<sub>2</sub>, 2H), 3.81 (br s, NH<sub>2</sub>, 2H), 7.08 (br s, Ar H, 2H), 7.15 (br s, Ar H, 1H). <sup>13</sup>C NMR (100 MHz, CDCl<sub>3</sub>, δ): 44.26 (CH<sub>3</sub>), 46.27 (N-CH<sub>2</sub>), 56.27 (N-CH<sub>2</sub>), 56.89 (N-CH<sub>2</sub>), 57.30 (N-CH<sub>2</sub>), 57.49 (N-CH<sub>2</sub>), 59.16 (N-CH<sub>2</sub>), 60.87, (Ar CH<sub>2</sub>), 67.90 (CH<sub>2</sub>-NH<sub>2</sub>), 125.93 (Ar CH), 127.79 (Ar CH), 140.55 (Ar C), 142.95 (Ar C). HRMS (*m/z*): [M + H]<sup>+</sup> calcd for C<sub>31</sub>H<sub>58</sub>N<sub>9</sub>, 556.4800; found, 556.4810.

**7.2.18. Synthesis of metal complexes of 1,1'-[3,5-dimethylaminobenzyl]-7,7'-[methyl]-bis(1,4,7,10-tetraazabicyclo[5.5.2]dodecane) (**20**)**



**General procedure I was followed**

**1,1'-[3,5-dimethylaminobenzyl]-7,7'-[methyl]-bis(1,4,7,10-tetraazabicyclo[5.5.2]dodecane) copper(II) acetate [Cu<sub>2</sub>**20**]<sup>4+</sup>**

Amounts: 1,1'-[3,5-Dimethylaminobenzyl]-7,7'-[methyl]-bis(1,4,7,10-tetraazabicyclo[5.5.2]dodecane) (**20**) (0.80 g, 1.4 mmol), MeOH (40 ml), copper(II) acetate monohydrate (0.63 g, 3.2 mmol), MeOH (20 ml). To yield a blue solid (1.01 g, 77%). HRMS (*m/z*): [M - 2CH<sub>3</sub>CO<sub>2</sub>]<sup>2+</sup> calcd for C<sub>35</sub>H<sub>63</sub>N<sub>9</sub>Cu<sub>2</sub>O<sub>4</sub>, 399.6791; found, 399.6792. Anal. calcd for C<sub>31</sub>H<sub>58</sub>N<sub>9</sub>Cu<sub>2</sub>·4CH<sub>3</sub>CO<sub>2</sub>·2CH<sub>3</sub>OH·2H<sub>2</sub>O: C, 47.48; H, 8.07; N, 12.15; Found: C, 47.32; H, 8.21; N, 11.75. UV-vis (CH<sub>3</sub>OH) λ<sub>max</sub>, nm (ε): 677 (520 M<sup>-1</sup> cm<sup>-1</sup>).

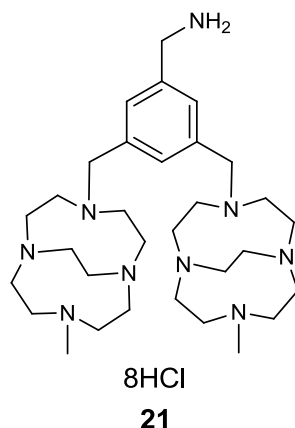
**1,1'-[3,5-dimethylaminobenzyl]-7,7'-[methyl]-bis(1,4,7,10-tetraazabicyclo[5.5.2]dodecane) zinc(II) acetate [Zn<sub>2</sub>20]<sup>4+</sup>**

Amounts: 1,1'-[3,5-Dimethylaminobenzyl]-7,7'-[methyl]-bis(1,4,7,10-tetraazabicyclo[5.5.2]dodecane) (**33**) (72.5 mg, 0.130 mmol), zinc(II) acetate (53 mg, 0.287 mmol). To yield a yellow/orange solid (106 mg, 88%). <sup>1</sup>H NMR (400 MHz, CD<sub>3</sub>OD, δ): 1.88 (br s, N-CH<sub>2</sub> + CH<sub>3</sub>, 8H), 2.37-3.14 (br m, N-CH<sub>2</sub>, 32H), 3.24-3.28 (m, N-CH<sub>2</sub>, 6H), 3.58 (br s, NH<sub>2</sub>, 2H), 3.89 (br s, Ar CH<sub>2</sub>, 4H), 7.35 (br m, Ar H, 3H). MS (*m/z*): 382 [M - 3CH<sub>3</sub>CO<sub>2</sub><sup>-</sup> + H<sub>2</sub>O]<sup>2+</sup>. Anal. calcd for C<sub>31</sub>H<sub>57</sub>N<sub>9</sub>Zn<sub>2</sub>·4CH<sub>3</sub>CO<sub>2</sub>·2.5CH<sub>3</sub>OH·6H<sub>2</sub>O: C, 44.87; H, 8.26; N, 11.35; Found: C, 44.91; H, 7.88; N, 11.10 (very hygroscopic compound).

**1,1'-[3,5-dimethylaminobenzyl]-7,7'-[methyl]-bis(1,4,7,10-tetraazabicyclo[5.5.2]dodecane) nickel(II) acetate [Ni<sub>2</sub>20]<sup>4+</sup>**

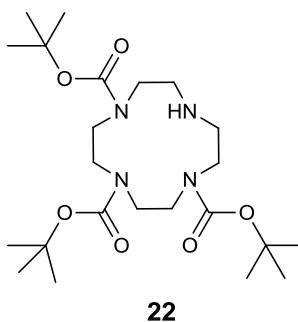
Amounts: 1,1'-[3,5-Dimethylaminobenzyl]-7,7'-[methyl]-bis(1,4,7,10-tetraazabicyclo[5.5.2]dodecane) (**33**) (72.5 mg, 0.130 mmol), nickel(II) acetate (51 mg, 0.287 mmol). To yield a pale orange solid (107 mg, 90%). MS (*m/z*): 376 [M - 3CH<sub>3</sub>CO<sub>2</sub><sup>-</sup> + H<sub>2</sub>O]<sup>2+</sup>. Anal. calcd for C<sub>31</sub>H<sub>57</sub>N<sub>9</sub>Ni<sub>2</sub>·4CH<sub>3</sub>CO<sub>2</sub>·9H<sub>2</sub>O: C, 43.71; H, 8.18; N, 11.76; Found: C, 43.78; H, 7.82; N, 11.40 (very hygroscopic compound). UV-vis (H<sub>2</sub>O) λ<sub>max</sub>, nm (ε): 476 (372 M<sup>-1</sup> cm<sup>-1</sup>).

**7.2.19. Synthesis of 1,1'-[3,5-dimethylaminobenzyl]-7,7'-[methyl]-bis(1,4,7,10-tetraazabicyclo[5.5.2]dodecane) octahydrochloride (21)**



1,1'-[3,5-dimethylaminobenzyl]-7,7'-[methyl]-bis(1,4,7,10-tetraazabicyclo[5.5.2]dodecane) (**20**) (300 mg, 0.54 mmol) was dissolved in ethanol (50 ml) and HCl(g) was bubbled through continuously for 5 min. The resulting precipitate was collected and dried to yield a cream solid (234 mg, 51%).  $^1\text{H}$  NMR (400 MHz,  $\text{D}_2\text{O}$ ,  $\delta$ ): 2.02 (s,  $\text{CH}_3$ , 6H), 2.23-5.54 (br m, N- $\text{CH}_2$  +  $\text{NH}_2$ , 45H), 3.68 (m,  $\text{CH}_2\text{NH}_2$ , 2H), 4.07-4.23 (m, Ar  $\text{CH}_2$ , 4H), 7.39-7.53 (m, Ar H, 3H).  $^{13}\text{C}$  NMR (100 MHz,  $\text{CDCl}_3$ ,  $\delta$ ): 30.28 ( $\text{CH}_3$ ), 42.78 (N- $\text{CH}_2$ ), 44.55 (N- $\text{CH}_2$ ), 44.83 (N- $\text{CH}_2$ ), 45.83 (N- $\text{CH}_2$ ), 46.35 (N- $\text{CH}_2$ ), 48.92 (N- $\text{CH}_2$ ), 50.81 (N- $\text{CH}_2$ ), 52.27 (N- $\text{CH}_2$ ), 52.51 (N- $\text{CH}_2$ ), 53.49 (N- $\text{CH}_2$ ), 55.33 (N- $\text{CH}_2$ ), 58.07 ( $\text{CH}_2\text{NH}_2$ ), 59.55 (Ar  $\text{CH}_2$ ), 123.51 (Ar CH), 130.44 (Ar CH), 132.37 (Ar C), 148.25 (Ar C). HRMS ( $m/z$ ):  $[\text{M} - 8\text{HCl} + \text{H}]^+$  calcd for  $\text{C}_{31}\text{H}_{58}\text{N}_9$ , 556.4804; found, 556.4810. Anal. calcd for  $\text{C}_{31}\text{H}_{58}\text{N}_9 \cdot 8\text{HCl} \cdot 2\text{CH}_3\text{OH}$ : C, 43.48; H, 8.07; N, 13.83; Found: C, 43.10; H, 8.08; N, 13.69.

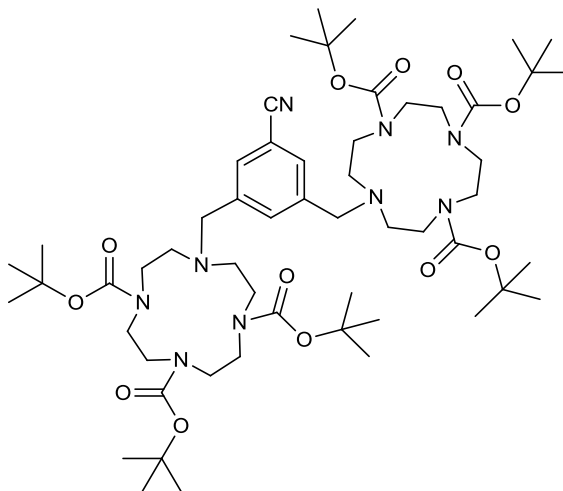
### 7.2.20. Synthesis of 1,4,7-tri-*tert*-butylcarbonate-1,4,7,10-tetraazacyclododecane (22)



Following the literature method outlined by Dessolin *et al.*<sup>158</sup>

To a solution of 1,4,7,10-tetraazacyclododecane (cyclen) (4.00 g, 23.2 mmol) in ice-cold DCM (400 ml) was added di-*tert*-butyl dicarbonate (9.12 g, 41.8 mmol) and the solution was stirred at RT for 4 hours. Solvent was removed *in vacuo* to give crude white solid. This was purified *via* flash chromatography (eluant, MeOH:DCM, 1:19) to yield a white, fluffy solid (4.20 g, 38%). <sup>1</sup>H NMR (400 MHz, CDCl<sub>3</sub>, δ): 1.38 (s, C(CH<sub>3</sub>)<sub>3</sub>, 18H), 1.40 (s, C(CH<sub>3</sub>)<sub>3</sub>, 9H), 2.78 (br s, N-CH<sub>2</sub>, 4H), 3.21-3.31 (m, N-CH<sub>2</sub>, 8H), 3.56 (br s, N-CH<sub>2</sub>, 4H). <sup>13</sup>C NMR (100 MHz, CDCl<sub>3</sub>, δ): 26.16 (C(CH<sub>3</sub>)<sub>3</sub>), 26.34 (C(CH<sub>3</sub>)<sub>3</sub>), 42.64 (N-CH<sub>2</sub>), 47.18 (N-CH<sub>2</sub>), 48.65 (N-CH<sub>2</sub>), 77.10 (C(CH<sub>3</sub>)<sub>3</sub>), 153.09 (C=O), 153.41 (C=O). HRMS (*m/z*): [M + H]<sup>+</sup> calcd for C<sub>23</sub>H<sub>45</sub>N<sub>4</sub>O<sub>6</sub>, 473.3330; found, 473.3334. Anal. calcd for C<sub>23</sub>H<sub>44</sub>N<sub>4</sub>O<sub>6</sub>: C, 58.45; H, 9.38; N, 11.85; Found: C, 58.46; H, 9.59; N, 11.83. R<sub>f</sub> = 0.69 (silica, MeOH:DCM, 1:19).

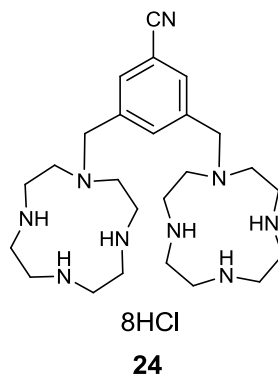
**7.2.21. Synthesis of 10,10'-(3,5-dimethylbenzonitrile)-bis-(1,4,7,10-tetraazacyclododecane)-1,4,7-hexa-*tert*-butylcarbonate (**23**)**



**23**

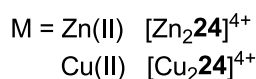
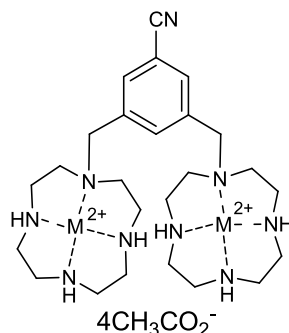
3,5-(Dibromomethyl)benzonitrile (**16**) (0.76 g, 2.63 mmol) and  $K_2CO_3$  (2.09 g, 14.44 mmol) were dissolved in dry MeCN (150 ml). 1,4,7-tri-*tert*-butylcarbonate-1,4,7,10-tetraazacyclododecane (**22**) (2.73 g, 5.79 mmol) was added in one portion. The mixture was refluxed for 18 hours under argon. The solution was filtered and solvents removed *in vacuo*. The residue was redissolved in ethyl acetate (200 ml) and washed with brine (4 x 100 ml). The organic layer was dried ( $MgSO_4$ ), filtered and solvent removed *in vacuo* to yield crude orange solid. This was purified *via* flash chromatography (eluant: MeOH:DCM, 1-5%) to yield a white, crispy solid (1.97 g, 70%).  $^1H$  NMR (400 MHz,  $CDCl_3$ ,  $\delta$ ): 1.38 (s,  $C(CH_3)_3$ , 18H), 1.40 (s,  $C(CH_3)_3$ , 36H), 2.53 (m, N- $CH_2$ , 8H), 3.23-3.39 (br m, N- $CH_2$ , 16H), 3.51 (br s, N- $CH_2$ , 8H), 3.69 (s, Ar  $CH_2$ , 4H), 7.23 (s, Ar H, 1H), 7.47 (s, 2H, Ar H).  $^{13}C$  NMR (100 MHz,  $CDCl_3$ ,  $\delta$ ): 25.82 ( $C(CH_3)_3$ ), 25.96 ( $C(CH_3)_3$ ), 45.38 (N- $CH_2$ ), 47.12 (N- $CH_2$ ), 50.75 (N- $CH_2$ ), 51.81 (N- $CH_2$ ), 52.83 (N- $CH_2$ ), 53.59 (N- $CH_2$ ), 74.69 ( $C(CH_3)_3$ ), 76.92 ( $C(CH_3)_3$ ), 77.08 (Ar  $CH_2$ ), 109.78 (Ar CH), 115.90 (CN), 129.41 (Ar CH), 132.97 (Ar C), 136.47 (Ar C), 152.77 (C=O), 153.11 (C=O), 153.57 (C=O). HRMS ( $m/z$ ):  $[M + H]^+$  calcd for  $C_{55}H_{94}N_9O_{12}$ , 1072.7015; found, 1072.7016. Anal. calcd for  $C_{55}H_{93}N_9O_{12} \cdot 1.5H_2O$ : C, 60.09; H, 8.80; N, 11.47; Found: C, 60.36; H, 9.32; N, 11.54.  $R_f$  = 0.64 (silica, MeOH:DCM, 1:19).

**7.2.22. Synthesis of 10,10'-(3,5-dimethylbenzonitrile)-bis(1,4,7,10-tetraazacyclododecane) octahydrochloride (24)**



10,10'-(3,5-dimethylbenzonitrile)-bis(1,4,7,10-tetraazacyclododecane)-1,4,7-hexa-*tert*-butyl carbonate (**23**) (0.74 g, 0.69 mmol) was dissolved in MeOH (15 ml), a 6 M solution of HCl (20 ml) was added and the resulting mixture was heated under reflux for 24 hours. After cooling solvents were removed *in vacuo* and the resulting cream solid was triturated with acetone (3 x 20 ml) after high vacuum drying a powdery, cream solid was obtained (0.50 g, 94%).  $^1\text{H}$  NMR (400 MHz,  $\text{D}_2\text{O}$ ,  $\delta$ ): 2.94 (s, NH, 6H), 3.01 (s, N- $\text{CH}_2$ , 2H), 3.19 (s, N- $\text{CH}_2$ , 7H), 3.29 (br s, N- $\text{CH}_2$ , 13H), 3.33 (m, N- $\text{CH}_2$ , 3H), 3.38 (m, N- $\text{CH}_2$ , 7H), 3.97 (m, Ar  $\text{CH}_2$ , 3H), 4.04 (s, Ar  $\text{CH}_2$ , 1H), 7.72 (s, Ar H, 1H), 7.80 (s, Ar H, 2H).  $^{13}\text{C}$  NMR (100 MHz,  $\text{D}_2\text{O}$ ,  $\delta$ ): 36.81 (N- $\text{CH}_2$ ), 42.09 (N- $\text{CH}_2$ ), 42.40 (N- $\text{CH}_2$ ), 42.69 (N- $\text{CH}_2$ ), 44.08 (N- $\text{CH}_2$ ), 44.28 (N- $\text{CH}_2$ ), 47.93 (N- $\text{CH}_2$ ), 48.42 (N- $\text{CH}_2$ ), 56.15 (Ar  $\text{CH}_2$ ), 112.55 (Ar CH), 119.37 (CN), 134.04 (Ar CH), 136.29 (Ar C), 137.40 (Ar C). HRMS ( $m/z$ ):  $[\text{M} - 8\text{HCl} + \text{H}]^+$  calcd for  $\text{C}_{25}\text{H}_{46}\text{N}_9$ , 472.3866; found, 472.3871. Anal. calcd for  $\text{C}_{25}\text{H}_{45}\text{N}_9 \cdot 8\text{HCl} \cdot 6\text{H}_2\text{O}$ : C, 34.46; H, 7.52; N, 14.47; Found: C, 34.86; H, 7.58; N, 14.92.

### 7.2.23. Synthesis of metal complexes of 10,10'-(3,5-dimethylbenzonnitrile)-bis(1,4,7,10-tetraazacyclododecane) (**24**)



#### General procedure J

10,10'-(3,5-dimethylbenzonnitrile)-bis(1,4,7,10-tetraazacyclododecane) octahydrochloride (**24**) (150 mg, 0.199 mmol) was dissolved in MeOH (15 ml), K<sub>2</sub>CO<sub>3</sub> (137 mg, 0.993 mmol) was added along with a methanolic (5 ml) solution of metal salt. This mixture was refluxed overnight under argon. After cooling, the mixture was filtered, solvents were removed *in vacuo* ~3 ml then purified *via* size exclusion chromatography (sephadex LH20).

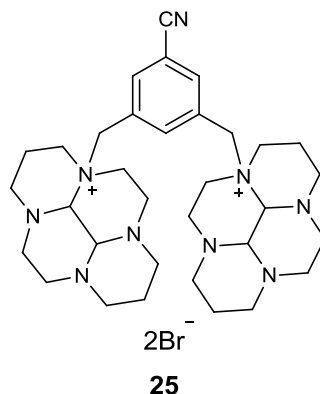
#### 10,10'-(3,5-dimethylbenzonnitrile)-bis(1,4,7,10-tetraazacyclododecane) zinc(II) acetate [Zn<sub>2</sub>**24**]<sup>4+</sup>

Amounts: Zinc(II) acetate (80 mg, 0.437 mmol). To yield a cream solid (121 mg, 72%). <sup>1</sup>H NMR (400 MHz, CD<sub>3</sub>OD, δ): 1.93 (s, N-CH<sub>2</sub>, 8H), 2.71-2.79 (m, N-CH<sub>2</sub>, 14H), 2.93 (m, N-CH<sub>2</sub>, 6H), 3.15 (m, N-CH<sub>2</sub>, 4H), 3.30 (s, Ar CH<sub>2</sub>, 4H), 4.05 (br s, NH, 6H), 7.81 (s, Ar H, 1H), 7.87 (m, Ar H, 2H). <sup>13</sup>C NMR (100 MHz, CD<sub>3</sub>OD, δ): 23.73 (N-CH<sub>2</sub>), 43.65 (N-CH<sub>2</sub>), 45.15 (N-CH<sub>2</sub>), 46.00 (N-CH<sub>2</sub>), 51.06 (Ar CH<sub>2</sub>), 114.26 (CN), 119.45 (Ar C), 131.57 (Ar CH), 135.89 (Ar CH), 161.62 (Ar C). HRMS (*m/z*): [M - 2CH<sub>3</sub>CO<sub>2</sub>]<sup>2+</sup> calcd for C<sub>29</sub>H<sub>45</sub>N<sub>9</sub>Zn<sub>2</sub>O<sub>4</sub>, 358.6323; found, 358.6318. Anal. calcd for C<sub>25</sub>H<sub>45</sub>N<sub>9</sub>Zn<sub>2</sub>·4CH<sub>3</sub>CO<sub>2</sub>·6.5H<sub>2</sub>O: C, 41.47; H, 7.38; N, 13.19; Found: C, 41.30; H, 7.57; N, 13.49 (very hygroscopic compound).

**10,10'-(3,5-dimethylbenzotrile)-bis(1,4,7,10-tetraazacyclododecane) copper(II) acetate [Cu<sub>2</sub>24]<sup>4+</sup>**

Amounts: Copper(II) acetate monohydrate (87 mg, 0.437 mmol). To yield a blue crystalline solid (150 mg, 90%). HRMS (*m/z*): [M – 2CH<sub>3</sub>CO<sub>2</sub>]<sup>2+</sup> calcd for C<sub>29</sub>H<sub>45</sub>N<sub>9</sub>Cu<sub>2</sub>O<sub>4</sub>, 357.6323; found, 357.6323. Anal. calcd for C<sub>25</sub>H<sub>45</sub>N<sub>9</sub>Cu<sub>2</sub>.4CH<sub>3</sub>CO<sub>2</sub>.10H<sub>2</sub>O: C, 39.05; H, 7.65; N, 13.29; Found: C, 41.30; H, 7.57; N, 13.49 (very hygroscopic compound). UV-vis (MeOH) λ<sub>max</sub>, nm (ε): 653 (578 M<sup>-1</sup> cm<sup>-1</sup>).

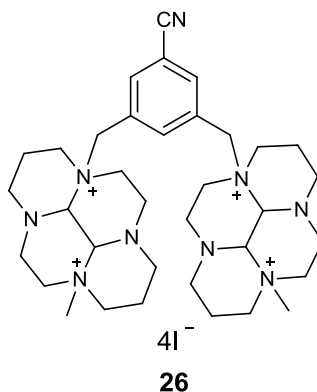
**7.2.24. Synthesis of 3a,3a'-[3,5-dimethylbenzonitrile]-bis(decahydro-3a,5a,8a,10a, tetraaza-pyrenium) dibromide (25)**



**General procedure B was followed**

Amounts: Bridged cyclam (**2**) (2.46 g, 11.07 mmol), MeCN (125 ml), 3,5-dibromomethylbenzonitrile (**16**) (1.60 g, 5.50 mmol), diethyl ether (2 x 50 ml). To yield a white solid (3.21 g, 79%).  $^1\text{H}$  NMR (400 MHz,  $\text{D}_2\text{O}$ ,  $\delta$ ): 1.45 (d,  $J = 14.1$  Hz, N- $\beta$ - $\text{CH}_2$ , 2H), 1.81 (d,  $J = 14.7$  Hz, N- $\beta$ - $\text{CH}_2$ , 2H), 2.22 (m, N- $\alpha$ - $\text{CH}_2$ , 4H), 2.34 (t,  $J = 11.6$  Hz, N- $\alpha$ - $\text{CH}_2$ , 2H), 2.48 (m, N- $\alpha$ - $\text{CH}_2$ , 4H), 2.67 (t,  $J = 9.9$  Hz, N- $\alpha$ - $\text{CH}_2$ , 2H), 3.00-3.15 (br m, N- $\alpha$ - $\text{CH}_2$ , 16H), 3.25 (m, N- $\alpha$ - $\text{CH}_2$ , 1H), 3.40 (m, N- $\alpha$ - $\text{CH}_2$ , 1H), 3.46-3.66 (m, N- $\alpha$ - $\text{CH}_2$ , 4H), 3.72 (s, N- $\alpha$ - $\text{CH}_2$ , 2H), 4.27 (t,  $J = 12.8$  Hz, Ar  $\text{CH}_2$ , 2H), 4.37 (s, Ar  $\text{CH}_2$ , 2H), 4.93 (d,  $J = 13.4$  Hz, CH, 2H), 5.27 (d,  $J = 13.4$  Hz, CH, 2H), 7.99 (s, Ar H, 1H), 8.15 (s, Ar H, 2H).  $^{13}\text{C}$  NMR (100 MHz,  $\text{D}_2\text{O}$ ,  $\delta$ ): 18.19 (N- $\beta$ - $\text{CH}_2$ ), 18.61 (N- $\beta$ - $\text{CH}_2$ ), 46.73 (N- $\alpha$ - $\text{CH}_2$ ), 49.19 (N- $\alpha$ - $\text{CH}_2$ ), 51.56 (N- $\alpha$ - $\text{CH}_2$ ), 52.00 (N- $\alpha$ - $\text{CH}_2$ ), 53.55 (N- $\alpha$ - $\text{CH}_2$ ), 54.13 (N- $\alpha$ - $\text{CH}_2$ ), 54.98 (N- $\alpha$ - $\text{CH}_2$ ), 60.33 (N- $\alpha$ - $\text{CH}_2$ ), 60.86 (Ar  $\text{CH}_2$ ), 69.67 (CH), 82.70 (CH), 114.39 (Ar C), 117.50 (CN), 128.93 (Ar CH), 139.34 (Ar CH), 142.58 (Ar C). HRMS ( $m/z$ ):  $[\text{M} - 2\text{Br}]^{2+}$  calcd for  $\text{C}_{33}\text{H}_{51}\text{N}_9$ , 286.7128; found, 286.7128. Anal. calcd for  $\text{C}_{33}\text{H}_{51}\text{N}_9^{79}\text{Br}_2 \cdot 2\text{H}_2\text{O}$ : C, 51.50; H, 7.20; N, 16.38; Found: C, 51.18; H, 7.25; N, 15.99.

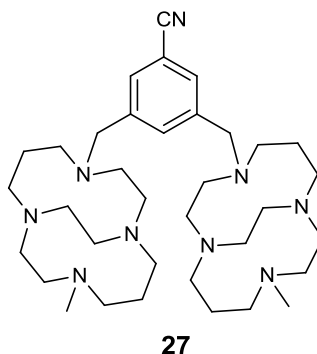
**7.2.25. Synthesis of 3a,3a'-[3,5-dimethylbenzonitrile]-8a,8a'-[methyl]-bis (decahydro-3a,5a,8a,10a-tetraaza-pyrenium) tetraiodide (26)**



**General procedure F was followed**

Amounts: 3a,3a'-[3,5-dimethylbenzonitrile]-bis(decahydro-3a,5a,8a,10a,tetraaza-pyrenium) dibromide (**25**) (3.00 g, 4.09 mmol), MeCN (80 ml), iodomethane (10 ml, 163.8 mmol then 5 ml, 81.90 mmol), diethyl ether (2 x 50 ml). To yield a yellow solid (3.43 g, 75%). <sup>1</sup>H NMR (400 MHz, DMSO, δ): 1.88 (m, N-β-CH<sub>2</sub>, 4H), 2.14 (m, N-β-CH<sub>2</sub>, 2H), 2.31 (m, N-β-CH<sub>2</sub>, 2H), 2.52 (s, CH<sub>3</sub> + N-α-CH<sub>2</sub>, 10H), 2.76 (m, N-α-CH<sub>2</sub>, 1H), 3.00-3.09 (m, N-α-CH<sub>2</sub>, 8H), 3.22 (d, *J* = 11.9 Hz, N-α-CH<sub>2</sub>, 4H), 3.52 (m, N-α-CH<sub>2</sub>, 4H), 3.71 (m, N-α-CH<sub>2</sub>, 4H), 3.83 (m, N-α-CH<sub>2</sub>, 2H), 4.32 (m, N-α-CH<sub>2</sub>, 5H), 5.10 (s, CH, 4H), 5.28-5.40 (m, Ar CH<sub>2</sub>, 4H), 8.14-8.35 (br ov, Ar H, 4H). <sup>13</sup>C NMR (100 MHz, DMSO, δ): 18.02 (N-β-CH<sub>2</sub>), 18.27 (N-β-CH<sub>2</sub>), 45.97 (CH<sub>3</sub>), 46.75 (CH<sub>3</sub>), 47.47 (N-α-CH<sub>2</sub>), 48.71 (N-α-CH<sub>2</sub>), 50.20 (N-α-CH<sub>2</sub>), 50.27(N-α-CH<sub>2</sub>), 59.16 (N-α-CH<sub>2</sub>), 59.57 (N-α-CH<sub>2</sub>), 63.88 (Ar CH<sub>2</sub>), 75.05 (CH), 75.56 (CH), 113.05 (Ar C), 117.10 (CN), 128.25 (Ar CH), 139.02 (Ar CH), 142.89 (Ar C). HRMS (*m/z*): [M – 2I<sup>-</sup>]<sup>2+</sup> calcd for C<sub>35</sub>H<sub>57</sub>N<sub>9</sub>I<sub>2</sub>, 428.6407; found, 428.6408. Anal. calcd for C<sub>35</sub>H<sub>57</sub>N<sub>9</sub>I<sub>4</sub>: C, 37.82; H, 5.17; N, 11.34; Found: C, 37.85; H, 5.30; N, 11.09.

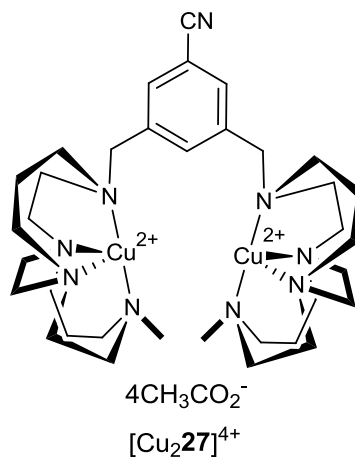
**7.2.26. Synthesis of 1,1'-[3,5-dimethylbenzonitrile]-8,8'-[methyl]-bis(1,4,8,11-tetraazabicyclo[10.2.2]hexadecane) (27)**



**General procedure G was followed**

Amounts: 3a,3a'-[3,5-dimethylbenzonitrile]-8a,8a'-[methyl]-bis(decahydro-3a,5a,8a,10a-tetraaza-pyrenium) tetraiodide (**26**) (3.35 g, 3.06 mmol), ethanol (200 ml), sodium borohydride (2.85 g, 75.35 mmol), water (100 ml, 100 ml), DCM (5 x 50 ml). To yield a yellow oil (1.25 g, 68%). <sup>1</sup>H NMR (400 MHz, D<sub>2</sub>O, δ): 1.37 (m, N-β-CH<sub>2</sub>, 4H), 1.52-1.60 (m, N-β-CH<sub>2</sub> + CH<sub>3</sub>, 10H), 2.29-2.34 (br m, N-α-CH<sub>2</sub>, 18H), 2.55 (m, N-α-CH<sub>2</sub>, 8H), 2.89 (m, N-α-CH<sub>2</sub>, 6H), 3.18 (m, N-α-CH<sub>2</sub>, 4H), 3.62 (m, N-α-CH<sub>2</sub>, 4H), 3.99 (m, Ar CH<sub>2</sub>, 4H), 7.42 (m, Ar H, 3H). <sup>13</sup>C NMR (100 MHz, D<sub>2</sub>O, δ): 24.94 (N-β-CH<sub>2</sub>), 25.46 (N-β-CH<sub>2</sub>), 41.74 (CH<sub>3</sub>), 42.98 (CH<sub>3</sub>), 51.33 (N-α-CH<sub>2</sub>), 51.79 (N-α-CH<sub>2</sub>), 52.05 (N-α-CH<sub>2</sub>), 52.77 (N-α-CH<sub>2</sub>), 53.11 (N-α-CH<sub>2</sub>), 53.29 (N-α-CH<sub>2</sub>), 53.39 (N-α-CH<sub>2</sub>), 53.72 (N-α-CH<sub>2</sub>), 55.70 (N-α-CH<sub>2</sub>), 56.61 (N-α-CH<sub>2</sub>), 57.32 (N-α-CH<sub>2</sub>), 57.84 (N-α-CH<sub>2</sub>), 58.39 (Ar CH<sub>2</sub>), 59.36 (Ar CH<sub>2</sub>), 112.00 (CN), 118.84 (Ar CH), 131.12 (Ar CH), 132.20 (Ar C), 137.61 (Ar C). HRMS (*m/z*): [M + 2H]<sup>2+</sup> calcd for C<sub>35</sub>H<sub>63</sub>N<sub>9</sub>, 304.7586; found, 304.7598.

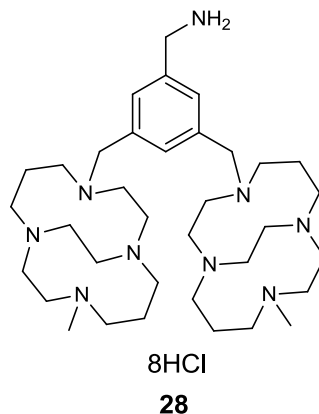
**7.2.27. Synthesis of 1,1'-[3,5-dimethylbenzonitrile]-8,8'-[methyl]-bis(1,4,8,11-tetraazabicyclo[10.2.2]hexadecane) copper(II) acetate [Cu<sub>2</sub>27]<sup>4+</sup>**



**General procedure I was followed**

Amounts: 1,1'-[3,5-dimethylbenzonitrile]-8,8'-[methyl]-bis(1,4,8,11-tetraazabicyclo[10.2.2]hexadecane (**27**) (100 mg, 0.164 mmol), copper(II) acetate monohydrate (72 mg, 0.362 mmol). To yield a blue, oil (132 mg, 83%). HRMS (*m/z*): [M + 2CH<sub>3</sub>CO<sub>2</sub>]<sup>2+</sup> calcd for C<sub>39</sub>H<sub>67</sub>Cu<sub>2</sub>N<sub>9</sub>O<sub>4</sub>, 425.6948; found, 425.6949. UV-vis (MeOH) λ<sub>max</sub>, nm (ε): 632 (492 M<sup>-1</sup> cm<sup>-1</sup>).

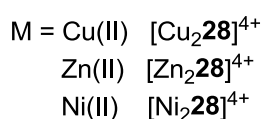
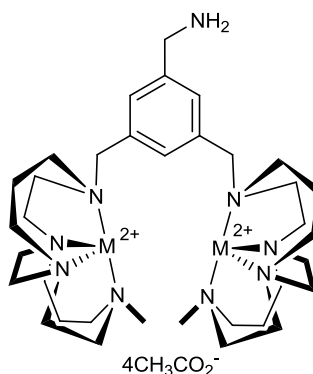
**7.2.28. Synthesis of 1,1'-[3,5-dimethylaminobenzyl]-8,8'-[methyl]-bis(1,4,8,11-tetraazabicyclo[10.2.2]hexadecane) octahydrochloride (28)**



Lithium aluminium hydride (0.19 g, 4.94 mmol) was dissolved in dry THF (30 ml). To this, 1,1'-[3,5-dimethylbenzyl]-8,8'-[methyl]-bis(1,4,8,11-tetraazabicyclo[10.2.2]hexadecane) (**27**) (1.00 g, 1.64 mmol) in dry THF (50 ml) was added dropwise under ice-cooling. After complete addition the mixture was stirred for 30 min then heated to reflux for 3 hours. The reaction was cooled in an ice-bath, water (0.2 ml) was added dropwise followed by 15% sodium hydroxide (0.2 ml) followed by a second portion of water (0.6 ml). The resulting white precipitate was filtered and washed with THF (2 x 20 ml) then water (2 x 50 ml). The aqueous layer was made strongly basic (pH > 14, KOH) and extracted with THF (5 x 20 ml). The organic phases were dried (Na<sub>2</sub>SO<sub>4</sub>), filtered and solvents removed *in vacuo*. The resulting oil was dissolved in ethanol (60 ml) and HCl(g) was bubbled through continuously for 5 min. The resulting precipitate was collected and dried to yield a cream solid (600 mg, 40%). <sup>1</sup>H NMR (400 MHz, D<sub>2</sub>O, δ): 1.26 (s, N-β-CH<sub>2</sub>, 2H), 1.71 (m, N-β-CH<sub>2</sub>, 2H), 2.15-2.38 (m, N-β-CH<sub>2</sub>, 4H), 2.71-3.83 (br m, N-α-CH<sub>2</sub> + NH<sub>2</sub> + CH<sub>3</sub>, 48H), 4.29 (m, CH<sub>2</sub>-NH<sub>2</sub>, 2H), 4.70 (m, Ar CH<sub>2</sub>, 4H), 7.22-8.10 (m, Ar H, 3H). <sup>13</sup>C NMR (100 MHz, D<sub>2</sub>O, δ): 13.49 (CH<sub>3</sub>), 18.63 (N-β-CH<sub>2</sub>), 19.01 (N-β-CH<sub>2</sub>), 40.05 (N-α-CH<sub>2</sub>), 45.67 (N-α-CH<sub>2</sub>), 48.92 (N-α-CH<sub>2</sub>), 49.10 (N-α-CH<sub>2</sub>), 49.23 (N-α-CH<sub>2</sub>), 50.07 (N-α-CH<sub>2</sub>), 50.18 (N-α-CH<sub>2</sub>), 53.07 (N-α-CH<sub>2</sub>), 58.49 (N-α-CH<sub>2</sub>), 59.26 (N-α-CH<sub>2</sub>), 62.79 (CH<sub>2</sub>-NH<sub>2</sub>), 73.88 (Ar CH<sub>2</sub>), 128.89 (Ar CH), 132.14 (Ar CH), 135.14 (Ar C), 140.07 (Ar C). HRMS (*m/z*): [M + H]<sup>+</sup> calcd for C<sub>35</sub>H<sub>66</sub>N<sub>9</sub>, 612.5435; found, 612.5436. Anal. calcd for

$C_{35}H_{65}N_9 \cdot 8HCl \cdot 4.5CH_3OH \cdot 5.5H_2O$ : C, 41.37; H, 8.96; N, 10.99; Found: C, 41.62; H, 8.58; N, 10.73.

**7.2.29. Synthesis of metal complexes of 1,1'-[3,5-dimethylaminobenzyl]-8,8'-[methyl]-bis(1,4,8,11-tetraazabicyclo[10.2.2]hexadecane) octahydrochloride (**28**)**



**General procedure K**

1,1'-[3,5-dimethylaminobenzyl]-8,8'-[methyl]-bis(1,4,8,11-tetraazabicyclo[10.2.2]hexadecane) octahydrochloride (**28**) and K<sub>2</sub>CO<sub>3</sub> were dissolved in anhydrous MeOH and stirred for 20 min under argon. An anhydrous methanolic solution of the metal salt was added dropwise and the mixture was refluxed for 24 hours under argon. Solids were filtered and solvent was concentrated ~ 5 ml and purified *via* size exclusion chromatography (sephadex LH20).

**1,1'-[3,5-dimethylaminobenzyl]-8,8'-[methyl]-bis(1,4,8,11-tetraazabicyclo[10.2.2]hexadecane) copper(II) acetate [Cu<sub>2</sub>**28**]<sup>4+</sup>**

Amounts: 1,1'-[3,5-dimethylaminobenzyl]-8,8'-[methyl]-bis(1,4,8,11-tetraazabicyclo[10.2.2]hexadecane) octahydrochloride (**28**) (75 mg, 0.12 mmol), K<sub>2</sub>CO<sub>3</sub> (133 mg, 0.96 mmol), MeOH (10 ml), copper(II) acetate monohydrate (54 mg, 0.27 mmol). To yield a blue solid (88 mg, 74%). HRMS (*m/z*): [M - 2CH<sub>3</sub>CO<sub>2</sub><sup>-</sup> - 4H]<sup>2+</sup> calcd for C<sub>39</sub>H<sub>67</sub>N<sub>9</sub>Cu<sub>2</sub>O<sub>4</sub>, 425.6948; found, 425.6949. Anal. calcd for C<sub>35</sub>H<sub>65</sub>Cu<sub>2</sub>N<sub>9</sub>·4CH<sub>3</sub>CO<sub>2</sub>·3H<sub>2</sub>O: C, 50.18; H, 8.13; N, 12.25; Found: C, 49.95; H, 8.26; N, 12.47 (very hygroscopic compound). UV-vis (MeOH) λ<sub>max</sub>, nm (ε): 657 (520 M<sup>-1</sup> cm<sup>-1</sup>).

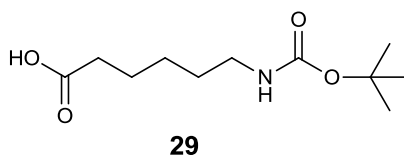
**1,1'-[3,5-dimethylaminobenzyl]-8,8'-[methyl]-bis(1,4,8,11-tetraazabicyclo[10.2.2]hexadecane) zinc(II) acetate [Zn<sub>2</sub>28]<sup>4+</sup>**

Amounts: 1,1'-[3,5-dimethylaminobenzyl]-8,8'-[methyl]-bis(1,4,8,11-tetraazabicyclo[10.2.2]hexadecane) octahydrochloride (**28**) (118 mg, 0.19 mmol), K<sub>2</sub>CO<sub>3</sub> (210 mg, 1.52 mmol), zinc(II) acetate (75 mg, 0.42 mmol). To yield a pale orange solid (111 mg, 58%). <sup>1</sup>H NMR (400 MHz, CD<sub>3</sub>OD, δ): 1.62 (br m, N-β-CH<sub>2</sub>, 8H), 1.94 (s, CH<sub>3</sub>, 6H) 2.13-3.25 (br m, N-α-CH<sub>2</sub> + CH<sub>2</sub>NH<sub>2</sub>, 44H), 3.90-4.58 (m, Ar CH<sub>2</sub>, 4H), 7.22 (m, Ar H, 3H). HRMS (*m/z*): [M - 2CH<sub>3</sub>CO<sub>2</sub>]<sup>2+</sup> calcd for C<sub>39</sub>H<sub>71</sub>N<sub>9</sub>Zn<sub>2</sub>O<sub>4</sub>, 428.7100; found, 428.7100. Anal. calcd for C<sub>35</sub>H<sub>65</sub>Zn<sub>2</sub>N<sub>9</sub>·4CH<sub>3</sub>CO<sub>2</sub>·6H<sub>2</sub>O: C, 47.43; H, 8.42; N, 11.58; Found: C, 47.59; H, 8.36; N, 11.41.

**1,1'-[3,5-dimethylaminobenzyl]-8,8'-[methyl]-bis(1,4,8,11-tetraazabicyclo[10.2.2]hexadecane) nickel(II) acetate [Ni<sub>2</sub>28]<sup>4+</sup>**

Amounts: 1,1'-[3,5-dimethylaminobenzyl]-8,8'-[methyl]-bis(1,4,8,11-tetraazabicyclo[10.2.2]hexadecane) octahydrochloride (**28**) (118 mg, 0.19 mmol), K<sub>2</sub>CO<sub>3</sub> (210 mg, 1.52 mmol), nickel(II) acetate (78 mg, 0.42 mmol). To yield a pale orange solid (91 mg, 46%). MS (*m/z*): 374 [M - 4CH<sub>3</sub>CO<sub>2</sub><sup>-</sup> + H<sub>2</sub>O]<sup>2+</sup>. UV-vis (MeOH) λ<sub>max</sub>, nm (ε): 593 (411 M<sup>-1</sup> cm<sup>-1</sup>).

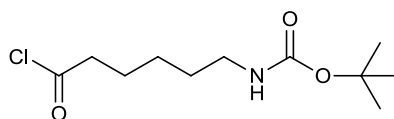
### 7.2.30. Synthesis of 6-((*tert*-butoxycarbonyl)amino)hexanoic acid (29)



Following the literature method outlined by Quelever *et al.*<sup>161</sup>

6-Aminohexanoic acid (2.62 g, 20 mmol) was dissolved in a dioxane:water mixture (120 ml, 2:1). The mixture was cooled to 0°C and a 1 M aqueous solution of NaOH (0.80 g, 20 ml, 20 mmol) was added, followed by di-*tert*-butyl dicarbonate (4.80 g, 22 mmol). The mixture was stirred at RT for 3 hours. Solvents were removed *in vacuo* and the basic residue was washed once with ethyl acetate (50 ml). The aqueous layer was acidified (1 M, HCl, pH 1) and extracted with ethyl acetate (3 x 50 ml). The organic layers were dried (MgSO<sub>4</sub>), filtered and solvents removed *in vacuo* to yield a white solid (slowly crystallised from an orange oil) (4.03 g, 100%).<sup>1</sup>H NMR (400 MHz, DMSO, δ): 1.17-1.25 (m, CH<sub>2</sub>, 4H), 1.37 (s, C(CH<sub>3</sub>)<sub>3</sub>, 9H), 1.47 (m, CH<sub>2</sub>, 2H), 2.51 (m, CH<sub>2</sub>, 2H), 2.88 (q, *J* = 6.6 Hz, CH<sub>2</sub>, 2H), 3.37 (br s, NH, 1H), 11.97 (br s, OH, 1H). <sup>13</sup>C NMR (100 MHz, DMSO, δ): 24.26 (CH<sub>2</sub>), 25.89 (CH<sub>2</sub>), 28.27 (C(CH<sub>3</sub>)), 29.26 (CH<sub>2</sub>), 33.66 (CH<sub>2</sub>), 59.76 (CH<sub>2</sub>), 77.31 (C(CH<sub>3</sub>)<sub>3</sub>), 155.62 (C=O), 174.45 (C=O). HRMS (*m/z*): [M + Na]<sup>+</sup> calcd for C<sub>11</sub>H<sub>21</sub>NONa, 254.1369; found, 254.1363.

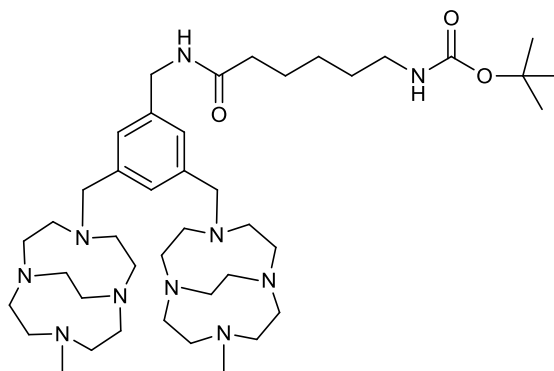
### 7.2.31. Attempted synthesis of *tert*-butyl(6-chloro-6-oxohexyl)carbamate (**30**)



**30**

To a cold (0°C) magnetically stirred solution of 6-((*tert*-butoxycarbonyl)amino) hexanoic acid (**29**) (0.5 g, 2.2 mmol) in DCM (30 ml) was added oxalyl chloride (0.3 g, 209  $\mu$ l, 2.4 mmol) under nitrogen along with one drop of DMF and the mixture was stirred at RT for 1 hour. Solvents were removed *in vacuo* to yield a colourless oil. The desired product was not isolated using this synthetic procedure. Analytical data indicates that the desired product was not obtained.

**7.2.32. Synthesis of *tert*-butyl(6-((3,5-bis((7,7'-[methyl]-1,4,7,10-tetraazabicyclo[5.5.2]tetradecan-4-yl)methyl)benzyl)amino)-6-oxohexyl) carbamate (31)**



**31**

**Method 1-Attempted synthesis**

To a cold (0°C) magnetically stirred solution of 6-((*tert*-butoxycarbonyl)amino) hexanoic acid (**30**) (0.1 g, 0.43 mmol) in DCM (30 ml) was added oxalyl chloride (41 µl, 0.47 mmol) under nitrogen, along with one drop of DMF, after 1 hour of stirring the solution was evaporated to yield colourless oil. The oil was redissolved in dry MeCN (10 ml) and added dropwise to a solution of 1,1'-[3,5-dimethylaminobenzyl]-7,7'-[methyl]-bis(1,4,7,10-tetraazabicyclo[5.5.2]dodecane) (**20**) (0.2 g, 0.36 mmol) in dry MeCN (10 ml). The resulting solution was stirred overnight. Solvents were removed *in vacuo* to yield an orange oil (>100%). HRMS: calcd. for C<sub>42</sub>H<sub>77</sub>N<sub>10</sub>O<sub>3</sub>: 769.6163 found 769.6175.

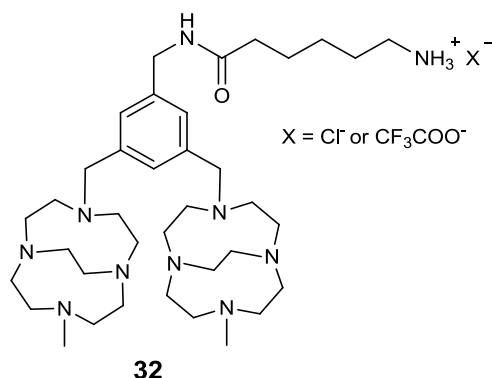
**Method 2-Preferred route**

**General procedure L**

Macrocycle and linker group were dissolved in a mixture of two solvents and heated for 4.5 hours at 40 °C. The resulting yellow mixture was extracted with chloroform. The aqueous layer was basified (pH 14, KOH) and extracted with chloroform. These organic washings were dried (MgSO<sub>4</sub>), filtered and solvents removed *in vacuo*.

Amounts: 1,1'-[3,5-dimethylaminobenzyl]-7,7'-[methyl]-bis(1,4,7,10-tetraazabicyclo [5.5.2]dodecane) (**20**) (200 mg, 0.36 mmol), 4-nitrophenyl-6-((*tert*-butoxycarbonyl) amino)hexanoate (**39**) (63 mg, 0.18 mmol), MeOH:DCM (1:1, 20 ml), chloroform (3 x 25 ml), chloroform (3 x 20 ml). To yield a yellow oil (110 mg, 80%).  $^1\text{H}$  NMR (400 MHz,  $\text{CD}_3\text{OD}$ ,  $\delta$ ): 1.22 (s,  $\text{CH}_3$ , 3H), 1.29-1.36 (m,  $\text{CH}_3$ , 3H), 1.40 (s,  $\text{CH}_2$ , 2H), 1.43 (s,  $\text{C}(\text{CH}_3)_3$ , 9H), 1.61 (m,  $\text{CH}_2$ , 2H), 2.22 (s,  $\text{CH}_2$ , 2H), 2.32 (m,  $\text{CH}_2$ , 2H), 2.65 (br s, N- $\text{CH}_2$ , 10H), 2.80-3.09 (br m, N- $\text{CH}_2$ , 30H), 3.35 (s,  $\text{CH}_2$ , 2H), 3.50-3.92 (br m, Ar  $\text{CH}_2$  +  $\text{CH}_2$ -NH, 6H), 7.21-7.26 (m, H-Ar, 3H).  $^{13}\text{C}$  NMR (100 MHz,  $\text{CD}_3\text{OD}$ ,  $\delta$ ): 16.91 ( $\text{CH}_3$ ), 21.09 ( $\text{CH}_2$ ), 22.71 ( $\text{CH}_2$ ), 24.26 ( $\text{C}(\text{CH}_3)_3$ ), 25.35 ( $\text{CH}_2$ ), 26.01 (N- $\text{CH}_2$ ), 26.43 (N- $\text{CH}_2$ ), 30.75 (N- $\text{CH}_2$ ), 30.82 (N- $\text{CH}_2$ ), 36.56 (N- $\text{CH}_2$ ), 39.04 (N- $\text{CH}_2$ ), 42.07 (N- $\text{CH}_2$ ), 45.34 (N- $\text{CH}_2$ ), 47.27 (N- $\text{CH}_2$ ), 47.65 (Ar  $\text{CH}_2$ -NH), 49.00 (CO- $\text{CH}_2$ ), 51.20 ( $\text{CH}_2$ -NH), 53.97 ( $\text{C}(\text{CH}_3)_3$ ), 75.11 (Ar  $\text{CH}_2$ ), 121.53 (Ar CH), 123.53 (Ar CH), 125.20 (Ar C), 134.65 (Ar C), 153.84 (C=O), 171.15 (C=O). HRMS ( $m/z$ ):  $[\text{M} + \text{H}]^+$  calcd for  $\text{C}_{42}\text{H}_{77}\text{N}_{10}\text{O}_3$ , 769.6165; found, 769.6175.

**7.2.33. Synthesis of 6-amino-*N*-(3,5-bis((7,7'-[methyl]-1,4,7,10-tetraazabicyclo[5.5.2]tetradecan-4-yl)methyl)benzyl)hexanamide (32)**



**Method 1-Attempted synthesis**

*tert*-Butyl(6-((3,5-bis((7,7'-[methyl]-1,4,7,10-tetraazabicyclo[5.5.2]tetradecan-4-yl)methyl)benzyl)amino)-6-oxohexyl)carbamate (**31**) (0.19 g, 0.25 mmol) was dissolved in MeOH (5 ml), 6M HCl (10 ml) was added and the orange solution was heated to reflux for 24 hours. After cooling, solvents were removed *in vacuo*. The residue was triturated with acetone (3 x 10 ml) to yield orange oil. The desired product was not isolated using this synthetic procedure. Analytical data indicates that the desired product was not obtained.

**Method 2-Attempted synthesis**

*tert*-Butyl(6-((3,5-bis((7,7'-[methyl]-1,4,7,10-tetraazabicyclo[5.5.2]tetradecan-4-yl)methyl)benzyl)amino)-6-oxohexyl)carbamate (**31**) (186 mg, 0.24 mmol) was dissolved in DCM (5 ml) and TFA (5 ml) and stirred at RT overnight. Solvents were removed *in vacuo*. The crude material was redissolved in water (30 ml) made strongly basic (KOH, pH 14) and extracted with DCM (5 x 50 ml). The organic phases were dried (Na<sub>2</sub>SO<sub>4</sub>), filtered and concentrated *in vacuo* to yield an orange oil. The desired product was not isolated using this synthetic procedure. Analytical data indicates that the desired product was not obtained.

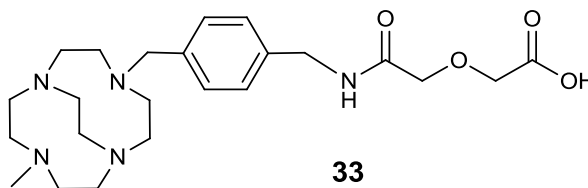
### Method 3-Preferred route

#### General procedure M

Macrocycle was dissolved in TFA and stirred at RT for 18 hours. Solvents were removed *in vacuo* and the residue was washed with ether followed by high vacuum drying.

Amounts: *tert*-Butyl-(6-((3,5-bis((7,7'-[methyl]-1,4,7,10-tetraazabicyclo[5.5.2] tetra decan-4-yl)methyl)benzyl)amino)-6-oxohexyl)carbamate (**31**) (100 mg, 0.13 mmol), TFA (5 ml), diethyl ether (2 x 10 ml). To yield a yellow/orange oil (81 mg, 79%). <sup>1</sup>H NMR (400 MHz, CD<sub>3</sub>OD,  $\delta$ ): 1.30 (m, CH<sub>3</sub>, 2H), 1.54 (m, CH<sub>3</sub>, 4H), 2.23 (t,  $J$  = 7.6 Hz, N-CH<sub>2</sub>, 2H), 2.77-2.85 (m, CH<sub>2</sub>, 7H), 2.94 (s, N-CH<sub>2</sub>, 9H), 3.07-3.39 (br m, N-CH<sub>2</sub>, 27H), 3.41 (d,  $J$  = 14.4 Hz, CH<sub>2</sub>, 3H), 3.52-3.57 (m, N-CH<sub>2</sub>, 3H), 3.66 (d,  $J$  = 12.0 Hz, NH<sub>2</sub>, 2H), 3.95 (s, 3H, Ar CH<sub>2</sub>), 4.05 (m, CH<sub>2</sub>-NH<sub>2</sub> + Ar CH<sub>2</sub>, 3H), 7.19-7.51 (m, Ar H, 3H). <sup>13</sup>C NMR (100 MHz, CD<sub>3</sub>OD,  $\delta$ ): 20.00 (CH<sub>3</sub>), 21.50(CH<sub>3</sub>), 22.85 (CH<sub>2</sub>), 29.04 (CH<sub>2</sub>), 35.21 (CH<sub>2</sub>), 35.31 (N-CH<sub>2</sub>), 38.63 (N-CH<sub>2</sub>), 41.41 (N-CH<sub>2</sub>), 44.57 (N-CH<sub>2</sub>), 47.35 (N-CH<sub>2</sub>), 48.65 (N-CH<sub>2</sub>), 48.88 (N-CH<sub>2</sub>), 49.00 (N-CH<sub>2</sub>), 49.11 (N-CH<sub>2</sub>), 49.34 (N-CH<sub>2</sub>), 49.57 (Ar CH<sub>2</sub>-NH), 51.72 (Ar CH<sub>2</sub>), 52.38 (Ar CH<sub>2</sub>), 106.46 (CO-CH<sub>2</sub>), 109.29 (CH<sub>2</sub>-NH<sub>2</sub>), 125.76 (Ar CH), 132.12 (Ar CH), 134.95 (Ar C), 145.50 (Ar C), 170.43 (C=O). MS ( $m/z$ ): 670 [M + H]<sup>+</sup>.

**7.2.34. Synthesis of 2-(2-((4-((7-[methyl]-1,4,7,10-tetraazabicyclo[5.5.2]tetradecan-4-yl)methyl)benzyl)amino)-2-oxoethoxy)acetic acid (33)**

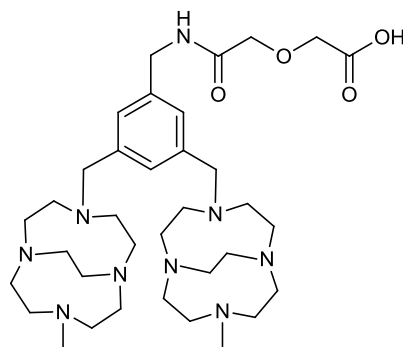


**General procedure N**

Macrocycle was dissolved in solvent, diglycolic anhydride was dissolved in MeOH and added dropwise. The mixture was stirred at RT for 2 hours. Solvents were removed *in vacuo*.

Amounts: 1-[4-Aminomethylbenzyl]-7-[methyl]-1,4,7,10-tetraazabicyclo[5.5.2]dodecane (**15**) (350 mg, 1.06 mmol), MeOH (15 ml), diglycolic anhydride (123 mg, 1.06 mmol), MeOH (5 ml). To yield a yellow/orange oil (0.47 g, 100%). <sup>1</sup>H NMR (400 MHz, D<sub>2</sub>O, δ): 1.30 (s, CH<sub>3</sub>, 3H), 2.56-2.59 (m, N-CH<sub>2</sub>, 2H), 2.66-3.05 (br m, N-CH<sub>2</sub> + OH, 16H), 4.00 (br s, N-CH<sub>2</sub> + NH, 4H), 4.05 (s, Ar CH<sub>2</sub>, 4H), 4.12 (s, CO-CH<sub>2</sub>-O, 4H), 7.17-7.45 (br ov, Ar H, 4H). <sup>13</sup>C NMR (100 MHz, CDCl<sub>3</sub>, δ): 30.37 (CH<sub>3</sub>), 31.11 (N-CH<sub>2</sub>), 44.48 (N-CH<sub>2</sub>), 52.50 (N-CH<sub>2</sub>), 53.18 (N-CH<sub>2</sub>), 53.35 (N-CH<sub>2</sub>), 53.77 (N-CH<sub>2</sub>), 54.01 (N-CH<sub>2</sub>), 56.44 (N-CH<sub>2</sub>), 56.78 (N-CH<sub>2</sub>), 63.03 (Ar CH<sub>2</sub>), 68.85 (C=O-CH<sub>2</sub>-COOH), 69.55 (C=O-CH<sub>2</sub>-O), 71.01 (Ar CH<sub>2</sub>), 126.32 (Ar C), 129.00 (Ar CH), 130.42 (Ar CH), 130.76 (Ar C), 172.58 (C=O), 174.48 (C=O). HRMS (*m/z*): [M + H]<sup>+</sup> calcd for C<sub>23</sub>H<sub>38</sub>N<sub>5</sub>O<sub>4</sub>, 448.2912; found, 448.2918.

**7.2.35. Synthesis of 2-(2-((3,5-bis((7,7'-[methyl]-1,4,7,10-tetraazabicyclo[5.5.2]tetradecan-4-yl)methyl)benzyl)amino)-2-oxoethoxy)acetic acid (34)**

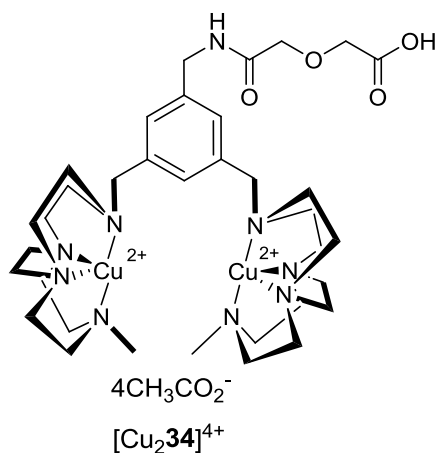


**34**

**General procedure N was followed**

Amounts: 1,1'-[3,5-Dimethylaminobenzyl]-7,7'-[methyl]-bis(1,4,7,10-tetraazabicyclo [5.5.2]dodecane) (**20**) (500 mg, 0.9 mmol), MeOH:MeCN (20 ml, 1:1), diglycolic anhydride (105 mg, 0.9 mmol), MeOH (10 ml). To yield a yellow oil (604 mg, 100%).  $^1\text{H}$  NMR (400 MHz,  $\text{CD}_3\text{OD}$ ,  $\delta$ ): 2.54 (m,  $\text{CH}_3$ , 6H), 2.43-3.00 (br m, N- $\text{CH}_2$ , 40H), 3.21 (m,  $\text{CH}_2$ -NH, 2H), 3.25 (s, NH, 1H), 3.87 (m, Ar  $\text{CH}_2$  + C=O- $\text{CH}_2$ -O, 6H), 3.94 (m, C=O- $\text{CH}_2$ -O, 1H), 4.16 (m, C=O- $\text{CH}_2$ -O, 1H), 5.10 (s, OH, 1H), 7.23-7.29 (m, Ar H, 3H).  $^{13}\text{C}$  NMR (100 MHz,  $\text{CD}_3\text{OD}$ ,  $\delta$ ): 23.69 ( $\text{CH}_3$ ), 24.76 ( $\text{CH}_3$ ), 37.36 (N- $\text{CH}_2$ ), 45.95 (N- $\text{CH}_2$ ), 46.16 (N- $\text{CH}_2$ ), 47.31 (N- $\text{CH}_2$ ), 48.08 (N- $\text{CH}_2$ ), 49.15 (N- $\text{CH}_2$ ), 49.65 ( $\text{CH}_2$ -NH), 52.62 (Ar  $\text{CH}_2$ ), 62.22 (Ar  $\text{CH}_2$ ), 64.96 (C=O- $\text{CH}_2$ -O), 65.25 (C=O- $\text{CH}_2$ -O), 119.93 (Ar CH), 122.46 (Ar CH), 123.97 (Ar C), 133.69 (Ar C), 166.76 (C=O), 170.71 (C=O). HRMS ( $m/z$ ):  $[\text{M} + \text{H}]^+$  calcd for  $\text{C}_{35}\text{H}_{62}\text{N}_9\text{O}_4$ , 672.4916; found, 672.4919.

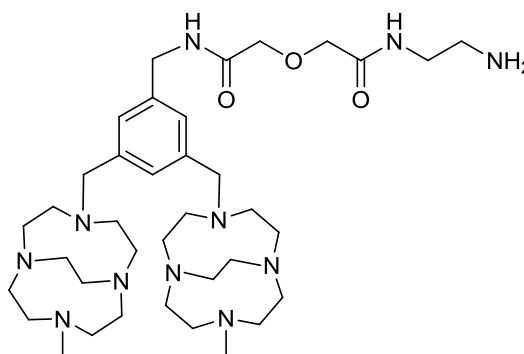
**7.2.36. Synthesis of 2-(2-((3,5-bis((7,7'-[methyl]-1,4,7,10-tetraazabicyclo[5.5.2]tetradecan-4-yl)methyl)benzyl)amino)-2-oxoethoxy)acetic acid copper(II) acetate [Cu<sub>2</sub>34]<sup>4+</sup>**



**General procedure I was followed**

Amounts: 2-(2-((3,5-Bis((7,7'-[methyl]-1,4,7,10-tetraazabicyclo[5.5.2]tetradecan-4-yl)methyl)benzyl)amino)-2-oxoethoxy)acetic acid (**34**) (85 mg, 0.13 mmol), MeOH (10 ml), copper(II) acetate monohydrate (56 mg, 0.28 mmol). To yield a blue solid (56 mg, 43%). HRMS (*m/z*): [M - 2CH<sub>3</sub>CO<sub>2</sub><sup>-</sup> + H]<sup>+</sup> calcd for C<sub>39</sub>H<sub>66</sub>N<sub>9</sub>Cu<sub>2</sub>O<sub>4</sub>, 914.3614; found, 914.3621. Anal. calcd for C<sub>35</sub>H<sub>61</sub>N<sub>9</sub>Cu<sub>2</sub>O<sub>4</sub>·4CH<sub>3</sub>CO<sub>2</sub>·4H<sub>2</sub>O: C, 46.64; H, 7.37; N, 11.39. Found: C, 46.38; H, 7.36; N, 11.58 (very hygroscopic compound). UV-vis (H<sub>2</sub>O) λ<sub>max</sub>, nm (ε): 656 (283 M<sup>-1</sup> cm<sup>-1</sup>).

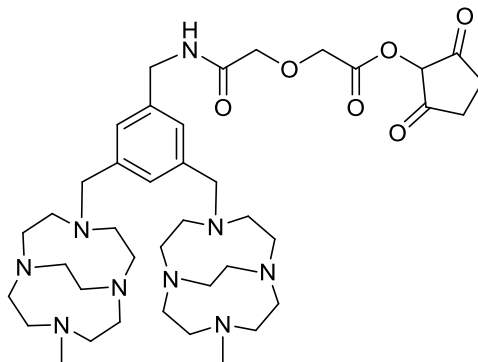
**7.2.37. Attempted synthesis of *N*-(2-aminoethyl)-2-(2-((3,5-bis((7,7'-[methyl]-1,4,7,10-tetraazabicyclo[5.5.2]tetradecan-4-yl)methyl)benzyl)amino)-2-oxoethoxy)acetamide (35)**



**35**

2-(2-((3,5-bis((7,7'-[methyl]-1,4,7,10-tetraazabicyclo[5.5.2]tetradecan-4-yl)methyl)benzyl)amino)-2-oxoethoxy)acetic acid (**34**) (200 mg, 0.30 mmol) and NHS (41 mg, 0.36 mmol) were dissolved in DCM (25 ml). EDC (68 mg, 0.36 mmol) was added to the mixture which was then stirred for 4 hours at RT. Ethylenediamine (179 mg, 0.20 ml, 3.00 mmol) was dissolved in DCM (3 ml) and added dropwise over 10 min. The resulting mixture was stirred for a further 2 days at RT. Solvents were removed *in vacuo* to yield a yellow oil. The desired product was not isolated using this synthetic procedure. Analytical data indicates that the desired product was not obtained.

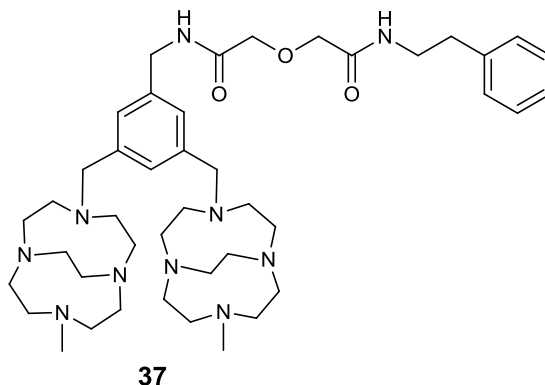
**7.2.38. Attempted synthesis of 2,5-dioxocyclopentyl-2-(2-((3,5-bis((7,7'-[methyl]-1,4,7,10-tetraazabicyclo[5.5.2]tetradecan-4-yl)methyl)benzyl)amino)-2-oxoethoxy)ester (36)**



**36**

2-(2-((3,5-bis((7,7'-[methyl]-1,4,7,10-tetraazabicyclo[5.5.2]tetradecan-4-yl)methyl)benzyl)amino)-2-oxoethoxy)acetic acid (**34**) (50 mg, 74.4  $\mu\text{mol}$ ) was dissolved in dry MeCN (10 ml), EDC (57 mg, 297.7  $\mu\text{mol}$ ) and NHS (34 mg, 297.7  $\mu\text{mol}$ ) were added and the mixture was stirred under argon overnight. Solvents were concentrated *in vacuo*. The crude was washed with water (3 x 1 ml) then dried to yield a yellow oil. The desired product was not isolating using this synthetic procedure. Analytical data indicates that the desired product was not obtained.

**7.2.39. Synthesis of *N*-(3,5-bis((7,7'-[methyl]-1,4,7,10-tetraazabicyclo[5.5.2]tetradecan-4-yl)methyl)benzyl)-2-(2-oxo-2-(phenethylamino)ethoxy)acetamide (37)**



**Method 1-Attempted synthesis**

2-(2-((3,5-Bis((7,7'-[methyl]-1,4,7,10-tetraazabicyclo[5.5.2]tetradecan-4-yl)methyl)benzyl)amino)-2-oxoethoxy)acetic acid (**34**) (40 mg, 59.5  $\mu$ mol) was dissolved in DMF (10 ml). DIC (9 mg, 71  $\mu$ mol) and DIPEA (9 mg, 71  $\mu$ mol) were added and the mixture was stirred at RT for 30 min. Phenylethylamine (22 mg, 178.6  $\mu$ mol) was added and the mixture was stirred at RT overnight. Solvents were removed *in vacuo*. The crude oil was re-dissolved in water (20 ml) and extracted with DCM (4 x 10 ml). The aqueous layer was concentrated and dried under high vacuum drying to yield an orange oil. The desired product was not isolated using this synthetic procedure. Analytical data indicates that the desired product was not obtained.

**General Procedure O**

Acid was dissolved in solvent, coupling reagents were added and the mixture was stirred at RT for 30 min. Amine was added and the mixture was stirred at RT overnight. Solvents were removed *in vacuo*.

### Method 2-Attempted synthesis

Amounts: 2-(2-((3,5-Bis((7,7'-[methyl]-1,4,7,10-tetraazabicyclo[5.5.2]tetradecan-4-yl)methyl)benzyl)amino)-2-oxoethoxy)acetic acid (**34**) (25 mg, 37  $\mu$ mol), MeOH:DCM (8 ml, 1:4), DCC (9 mg, 45  $\mu$ mol), phenylethylamine (5 mg, 45  $\mu$ mol). To yield an orange oil. The desired product was not isolated using this synthetic procedure. Analytical data indicates that the desired product was not obtained.

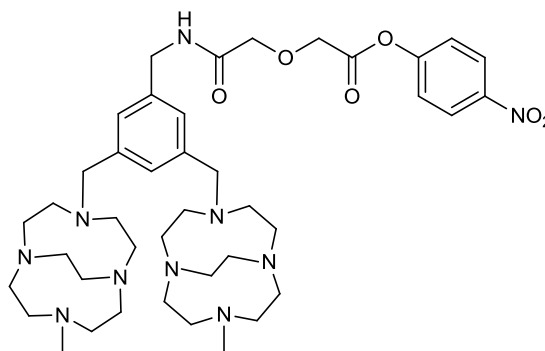
### Method 3-Attempted synthesis

Amounts: 2-(2-((3,5-Bis((7,7'-[methyl]-1,4,7,10-tetraazabicyclo[5.5.2]tetradecan-4-yl)methyl)benzyl)amino)-2-oxoethoxy)acetic acid (**34**) (63 mg, 93  $\mu$ mol), MeOH:DCM (10 ml, 1:4), DCC (23 mg, 133  $\mu$ mol), phenylethylamine (9 mg, 78  $\mu$ mol). To yield orange oil (>100%).  $^1\text{H}$  NMR (400 MHz,  $\text{CD}_3\text{OD}$ ,  $\delta$ ): 1.02-1.30 (br m, N- $\text{CH}_2$ , 20H), 1.46-1.50 (m,  $\text{CH}_3$ , 6H), 1.63-1.65 (m,  $\text{CH}_2$ -NH, 2H), 1.79-1.81 (m, N- $\text{CH}_2$ , 4H), 2.54 (br s, NH, 2H), 2.72-2.99 (br m, N- $\text{CH}_2$ , 16H), 3.21 (m, CO- $\text{CH}_2$ -O, 2H), 3.25 (s, CO- $\text{CH}_2$ -O, 2H), 3.37-3.39 (m, Ar  $\text{CH}_2$ , 2H), 3.79-3.85 (m, Ar  $\text{CH}_2$ , 4H), 4.09 (s,  $\text{CH}_2$ -NH, 2H), 7.11-7.31 (br m, 8H, Ar H).  $^{13}\text{C}$  NMR (100 MHz,  $\text{CD}_3\text{OD}$ ,  $\delta$ ): 18.67 ( $\text{CH}_3$ ), 20.09 ( $\text{CH}_3$ ), 21.33 (N- $\text{CH}_2$ ), 21.51 (N- $\text{CH}_2$ ), 21.62 (N- $\text{CH}_2$ ), 21.97 (N- $\text{CH}_2$ ), 22.15 (N- $\text{CH}_2$ ), 29.19 (N- $\text{CH}_2$ ), 29.54 (N- $\text{CH}_2$ ), 30.19 (N- $\text{CH}_2$ ), 30.65 (N- $\text{CH}_2$ ), 31.44 (N- $\text{CH}_2$ ), 45.44 ( $\text{CH}_2$ -NH), 47.71 ( $\text{CH}_2$ -NH), 48.10 (CO- $\text{CH}_2$ -O), 49.00 (CO- $\text{CH}_2$ -O), 52.40 (Ar  $\text{CH}_2$ ), 66.51 (Ar  $\text{CH}_2$ ), 122.26 (Ar CH), 122.33 (Ar CH), 123.30 (Ar CH), 124.36 (Ar C), 124.93 (Ar CH), 125.46 (Ar CH), 139.74 (Ar C), 149.99 (Ar C), 172.76 (C=O). MS: (ESI)  $m/z$  556 (100[**20** + H] $^+$ ).

#### Method 4-Preferred method

Amounts: 2-(2-((3,5-Bis((7,7'-[methyl]-1,4,7,10-tetraazabicyclo[5.5.2]tetradecan-4-yl)methyl)benzyl)amino)-2-oxoethoxy)acetic acid (**34**) (60 mg, 89.3  $\mu\text{mol}$ ), MeOH (10 ml), PyBOP (46 mg, 89.3  $\mu\text{mol}$ ), phenylethylamine (9.0 mg, 74.4  $\mu\text{mol}$ ). To yield a yellow/orange oil (>100%).  $^1\text{H}$  NMR (400 MHz,  $\text{CD}_3\text{OD}$ ,  $\delta$ ): 1.31 (m, 6H,  $\text{CH}_3$ ), 2.57 (m, N- $\text{CH}_2$ , 2H), 2.71-3.01 (br m, N- $\text{CH}_2$ , 20H), 3.09-3.11 (m, N- $\text{CH}_2$  +  $\text{CH}_2$ -NH, 24H), 3.26 (s, CO- $\text{CH}_2$ -O, 2H), 3.69 (s, CO- $\text{CH}_2$ -O, 2H), 3.86-3.89 (m,  $\text{CH}_2$ -NH, 2H), 4.19 (m, Ar  $\text{CH}_2$ , 2H), 4.42 (m, Ar  $\text{CH}_2$ , 2H), 7.21 (m, 3H, Ar H), 7.38 (m, 2H, Ar H), 7.62 (m, 3H, Ar H).  $^{13}\text{C}$  NMR (100 MHz,  $\text{CD}_3\text{OD}$ ,  $\delta$ ): 18.57 ( $\text{CH}_3$ ), 20.06 ( $\text{CH}_3$ ), 21.43 (N- $\text{CH}_2$ ), 21.45 (N- $\text{CH}_2$ ), 21.32 (N- $\text{CH}_2$ ), 21.99 (N- $\text{CH}_2$ ), 21.96 (N- $\text{CH}_2$ ), 29.05 (N- $\text{CH}_2$ ), 29.60 (N- $\text{CH}_2$ ), 30.20 (N- $\text{CH}_2$ ), 30.57 (N- $\text{CH}_2$ ), 31.32 (N- $\text{CH}_2$ ), 45.46 ( $\text{CH}_2$ -NH), 47.77 ( $\text{CH}_2$ -NH), 48.20 (CO- $\text{CH}_2$ -O), 48.89 (CO- $\text{CH}_2$ -O), 52.47 (Ar  $\text{CH}_2$ ), 66.55 (Ar  $\text{CH}_2$ ), 122.26 (Ar CH), 122.32 (Ar CH), 123.34 (Ar CH), 124.40 (Ar C), 125.03 (Ar CH), 125.44 (Ar CH), 139.74 (Ar C), 150.12 (Ar C), 172.73 (C=O). HRMS: calcd. for  $\text{C}_{43}\text{H}_{71}\text{N}_{10}\text{O}_3$ : 775.5703 found 775.5705.

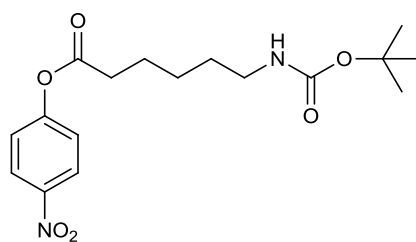
**7.2.40. Synthesis of 2-(2-((3,5-bis((7,7'-[methyl]-1,4,7,10-tetraazabicyclo[5.5.2]tetradecan-4-yl)methyl)benzyl)amino)-2-oxoethoxy)nitrophenyl ester (38)**



**38**

2-(2-((3,5-Bis((7,7'-[methyl]-1,4,7,10-tetraazabicyclo[5.5.2]tetradecan-4-yl)methyl)benzyl)amino)-2-oxoethoxy)acetic acid (**34**) (100 mg, 0.149 mmol) and DCC (31 mg, 0.149 mmol) were dissolved in a mixture of MeOH/DCM (30 ml, 1:5) and stirred for 20 min. *p*-Nitrophenol (31 mg, 0.223 mmol) in DCM (5 ml) was added and the mixture was stirred for 1 hour. Solids were filtered. Aqueous KOH (pH 14, 25 ml) was added to the filtrate which was then extracted with DCM (5 x 50 ml). The organic extracts were combined, dried (MgSO<sub>4</sub>), filtered and solvents removed *in vacuo* to yield a yellow oily solid (90 mg, 76%). <sup>1</sup>H NMR (400 MHz, CDCl<sub>3</sub>, δ): 1.11-1.37 (br m, N-CH<sub>2</sub>, 16H), 1.66-1.91 (br m, N-CH<sub>2</sub>, 14H), 2.31-3.16 (br m, N-CH<sub>2</sub> + Ar CH<sub>2</sub>, 20H), 3.32-3.48 (m, CO-CH<sub>2</sub>-O, 4H), 3.65-3.74 (m, CH<sub>2</sub>-NH, 1H), 3.90 (s, CH<sub>2</sub>-NH, 1H), 6.43 (d, *J* = 6.5 Hz, Ar H, 2H), 7.22 (br s, Ar H, 3H), 7.96 (d, *J* = 6.5 Hz, Ar H, 2H). <sup>13</sup>C NMR (100 MHz, CDCl<sub>3</sub>, δ): 25.69 (CH<sub>3</sub>), 26.04 (N-CH<sub>2</sub>), 26.16 (N-CH<sub>2</sub>), 26.45 (N-CH<sub>2</sub>), 26.72 (N-CH<sub>2</sub>), 29.90 (N-CH<sub>2</sub>), 33.91 (N-CH<sub>2</sub>), 34.04 (N-CH<sub>2</sub>), 34.72 (N-CH<sub>2</sub>), 35.17 (N-CH<sub>2</sub>), 51.55 (CH<sub>2</sub>-NH), 52.37 (Ar CH<sub>2</sub>), 71.31 (CO-CH<sub>2</sub>-O), 117.80 (Ar CH), 124.95 (Ar CH), 143.70 (Ar CH), 152.18 (Ar CH), 153.15 (Ar C), 156.27 (Ar C), 157.96 (Ar C), 166.00 (Ar C), 167.32 (C=O), 174.56 (C=O).

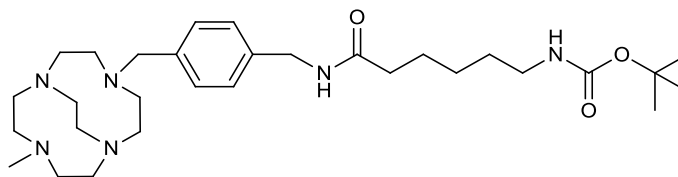
### 7.2.41. Synthesis of 4-nitrophenyl-6-((*tert*-butoxycarbonyl)amino)hexanoate (39)



39

6-((*tert*-Butoxycarbonyl)amino)hexanoic acid (**29**) (1.00 g, 4.3 mmol) and *p*-nitrophenol (0.75 g, 6.5 mmol) were dissolved in DCM (50 ml). DCC (0.89 g, 4.3 mmol) in DCM (25 ml) was added and the mixture was stirred for 1 hour at RT. The mixture was filtered and the solvent removed *in vacuo*. The crude solid was purified *via* flash chromatography (silica, eluent MeOH /DCM, 1:49) to yield a cream solid (1.93 g, 84%).  $^1\text{H}$  NMR (400 MHz,  $\text{CDCl}_3$ ,  $\delta$ ): 1.05 (m,  $\text{CH}_2$ , 2H), 1.35-1.44 (s,  $\text{C}(\text{CH}_3)_3$ , 9H), 1.70 (m,  $\text{CH}_2$ , 2H), 2.54 (t,  $J = 7.3$  Hz,  $\text{CH}_2$ , 2H), 3.08 (m,  $\text{CH}_2$ , 4H), 4.58 (br s, NH, 1H), 7.20 (d,  $J = 9.2$  Hz, Ar H, 2H), 8.20 (d,  $J = 9.2$  Hz, Ar H, 2H).  $^{13}\text{C}$  NMR (100 MHz,  $\text{CDCl}_3$ ,  $\delta$ ): 24.81 ( $\text{CH}_2$ ), 25.46 ( $\text{CH}_2$ ), 28.35 ( $\text{C}(\text{CH}_3)_3$ ), 29.68 ( $\text{CH}_2$ ), 33.76 ( $\text{CH}_2$ ), 40.25 ( $\text{CH}_2$ ), 49.17 ( $\text{C}(\text{CH}_3)_3$ ), 115.63 (Ar C), 122.68 (Ar CH), 125.13 (Ar CH), 126.04 (Ar C), 155.36 (C=O), 171.02 (C=O). HRMS ( $m/z$ ):  $[\text{M} + \text{H}]^+$  calcd for  $\text{C}_{17}\text{H}_{25}\text{N}_2\text{O}_6$ , 353.1711; found, 353.1707. Anal. calcd for  $\text{C}_{17}\text{H}_{24}\text{N}_2\text{O}_6$ : C, 57.94; H, 6.86; N, 7.95. Found: C, 57.68; H, 7.05; N, 7.69.  $R_f = 0.36$  (silica, MeOH:DCM, 1:49).

**7.2.42. Synthesis of *tert*-butyl-(6-((1,4-((7-[methyl]-1,4,7,10-tetraazabicyclo[5.5.2]tetradecan-4-yl)methyl)benzyl)amino)-6-oxohexyl)carbamate (40)**

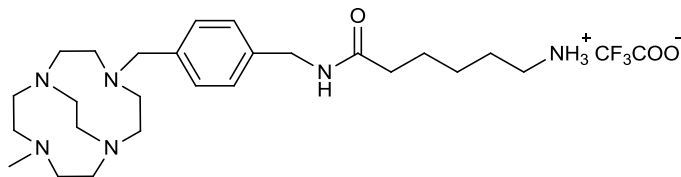


**40**

**General procedure L was followed**

Amounts: 1-[4-Aminomethylbenzyl]-7-[methyl]-1,4,7,10-tetraazabicyclo[5.5.2] dodecane (**15**) (100 mg, 0.30 mmol), 4-nitrophenyl-6-((*tert*-butoxycarbonyl) amino)hexanoate (**39**) (106 mg, 0.15 mmol), water:dioxane (10 ml, 1:1), chloroform (3 x 10 ml then 3 x 10 ml). To yield a yellow oil (145 mg, 58%).  $^1\text{H}$  NMR (400 MHz,  $\text{CDCl}_3$ ,  $\delta$ ): 1.25 (m,  $\text{CH}_3$ , 3H), 1.36 (s,  $\text{C}(\text{CH}_3)_3$ , 9H), 1.56 (m,  $\text{CH}_2$ , 2H), 2.21 (m,  $\text{CH}_2$ , 2H), 2.41 (m,  $\text{CH}_2$ , 2H), 2.52-2.71 (br m, N- $\text{CH}_2$ , 8H), 2.86-3.00 (br m, N- $\text{CH}_2$ , 8H), 3.24 (m,  $\text{CH}_2$ , 2H), 3.59-3.82 (m, N- $\text{CH}_2$  +  $\text{CH}_2$ , 6H), 4.34 (s,  $\text{CH}_2$ -NH, 2H), 4.75 (s, Ar  $\text{CH}_2$ , 2H), 7.21-7.22 (m, Ar H, 4H), 7.67 (br s, NH, 1H), 12.00 (br s, NH, 1H).  $^{13}\text{C}$  NMR (100 MHz,  $\text{CDCl}_3$ ,  $\delta$ ): 25.30 ( $\text{CH}_3$ ), 26.33 ( $\text{CH}_2$ ), 28.39 ( $\text{C}(\text{CH}_3)_3$ ), 29.66 ( $\text{CH}_2$ ), 34.01 ( $\text{CH}_2$ ), 36.72 (N- $\text{CH}_2$ ), 40.04 (N- $\text{CH}_2$ ), 44.00 (N- $\text{CH}_2$ ), 47.53 (N- $\text{CH}_2$ ), 52.53 (N- $\text{CH}_2$ ), 52.97 (N- $\text{CH}_2$ ), 53.37 ( $\text{CH}_2$ -NH), 55.54 ( $\text{C}=\text{O}$ - $\text{CH}_2$ ), 56.09 ( $\text{C}(\text{CH}_3)_3$ ), 61.14 (Ar  $\text{CH}_2$ -NH), 78.83 (Ar  $\text{CH}_2$ ), 128.09 (Ar C), 128.32 (Ar CH), 128.76 (Ar CH), 129.17 (Ar C), 156.64 ( $\text{C}=\text{O}$ ). HRMS ( $m/z$ ):  $[\text{M} + \text{H}]^+$  calcd for  $\text{C}_{30}\text{H}_{53}\text{N}_6\text{O}_3$ , 545.4167; found, 545.4174.

**7.2.43. Synthesis of 6-amino-*N*-(6-((1,4-((7-[methyl]-1,4,7,10-tetraazabicyclo[5.5.2]tetradecan-4-yl)methyl)benzyl))hexanamide (41)**

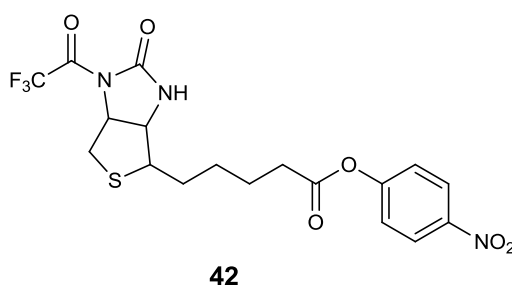


**41**

**General procedure M was followed**

Amounts: *tert*-butyl-(6-((1,4-((7-[methyl]-1,4,7,10-tetraazabicyclo[5.5.2]tetradecan-4-yl)methyl)benzyl)amino)-6-oxohexyl)carbamate (**40**) (100 mg, 0.18 mmol), TFA (5 ml), diethyl ether (2 x 10 ml). To yield an orange oil (63 mg, 63%). <sup>1</sup>H NMR (400 MHz, CDCl<sub>3</sub>, δ): 1.26 (m, CH<sub>3</sub>, 3H), 1.51 (m, CH<sub>2</sub>, 6H), 2.12 (m, CH<sub>2</sub>, 2H), 2.64 (s, CH<sub>2</sub>, 2H), 2.76-2.98 (br m, N-CH<sub>2</sub>, 20H), 3.16 (s, CH<sub>2</sub>-NH, 2H), 3.81-3.89 (m, Ar CH<sub>2</sub>, 2H), 4.21 (br s, NH<sub>2</sub>, 2H), 7.16-7.32 (m, Ar H, 4H). <sup>13</sup>C NMR (100 MHz, CDCl<sub>3</sub>, δ): 27.89 (CH<sub>3</sub>), 28.91 (CH<sub>2</sub>), 29.59 (CH<sub>2</sub>), 30.82 (N-CH<sub>2</sub>), 39.22 (N-CH<sub>2</sub>), 43.14 (N-CH<sub>2</sub>), 46.39 (N-CH<sub>2</sub>), 51.02 (N-CH<sub>2</sub>), 55.49 (N-CH<sub>2</sub>), 55.76 (N-CH<sub>2</sub>), 55.95 (N-CH<sub>2</sub>), 58.18 (CH<sub>2</sub>-NH<sub>2</sub>), 59.14 (CO-CH<sub>2</sub>), 59.49 (CH<sub>2</sub>-NH), 60.25 (Ar CH<sub>2</sub>), 119.21 (Ar CH), 129.69 (Ar CH), 131.41 (Ar C), 133.36 (Ar C), 167.86 (C=O). HRMS (*m/z*): [M + H]<sup>+</sup> calcd for C<sub>25</sub>H<sub>45</sub>N<sub>6</sub>O, 445.3647; found, 445.3649.

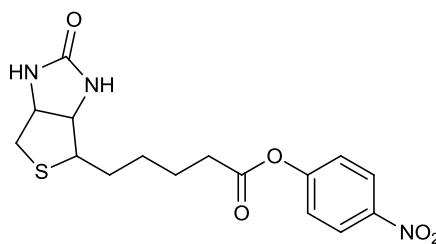
#### 7.2.44. Synthesis of *N*-trifluoroacetyl-biotin-*p*-nitrophenyl ester (42)



Following the literature method outlined by Bodanszky *et al.*<sup>177</sup>

Biotin (2.44 g, 10 mmol) was suspended in dry pyridine (60 ml), *p*-nitrophenyl (1.40 g, 10 mmol) and *p*-nitrophenyl trifluoroacetate (10.00 g, 42.5 mmol) were added. The mixture was stirred and heated to 50°C for 1 hour. The clear solution was allowed to cool to RT and the solvent was removed *in vacuo*. The resulting orange oil was dried over P<sub>2</sub>O<sub>5</sub> for 2 days until a semi-solid formed. This was triturated with ether (20 ml), filtered and washed with ether (10 ml), water (10 ml) and once again with ether (20 ml). The resulting white solid was dried under high vacuum to yield a white, powdery solid (4.05 g, 88%). <sup>1</sup>H NMR (400 MHz, CDCl<sub>3</sub>, δ): 1.46-1.62 (m, CH<sub>2</sub>, 3H), 1.71-1.72 (m, CH<sub>2</sub>, 3H), 2.67 (t, *J* = 14.7 Hz, CH<sub>2</sub>, 2H), 2.94 (m, S-CH<sub>2</sub>, 1H), 3.05 (m, S-CH<sub>2</sub>, 1H), 3.31 (m, S-CH, 1H), 4.30 (m, CH, 1H), 4.92 (t, *J* = 12.8 Hz, CH, 1H), 7.45 (d, *J* = 9.1 Hz, Ar H, 2H), 8.31 (d, *J* = 9.1 Hz, Ar H, 2H), 8.44 (s, NH, 1H). <sup>13</sup>C NMR (100 MHz, CDCl<sub>3</sub>, δ): 24.02 (CH<sub>2</sub>), 27.82 (CH<sub>2</sub>), 27.94 (CH<sub>2</sub>), 33.21 (CH<sub>2</sub>), 36.25 (S-CH<sub>2</sub>), 54.41 (S-CH), 58.30 (CH), 62.09 (CH), 115.76 (CF<sub>3</sub>), 125.24 (Ar CH), 125.71 (Ar CH), 126.14 (Ar C), 144.97 (Ar C), 152.76 (CF<sub>3</sub>-C=O), 155.37 (NC=O), 171.11 (OC=O). MS (*m/z*): 366 [M - CF<sub>3</sub>CO<sup>-</sup> + H]<sup>+</sup>. Anal. calcd for C<sub>18</sub>H<sub>18</sub>F<sub>3</sub>N<sub>3</sub>O<sub>6</sub>S: C, 46.85; H, 3.93; N, 9.11; Found: C, 46.58; H, 3.64; N, 8.86.

### 7.2.45. Synthesis of biotin-*p*-nitrophenyl ester (**43**)

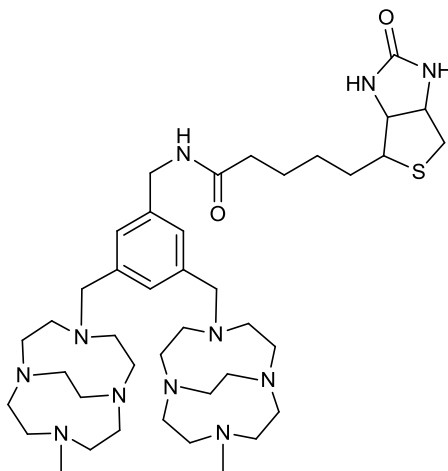


**43**

Following the literature method outlined by Bodanszky *et al.*<sup>177</sup>

*N*-trifluoroacetyl-biotin-*p*-nitrophenyl ester (**42**) (3.00 g, 6.5 mmol) was suspended in 95% ethanol (30 ml) and heated to the boil. Once all the material had dissolved the solution was refluxed for a further 5 min. The solution was cooled in an ice-water bath and the resulting crystals were collected, washed with ice-cold ethanol (95%) and dried over P<sub>2</sub>O<sub>5</sub> to yield a white solid (2.05 g, 86%). <sup>1</sup>H NMR (400 MHz, DMSO, δ): 1.43-1.58 (m, CH<sub>2</sub>, 3H), 1.65-1.71 (m, CH<sub>2</sub>, 3H), 2.66 (m, CH<sub>2</sub>, 2H), 2.84 (m, S-CH<sub>2</sub>, 1H), 3.15 (m, S-CH<sub>2</sub>, 1H), 3.46 (m, S-CH, 1H), 4.17 (m, CH, 1H), 4.33 (m, CH, 1H), 6.40 (br s, NH, 1H), 6.50 (br s, NH, 1H), 7.45 (d, *J* = 9.1 Hz, Ar H, 2H), 8.31 (d, *J* = 9.1 Hz, Ar H, 2H). <sup>13</sup>C NMR (100 MHz, DMSO, δ): 24.79 (CH<sub>2</sub>), 28.48 (CH<sub>2</sub>), 28.59 (CH<sub>2</sub>), 33.89 (CH<sub>2</sub>), 40.48 (S-CH<sub>2</sub>), 55.90 (S-CH), 59.84 (CH), 61.65 (CH), 123.80 (Ar CH), 125.86 (Ar CH), 145.59 (Ar C), 156.01 (Ar C), 163.36 (NHC=O), 171.78 (OC=O). HRMS (*m/z*): [M + H]<sup>+</sup> calcd for C<sub>16</sub>H<sub>20</sub>N<sub>3</sub>SO<sub>5</sub>, 366.1122; found, 366.1118. Anal. calcd for C<sub>16</sub>H<sub>19</sub>N<sub>3</sub>O<sub>5</sub>·0.5H<sub>2</sub>O: C, 51.33; H, 5.38; N, 11.22; Found: C, 51.16; H, 5.19; N, 11.15.

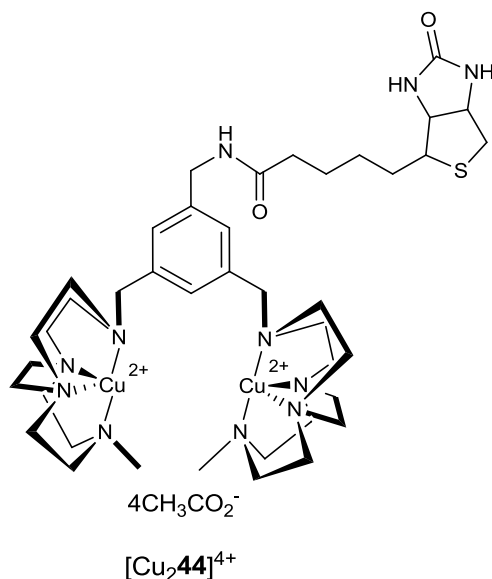
**7.2.46. Synthesis of 1,1'-[3,5-dimethylamino-(biotin-*p*-nitrophenyl ester)benzyl]-7,7'-[methyl]-bis(1,4,7,10-tetraazabicyclo[5.5.2]dodecane) (**44**)**



**44**

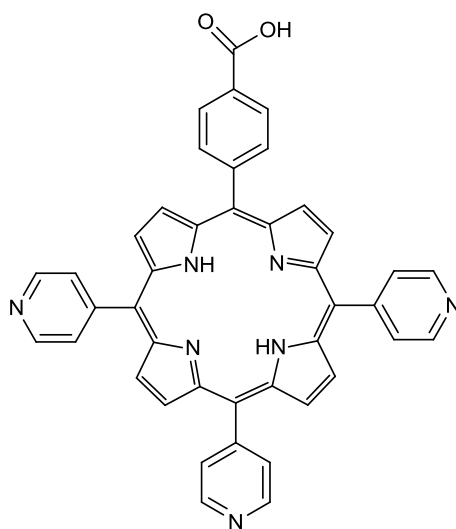
1,1'-[3,5-dimethylaminobenzyl]-7,7'-[methyl]-bis(1,4,7,10-tetraazabicyclo[5.5.2]dodecane) (**20**) (330 mg, 0.59 mmol) was dissolved in water (10 ml) and a solution of biotin-*p*-nitrophenyl ester (**43**) (217 mg, 0.59 mmol) in dioxane (10 ml) was added. The mixture was allowed to stir at 40°C for 4.5 hours, then extracted with DCM (4 x 20 ml). The aqueous layer was made strongly basic (pH 14, KOH), then extracted with DCM (4 x 20 ml). The organic extractions were dried (MgSO<sub>4</sub>), filtered and solvents removed *in vacuo* to yield a yellow, oily solid (330 mg, 71%). <sup>1</sup>H NMR (400 MHz, CDCl<sub>3</sub>, δ): 1.39-1.70 (m, CH<sub>2</sub>, 6H), 2.20-3.07 (br m, CH<sub>3</sub> + CH<sub>2</sub> + N-CH<sub>2</sub> + S-CH<sub>2</sub> + NH, 51H), 3.29 (s, S-CH + CH, 2H), 3.61 (m, CH, 1H), 3.89 (s, CH<sub>2</sub>-NH<sub>2</sub>, 2H), 4.28 (s, Ar CH<sub>2</sub>, 2H), 4.47 (s, Ar CH<sub>2</sub>, 2H), 4.48 (br s, NH, 2H), 7.16-7.19 (m, Ar H, 3H). <sup>13</sup>C NMR (100 MHz, CDCl<sub>3</sub>, δ): 25.35 (CH<sub>2</sub>), 7.95 (CH<sub>2</sub>), 35.57 (CH<sub>2</sub>), 40.17 (S-CH<sub>2</sub>), 43.33 (CH<sub>3</sub>), 44.17 (N-CH<sub>2</sub>), 48.04 (N-CH<sub>2</sub>), 49.62 (N-CH<sub>2</sub>), 49.88 (N-CH<sub>2</sub>), 51.32 (N-CH<sub>2</sub>), 52.85 (Ar CH<sub>2</sub>), 53.72 (CH<sub>2</sub>NH<sub>2</sub>), 55.34 (S-CH), 59.88 (CH), 61.65 (CH), 125.93 (Ar CH), 127.79 (Ar CH), 140.55 (Ar C), 142.95 (Ar C), 164.22 (C=O), 174.07 (C=O). HRMS (*m/z*): [M + H]<sup>+</sup> calcd for C<sub>41</sub>H<sub>72</sub>N<sub>11</sub>SO<sub>2</sub>, 782.5583; found, 782.5586.

**7.2.47. Synthesis of 1,1'-[3,5-dimethylamino-(biotin-*p*-nitrophenyl ester)benzyl]-7,7'-[methyl]-bis(1,4,7,10-tetraazabicyclo[5.5.2]dodecane) copper(II) acetate [Cu<sub>2</sub>44]<sup>4+</sup>**



1,1'-[3,5-dimethylamino-(biotin-*p*-nitrophenylester)benzyl]-7,7'-[methyl]-bis(1,4,7,10-tetraazabicyclo[5.5.2]dodecane) (**44**) (300 mg, 0.38 mmol) was dissolved in dry MeOH (15 ml). A methanolic (10 ml) solution of copper(II) acetate monohydrate (168 mg, 0.38 mmol) was added dropwise and the mixture was refluxed for 2 hours then allowed to stir at RT overnight. Solvent was concentrated ~5 ml and the crude solution was purified *via* size exclusion chromatography (sephadex LH20) to yield a blue solid (411 mg, 94%). HRMS (*m/z*): [M – 2CH<sub>3</sub>CO<sub>2</sub><sup>-</sup>]<sup>2+</sup> calcd for C<sub>45</sub>H<sub>77</sub>Cu<sub>2</sub>N<sub>11</sub>SO<sub>6</sub>, 512.7171; found, 512.7180. Anal. calcd for C<sub>49</sub>H<sub>83</sub>Cu<sub>2</sub>N<sub>11</sub>O<sub>10</sub>S·3H<sub>2</sub>O·CH<sub>3</sub>OH: C, 48.76; H, 7.61; N, 12.51; Found: C, 49.01; H, 8.07; N, 12.56. UV-vis (CH<sub>3</sub>OH) λ<sub>max</sub>, nm (ε): 683 (552 M<sup>-1</sup> cm<sup>-1</sup>).

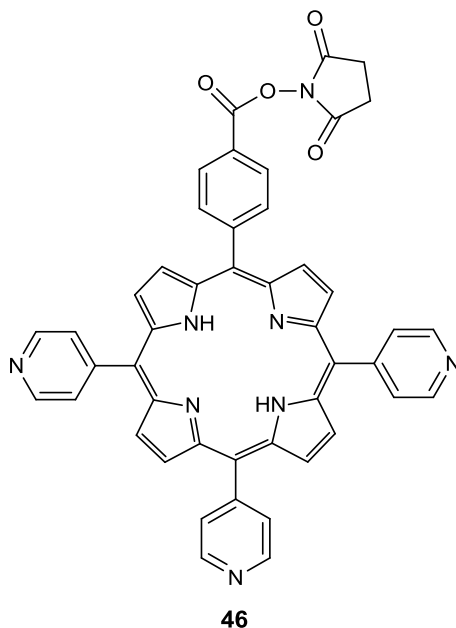
### 7.2.48. Synthesis of 5-(4-carboxyphenyl)-10,15,20-tris-(4-pyridyl) porphyrin (45)



**45**

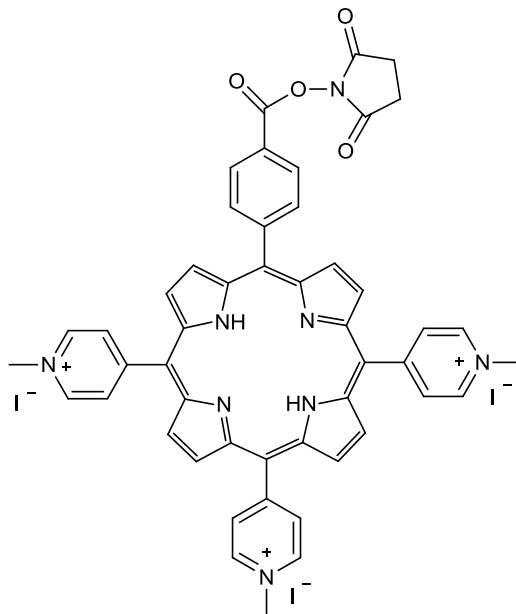
A mixture of 4-formylbenzoic acid (2.54 g, 17.0 mmol) and 4-pyridine carboxaldehyde (4 ml, 43.0 mmol) in propionic acid (150 ml) were heated to reflux with stirring. To this mixture, pyrrole (4 ml, 58.0 mmol) was added dropwise, and the reaction mixture stirred for 1 hour under reflux. Solvents were removed *in vacuo*, and the residue purified using flash chromatography using a gradient (eluent, MeOH:DCM, 8-30%). The product was precipitated from MeOH over DCM to yield a purple solid (110 mg, 1%).  $^1\text{H}$  NMR (400 MHz,  $\text{CDCl}_3$ ,  $\delta$ ): -2.04 (s, internal NH, 2H), 8.05 (m, 5-o-Py H, 8H), 8.10 (d,  $J = 8.4$  Hz, 5-m-Ph H, 2H), 8.28 (d,  $J = 8.4$  Hz, 5-o-Ph H, 2H), 8.68 (br s,  $\beta\text{H}$ , 8H), 8.80 (m, 5-m-Py H, 6H). HRMS ( $m/z$ ):  $[\text{M} + \text{H}]^+$  calcd for  $\text{C}_{42}\text{H}_{28}\text{N}_7\text{O}_2$ , 662.2297; found, 662.2299. UV-vis ( $\text{CH}_3\text{OH}$ )  $\lambda_{\text{max}}$ , nm ( $\log \epsilon$ ): 412 (5.0), 504, 540, 584, 639.  $R_f = 0.81$  (silica, MeOH:DCM, 1:10).

**7.2.49. Synthesis of 5-[4-(succinimide-*N*-oxycarbonyl)phenyl]-10,15,20-tris-(4-pyridyl) porphyrin (46)**



Thionyl chloride (0.22 ml, 3.75 mmol) was slowly added to a stirred mixture of 5-(4-carboxyphenyl)-10,15,20-tri-(4-pyridyl)porphyrin (**45**) (110 mg, 0.17 mmol) in dry pyridine (10 ml). The mixture was stirred at 50°C for 30 min and protected from light and moisture. *N*-Hydroxysuccinimide (430 mg, 3.75 mmol) was added, and the mixture stirred under these conditions for a further 3 hours. The solvent was removed *in vacuo*, and the residue dissolved in DCM and washed with a saturated solution of sodium carbonate in water. The organic layer was dried (Na<sub>2</sub>SO<sub>4</sub>), and solvent removed *in vacuo*. The product was crystallised in light petroleum over chloroform to yield a purple solid (115 mg, 92%). <sup>1</sup>H NMR (400 MHz, CDCl<sub>3</sub>, δ): -2.08 (s, internal NH, 2H), 3.53 (br s, CH<sub>2</sub>, 4H), 8.24 (d, *J* = 6.5 Hz, 5-*o*-Py H, 6H), 8.40 (d, *J* = 5.4 Hz, 5-*m*-Ph H, 2H), 8.59 (d, *J* = 8.4 Hz, 5-*o*-Ph H, 2H), 8.89 (br s, βH, 8H), 9.04 (d, *J* = 5.9 Hz, 5-*m*-Py H, 6H). HRMS (*m/z*): [M + H]<sup>+</sup> calcd for C<sub>46</sub>H<sub>31</sub>N<sub>8</sub>O<sub>4</sub>, 759.2453; found, 759.2463. UV-vis (CH<sub>3</sub>OH) λ<sub>max</sub>, nm (log ε): 413 (5.2), 509, 541, 585, 642. R<sub>f</sub> = 0.82 (silica, MeOH:DCM, 1:10).

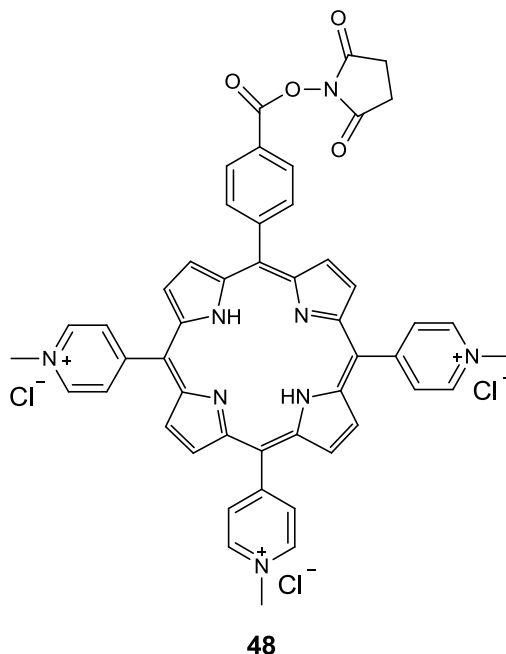
**7.2.50. Synthesis of 5-[4-(succinimide-*N*-oxycarbonyl)phenyl]-10,15,20-tris-(4-*N*-methyl pyridinium)porphyrin triiodide (47)**



**47**

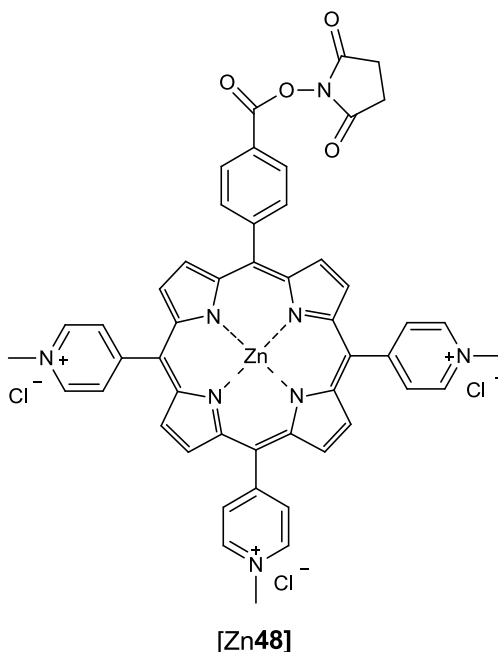
Iodomethane (1.92 ml, 30.88 mmol) was added to a stirred solution of 5-[4-(succinimide-*N*-oxycarbonyl)phenyl]-10,15,20-tri-(4-pyridyl)porphyrin (**46**) (100 mg, 0.13 mmol) in dry DMF (5 ml), and the mixture was stirred overnight at 40°C, protected from light and moisture. The product was then precipitated in ether in order to remove any residual solvent and iodomethane. The product was filtered, dissolved in a mixture of acetone and water (50:50) and the solvents removed *in vacuo*. The product was precipitated in acetone over water to yield a purple solid (101 mg, 74%). <sup>1</sup>H NMR (400 MHz, DMSO,  $\delta$ ): -2.10 (s, internal NH, 2H), 2.49 (s, CH<sub>2</sub>, 4H), 4.71 (s, CH<sub>3</sub>, 9H), 8.50 (d,  $J = 8.3$  Hz, 5-*m*-Ph H, 2H), 8.59 (d,  $J = 8.3$  Hz, 5-*o*-Ph H, 2H), 8.99 (m, 5-*o*-Py H, 6H), 9.09 (s,  $\beta$ H, 4H), 9.18 (s,  $\beta$ H, 4H), 9.47 (d,  $J = 5.7$  Hz, 5-*m*-Py H, 6H). HRMS ( $m/z$ ): [M - 3I<sup>-</sup> + CH<sub>3</sub>OH]<sup>3+</sup> calcd for C<sub>50</sub>H<sub>43</sub>N<sub>8</sub>O<sub>5</sub>, 278.4448; found, 278.4447. UV-vis (H<sub>2</sub>O)  $\lambda_{\max}$ , nm (log  $\epsilon$ ): 420 (5.2), 517, 554, 582, 636. R<sub>f</sub> = 0.29 (silica, saturated potassium nitrate:H<sub>2</sub>O:MeCN, 1:1:8).

**7.2.51. Synthesis of 5-[4-(succinimide-*N*-oxycarbonyl)phenyl]-10,15,20-tris-(4-*N*-methyl pyridinium)porphyrin trichloride (**48**)**



Amberlite IRA 400 ( $\text{Cl}^-$  form) (2.86 g) was added to a stirred solution of 5-[4-(succinimide-*N*-oxycarbonyl)phenyl]-10,15,20-tris-(4-*N*-methylpyridiniumyl) porphyrin triiodide (**47**) (90 mg, 0.08 mmol) in dry MeOH (114 ml). The mixture was stirred for 1 hour and protected from light and moisture. The amberlite IRA 400 ( $\text{Cl}^-$  form) was then separated from the mixture by filtration, and the residue concentrated *in vacuo*. The product was precipitated with acetone to yield a brown/purple solid (66 mg, 96%).  $^1\text{H}$  NMR (400 MHz, DMSO,  $\delta$ ): -2.07 (s, internal NH, 2H), 1.82 (s,  $\text{CH}_2$ , 4H), 3.74 (s,  $\text{CH}_3$ , 9H), 6.74 (d,  $J = 8.3$  Hz, 5-*m*-Ph H, 2H), 7.04 (d,  $J = 8.3$  Hz, 5-*o*-Ph H, 2H), 7.63 (m, 5-*o*-Py H, 6H), 8.60 (s,  $\beta\text{H}$ , 4H), 8.68 (s,  $\beta\text{H}$ , 4H), 9.17 (d,  $J = 5.7$  Hz, 5-*m*-Py H, 6H). HRMS ( $m/z$ ):  $[\text{M} - 3\text{Cl}]^{3+}$  calcd for  $\text{C}_{45}\text{H}_{35}\text{N}_7\text{O}_2$ , 352.6423; found, 352.6421. UV-vis ( $\text{H}_2\text{O}$ )  $\lambda_{\text{max}}$ , nm (log  $\epsilon$ ): 420 (5.4), 517, 554, 581, 636.  $R_f = 0.25$  (silica, saturated potassium nitrate: $\text{H}_2\text{O}$ :MeCN, 1:1:8).

### 7.2.52. Synthesis of zinc-5-[4-(succinimide-*N*-oxycarbonyl)phenyl]-10,15,20-tris-(4-*N*-methylpyridinium)porphyrin trichloride [Zn48]

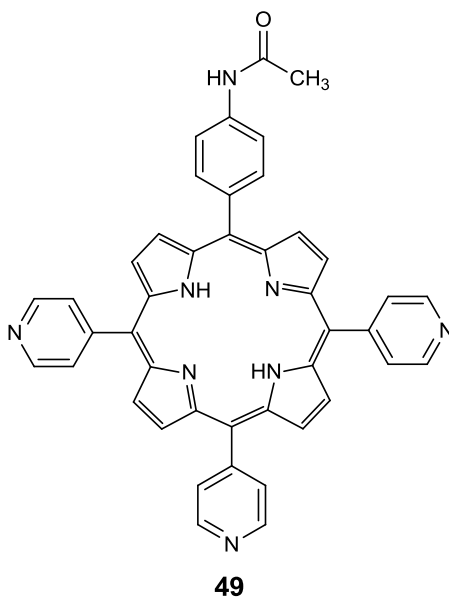


#### General procedure P

Porphyrin was dissolved in MeOH. Zinc(II) acetate in MeOH was added and the mixture was stirred at RT for 1 hour. Aqueous ammonium hexafluorophosphate was added until no more precipitation occurred and the resulting solid was collected. This crude solid was re-dissolved in acetone and an aqueous solution of tetrabutylammonium chloride was added until no more precipitation occurred and the resulting solid was collected and dried to yield green/purple solid.

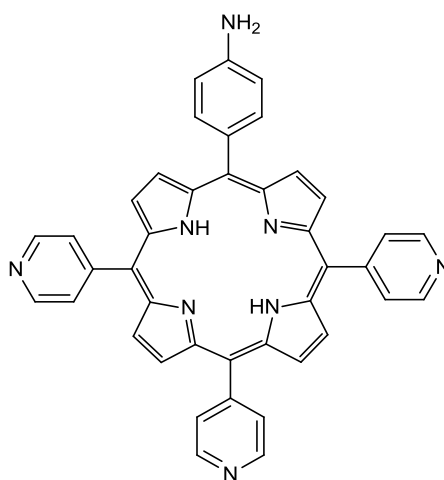
Amounts: 5-[4-(succinimide-*N*-oxycarbonyl)phenyl]-10,15,20-tris-(4-*N*-methylpyridinium) porphyrin trichloride (**48**) (50 mg, 55.1  $\mu\text{mol}$ ), MeOH (10 ml), zinc(II) acetate (50 mg, 274.8  $\mu\text{mol}$ ), MeOH (10 ml). To yield a green/purple solid (44 mg, 82%).  $^1\text{H}$  NMR (400 MHz,  $\text{CD}_3\text{OD}$ ,  $\delta$ ): 1.82 (s,  $\text{CH}_2$ , 4H), 3.71 (s,  $\text{CH}_3$ , 9H), 6.84 (d,  $J = 8.3$  Hz, 5-*m*-Ph H, 2H), 7.34 (d,  $J = 8.3$  Hz, 5-*o*-Ph H, 2H), 7.62 (m, 5-*o*-Py H, 6H), 8.60 (s,  $\beta\text{H}$ , 4H), 8.68 (s,  $\beta\text{H}$ , 4H), 9.20 (d,  $J = 5.7$  Hz, 5-*m*-Py H, 6H). HRMS ( $m/z$ ):  $[\text{M} - 3\text{Cl}]^{3+}$  calcd for  $\text{C}_{49}\text{H}_{37}\text{N}_8\text{O}_4\text{Zn}$ , 288.4097; found, 288.4094. UV-vis ( $\text{H}_2\text{O}$ )  $\lambda_{\text{max}}$ , nm (log  $\epsilon$ ): 443 (4.8), 565, 612.

### 7.2.53. Synthesis of 5-(4-acetamidophenyl)-10,15,20-tris-(4-pyridyl)porphyrin (49)



4-Acetamidobenzaldehyde (3.26 g, 0.02 mol) and 4-pyridinecarboxaldehyde (5.7 ml, 0.06 mol) were dissolved in propionic acid (300 ml) and the solution heated to the point of reflux. Pyrrole (5.4 ml 0.08 mol) was added dropwise to the solution and the reaction mixture heated under reflux for 40 min. The cooled reaction mixture was then concentrated *in vacuo* to yield a dark purple solid. The crude solid was purified by column chromatography using 5% MeOH/DCM as the eluant. Fractions were concentrated *in vacuo* to yield purple solid (280 mg, 2%).  $^1\text{H}$  NMR (400 MHz,  $\text{CDCl}_3$ ,  $\delta$ ): -2.08 (s, internal NH, 2H), 1.76 (br s, NH, 1H), 2.39 (s,  $\text{COCH}_3$ , 3H), 7.95 (d,  $J = 7.7$  Hz, o-Ph-H, 2H), 8.14 (d,  $J = 5.5$  Hz, 5-o-Py-H + m-Ph-H, 8H), 8.81-8.85 (m,  $\beta$ -H, 6H), 8.94 (s,  $\beta$ -H, 2H), 9.03 (s, 5-m-Py-H, 6H). HRMS ( $m/z$ ):  $[\text{M} + \text{H}]^+$  calcd for  $\text{C}_{43}\text{H}_{31}\text{N}_8\text{O}$ , 675.2605; found, 675.2615. UV-vis ( $\text{H}_2\text{O}$ )  $\lambda_{\text{max}}$ , nm (log  $\epsilon$ ): 414 (4.9), 511, 547, 587, 622.  $R_f = 0.30$  (silica, MeOH:DCM, 2:23).

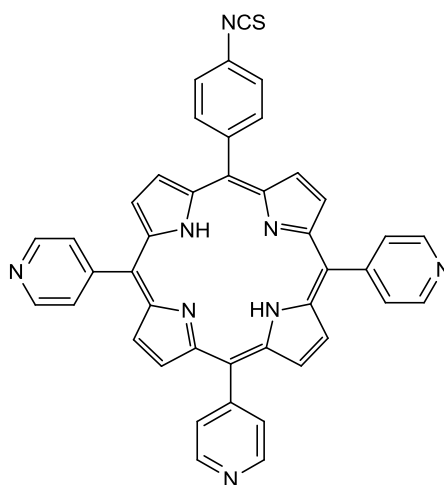
#### 7.2.54. Synthesis of 5-(4-aminophenyl)-10,15,20-tris-(4-pyridyl)porphyrin (50)



50

5-(4-Acetamidophenyl)-10,15,20-tris-(4-pyridyl)porphyrin (**49**) (260 mg, 0.39 mmol) was dissolved in 18% HCl (25 ml) and the solution was heated under reflux for 2 hours. The hot reaction mixture was concentrated *in vacuo* to yield a crude green solid. The solid was redissolved in a mixture of DCM / triethylamine (9:1, 72:8 ml) and stirred for 10 min. The solution was washed with water (3 x 100 ml) then brine (100ml). The organic layers were combined, dried (Na<sub>2</sub>SO<sub>4</sub>), filtered and concentrated *in vacuo* to yield a crude purple solid. The crude was purified *via* column chromatography (eluent, MeOH:DCM, 3:37). Fractions were combined and concentrated *in vacuo* to yield a purple solid (235 mg, 96%). <sup>1</sup>H NMR (400 MHz, CDCl<sub>3</sub>, δ): -2.10 (s, internal NH, 2H), 3.15-3.39 (br, s, NH, 2H), 7.99 (d, *J* = 10.8 Hz, 5-m-ArH, 2H), 8.21 (d, *J* = 5.9 Hz, 5-o-ArH + 10+15+20-o-PryH, 8H), 8.84 (br, s, βH, 8H), 9.01 (s, 10+15+20-m-PryH, 6H). HRMS (*m/z*): [M + H]<sup>+</sup> calcd for C<sub>41</sub>H<sub>29</sub>N<sub>8</sub>, 633.2501; found, 633.2510. UV-vis (CH<sub>3</sub>OH) λ<sub>max</sub>, nm (log ε): 414 (5.0), 511, 547, 587, 622. R<sub>f</sub> = 0.48 (silica, MeOH:DCM, 3:37).

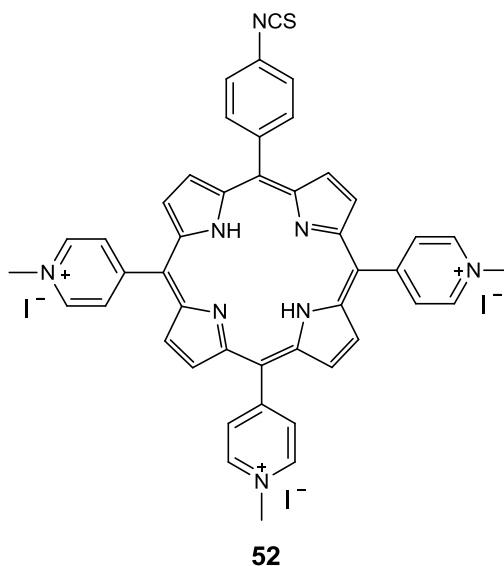
### 7.2.55. Synthesis of 5-(4-isothiocyanatophenyl)-10,15,20-tris-(4-pyridyl)porphyrin (51)



**51**

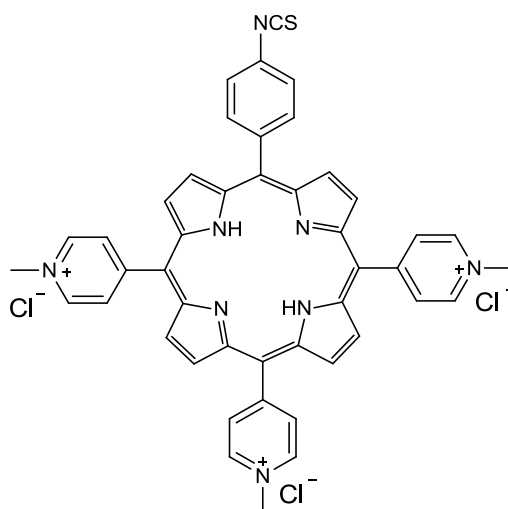
1,1'-Thiocarbonyldi-2(1H)-pyridone (161 mg, 0.69 mmol) was added to a stirred solution of 5-(4-aminophenyl)-10,15,20-tris-(4-pyridyl)porphyrin (**50**) (220 mg, 0.35 mmol) dissolved in dry DCM (50 ml). The reaction mixture was allowed to stir under argon for 6 hours and upon completion was concentrated *in vacuo* to yield a dark purple solid. The crude solid was purified *via* column chromatography (eluent, MeOH:DCM, 1:19). Fractions were combined and solvent was removed *in vacuo* to yield a purple solid (130 mg, 55%).  $^1\text{H}$  NMR (400 MHz,  $\text{CDCl}_3$ ,  $\delta$ ): -2.11 (s, internal NH, 2H), 7.65 (d,  $J = 10.6$  Hz, m-Ph-H, 2H), 8.19 (d,  $J = 7.5$  Hz, 5-o-Py-H + o-Ph-H, 8H), 8.87 (br s,  $\beta$ -H, 8H), 9.03 (d,  $J = 5.9$  Hz, 5-m-Py-H, 6H). HRMS ( $m/z$ ):  $[\text{M}]^+$  calcd for  $\text{C}_{42}\text{H}_{26}\text{N}_8\text{S}$ , 674.1992; found, 674.1996. UV-vis ( $\text{CH}_3\text{OH}$ )  $\lambda_{\text{max}}$ , nm ( $\log \epsilon$ ): 415 (5.0), 514, 551, 593, 655.  $R_f = 0.17$  (silica, MeOH:DCM, 1:19).

**7.2.56. Synthesis of 5-(4-isothiocyanatophenyl)-10,15,20-tris-(4-*N*-methylpyridiniumyl) porphyrin triiodide (52)**



Iodomethane (2.4 ml, 39.00 mmol) was added to a stirred solution of 5-(4-isothiocyanatophenyl)-10,15,20-tris-(4-pyridyl)porphyrin (**51**) (120 mg, 0.18 mmol) in anhydrous DMF (20 ml). The reaction mixture was allowed to stir under argon for 3.5 hours. Upon completion the reaction mixture was washed with ether (3 x 30 ml), solids were collected by filtration. The crude was precipitated in ether over MeOH to yield a purple solid (116 mg, 59%).  $^1\text{H}$  NMR (400 MHz,  $\text{CDCl}_3$ ,  $\delta$ ): -2.04 (s, internal NH, 2H), 3.30 (s,  $\text{CH}_3$ , 9H), 7.89 (d,  $J = 8.4$  Hz, m-Ph-H, 2H), 8.24 (d,  $J = 8.4$  Hz, o-Ph-H, 2H), 8.92-9.02 (m,  $\beta$ -H, 8H), 9.11 (s, 5-o-Py-H, 6H), 9.41 (d,  $J = 6.4$  Hz, 5-m-Py-H, 6H). HRMS ( $m/z$ ):  $[\text{M} - 3\text{I}]^{3+}$  calcd for  $\text{C}_{45}\text{H}_{35}\text{N}_8\text{S}$ , 239.7565; found, 239.7563. UV-vis ( $\text{H}_2\text{O}$ )  $\lambda_{\text{max}}$ , nm (log  $\epsilon$ ): 423 (5.2), 522, 559, 582, 643.  $R_f = 0.38$  (silica, saturated potassium nitrate: $\text{H}_2\text{O}$ :MeCN, 1:1:8).

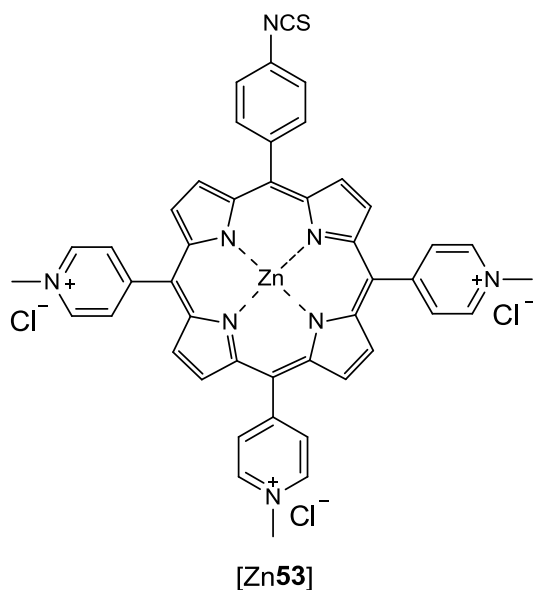
**7.2.57. Synthesis of 5-(4-isothiocyanatophenyl)-10,15,20-tris-(4-*N*-methylpyridiniumyl) porphyrin trichloride (53)**



**53**

Amberlite IRA 400 (Cl<sup>-</sup> form) (3.50 g) was added to a stirred solution of 5-(4-isothiocyanatophenyl)-10,15,20-tris-(4-*N*-methylpyridiniumyl) porphyrin triiodide (**52**) (105 mg, 95 μmol) in anhydrous MeOH (70 ml). The reaction mixture was allowed to stir under argon for 1 hour. The amberlite IRA 400 (Cl<sup>-</sup> form) resin was filtered and washed with a small amount of anhydrous MeOH (2 x 20 ml). The filtrate was concentrated *in vacuo* to yield a purple solid (70 mg, 89%). <sup>1</sup>H NMR (400 MHz, DMSO, δ): -2.13 (s, internal NH, 2H), 3.32 (s, CH<sub>3</sub>, 9H), 7.59 (d, *J* = 8.3 Hz, m-Ph-H, 2H), 8.24 (d, *J* = 8.3 Hz, o-Ph-H, 2H), 8.84-9.02 (m, β-H, 8H), 9.11 (s, 5-o-Py-H, 6H), 9.35 (d, *J* = 6.4 Hz, 5-m-Py-H, 6H). MS: (ESI) *m/z* 240 (100[M - 3Cl]<sup>3+</sup>). UV-vis (H<sub>2</sub>O) λ<sub>max</sub>, nm (log ε): 424 (5.3), 521, 559, 585, 655. R<sub>f</sub> = 0.35 (silica, saturated potassium nitrate:H<sub>2</sub>O:MeCN, 1:1:8).

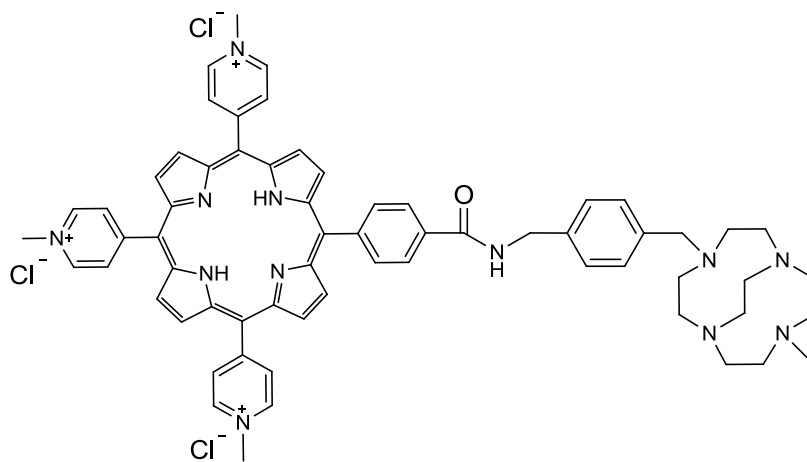
**7.2.58. Synthesis of zinc-5-(4-isothiocyanatophenyl)-10,15,20-tris-(4-*N*-methylpyridiniumyl) porphyrin trichloride [Zn53]**



**General procedure P was followed**

Amounts: 5-(4-isothiocyanatophenyl)-10,15,20-tris-(4-*N*-methylpyridiniumyl) porphyrin trichloride (**53**) (70 mg, 85  $\mu\text{mol}$ ), MeOH (10 ml), zinc(II) acetate (70 mg, 385  $\mu\text{mol}$ ), MeOH (10 ml). To yield a green/purple solid (70 mg, 93%).  $^1\text{H}$  NMR (400 MHz,  $\text{CD}_3\text{OD}$ ,  $\delta$ ): 3.30 (s,  $\text{CH}_3$ , 9H), 7.59 (d,  $J = 8.3$  Hz, m-Ph-H, 2H), 8.14 (d,  $J = 8.3$  Hz, o-Ph-H, 2H), 8.84-9.02 (m,  $\beta$ -H, 8H), 9.19 (s, 5-o-Py-H, 6H), 9.42 (d,  $J = 6.4$  Hz, 5-m-Py-H, 6H). HRMS ( $m/z$ ):  $[\text{M} - 3\text{Cl}]^+$  calcd for  $\text{C}_{45}\text{H}_{33}\text{N}_8\text{SZn}$ , 781.18367; found, 781.18349. UV-vis ( $\text{H}_2\text{O}$ )  $\lambda_{\text{max}}$ , nm (log  $\epsilon$ ): 447 (4.9), 566, 605.

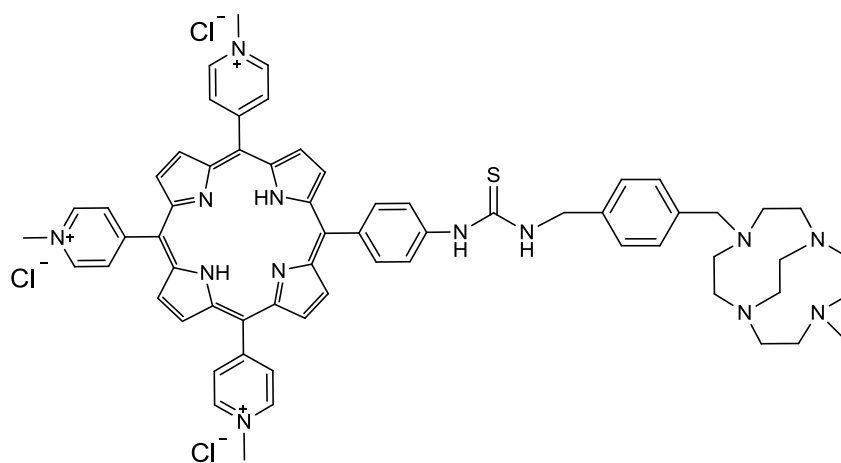
7.2.59. Attempted conjugation of 1-[4-aminomethylbenzyl]-7-[methyl]-1,4,7,10-tetraaza bicyclo[5.5.2]dodecane (**15**) with 5-[4-(succinimide-*N*-oxycarbonyl)phenyl]-10,15,20-tris-(4-*N*-methylpyridinium)porphyrin trichloride (**48**)



**54**

5-[4-(Succinimide-*N*-oxycarbonyl)phenyl]-10,15,20-tris-(4-*N*-methylpyridinium) porphyrin trichloride (**48**) (5.0 mg, 5.5  $\mu$ mol) and 1-[4-aminomethylbenzyl]-7-[methyl]-1,4,7,10-tetraazabicyclo[5.5.2]dodecane (**15**) (1.8 mg, 5.5  $\mu$ mol) were dissolved in PBS (1 ml, 0.1 mmol, pH 7.6) and stirred for 20 hours. Solvent was removed on a Schlenk line. The crude solid was redissolved in MeOH (1 ml) and purified *via* size exclusion chromatography. The desired product was not isolated using this synthetic procedure.

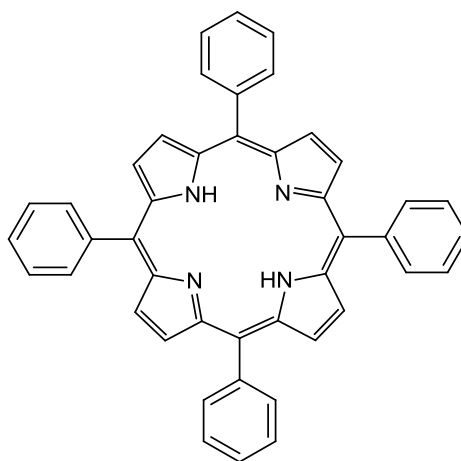
**7.2.60. Attempted conjugation of 1-[4-aminomethylbenzyl]-7-[methyl]-1,4,7,10-tetraaza bicyclo[5.5.2]dodecane (15) with 5-(4-isothiocyanatophenyl)-10,15,20-tris-(4-*N*-methyl pyridiniumyl) porphyrin trichloride (53)**



**55**

5-(4-Isothiocyanatophenyl)-10,15,20-tris-(4-*N*-methylpyridiniumyl) porphyrin trichloride (**53**) (5.0 mg, 6  $\mu$ mol) and 1-[4-aminomethylbenzyl]-7-[methyl]-1,4,7,10-tetraazabicyclo [5.5.2]dodecane (**15**) (2.0 mg, 6  $\mu$ mol) were dissolved in aqueous sodium hydrogen carbonate (1 ml, 0.1 mmol, pH 9.2) and stirred for 20 hours. Solvent was removed on a Schlenk line. The crude solid was redissolved in MeOH (1 ml) and purified *via* size exclusion chromatography. The desired product was not isolated using this synthetic procedure.

### 7.2.61. Synthesis of tetraphenyl porphyrin (TPP) (56)

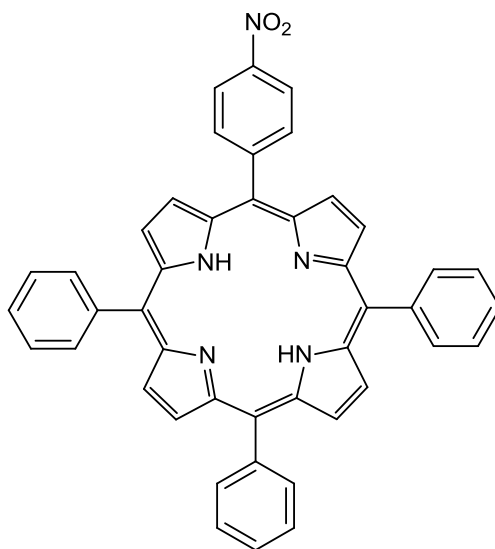


56

Following the literature method outlined by Adler *et al.*<sup>213</sup>

Benzaldehyde (14.6 g, 0.14 mol, 14 ml) and freshly distilled pyrrole (9.67 g, 0.14 mol, 10 ml) were dissolved in propionic acid (500 ml) and refluxed under nitrogen for 1 hour, whilst being protected from light. With the use of MeOH (~100 ml) the mixture was transferred to a suitable flask and solvents were removed *in vacuo*. The crude was run down a pre-column (eluant: DCM), suitable fractions were precipitated from DCM: MeOH (300 ml, 1:10) to yield a shiny, purple solid (4.77 g, 23%). <sup>1</sup>H NMR (400 MHz, CDCl<sub>3</sub>, δ): -2.84 (s, internal NH, 2H), 7.73 (m, p-Ph H + m-Ph H, 12H), 8.21-8.24 (m, β H, 8H), 8.86 (br s, o-Ph H, 8H). HRMS (*m/z*): [M + H]<sup>+</sup> calcd for C<sub>44</sub>H<sub>30</sub>N<sub>4</sub>, 614.2460; found, 614.2465. UV-vis (DCM) λ<sub>max</sub>, nm (log ε): 418 (4.7), 514, 549, 590, 647. R<sub>f</sub> = 0.49 (silica, DCM:hexane, 1:1).

### 7.2.62. Synthesis of nitro-tetraphenyl porphyrin (TPP-NO<sub>2</sub>) (**57**)

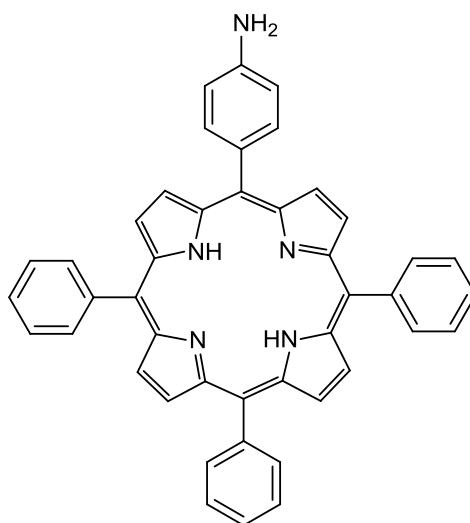


**57**

Following the literature method outlined by Smith *et al.*<sup>233</sup>

A solution of TPP (**56**) (0.93 g, 1.51 mmol) in DCM (180 ml) was purged with nitrogen for 10 min at RT. [NO<sub>2</sub>][BF<sub>4</sub>] (2.74 ml, 1.37 mmol) was added dropwise over 30 min (~0.1 ml/min). The mixture was stirred for 30 min and another portion of [NO<sub>2</sub>][BF<sub>4</sub>] (2.74 ml, 1.37 mmol) was added dropwise over 30 min (~0.1 ml/min). TLC showed the presence of TPP so a further portion of [NO<sub>2</sub>][BF<sub>4</sub>] (1.00 ml, 0.5 mmol) was added. The mixture was then allowed to stir for a further 30 min. The mixture was quenched by addition of water (100 ml), then extracted with a further two portions of water (2 x 200 ml). The organic layer was concentrated, the crude was re-dissolved in acetone (50 ml) and precipitated with water (500 ml). The resulting solid was purified *via* flash chromatography (silica, eluant: DCM:hexane, 1:1), pure fractions were collected, dried (MgSO<sub>4</sub>), filtered and solvent removed *in vacuo* to yield a purple solid (860 mg, 86%). <sup>1</sup>H NMR (400 MHz, CDCl<sub>3</sub>, δ): -2.86 (s, internal NH, 2H), 7.66-7.71 (br m, β H + o-Ph H, 10H), 8.12-8.14 (m, m-Ph H, 6H), 8.30-8.32 (d, *J* = 8.8 Hz, o-Ph H, 2H), 8.53-8.56 (d, *J* = 8.8 Hz, o-Ph H, 2H), 8.65 (d, *J* = 4.7 Hz, o-Ph H, 2H), 8.78 (s, p-Ph H, 3H), 8.81 (d, *J* = 4.7 Hz, NO<sub>2</sub>-Ph H, 2H). HRMS (*m/z*): [M + H]<sup>+</sup> calcd for C<sub>44</sub>H<sub>30</sub>N<sub>5</sub>O<sub>2</sub>, 660.2389; found, 660.2394. UV-vis (DCM) λ<sub>max</sub>, nm (log ε): 419 (4.6), 515, 551, 590, 646. R<sub>f</sub> = 0.31 (silica, DCM:hexane, 1:1).

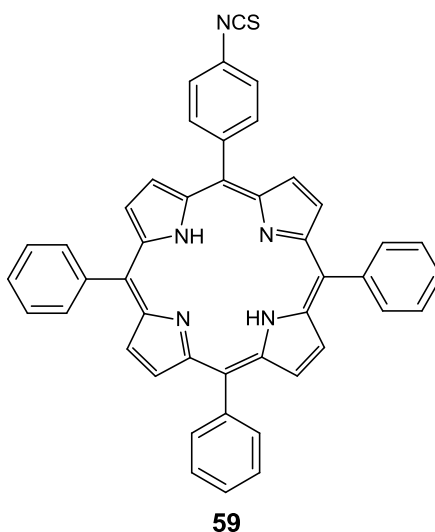
### 7.2.63. Synthesis of amino-tetraphenyl porphrin (TPP-NH<sub>2</sub>) (**58**)



**58**

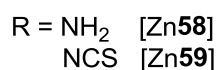
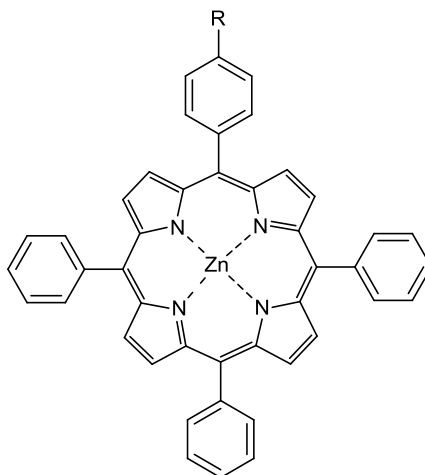
To a solution of TPP-NO<sub>2</sub> (**57**) (680 mg, 1.03 mmol) in HCl (150 ml) was added to tin(II) chloride dihydrate (699 mg, ) and the mixture was stirred at 60°C under N<sub>2</sub> for 1 hour. Solvent was removed *in vacuo* and re-dissolved in DCM:Et<sub>3</sub>N (9:1, 100 ml) and washed with water (3 x 100 ml). The organic layer was dried (MgSO<sub>4</sub>), filtered and concentrated *in vacuo*. The crude solid was precipitated from DCM:MeOH (1:12, 300 ml) to yield a purple solid (611 mg, 94%). <sup>1</sup>H NMR (400 MHz, CDCl<sub>3</sub>, δ): -2.73 (s, internal NH, 2H), 3.95 (s, NH<sub>2</sub>, 2H), 7.02 (d, *J* = 8.1 Hz, NH<sub>2</sub>-Ph H, 4H), 7.74-7.77 (m, o-Ph H + p-Ph H, 9H), 7.99 (d, *J* = 8.1 Hz, β H, 2H), 8.22-8.24 (m, β H, 6H), 8.85 (s, m-Ph H, 6H), 8.95 (d, *J* = 4.7 Hz, m-Ph H, 2H). HRMS (*m/z*): [M]<sup>+</sup> calcd for C<sub>44</sub>H<sub>31</sub>N<sub>5</sub>, 629.2560; found, 629.2574. UV-vis (DCM) λ<sub>max</sub>, nm (log ε): 420 (4.7), 516, 553, 592, 648. R<sub>f</sub> = 0.29 (silica, DCM).

#### 7.2.64. Synthesis of isothiocyano-tetraphenyl porphyrin (TPP-NCS) (**59**)



1,1'-Thiocarbonyldi-2(1H)-pyridone (295 mg, 1.270 mmol) was added to a stirred solution of TPP-NH<sub>2</sub> (**58**) (400 mg, 0.635 mmol) dissolved in dry DCM (100 ml). The reaction mixture was allowed to stir under argon for 6 hours and upon completion, solvents were removed *in vacuo* to yield a dark purple solid. The crude solid was purified *via* column chromatography (eluent, MeOH:DCM, 1:24). Fractions were combined and solvent removed *in vacuo* to yield a purple solid (420 mg, 98%). <sup>1</sup>H NMR (400 MHz, CDCl<sub>3</sub>, δ): -2.74 (s, NH, 2H), 7.60 (d, *J* = 8.4 Hz, Ar H, 2H), 7.77 (m, Ar H, 9H), 8.23 (m, β-H, 8H), 8.80 (d, *J* = 4.7 Hz, Ar H, 2H), 8.91 (m, Ar H, 6H). HRMS (*m/z*): [M + H]<sup>+</sup> calcd for C<sub>45</sub>H<sub>30</sub>N<sub>5</sub>S, 672.2211; found, 672.2216. UV-vis (DCM) λ<sub>max</sub>, nm (log ε): 419 (4.8), 515, 550, 590, 646. R<sub>f</sub> = 0.47 (silica, DCM:hexane, 1:1).

### 7.2.65. Synthesis of zinc-amino-tetraphenyl porphyrin [Zn58] and zinc-isothiocyano-tetraphenyl porphyrin [Zn59]



#### General procedure Q

Porphyrin was dissolved in DCM. Zinc(II) acetate was added in MeOH and the mixture was stirred for 1 hour at RT. Solvents were concentrated ~ 5 ml. MeOH was added and the resulting precipitate was filtered.

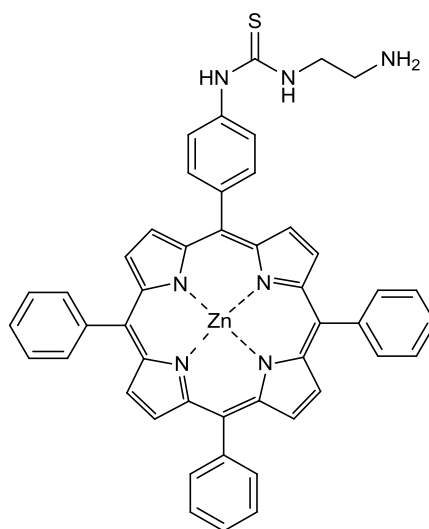
#### Zinc-amino-tetraphenyl porphyrin [Zn58]

Amounts: TPP-NH<sub>2</sub> (**58**) (500 mg, 0.793 mmol), DCM (100 ml), zinc(II) acetate (582 mg, 3.171 mmol), MeOH (10 ml), MeOH (80 ml). To give a purple solid (403 mg, 73%). <sup>1</sup>H NMR (400 MHz, CDCl<sub>3</sub>, δ): 5.49 (br s, NH<sub>2</sub>, 2H), 6.97 (d, *J* = 7.8 Hz, Ar H, 2H), 7.81 (m, Ar H, 9H), 8.17 (s, β-H, 8H), 8.74 (s, Ar H, 6H), 8.90 (d, *J* = 4.0 Hz, Ar H, 2H). HRMS (*m/z*): [M]<sup>+</sup> calcd for C<sub>44</sub>H<sub>29</sub>N<sub>5</sub>Zn, 691.1702; found, 691.1709. UV-vis (DCM) λ<sub>max</sub>, nm (log ε): 423 (4.7), 555, 597. R<sub>f</sub> = 0.61 (silica, DCM).

### Zinc-isothiocyano-tetraphenyl porphyrin [Zn59]

Amounts: TPP-NCS (**59**) (350 mg, 0.521 mmol), DCM (30 ml), zinc(II) acetate (478 mg, 2.605 mmol), MeOH (5 ml), MeOH (80 ml). To yield a purple solid (295 mg, 77%).  $^1\text{H}$  NMR (400 MHz,  $\text{CDCl}_3$ ,  $\delta$ ): 7.63 (d,  $J = 8.3$  Hz, Ar H, 2H), 7.77 (m, Ar H, 9H), 8.25 (m,  $\beta$ -H, 8H), 8.91 (d,  $J = 4.4$  Hz, Ar H, 2H), 8.99 (m, Ar H, 6H). HRMS ( $m/z$ ):  $[\text{M} + \text{H}]^+$  calcd for  $\text{C}_{45}\text{H}_{27}\text{N}_5\text{SZn}$ , 733.1261; found, 733.1273. UV-vis (DCM)  $\lambda_{\text{max}}$ , nm (log  $\epsilon$ ): 420 (4.6), 548, 629.  $R_f = 0.42$  (silica, DCM:hexane, 1:1).

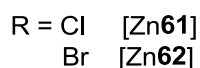
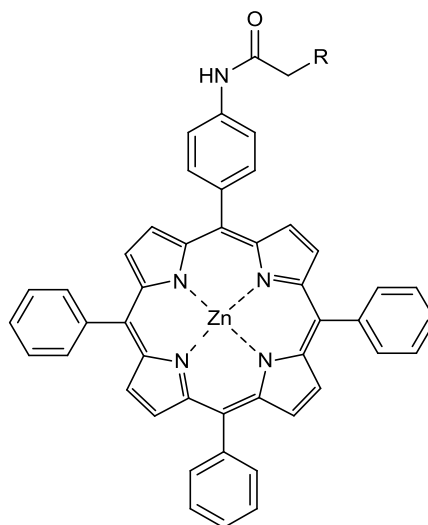
### 7.2.66. Synthesis of zinc-(aminoethyl)thiourea-tetraphenyl porphyrin [Zn60]



[Zn60]

To a stirred solution of zinc-isothiocyano-tetraphenyl porphyrin ([Zn59] (100 mg, 0.136 mmol) was dissolved in ethylenediamine (5 ml) and the mixture was stirred at RT for 3 hours. Solvents were removed *in vacuo*, followed by addition and subsequent removal of MeOH (3 x 20 ml) to yield a purple solid (100 mg, 93%).  $^1\text{H}$  NMR (400 MHz,  $\text{CDCl}_3$ ,  $\delta$ ): 1.89 (s,  $\text{CH}_2\text{NH}_2$ , 1H), 2.01 (d,  $J = 8.8$  Hz,  $\text{CH}_2\text{NH}_2$ , 1H), 2.21 (d,  $J = 8.8$  Hz,  $\text{CH}_2\text{NH}_2$ , 1H), 2.52 (s,  $\text{CH}_2\text{NH}_2$ , 1H), 3.40 (s, NH, 2H), 6.40 (br s, NH, 2H), 7.63 (m, Ar H, 10H), 8.10 (d,  $J = 6.0$  Hz, Ar H, 9H), 8.76 (m,  $\beta$ -H, 8H). HRMS ( $m/z$ ):  $[\text{M} + \text{H}]^+$  calcd for  $\text{C}_{47}\text{H}_{36}\text{N}_7\text{SZn}$ , 794.2039; found, 794.2039. UV-vis (DCM)  $\lambda_{\text{max}}$ , nm ( $\log \epsilon$ ): 425 (5.7), 562, 605.

### 7.2.67. Synthesis of zinc-chloroacetamido-tetraphenyl porphyrin [Zn61] and zinc-2-bromo acetamido-tetraphenyl porphyrin [Zn62]



#### General procedure R

To Zn-TPP-NH<sub>2</sub> ([Zn58]) and DIPEA in chloroform (20 ml) was added the acetyl compound. The mixture was stirred at RT for 2 hours. Solvents were concentrated *in vacuo* and the resulting crude solid was purified *via* flash chromatography (silica, eluant DCM).

#### Zinc-chloroacetamido-tetraphenyl porphyrin [Zn61]

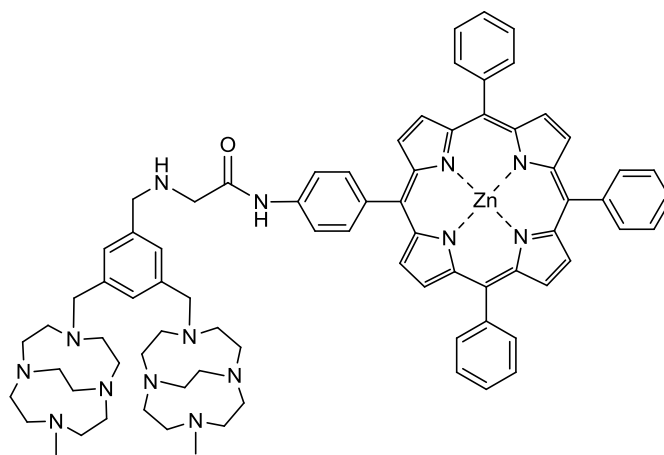
Amounts: Zn-TPP-NH<sub>2</sub> ([Zn58]) (100 mg, 0.144 mmol), DIPEA (19 mg, 0.144 mmol, 26  $\mu$ l), chloroacetyl chloride (16 mg, 0.144 mmol, 12  $\mu$ l). To yield a purple solid (102 mg, 92%). <sup>1</sup>H NMR (400 MHz, CD<sub>3</sub>OD,  $\delta$ ): 4.27 (s, CH<sub>2</sub>, 2H), 7.67 (m, 10H), 7.90 (d, *J* = 4.5 Hz, Ar H, 2H), 8.08 (m,  $\beta$ -H, 8H), 8.71 (m, 7H). HRMS (*m/z*): [M]<sup>+</sup> calcd for C<sub>46</sub>H<sub>30</sub>N<sub>5</sub>O<sup>35</sup>ClZn, 767.1440; found, 767.1425. UV-vis (DCM)  $\lambda_{\text{max}}$ , nm (log  $\epsilon$ ): 421 (4.7), 555, 595. R<sub>f</sub> = 0.22 (silica, DCM:hexane, 1:1).

### Zinc-bromoacetamido-tetraphenyl porphyrin [Zn62]

Amounts: Zinc-amino-tetraphenyl porphyrin ([Zn58]) (100 mg, 0.144 mmol), DIPEA (19 mg, 0.144 mmol, 26  $\mu$ l), bromoacetyl bromide (16 mg, 0.144 mmol, 12  $\mu$ l). To yield a purple solid (67 mg, 57%).

$^1\text{H}$  NMR (400 MHz,  $\text{CDCl}_3$ ,  $\delta$ ): 4.06 (s,  $\text{CH}_2$ , 2H), 7.67 (m, 10H), 7.89 (d,  $J = 8.6$  Hz, Ar H, 2H), 8.10 (m,  $\beta$ -H, 8H), 8.72 (s, 3H), 8.74 (d,  $J = 4.5$  Hz, 2H), 8.77 (d,  $J = 4.7$  Hz, Ar H, 2H). HRMS ( $m/z$ ):  $[\text{M}]^+$  calcd for  $\text{C}_{46}\text{H}_{30}\text{N}_5\text{O}^{79}\text{BrZn}$ , 811.0924; found, 811.0920. UV-vis (DCM)  $\lambda_{\text{max}}$ , nm ( $\log \epsilon$ ): 424 (5.1), 555, 592.  $R_f = 0.22$  (silica, DCM:hexane, 1:1).

7.2.68. Attempted conjugation of 1,1'-[3,5-dimethylaminobenzyl]-7,7'-[methyl]-bis (1,4,7,10-tetraazabicyclo [5.5.2]dodecane (20) with zinc-chloroacetamido-tetraphenyl porphyrin [Zn61] or zinc-bromoacetamido-tetraphenyl porphyrin [Zn62]



### General procedure S

The bismacrocycle was dissolved in MeOH,  $K_2CO_3$  was added and the mixture was stirred for 10 min. The metalloporphyrin was added and the mixture was refluxed for 24 hours, whilst being protected from light. Solvents were removed *in vacuo*.

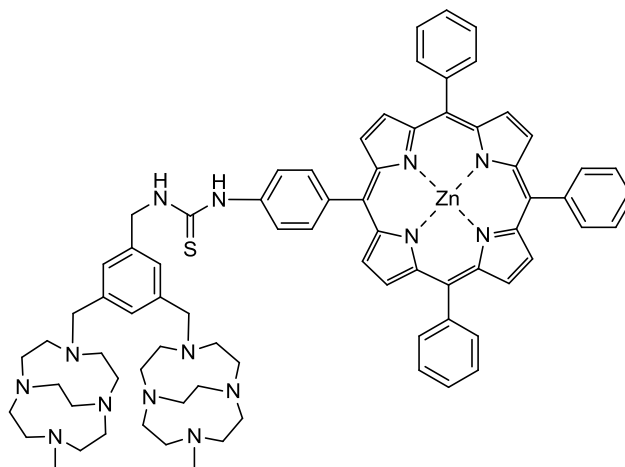
### Method 1-Attempted synthesis

Amounts: 1,1'-[3,5-dimethylaminobenzyl]-7,7'-[methyl]-bis(1,4,7,10-tetraazabicyclo [5.5.2] dodecane (20) (25 mg, 45  $\mu$ mol), MeOH (5 ml),  $K_2CO_3$  (31 mg, 225  $\mu$ mol), zinc-chloroacetamido-tetraphenyl porphyrin (23 mg, 30  $\mu$ mol). To yield a green/purple solid. The desired product was not isolated using this synthetic procedure.

### Method 2-Attempted synthesis

Amounts: 1,1'-[3,5-dimethylaminobenzyl]-7,7'-[methyl]-bis(1,4,7,10-tetraazabicyclo [5.5.2] dodecane (20) (25 mg, 45  $\mu$ mol), MeOH (5 ml),  $K_2CO_3$  (31 mg, 225  $\mu$ mol), zinc-bromoacetamido-tetraphenyl porphyrin (24 mg, 30  $\mu$ mol). To yield a green/purple solid. The desired product was not isolated using this synthetic procedure.

**7.2.69. Conjugation of 1,1'-[3,5-dimethylaminobenzyl]-7,7'-[methyl]-bis (1,4,7,10-tetraazabicyclo [5.5.2]dodecane (20) and Zn-TPP-NCS [Zn59]**



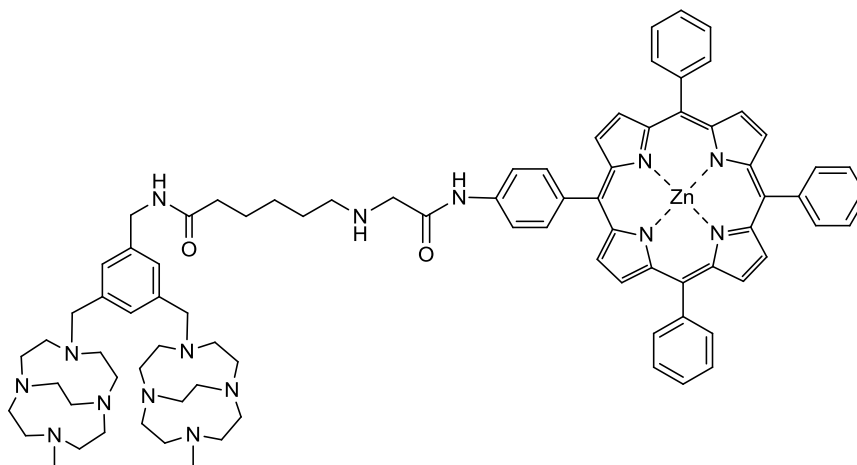
**64**

**General method T**

The bismacrocycle was dissolved in MeOH, Zn-TPP-NCS [Zn59] in DCM (2.5 ml) was added and the mixture was stirred at RT for 2 hours. TLC indicated complete consumption of starting material. Solvents were removed *in vacuo*.

Amounts: 1,1'-[3,5-dimethylaminobenzyl]-7,7'-[methyl]-bis(1,4,7,10-tetraazabicyclo [5.5.2] dodecane (**20**) (29 mg, 51  $\mu\text{mol}$ ), MeOH (2.5 ml), Zn-TPP-NCS [Zn**59**] (25 mg, 34  $\mu\text{mol}$ ), DCM (2.5 ml). To yield a green/purple solid. MS ( $m/z$ ): 1293  $[\text{M} + \text{H}]^+$ , 647  $[\text{M} + 2\text{H}]^{2+}$ . UV-vis (DCM) )  $\lambda_{\text{max}}$ , nm (log  $\epsilon$ ): 431 (4.6), 565, 606.

**7.2.70. Attempted conjugation of 6-amino-*N*-(3,5-bis((10-methyl-1,4,7,10-tetraazabicyclo [5.5.2] tetradecan-4-yl)methyl)benzyl)hexanamide (32) and zinc-chloroacetamido-tetraphenyl porphyrin [Zn61]**



65

**Method 1-Attempted synthesis**

**General procedure S was followed**

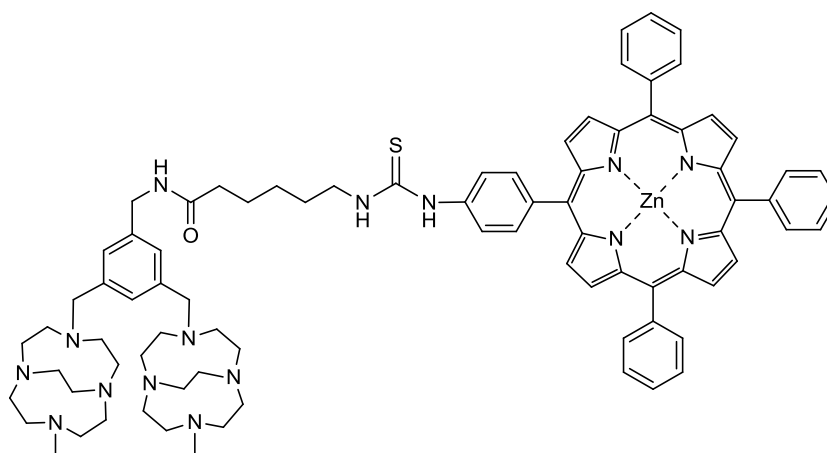
Amounts: 6-amino-*N*-(3,5-bis((10-methyl-1,4,7,10-tetraazabicyclo[5.5.2]tetradecan-4-yl)methyl)benzyl)hexanamide (**32**) (20 mg, 20.8  $\mu\text{mol}$ ), MeOH (5 ml),  $\text{K}_2\text{CO}_3$  (23 mg, 166.6  $\mu\text{mol}$ ) zinc-chloroacetamido-tetraphenyl porphyrin [Zn**61**] (11 mg, 13.9  $\mu\text{mol}$ ). To yield a green/purple solid. The desired product was not isolated using this synthetic procedure.

**Method 2-Attempted synthesis**

**General procedure S was followed**

Amounts: 6-amino-*N*-(3,5-bis((10-methyl-1,4,7,10-tetraazabicyclo[5.5.2]tetradecan-4-yl)methyl)benzyl)hexanamide (**32**) (20 mg, 20.8  $\mu\text{mol}$ ), MeOH (5 ml),  $\text{K}_2\text{CO}_3$  (23 mg, 166.6  $\mu\text{mol}$ ) zinc-bromoacetamido-tetraphenyl porphyrin [Zn**62**] (11 mg, 13.9  $\mu\text{mol}$ ). To yield a green/purple solid. The desired product was not isolated using this synthetic procedure.

7.2.71. Attempted conjugation of 6-amino-*N*-(3,5-bis((10-methyl-1,4,7,10-tetraazabicyclo [5.5.2]tetradecan-4-yl)methyl)benzyl)hexanamide (**32**) and Zn-TPP-NCS [Zn59]

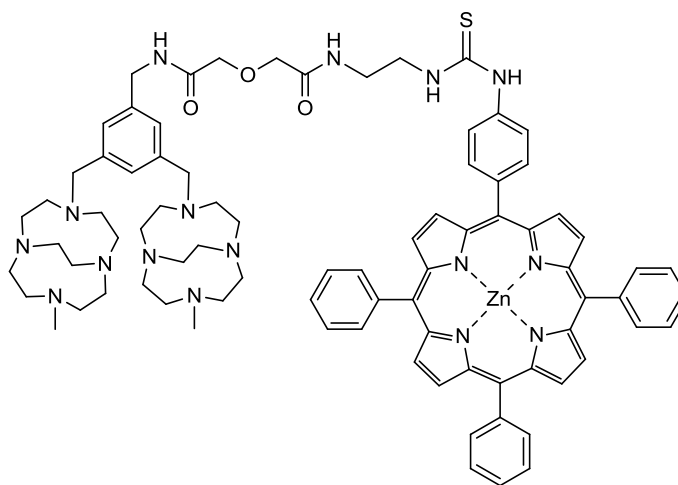


66

**General procedure T was followed**

Amounts: 6-amino-*N*-(3,5-bis((10-methyl-1,4,7,10-tetraazabicyclo[5.5.2]tetradecan-4-yl)methyl)benzyl)hexanamide (**32**) (30 mg, 31.2  $\mu$ mol), MeOH (2.5 ml), Zn-TPP-NCS [Zn59] (15 mg, 20.8  $\mu$ mol), DCM (2.5 ml). To yield a green/purple solid. The desired product was not isolated using this synthetic procedure.

7.2.72. Attempted conjugation of 2-(2-((3,5-bis((10-methyl-1,4,7,10-tetraaza bicyclo[5.5.2]tetradecan-4-yl)methyl)benzyl)amino)-2-oxoethoxy) nitrophenyl ester (**38**) and zinc-(aminoethyl)thiourea-tetraphenyl porphyrin [**Zn60**]



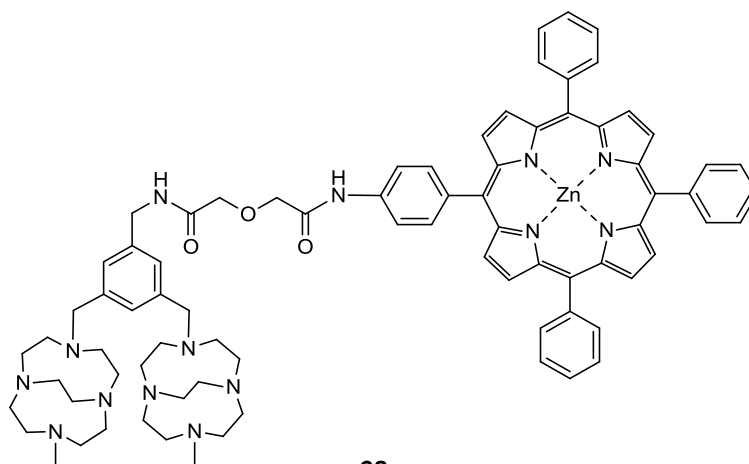
67

#### General procedure U

The bismacrocycle was dissolved in MeOH, the metalloporphyrin in DCM was added and the mixture was heated to 40°C for 4 hours. TLC indicated a reaction had occurred. Solvents were removed *in vacuo*.

2-(2-((3,5-bis((10-methyl-1,4,7,10-tetraazabicyclo[5.5.2]tetradecan-4-yl)methyl)benzyl)amino)-2-oxoethoxy) nitrophenyl ester (**38**) (20 mg, 25.2  $\mu\text{mol}$ ), MeOH (2 ml), zinc-(aminoethyl)thiourea-tetraphenyl porphyrin [**Zn60**] (15 mg, 18.7  $\mu\text{mol}$ ), DCM (2 ml). To yield a green/purple solid. The desired product was not isolated using this synthetic procedure.

7.2.73. Attempted conjugation of 2-(2-((3,5-bis((10-methyl-1,4,7,10-tetraaza bicyclo[5.5.2]tetradecan-4-yl)methyl)benzyl)amino)-2-oxoethoxy) nitrophenyl ester (**38**) or 2-(2-((3,5-bis((10-methyl-1,4,7,10-tetraazabicyclo[5.5.2]tetradecan-4-yl)methyl)benzyl)amino)-2-oxoethoxy)acetic acid (**34**) with Zn-TPP-NH<sub>2</sub> [Zn58]



#### Method 1-Attempted synthesis

##### General procedure U was followed

Amounts: 2-(2-((3,5-bis((10-methyl-1,4,7,10-tetraazabicyclo[5.5.2]tetradecan-4-yl)methyl)benzyl)amino)-2-oxoethoxy) nitrophenyl ester (**38**) (20 mg, 25.2  $\mu$ mol), MeOH (2 ml), Zn-TPP-NH<sub>2</sub> [Zn58] (13 mg, 18.7  $\mu$ mol), DCM (2 ml). To yield a green/purple solid. The desired product was not isolated using this synthetic procedure.

##### General procedure V

The bismacrocycle was dissolved in MeOH, coupling reagents were added and allowed to stir at RT for 10 min. The metalloporphyrin in DCM was added and the mixture was heated to 40°C for 4 hours. TLC indicated a reaction had occurred. Solvents were removed *in vacuo*.

### **Method 2-Attempted synthesis**

Amounts: 2-(2-((3,5-bis((10-methyl-1,4,7,10-tetraazabicyclo[5.5.2]tetradecan-4-yl)methyl)benzyl)amino)-2-oxoethoxy)acetic acid (**34**) (30 mg, 44.6  $\mu\text{mol}$ ), MeOH (2.5 ml), PyBOP (24 mg, 44.6  $\mu\text{mol}$ ), DIPEA (18 mg, 136.3  $\mu\text{mol}$ , 24  $\mu\text{l}$ ), Zn-TPP-NH<sub>2</sub> [**Zn58**] (21 mg, 29.8  $\mu\text{mol}$ ), DCM (2.5 ml). To yield a green/purple solid. The desired product was not isolated using this synthetic procedure.

### **Method 3-Attempted synthesis**

Amounts: 2-(2-((3,5-bis((10-methyl-1,4,7,10-tetraazabicyclo[5.5.2]tetradecan-4-yl)methyl)benzyl)amino)-2-oxoethoxy)acetic acid (**34**) (30 mg, 44.6  $\mu\text{mol}$ ), MeOH (2.5 ml), DCC (9 mg, 44.6  $\mu\text{mol}$ ), DIPEA (18 mg, 136.3  $\mu\text{mol}$ , 24  $\mu\text{l}$ ), Zn-TPP-NH<sub>2</sub> [**Zn58**] (21 mg, 29.8  $\mu\text{mol}$ ), DCM (2.5 ml). To yield a green/purple solid. The desired product was not isolated using this synthetic procedure.

## **7.3. Biological experimental**

### **7.3.1. Experimental for competition binding assays**

#### ***7.3.1.1. General methods and preparation of cell cultures***

Human leukaemia T cell lymphoblasts (Jurkat) were obtained from the MRL (University of Hull). These cells were cultured in RPMI 1640 media (Invitro technologies, UK) containing 10% (v/v) heat inactivated FBS (Biowest, France), 1% glutamate (2 mM), 1% (v/v) penicillin and streptomycin (100 units/ml) antibiotics. The cell cultures were maintained at 37°C in a humidified, CO<sub>2</sub> (5%) controlled atmosphere with subculturing done every 2-3 days. To handle the cells aseptic techniques were conducted in a Class II microbiological safety cabinet fitted with a UV sterilising lamp. All glassware and heat stable solutions were autoclaved prior to use at 121°C for 10 min, disposable equipment and all solutions were of sterile tissue culture grade.

#### ***7.3.1.2. Antibodies and fluorescent dyes***

Unconjugated mouse anti-human CXCR4 mAb clone 44717.111 was purchased from R & D systems Europe, Abingdon, UK. Secondary FITC conjugated anti-mouse antibody was purchased from Serotec, UK. Dilutions of mAbs were prepared using PBS supplemented with 0.25% (v/v) BSA and NaN<sub>3</sub> (0.001 M). All reagents, antibodies and fluorescent dyes were reconstituted and stored according to the manufacturer's instructions unless otherwise stated.

#### ***7.3.1.3. Cell counting***

The concentration of the cells was determined using a Neubauer hemacytometer. Cells in suspension were diluted 1:1 with 0.2% (v/v) Trypan blue stain. This dilution was placed into a hemacytometer chamber and the cell density was determined using light microscopy by counting the number of viable cells in a set area. Equation 2 is then used to determine the concentration of cells.

Equation 2:

Cell concentration (cells / ml) = Averaged cell count x 2 (dilution factor) x 10<sup>4</sup>  
(volume of chamber)

#### ***7.3.1.4. Antibody binding and subsequent fluorescent tagging for flow cytometry***

The Jurkat cell culture was centrifuged (180 x g for 3 min), resuspended in 10 ml PBS and centrifuged (180 x g for 3 min) further. The cell pellet was resuspended in 1.0 ml PBS and counted using the Trypan-blue test. Cells at a density of ~200000 were aliquoted into polypropylene FACS tubes (Falcon 2054 tubes), and then incubated with 10 µl of the compound under study (small molecule antagonist) for 1 hour 4°C. Each compound was run in duplicate. Cells were then washed (centrifuged 180 x g for 3 min) with 1.0 ml PBS and incubated with the CXCR4 mAb (10 µl) for 1 h at 4°C. Thereafter cells were washed (centrifuged at 180 x g for 3 min) with 1.0 ml PBS, and incubated with secondary fluorescently tagged antibody (diluted 1:100 in PBS) for 30 min at 4°C. After further washing (centrifuged at 180 x g for 3 min) with 1.0 ml PBS, the cells samples were fixed in 300 µl of PBS and analysed on a FACScan flow cytometer (BD Biosciences Europe, Erembodegem, Belgium). Data were acquired and analysed with CellQuest software (Becton Dickinson). A positive and negative control was run alongside the other samples to set the boundaries. The negative control measures for non-specific background staining; the cells were suspended in 10 µl PBS only. The positive control measures 100% antibody binding, the cells are incubated with 10 µl CXCR4 antibody and secondary fluorescently tagged antibody (diluted 1:100 in PBS).

## **7.4. Experimental for calcium signaling assays**

### **7.4.1. Cell cultures**

U87.CD4.CXCR4 cells were obtained from the American Type Culture Collection (ATCC) (Rockville, MD). Cells were cultured in RPMI-1640 medium (Gibco BRL, Gaithersburg, MD) supplemented with 10% heat-inactivated FBS and 1% glutamine (Gibco BRL). The cell cultures were maintained at 37°C in a humidified CO<sub>2</sub>-

controlled atmosphere. Subcultivations were done every 2-3 days and cells were used in stationary growth phase (3 days after two thirds subcultivation).

#### **7.4.2. Loading of the cells with the Ca<sup>2+</sup> indicator Fluo-3**

A detailed experimental is provided by Princen *et al.* (**Princen 2003 Cytometry**) but briefly, a 2 mM stock solution of Fluo-3 acetoxymethylester (Fluo-3/AM; Molecular Probes, Leiden, The Netherlands) was prepared with anhydrous dimethyl sulfoxide. The acetoxymethyl ester bound to Fluo-3 masks the negative charges in the indicator molecule and makes it hydrophobic and, hence, cell membrane permeable. Once inside the cell, the acetoxymethyl group is hydrolyzed by cytosol esterases, and the Ca<sup>2+</sup> sensitive polycarboxylate form of the indicator is formed ( $\lambda_{\text{ex}} = 488 \text{ nm}$ ,  $\lambda_{\text{em}} = 530 \text{ nm}$ ). A 20% w/v stock solution of the detergent Pluronic acid F-127 (Molecular Probes) was also prepared in dimethyl sulfoxide. An equal volume of Pluronic acid stock was added to the dye stock, just before use, to increase Fluo-3/AM solubility and improve dye loading into the cells. Cells were centrifuged and resuspended in RPMI-1640 medium supplemented with 2% FBS, for a final Fluo-3/AM concentration of 4  $\mu\text{M}$ . After incubation for 45 min at room temperature, cells were washed two times at room temperature in Ca<sup>2+</sup> flux assay buffer (Hank's balanced salt solution containing 20 mM HEPES and 0.2% bovine serum albumin, pH 7.4) to remove extracellular dye. After the second wash, cells were incubated for 10 min at room temperature. In the meantime, cells were counted with the use of trypan blue staining to determine the percentage of dead cells (blue cells). Then cells were centrifuged and resuspended at a density of  $3 \times 10^6$  cells/ml.

#### **7.4.3. Measurement of intracellular Ca<sup>2+</sup> mobilization and evaluation of receptor antagonists by the Fluorometric Imaging Plate Reader (FLIPR)**

The CXC chemokine CXCL12 was provided by Dr. I. Clark-Lewis (University of British Columbia, Vancouver, BC, Canada). After loading with Fluo-3, the cells were seeded (at a density of  $0.3 \times 10^6$  cells/ml) in a black-wall microplate (Costar, Cambridge, UK) that already contained 50  $\mu\text{l}$  of the CXCR4 antagonist. To form a uniform monolayer of cells on the bottom of the wells, the microplate was gently centrifuged for 3 min

with low acceleration and without break. After a 10 min incubation in the FLIPR test chamber, which was maintained at 37°C, fluorescence was recorded over a 4 min period, with measurements every 2 seconds during the first 2 min and subsequently every 6 seconds. At the beginning of a data run, a “signal test” is performed to check the background fluorescence and the basal fluorescence signal from the cells. Background fluorescence is produced by autofluorescence of the cells and by the test plate and tips. The autofluorescence of plates and tips is already very low  $\text{Ca}^{2+}$  because the black-wall microplate and black tips are used to avoid this. The basal fluorescence of the cells or the green fluorescence of unstimulated cells should be in the range of 8,000–10,000 counts (saturation of the camera occurs at 65,000 counts). Acceptable basal fluorescence values can be obtained by adjusting the exposure length of the CCD camera and/or increasing or decreasing the laser power, but the latter should be weaker than 0.150 W and no stronger than 0.800 W during the assay. After a 20 second baseline monitoring, 50  $\mu\text{l}$  of chemokine CXCL12, diluted in  $\text{Ca}^{2+}$  flux assay buffer at four times the final concentration was transferred to the test plate from a second 96 well microplate (Sero-wel, Sterilin Ltd, Stone, Staffs, UK). For each condition, the average of four identical microplate wells was measured. The data was expressed as fluorescence units versus time and was analyzed using the Softmax PRO 4.0 program (Molecular Devices) and  $\text{IC}_{50}$  values were calculated using the GraphPad Prism 4.0 software (San Diego, CA).

## **7.5. Experimental for anti-HIV assays**

Anti-HIV activity and cytotoxicity measurements in MT-4 and other cells were based on the viability of the cells that had been infected or not infected with HIV-1, HIV-2 or SIV and exposed to various concentrations of the test compound.<sup>237</sup> After the cells were allowed to proliferate for 5 days, the number of viable cells was quantified by a tetrazolium-based colorimetric method, as described by Pauwels *et al.*<sup>238, 239</sup> PBMCs were purified and infected with HIV and SIV, as described in detail by Schols *et al.*<sup>240</sup>

## **7.6. Experimental for internalisation, phosphorylation and degradation assays.**

### **7.6.1. Antibodies and reagents**

Goat polyclonal anti-CXCR4 was obtained from Abcam. Mouse monoclonal anti-GFP (clone 3E1), anti-EEA1, anti-ERK1/2, and anti-GAPDH were purchased from the Monoclonal Antibody Service of Cancer Research UK, BD Bioscience, Sigma, and Calbiochem, respectively. Rabbit monoclonal antibodies against p38 MAPK and Hsp27 were from Cell Signaling Technologies. Rabbit anti-phospho S324/S325 was raised against the phospho-peptide RG(pS)(pS)LKIL coupled to hemocyanin, affinity-purified, and purified against the phospho-peptide (contracted to AMSbio). Phosphor-specific antibodies against ERK1/2, p38 MAPK, and Hsp27 were purchased from Cell Signaling Technologies. Cy5-conjugated anti-Mouse and HRP-conjugated secondary antibodies were purchased from Jackson ImmunoResearch and Dako, respectively. Recombinant CXCL12/SDF1 $\alpha$  was obtained from Peprotech and generally used at 100 nM (unless otherwise indicated). AMD3100, cycloheximide (CHX), paraformaldehyde (PFA), and all standard laboratory chemicals were purchased from Sigma, PAA or VWR unless otherwise indicated.

### **7.6.2. Plasmids, cell lines, and cell culture conditions**

The EGFP-tagged CXCR4 construct has been described in detail.<sup>241, 242</sup> Briefly, it was obtained by sub-cloning the human CXCR4 coding sequence into the HindIII and EcoRI sites of pEGFP-N1 (Clontech), followed by further sub-cloning into the retroviral expression vector pLPCX (Clontech), and verification by DNA sequencing.

The retroviral plasmid and appropriate retroviral packaging plasmids were transfected into 293T cells by calcium phosphate transfection. Before transfection  $1 \times 10^6$  293T cells were seeded into 25 cm<sup>3</sup> flasks. Cells were transfected with 7  $\mu$ g pLPCX or pLHCX vectors carrying the desired constructs, together with 7  $\mu$ g of pVSV-G and 7  $\mu$ g of pGag-pol. After 8 h of incubation, the transfection media was replaced with fresh culture media. Two days later, the retrovirus containing supernatant was collected, sieved (40  $\mu$ m pores) and filtered (0.45  $\mu$ m pores)

before being aliquoted and stored at  $-80^{\circ}\text{C}$  until infection of target cells. Sub-confluent target cells were infected by overlaying the culture with retrovirus containing supernatant supplemented with  $8\ \mu\text{g}/\text{ml}$  polybrene and left for 8-16 h at  $37^{\circ}\text{C}$ . Subsequently, cells were washed and grown for 24 h before being added into selection medium (growth medium supplemented with  $2\ \mu\text{g}/\text{ml}$  puromycin). Single clones were expanded and grown until fluorescence levels were stable.

MTLn3E cells and all derived cell lines were maintained in an atmosphere of 5%  $\text{CO}_2$ /95% air in  $\alpha$ MEM medium (Sigma) supplemented with 5% FBS, with admixtures of selection antibiotics (puromycin and/or hygromycin) when necessary. 293T cells (ATCC) were grown in Dulbecco's modified MEM (Sigma) supplemented with 10% FBS in an atmosphere of 5%  $\text{CO}_2$ /95% air. In addition, all growth media contained 10 mg/ml L-glutamate, 100 U/ml penicillin, and 0.1 mg/ml streptomycin.

### **7.6.3. Receptor degradation assay**

Sub-confluent cells were stimulated with 100 nM CXCL12 in the presence of 40  $\mu\text{g}/\text{ml}$  CHX for indicated times and receptor degradation was quantified *via* immunoblot analysis using the indicated antibodies.

### **7.6.4. Immunoblot analysis**

Cells were lysed in 1.5-fold sample buffer (92.5 mM Tris/HCl pH 8.5, 0.75% (w/w) lithium dodecylsulfate, 3.75% (w/w) glycerol, 0.2 mM EDTA) and the protein concentrations of the resulting lysates were determined using the BCA protein assay kit (Pierce). Equal amounts of protein were supplemented with 100 mM DTT and 0.06 mM Serva Blue G250 (Serva), boiled, and subjected to electrophoresis using SDS-PAGE before being transferred to PVDF Immobilon membranes (Millipore). Membranes were blocked with 4% (w/v) BSA in TBS-T for 30 min, followed by incubation with primary antibody over night at  $4^{\circ}\text{C}$ , washed four times with TBS-T, and incubated with the appropriated HRP-conjugated secondary antibody for 45 min at RT. The signal was detected with the ECL kit (Pierce) following the manufacturer's instructions. Quantification was afforded by densitometry using ImageJ software (NIH).

### **7.6.5. Confocal microscopy**

For immunofluorescence experiments sub-confluent cells were treated as indicated, fixed with 4% (w/v) PFA, permeabilized (0.3% (v/v) Triton X-100 in PBS), treated with NaBH<sub>4</sub> (1 mg/ml in PBS) and stained with indicated antibodies and the nuclear stain Hoechst 33342 (Merck). Samples were mounted in MOWIOL® containing 2.5% (w/w) DABCO as antifade before being imaged by confocal microscopy using a LSM 510 META (Zeiss). Identical channel settings were used for acquiring all images in one experiment. For the purpose of better visualization to the reader contrast-enhancements were made in merged images only. Co-localization analysis was performed on raw data using the ImageJ plug-in JACoP.<sup>243</sup>

### **7.6.6. Statistical methods**

All statistical analyses were performed with the Student's *t*-test and *P*-values were calculated underlying the Student distribution. Numbers included in the various sections as well as error bars in diagrams of pooled data indicate mean ± SEM.

## References

1. W. Y. Huang and J. J. Davis, *Dalton Trans.*, 2011, **40**, 6087-6103.
2. E. S. Olson, T. Jiang, T. A. Aguilera, Q. T. Nguyen, L. G. Ellies, M. Scadeng and R. Y. Tsien, *Proc. Natl. Acad. Sci. U. S. A.*, 2010, **107**, 4311-4316.
3. N. Rapoport, A. M. Kennedy, J. E. Shea, C. L. Scaife and K. H. Nam, *Mol. Pharmaceut.*, 2010, **7**, 22-31.
4. Q. T. Nguyen, E. S. Olson, T. A. Aguilera, T. Jiang, M. Scadeng, L. G. Ellies and R. Y. Tsien, *Proc. Natl. Acad. Sci. U. S. A.*, 2010, **107**, 4317-4322.
5. J. Kim, Y. Piao and T. Hyeon, *Chem. Soc. Rev.*, 2009, **38**, 372-390.
6. J. S. Guthi, S. G. Yang, G. Huang, S. Z. Li, C. Khemtong, C. W. Kessinger, M. Peyton, J. D. Minna, K. C. Brown and J. M. Gao, *Mol. Pharmaceut.*, 2010, **7**, 32-40.
7. Z. M. Li, P. Huang, X. J. Zhang, J. Lin, S. Yang, B. Liu, F. Gao, P. Xi, Q. S. Ren and D. X. Cui, *Mol. Pharmaceut.*, 2010, **7**, 94-104.
8. C. K. Huang, C. L. Lo, H. H. Chen and G. H. Hsiue, *Adv. Funct. Mater.*, 2007, **17**, 2291-2297.
9. M. Shokeen and C. J. Anderson, *Acc. Chem. Res.*, 2009, **42**, 832-841.
10. D. Raman, P. J. Baugher, Y. M. Thu and A. Richmond, *Cancer Lett.*, 2007, **256**, 137-165.
11. M. M. Martinez, R. D. Reif and D. Pappas, *Anal. Methods*, 2010, **2**, 996-1004.
12. G. J. Kelloff, K. A. Krohn, S. M. Larson, R. Weissleder, D. A. Mankoff, J. M. Hoffman, J. M. Link, K. Z. Guyton, W. C. Eckelman, H. I. Scher, J. O'Shaughnessy, B. D. Cheson, C. C. Sigman, J. L. Tatum, G. Q. Mills, D. C. Sullivan and J. Woodcock, *Clin. Cancer Res.*, 2005, **11**, 7967-7985.
13. P. T. Winnard, A. P. Pathak, S. Dhara, S. Y. Cho, V. Raman and M. G. Pomper, *J. Nucl. Med.*, 2008, **49**, 96-112.
14. R. N. Moule, I. Kayani, S. A. Moinuddin, K. Meer, C. Lemon, K. Goodchild and M. I. Saunders, *Radiother. Oncol.*, 2010, **97**, 189-193.
15. R. M. Glasspool and T. R. J. Evans, *Eur. J. Cancer*, 2000, **36**, 1661-1670.
16. D. A. Torigan, S. S. Huang, M. Houseni and A. Alavi, *Ca-Cancer J. Clin.*, 2007, **57**, 206-224.
17. D. A. Mankoff, J. M. Link, H. M. Linden, L. Sundararajan and K. A. Krohn, *J. Nucl. Med.*, 2008, **49**, 149-163.
18. A. Signore, A. Annovazzi, M. Chianelli, F. Corsetti, C. Van de Wiele, R. N. Watherhouse and F. Scopinaro, *Eur. J. Nucl. Med.*, 2001, **28**, 1555-1565.
19. J. L. Wang and L. Maurer, *Curr. Top. Med. Chem.*, 2005, **5**, 1053-1075.
20. K. Serdons, A. Verbruggen and G. M. Bormans, *Methods*, 2009, **48**, 104-111.
21. M. Baggiolini, B. Dewald and B. Moser, *Annu. Rev. Immunol.*, 1997, **15**, 675-705.
22. A. E. I. Proudfoot, *Nat. Rev. Immunol.*, 2002, **2**, 106-115.
23. K. Sokolov, J. Aaron, B. Hsu, D. Nida, A. Gillenwater, M. Follen, C. MacAulay, K. Adler-Storthz, B. Korgel, M. Descour, R. Pasqualini, W. Arap, W. Lam and R. Richards-Kortum, *Technol. Cancer. Res. T.*, 2003, **2**, 491-504.
24. J. Kovar, M. Simpson, A. Schutz-Geschwender and D. M. Olive, *Anal. Biochem.*, 2007, **367**, 1-12.

25. H. Schoder, E. C. Glass, A. P. Pecking, J. K. Harness, A. M. Wallace, P. Hirnle, J. L. Alberini, D. Vilain, S. M. Larson, C. K. Hoh and D. R. Vera, *Cancer Metast. Rev.*, 2006, **25**, 185-201.
26. T. Betancourt, K. Shah and L. Brannon-Peppas, *J. Mater. Sci: Mater. Med.*, 2009, **20**, 387-395.
27. V. Tolmachev, F. Y. Nilsson. C. Widstrom, K. Anderson, D. Rosik, L. Gedda, A. Wennborg and A. Orlova, *J. Nucl. Med.*, 2006, **47**, 846-853.
28. H. Zhang, D. Yee and C. Wang, *Nanomedicine*, 2008, **3**, 83-91.
29. X. Gao, L. W. K. Chung and S. Nie, *Methods Mol. Biol.*, 2007, **374**, 135-145.
30. J. J. Onuffer and R. Horuk, *Trends Pharmacol. Sci.*, 2002, **23**, 459-467.
31. A. Khan, J. Greenman and S. J. Archibald, *Curr. Med. Chem.*, 2007, **14**, 2257-2277.
32. A. Kalinkovich, S. Tavor, A. Avigdor, J. Kahn, A. Brill, I. Petit, P. Goichberg, M. Tesio, N. Netzer, E. Naparstek, I. Hardan, A. Nagler, I. Resnick, A. Tsimanis and T. Lapidot, *Cancer Res.*, 2006, **66**, 11013-11020.
33. O. Salvucci, A. Bouchard, A. Baccarelli, J. Dechenes, G. Sauter, R. Simon, R. Bianchi and M. Basik, *Breast Cancer Res. T.*, 2006, **97**, 275-283.
34. N. M. Zhou, Z. W. Luo, J. S. Luo, D. X. Liut, J. W. Hall, R. J. Pomerantz and Z. W. Huang, *J. Biol. Chem.*, 2001, **276**, 42826-42833.
35. L. O. Gerlach, R. T. Skerlj, G. J. Bridger and T. W. Schwartz, *J. Biol. Chem.*, 2001, **276**, 14153-14160.
36. K. Palczewski, T. Kumasaka, T. Hori, C. A. Behnke, H. Motoshima, B. A. Fox, I. Le Trong, D. C. Teller, T. Okada, R. E. Stenkamp, M. Yamamoto and M. Miyano, *Science*, 2000, **289**, 739-745.
37. B. L. Wu, E. Y. T. Chien, C. D. Mol, G. Fenalti, W. Liu, V. Katritch, R. Abagyan, A. Brooun, P. Wells, F. C. Bi, D. J. Hamel, P. Kuhn, T. M. Handel, V. Cherezov and R. C. Stevens, *Science*, 2010, **330**, 1066-1071.
38. K. Koizumi, S. Hojo, T. Akashi, K. Yasumoto and I. Saiki, *Cancer Science*, 2007, **98**, 1652-1658.
39. O. Jacobson, I. D. Weiss, L. Szajek, J. M. Farber and D. O. Kiesewetter, *Bioorg. Med. Chem.*, 2009, **17**, 1486-1493.
40. Y. Chen, G. Stamatoyannopoulos and C. Z. Song, *Cancer Res.*, 2003, **63**, 4801-4804.
41. G. Lazennec and A. Richmond, *Trends Mol. Med.*, 2010, **16**, 133-144.
42. S. P. Fricker, V. Anastassov, J. Cox, M. C. Darkes, O. Grujic, S. R. Idzan, J. Labrecque, G. Lau, R. M. Mosi, K. L. Nelson, L. Qin, Z. Santucci and R. S. Y. Wong, *Biochem. Pharmacol.*, 2006, **72**, 588-596.
43. A. Muller, B. Homey, H. Soto, N. Ge, D. Catron, M. E. Buchanan, T. McClanahan, E. Murphy, W. Yuan, S. N. Wagner, J. L. Barrera, A. Mohar, E. Verastegui and A. Zlotnik, *Nature*, 2001, **410**, 50-56.
44. H. Elias, *Coord. Chem. Rev.*, 1999, **187**, 37-73.
45. G. Alkhatib, C. Combadiere, C. C. Broder, Y. Feng, P. E. Kennedy, P. M. Murphy and E. A. Berger, *Science*, 1996, **272**, 1955-1958.
46. Y. Feng, C. C. Broder, P. E. Kennedy and E. A. Berger, *Science*, 1996, **272**, 872-877.

47. E. De Clercq, N. Yamamoto, R. Pauwels, M. Baba, D. Schols, H. Nakashima, J. Balzarini, Z. Debyser, B. A. Murrer and D. Schwartz, *Proc. Natl. Acad. Sci. U.S.A.*, 1992, **89**, 5286-5290.
48. E. De Clercq, N. Yamamoto, R. Pauwels, J. Balzarini, M. Witvrouw, K. Devreese, Z. Debyser, B. Rosenwirth, P. Peichl, R. Datema, D. Thornton, R. Skerlj, F. Gaul, S. Padmanabhan, G. Bridger, G. Henson and M. Abrams, *Antimicrob. Agents Chemother.*, 1994, **38**, 668-674.
49. A. Ross, D. C. Soares, D. Covelli, C. Pannecouque, L. Budd, A. Collins, N. Robertson, S. Parsons, E. De Clercq, P. Kennepohl and P. J. Sadler, *Inorg. Chem.*, 2010, **49**, 1122-1132.
50. D. K. Cabbiness and D. W. Margerum, *J. Am. Chem. Soc.*, 1969, **91**, 6540-6541.
51. N. F. Curtis, *J. Chem.Soc.*, 1964, 2644-2650.
52. J. Plutnar, J. Havlickova, J. Kotek, P. Hermann and I. Lukes, *New J. Chem.*, 2008, **32**, 496-504.
53. J. D. Silversides, C. C. Allan and S. J. Archibald, *Dalton Trans.*, 2007, 971-978.
54. S. Hatse, K. Princen, E. De Clercq, M. M. Rosenkilde, T. W. Schwartz, P. E. Hernandez-Abad, R. T. Skerlj, G. J. Bridger and D. Schols, *Biochem. Pharmacol.*, 2005, **70**, 752-761.
55. A. Y. Odendaal, A. L. Fiamengo, R. Ferdani, T. J. Wadas, D. C. Hill, Y. J. Peng, K. J. Heroux, J. A. Golen, A. L. Rheingold, C. J. Anderson, G. R. Weisman and E. H. Wong, *Inorg. Chem.*, 2011, **50**, 3078-3086.
56. J. A. Este, C. Cabrera, E. De Clercq, S. Struyf, J. Van Damme, G. Bridger, R. T. Skerlj, M. J. Abrams, G. Henson, A. Gutierrez, B. Clotet and D. Schols, *Mol. Pharmacol.*, 1999, **55**, 67-73.
57. S. J. Paisey and P. J. Sadler, *Chem. Commun.*, 2004, 306-307.
58. G. C. Valks, G. McRobbie, E. A. Lewis, T. J. Hubin, T. M. Hunter, P. J. Sadler, C. Pannecouque, E. De Clercq and S. J. Archibald, *J. Med. Chem.*, 2006, **49**, 6162-6165.
59. B. Bosnich, C. K. Poon and M. L. Tobe, *Inorg. Chem.*, 1965, **4**, 1102-1108.
60. T. M. Hunter, I. W. McNae, D. P. Simpson, A. M. Smith, S. Moggach, F. White, M. D. Walkinshaw, S. Parsons and P. J. Sadler, *Chemistry*, 2007, **13**, 40-50.
61. X. Y. Liang, M. Weishaupl, J. A. Parkinson, S. Parsons, P. A. McGregor and P. J. Sadler, *Chem-Eur. J.*, 2003, **9**, 4709-4717.
62. X. Y. Liang and P. J. Sadler, *Chem. Soc. Rev.*, 2004, **33**, 246-266.
63. A. Khan, G. Nicholson, J. Greenman, L. Madden, G. McRobbie, C. Pannecouque, E. De Clercq, R. Ullom, D. L. Maples, R. D. Maples, J. D. Silversides, T. J. Hubin and S. J. Archibald, *J. Am. Chem. Soc.*, 2009, **131**, 3416-3417.
64. R. D. Hancock, S. M. Dobson, A. Evers, P. W. Wade, M. P. Ngwenya, J. C. A. Boeyens and K. P. Wainwright, *J. Am. Chem. Soc.*, 1988, **110**, 2788-2794.
65. K. P. Wainwright, *Inorg. Chem.*, 1980, **19**, 1396-1398.
66. G. R. Weisman, M. E. Rogers, E. H. Wong, J. P. Jasinski and E. S. Paight, *J. Am. Chem. Soc.*, 1990, **112**, 8604-8605.
67. T. J. Wadas, E. H. Wong, G. R. Weisman and C. J. Anderson, *Chem. Rev.*, 2010, **110**, 2858-2902.

68. J. D. Silversides, R. Smith and S. J. Archibald, *Dalton Trans.*, 2011, **40**, 6289-6297.
69. E. De Clercq, *Mol. Pharmacol.*, 2000, **57**, 833-839.
70. C. A. Boswell, C. A. S. Regino, K. E. Baidoo, K. J. Wong, D. E. Milenic, J. A. Kelley, C. C. Lai and M. W. Brechbiel, *Bioorg. Med. Chem.*, 2009, **17**, 548-552.
71. I. Sehgal, M. Sibrian-Vazquez and M. G. H. Vicente, *J. Med. Chem.*, 2008, **51**, 6014-6020.
72. C. Alonso, R. W. Boyle, in *Handbook of Porphyrin Science*, World Scientific, London, 2010.
73. L. B. Josefsen and R. W. Boyle, *Metal Based Drugs*, 2008, **2008**, 1-24.
74. M. Bhatti, G. Yahiolu, L. R. Milgrom, M. Garcia-Maya, K. A. Chester and M. P. Deonarain, *Int. J. Cancer*, 2008, **123**, 245-245.
75. R. Bonnett, *Chem. Soc. Rev.*, 1995, **24**, 19-33.
76. F. Giuntini, C. M. A. Alonso and R. W. Boyle, *Photochem. Photobiol. Sci.*, 2011, **10**, 759-791.
77. H. R. Li, T. J. Jensen, F. R. Fronczek and M. G. H. Vicente, *J. Med. Chem.*, 2008, **51**, 502-511.
78. H. R. Li, N. Nguyen, F. R. Fronczek and M. G. H. Vicente, *Tetrahedron*, 2009, **65**, 3357-3363.
79. M. K. Kuimova, M. Bhatti, M. Deonarain, G. Yahiolu, J. A. Levitt, I. Stamati, K. Suhling and D. Phillips, *Photochem. Photobiol. Sci.*, 2007, **6**, 933-939.
80. B. Di Stasio, C. Frochot, D. Dumas, P. Even, J. Zwier, A. Muller, J. Didelon, F. Guillemin, M. L. Viriot and M. Barberi-Heyob, *Eur. J. Med. Chem.*, 2005, **40**, 1111-1122.
81. M. Sibrian-Vazquez, T. J. Jensen, R. P. Hammer and M. G. H. Vicente, *J. Med. Chem.*, 2006, **49**, 1364-1372.
82. C. M. A. Alonso, A. Palumbo, A. J. Bullous, F. Pretto, D. Neri and R. W. Boyle, *Bioconjug. Chem.*, 2010, **21**, 302-313.
83. G. A. M. S. van Dongen, G. W. M. Visserb, M. B. Vrouenraets, *Adv. Drug Deliv. Rev.*, 2004, **56**, 31-52.
84. Y. Zorlu, F. Dumoulin, D. Bouchu, V. Ahsen and D. Lafont, *Tetrahedron Lett.*, 2010, **51**, 6615-6618.
85. M. Sibrian-Vazquez, T. J. Jensen and M. G. H. Vicente, *J. Med. Chem.*, 2008, **51**, 2915-2923.
86. L. Chaloin, P. Bigey, C. Loup, M. Marin, N. Gaelotti, M. Piechaczyk, F. Heitz and B. Meunier, *Bioconjug. Chem.*, 2001, **12**, 691-700.
87. M. Qin, H. J. Hah, G. Kim, G. C. Nie, Y. E. K. Lee and R. Kopelman, *Photochem. Photobiol. Sci.*, 2011, **10**, 832-841.
88. K. Zaruba, J. Kralova, P. Rezanka, P. Pouckova, L. Veverkova and V. Kral, *Org. Biomol. Chem.*, 2010, **8**, 3202-3206.
89. T. Stuchinskaya, M. Moreno, M. J. Cook, D. R. Edwards and D. A. Russell, *Photochem. Photobiol. Sci.*, 2011, **10**, 822-831.
90. P. Blower, *Dalton Trans.*, 2006, 1705-1711.
91. M. E. Phelps, E. J. Hoffman, N. A. Mullani and M. M. Terpogossian, *J. Nucl. Med.*, 1975, **16**, 210-224.
92. P. W. Miller, *J. Chem. Tech. Biot.*, 2009, **84**, 309-315.

93. P. W. Miller, N. J. Long, R. Vilar and A. D. Gee, *Angew. Chem. Int. Edit.*, 2008, **47**, 8998-9033.
94. S. J. Mather, *Mol. Biosyst.*, 2007, **3**, 30-35.
95. R. E. Coleman, *Cancer*, 1991, **67**, 1261-1270.
96. K. A. Wood, P. J. Hoskin and M. I. Saunders, *Clin. Oncol.*, 2007, **19**, 237-255.
97. D. A. Mankoff, J. F. Eary, J. M. Link, M. Muzi, J. G. Rajendran, A. M. Spence and K. A. Krohn, *Clin. Cancer Res.*, 2007, **13**, 3460-3469.
98. N. E. Avril and W. A. Weber, *Radiol. Clin. North Am.*, 2005, **43**, 189-204.
99. Z. B. Li and P. S. Conti, *Adv. Drug Deliver. Rev.*, 2010, **62**, 1031-1051.
100. B. M. Zeglis and J. S. Lewis, *Dalton Trans.*, 2011, **40**, 6168-6195.
101. C. J. Anderson and R. Ferdani, *Cancer Biother. Radio.*, 2009, **24**, 379-393.
102. K. Abbas, J. Kozempel, M. Bonardi, F. Groppi, A. Alfarano, U. Holzwarth, F. Simonelli, H. Hofman, W. Horstmann, E. Menapace, L. Leseticky and N. Gibson, *Appl. Radiat. Isot.*, 2006, **64**, 1001-1005.
103. T. J. Wadas, E. H. Wong, G. R. Weisman and C. J. Anderson, *Curr. Pharm. Des.*, 2007, **13**, 3-16.
104. R. E. Mewis and S. J. Archibald, *Coord. Chem. Rev.*, 2010, **254**, 1686-1712.
105. L. Wei, Y. Ye, T. J. Wadas, J. S. Lewis, M. J. Welch, S. Achilefu and C. J. Anderson, *Nucl. Med. Biol.*, 2009, **36**, 277-285.
106. P. D. Bonnitcho, S. R. Bayly, M. B. M. Theobald, H. M. Betts, J. S. Lewis and J. R. Dilworth, *J. Inorg. Biochem.*, 2010, **104**, 126-135.
107. C. J. Anderson, J. M. Connett, S. W. Schwarz, P. A. Rocque, L. W. Guo, G. W. Philpott, K. R. Zinn, C. F. Meares and M. J. Welch, *J. Nucl. Med.*, 1992, **33**, 1685-1691.
108. X. K. Sun, M. Wuest, G. R. Weisman, E. H. Wong, D. P. Reed, C. A. Boswell, R. Motekaitis, A. E. Martell, M. J. Welch and C. J. Anderson, *J. Med. Chem.*, 2002, **45**, 469-477.
109. L. A. Bass, M. Wang, M. J. Welch and C. J. Anderson, *Bioconjug. Chem.*, 2000, **11**, 527-532.
110. C. A. Boswell, X. K. Sun, W. J. Niu, G. R. Weisman, E. H. Wong, A. L. Rheingold and C. J. Anderson, *J. Med. Chem.*, 2004, **47**, 1465-1474.
111. S. Nimmagadda, M. Pullambhatla, K. Stone, G. Green, Z. M. Bhujwalla and M. G. Pomper, *Cancer Res.*, 2010, **70**, 3935-3944.
112. I. D. Weiss, O. Jacobson, D. O. Keisewetter, J. P. Jacobus, L. P. Szajek, X. Chen, and J. M. Farber, *Mol. Imaging Biol.*, 2012, **14**, 106-114.
113. X. Y. Liang, J. A. Parkinson, M. Weishaupl, R. O. Gould, S. J. Paisey, H. S. Park, T. M. Hunter, C. A. Blindauer, S. Parsons and P. J. Sadler, *J. Am. Chem. Soc.*, 2002, **124**, 9105-9112.
114. J. R. Morphy, D. Parker, R. Katakya, M. A. W. Eaton, A. T. Millican, R. Alexander, A. Harrison and C. Walker, *J. Chem. Soc.-Perkin Trans. 2*, 1990, 573-585.
115. E. A. Lewis, C. C. Allan, R. W. Boyle and S. J. Archibald, *Tetrahedron Lett.*, 2004, **45**, 3059-3062.
116. E. A. Lewis, R. W. Boyle and S. J. Archibald, *Chem. Commun.*, 2004, 2212-2213.

117. C. S. Cutler, M. Wuest, C. J. Anderson, D. E. Reichert, Y. Z. Sun, A. E. Martell and M. J. Welch, *Nucl. Med. Biol.*, 2000, **27**, 375-380.
118. A. E. Goeta, J. A. K. Howard, D. Maffeo, H. Puschmann, J. A. G. Williams and D. S. Yufit, *J. Chem. Soc.-Dalton Trans.*, 2000, 1873-1880.
119. J. M. Slocik, M. S. Ward and R. E. Shepherd, *Inorg. Chim. Acta*, 2001, **317**, 290-303.
120. Y. Rousselin, N. Sok, F. Boschetti, R. Guilard and F. Denat, *Eur. J. Org. Chem.*, 2010, 1688-1693.
121. R. D. Hancock, G. Pattrick, P. W. Wade and G. D. Hosken, *Pure Appl. Chem.*, 1993, **65**, 473-476.
122. A. Ramasubbu and K. P. Wainwright, *J. Chem. Soc.- Chem. Commun.*, 1982, 277-278.
123. A. Khan, J. D. Silversides, L. Madden, J. Greenman and S. J. Archibald, *Chem. Commun.*, 2007, **1**, 416-418.
124. A. B. A. Bencini, C. Bazzicalupi, M. Ciampolini, V. Fusi, M. Micheloni, N. Nardi, P. Paoli, B. Valtancoli, *Supramol. Chem.*, 1994, **3**, 141-146.
125. T. J. Hubin, J. M. McCormick, N. W. Alcock, H. J. Clase and D. H. Busch, *Inorg. Chem.*, 1999, **38**, 4435-4446.
126. E. H. Wong, G. R. Weisman, D. C. Hill, D. P. Reed, M. E. Rogers, J. S. Condon, M. A. Fagan, J. C. Calabrese, K. Lam, I. A. Guzei and A. L. Rheingold, *J. Am. Chem. Soc.*, 2000, **122**, 10561-10572.
127. W. J. Niu, E. H. Wong, G. R. Weisman, L. N. Zakharov, C. D. Incarvito and A. L. Rheingold, *Polyhedron*, 2004, **23**, 1019-1025.
128. K. J. Heroux, K. S. Woodin, D. J. Tranchemontagne, P. C. B. Widger, E. Southwick, E. H. Wong, G. R. Weisman, S. A. Tomellini, T. J. Wadas, C. J. Anderson, S. Kassel, J. A. Golen and A. L. Rheingold, *Dalton Trans.*, 2007, 2150-2162.
129. R. Ferdani, D. J. Stigers, A. L. Fiamengo, L. Wei, B. T. Y. Li, J. A. Golen, A. L. Rheingold, G. R. Weisman, E. H. Wong and C. J. Anderson, *Dalton Trans.*, 2012, **41**, 1938-1950.
130. E. K. Barefield, F. Wagner, A. W. Herlinger and A. R. Dahl, *Inorg. Synth.*, 1976, **16**, 220-225.
131. M. Le Baccon, F. Chuburu, L. Toupet, H. Handel, M. Soibinet, I. Dechamps-Olivier, J. Barbier and M. Aplincourt, *New J. Chem.*, 2001, **25**, 1168-1174.
132. R. Smith, D. Huskens, D. Daelemans, R. E. Mewis, C. D. Garcia, A. N. Cain, T. N. C. Freeman, C. Pannecouque, E. De Clercq, D. Schols, T. J. Hubin and S. J. Archibald, *Dalton Trans.*, 2012, **41**, 11369-11377.
133. R. A. Kolinski, *Pol. J. Chem.*, 1995, **69**, 1039-1045.
134. L. Lukesova, J. Ludvik, I. Cisarova and P. Stepnicka, *Collect. Czech. Chem. Commun.*, 2000, **65**, 1897-1910.
135. I. M. Helps, D. Parker, J. R. Morphy and J. Chapman, *Tetrahedron*, 1989, **45**, 219-226.
136. Y. Zhang, C. E. Ballard, S. Zheng, X. Gao, K. Ko, H. Yang, G. Brandt, X. Lou, P. C. Tai, C. Lu, and B. Wang, *Bioorg. Med. Chem. Lett.*, 2007, 707-711.

137. A. Hackling, R. Ghosh, S. Perachon, A. Mann, H. D. Holtje, C. G. Wermuth, J. C. Schwartz, W. Sippl, P. Sokoloff and H. Stark, *J. Med. Chem.*, 2003, **46**, 3883-3899.
138. L. Leonard, B. Lygo, G. Procter, *Advanced Practical Organic Chemistry*, Chapman and Hall, UK, 1995.
139. L. Ronconi and P. J. Sadler, *Coord. Chem. Rev.*, 2007, **251**, 1633-1648.
140. E. De Clercq, *Nat. Rev. Drug Discov.*, 2003, **2**, 581- 587.
141. G. J. Bridger, R. T. Skerlj, D. Thornton, S. Padmanabhan, S. A. Martellucci, G. W. Henson, M. J. Abrams, N. Yamamoto, K. Devreese, R. Pauwels and E. De Clercq, *J. Med. Chem.*, 1995, **38**, 366-378.
142. G. J. Bridger, R. T. Skerlj, S. Padmanabhan, S. A. Martellucci, G. W. Henson, M. J. Abrams, H. C. Joao, M. Witvrouw, K. DeVreese, R. Pauwels and E. De Clercq, *J. Med. Chem.*, 1996, **39**, 109-119.
143. M. Ramli, S. V. Smith and L. F. Lindoy, *Bioconjug. Chem.*, 2009, **20**, 868-876.
144. N. Bernier, R. Tripier, V. Patinec, M. Le Baccon and H. Handel, *C. R. Chimie*, 2007, **10**, 832-838.
145. J. Costa, E. Balogh, V. Turcry, R. Tripier, M. Le Baccon, F. Chuburu, H. Handel, L. Helm, E. Toth and A. E. Merbach, *Chem-Eur. J.*, 2006, **12**, 6841-6851.
146. T. Gunnlaugsson, J. P. Leonard, S. Mulready and M. Nieuwenhuyzen, *Tetrahedron*, 2004, **60**, 105-113.
147. S. J. A. Pope, A. M. Kenwright, V. A. Boote and S. Faulkner, *Dalton Trans.*, 2003, 3780-3784.
148. S. Develay, R. Tripier, M. Le Baccon, V. Patinec, G. Serratrice and H. Handel, *Dalton Trans.*, 2006, 3418-3426.
149. T. Tanaka, T. Narumi, T. Ozaki, A. Sohma, N. Ohashi, C. Hashimoto, K. Itotani, W. Nomura, T. Murakami, Y. B. Naoki and H. Tamamura, *Chemmedchem*, 2011, **6**, 834-839.
150. H. P. Xi, C. L. D. Gibb and B. C. Gibb, *J. Org. Chem.*, 1999, **64**, 9286-9288.
151. M. W. Easson, F. R. Fronczek, T. J. Jensen and M. G. H. Vicente, *Bioorg. Med. Chem.*, 2008, **16**, 3191-3208.
152. K. D. Karlin, M. S. Nasir, B. I. Cohen, R. W. Cruse, S. Kaderli and A. D. Zuberbuhler, *J. Am. Chem. Soc.*, 1994, **116**, 1324-1336.
153. G. J. Bodwell, J. N. Bridson, T. J. Houghton and B. Yarlagadda, *Tetrahedron Lett.*, 1997, **38**, 7475-7478.
154. J. L. Segura, R. Gomez, N. Martin and D. M. Guldi, *Org. Lett.*, 2001, **3**, 2645-2648.
155. T. H. Fisher, S. M. Dershem and M. L. Prewitt, *J. Org. Chem.*, 1990, **55**, 1040-1043.
156. T. J. Hubin, J. M. McCormick, S. R. Collinson, N. W. Alcock and D. H. Busch, *Chem. Commun.*, 1998, 1675-1676.
157. D. Oltmanns, S. Zitzmann-Kolbe, A. Mueller, U. Bauder-Wuest, M. Schaefer, M. Eder, U. Haberkorn and M. Eisenhut, *Bioconjug. Chem.*, 2011, **22**, 2611-2624.
158. J. Dessolin, P. Galea, P. Vlieghe, J. C. Chermann and J. L. Kraus, *J. Med. Chem.*, 1999, **42**, 229-241.
159. C. Montalbetti and V. Falque, *Tetrahedron*, 2005, **61**, 10827-10852.

160. J. Kuril, T. Buckle, H. Yuan, N. S. van den Berg, S. Oishi, N. Fujii, L. Josephson and F. W. B. van Leeuwen, *Bioconjug. Chem.*, 2011, **22**, 859-864.
161. G. Quelever, P. Kachidian, C. Melon, C. Garino, Y. Laras, N. Pietrancosta, M. Sheha and J. L. Kraus, *Org. Biomol. Chem.*, 2005, **3**, 2450-2457.
162. L. A. Carpino, B. J. Cohen, K. E. Stephens, S. Y. Sadataalae, J. H. Tien and D. C. Langridge, *J. Org. Chem.*, 1986, **51**, 3732-3734.
163. T. F. Buckley and H. Rapoport, *J. Am. Chem. Soc.*, 1982, **104**, 4446-4450.
164. Q. I. M. de Chermont, C. Chaneac, J. Seguin, F. Pelle, S. Maitrejean, J.-P. Jolivet, D. Gourier, M. Bessodes and D. Scherman, *Proc. Natl. Acad. Sci. U. S. A.*, 2007, **104**, 9266-9271.
165. W. B. Bruner and L. T. Sherwood, *Ind. Eng. Chem.*, 1949, **41**, 1653-1656.
166. Daiichi Pure Chemicals, 2005, **US2005/49313A1**.
167. C. A. Boswell, C. A. S. Regino, K. E. Baidoo, K. J. Wong, A. Bumb, H. Xu, D. E. Milenic, J. A. Kelley, C. C. Lai and M. W. Brechbiel, *Bioconjug. Chem.*, 2008, **19**, 1476-1484.
168. J. E. Sprague, Y. J. Peng, X. K. Sun, G. R. Weisman, E. H. Wong, S. Achilefu and C. J. Anderson, *Clin. Cancer Res.*, 2004, **10**, 8674-8682.
169. S. De Luca, D. Tesauro, P. Di Lello, R. Fattorusso, M. Saviano, C. Pedone and G. Morelli, *J. Pept. Sci.*, 2001, **7**, 386-394.
170. S. Rahimipour, N. Ben-Aroya, K. Ziv, A. Chen, M. Fridkin and Y. Koch, *J. Med. Chem.*, 2003, **46**, 3965-3974.
171. N. M. Green, *Methods Enzymol.*, 1990, **184**, 51-67.
172. E. A. Gould, A. Buckley and N. Cammack, *J. Virol. Methods*, 1985, **11**, 41-48.
173. P. C. Weber, D. H. Ohlendorf, J. J. Wendoloski and F. R. Salemme, *Science*, 1989, **243**, 85-88.
174. D. S. Wilbur, P. M. Pathare, D. K. Hamlin, P. S. Stayton, R. To, L. A. Klumb, K. R. Buhler and R. L. Vessella, *Biomol. Eng.*, 1999, **16**, 113-118.
175. U. Piran and W. J. Riordan, *J. Immunol. Methods*, 1990, **133**, 141-143.
176. D. L. Meyer, J. Schultz, Y. K. Lin, A. Henry, J. Sanderson, J. M. Jackson, S. Goshorn, A. R. Rees and S. S. Graves, *Protein Sci.*, 2001, **10**, 491-503.
177. M. Bodanszky and D. T. Fagan, *J. Am. Chem. Soc.*, 1977, **99**, 235-239.
178. J. A. Burger and T. J. Kipps, *Blood*, 2006, **107**, 1761-1767.
179. B. A. Teicher and S. P. Fricker, *Clin. Cancer Res.*, 2010, **16**, 2927-2931.
180. V. Saini, A. Marchese and M. Majetschak, *J. Biol. Chem.*, 2010, **285**, 15566-15576.
181. F. Sierro, C. Biben, L. Martinez-Munoz, M. Mellado, R. M. Ransohoff, M. Li, B. Woehl, H. Leung, J. Groom, M. Batten, R. P. Harvey, C. Martinez-A, C. R. Mackay and F. Mackay, *Proc. Natl. Acad. Sci. U. S. A.*, 2007, **104**, 14759-14764.
182. W. C. Liles, H. E. Broxmeyer, E. Rodger, B. Wood, K. Hubel, S. Cooper, G. Hangoc, G. J. Bridger, G. W. Henson, G. Calandra and D. C. Dale, *Blood*, 2003, **102**, 2728-2730.
183. C. C. Bleul, J. L. Schultze and T. A. Springer, *J. Exp. Med.*, 1998, **187**, 753-762.
184. A. E. Hauser, G. F. Debes, S. Arce, G. Cassese, A. Hamann, A. Radbruch and R. A. Manz, *J. Immunol.*, 2002, **169**, 1277-1282.

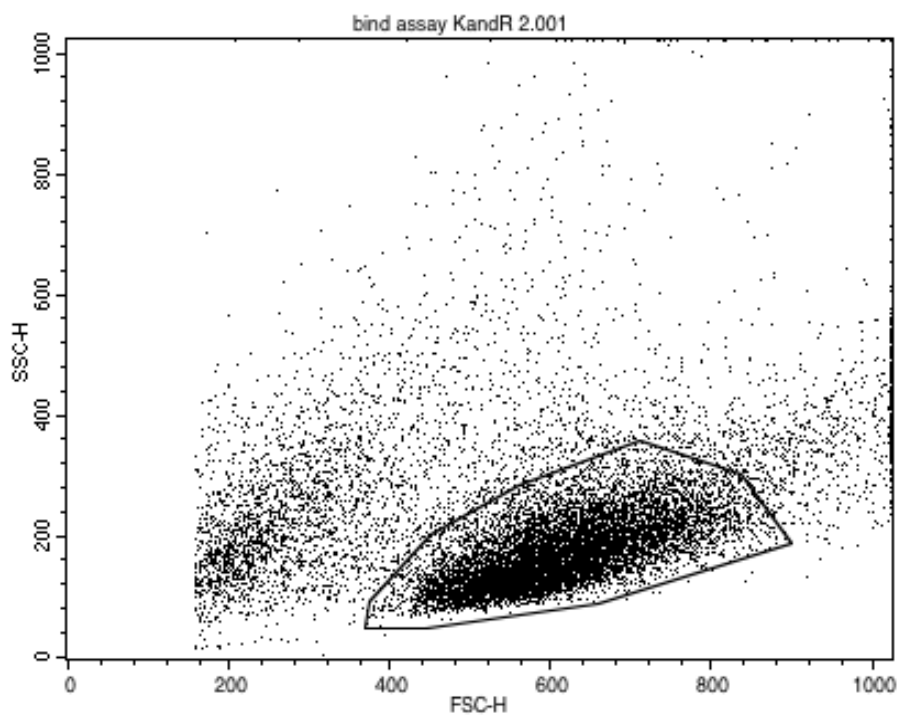
185. W. Lu, J. A. Gersting, A. Maheshwari, R. D. Christensen and D. A. Calhoun, *Early Hum. Dev.*, 2005, **81**, 489-496.
186. E. A. Berger, P. M. Murphy and J. M. Farber, *Annu. Rev. Immunol.*, 1999, **17**, 657-700.
187. X. Sun, G. Cheng, M. Hao, J. Zheng, X. Zhou, J. Zhang, R. S. Taichman, K. J. Pienta and J. Wang, *Cancer Metast. Rev.*, 2010, **29**, 709-722.
188. T. Murakami, A. R. Cardones and S. T. Hwang, *J. Dermatol. Sci.*, 2004, **36**, 71-78.
189. H. Tamamura, Y. O. Xu, T. Hattori, X. Y. Zhang, R. Arakaki, K. Kanbara, A. Omagari, A. Otaka, T. Ibuka, N. Yamamoto, H. Nakashima and N. Fujii, *Biochem. Biophys. Res. Commun.*, 1998, **253**, 877-882.
190. D. Schols, *Curr. Top. Med. Chem.*, 2004, **4**, 883-893.
191. D. Daelemans, D. Schols, M. Witvrouw, C. Pannecouque, S. Hatse, S. van Dooren, F. Hamy, T. Klimkait, E. De Clercq and A. M. Vandamme, *Mol. Pharmacol.*, 2000, **57**, 116-124.
192. K. Ichiyama, S. Yokoyama-Kumakura, Y. Tanaka, R. Tanaka, K. Hirose, K. Bannai, T. Edamatsu, M. Yanaka, Y. Niitani, N. Miyano-Kurosaki, H. Takaku, Y. Koyanagi and N. Yamamoto, *Proc. Natl. Acad. Sci. U. S. A.*, 2003, **100**, 4185-4190.
193. V. Bodart, V. Anastassov, M. C. Darkes, S. R. Idzan, J. Labrecque, G. Lau, R. M. Mosi, K. S. Neff, K. L. Nelson, M. C. Ruzek, K. Patel, Z. Santucci, R. Scarborough, R. S. Y. Wong, G. J. Bridger, R. T. MacFarland and S. P. Fricker, *Biochem. Pharmacol.*, 2009, **78**, 993-1000.
194. D. Schols, S. Claes, S. Hatse, K. Princen, K. Vermeire, E. De Clercq, R. Skerlj, G. Bridger and G. Calandra, *Antiviral Res.*, 2003, **57**, A39-A39.
195. H. E. Broxmeyer, C. M. Orschell, D. W. Clapp, G. Hangoc, S. Cooper, P. A. Plett, W. C. Liles, X. X. Li, B. Graham-Evans, T. B. Campbell, G. Calandra, G. Bridger, D. C. Dale and E. F. Srouf, *J. Exp. Med.*, 2005, **201**, 1307-1318.
196. T. M. Hunter, I. W. McNae, X. Y. Liang, J. Bella, S. Parsons, M. D. Walkinshaw and P. J. Sadler, *Proc. Natl. Acad. Sci. U. S. A.*, 2005, **102**, 2288-2292.
197. M. M. Rosenkilde, L. O. Gerlach, S. Hatse, R. T. Skerlj, D. Schols, G. J. Bridger and T. W. Schwartz, *J. Biol. Chem.*, 2007, **282**, 27345-27365.
198. G. J. Bridger, R. T. Skerlj, P. E. Hernandez-Abad, D. E. Bogucki, Z. R. Wang, Y. X. Zhou, S. Nan, E. M. Boehringer, T. Wilson, J. Crawford, M. Metz, S. Hatse, K. Princen, E. De Clercq and D. Schols, *J. Med. Chem.*, 2010, **53**, 1250-1260.
199. G. McRobbie, G. C. Valks, C. J. Empson, A. Khan, J. D. Silversides, C. Pannecouque, E. De Clercq, S. G. Fiddy, A. J. Bridgeman, N. A. Young and S. J. Archibald, *Dalton Trans.*, 2007, 5008-5018.
200. U. M. Domanska, R. C. Kruizinga, W. B. Nagengast, H. Timmer-Bosscha, G. Huls, E. G. E. de Vries and A. M. E. Walenkamp, *Eur. J. Cancer*, 2013, **49**, 219-230.
201. K. Princen, S. Hatse, K. Vermeire, E. De Clercq and D. Schols, *Cytometry Part A*, 2003, **51A**, 35-45.
202. T. M. Hunter, S. J. Paisey, H. S. Park, L. Cleghorn, A. Parkin, S. Parsons and P. J. Sadler, *J. Inorg. Biochem.*, 2004, **98**, 713-719.

203. J. P. C. Tome, M. Neves, A. C. Tomes, J. A. S. Cavaleiro, M. Soncin, M. Magaraggia, S. Ferro and G. Jori, *J. Med. Chem.*, 2004, **47**, 6649-6652.
204. M. Boisbrun, R. Vanderesse, P. Engrand, A. Olie, S. Hupont, J.-B. Regnouf-de-Vains and C. Frochot, *Tetrahedron*, 2008, **64**, 3494-3504.
205. J. R. Starkey, A. K. Rebane, M. A. Drobizhev, F. Meng, A. Gong, A. Elliott, K. McInnerney and C. W. Spangler, *Clin. Cancer Res.*, 2008, **14**, 6564-6573.
206. Y. Choi, J. R. McCarthy, R. Weissleder and C.-H. Tung, *Chemmedchem*, 2006, **1**, 458-463.
207. T. Arai, N. Maruo, Y. Sumida, C. Korosue and N. Nishino, *Chem. Commun.*, 1999, 1503-1504.
208. J. Shi, T. W. B. Liu, J. Chen, D. Green, D. Jaffray, B. C. Wilson, F. Wang and G. Zheng, *Theranostics*, 2011, **1**, 363-370.
209. M. Sibrian-Vazquez, T. J. Jensen, F. R. Fronczek, R. P. Hammer and M. G. H. Vicente, *Bioconjug. Chem.*, 2005, **16**, 852-863.
210. E. Biron and N. Voyer, *Chem. Commun.*, 2005, 4652-4654.
211. S. Weimin, Z. Gen, D. Guifu, Z. Yunxiao, Z. Jin and T. Jingchao, *Bioorg. Med. Chem.*, 2008, **16**, 5665-5671.
212. P. Rothmund, *J. Am. Chem. Soc.*, 1935, **57**, 2010-2011.
213. A. D. Adler, F. R. Longo, J. D. Finarelli, J. Goldmacher, J. Assour and L. Korsakoff, *J. Org. Chem.*, 1967, **32**, 476.
214. J. S. Lindsey, I. C. Schreiman, H. C. Hsu, P. C. Kearney and A. M. Marguerettaz, *J. Org. Chem.*, 1987, **52**, 827-836.
215. D. Gryko and J. S. Lindsey, *J. Org. Chem.*, 2000, **65**, 2249-2252.
216. A. D. Adler, F. R. Longo, J. D. Finarelli, L. Sklar and M. G. Finarelli, *J. Heterocycl. Chem.*, 1968, **5**, 669-678.
217. O. B. Locos, C. C. Heindl, A. Corral, M. O. Senge and E. M. Scanlan, *Eur. J. Org. Chem.*, 2010, 1026-1028.
218. J. M. Sutton, O. J. Clarke, N. Fernandez and R. W. Boyle, *Bioconjug. Chem.*, 2002, **13**, 249-263.
219. H. L. Anderson, *Chem. Commun.*, 1999, 2323-2330.
220. I. J. MacDonald and T. J. Dougherty, *J. Porphyr. Phthalocya.*, 2001, **5**, 105-129.
221. T. Elangovan and V. Krishnan, *Chem. Phys. Lett.*, 1992, **194**, 139-146.
222. A. Wickramasinghe, L. Jaquinod, D. J. Nurco and K. M. Smith, *Tetrahedron*, 2001, **57**, 4261-4269.
223. M. M. Catalano, M. J. Crossley, M. M. Harding and L. G. King, *J. Chem. Soc.-Chem. Commun.*, 1984, 1535-1536.
224. O. Siri, L. Jaquinod and K. M. Smith, *Tetrahedron Lett.*, 2000, **41**, 3583-3587.
225. J. E. Baldwin, M. J. Crossley and J. Debernardis, *Tetrahedron*, 1982, **38**, 685-692.
226. A. Giraudeau, H. J. Callot, J. Jordan, I. Ezhar and M. Gross, *J. Am. Chem. Soc.*, 1979, **101**, 3857-3862.
227. H. K. Hombrecher, V. M. Gherdan, S. Ohm, J. A. S. Cavaleiro, M. Neves and M. D. Condesso, *Tetrahedron*, 1993, **49**, 8569-8578.
228. P. Wyrebek and S. Ostrowski, *J. Porphyr. Phthalocya.*, 2007, **11**, 822-828.

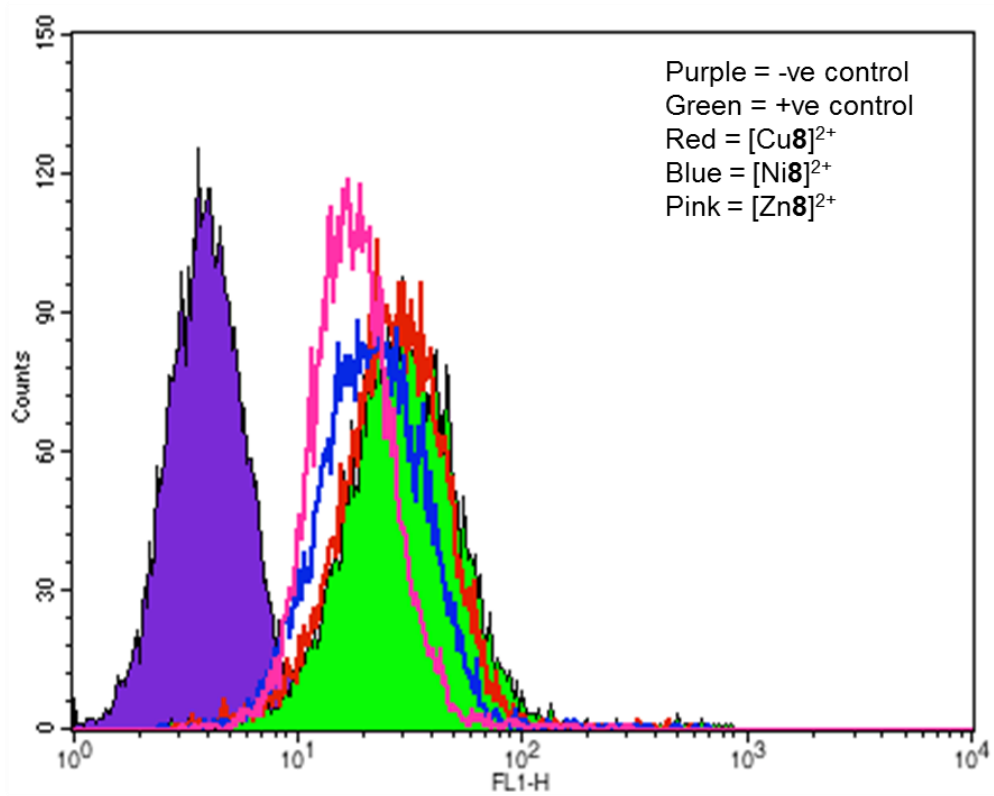
229. W. J. Kruper, T. A. Chamberlin and M. Kochanny, *J. Org. Chem.*, 1989, **54**, 2753-2756.
230. G. Z. G. Meng, B. R. James and K. A. Skov, *Can. J. Chem.*, 1994, **72**, 1894-1909.
231. S. Ostrowski, A. Mikus and B. Lopuszynska, *Tetrahedron*, 2004, **60**, 11951-11957.
232. R. Luguay, L. Jaquinod, F. R. Fronczek, A. G. H. Vicente and K. M. Smith, *Tetrahedron*, 2004, **60**, 2757-2763.
233. N. W. Smith and S. V. Dzyuba, *Arkivoc*, 2010, 10-18.
234. J. P. Collman, R. R. Gagne, C. A. Reed, T. R. Halbert, G. Lang and W. T. Robinson, *J. Am. Chem. Soc.*, 1975, **97**, 1427-1439.
235. A. Eggenspiller, *Personal Communication*, 2012.
236. D. Bradley, G. Williams and M. Lawton, *J. Org. Chem.*, 2010, **75**, 8351-8354.
237. S. Harada, Y. Koyanagi and N. Yamamoto, *Science*, 1985, **229**, 563-566.
238. C. Pannecoque, D. Daelemans and E. De Clercq, *Nat. Protoc.*, 2008, **3**, 427-434.
239. R. Pauwels, J. Balzarini, M. Baba, R. Snoeck, D. Schols, P. Herdewijn, J. Desmyter and E. De Clercq, *J. Virol. Methods*, 1988, **20**, 309-321.
240. D. Schols, S. Struyf, J. VanDamme, J. A. Este, G. Henson and E. De Clercq, *J. Exp. Med.*, 1997, **186**, 1383-1388.
241. N. I. Cade, G. Fruhwirth, S. J. Archibald, T. Ng and D. Richards, *Biophys. J.*, 2010, **98**, 2752-2757.
242. G. O. Fruhwirth, S. Ameer-Beg, R. Cook, T. Watson, T. Ng and F. Festy, *Opt. Express*, 2010, **18**, 11148-11158.
243. S. Bolte and F. P. Cordelieres, *J. Microsc-Oxford*, 2006, **224**, 213-232.

## Appendix

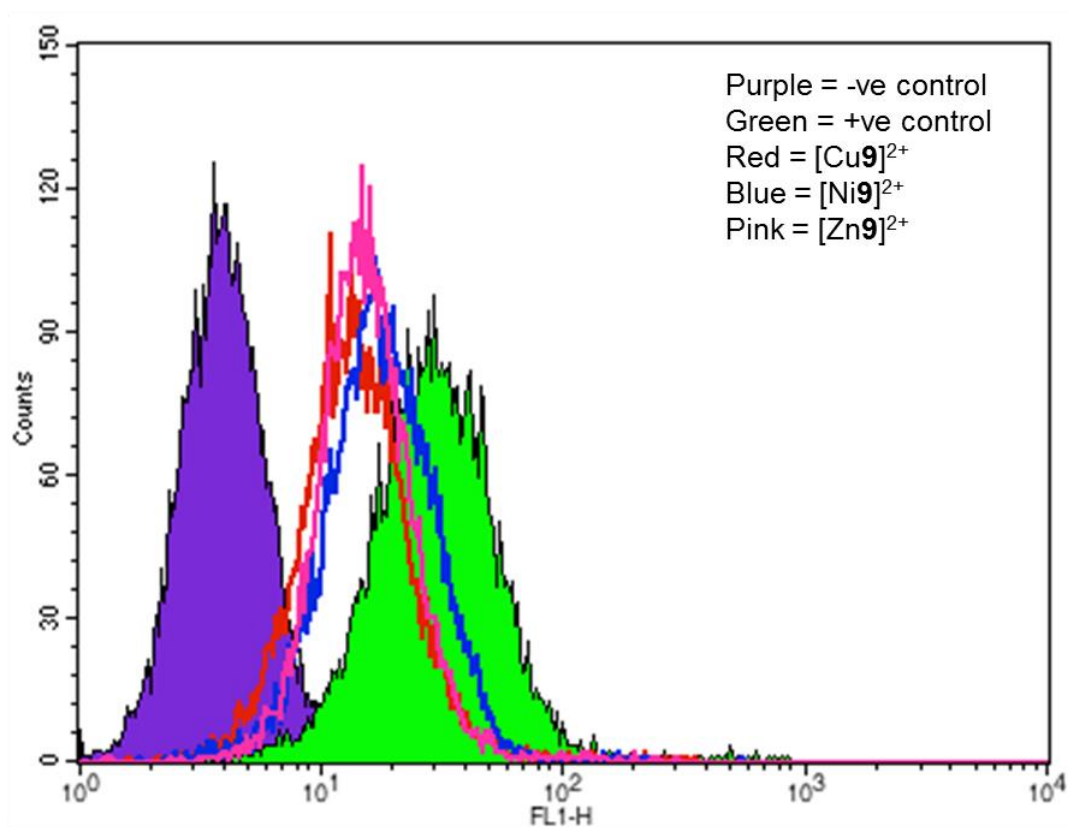
A. Dot plot – gridded area was used for histogram plots B - E.



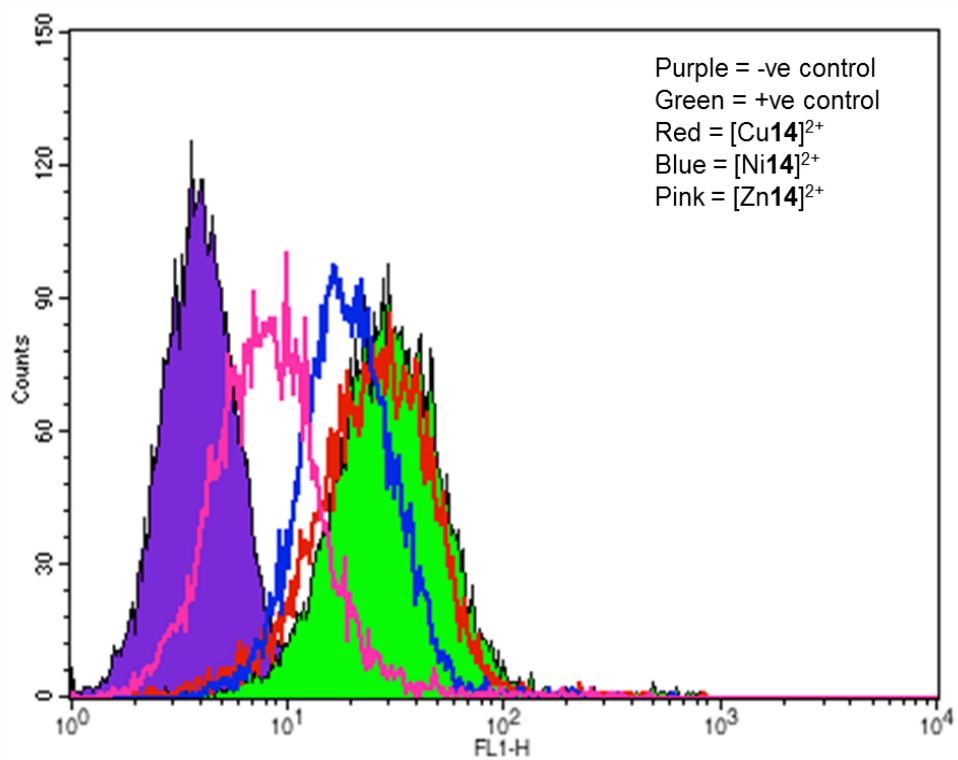
B. Histogram plot for the copper(II), zinc(II) and nickel(II) complexes for ligand **8**.



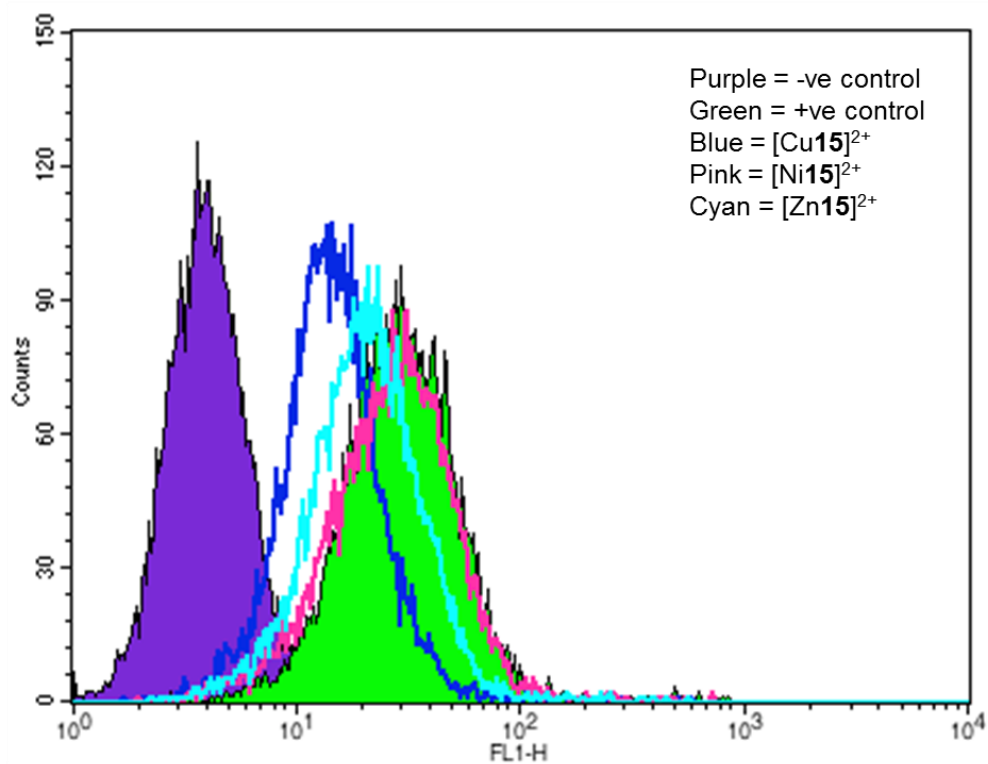
C. Histogram plot for the copper(II), zinc(II) and nickel(II) complexes for ligand **9**.



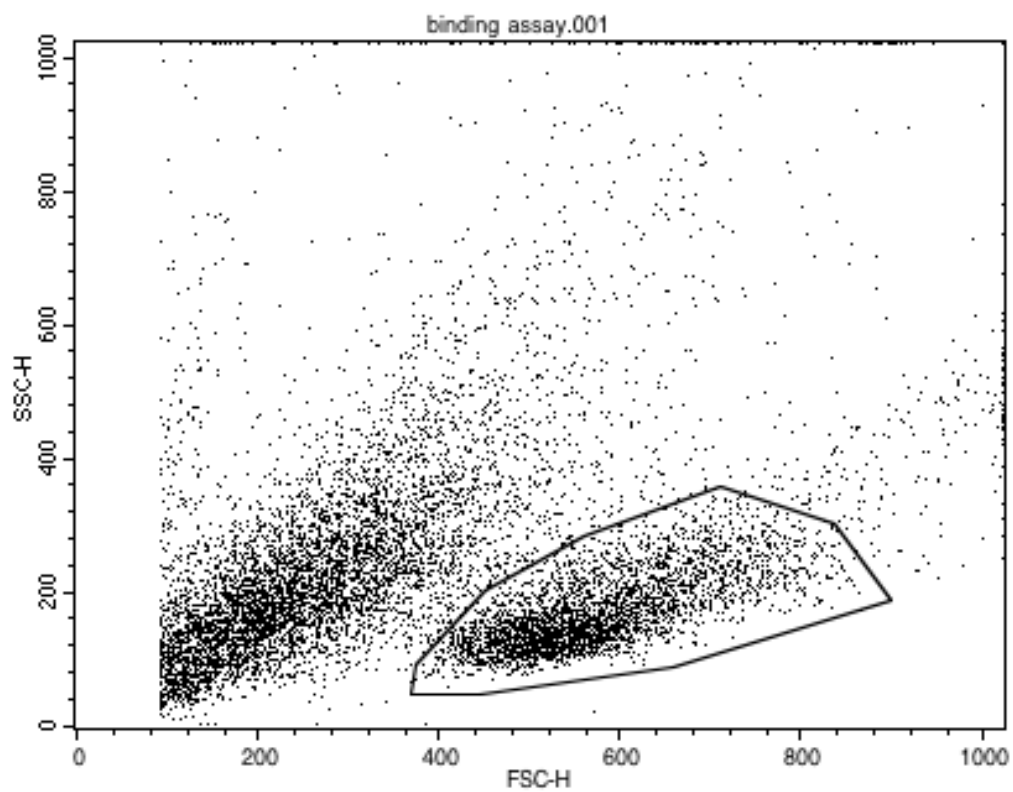
D. Histogram plot for the copper(II), zinc(II) and nickel(II) complexes for ligand **14**.



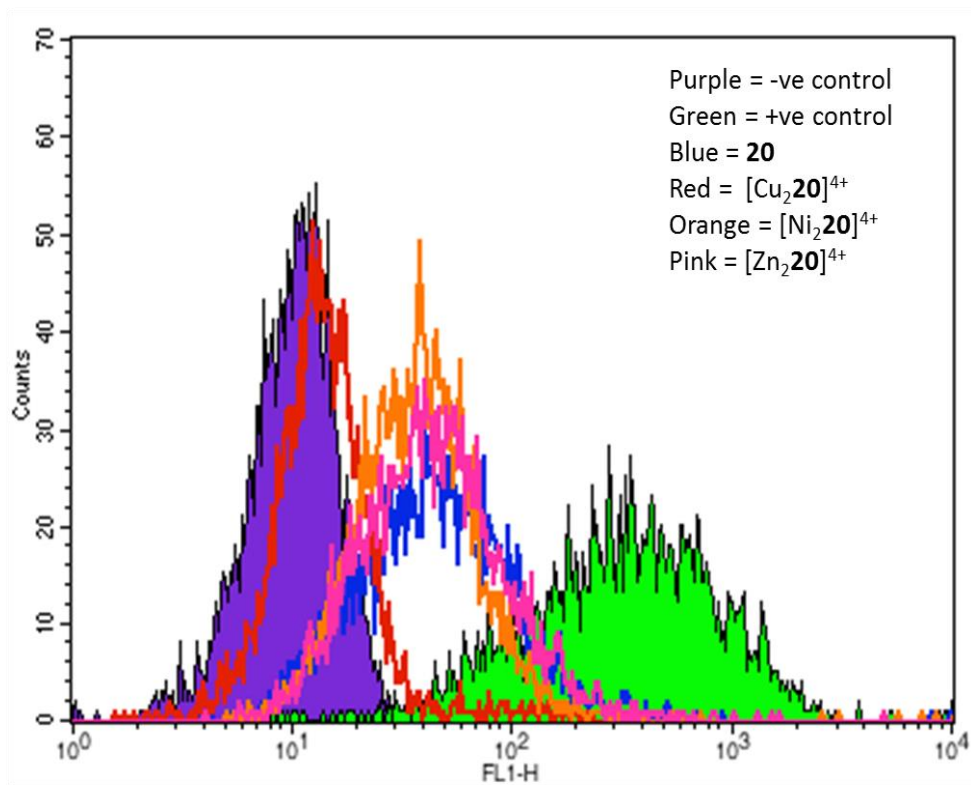
E. Histogram plot for the copper(II), zinc(II) and nickel(II) complexes for ligand **15**.



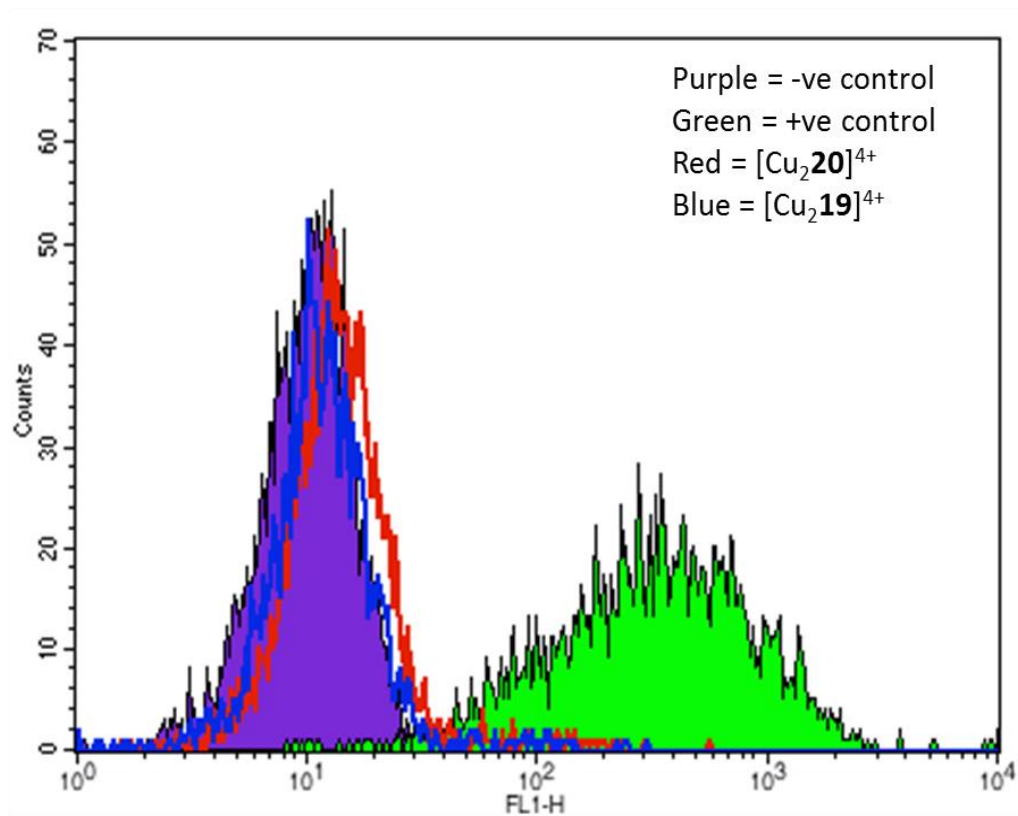
F. Dot plot – gridded area was used for histogram plots G, H and M - Q.



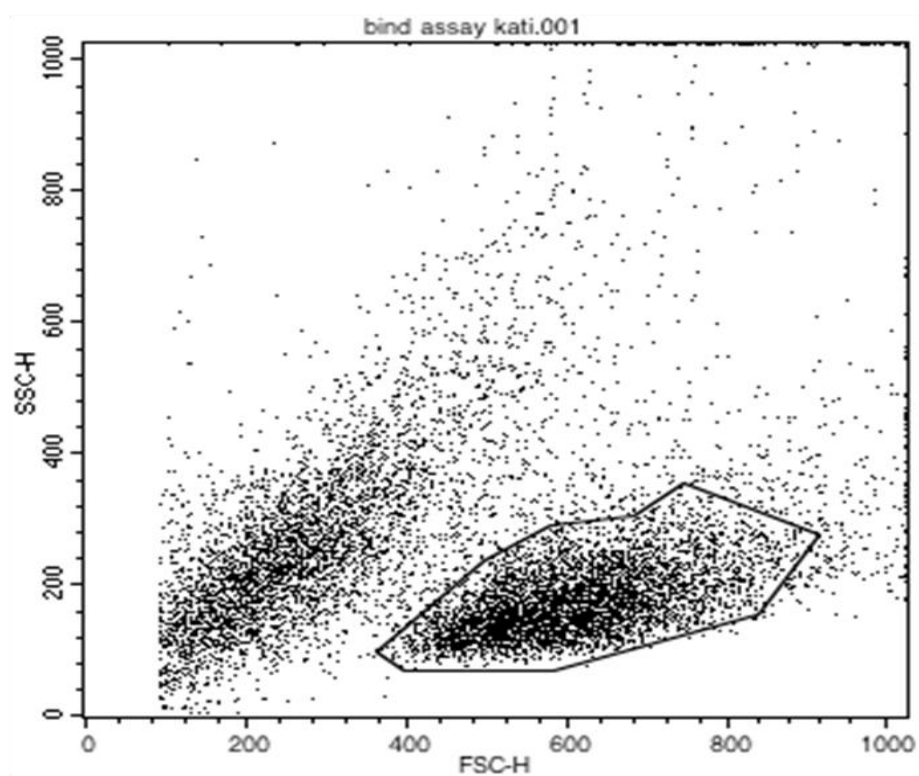
G. Histogram plot for ligand **20** and its copper(II), zinc(II) and nickel(II) complexes.



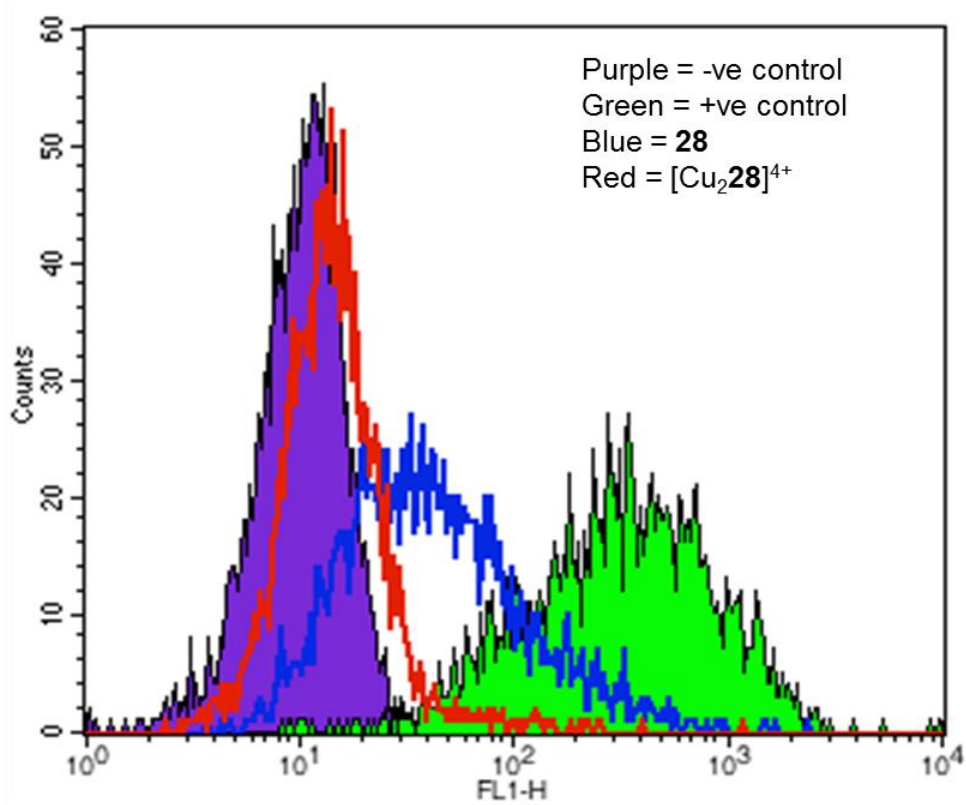
H. Histogram plot comparing the copper(II) complexes of ligand **19** and **20**.



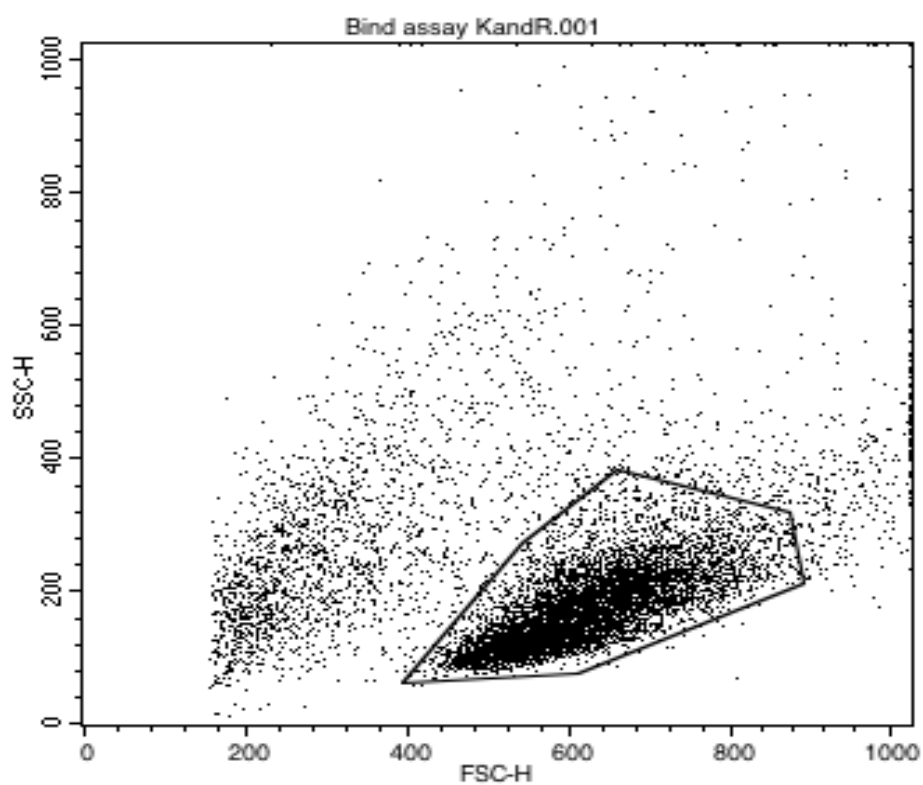
I. Dot plot – gridded area was used for histogram J.



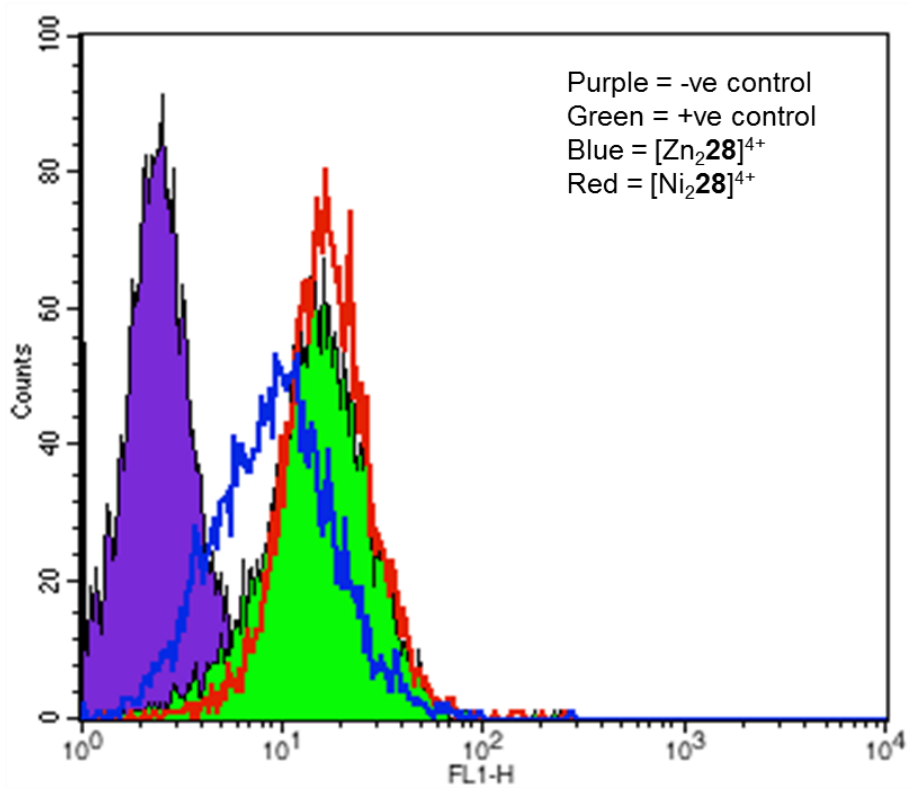
J. Histogram plot for ligand **28** and its copper(II) complex.



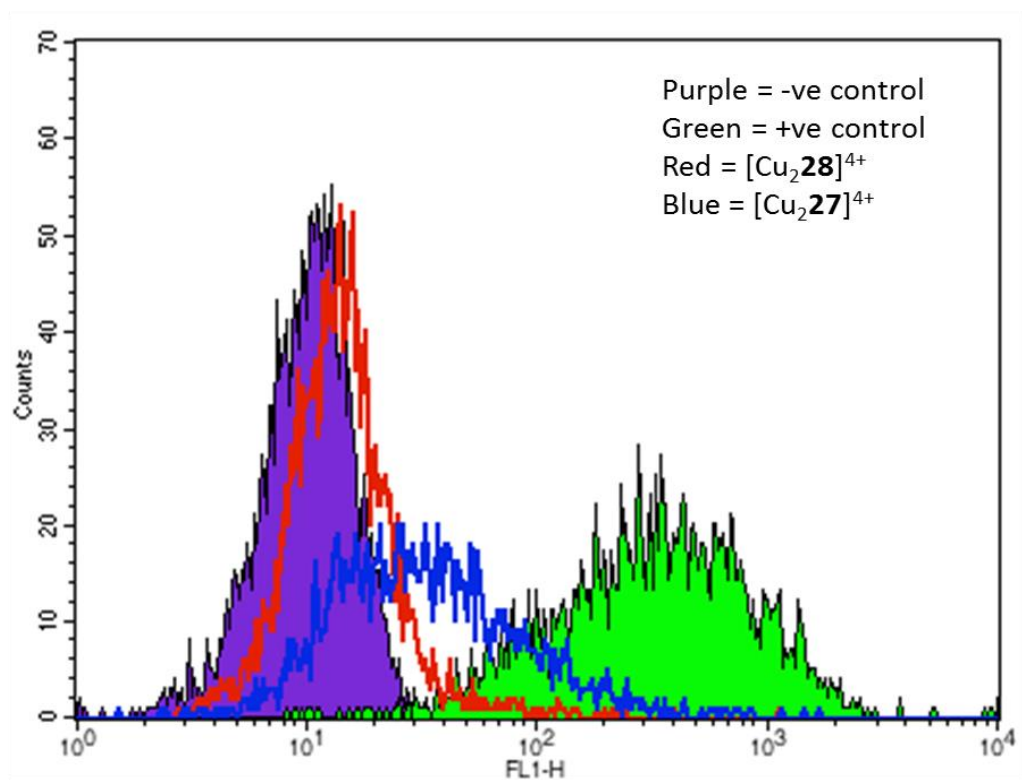
K. Dot plot – gridded area was used for histogram L.



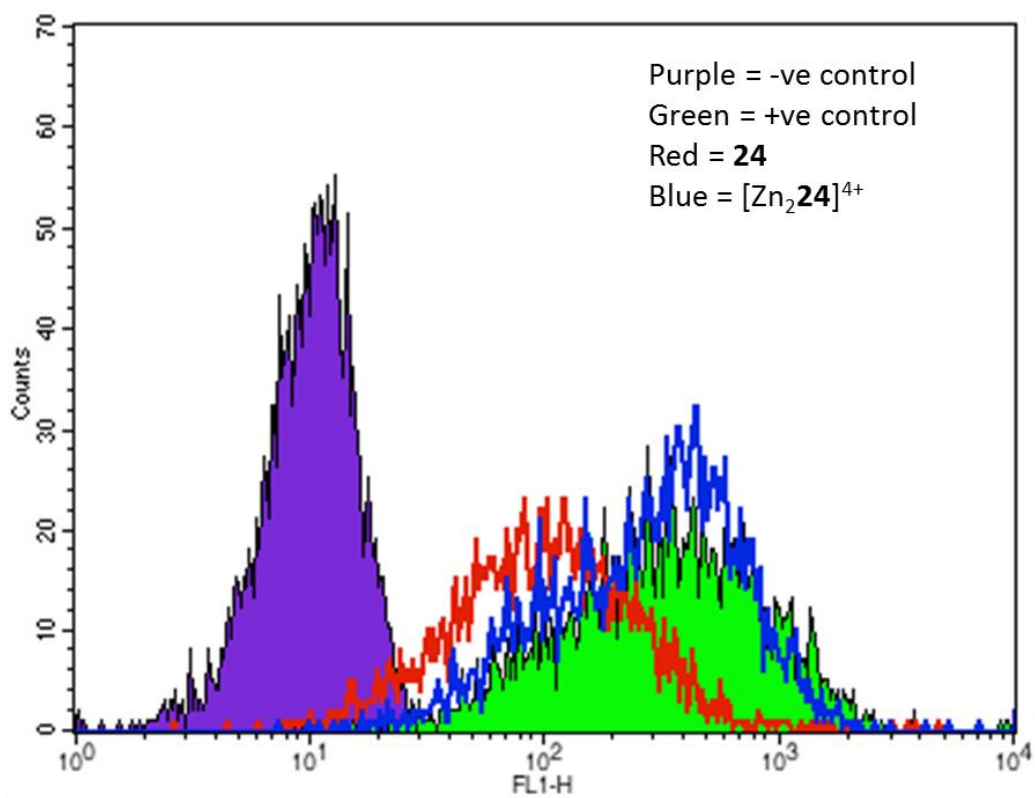
L. Histogram plot for the zinc(II) and nickel(II) complexes of ligand **28**.



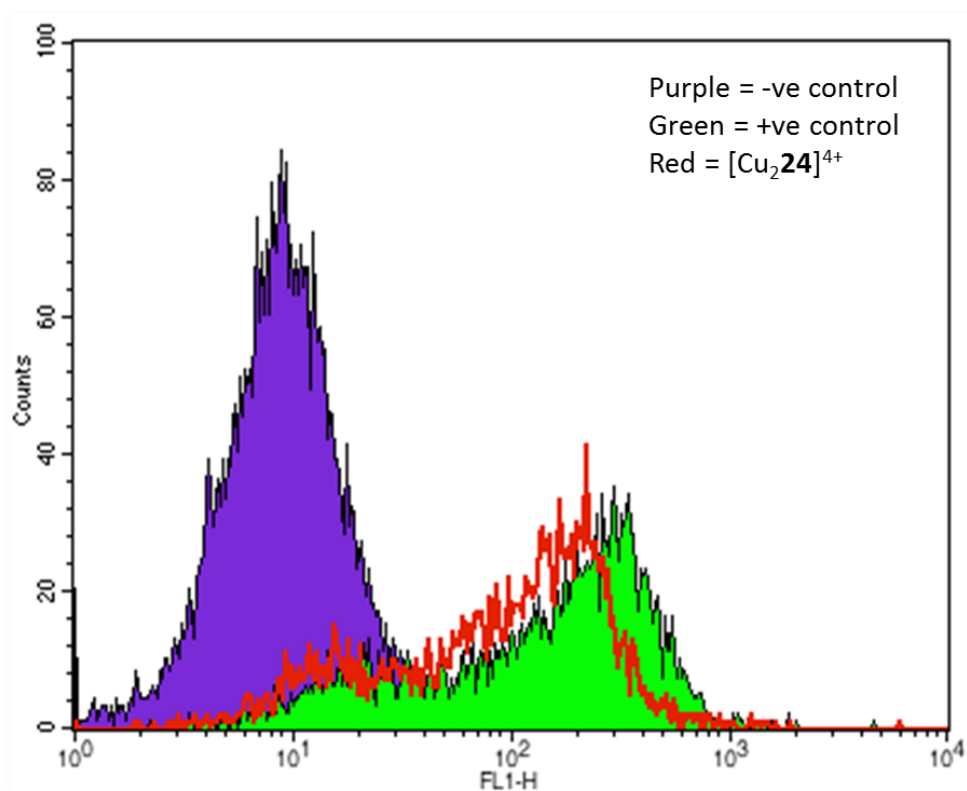
M. Histogram plot comparing the copper(II) complexes of ligand **27** and **28**.



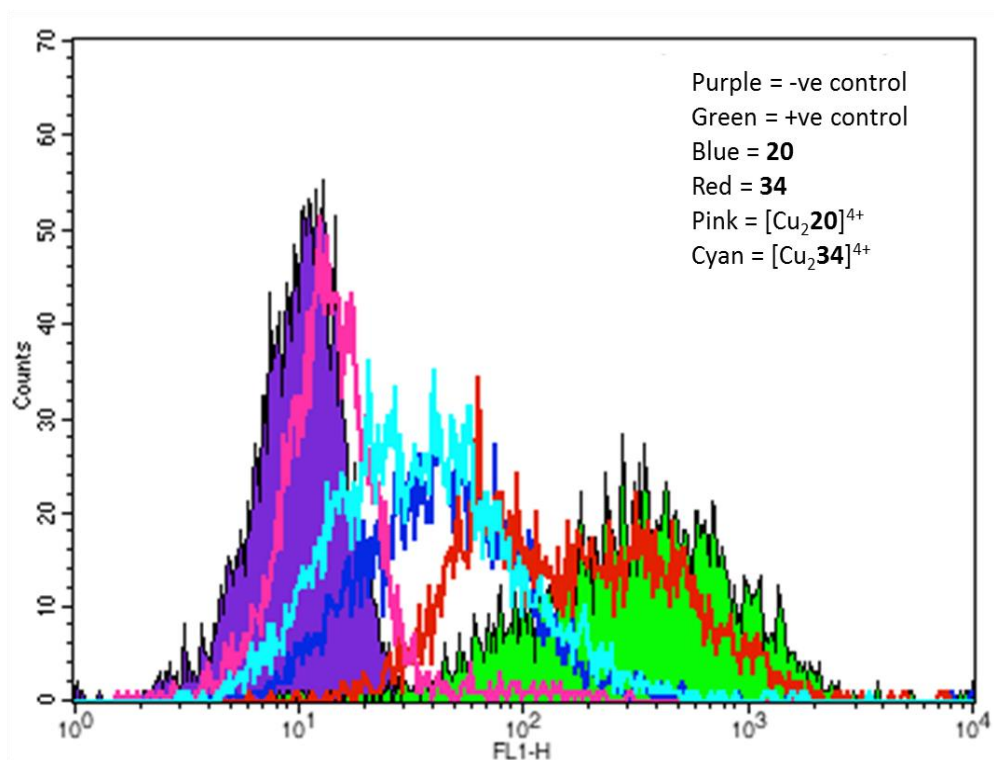
N. Histogram plot for ligand **24** and its zinc(II) complex.



O. Histogram plot for  $[\text{Cu}_2\mathbf{24}]^{4+}$ .



P. Histogram plot comparing the methylamine terminating ligand **20** with the acid terminating ligand **34** along with their respective copper(II) complexes.



Q. Histogram plot comparing the methylamine terminating ligand  $[\text{Cu}_2\mathbf{20}]^{4+}$  with the biotin tagged ligand  $[\text{Cu}_2\mathbf{44}]^{4+}$ .

